Hashemite Kingdom of Jordan

Jordan Journal of Biological Sciences

An International Peer-Reviewed Scientific Journal

Financed by the Scientific Research and Innovation Support Fund

This title is indexed in Scopus

http://jjbs.hu.edu.jo/

المجلة الأردنية للعلوم الحياتية
Jordan Journal of Biological Sciences (JJBS)
http://jjbs.hu.edu.jo

Jordan Journal of Biological Sciences (JJBS) (ISSN: 1995–6673 (Print); 2307-7166 (Online)): An International Peer- Reviewed Open Access Research Journal financed by the Scientific Research and Innovation Support Fund, Ministry of Higher Education and Scientific Research, Jordan and published quarterly by the Deanship of Scientific Research , The Hashemite University, Jordan.

Submission Address
Professor Wedyan, Mohammed A.
The Hashemite Universit y
P.O. Box 330127, Zarqa, 13115, Jordan
Phone: +962-5-3903333 ext.4147
E-Mail: jjbs@hu.edu.jo

المجلة الاردنية للعلوم الحياتية
Jordan Journal of Biological Sciences (JJBS)
http://jjbs.hu.edu.jo

International Advisory Board (Arranged alphabetically)

Instructions to Authors

Scopes

Study areas include cell biology, genomics, microbiology, immunology, molecular biology, biochemistry, embryology, immunogenetics, cell and tissue culture, molecular ecology, genetic engineering and biological engineering, bioremediation and biodegradation, bioinformatics, biotechnology regulations, gene therapy, organismal biology, microbial and environmental biotechnology, marine sciences. The JJBS welcomes the submission of manuscript that meets the general criteria of significance and academic excellence. All articles published in JJBS are peer-reviewed. Papers will be published approximately one to two months after acceptance.

Type of Papers

The journal publishes high-quality original scientific papers, short communications, correspondence and case studies. Review articles are usually by invitation only. However, Review articles of current interest and high standard will be considered.

Submission of Manuscript

Manuscript, or the essence of their content, must be previously unpublished and should not be under simultaneous consideration by another journal. The authors should also declare if any similar work has been submitted to or published by another journal. They should also declare that it has not been submitted/ published elsewhere in the same form, in English or in any other language, without the written consent of the Publisher. The authors should also declare that the paper is the original work of the author(s) and not copied (in whole or in part) from any other work. All papers will be automatically checked for duplicate publication and plagiarism. If detected, appropriate action will be taken in accordance with International Ethical Guideline. By virtue of the submitted manuscript, the corresponding author acknowledges that all the co-authors have seen and approved the final version of the manuscript. The corresponding author should provide all co-authors with information regarding the manuscript, and obtain their approval before submitting any revisions. Electronic submission of manuscripts is strongly recommended, provided that the text, tables and figures are included in a single Microsoft Word file. Submit manuscript as e-mail attachment to the Editorial Office at: JJBS@hu.edu.jo. After submission, a manuscript number will be communicated to the corresponding author within 48 hours.

Peer-review Process

It is requested to submit, with the manuscript, the names, addresses and e-mail addresses of at least 4 potential reviewers. It is the sole right of the editor to decide whether or not the suggested reviewers to be used. The reviewers' comments will be sent to authors within 6-8 weeks after submission.
Manuscripts and figures for review will not be returned to authors whether the editorial decision is to accept, revise, or reject. All Case Reports and Short Communication must include at least one table and/ or one figure.

Preparation of Manuscript

The manuscript should be written in English with simple lay out. The text should be prepared in single column format. Bold face, italics, subscripts, superscripts etc. can be used. Pages should be numbered consecutively, beginning with the title page and continuing through the last page of typewritten material.

The text can be divided into numbered sections with brief headings. Starting from introduction with section 1. Subsections should be numbered (for example 2.1 (then 2.1.1, 2.1.2, 2.2, etc.), up to three levels. Manuscripts in general should be organized in the following manner:

Title Page

The title page should contain a brief title, correct first name, middle initial and family name of each author and name and address of the department(s) and institution(s) from where the research was carried out for each author. The title should be without any abbreviations and it should enlighten the contents of the paper. All affiliations should be provided with a lower-case superscript number just after the author's name and in front of the appropriate address.
The name of the corresponding author should be indicated along with telephone and fax numbers (with country and area code) along with full postal address and e-mail address.

Abstract

The abstract should be concise and informative. It should not exceed **350 words** in length for full manuscript and Review article and **150 words** in case of Case Report and/ or Short Communication. It should briefly describe the purpose of the work, techniques and methods used, major findings with important data and conclusions. No references should be cited in this part. Generally non-standard abbreviations should not be used, if necessary they should be clearly defined in the abstract, at first use.

Keywords

Immediately after the abstract, **about 4-8 keywords** should be given. Use of abbreviations should be avoided, only standard abbreviations, well known in the established area may be used, if appropriate. These keywords will be used for indexing.

Abbreviations

Non-standard abbreviations should be listed and full form of each abbreviation should be given in parentheses at first use in the text.

Introduction

Provide a factual background, clearly defined problem, proposed solution, a brief literature survey and the scope and justification of the work done.

Materials and Methods

Give adequate information to allow the experiment to be reproduced. Already published methods should be mentioned with references. Significant modifications of published methods and new methods should be described in detail. Capitalize trade names and include the manufacturer's name and address. Subheading should be used.

Results

Results should be clearly described in a concise manner. Results for different parameters should be described under subheadings or in separate paragraph. Results should be explained, but largely without referring to the literature. Table or figure numbers should be mentioned in parentheses for better understanding.

Discussion

The discussion should not repeat the results, but provide detailed interpretation of data. This should interpret the significance of the findings of the work. Citations should be given in support of the findings. The results and discussion part can also be described as separate, if appropriate. The Results and Discussion sections can include subheadings, and when appropriate, both sections can be combined

Conclusions

This should briefly state the major findings of the study.

Acknowledgment

A brief acknowledgment section may be given after the conclusion section just before the references. The acknowledgment of people who provided assistance in manuscript preparation, funding for research, etc. should be listed in this section.

Tables and Figures

Tables and figures should be presented as per their appearance in the text. It is suggested that the discussion about the tables and figures should appear in the text before the appearance of the respective tables and figures. No tables or figures should be given without discussion or reference inside the text.

Tables should be explanatory enough to be understandable without any text reference. Double spacing should be maintained throughout the table, including table headings and footnotes. Table headings should be placed above the table. Footnotes should be placed below the table with superscript lowercase letters. Each table should be on a separate page, numbered consecutively in Arabic numerals.

Each figure should have a caption. The caption should be concise and typed separately, not on the figure area. Figures should be self-explanatory. Information presented in the figure should not be repeated in the table. All symbols and abbreviations used in the illustrations should be defined clearly. Figure legends should be given below the figures.

References

References should be listed alphabetically at the end of the manuscript. Every reference referred in the text must be also present in the reference list and vice versa. In the text, a reference identified by means of an author's name should be followed by the year of publication in parentheses (e.g.(Brown,2009)). For two authors, both authors' names followed by the year of publication (e.g.(Nelson and Brown, 2007)). When there are more than two authors, only the first author's name followed by "*et al*." and the year of publication (e.g. (Abu-Elteen *et al*., 2010)). When two or more works of an author has been published during the same year, the reference should be identified by the letters "a", "b", "c", etc., placed after the year of publication. This should be followed both in the text and reference list. e.g., Hilly, (2002a, 2002b); Hilly, and Nelson, (2004). Articles in preparation or submitted for publication, unpublished observations, personal communications, etc. should not be included in the reference list but should only be mentioned in the article text (e.g., Shtyawy,A., University of Jordan, personal communication). Journal titles should be abbreviated according to the system adopted in Biological Abstract and Index Medicus, if not included in Biological Abstract or Index Medicus journal title should be given in full. The author is responsible for the sccuracy and completeness of the references and for their correct textual citation. Failure to do so may result in the paper being withdraw from the evaluation process. Example of correct reference form is given as follows:-

Reference to a journal publication:

Bloch BK. 2002. Econazole nitrate in the treatment of *Candida vaginitis*. *S Afr Med J.* , **58**:314-323.

Ogunseitan OA and Ndoye IL. 2006. Protein method for investigating mercuric reductase gene expression in aquatic environments. *Appl Environ Microbiol.*, **64**: 695-702.

Hilly MO, Adams MN and Nelson SC. 2009. Potential fly-ash utilization in agriculture. *Progress in Natural Sci.*, **19**: 1173-1186.

Reference to a book:

Brown WY and White SR.1985. **The Elements of Style**, third ed. MacMillan, New York.

Reference to a chapter in an edited book:

Mettam GR and Adams LB. 2010. How to prepare an electronic version of your article. In: Jones BS and Smith RZ (Eds.), **Introduction to the Electronic Age**. Kluwer Academic Publishers, Netherlands, pp. 281–304.

Conferences and Meetings:

Embabi NS. 1990. Environmental aspects of distribution of mangrove in the United Arab Emirates. Proceedings of the First ASWAS Conference. University of the United Arab Emirates. Al-Ain, United Arab Emirates.

Theses and Dissertations:

El-Labadi SN. 2002. Intestinal digenetic trematodes of some marine fishes from the Gulf of Aqaba. MSc dissertation, The Hashemite University, Zarqa, Jordan.

Nomenclature and Units

Internationally accepted rules and the international system of units (SI) should be used. If other units are mentioned, please give their equivalent in SI.

For biological nomenclature, the conventions of the *International Code of Botanical Nomenclature, the International Code of Nomenclature of Bacteria,* and the *International Code of Zoological Nomenclature* should be followed.

Scientific names of all biological creatures (crops, plants, insects, birds, mammals, etc.) should be mentioned in parentheses at first use of their English term.

Chemical nomenclature, as laid down in the *International Union of Pure and Applied Chemistry* and the official recommendations of the *IUPAC-IUB Combined Commission on Biochemical Nomenclature* should be followed. All biocides and other organic compounds must be identified by their Geneva names when first used in the text. Active ingredients of all formulations should be likewise identified.

Math formulae

All equations referred to in the text should be numbered serially at the right-hand side in parentheses. Meaning of all symbols should be given immediately after the equation at first use. Instead of root signs fractional powers should be used. Subscripts and superscripts should be presented clearly. Variables should be presented in italics. Greek letters and non-Roman symbols should be described in the margin at their first use.

To avoid any misunderstanding zero (0) and the letter O, and one (1) and the letter l should be clearly differentiated. For simple fractions use of the solidus (/) instead of a horizontal line is recommended. Levels of statistical significance such as: $^{*}P < 0.05$, $^{**}P < 0.01$ and $^{***}P < 0.001$ do not require any further explanation.

Copyright

Submission of a manuscript clearly indicates that: the study has not been published before or is not under consideration for publication elsewhere (except as an abstract or as part of a published lecture or academic thesis); its publication is permitted by all authors and after accepted for publication it will not be submitted for publication anywhere else, in English or in any other language, without the written approval of the copyright-holder. The journal may consider manuscripts that are translations of articles originally published in another language. In this case, the consent of the journal in which the article was originally published must be obtained and the fact that the article has already been published must be made clear on submission and stated in the abstract. It is compulsory for the authors to ensure that no material submitted as part of a manuscript infringes existing copyrights, or the rights of a third party.

Ethical Consent

All manuscripts reporting the results of experimental investigation involving human subjects should include a statement confirming that each subject or subject's guardian obtains an informed consent, after the approval of the experimental protocol by a local human ethics committee or IRB. When reporting experiments on animals, authors should indicate whether the institutional and national guide for the care and use of laboratory animals was followed.

Plagiarism

The JJBS hold no responsibility for plagiarism. If a published paper is found later to be extensively plagiarized and is found to be a duplicate or redundant publication, a note of retraction will be published, and copies of the correspondence will be sent to the authors' head of institute.

Galley Proofs

The Editorial Office will send proofs of the manuscript to the corresponding author as an e-mail attachment for final proof reading and it will be the responsibility of the corresponding author to return the galley proof materials appropriately corrected within the stipulated time. Authors will be asked to check any typographical or minor clerical errors in the manuscript at this stage. No other major alteration in the manuscript is allowed. After publication authors can freely access the full text of the article as well as can download and print the PDF file.

Publication Charges

There are no page charges for publication in Jordan Journal of Biological Sciences, except for color illustrations,

Reprints

Ten (10) reprints are provided to corresponding author free of charge within two weeks after the printed journal date. For orders of more reprints, a reprint order form and prices will be sent with article proofs, which should be returned directly to the Editor for processing.

Disclaimer

Articles, communication, or editorials published by JJBS represent the sole opinions of the authors. The publisher shoulders no responsibility or liability what so ever for the use or misuse of the information published by JJBS.

Indexing

JJBS is indexed and abstracted by:

DOAJ (Directory of Open Access Journals)	CABI
Google Scholar	EBSCO
Journal Seek	CAS (Chemical Abstract Service)
HINARI	ETH- Citations
Index Copernicus	Open J-Gat
NDL Japanese Periodicals Index	SCImago
SCIRUS	Clarivate Analytics (Zoological Abstract)
OAJSE	Scopus
ISC (Islamic World Science Citation Center)	AGORA (United Nation's FAO database)
Directory of Research Journal Indexing (DRJI)	SHERPA/RoMEO (UK)
Ulrich's	

المجلة الأردنية للعلوم الحياتية
Jordan Journal of Biological Sciences (JJBS)
ISSN 1995- 6673 (Print), 2307- 7166 (Online)
http://jjbs.hu.edu.jo

The Hashemite University

Deanship of Scientific Research

TRANSFER OF COPYRIGHT AGREEMENT

Journal publishers and authors share a common interest in the protection of copyright: authors principally because they want their creative works to be protected from plagiarism and other unlawful uses, publishers because they need to protect their work and investment in the production, marketing and distribution of the published version of the article. In order to do so effectively, publishers request a formal written transfer of copyright from the author(s) for each article published. Publishers and authors are also concerned that the integrity of the official record of publication of an article (once refereed and published) be maintained, and in order to protect that reference value and validation process, we ask that authors recognize that distribution (including through the Internet/WWW or other on-line means) of the authoritative version of the article as published is best administered by the Publisher.

To avoid any delay in the publication of your article, please read the terms of this agreement, sign in the space provided and return the complete form to us at the address below as quickly as possible.

Article entitled:----------

Corresponding author: ----------

To be published in the journal: Jordan Journal of Biological Sciences (JJBS)

I hereby assign to the Hashemite University the copyright in the manuscript identified above and any supplemental tables, illustrations or other information submitted therewith (the "article") in all forms and media (whether now known or hereafter developed), throughout the world, in all languages, for the full term of copyright and all extensions and renewals thereof, effective when and if the article is accepted for publication. This transfer includes the right to adapt the presentation of the article for use in conjunction with computer systems and programs, including reproduction or publication in machine-readable form and incorporation in electronic retrieval systems.
Authors retain or are hereby granted (without the need to obtain further permission) rights to use the article for traditional scholarship communications, for teaching, and for distribution within their institution.

☐ **I am the sole author of the manuscript**

☐ **I am signing on behalf of all co-authors of the manuscript**

☐ **The article is a 'work made for hire' and I am signing as an authorized representative of the employing company/institution**

Please mark one or more of the above boxes (as appropriate) and then sign and date the document in black ink.

Signed:_____ **Name printed:** _____
Title and Company (if employer representative) : _____
Date: _____

Data Protection: By submitting this form you are consenting that the personal information provided herein may be used by the Hashemite University and its affiliated institutions worldwide to contact you concerning the publishing of your article.

Please return the completed and signed original of this form by mail or fax, or a scanned copy of the signed original by e-mail, retaining a copy for your files, to:

Hashemite University
Jordan Journal of Biological Sciences
Zarqa 13115 Jordan
Fax: +962 5 3903338
Email: jjbs@hu.edu.jo

Editorial Preface

Jordan Journal of Biological Sciences (JJBS) is a refereed, quarterly international journal financed by the Scientific Research and Innovation Support Fund, Ministry of Higher Education and Scientific Research in cooperation with the Hashemite University, Jordan. JJBS celebrated its 12th commencement this past January, 2020. JJBS was founded in 2008 to create a peer-reviewed journal that publishes high-quality research articles, reviews and short communications on novel and innovative aspects of a wide variety of biological sciences such as cell biology, developmental biology, structural biology, microbiology, entomology, molecular biology, biochemistry, medical biotechnology, biodiversity, ecology, marine biology, plant and animal biology, plant and animal physiology, genomics and bioinformatics.

We have watched the growth and success of JJBS over the years. JJBS has published 14 volumes, 60 issues and 800 articles. JJBS has been indexed by SCOPUS, CABI's Full-Text Repository, EBSCO, Clarivate Analytics- Zoological Record and recently has been included in the UGC India approved journals. JJBS Cite Score has improved from 0.7 in 2019 to 1.4 in 2021 (Last updated on 6 March, 2022) and with Scimago Institution Ranking (SJR) 0.22 (Q3) in 2021.

A group of highly valuable scholars have agreed to serve on the editorial board and this places JJBS in a position of most authoritative on biological sciences. I am honored to have six eminent associate editors from various countries. I am also delighted with our group of international advisory board members coming from 15 countries worldwide for their continuous support of JJBS. With our editorial board's cumulative experience in various fields of biological sciences, this journal brings a substantial representation of biological sciences in different disciplines. Without the service and dedication of our editorial; associate editorial and international advisory board members, JJBS would have never existed.

In the coming year, we hope that JJBS will be indexed in Clarivate Analytics and MEDLINE (the U.S. National Library of Medicine database) and others. As you read throughout this volume of JJBS, I would like to remind you that the success of our journal depends on the number of quality articles submitted for review. Accordingly, I would like to request your participation and colleagues by submitting quality manuscripts for review. One of the great benefits we can provide to our prospective authors, regardless of acceptance of their manuscripts or not, is the feedback of our review process. JJBS provides authors with high quality, helpful reviews to improve their manuscripts.

Finally, JJBS would not have succeeded without the collaboration of authors and referees. Their work is greatly appreciated. Furthermore, my thanks are also extended to The Hashemite University and the Scientific Research and Innovation Support Fund, Ministry of Higher Education and Scientific Research for their continuous financial and administrative support to JJBS.

Professor Wedyan ,Mohammed A.
March, 2024

JJBS

Volume 19, Number 1, June 2026
ISSN 1995-6673

Jordan Journal of Biological Sciences

CONTENTS

Original Articles

JJBS

Volume 19, Number 1,March 2026
ISSN 1995-6673
Pages 1 – 11
https://doi.org/10.54319/jjbs/190101

Jordan Journal of Biological Sciences

Ecological testing of foreign melon varieties (*Cucumis melo L.*) in the climatic conditions of the Kazakhstan's Aral Sea region

Kanagat Begaliev[1], Sultanbek Tauipbaev[1], Serikbai Umirzakov[2], Marat Zhanzakov[3], Laura Tokhetova[4,*]

[1]Department of Vegetable and Potato Crops, Kazakh Scientific Research Institute of Rice Cultivation named after Ibray Zhakhaev, Kyzylorda, Republic of Kazakhstan; [2]Department of Rice Seed Production and Rice Crop Rotation, Kazakh Scientific Research Institute of Rice Cultivation named after Ibray Zhakhaev, Kyzylorda, Republic of Kazakhstan; [3]Research Institute "Bolashak", Bolashak University, Kyzylorda, Republic of Kazakhstan; [4]Department of Agricultural Technologies, Korkyt Ata Kyzylorda University, Kyzylorda, Republic of Kazakhstan

Received: May 1, 2025; Revised: June 10, 2025; Accepted: June 27, 2025

Abstract

The study is relevant for assessing the adaptability of foreign watermelon varieties (Cucumis melo L.) to climate change in Kazakhstan's Aris region, aiming to enhance sustainability and yield. The aim of this study was to assess the yield of several foreign melon varieties with different ripening times in the conditions of the Kyzylorda region of Kazakhstan. The research was conducted on experimental fields of the Kazakh Research Institute of Rice Farming named after I. Zhakhaev, located in the village of Karaultyube, Kyzylorda region, under the conditions of a sharply continental climate. The melon varieties tested included selections from Uzbekistan, Ukraine, Russia, and Israel, with a total of 14 varieties included in the study. The results showed a slight correlation between laboratory seed germination and the emergence of seedlings in the "open" soil, although it was not statistically significant ($P>0.05$). The experimental results showed that Uzbek varieties had longer germination periods, with the growing season length determined by the melon variety. On average, 2-3 fruits developed per plant, and the fruit weight variation within each variety was minimal, with a coefficient of variation not exceeding 6%. During storage tests, it was found that skin thickness significantly influenced fruit preservation ($r=0.59$, $P<0.05$). As for the taste quality of the fruits, the sugar content in the flesh ($r=0.56$, $P<0.05$) and the dissolved solids content ($r=0.61$, $P<0.05$) were statistically significant factors. All the foreign melon varieties tested showed good yields and could be used for cultivation in the Aral Sea region.

Key words: Soluble solids, Transportability, Rind thickness, Germination, Taste quality, Correlation.

1. Introduction

Melons are an important food product for the population of Kazakhstan, as they contain a significant amount of easily digestible carbohydrates, vitamins A, D, C, K, E, and some B vitamins. Biologically active compounds such as tocopherols, phospholipids, sterols, organic acids, and trace elements also provide beneficial effects on human health. According to W. Khalid et al. (2021), melons are cultivated in many countries and have high economic importance worldwide due to their high adaptation to various climates and soil types. In recent decades, melons have also been used for the production of long-storage products, as methods for their long-term preservation have been developed.

As a result, since 2019, Kazakhstan has seen an annual increase in the area allocated for melon cultivation as well as the overall yield. According to the National Statistics Bureau of the Agency for Strategic Planning and Reforms of the Republic of Kazakhstan, melon yields increased from 206.8 centners per hectare in 2012 to 255.6 centners per hectare in 2022 (Statistical Collection "Agriculture…, 2023). Similar data are cited by I. Urazbaev and N.K. Masharipov (2021), indicating that the area of melon cultivation in Eurasian countries reached 9%, and the total yield was 31.2 million tonnes.

In Kazakhstan, melon crops such as watermelon, melon, pumpkin, and cucumber are widespread and cultivated in almost all regions, with commercial production concentrated in areas most favorable for these plants (Zymaroieva et al., 2021; Faichuk et al., 2022). One such region is the southern part of Kazakhstan, including the Kyzylorda region, which, due to the accumulated heat during the growing season, is conducive to growing various melon varieties with different ripening times and high taste qualities. This is confirmed by research from S.U. Kosanov et al. (2022), who note that it is in the Kyzylorda region where high melon yields (watermelons, melons, etc.) are obtained annually, aided by the region's vast territory with a sandy landscape ideal for melon cultivation. Long-standing selection of the available genetic material has led to the creation of local varieties, which, by many indicators, significantly lag behind the modern gene pool of melons from other countries (Serhienko et al., 2023; Novruzova, 2016). Therefore, in

* Corresponding author. e-mail: ltokhetova@gmail.com.

order to maintain high yields of melon crops and meet the population's demand for various types of melons, regular genetic material exchange is necessary, as emphasized by Zh.Zh. Mamyrbekov et al. (2024), alongside ongoing research on developing new varieties with required properties and the acclimatization of imported varieties to the country's conditions.

According to M. Lija and S. Beevy (2021), there are many botanical and horticultural varieties of melons worldwide. These varieties vary significantly in shape, skin and flesh colour, flesh thickness, sweetness, seed cavity, seed size, and more, which influences the market value of melons. Thus, the breeding work in Kazakhstan's melon farming is multifaceted and not limited to the use of foreign gene pools of these plants, but also includes active efforts to create local disease-resistant melon varieties. Given the constant global population growth, R. Turamatov et al. (2021) believe that high-yielding, intensive agricultural varieties are of significant interest. Consequently, all work in melon farming is focused on research aimed at increasing the total volume of fruit not by expanding the cultivation area but by increasing yields several times over. Additionally, the country is actively working on preserving indigenous plant varieties, including melons, as highlighted by N. Kiseleva and M. Yessimbekova (2024).

Considering that the Kyzylorda region is the main and unique natural area for melon production in Kazakhstan, the issues of increasing melon crop yields are particularly relevant. These include expanding the variety and yield of melon products as well as exploring the possibility of exporting them to other regions of the country and beyond. However, these issues remain largely unexplored.

The aim of this research was to evaluate the adaptation of foreign melon varieties (Cucumis melo L.) to the climatic conditions of the Aral region in Kazakhstan, in particular to study their growth, yield, transport characteristics, fruit quality, and storage capacity. The task of the study was to identify the most suitable varieties for cultivation in conditions of low soil fertility and climate change, as well as to assess the prospects for the use of foreign genetic material in agriculture in Kazakhstan.

2. Literature Review

Melon (Cucumis melo L.) is a member of the Cucurbitaceae family, a heat- and light-loving plant, resistant to soil salinity and drought, but poorly tolerates high air humidity. The most well-known melon-exporting countries include China, the USA, Spain, Turkey, Australia, and Iran, as noted by K. Kubo et al. (2021). In 2022-2023, Australia produced 226,022 tonnes of melons worth USD 248 million, according to S.P. Singh (2023). Japan and Singapore are the largest export markets (accounting for 75%), with New Zealand and the UAE also being significant export markets. S. Yunusov et al. (2023) highlight that the current focus of melon breeding is on developing varieties suitable for growing at different times, particularly in isolated and protected environments, as well as refining greenhouse cultivation methods.

Among the research on melon breeding in open fields worldwide, the following directions are prominent: the study of water and temperature stress effects on melon growth and productivity, as explored by D. Yavuz et al. (2021); the impact of seasonal and weather factors on melon cultivation, studied by Y. Qian Ong and M. Moneruzzaman Khandaker (2021); and breeding melons for sweetness, firmness, and fruit colour, as well as early ripening, which has been investigated by F. Soltani (2021). The use of fertilisers to accelerate growth and fruit ripening has been examined by N.F. Mukhtar and A.B. Abd Samad (2022). Ecological conditions for growing organic produce were explored by G. Chen (2022). In recent years, numerous studies have focused on growing melons in greenhouse conditions, including the effect of substrate on melon growth and yield, studied by C.S. Nascimento et al. (2020); comparison of stem load in different growing conditions, examined by D.S. Lee et al. (2021); and pesticide management to prevent melon diseases, researched by G.R. dos Santos et al. (2021).

However, the most in-depth research has been in the genetic field, with studies using SSRs and SNPs markers to assess genetic differences between melon varieties, as conducted by J. Zhang et al. (2023), and examining the relationship between phenotypic traits and the yield of different varieties, as explored by F. Soltani et al. (2022), who found positive correlations between the number of female flowers, fruit count, and yield. However, the number of fruits negatively correlated with leaf area. H. Chikh-Rouhou et al. (2021) found that the “Galaoui” genotype had the highest β-carotene (6.6 mg) and flavonoid content (45.4), while the “Dzeri” genotype contained significant phenolic compounds (896.67 mg), the “Rupa” genotype had the highest antioxidant activity (14.61%), and the “Asli” genotype contained vitamin C (0.15 g/100 ml of fresh juice).

One-sided selection focused solely on increasing yield decreases the expected benefits of modern melon varieties. S. Manchali et al. (2021) report that wild and local melon varieties in India had higher soluble solids content and reducing sugars, as well as other biologically active compounds, making them more marketable. Similar conclusions were made by H. Kesh and P. Kaushik (2021), who noted the valuable genetic and metabolic variability of local and wild melon species, which helps increase yield and expand the genetic base of cultivated melons.

In the post-Soviet countries, one of the main areas of melon research is the acclimatisation and adaptation of foreign varieties to local conditions. B. Asabaev and A.K. Kostakov (2020) conducted a comprehensive study on the comparative productivity of foreign melon varieties, highlighting how different climatic conditions influence yield and quality. Zh.Zh. Mamyrbekov et al. (2021) also focused on similar research, providing valuable insights into the performance of these varieties in various regions, and assessing the genetic and agronomic traits that contribute to their adaptability. M. Yessimbekova et al. (2024) examined the introduction of genetic material, with a particular emphasis on the potential for improving local melon varieties through the incorporation of foreign genetic traits, enhancing both their resistance to disease and their overall productivity.

For example, in the study by Zh.Zh. Mamyrbekov et al. (2021), it was concluded that the highest yields in southern Kazakhstan came from four melon hybrids – Sari Ball, Darvina F1, AH 6404 F1, and Giallo da Inverno. Varieties such as Darimo F1, Darvina F1, Ah70-158 F1, Pirona F1, and DC 45-160 F1 were also found to be more resistant to

a range of melon diseases, including powdery mildew, peronosporosis, and fusariosis, making them promising for cultivation in Kazakhstan. A similar study was conducted by S. Yunusov et al. (2023), in which late-ripening varieties such as L-Oybek yielded 45.2 t/ha, while the mid-season variety Non Gosht Khorezm produced 27.1 t/ha. Thus, given the different experimental conditions used by the authors, it is not possible to directly compare their findings. Furthermore, neither study included the use of mineral fertilisers or plant protection measures in their variety testing, making it difficult to determine the optimal melon varieties for cultivation in Kazakhstan's Aral Sea region.

The review of recent literature suggests that genetic research aimed at increasing melon yields under different environmental and climatic conditions is a promising direction in melon farming. As there is no definitive conclusion regarding the most promising melon varieties adapted to the conditions of the Aral Sea region, further research in this area is both necessary and promising for improving the economic potential of Kazakhstan's agricultural production.

3. Materials and Methods

A series of experiments on the yield of foreign melon varieties under the conditions of the Aral Sea region were conducted at the experimental fields of the Kazakh Research Institute of Rice Cultivation named after I. Zhakhaev, located in the village of Karaultyube, Kyzylorda region. The experiments took place under the conditions of a sharply continental climate, with an annual temperature range from -34°C to +41°C. During the experiment, the average annual air temperature was 9°C, and the total precipitation was only 105 mm per year. Melons were grown on low-fertility meadow-swamp soils on areas previously used for rice cultivation.

During the variety testing, melons from foreign breeding varieties from the following countries were used: Uzbekistan – 4 varieties (Myrzashop, Sary Kauyn, Syrnaval, Kyzyl Kauyn), Ukraine – 3 varieties (July, Zolotistaya, Titovka), Russia – 5 varieties (Yuzhanka, Ananas, Muza, Ethiopka, Princess Elizabeth), and Israel – 2 varieties (Can-4, Israel). These were randomly sown in designated areas of the station's nursery, with each variety allocated at least 9 m², and each variety was planted in triplicates. During the vegetation period, manual weeding was performed three times, the holes were loosened, vines were laid out, and fruits were harvested as they ripened. Up to 10 vegetation irrigations were carried out during the growing period. Since the experiment was focused on ecological fruit cultivation, plant protection means and pesticides were not used.

The selection of the 14 foreign melon varieties from Uzbekistan, Ukraine, Russia, and Israel was based on several criteria, including their proven yield potential, resistance to environmental stress factors, flavor profile, and transportability. These varieties were chosen because of their adaptability to diverse climatic conditions and their relevance to melon cultivation in regions similar to Kazakhstan's Aral Sea area. Previous studies on the performance of these varieties in different environmental conditions suggested their suitability for testing in the sharply continental climate of the Aral Sea region. The aim was to identify varieties that could not only provide high yields but also demonstrate resilience against common agricultural stresses such as drought and soil salinity, and possess desirable flavor and transportability characteristics that would be important for both local consumption and potential export.

The yield of the experimental samples was determined by comparing the number and weight of fruits among the varieties. The yield was divided into standard and non-standard products according to GOST 7178-2015 "Fresh melons. Specifications" (2015). Fruits affected by anthracnose, bacterial disease, fusarium, powdery mildew, or damaged by pests and sunburns were considered as defective. To maintain the purity of the experiment and prevent inter-variety hybridization that could affect the results, self-pollination or intra-varietal pollination was performed.

Initial data on the variety testing were recorded based on characteristics such as seed germination, yield, and fruit weight, which were directly measured on the experimental plots using third-class accuracy scales. Fruits of medium size were selected for laboratory and tasting tests. Laboratory analysis, namely the content of dry soluble substances and sugars, was conducted at the "Department of Vegetable and Melon Crops and Potatoes" laboratory. Digital refractometers Atago (Japan) of the PAL series (PAL-1 and PAL-3) with automatic temperature compensation were used to minimize errors during the research. For tasting, melons were evaluated based on criteria such as pulp structure, juiciness, and flavor, with a total score given. The suitability of melons of different varieties for export to other regions and countries was determined by assessing their transportability and storage qualities. This was done by transporting the fruits by car to a laboratory after harvesting, where they were stored at 5°C and 85-90% relative humidity for six days, followed by a day at room temperature to determine their preservation rate.

The results obtained were recorded in an electronic spreadsheet file for statistical and correlation analysis using the Tibco Statistica 14.0.1 software. The results of the mathematical analysis were used to compare growth indicators, transport, and flavour characteristics of the fruits, which were then converted into conclusions and recommendations for further characteristics.

4. Results

4.1. Quality of Genetic Material and Seed Germination

The first stage of the work was to check the quality of the genetic material of the various melon varieties in laboratory conditions. The seed material from foreign breeding varieties, selected for the ecological variety testing in the Aral Sea region, showed slight differences in seed germination levels under laboratory conditions. The results of this work are presented in Table 1.

Table 1. Results of seed germination tests for the controlled melon varieties in laboratory conditions

No.	Sample name	Seed origin, country	Laboratory seed germination, %
1	Myrzashop	Uzbekistan	87.4±2.1
2	Sary Kauyn	Uzbekistan	93.1±3.7
3	Syrnaval	Uzbekistan	91.6±5.2
4	Kyzyl Kauyn	Uzbekistan	98.1±1.9
5	July	Ukraine	87±4.6
6	Zolotistaya	Ukraine	89.3±3.7
7	Titovka	Ukraine	94.4±5.5
8	Yuzhanka	Russia	93.7±2.2
9	Ananas	Russia	89.3±1.9
10	Muza	Russia	95.5±0.9
11	Ethiopka	Russia	97.1±1.1
12	Princess Elizabeth	Russia	89.3±2.1
13	Israel	Israel	95.6±1.5
14	Can-4	Israel	87.3±3.4

The results presented in Table 1 show the seed germination rates for the 14 foreign melon varieties tested under laboratory conditions. The germination rates ranged from 87.3% to 98.1%, with the highest germination observed in the Uzbek variety Kyzyl Kauyn (98.1%) and the lowest in Can-4 from Israel (87.3%). While the seed germination rates varied slightly across the varieties, there were no significant differences between them based on their country of origin. The variability observed in germination rates can be attributed to minor genetic differences between the varieties, but the overall performance of the genetic material was satisfactory.

The results also suggest that the seed material used in the experiment was of good quality and suitable for further testing in the Aral Sea region's growing conditions. The small differences in germination percentages between varieties can be considered within the acceptable range for agricultural research, especially given that the differences were not statistically significant.

The analysis of seed germination confirms that the foreign melon varieties selected for this study exhibit reliable germination rates, ensuring that the experiment could proceed with consistent material. While there were minor differences in germination percentages, these differences did not affect the overall quality of the genetic material. Therefore, the genetic material selected for the variety testing is suitable for further examination in subsequent stages of the research, focusing on growth, yield, and other critical traits under the Aral Sea region's climatic conditions.

4.2. Plant Development and Growing Period

Subsequently, after performing pre-sowing soil treatment, seeds of all varieties were sown simultaneously in the control plots. Daily monitoring of the first sprouts and further plant development was carried out (Figure 1).

Figure 1. Appearance of the first melon sprouts

During the experiment, the day of the first sprout emergence, the day of maximum sprout numbers, and the length of the growing period were recorded (Table 2).

Table 2. Seed germination indicators in open ground and the length of the growing period for foreign melon varieties

No.	Sample name	Sowing date	First sprouts, day	% of sown seeds	Maximum sprouts, day	Growing period length, days
1	Myrzashop	13.05	6	35	9	63
2	Sary Kauyn	13.05	5	35	8	63
3	Syrnaval	13.05	6	45	8	79
4	Kyzyl Kauyn	13.05	6	30	10	106
5	July	13.05	6	60	7	74
6	Zolotistaya	13.05	4	50	8	69
7	Titovka	13.05	6	50	7	87
8	Yuzhanka	13.05	5	40	8	69
9	Ananas	13.05	6	45	8	85
10	Muza	13.05	5	50	9	79
11	Ethiopka	13.05	5	40	9	91
12	Princess Elizabeth	13.05	4	30	9	92
13	Israel	13.05	6	35	7	79
14	Can-4	13.05	5	30	7	79

It is important to note that there was a slight correlation between the laboratory seed germination results and the emergence of sprouts in open ground, but this correlation was not statistically significant ($p>0.05$). Sprouts appeared in the experimental plots on days 4-6, with the germination rate in the first days ranging from 35% to 60% of the sown seeds, depending on the variety. It was expected that earlier varieties would have the highest germination and growth rates, but under the same conditions, the differences between varieties were relatively small. This may be due to some varieties originating from countries with cooler climates, and under the warmer conditions of the Aral Sea region, where average daily temperatures were significantly higher, these varieties accelerated their growth and development (Yessimbekova et al., 2024). This hypothesis requires further research over several years to determine the causes of accelerated development in foreign varieties, which may become the focus of future work.

The plant development and growing period results indicate that the varieties showed a range of germination and growth rates, with sprouts emerging between days 4

and 6 across the varieties. Although earlier varieties were expected to show faster germination and growth, the differences between the varieties were relatively small, possibly due to the adaptation of some varieties from cooler climates to the warmer conditions of the Aral Sea region. These findings suggest that, while the varieties demonstrated similar initial growth patterns, further research is necessary to better understand the factors influencing the accelerated development of some varieties. Overall, the results provide a solid foundation for the next stages of the experiment, focusing on yield, fruit quality, and other performance indicators under the region's environmental conditions.

4.3. Fruit Yield and Transportability

Full seed germination was observed between days 7-10, depending on the variety, with Uzbek varieties showing the longest germination period. The reason for this phenomenon may be the similarity of conditions between Uzbekistan and Kazakhstan, which did not contribute to their more intense growth, while the higher temperatures for other varieties may have acted as a growth catalyst. The length of the growing period was already determined by the variety, with longer periods typical of late and medium-early varieties, while early varieties had shorter growing periods of 63 to 74 days. Yield monitoring was carried out as fruits matured on plants of each variety. The results of this variety testing are presented in Table 3.

Table 3. Yield and transportability results of fruits from different foreign melon varieties

Sample name	Number of fruits, pcs/plant	Fruit weight, kg	Skin thickness, cm	Transportability, points	Storage, points
Myrzashop	3	4.5±0.22	0.2±0.01	3.7	2.1
Sary Kauyn	2	1.2±0.05	0.3±0.01	4.5	4.7
Syrnaval	2	1.9±0.1	0.5±0.02	4.1	4.7
Kyzyl Kauyn	2	2.8±0.18	0.4±0.01	4.4	4.7
July	3	1.1±0.06	0.3±0.01	4.7	4.5
Zolotistaya	2	3.6±0.16	0.3±0.01	2.1	1.8
Titovka	3	0.8±0.03	0.4±0.01	3.4	4.7
Yuzhanka	2	1.9±0.11	0.6±0.02	4.2	4.4
Ananas	2	1±0.04	0.2±0.01	1.9	1.9
Muza	3	1.7±0.09	0.2±0.01	2.1	1.8
Ethiopka	2	2.4±0.13	0.4±0.01	3.8	3.9
Princess Elizabeth	3	4.5±0.31	0.4±0.01	3.9	3.7
Israel	3	0.6±0.03	0.3±0.01	1.3	1.9
Can-4	2	2.9±0.14	0.2±0.01	4.7	4.3

Based on the tabular data presented, it can be concluded that, under the conditions of the Aral Sea region, most foreign melon varieties developed an average of two fruits per plant, with the exception of certain varieties such as Myrzashan, Iulyskaya, Titovka, Muza, Princess Elizabeth, and Israel, which supported the simultaneous development of three fruits on a single stem. The relative multi-fruiting of these varieties did not depend on the country of origin, the time of fruit ripening, or the size of the fruits. The difference in fruit weight within a single variety was almost negligible and fell within the range of statistical error. The coefficient of variation did not exceed 6% (Figure 2).

Figure 2. Fruits of several melon varieties of foreign breeding (Ananas, Zolotistaya, Efiofka)

Source: compiled by the authors.

Therefore, a preliminary conclusion can be made that such relative multi-fruiting, associated with a higher adaptability of these varieties to the growing conditions, makes them more preferable for continued breeding and adaptation work for growing these varieties in the conditions of Kazakhstan's Aral Sea region.

An equally important indicator in the decision-making process regarding the further acclimatization of a variety in Kazakhstan, alongside yield, is the ability to transport the fruits to places of sale and their storage within a short period. Melon products have a high export value for Kazakhstan's agriculture (Kulazhanov et al., 2021; Uikassova et al., 2022). To assess this, experiments were conducted on the influence of fruit transportation by road from the growing areas to the laboratory, where studies on fruit preservation and taste quality were carried out. The main indicator that directly affects the transportation potential of melons and their shelf life during sale is the thickness of the fruit's rind. As a result of the variety trials of foreign melon varieties in the conditions of Kazakhstan's Aral Sea region, mid- and late-ripening varieties with thicker rinds were better adapted to transportation. Meanwhile, most early-ripening varieties of foreign breeding exhibited poor storage characteristics. To assess the suitability of varieties for export, a study was conducted on the effect of rind thickness on fruit transportability and storage over six days in a refrigerator. For convenience, the above indicators were rated on a 5-point scale, with the following principles: 5 points – no damage during transport (no soft spots or mechanical damage), and no visible signs of decay or rot during

storage; the lowest rating, 1 point, was assigned when fruits were damaged after transportation or became unsuitable for consumption after storage. Considering that this method is quite subjective and depends on the expert's viewpoint, a more accurate evaluation was made using the average score obtained from three independent assessments.

To determine the influence of rind thickness on transportability, a correlation analysis was performed between these indicators. The graphical result of the relationship between these indicators is presented in Figure 3.

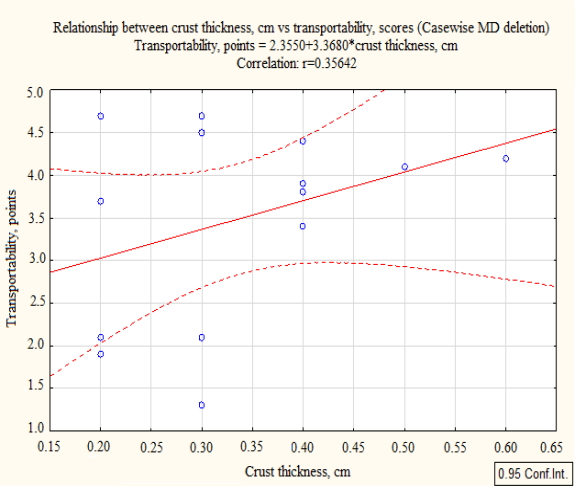

Figure 3. Correlation between melon rind thickness and its transportability

The correlation analysis did not reveal a significant influence of rind thickness on the level of fruit damage during transport (Table 4).

Table 4. Results of the correlation analysis between rind thickness and melon transportability

Indicator	Correlation matrix						
	Mean	Std.Dv.	r(X,Y)	r?	t	p	N
Rind thickness, cm	0.335	0.121	-	-	-	-	-
Transportability, points	3.485	1.149	0.356	0.127	1.321	0.211	14

Note: Mean – mean, Std. Dev. – standard deviation, r(X,Y) – correlation coefficient, r^2 – error in the correlation coefficient, p – significance level.

Source: compiled by the authors.

Table 4 presents the results of the correlation analysis between rind thickness and melon transportability. The mean rind thickness for the varieties tested was 0.335 cm, with a standard deviation of 0.121 cm. The correlation coefficient (r) between rind thickness and transportability was 0.356, which indicates a moderate positive correlation. However, the p-value of 0.211 suggests that this correlation is not statistically significant at the 0.05 level, meaning that rind thickness does not have a significant impact on the transportability of the melons during transportation. This finding suggests that factors other than rind thickness such as road quality, transportation conditions, and fruit handling might have a more substantial influence on the level of fruit damage during transport.

The results from the fruit yield and transportability tests indicate that most foreign melon varieties developed an average of two fruits per plant, with some varieties showing the ability to support three fruits per stem. The variation in fruit weight within a single variety was minimal, and the coefficient of variation did not exceed 6%, suggesting that the varieties were relatively consistent in their yield characteristics. The transportability and storage characteristics, particularly rind thickness, were evaluated as key factors affecting fruit preservation. While mid- and late-ripening varieties with thicker rinds were better suited for transport, early-ripening varieties showed poorer storage qualities. Correlation analysis revealed that rind thickness had a significant impact on the preservation of fruits during storage but did not significantly affect the level of damage during transport. These findings provide valuable insights into the potential for exporting melons and the factors that influence their quality under the conditions of Kazakhstan's Aral Sea region, guiding future breeding and adaptation efforts.

4.4. Transportability and Storage Characteristics

Other factors have a greater influence on the degree of fruit damage during transport – road quality, the suitability of the vehicle for transporting this type of agricultural product, the degree of load, the professional skills of the driver, etc. Therefore, no significant relationship between these indicators was found, while rind thickness had a significant impact on the preservation of fruits during storage (Figure 4).

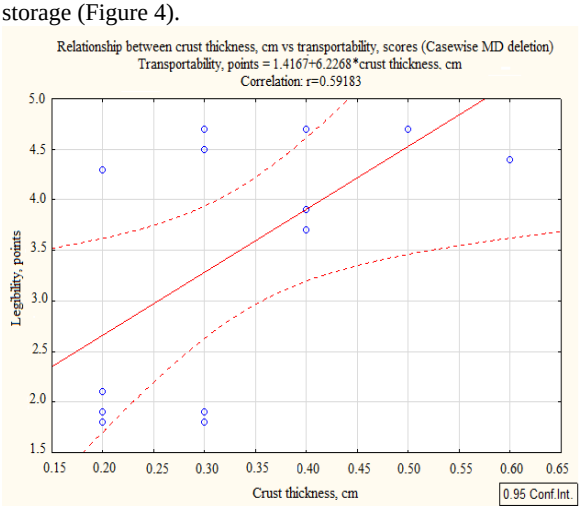

Figure 4. Graphical representation of the relationship between rind thickness and fruit preservation during storage

The data presented in Table 5 offer a statistically grounded insight into the relationship between rind thickness and melon storage potential. The average rind thickness among the examined melon varieties was 0.335 cm, with a standard deviation of 0.121 cm, indicating a relatively narrow variation in this morphological trait. Meanwhile, the storage potential assessed in points based on post-harvest longevity and visual/organoleptic quality preservation had a mean score of 3.507 with a broader standard deviation of 1.279, suggesting greater variability in storability among the samples. The statistically calculated correlation coefficient between these indicators was significant, at r=0.59 (P<0.05).

Table 5. Results of the correlation analysis between rind thickness and melon storage potential

Indicator	Correlation Matrix						
	Mean	Std.Dv	r(X,Y)	r?	t	p	N
Rind thickness, cm	0.335	0.121	-	-	-	-	-
Storage potential, points	3.507	1.279	0.592	0.35	2.543	0.026	14

The thickness and hardness of the melon rind prevents microorganisms from causing decay during storage, as confirmed by statistical analysis. Thus, the rind thickness indicator can be used as a selection criterion for further improvement of melons and their preservation during export-import operations. Among the foreign melon varieties used in the trials, the highest transportability and preservation rates were found in most varieties from Uzbekistan, while those from other countries showed lower results. This could be linked to the breeding work of local specialists, who developed varieties intended for export, whereas varieties from Russia and Ukraine were meant for domestic consumption, with no significant requirements for transportability.

Another aspect of evaluating melon quality during the trials was their taste qualities. The evaluation was carried out by employees of the Department of Melon and Potato Crops of the Kazakh Research Institute of Rice Production, named after I. Zhakaev, using a 5-point scale. Parameters such as sweetness, juiciness, aroma, and aftertaste were considered. The results of the taste evaluation are presented in Table 6.

Table 6. Taste evaluation of foreign melon varieties

Sample name	Flesh thickness, cm	Taste evaluation, points	Soluble solids content, %	Sugar content, %
Myrzashop	3.8±0.11	4.9	12	7.8
Sary Kauyn	3.9±0.1	4.9	10	6.5
Syrnaval	3.8±0.11	4.7	10	6.8
Kyzyl Kauyn	4.6±0.13	4.9	15	7.8
July	4±0.12	4.7	4.7	3.8
Zolotistaya	4.2±0.12	4.7	8	4.9
Titovka	2.9±0.09	4.7	7.1	4.6
Yuzhanka	4.5±0.12	4.7	9	5.9
Ananas	4.5±0.12	4.8	6	3.9
Muza	4.5±0.13	4.8	8.5	4.9
Ethiopka	4±0.11	4.9	10.5	6.5
Princess Elizabeth	4.3±0.12	4.8	7	4.7
Israel	2.8±0.1	4.6	4.7	3.3
Can-4	3.4±0.1	4.8	8	6.2

According to the subjective evaluation of the tasters, the taste qualities of melons from all foreign varieties received high scores ranging from 4.7 to 4.9 on a 5-point scale. The lowest taste quality score was for the Israel variety. Upon analysing this low score, it was found that the sugar content in the flesh of these melons was the lowest, as was the content of soluble solids. Based on these results, a correlation analysis was conducted between the taste score given by the tasters and the laboratory analysis of the flesh, including the content of soluble solids and sugar. The results are presented in Tables 7 and 8.

Table 7. Correlation analysis between taste qualities of flesh and soluble solids content

Indicator	Correlation matrix						
	Mean	Std.Dv.	r(X,Y)	r?	t	p	N
Taste evaluation, points	4.771	0.107	-	-	-	-	-
Soluble solids content, %	8.607	2.814	0.607	0.368	2.644	0.021	14

Table 8. Correlation analysis between taste qualities of flesh and sugar content

Indicator	Correlation Matrix						
	Mean	Std.Dv.	r(X,Y)	r?	t	p	N
Taste evaluation, points	4.771	0.107	-	-	-	-	-
Sugar content, %	5.543	1.451	0.564	0.318	2.366	0.036	14

Thus, the results of the analysis indicate a significant and reliable impact of the sugar content ($r=0.56$) ($P<0.05$) and soluble solids content ($r=0.61$) ($P<0.05$) on the taste evaluation. The testing of several foreign melon varieties in the Aral Sea region (Kazakhstan) showed no significant differences in quality characteristics between varieties. However, quantitative characteristics, including transportability and storage potential, met varietal standards and remained unchanged when grown under different conditions.

5. Discussion

The findings of this study offer several key insights into the adaptation of foreign melon varieties to the conditions of the Aral Sea region in Kazakhstan, providing valuable information for future agricultural strategies and regional policy. The results indicate that the quality of genetic material used for testing was generally high, with only slight variations in seed germination across the 14 melon varieties. While the differences in seed germination rates were not statistically significant, they suggest that genetic material from various regions, including Uzbekistan, Ukraine, Russia, and Israel, can perform well under the harsh climatic conditions of Kazakhstan's Aral Sea region. This supports the potential of introducing these foreign varieties for further testing and possible cultivation in the area, contributing to efforts to diversify crop production and enhance local agriculture.

The observed variation in plant development and growing periods, particularly the relatively consistent performance of the varieties, is also noteworthy (Shahwar et al., 2024). Despite expectations that varieties from cooler climates would show slower growth, the results indicated that the warmer conditions of the Aral Sea region acted as a growth catalyst, speeding up development in several varieties. This highlights the adaptability of foreign melon varieties and suggests that climate factors may be leveraged to accelerate crop development. However, further research is needed to better understand the underlying mechanisms of this accelerated growth, especially since the observed differences were minor.

In terms of yield and fruit quality, the study provides important information about the relative multi-fruiting ability of various melon varieties. The ability of certain varieties to produce more than two fruits per plant is a desirable trait, as it suggests these varieties are more adaptable and capable of yielding higher productivity under the region's conditions (Komala and Kuni, 2022). Moreover, the relatively low variation in fruit weight within each variety (with a coefficient of variation not exceeding 6%) supports the reliability of the foreign varieties for consistent yields. This is critical for agricultural practices aimed at enhancing food security in the region.

The results of the transportability and storage trials also have important implications for regional agricultural policy, especially with regard to export potential. The findings suggest that mid- and late-ripening varieties with thicker rinds were better suited for transportation, an essential factor for ensuring melons can be successfully exported. As Kazakhstan looks to expand its agricultural exports, especially in regions with difficult transportation infrastructure, focusing on varieties with better preservation characteristics could increase the viability of melon exports to international markets. The lack of significant correlation between rind thickness and transport damage implies that other factors, such as handling and road conditions, play a more significant role in determining the fruit's transportation success (Tlevlessova et al., 2023; Ismanzhanov and Tashiev, 2016). This information can be used to improve post-harvest handling and logistics, which are key to ensuring quality export products.

Considering the complex global food situation, the primary task of agricultural production is to provide the population with quality food products. The "global food crisis" refers to a widespread shortage of food that is affecting many regions around the world. This crisis is caused by a combination of factors, both natural and human-made. Climate change, for instance, has led to rising global temperatures, unpredictable rainfall patterns, and extreme weather events like droughts and floods, all of which severely impact agricultural productivity (Fedoniuk et al., 2024; Murabildayeva et al., 2024). These shifts in climate make it difficult to grow crops in traditional farming regions, leading to reduced yields and higher prices for essential food items. This situation demands continuous work by breeders aimed at increasing the yield of major agricultural crops and improving their quality. Climatic changes, such as the rise in average annual temperatures, the reduction in rainfall, and partial soil salinization, decrease the yields of traditionally grown crops in this area. This necessitates not only selective breeding aimed at improving local plant varieties but also the search for high-yield crops developed in other countries that are best suited for industrial cultivation under Kazakhstan's conditions.

Equally important is achieving high yields on soils not adapted for this purpose – such as in the case of the Aral Sea region, where the land has high salinity. Research by C. Erdinc et al. (2021) indicates significant differences in the genotypes of melons grown on saline soils. For instance, some Turkish melon varieties showed an increase in chlorophyll content in the plants' vegetative mass, leading to increased yields on saline soils. S. Chevilly et al. (2021) also suggest that growing different melon varieties under controlled drought or salt stress conditions will help identify crops that will be promising in the face of future climate changes. Therefore, such research results led to experiments studying the yield of different foreign-bred melon varieties in the saline plots of the Aral Sea region in Kazakhstan's Kyzylorda region to create a list of varieties suitable for future climatic changes. Varieties selected for this purpose were developed and adapted for cultivation in this climate zone – some from neighbouring Uzbekistan, others from Israel, a country with similar climatic conditions, and also from Russia and Ukraine, countries with cooler climates.

As a result of this variety testing, the vegetative characteristics of the varieties from countries with similar climatic conditions were almost identical when grown in Kazakhstan, while the melon varieties from Russia and Ukraine exhibited more accelerated growth. These changes might be due to the higher sum of daily average temperatures during the growing season compared to the countries of origin of these varieties, which could have acted as a catalyst for more intensive plant growth and accelerated fruit ripening. Additionally, the variety testing showed that almost all modern melon varieties, regardless of their country of origin, are drought-resistant, as the limited watering conditions used in the experimental plots resulted in significant melon yields.

According to A. Rehman et al. (2023), A. Galil Tzuri et al. (2025), varieties characterized by significant activation of genes and antioxidant enzyme activity in drought conditions represent the future of breeding work. The genetic potential of these plants led to a reduction in oxidative damage to their cells, improving their vegetative growth and photosynthetic functions. Thus, all the varieties tested in this experiment can be used for industrial cultivation in Kazakhstan's Aral Sea region. However, recent studies over the past five years have presented a different opinion, as stated in the work of S. Walters et al. (2021), who argue that under changing climatic conditions, the main yield will come from local varieties. This would allow for the identification of new gene combinations with resistance and specific fruit qualities, which L. Xu et al. (2022) emphasize as necessary for developing effective and useful melon breeding technologies. Therefore, the experiments described in this article on the study of adaptation properties of different melon varieties from various climatic and agronomic zones fit well into the modern global system of melon crop breeding.

Another important indicator after melon yield is its ability to be transported over long distances while maintaining its marketable qualities. Given that the melon cultivation area is limited by specific climatic conditions, these fruits are consumed worldwide due to their taste qualities. Therefore, transportability and the preservation of melons during distribution are important breeding traits. The spoilage of melons during storage is primarily due to the continuation of physiological reactions in the fruit after harvest, and if the surface layer has poor barrier function, microbial contamination may occur, leading to fruit spoilage (Kizatova et al., 2017; Safarova and Novruzova, 2021). Therefore, the research used the rind thickness as a parameter for transportation and storage adaptability, similar to what was proposed for

watermelons (Wan Azman et al., 2024). The research demonstrated a reliable correlation between this parameter and fruit preservation during storage. This can be explained by T. Puthmee et al. (2013), who established that during storage, cracks form in the rind of the fruit through which both moisture loss occurs, leading to fruit softening, and microbial contamination can take place. However, rind thickness did not significantly affect transport losses of melons. This corresponds with the research by R. Tursunkhodjaeva and S. Saidivaliev (2024), who indicated that factors such as temperature, humidity, and packaging conditions significantly impact microorganism growth and contribute to product spoilage during transportation. This could explain why the rind thickness had less impact on melon transportability.

The next factor used to compare foreign-bred melon varieties grown in the Aral Sea region was their taste characteristics. The sensory evaluation of the fruit showed that almost all melon varieties received fairly high scores, and changing growing conditions had little impact on the taste and aroma. According to M. Kaleem et al. (2022), these characteristics are largely influenced by the concentration of dissolved sugars in the melon flesh, which accumulate during fruit ripening. Significant sugar accumulation in the melons grown during the variety testing indicates that all varieties are adapted for cultivation in Kazakhstan's Kyzylorda region. High correlation was also found between sugar content and dissolved solids in the fruit and sensory evaluation results. The correlation coefficient for dissolved solids was higher ($r=0.61$) compared to sugar content ($r=0.56$).

The only exception was the “Israel” variety, which received the lowest taste ratings, with the lowest concentration of sugars in the fruit flesh. This may suggest that this variety is not well adapted to the conditions of the Aral Sea region. However, such results require further long-term research and comparison with results from other experiments conducted in the country of origin of this variety. Therefore, these studies represent only the initial phase of variety testing and will continue in a series of follow-up works comparing foreign-bred varieties with local varieties and their yields under optimal conditions.

6. Conclusions

The results of study provide important data on the adaptation of foreign melon varieties to the conditions of the Aral region of Kazakhstan, which is key to the future development of agriculture in this part of the country. The high germination rate of foreign varieties indicates their high quality and potential for further testing. This underscores the importance of using genetic resources from different countries, as variety diversity allows agricultural production to be adapted to specific climatic and environmental conditions, particularly in conditions of drought and high temperatures.

Although some varieties, particularly Uzbek ones, had a longer germination period, the general trend indicates that high temperatures in the Aral region accelerate plant development, opening up new opportunities for the accelerated cultivation of certain varieties. This could be an important factor in the development of fast-growing crops that are capable of high productivity in a shorter period, which is particularly important for agricultural practices in the context of climate change.

The results also highlight the importance of yield and transport characteristics for melon variety selection. Thicker skin in late and mid-early varieties was found to be a key factor in increasing their resistance to mechanical damage during transport. These findings may be important for the further development of Kazakhstan's export opportunities in the agricultural sector. Since melons are one of the promising export products, varieties with better preservation and transportability characteristics can contribute to the growth of the country's agricultural export potential. The results of the research also allow us to consider the adaptation of foreign varieties as a strategic direction for improving environmental sustainability and food security. In the context of climate change, it is important to select crops that can withstand extreme temperatures, low humidity, and soil salinity while maintaining high yields and product quality. Breeding work with such varieties can ensure the sustainability of agricultural production and reduce dependence on external suppliers.

Prospects for further research include a more detailed analysis of the reasons for the accelerated development of some varieties, which requires long-term observations and comparative tests. Another important area is the expansion of breeding work, taking into account environmental factors that affect yield and fruit quality. The practical application of the research results can form the basis for the development of effective methods for the acclimatization of new crops and the optimization of agrotechnical cultivation techniques.

Acknowledgement

The work was carried out within the framework of scientific and technical programme BR22885335 “Ensuring sustainable development of potato, vegetable and melon growing in Kazakhstan based on selection, seed production, biotechnology and innovative technologies” for 2024-2026 under budget programme 267 “Increasing the availability of knowledge and scientific research” under subprogramme 101 “Programme-targeted financing of scientific research and activities.”

References

Abdyvalieva K, Botaev S and Zhumadilova Zh. 2020. Creation of perspective models of foreign and farm varieties in Risovodchesky regions of Almaty region. Bull Korkyt Ata Kyzylorda Univ., 54(1): 22-27.

Adıgüzel P, Nyirahabimana F, Shimira F, Solmaz I and Taşkın H. 2023. Applied biotechnological approaches for reducing yield gap in melon grown under saline and drought stresses: An overview. J Soil Sci Plant Nutr., 23: 139-151. https://doi.org/10.1007/s42729-022-01044-y

Asabaev B and Kostakov AK. 2020. Testing of melon varieties of high-yielding and resistant to a complex of diseases. In: Proceedings of the International Scientific-Theoretical Conference “Seifullin Readings – 16: Youth Science, New Formation – The Future of Kazakhstan” (pp. 8-12). Astana: Ministry of Agriculture of the Republic of Kazakhstan. https://kazatu.edu.kz/assets/i/science/sf16-agro-103.pdf

Chen G. 2022. Study of non-pollution cultivation techniques of organic ecotype of melon crops considering population characteristics. Cell Mol Biol., 67(6): 330-338. https://doi.org/10.14715/cmb/2021.67.6.43

Chevilly S, Dolz-Edo L, Martínez-Sánchez G, Morcillo L, Vilagrosa A, López-Nicolás JM, Blanca J, Yenush L and Mulet JM. 2021. Distinctive traits for drought and salt stress tolerance in melon (*Cucumis melo* L.). Front Plant Sci., 12: 777060. https://doi.org/10.3389/fpls.2021.777060

Chikh-Rouhou H, Mezghani N, Mnasri S, Mezghani N and Garcés-Claver A. 2021. Assessing the genetic diversity and population structure of a Tunisian melon (*Cucumis melo* L.) collection using phenotypic traits and SSR molecular markers. Agronomy, 11(6): 1121. https://doi.org/10.3390/agronomy11061121

dos Santos GR, Tschoeke PH, Sarmento RA, Oliveira EE, Rodrigues-Silva N, Dalcin MS, Haddi K and Silva RS. 2021. Impact of growing seasons and pesticides used on the occurrence and severity of the gummy stem blight in melon cultivation in Brazil. Eur J Plant Pathol., 161: 171-184. https://doi.org/10.1007/s10658-021-02312-w

Erdinc C, Inal B, Erez E, Ekincialp A and Sensoy S. 2021. Comparative adaptation responses of melon (*Cucumis melo* L.) genotypes to salinity stress. J Agric Sci Technol., 23(2): 403-418. https://jast.modares.ac.ir/article-23-35313-en.pdf

Faichuk O, Voliak L, Hutsol T, Glowacki S, Pantsyr Y, Slobodian S, Szeląg-Sikora A and Gródek-Szostak Z. 2022. European Green Deal: Threats Assessment for Agri-Food Exporting Countries to the EU. Sustainability Switz., 14(7): 3712. https://doi.org/10.3390/su14073712

Fedoniuk T, Zhuravel S, Kravchuk M, Pazych V and Bezvershuck I. 2024. Historical sketch and current state of weed diversity in continental zone of Ukraine. Agricult Nat Resour., 58(5): 631-642. https://doi.org/10.34044/j.anres.2024.58.5.10

Galil Tzuri A, Dafna A, Ben Itzhaki I, Halperin I, Oren E, Isaacson T, Faigenboim A, Yeselson Y, Paris HS, Mazourek M, Burger J, Schaffer AA and Gur A. 2025. Meta-genetic analysis of melon sweetness. Theor Appl Genet., 138: 68. https://doi.org/10.1007/s00122-025-04863-6

GOST 7178-2015. 2015. Fresh melons. Specifications. https://online.zakon.kz/Document/?doc_id=34554222&pos=1;-16#pos=1;-16

Ismanzhanov AI and Tashiev NM. 2016. Development and research of the technology for powdering agricultural products using solar energy. Appl Solar Energy Eng Transl Geliotekh., 52(4): 256-258. https://doi.org/10.3103/S0003701X16040101

Kaleem MM, Nawaz MA, Ding X, Wen S, Shireen F, Cheng J and Bie Z. 2022. Comparative analysis of pumpkin rootstocks mediated impact on melon sensory fruit quality through integration of non-targeted metabolomics and sensory evaluation. Plant Physiol Biochem., 192: 320-330. https://doi.org/10.1016/j.plaphy.2022.10.010

Kesh H and Kaushik P. 2021. Advances in melon (*Cucumis melo* L.) breeding: An update. Scientia Hortic., 282: 110045. https://doi.org/10.1016/j.scienta.2021.110045

Khalid W, Ikram A, Rehan M, Afzal FA, Ambreen S, Ahmad M, Aziz A and Sadiq A. 2021. Chemical composition and health benefits of melon seed: A review. Pak J Agric Res., 34(2): 309-317. https://doi.org/10.17582/journal.pjar/2021/34.2.309.317

Kiseleva N and Yessimbekova M. 2024. Formation of the gene pool of vegetable plants in Kazakhstan. Izdenister Natigeler, 2-1: 342-348. https://doi.org/10.37884/2-1-2024/570

Kizatova MY, Medvedkov YB, Shevtsov AA, Drannikov AV and Tlevlessova DA. 2017. Experimental-statistical analysis and multifactorial process optimization of the crust from melon pulp separation process. J Eng Appl Sci., 12(7): 1762-1771. https://doi.org/10.3923/jeasci.2017.1762.1771

Komala M and Kuni P. 2022. Genetic diversity and molecular breeding of melon (*Cucumis melo* L.): A review. Curr Agric Res., 10(3). https://doi.org/10.12944/CARJ.10.3.03

Kosanov SU, Maslovsky SA, Shapovalova PN, Karpova NA, Salmina DA and Kovalenko AS. 2022. Justification of the technology of production of snack products from melon fruits. Int Res J., 119(5): 57-61. https://doi.org/10.23670/IRJ.2022.119.5.009

Kubo K, Pritchard B and Phyo AS. 2021. How Chinese demand for fresh fruit and vegetables is creating new landscapes of rural development and vulnerability in Southeast Asia: Insights from the Myanmar melon frontier. Geoforum, 122: 32-40. https://doi.org/10.1016/j.geoforum.2021.03.008

Kulazhanov T, Baibolova L, Shaprov M, Tlevlessova D, Admaeva A, Kairbayeva A, Azimova S, Kizatova M and Nazymbekova A. 2021. Means of mechanization and technologies for melons processing. In: Prudius I, editors. Means of Mechanization and Technologies for Melons Processing. Kharkiv: PC TECHNOLOGY CENTER; p. 1-174. https://doi.org/10.15587/9786177319398

Lee DS, Kwon JK, Yun SW, Lee SY, Seo MT, Lee HJ, Lee SG and Kang TG. 2021. Comparison of yield and workload depending on stem training methods in oriental melon hydroponics. J Bio-Env Control., 30(4): 377-382. https://doi.org/10.12791/KSBEC.2021.30.4.377

Lija M and Beevy S. 2021. A review on the diversity of Melon. Plant Sci Today, 8(4): 995-1003. https://doi.org/10.14719/pst.1300

Mamyrbekov ZhZh, Taishibaeva EU and Aitbaeva AT. 2021. Ecological testing of foreign variety samples of melon in the conditions of the south-east of Kazakhstan. In: Proc Int Sci-Practical Conf “Actual Problems of Agro-Science in the Context of Adaptation to Global Climate Change” (pp. 203-207). Almaty: Asyl Kitan LLP. https://kazniizr.kz/wp-content/uploads/2021/06/Sbornik-konf.-75-let.-Mejrman-G.T.-08.06.21.pdf

Mamyrbekov ZhZh, Tayshibaeva EU and Aitbaeva AT. 2024. Sowing qualities of seeds and development of the root system of melon varieties of different maturation dates in the conditions of the pedimountain steppe and pedmountary zones of Kazakhstan. Izdenister Natigeler, 102(2): 200-209. https://doi.org/10.37884/2-2024/19

Manchali S, Chidambara Murthy KN and Vishnuvardana Patil BS. 2021. Nutritional composition and health benefits of various botanical types of melon (*Cucumis melo* L.). Plants, 10(9): 1755. https://doi.org/10.3390/plants10091755

Mukhtar NF and Abd Samad AB. 2022. Optimization of growth parameters on rock melon quality via fertigation system. Proc Sci Math., 12: 210-219. https://science.utm.my/procscimath/wp-content/uploads/sites/605/2022/11/22_Noor-Farrah-Aminah-Mukhtar_210-219.pdf

Murabildayeva R, Bimendiyeva L, Kondybayeva S and Yermekova Zh. 2024. Climate change and agricultural productivity: Economic implications for food security. Sci Horiz., 27(12): 168-179. https://doi.org/10.48077/scihor12.2024.168

Nascimento CS, Nascimento CS and Cecilio Filho AB. 2020. N:K ratio for phenological growth stages of net melon cultivated in NFT hydroponic system. Rev Caatinga, 33(1): 108-115. http://dx.doi.org/10.1590/1983-21252020v33n112rc

Novruzova E. 2016. The features of ferns for their moisture demand and life form including in the flora of Nakhchivan Autonomous Republic Azerbaijan. Int J Multidiscip Res Develop., 3(11): 65-67.

Puthmee T, Takahashi K, Sugawara M, Kawamata R, Motomura Y, Nishizawa T, Aikawa T and Kumpoun W. 2013. The role of net development as a barrier to moisture loss in netted melon fruit (*Cucumis melo* L.). HortScience Horts, 48(12): 1463-1469. https://doi.org/10.21273/HORTSCI.48.12.1463

Qian Ong Y and Moneruzzaman Khandaker M. 2021. Growth and development of melon Manis Terengganu in response to seasonal variation. Asian J Plant Sci., 20(4): 659-664. https://doi.org/10.3923/ajps.2021.659.664

Rehman A, Weng J, Li P, Yu J, Rahman S, Khalid M, Shah IH, Gulzar S, Chang L and Niu Q. 2023. Differential response of two contrasting melon (*Cucumis melo* L.) genotypes to drought stress. J Plant Biol., 66: 519-534. https://doi.org/10.1007/s12374-023-09398-1

Safarova F and Novruzova E. 2021. Self-defense Mechanisms of Plants in Nature. Bull Sci Pract., 7(8): 73-77.

Serhienko O, Shabetia O, Linnik Z, Serhiienko M and Melnyk O. 2023. Selection of highly adaptive source material of watermelon for selection for early ripening. Sci Horiz., 26(8): 42-51. https://doi.org/10.48077/scihor8.2023.42

Shahwar D, Khan Z and Park Y. 2024. Molecular markers for marker-assisted breeding for biotic and abiotic stress in melon (*Cucumis melo* L.): A review. Int J Mol Sci., 25(12): 6307. https://doi.org/10.3390/ijms25126307

Singh SP. 2023. Flooding adversely impacts fresh produce safety. Microbiol Aust., 44(4): 185-189. https://doi.org/10.1071/MA23054

Soltani F, Shajari M, Mirbehbahani GS, and Bihamta MR. 2022. Assessment of melon genetic diversity based on fruit phenotypic traits and flowering habits. Int J Hortic Sci Technol., 9(1): 97-116. https://doi.org/10.22059/ijhst.2021.313939.415

Soltani F. 2021. Breeding of melon (Cucumis melo L. groups Dudaim and Flexuosus). In: Al-Khayri JM, Jain SM, Johnson DV, editors. Advances in Plant Breeding Strategies: Vegetable Crops. Cham: Springer; p. 333-361. https://doi.org/10.1007/978-3-030-66961-4_9

Statistical Collection “Agriculture, Forestry and Fishery in the Republic of Kazakhstan, 2018-2022”. 2023. https://stat.gov.kz/upload/iblock/1d8/g9qb3n8u30g1jftcy900a0v4exegme8b/C-11-%D0%93-2018-2020%20(%D0%BA%D0%B0%D0%B7-%D1%80%D1%83%D1%81).pdf

Tlevlessova D, Medvedkov Y, Kairbayeva A and Nazymbekova A. 2023. Mechanisation of the primary processing of watermelons without destroying the rind. Food Sci Tech Braz., 43: e86622. https://doi.org/10.1590/fst.86622

Turamatov RG, Rasulov F and Shokirov AJ. 2021. Determining the possible sowing times for morning pumpkin growing. Acad Int Multidiscip Res J., 11(11): 885-891. https://doi.org/10.5958/2249-7137.2021.02532.5

Tursunkhodjaeva R and Saidivaliev S. 2024. Evaluation of factors in the transportation of melons by railway. BIO Web Conf., 141: 01023. https://doi.org/10.1051/bioconf/202414101023

Uikassova Z, Azimova S, Tlevlessova D and Galoburda R. 2022. Determining critical control points for processing melon fruits. East Eur J Enterp Tech., 4(11-118): 97-104. https://doi.org/10.15587/1729-4061.2022.262850

Urazbaev IU and Masharipov NK. 2021. Fundamental scale of evaluation of productivity of irrigated gray-meadow soils which are appointed for growing melon crops. Alinteri J Agric Sci., 36(1): 257-259. https://doi.org/10.47059/alinteri/V36I1/AJAS21038

Walters SA, Abdelaziz M and Bouharroud R. 2021. Local melon and watermelon crop populations to moderate yield responses to climate change in North Africa. Climate, 9(8): 129. https://doi.org/10.3390/cli9080129

Wan Azman WM, Shahar A, Azizan SA and Rahim AA. 2024. Physical and mechanical properties of watermelon rind. Adv Agric Food Res J., 5(2): a0000318. https://doi.org/10.36877/aafrj.a0000318

Xu L, He Y, Tang L, Xu Y and Zhao G. 2022. Genetics, genomics, and breeding in melon. Agronomy, 12(11): 2891. https://doi.org/10.3390/agronomy12112891

Yavuz D, Seymen M, Yavuz N, Çoklar H and Ercan M. 2021. Effects of water stress applied at various phenological stages on yield, quality, and water use efficiency of melon. Agric Water Manag., 246: 106673. https://doi.org/10.1016/j.agwat.2020.106673

Yessimbekova M, Mukin K, Dolinny Y, Ainebekova B, Espanov A, Didenko I and Kenebaev A. 2024. The results of agricultural crops genetic resources mobilization in Kazakhstan. Izdenister Natigeler, 2-1: 316-331. https://doi.org/10.37884/2-1-2024/568

Yunusov S, Sadullayev S, Khaitboyeva G and Sharipova M. 2023. Selection of high-yielding, disease-resistant, promising, and export-oriented varieties of melons. E3S Web Conf., 389: 03044. https://doi.org/10.1051/e3sconf/202338903044

Zhang J, Yang J, Lv Y, Zhang X, Xia C, Zhao H and Wen C. 2023. Genetic diversity analysis and variety identification using SSR and SNP markers in melon. BMC Plant Biol., 23: 39. https://doi.org/10.1186/s12870-023-04056-7

Zymaroieva A, Zhukov O, Fedoniuk T, Pinkina T and Hurelia V. 2021. The relationship between landscape diversity and crops productivity: Landscape scale study. J Landscape Eco Czech Rep., 14(1): 39-58. https://doi.org/10.2478/jlecol-2021-0003

JJBS

Volume 19, Number 1,March 2026
ISSN 1995-6673
Pages 13 – 21
https://doi.org/10.54319/jjbs/190102

Jordan Journal of Biological Sciences

Morphological and molecular data reveal two distinct clades of *Xanthosoma undipes* (Araceae) on Mount Karang, Banten, Indonesia

Gut Windarsih[1,*] , Muhammad Rifqi Hariri[2], Ina Erlinawati[2], I Putu Gede P. Damayanto[2], Indira Riastiwi[3] , Surya Diantina[3], Andi Salamah[4]

[1] *Program of Biology, Faculty of Science and Technology, Universitas Islam Negeri Sultan Maulana Hasanuddin Banten. Jl. Syech Nawawi Al Bantani, Serang, 42116, Banten, Indonesia;* [2] *Research Center for Biosystematics and Evolution, Herbarium Bogoriense, National Research and Innovation Agency, Indonesia. Jl. Raya Jakarta-Bogor, km 46, Cibinong, Bogor, 16911, West Java, Indonesia;* [3] *Research Center for Applied Botany, National Research and Innovation Agency, Indonesia. Jl. Raya Jakarta-Bogor, km 46, Cibinong, Bogor, 16911, West Java, Indonesia;* [4] *Department of Biology, Faculty of Mathematics and Natural Sciences, Universitas Indonesia. Jl. Margonda Raya, Pondok Cina, Beji, Depok, 16424, West Java, Indonesia*

Received: January 21, 2025; Revised: May 27, 2025; Accepted: June 30, 2025

Abstract

Xanthosoma undipes, locally known in Indonesia as *talas beneng*, is a taro plant with edible corms. Two distinct morphological groups have been identified in three locations on Mount Karang, Banten, Indonesia. This study investigates the variation among *X. undipes* accessions from Mount Karang based on morphological traits and the chloroplast *psb*A-*trn*H intergenic spacer (IGS) marker. Accessions of *X. undipes* were collected from Mount Karang as herbarium specimens and DNA samples. Morphological data were gathered, scored, and analyzed using the UPGMA method. DNA was isolated using a modified CTAB method with 2% polyvinylpyrrolidone, leaf tissue was ground in CTAB buffer, incubated, extracted with chloroform:isoamyl alcohol (24:1), and DNA was precipitated with isopropanol, washed with 70% ethanol, and resuspended in TE. PCR amplification was performed using *psb*A-*trn*H IGS primers (forward: 5'-GTT ATG CAT GAA CGT AAT GCT C-3' and reverse: 5'-CGC GCA TGG TGG ATT CAC ATT CAC AAT-3'). DNA sequencing was conducted by 1st Base. A phylogenetic tree was constructed using the Maximum Likelihood method with 1000 bootstrap replications, using *Alocasia macrorrhizos* as an outgroup because it belongs to the same family but a different genus, with sequences available in NCBI. Nucleotide variations were visualized using Multalin. Morphological analysis revealed two distinct clades of *X. undipes* accessions from Mount Karang. Clade I consists of accessions GW1, GW3, GW12, GW14, and GW22, while Clade II consists of GW6, GW18, GW19, GW20, and GW21. Morphological characters, including corms, cormels, leaf petiole junctions, leaf sheaths, peduncles, spathes, sterile flowers, and male flowers, distinguish *X. undipes* accessions into two clades. Molecular analysis using the chloroplast *psb*A-*trn*H IGS marker supported the clustering observed in the morphological data. A notable difference between the two clades was found at nucleotide base position 156, where clade I had a cytosine, while clade II had a thymine. In the end, morphological and molecular evidence revealed two distinct clades among *X. undipes* accessions from Mount Karang.

Keywords: dendrogram, phylogeny, *talas beneng*, taro, *psb*A-*trn*H IGS, *Xanthosoma undipes*

1. Introduction

Xanthosoma undipes (K.Koch & C.D.Bouché) K.Koch (Araceae), locally known as *talas beneng* in Indonesia, is a taro plant with the main tuber being an edible corm that serve as a source of carbohydrates. According to Windarsih *et al.* (2023), morphologically, *X. undipes* has corms that range from rounded to elongated in shape, which develop into a pseudostem that can grow up to 2 meters tall in height. The underground corms branch into lateral tubers (cormels). The leaf blades are sagittate, green, thin, soft, with undulate margins, acute tips, and a bowl-shaped surface. The inflorescence is erect, featuring spoon-shaped bracts with a tubular form at the lower part and a flattened shape at the upper part. The female and sterile flowers are enclosed within a spathe tube, while the male flowers become visible when the spathe opens. Milky-white, sticky exudates are present in nearly all parts of the plant.

Xanthosoma undipes has significant economic value, as various plant parts are utilized for multiple purposes, including food, raw materials for crafts, clothing, ornamental plants, and traditional medicine. It has been reported to possess anti-diabetic (Windarsih *et al*., 2023), anti-malarial (Frausin *et al*., 2015), and potential heart disease and cancer treatment properties (Nurtiana *et al*., 2022). Additionally, it is used in the production of cigarettes (Fitriyah and Wahyudi, 2022), and the tannin content in leaves suggests their potential as a raw material

* Corresponding author. e-mail: gut_windarsih@yahoo.com.

for biopesticides (Fatmawaty *et al*., 2019). *Xanthosoma undipes* grows in tropical humid areas and is native to tropical America (POWO, 2024) at elevations between 200 and 2700 m above sea level (Kerbs, 2015; Croat *et al*., 2017). During the era of the transatlantic slave trade, *Xanthosoma* was introduced to Africa, and by the 19th and early 20th centuries, it spread throughout Oceania and into Asia (Jansen and Premchand, 1996). In Indonesia, *X. undipes* has been found in Java, particularly on Mount Karang, Banten (Budiarto and Rahayuningsih, 2017; Fatmawaty *et al*., 2019; Hakiki *et al*., 2019; Yursak *et al*., 2021; Windarsih *et al*., 2023). Since *Xanthosoma* often escapes cultivation and becomes naturalized (Jansen and Premchand, 1996), it is unsurprising that *X. undipes* has also naturalized in mountainous areas.

Two distinct groups of *X. undipes* are found in Mount Karang based on morphological observation, one with a green leaf sheath and the other with a red sheath (Windarsih *et al*., 2023). Morphological data are commonly used for initial evaluations due to their simplicity and speed (Beyene *et al*., 2005). However, this method is vulnerable to environmental factors and subjective interpretation (Fendiyanto *et al*., 2024). Therefore, molecular techniques, such as DNA sequencing, which is a powerful tool for species identification and evaluation, should be used to support morphological data (Kress *et al*., 2015). DNA-based analysis has been applied to various plants, including *Colocasia esculenta* (L.) Schott (Nunes *et al*., 2015), *Cynosurus cristatus* L., *Dactylis glomerata* L., and *Trisetum flavescens* (L.) P.Beauv. (Loera-Sánchez *et al*., 2020), as well as several plants that produce nectar (Balkanska *et al*., 2020).

The DNA loci commonly used as markers in plant variety analyses are *rbc*L (Talley and Kolondam, 2015), *mat*K (Ali *et al*., 2015), Internal Transcribed Spacer (ITS) (Chen *et al*., 2010) and the *psb*A-*trn*H intergenic spacer (IGS) (Kress *et al*., 2005). The *psb*A-*trn*H IGS locus is an intergenic spacer region in the plant chloroplast genome. It is the most variable barcode region within the Angiospermae group (Kress *et al*., 2005). Due to its tendency to accumulate mutations rapidly, the sequence of the *psb*A-*trn*H IGS locus is currently utilized for establishing lower taxonomic levels, such as genus, species, and subspecies (Kress and Erickson, 2007).

As mentioned earlier, several accessions of *X. undipes* from Mount Karang exhibit variations in morphological characteristics (Windarsih *et al*., 2023). This morphological variation should be validated using *psb*A-*trn*H IGS molecular data. Therefore, a study was conducted to evaluate variation among *X. undipes* accessions from Mount Karang, using morphological characteristics and the *psb*A-*trn*H IGS marker. The integration of molecular analysis with morphological data presented in this study provides a critical foundation for a new formal classification of the Araceae. It also enhances our understanding of the evolutionary history of this ancient family (Cusimano *et al*., 2011), as *Xanthosoma* is considered as one of the least understood genera in the Araceae family (Croat and Ortiz, 2020).

2. Materials and Methods

2.1. Study area

Samples of *X. undipes* were collected from the Mount Karang area in Pandeglang Regency, Banten Province, Indonesia, between August and October 2023 at three locations: Pandeglang Village in Pandeglang District, Juhut Village in Karang Tanjung District, and Saninten Village in Kaduhejo District (Figure 1). The study sites were selected using purposive sampling.

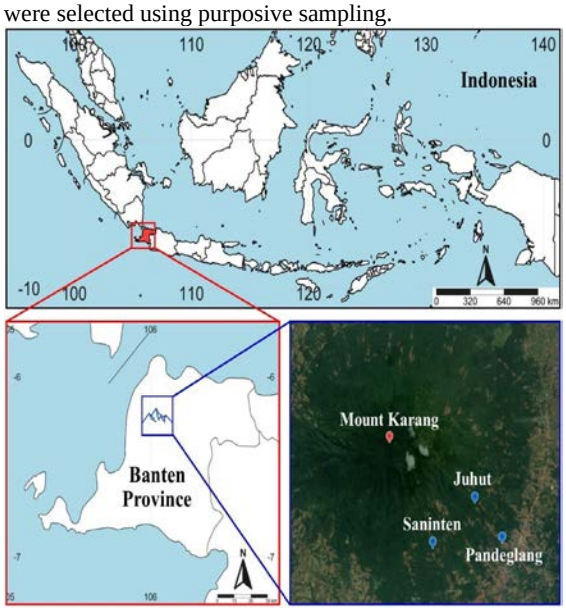

Figure 1. Map showing the sample collection sites in three villages (Pandeglang, Juhut, and Saninten) on Mount Karang, Banten Province, Indonesia.

2.2. Sampling methods

Samples of *X. undipes* were collected as herbarium specimens for morphological study using the method of taxonomic data collection from Rugayah *et al*. (2004). Herbarium specimens were processed using the method of Djarwaningsih *et al*. (2002) and stored at the Herbarium Bogoriense (BO), Herbarium Bandungense (FIPIA), and Herbarium Faculty of Science and Technology Universitas Islam Negeri Sultan Maulana Hasanuddin Banten. Young leaves were also collected for molecular analysis (Table 1), placed in tea bags, and dried using silica gel. Data of *X. undipes* habitat were recorded, including altitude, soil pH and temperature, relative humidity, and air temperature. Measurements were taken three times daily at 10:00, 12:00, and 14:00, respectively, and the average values were calculated.

Table 1. Accessions of *Xanthosoma undipes* from Mount Karang used for molecular analysis.

Accessions	Locations	Coordinates
GW1	Pandeglang Village	6°18'23.8"S 106°06'01.0"E
GW3	Pandeglang Village	6°18'23.2"S 106°06'01.6"E
GW6	Pandeglang Village	6°18'25.1"S 106°05'58.9"E
GW12	Juhut Village	6°17'40.8"S 106°05'27.6"E
GW14	Juhut Village	6°17'33.3"S 106°05'13.2"E
GW18	Saninten Village	6°18'14.5"S 106°03'59.4"E
GW19	Saninten Village	6°18'14.2"S 106°03'59.4"E
GW20	Saninten Village	6°18'15.2"S 106°03'58.2"E
GW21	Saninten Village	6°18'15.4"S 106°04'00.4"E
GW22	Saninten Village	6°18'30.1"S 106°04'05.8"E

2.3. Morphological observation

Herbarium specimens were observed, and morphological data were gathered following the method of Minantyorini and Hanarida (2002). The plant parts observed included corms, cormels, stems, leaves, and inflorescences (Table 2).

Table 2. Morphological characteristics used for scoring in the morphological analysis.

Morphological characters	Scoring
Stem habits	0 = erect; 1 = creeping
Color of corms cortex	0 = white; 1 = pink
Color of corms bud	0 = greenish-yellow; 1 = pink
Color of cormel cortex	0 = white; 1 = white-pink
Color of cormel apex	0 = white-cream/yellowish; 1 = pink
Color of abaxial leaf veins	0 = green; 1 = reddish-green
Color of abaxial leaf petiole junction	0 = green; 1 = pink
Color of leaf sheath margin	0 = yellow with brownish-red spots; 1 = purplish-red
Leaf sheath margin	0 = overlapping; 1 = curving inward
Color of leaf sheath base	0 = whitish; 1 = pink
Color of peduncles	0 = green; 1 = reddish-green
Color of leaf flag	0 = purplish; 1 = pink; 2 = green
Color of outer surface of spathe tube	0 = green; 1 = purplish-dark red
Color of inner surface of spathe tube	0 = light green; 1 = upper part is yellow, lower part is purplish-dark red
Color of outer surface of spathe blade	0 = yellow; 1 = pink
Color of inner surface of curved portion of spathe	0 = yellowish-green; 1 = yellow
Spadix apex	0 = capitate; 1 = rounded; 2 = obtuse
Color of sterile flower	0 = yellowish-cream; 1 = pink
Color of male flower	0 = cream; 1 = pink

2.4. Molecular analyses

DNA isolation was performed using the modified CTAB method (Doyle and Doyle, 1987) with 2% polyvinylpyrrolidone (PVP). PCR amplification was performed using the *psb*A-*trn*H IGS primers (forward: 5'-GTT ATG CAT GAA CGT AAT GCT C-3' and reverse: 5'-CGC GCA TGG TGG ATT CAC ATT CAC AAT-3'). The PCR reaction was carried out in a 50 µL total volume, containing 25 µL MyTaq Master Mix (Bioline), 10 µL DNA 10 ng/µL, 5 µM of each primer, and 5 µL ddH_2O. The PCR conditions involved an initial denaturation step at 94°C for 5 minutes, followed by 35 cycles of denaturation at 94°C for 30 seconds, annealing at 54°C for 30 seconds, and extension at 72°C for 30 seconds. A final extension was performed at 72°C for 5 minutes. DNA sequencing was performed by 1st Base (https://base-asia.com) with assistance from PT Genetika Science Indonesia.

2.5. Data analyses

The scoring morphological data were analyzed using the Simple Matching (SM) index to assess the similarity among *X. undipes* accessions. Grouping was performed using the Unweighted Pair Group Method with Arithmetic Mean (UPGMA) in NTSYs software version 2.02 (Rohlf, 1997). The similarity data were visualized as a dendrogram in TREE format.

Forward and reverse sequences were edited using BioEdit software (Hall, 1999), and their chromatograms were validated to avoid nucleotide reading bias. The two sequences were assembled into a contig and matched against the National Center for Biotechnology Information (NCBI) database. Sequences of *Alocasia macrorrhizos* (L.) G.Don (JN406925.2 and MW940647.1) from NCBI were used as outgroups. All sequences were aligned using the ClustalW method. The phylogenetic tree was constructed using the Maximum Likelihood (ML) method with the Kimura-2-Parameter substitution model and 1000 bootstrap replications. The analysis was performed using MEGA 11 software (Tamura *et al*., 2021). A clade with an ML bootstrap value above 85 indicates strong support, while below 85 indicates low support (Cusimano *et al*., 2011). Nucleotide variations were visualized through multiple sequence alignment using hierarchical clustering on the Multalin web tool (http://multalin.toulouse.inra.fr/multalin) (Corpet, 1988).

3. Results

3.1. Habitat conditions

Habitat conditions varied among *X. undipes* accessions collected from the three locations in Mount Karang, with altitudes ranging from 444–604 m above sea level (a.s.l.), soil pH 6.5–7.0, soil temperature 24–28°C, relative humidity 46–73%, and air temperature 26.8–36.1°C (Table 3).

Table 3. Habitat conditions of *Xanthosoma undipes* collected from Mount Karang.

Accession number	Location (Village)	Altitude (m a.s.l.)	Soil pH	Soil temperature (°C)	Relative humidity (%)	Air temperature (°C)
GW1	Pandeglang	444	7.0	27	46	36.1
GW3	Pandeglang	461	6.5	25	58	34.4
GW6	Pandeglang	486	7.0	26	65	30.2
GW12	Juhut	567	7.0	26	73	28.5
GW14	Juhut	604	7.0	26	72	26.8
GW18	Saninten	585	7.0	25	59	29.0
GW19	Saninten	599	7.0	25	63	28.5
GW20	Saninten	590	7.0	28	65	28.1
GW21	Saninten	601	7.0	24	65	28.3
GW22	Saninten	541	7.0	27	56	30.5

3.2. Morphological observation

Xanthosoma undipes accessions from Mount Karang exhibited morphological variation (Table 4). UPGMA analysis revealed high morphological diversity, with similarity coefficients ranging from 0.14 to 1. The dendrogram grouped the *X. undipes* accessions from Mount Karang into two main clades with a similarity coefficient of 0.14, with Clade I including accessions GW1, GW3, GW12, GW14, and GW22, and Clade II comprising GW6, GW18, GW19, GW20, and GW21 (Figure 2). The highest similarity (similarity coefficient = 1) was observed among accessions GW1, GW3, and GW14 in Clade I. Similarly, in Clade II, the highest similarity (similarity coefficient = 1) is observed between GW6 and GW20, as well as between GW18 and GW21.

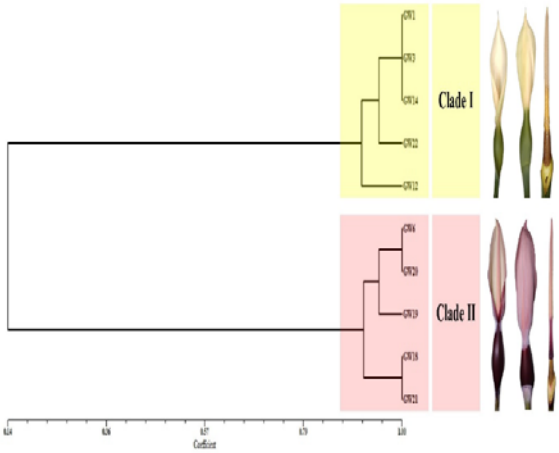

Figure 2. Dendrogram of *Xanthosoma undipes* accessions collected from Mount Karang based on morphological characters, analyzed using UPGMA.

Table 4. Morphological variation of *Xanthosoma undipes* accessions from Mount Karang.

Morphological characters	Accession numbers GW…)
Stem is erect	1, 3, 12, 14, 18, 19, 21, 22
Stem is creeping	6, 20
Corms cortex is white	1, 3, 12, 14, 22
Corms cortex is pink	6, 18, 19, 20, 21
Corms bud is greenish-yellow	1, 3, 12, 14, 22
Corms bud is pink	6, 18, 19, 20, 21
Cormel cortex is white	1, 3, 12, 14, 22
Cormel cortex is white-pink	6, 18, 19, 20, 21
Cormel apex is white-cream/yellowish	1, 3, 12, 14, 22
Cormel apex is pink	6, 18, 19, 20, 21
Abaxial leaf veins is green	1, 3, 6, 12, 14, 19, 20, 22
Abaxial leaf veins is reddish-green	18, 21
Abaxial leaf petiole junction is green	1, 3, 12, 14, 22
Abaxial leaf petiole junction is pink	6, 18, 19, 20, 21
Leaf sheath margin is yellow with brownish-red dots	1, 3, 12, 14, 22
Leaf sheath margin is purplish-red	6, 18, 19, 20, 21
Leaf sheath margin is overlapping	1, 3, 12, 14, 22
Leaf sheath margin is curving inward	6, 18, 19, 20, 21
Leaf sheath base is whitish	1, 3, 12, 14, 22
Leaf sheath base is pink	6, 18, 19, 20, 21
Peduncle is green	1, 3, 12, 14, 22
Peduncle is reddish-green	6, 18, 19, 20, 21
Leaf flag is purplish	1, 3, 12, 14
Leaf flag is pink	6, 18, 19, 20, 21
Leaf flag is green	22
Outer surface of spathe tube is green	1, 3, 12, 14, 22
Outer surface of spathe tube is purplish-dark red	6, 18, 19, 20, 21
Inner surface of spathe tube is light green	1, 3, 12, 14, 22
Inner surface of spathe tube in upper part is yellow, in lower part is purplish-dark red	6, 18, 19, 20, 21
Outer surface of spathe blade is yellow	1, 3, 12, 14, 22
Outer surface of spathe blade is pink	6, 18, 19, 20, 21
Inner surface of curved portion of spathe is yellowish-green	1, 3, 12, 14, 22
Inner surface of curved portion of spathe is yellow	6, 18, 19, 20, 21
Spadix apex is capitate	1, 3, 6, 14, 18, 19, 20, 21, 22
Spadix apex is rounded	12
Spadix apex is obtuse	12
Sterile flower is yellowish-cream	1, 3, 12, 14, 22
Sterile flower is pink	6, 18, 19, 20, 21
Male flower is cream	1, 3, 12, 14, 22
Male flower is pink	6, 18, 19, 20, 21

Morphological characters distinguish *X. undipes* accessions from Mount Karang into two clades, including features such as corm cortex, corm buds, cormel cortex, cormel tips, petiole junction on the underside of the leaf, leaf sheath edges, leaf sheath base, peduncles, outer and inner tube of the spathe, outer and inner spathe blade, sterile flowers, and male flowers (Table 5 and Figure 3).

Tabel 5. Morphological comparison of *Xanthosoma undipes* clades from Mount Karang.

Morphological characters	Clade I	Clade II
Corm cortex	White	Pink
Corm bud	Yellowish-green	Pink
Cormel cortex	White, tip white to cream or yellowish	White with pink hues, tip pink
Abaxial petiole junction	Green	Pink
Leaf sheath margin	Yellow with reddish-brown spots, overlapping	Reddish-purple, curving inward
Leaf sheath base	Whitish	Pink
Peduncle	Green	Greenish-red
Outer spathe tube	Green	Dark red to purplish
Inner spathe tube	Bright green	Yellow at top, dark red to purplish at base
Outer spathe blade	Yellow	Pink
Inner spathe groove	Yellowish-green	Yellow
Sterile flowers	Cream to yellowish	Pink
Male flowers	Cream	Pink

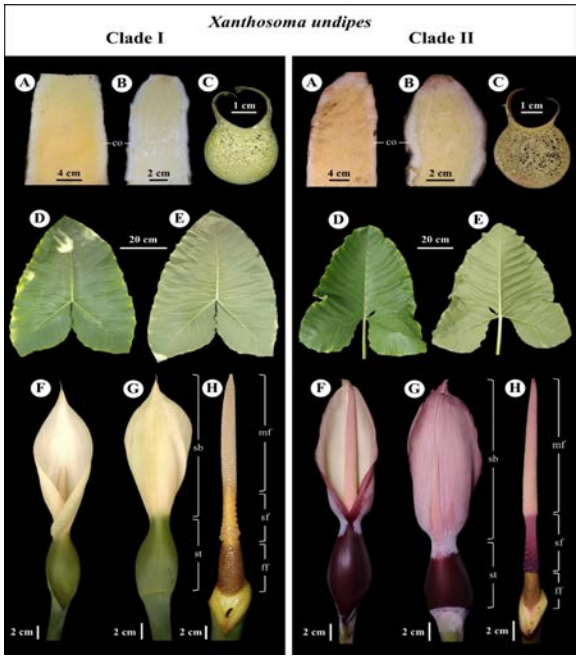

Figure 3. Representative morphological traits of two *Xanthosoma undipes* clades from Mount Karang. A. Corm showing cortex (co); B. Cormel showing cortex (co); C. Cross section of leaf sheath; D. Adaxial leaf; E. Abaxial leaf; F. The front part of inflorescence; G. The back part of inflorescence showing spathe blade (sb) and spathe tube (st); H. Inflorescence, spathe is removed, showing male flowers (mf), sterile flowers (sf), and female flower (ff). Photos: Gut Windarsih.

3.3. Molecular analyses

Based on the phylogenetic tree using the *psb*A-*trn*H IGS marker with Maximum Likelihood method and 1000 Bootstrap, *X. undipes* accessions were grouped into two main clades. Clade I, comprising accessions GW1, GW3, GW12, GW14, and GW22, and Clade II, consisting of GW6, GW18, GW19, GW20, and GW21, were strongly supported by bootstrap values of 100 (Figure 4). A bootstrap value of 100 means that every resampled dataset consistently grouped those accessions into the same clade.

Based on the alignment results and analysis of nucleotide variations (Figure 5), *X. undipes* accessions showed distinct sequence differences from the outgroup, *A. macrorrhizos*, at nucleotide base positions 124–128, 131–135, and 150. A notable difference between the two clades was found at nucleotide base position 156, where clade I had a cytosine (C), while clade II had a thymine (T) (Figure 5).

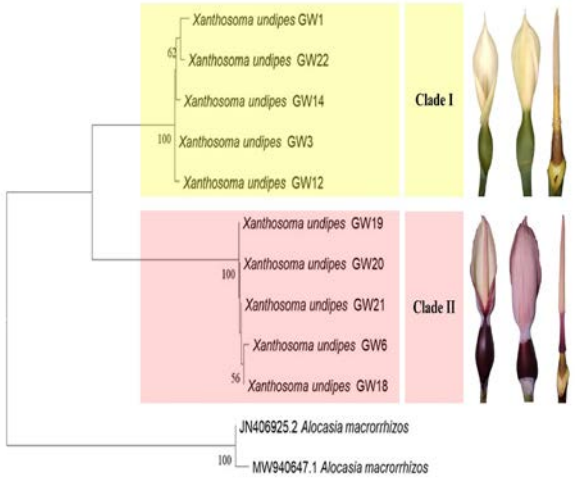

Figure 4. Phylogenetic tree of *Xanthosoma undipes* accessions collected from Mount Karang using the *psb*A-*trn*H IGS marker with Maximum Likelihood and 1000 Bootstrap. Bootstrap percentages are shown next to branches.

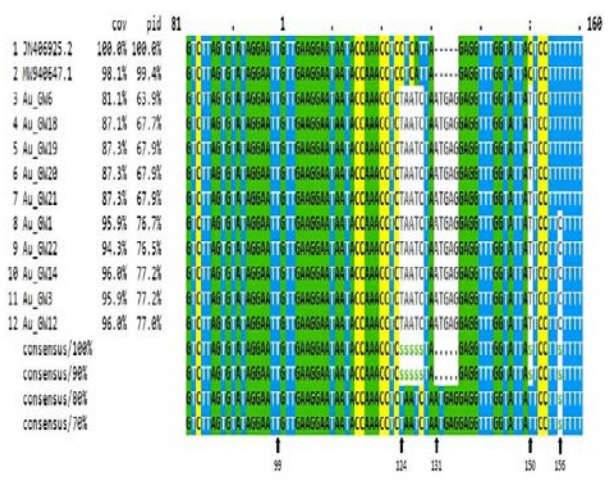

Figure 5. Nucleotide base variation based on the *psb*A-*trn*H IGS locus in *Xanthosoma undipes* accessions collected from Mount Karang.

4. Discussion

Xanthosoma undipes was first described in 1856, highlighting its morphological characteristics (Seemann and Seemann, 1856) and is native to tropical America (POWO, 2024). According to its protologue (Seemann and Seemann, 1856), *X. undipes* features a conspicuous stem, triangular leaves with pointed lobes at the base, and petioles with a wavy sheath. The spadix is slightly curved in the middle, narrower, and shorter than the spathe. Its antheridia, or male reproductive organs, are numerous and have a slightly flattened top (Seemann and Seemann, 1856). Croat *et al.* (2017) in a taxonomic revision of *Xanthosoma* in Central America, further described *X. undipes* as having a large stem, broad leaves with convex major veins, and 5–7 inflorescences per axil. The peduncles are pale green, the spathe blade is pale yellow-green to white outside and white inside, and the tube is usually green with reddish-purple tinges near the tip (sometimes purplish) outside and dark purple-violet inside, especially at the base. The sterile male flowers are white to yellowish cream, while the female flowers are bright orange (Croat *et al*., 2017).

In contrast, *X. undipes* from Indonesia, particularly Mount Karang, exhibit a green or greenish-red peduncle. The outer spathe tube varies from green to dark red or purplish, while the inner spathe tube is bright green or yellow at the top and transitions to dark red or purplish at the base. Additionally, the outer spathe blade is yellow or pink. These findings align with the observations of Windarsih *et al.* (2023) for *X. undipes* in Indonesia. The spathe coloration of *X. undipes* from Central America, as described by Croat *et al.* (2017), appears to exhibit a combination of morphological characteristics observed in the two distinct clades identified among *X. undipes* accessions on Mount Karang. On Mount Karang, *X. undipes* displays spathe colour variations that clearly differentiate the accessions into two clades: Clade I is characterized by a green outer spathe tube, a bright green inner spathe tube, and a yellow outer spathe blade, whereas Clade II exhibits a dark red to purplish outer spathe tube, an inner spathe tube that is yellow at the apex and transitions to dark red-purple at the base, and a pink outer spathe blade.

Beyond spathe coloration, other morphological features, including corm cortex and bud colour, cormel cortex and tip colour, petiole junction colour on the leaf underside, leaf sheath coloration, peduncle colour, and the coloration of both sterile and male flowers, further support the delineation of these two clades. This observation is corroborated by a morphological similarity analysis, which clustered the *X. undipes* accessions from Mount Karang into two primary clades with a similarity coefficient of 0.14 using the UPGMA method (Figure 2). A detailed morphological comparison of these clades is presented in Table 5 and Figure 3. Notably, the most prominent distinctions between the two clades are associated with colour variations in various plant structures.

As well established, the phenotypes or morphological characteristics of a plant are determined by its genes and their interactions (Campbell *et al*., 2002). Environmental factors can influence gene expression, potentially leading to different phenotypes. However, based on the habitat conditions of *X. undipes* collected from Mount Karang (Table 3), no specific habitat conditions were identified as being associated with the phenotype of two clades *X. undipes* on Mount Karang. Further research is needed on the influence of environmental factors on spathe colour

variations in *X. undipes*. Nevertheless, it is undeniable that the environment can affect plant phenotypes (Fritz *et al*., 2018). A classic example of environmental factors affecting gene expression is seen in hydrangeas (*Hydrangea* sp.) (Campbell *et al*., 2002; Rahmati *et al*., 2022). In acidic soil (pH < 5.5), hydrangea flowers appear blue due to the availability of aluminium ions, which influence anthocyanin pigments. Conversely, limited aluminium ions result in pink flowers in neutral to alkaline soil (pH > 6.5).

Phylogenetically, molecular analysis using the ML method on *X. undipes* accessions collected from Mount Karang, which utilizing chloroplast DNA sequences from the *psb*A-*trn*H IGS region, revealed results consistent with the UPGMA analysis based on morphological characteristics. This ML analysis of DNA sequencing at the *psb*A-*trn*H IGS locus strongly differentiated (bootstrap = 100) the *X. undipes* accessions from Mount Karang into two distinct clades (Figure 4), with each clade comprising the same set of *X. undipes* accessions as identified in the morphological analysis. The ML clustering with a bootstrap value of 100 is considered strongly supported, according to Cusimano *et al.* (2011). Nucleotide base position 156 at the *psb*A-*trn*H IGS locus (Figure 5) serves as a distinguishing marker between the two clades.

A similar pattern was observed in a phylogenetic study of Araceae, where comparisons were made between morphological characteristics and molecular phylogenies. The clustering analyses based on qualitative morphological characteristics and Simple Sequence Repeat (SSR) markers effectively distinguished the purple *X. sagittifolium* (L.) Schott accessions from the green accessions (Wada *et al*., 2021). Meanwhile, the resulting ML phylogeny is well-resolved and strongly supported, with most of the 44 larger clades of Araceae also exhibiting synapomorphies in morphology (Cusimano *et al*., 2011). Synapomorphies are derived characteristics shared by two or more taxonomic groups (Assis and Rieppel, 2011). In this study, the inflorescence characters (‘spathe + spadix’ model) of *X. undipes* represent a synapomorphic trait that distinguishes the two clades. However, it is crucial to note that the ‘spathe + spadix’ model inflorescence is not exclusively a synapomorphy of Araceae, as plants in the order Acorales also produce a similar type of inflorescence (Tippery *et al*., 2021).

In this study, the accessions *X. undipes* GW18, GW19, GW20, GW21, and GW22, collected from Saninten Village, are known to be the source of planting material for the five other accessions cultivated in Pandeglang Village and Juhut Village. The phenomenon of farmer-to-farmer exchange of planting materials is also commonly observed with *X. sagittifolium* accessions in Ethiopia (Wada *et al*., 2021). The clustering phenomenon suggests that, in the past, clonal propagation of *X. undipes* likely occurred, involving the multiplication of genetically identical individuals through asexual reproduction. Additionally, *X. undipes* may have also reproduced sexually through seeds resulting from cross-pollination, similar to what has been observed in Araceae species, such as *Amorphophallus variabilis* Blume (Santosa *et al*., 2012), *A. konjac* K. Koch (Pan *et al*., 2015), and *Cyrtosperma merkusii* (Hassk.) Schott (Erlinawati *et al*., 2018).

Xanthosoma undipes has strong potential to support food security. Its tubers are a source of carbohydrates, while the leaves can be used as a tobacco substitute and herbal tea. However, the plant remains poorly known (Suhaendah *et al*., 2025). This study contributes to expanding current knowledge of *X. undipes.* On the other hand, traditional vegetative propagation methods often result in limited phenotypic diversity of *X. undipes* (Wardhani *et al*., 2025), thus the findings of this study can serve as baseline data for experimental research, such as propagation.

5. Conclusion

Morphological data reveal two distinct clades of *X. undipes* accessions on Mount Karang, Banten, Indonesia. Some distinguishing morphological characters differentiate the two clades of *X. undipes*, including corms, cormels, leaf petiole junctions, leaf sheaths, peduncles, spathes, sterile flowers, and male flowers. Molecular analysis using the *psb*A-*trn*H IGS marker supports the clustering observed in the morphological data. In the end, morphological and molecular evidence clearly confirmed the presence of two distinct clades among *X. undipes* accessions from Mount Karang.

Acknowledgments

We extend our gratitude to the Faculty of Science, UIN Sultan Maulana Hasanuddin Banten, for funding this research. We extend our sincere gratitude to the Director of Scientific Collection Management (Herbarium Bogoriense), National Research and Innovation Agency, Indonesia, Herbarium Bandungense (FIPIA), and Herbarium Faculty of Science and Technology UIN Sultan Maulana Hasanuddin Banten, for permitting us to deposit the specimens. We also express our sincere appreciation to Maman, Ddedi Muhadi, Azizah Fauziah Rahma, Deni Mulyana, Saiful Iman Maulana, and Fitri Novianti for their valuable assistance in characterizing the morphological features and collecting *Xanthosoma undipes* leaves for molecular analysis. We acknowledge the National Center for Biotechnology Information (NCBI) database for their valuable data. We sincerely thank the Directorate of Repositories, Multimedia, and Scientific Publishing, National Research and Innovation Agency, for the linguistic review (ID: LG20241734903718).

References

Ali MA, Gabor G and Al-Hemaid F. 2015. **Plant DNA Barcoding and Phylogenetics**. Lambert Academic Publishing, Germany. pp. 155-170.

Assis LCS and Rieppel O. 2011. Are monophyly and synapomorphy the same or different? Revisiting the role of morphology in phylogenetics. *Cladistics*., **27(1)**: 94–102. https://doi.org/10.1111/j.1096-0031.2010.00317.x

Balkanska R, Stefanova K, Stoikova-Grigorova R and Ignatova M. 2020. A preliminary assessment of *trn*H-*psb*A as DNA barcode for botanical identification of polyfloral honey samples and comparison with *rbcL* marker. *Bulg J Agric Sci*., **26(1)**: 238–242.

Beyene P, Botha A and Myburg AA. 2005. A comparative study of molecular and morphological methods of describing genetic

relationships in traditional Ethiopian highland maize. *Afr J Biotechnol*., **4(7)**: 586–595. https://doi.org/10.5897/AJB2005.000-3107

Budiarto MS and Rahayuningsih Y. 2017. Economic value potency of talas beneng (*Xanthosoma undipes* K. Koch) based on nutrient content. *J Kebij Pembang Daer*., **1(1)**: 1–12. https://doi.org/10.56945/jkpd.v1i1.1

Campbell NA, Reece JB and Mitchell LG. 2002. **Biologi**, edisi kelima, jilid I. Erlangga, Jakarta.

Chen S, Yao H, Han J, Liu C, Song J, Shi L, Zhu Y, Ma X, Gao T, Pang X, Luo K, Li Y, Li X, Jia X, Lin Y and Leon C. 2010. Validation of the ITS2 region as a novel DNA barcode for identifying medicinal plant species. *PLoS One*., **5(1)**: e8613. https://doi.org/10.1371/journal.pone.0008613

Corpet F. 1988. Multiple sequence alignment with hierarchical clustering. *Nucleic Acids Res*., **16(22)**: 10881–10890. https://doi.org/10.1093/nar/16.22.10881

Croat TB and Ortiz OO. 2020. Distribution of Araceae and the diversity of life forms. *Acta Soc Bot Pol*., **89(3)**: 8939. https://doi.org/10.5586/asbp.8939

Croat TB, Delannay X and Ortiz OO. 2017. A revision of *Xanthosoma* (Araceae). Part 2: Central America. *Aroideana*., **40(2)**: 504–581.

Cusimano N, Bogner J, Mayo SJ, Boyce PC, Wong SY, Hesse M, Hetterscheid WLA, Keating RC and French JC. 2011. Relationships within the Araceae: Comparison of morphological patterns with molecular phylogenies. *Am J Bot*., **98(4)**: 654–668. https://doi.org/10.3732/ajb.1000158

Djarwaningsih T, Sunarti S and Kramadibrata K. 2002. **Panduan Pengolahan dan Pengelolaan Material Herbarium serta Pengendalian Hama Terpadu di Herbarium Bogoriens**e. Herbarium Bogoriense-Bidang Botani, Pusat Penelitian Biologi, Lembaga Ilmu Pengetahuan Indonesia, Bogor.

Doyle JJ and Doyle JL. 1987. A rapid DNA isolation from small amount of fresh leaf tissue. *Phytochem Bull*., **19**: 11−15.

Erlinawati I, Abinawanto, Salamah A and Rugayah. 2018. Genetic diversity analysis of daluga (*Cyrtosperma merkusii*) using sequence-related amplified polymorphism in Siau, Sangihe and Talaud Islands, North Sulawesi, Indonesia. *Biodiversitas*., **19(6)**: 2374–2380. https://doi.org/10.13057/biodiv/d190648

Fatmawaty AA, Hermita N, Hastuti D, Kartina AM and Hilal S. 2019. Phytochemical analysis of beneng taro (*Xanthosoma undipes* K. Koch) leaves: Cultivation as raw material for biopesticides for eco-friendly agriculture. *IOP Conf Ser: Earth Environ Sci*., **383:** 012006. https://doi.org/10.1088/1755-1315/383/1/012006

Fendiyanto MH, Supena EDJ, Sari IE, Pratami MP, Satrio RD and Nikmah IA. 2024. Biological diversity of seawater microalgae isolated from Ujung Genteng Sukabumi and their novel genomic DNA isolation technique. *Jordan J Biol Sci*., **17(3)**: 495–505. https://doi.org/10.54319/jjbs/170312

Fitriyah N and Wahyudi M. 2022. Efektivitas penambahan zat pengatur tumbuh pada stek mikro tanaman porang (*Amorphophallus muelleri* Blume) dan talas beneng (*Xanthosoma undipes* K. Koch). *Innofarm*., **24(2)**: 64–72.

Frausin G, Lima RBS, Hidalgo AF, Ming LC and Pohlit AM. 2015. Plants of the Araceae for malaria and related diseases: A review. *Rev Bras Plantas Med*., **17(4)**: 1–21. https://doi.org/10.1590/1983-084X/14_024

Fritz MA, Rosa S and Sicard A. 2018. Mechanisms underlying the environmentally induced plasticity of leaf morphology. *Front Genet*., **9**: 478. https://doi.org/10.3389/fgene.2018.00478

Hakiki DN, Rostianti T, Nasir and Nursuciyoni. 2019. Development of local food biodiversity of nata de taro from talas beneng (*Xanthosoma undipes* K. Koch). *IOP Conf Ser: Earth Environ Sci*., **309:** 012030. https://doi.org/10.1088/1755-1315/309/1/012030

Hall TA. 1999. BioEdit: a user-friendly biological sequence alignment editor and analysis program for Windows 95/98/NT. *Nucleic Acids Symp Ser*., **41**: 95–98.

Jansen PCM and Premchand V. 1996. *Xanthosoma* Schott. In: Flach, M., & Rumawas, F. (Editors). **Plant Resources of South-East Asia** No. 9: Plants yielding non-seed carbohydrates. PROSEA Foundation, Bogor, Indonesia. pp. 159–164.

Kerbs B. 2015. *Xanthosoma undipes* (Araceae) as a food source for black-chinned mountain-tanager (*Anisognathus notabilis*) and orange-bellied euphonia (*Euphonia xanthogaster*) in northwest Ecuador. *Ornitol Neotrop*., **26(1)**: 103–107. https://doi.org/10.58843/ornneo.v26i1.16

Kress WJ and Erickson DL. 2007. A Two-locus global DNA barcode for land plants: The coding *rbc*L gene complements the non-coding *trn*H–*psb*A spacer region. *PLoS One*., **2(6):** e508. https://doi.org/10.1371/journal.pone.0000508

Kress WJ, Garcia-lobredo C, Uriarte M and Erickson DL. 2015. DNA Barcodes for Ecology, Evolution, and Conversation. *Trends Ecol Evol*., **30(1)**: 25–35. https://doi.org/10.1016/j.tree.2014.10.008

Kress WJ, Wurdack KJ, Zimmer EA, Weigt LA and Janzen DH. 2005. Use of DNA barcodes to identify flowering plants. *Proc Natl Acad Sci U S A*., **102(23):** 8369–8374. https://doi.org/10.1073/pnas.0503123102

Loera-Sánchez M, Studer B and Kölliker R. 2024. DNA barcode *trn*H-*psb*A is a promising candidate for efficient identification of forage legumes and grasses. *BMC Res Notes*., **13(35)**: 1–6. https://doi.org/10.1186/s13104-020-4897-5

Minantyorini and Hanarida I. 2002. **Panduan Karakterisasi dan Evaluasi Plasma Nutfah Talas**. Departemen Pertanian Badan Penelitian dan Pengembangan Pertanian Komisi Nasional Plasma Nutfah, Bogor, Indonesian.

Nunes RSC, Aguila EMD, Paschoalin VMF and da Silva JT. 2015. DNA barcoding assessment of the genetic diversity of varieties of taro, *Colocasia esculenta* (L.) Schott in Brazil. **Breeding and Genetic Engineering**. iConcept Press Ltd., Queensland.

Nurtiana W, Rismaya R, Sulistyawati EYE, Fauziyyah A, Hakiki DN, Radiansyah MR and Rahmawan A. 2022. The effect of beneng taro (*Xanthosoma undipes* K.Koch) flour substitution on physical and sensory characteristics of muffins. ~~*Food Sci Tech J*~~ *Food ScienTech J*., **4(2)**: 129–144. https://doi.org/10.33512/fsj.v4i2.17413

Pan C, Gichira AW and Chen JM. 2015. Genetic variation in wild populations of the tuber crop *Amorphophallus konjac* (Araceae) in central China as revealed by AFLP markers. *Genet Mol Res*., **14(4)**: 18753–18763. https://doi.org/10.4238/2015.December.28.24

POWO [Plants of the World Online]. 2023. **Plants of the World Online**. Facilitated by the Royal Botanic Gardens, Kew. http://www.plantsoftheworldonline.org/. [2 December 2023].

Rahmati R, Hamid R, Ghorbanzadeh Z, Jacob F, Azadi P, Zeinalabedini M, Farsad LK, Kazemi M, Ebrahimi MA, Shahinnia F, Salekdeh GH, Ghaffari MR and Hajirezaei MR. 2022. Comparative transcriptome analysis unveils the molecular mechanism underlying sepal colour changes under acidic pH substratum in *Hydrangea macrophylla*. *Int J Mol Sci*., **23(23)**: 15428. https://doi.org/10.3390/ijms232315428

Rohlf FJ. 1997. **NTSYS-pc. Numerical taxonomy and multivariate analysis. Version 2.0**. Exeter Software, New York.

Rugayah, Retnowati A, Windadri FI and Hidayat A. 2004. Pengumpulan Data Taksonomi. In: Rugayah, Widjaja EA and Praptiwi (Eds.). **Pedoman Pengumpulan Data Keanekaragaman Flora**. Pusat Penelitian Biologi-LIPI, Bogor, Indonesia. pp. 5–42.

Santosa E, Sugiyama N, Kawabata S and Hikosaka S. 2012. Genetic variations of *Amorphophallus variabilis* Blume (Araceae) in Java using AFLP. *J Agron Indones*., **40(1)**: 62–68. https://doi.org/10.24831/jai.v40i1.14941

Seemann WEG and Seemann B. 1856. **Bonplandia**. Zeitschrift für die gesammte Botanik. C. Rümpler, Hannover.

Suhaendah E, Sudomo A, Suhartono S, Fauziyah E and Geraldine LA. 2025. Understory cultivation practices of *Xanthosoma undipes* K.Koch: Lessons learned from private forests in Sukabumi, West Java, Indonesia. *AIP Conf Proc*., **3172(1)**: 020012. https://doi.org/10.1063/5.0240941

Talley TE and Kolondam BJ. 2015. DNA barcoding of Sangihe Nutmeg (*Myristica fragrans*) using *mat*K gene. *Hayati J Biosci*., **22(1)**: 41–47. https://doi.org/10.4308/hjb.22.1.41

Tamura K, Stecher G and Kumar D. 2021. MEGA11: Molecular evolutionary genetics analysis version 11. *Mol Biol Evol*., **38(7)**: 3022–3027. https://doi.org/10.1093/molbev/msab120

Tippery NP, Les DH, Appenroth KJ, Sree KS, Crawford DJ and Bog M. 2021. Lemnaceae and Orontiaceae are phylogenetically and morphologically distinct from Araceae. *Plants*., **10(12)**: 2639. https://doi.org/10.3390/plants10122639

Wada E, Feyissa T, Tesfaye K, Asfaw Z and Potter D. 2021. Genetic diversity of Ethiopian cocoyam (*Xanthosoma sagittifolium* (L.) Schott) accessions as revealed by morphological traits and SSR markers. *PLoS One*., **16(1)**: e0245120. https://doi.org/10.1371/journal.pone.0245120

Wardhani KA, Dinarti D, Santosa E and Nurcholis W. 2025. Gamma ray irradiation effects on embryogenic calli growth in Indonesian taro. *Pertanika J Trop Agric Sci*., **48(3)**: 733–746. https://doi.org/10.47836/pjtas.48.3.05

Windarsih G, Rahma AF, Mulyana D, Hariri MR, Erlinawati I, Riastiwi I and Efendi M. 2023. Pragmatical utilization of beneng taro (*Xanthosoma undipes* K.Koch) based on local knowledge of the community of Mount Karang, Pandeglang, Indonesia. *Biodiversitas*., **24(12)**: 6415–6424. https://doi.org/10.13057/biodiv/d241202

Yursak Z, Hidayah I, Saryoko A, Kurniawati S, Ripasonah O and Susilawati PN. 2021. Morphological characterization and development potential of beneng variety (*Xanthosoma undipes* K. Koch) Pandeglang - Banten. *IOP Conf Ser: Earth Environ Sci*., **715**: 012022. https://doi.org/10.1088/1755-1315/715/1/012022

JJBS

Volume 19, Number 1,March 2026
ISSN 1995-6673
Pages 23 – 33
https://doi.org/10.54319/jjbs/190103

Jordan Journal of Biological Sciences

Structural and antigenic impact of RpfE (Rv2450c) mutations in *Mycobacterium tuberculosis* clinical isolates from South Sulawesi, Indonesia: insights from molecular docking, molecular dynamics, and epitope prediction

Sadiya Ramli[1], Israini Wiyulanda Iskandar[1], Astutiati Nurhasanah[2,*], Nihayatul Karimah[2], Najdah Hidayah[3], Muhammad Nasrum Massi[4,*], Doddy Irawan Setyo Utomo[2], Rizalinda Sjahril[4], Fadhilah Syamsuri[4], Irda Handayani[5]

[1]*Biomedical Science Master Program, Postgraduate School, Faculty of Medicine, Universitas Hasanuddin, Makassar, South Sulawesi 90245, Indonesia;* [2]*Centre for Vaccine and Drugs Research, Health Research Organization, National Research and Innovation Agency (BRIN), Banten 15314, Indonesia;* [3]*Institute for Research and Community Services, Universitas Hasanuddin, Makassar, South Sulawesi 90245, Indonesia;* [4]*Department of Microbiology, Faculty of Medicine, Universitas Hasanuddin, Makassar, South Sulawesi 90245, Indonesia;* [5]*Department of Clinical Pathology, Faculty of Medicine, Universitas Hasanuddin, Makassar, South Sulawesi 90245, Indonesia*

Received: April 18, 2025; Revised: June 26, 2025; Accepted: July 2, 2025

Abstract

Tuberculosis (TB), caused by *Mycobacterium tuberculosis* (Mtb), remains a global health threat. Resuscitation-Promoting Factor E (RpfE), encoded by *Rv2450c*, plays a key role in bacterial reactivation and is a promising vaccine and therapeutic target. However, mutations in *Rv2450c* may alter RpfE's structure, function, and antigenicity, affecting immune recognition.

This study analysed *Rv2450c* variations in 40 Mtb clinical isolates from South Sulawesi, Indonesia, using *in silico* approaches to predict structural and functional impacts. Structural modelling, molecular dynamics simulations, epitope binding predictions, and antigenicity analyses were conducted, alongside molecular docking with TLR4 and ligand-binding assessment with NAG3.

Three missense mutations were identified: Arg126Gln (ubiquitous), Thr20Arg (lineage-specific), and Pro35Ser (novel), resulting in three RpfE variants: M1 (containing double mutations Arg126Gln, Thr20Arg), M2 (containing double mutations Arg126Gln, Pro35Ser), and M3 (containing single mutation Arg126Gln). These mutations induced moderate conformational changes with minimal effects on stability or immunogenicity. VaxiJen analysis indicated moderate antigenicity across all variants. Notably, M2 showed the strongest binding to TLR4, while docking with NAG3 also showed affinity alterations.

These findings highlight the genetic diversity of *Rv2450c* and its potential implications for immune recognition and vaccine design. Experimental validation is needed to confirm these predictions.

Key words: molecular modelling, Mycobacterium tuberculosis, mutation, RpfE, Rv2450c

1. Introduction

Tuberculosis, caused by Mycobacterium tuberculosis (Mtb), is a significant global health concern, with more than ten million new cases and approximately 1.25 million deaths reported in 2023 (WHO, 2024). The pathogen's ability to persist in dormancy and reactivate underlies the chronicity and global burden of TB. Resuscitation-Promoting Factors (Rpfs) are crucial in reactivating dormant bacilli (Kana et al., 2008), functioning alongside partnering proteins in hydrolysis of peptidoglycan. Mtb possesses five *rpf* homologues, *rpfA-E* (Mukamolova et al., 2002), all of which are expressed during *in vitro* growth and detected in human tissues infected by the bacteria (Davies et al., 2008). In addition, *M. tuberculosis* H37Rv with combinations of three deleted *rpf*-like genes showed reduced ability to resuscitate from a 'non-culturable' state and exhibited differential growth attenuation in mice (Downing et al., 2005). RpfB and RpfE are also known to interact with Rpf-interacting protein A (RipA), colocalising at the septa of dividing cells, suggesting a role for the RipA–Rpf complex in peptidoglycan hydrolysis during cell division (Hett et al., 2007). RipA is known to hydrolyse several cell wall substrates and synergises with RpfB (Hett et al., 2008). However, RipA does not interact with RpfA, C, and D, suggesting that these proteins act on different pathways, perhaps involving other RipA-like proteins.

The crystal structure of the RpfE catalytic domain revealed that the protein adopts the characteristic Rpf fold, with narrower catalytic cleft in comparison to Mtb RpfB. Also, unlike RpfB, RpfE's predicted peptide-binding sites are more positively charged at neutral pH (Mavrici et al., 2014). The reversal of the electrostatic potential at the substrate-binding site indicates that RpfE may function optimally at a different pH than RpfB, or preferentially

* Corresponding author. e-mail: astutiati.nurhasanah@brin.go.id; nasrumm@unhas.ac.id

hydrolyse distinct micro-domains of the peptidoglycan (Mavrici et al., 2014).

RpfE's immunogenic properties, including T-cell activation and TLR4 binding (Choi et al., 2015; Park et al., 2021), make it a promising candidate for molecular adjuvants and vaccine development. However, since variations in other genes, such as *accD3* (Jalil et al., 2018), involved in Mtb cell wall biosynthesis, had been previously reported, it is also possible that the mutations in *rpfE* (also known as *Rv2450c)* gene may alter RpfE's structure, function, or antigenicity, potentially affecting bacterial persistence, immune evasion and potentially compromise vaccine efficacy.

Given that RpfE-treated dendritic cells induce PGE2 production through MAPK and COX-2 signalling, which in turn promotes Th1 and Th17 responses via EP4 receptor signalling (Choi et al., 2015), mutations in RpfE could potentially impair this immunostimulatory function. RpfE, like other members of the resuscitation-promoting factor (Rpf) family, possesses muralytic (peptidoglycan-hydrolysing) activity via its conserved catalytic domain, which is structurally similar to lysozymes (Mavrici et al., 2014). Mutations affecting key residues involved in peptidoglycan binding or hydrolysis—such as conserved glutamic acid residues essential for catalytic activity (Mavrici et al., 2014; Squeglia et al., 2013)—could reduce RpfE's ability to generate the muropeptide fragments that act as potent pathogen-associated molecular patterns (PAMPs). These muropeptides are thought to be crucial for dendritic cell activation and the subsequent induction of cytokines like PGE2 (Park et al., 2021). A mutation affecting the conserved catalytic residues could drastically impair muralytic activity, thereby reducing the availability of peptidoglycan-derived ligands for innate immune recognition, leading to suboptimal PGE2 production and consequently weaker Th1/Th17 polarisation. This could represent a potential mechanism of immune evasion by Mtb clinical isolates. Moreover, reduced muralytic activity due to such mutations may simultaneously hinder peptidoglycan remodeling, potentially impairing bacterial resuscitation from dormancy but favouring persistence under immune pressure—a classical trade-off seen in pathoadaptation (Kana et al., 2008). Thus, specific mutations in the catalytic domain of RpfE may confer a selective advantage by diminishing immune detection (via impaired PGE2-mediated Th1/Th17 priming) while modulating the bacterial life cycle balance between dormancy and active growth.

This study is the first to characterize RpfE mutations in clinical Mtb isolates from South Sulawesi, Indonesia, using in silico functional prediction. Indonesia is a high-incidence region reporting over one million TB cases in 2024 (Arlinta, 2024). Using in silico analyses, we identified mutations in *Rv2450c* and evaluated their effects on protein structure, antigenicity, and enzymatic activity. These findings provide insights into the role of RpfE variations in TB pathogenesis and implications for vaccine and therapeutic development.

2. Materials and Methods

2.1. Sample Collection

This study analysed 40 *M. tuberculosis* clinical isolates (Supplementary Table 1) stored at the HUMRC Laboratory, Universitas Hasanuddin, Makassar, Indonesia. The isolates originated from the South Sulawesi Referral Laboratory for Tuberculosis Culture and Drug Susceptibility Testing (DST), Faculty of Medicine, Universitas Hasanuddin, and were collected from patients with confirmed active pulmonary tuberculosis between 2016 and 2018. Each isolate was cultured, species identified, and DST-ed for first- and second-line anti-tuberculosis drugs. Based on DST results, isolates were categorised as drug-sensitive, rifampicin-resistant, multidrug-resistant (MDR), or extensively drug-resistant (XDR). Isolates that failed DNA quality standard were excluded from further molecular analysis. Ethical approval for the use of human-derived samples was granted by the Research Ethics Committee of Universitas Hasanuddin (Ethics Approval No: 678/UN4.6.4.5.3.1/PP36/2023). All procedures involving *M. tuberculosis* cultures were carried out in a certified Biosafety Level 3 (BSL-3) facility at the HUMRC Laboratory. Handling of live bacteria—including inoculation, subculturing, and sample processing—was strictly conducted within a Class II Biological Safety Cabinet (BSC) to minimise the risk of aerosol exposure. The laboratory was equipped with HEPA-filtered negative pressure airflow systems, and access was restricted to personnel with appropriate training.

2.2. DNA extraction

Genomic DNA was extracted using the gSYNC™ DNA Extraction Kit (Geneaid™), following the manufacturer's instructions with slight modifications to accommodate the characteristics of mycobacterial cells. Approximately 200 µL of bacterial pellet was collected from Mtb cultures grown in Löwenstein–Jensen (LJ) medium after 4 to 6 weeks of incubation at 37°C. The pellet was transferred into a sterile 1.5 mL microcentrifuge tube and resuspended in 200 µL of PBS. The suspension was heat-inactivated at 95°C for 30 minutes to ensure biosafety, then centrifuged at 13,000 rpm for 5 minutes. The supernatant was discarded, and the pellet underwent enzymatic lysis by adding 200 µL of GS1 buffer and 20 µL of Proteinase K, followed by incubation at 60°C for 30 minutes.

Following lysis, 200 µL of GS2 buffer was added, mixed thoroughly, and incubated at room temperature for 10 minutes. DNA binding was achieved by adding 200 µL of absolute ethanol, mixing well, and transferring the mixture into the gSYNC™ DNA mini column. After centrifugation at 14,000 rpm for 1 minute, the column was washed with 400 µL of W1 buffer and twice with 600 µL of wash buffer (ethanol-based). The column was dried through additional centrifugation to remove any residual ethanol. DNA was eluted by adding 50 µL of pre-warmed elution buffer (provided in the kit) directly to the center of the column membrane, incubated at room temperature for 3 minutes, and centrifuged at 14,000 rpm for 1 minute. The eluted genomic DNA was stored at -20°C until further analysis. DNA purity and concentration were assessed using a NanoDrop™ 2000 spectrophotometer (Thermo Scientific™).

2.3. PCR Amplification of RpfE Gene

The Rv2450c (RpfE) gene was amplified using PCR with primers designed via Primer-BLAST based on the Mtb H37Rv reference genome (NC_000962.3). The PCR was performed with an annealing temperature of 58°C, resulting in an amplicon size of 683 bp. The full primer sequences, PCR cycling parameters, and electrophoresis conditions are detailed in Table 1.

Table 1. *Mtb* RpfE PCR amplification primers

Gene	Identifier	Size	Primer sequence	Tm (°C)	Amplicon size
RpfE	Rv2450c	519	F 5' GTCACGGGTTTGACGCTACT 3'	58°C	683
			R 5' AATGCACCTGGCAGCTAACC 3'		
PCR Conditions		95°C (3 min); 30 cycles of 95°C (30 s), 58°C (15 s), 72°C (1 min); final extension at 72°C (10 min)			
Gel Electrophoresis		0.8% agarose gel, 1X TAE buffer, 5 - 7V/cm, 40 mins; UV transilluminator			

2.4. DNA Sequencing and Data Analysis

Amplicons were purified and subjected to bidirectional Sanger sequencing using the BigDye® Terminator v3.1 Cycle Sequencing Kit on an ABI PRISM® 3730xl DNA Analyzer platform at 1st BASE Laboratories (Selangor, Malaysia). The same primers as used for PCR amplification (Table 1) were used for the sequencing. Resulting chromatograms were manually checked for quality and contigs were assembled using BioEdit v7.2.5 (Hall, 1999). Contigs were aligned to the H37Rv reference genome (NC_000962.3) and compared with GenBank database sequences (Supplementary Table 2). Homologous sequences and protein variants were identified using BLASTp (Altschul et al., 1990).

2.5. Phylogenetic Analysis

Phylogenetic trees were constructed using the Tamura 3-parameter (T92) model in MEGA 11 (Tamura et al., 2021), incorporating six *Rv2450c* sequences from different Mtb lineages (Supplementary Table 2)

2.6. Construction and Validation of the RpfE Model Structure

RpfE protein structures were modelled using I-TASSER (http://zhang.bioinformatics.ku.edu/I-TASSER) (Yang & Zhang, 2015) and AlphaFold (https://alphafold.ebi.ac.uk/) (Jumper et al., 2021), then validated using SAVES v6.0 server (https://saves.mbi.ucla.edu/) (Laskowski et al., 1993).

2.7. Structural Alignment

Structural similarity was assessed by aligning modelled structures, with Root Mean Square Deviation (RMSD) and coverage calculated using PyMOL 3.0.3.

2.8. Prediction of Protein Stability and Solubility

The stability and solubility of the proteins were computed using Protparam (https://web.expasy.org/protparam/) (Gasteiger E. et al., 2005).

2.9. Prediction of T cell epitopes

Cytotoxic T Lymphocyte (CTL) and Helper T Lymphocyte (HTL) epitopes were predicted using IEDB tools (http://tools.iedb.org/mhci/ and http://tools.iedb.org/mhcii/), with NetMHCPan 4.1 BA (HLA-I) and NetMHCIIPan 4.0 BA (HLA-II) (Reynisson et al., 2020) methods, and HLA reference sets covering >97% (HLA-I) (Weiskopf et al., 2013) and 99% (HLA-II) (Greenbaum et al., 2011) of the population. IC50 thresholds <500 nM for binding affinity, <50 nM for strong binders were used.

2.10. Prediction of Epitope Antigenicity

Antigenicity was assessed using VaxiJen 2.0 (https://www.ddg-pharmfac.net/vaxijen/VaxiJen/VaxiJen.html) (Doytchinova & Flower, 2007), with 0.4 threshold indicating antigenicity, and scores > 1.0 indicating high antigenicity, whereas 0.4 < scores < 1.0 indicating intermediate antigenicity.

2.11. Prediction of Signal Peptide

Signal peptides were identified using SignalP 6.0 (https://services.healthtech.dtu.dk/services/SignalP-6.0/) (Teufel et al., 2022).

2.12. TLR4 – RpfE Molecular Docking

Potential binding interfaces of TLR4 (PDB ID: 3FXI)-H37Rv RpfE was initially predicted by ClusPro (Kozakov et al., 2017) blind docking. The interfaces were then used as restraints for guided TLR4-RpfE (H37Rv and the mutants M1, M2, M3) dockings in HADDOCK 2.4 (Honorato et al., 2024). LRR positions were from UniProt TLR4_Human (Accession Number O00206). Interaction interfaces were analysed with PDBsum Generate (Laskowski, 2022) and the Protein–Ligand Interaction Profiler (PLIP) (Adasme et al., 2021), with visualisations prepared using PyMOL.

2.13. RpfE Catalytic Domain – NAG3 Ligand Molecular Docking

Docking of RpfE with its ligand, NAG3 (PDB ID: 4KPM) (Mavrici et al., 2014), was performed using AutoDock Vina v1.2.3 (parameters in Supplementary Table 3). The docking results were analysed for binding energy, pose or conformation relative to the binding site, and molecular interactions involving residues within 5Å. Validation was conducted by superimposing the re-docked NAG3 structure with the original 4KPM (RMSD <2Å). Models were visualised using BIOVIA Discovery Studio 2021.

2.14. Molecular Dynamics (MD) Simulations

MD simulations (100 ns) were conducted using GROMACS v2023.2 (Abraham et al., 2023), with TIP3P water and ionic conditions. Binding free energy was calculated using gmx_MMPBSA from trajectory data.

3. Results

3.1. PCR Amplification and Sequencing of the Amplicons

PCR amplification of the RpfE gene from 40 clinical isolates produced 683-bp amplicons. Sanger sequencing identified three nucleotide substitutions: 377G>A (all

isolates), 59C>G (4 isolates), and 103C>T (2 isolates) (Figure 1, Supplementary Figure 1). These substitutions resulted in three missense mutations (Supplementary Figure 1D)—Thr20Arg, Pro35Ser, and Arg126Gln. All isolates carried Arg126Gln, with subsets carrying either Thr20Arg (M1, hence Arg126Gln, Thr20Arg) or Pro35Ser (M2, Arg126Gln, Pro35Ser), or neither (M3, Arg126Gln). Representative isolates of each mutant were submitted to GenBank with the following accession numbers M1 (isolate R042SUS, Accession: PV075057), M2 (MDR162R, Accession: PV075056), M3 (MDR322SUS, Accession: PV075058).

3.2. Sequence Diversity

Sequence alignment with six Mtb lineages (L1–L6) revealed lineage-specific mutation patterns (Supplementary Figure 2). The Arg126Gln mutation (M3) was observed in lineages L1, L3, L4, L5, and L6 but absent in H37Rv. M1 (Arg126Gln, Thr20Arg) was found in Beijing/NITR203 (L2) and FDAARGOS_756, while M2 (Arg126Gln, Pro35Ser) was unique to this study. BLASTp confirmed that Pro35Ser is novel, not reported in GenBank.

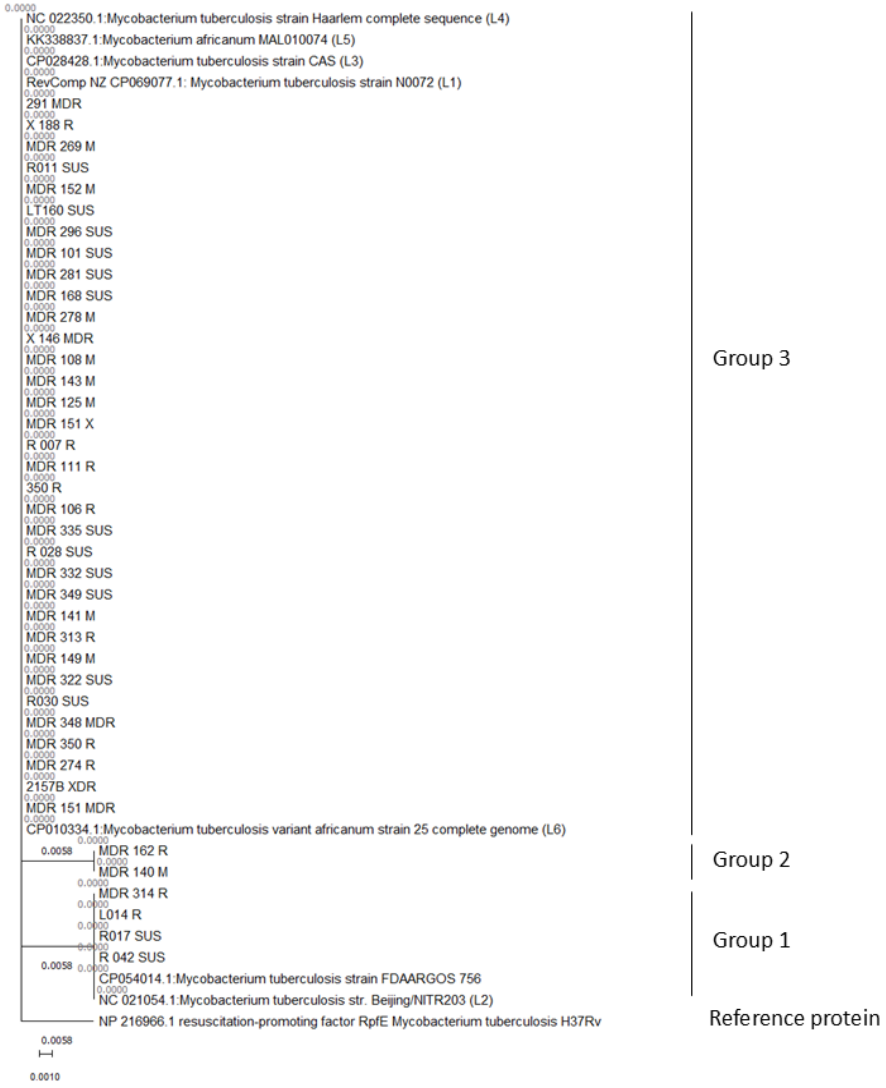

Isolate code	Nucleotide Substitution	Amino acid Substitution	Percentage of Clinical Isolates Containing the Sequence Variation
All clinical isolates	377G>A	*Arg*126*Gln*	100
R017SUS R042SUS L014R MDR314R	59C>G	*Thr*20*Arg*	10
MDR162R MDR140M	103C>T	*Pro*35*Ser*	5

Figure 1. Mutation sites (Arg: Arginine; Gln: Glutamine; Thr: Threonine; Pro: Proline; Ser: Serine; A: Adenine; C: Cytosine; G: Guanine; T: Thymine) found in the clinical Mtb isolates and phylogenetic tree of the RpfE gene, constructed using sequences from H37Rv, the mutant sequences identified in this study, and previously reported sequences from the NCBI-GenBank database. The divergence scale at the bottom of the tree represents the genetic divergence in terms of the number of substitutions per site. A value of 0.0010 indicates a genetic difference of 0.0010 substitutions per DNA site between the compared strains.

3.3. Phylogenetic Analysis

Maximum Likelihood phylogenetic analysis grouped isolates into four clusters (Figure 1). M1 was linked to FDAARGOS_756 and Beijing/NITR203 (L2), M2 to a distinct cluster, and M3 to N0072 (L1), CAS (L3), Haarlem (L4), *M. africanum* MAL010074 (L5), and *M. tuberculosis* africanum strain 25 (L6). H37Rv formed a separate cluster, confirming evolutionary divergence.

3.4. Impact of Nucleotide Variations on RpfE Protein Structure and Antigenicity

3.4.1. RpfE Modelling and Validation

I-TASSER-derived 3D models (Supplementary Figure 3) demonstrated higher reliability than AlphaFold models (Supplementary Table 5). MD simulations (100 ns) confirmed stability, with Ramachandran plots indicating that the majority of residues were located within favoured regions.

3.4.2. Effect of Amino Acid Variations on RpfE Protein Structure, Stability, Solubility, and Signal Peptide Position

Secondary structure analysis (Supplementary Figure 4) showed no significant changes in the number of helices (three) or beta strands (three) across the reference and mutant proteins, though beta strand lengths varied. M1 retained the same beta strand positions as the reference (6–13, 17–19, and 123–125), while M2 exhibited slightly shorter strands (6–12, 17–18). M3 displayed an extended N-terminal beta strand (5–13), with other strand positions matching those of the reference and M1.

Three-dimensional structural alignments (Supplementary Figure 5) revealed RMSD scores and coverage of 1.70 Å (74.84%) for M1, 1.32 Å (56.79%) for M2, and 0.92 Å (64.65%) for M3, reflecting moderate deviations from the reference.

According to the Protparam results (Table 2), all the proteins might be considered unstable, with Instability Indexes exceeding 40, and they are likely hydrophilic, based on the negative GRAVY scores.

SignalP 6.0 predicted the signal peptide position (amino acids 1–28) and cleavage site (between residues 28 and 29) to be unchanged across all mutants compared to the reference RpfE protein. Detailed results are provided in Supplementary Figure 6.

Table 2. Instability index and GRAVY score of RpfE reference and variant proteins, as predicted using Protparam

Protein	Instability Index	Grand average of hydropathicity (GRAVY) score
Reference protein (H37Rv)	47.84	-0.269
M1 (Thr20Arg, Arg126Gln)	50.73	-0.285
M2 (Pro35Ser, Arg126Gln)	49.29	-0.259
M3 (Arg126Gln)	48.17	-0.263

3.4.3. Effect of Amino Acid Variations on Protein's Antigenicity

The VaxiJen scores for the RpfE reference protein and its M1, M2, and M3 mutants were 0.8023, 0.7946, 0.8068, and 0.7996, respectively, indicating medium antigenicity (0.4 < VaxiJen scores < 1.0).

3.4.4. Effect of Amino Acid Variations on T-cell Epitopes

The overall antigenicity of mutated epitopes is largely unchanged, even though binding affinities with MHC-I and MHC-II vary with mutations. Amino acid variations in the RpfE protein influenced predicted MHC-I and MHC-II T-cell epitopes affinity towards HLA alleles (Supplementary Files 1–8), although the effect seems to be allele and mutation specific, and to a varying degree.

The reference RpfE protein (H37Rv) contained ten high-affinity MHC-I epitopes (IC50 < 50 nM), none of which includes the positions of amino acid variations (Thr20, Pro35, or Arg126). Increasing the IC50 threshold to <500 nM, showed Thr20 and Arg126 as part of medium-affinity epitopes, but not Pro35. The Thr20Arg mutation (Supplementary Table 6) reduced binding affinity for three epitopes across five alleles but enhanced seven others, generating two new strong-binding epitopes (IC50 < 50 nM) with medium antigenicity (0.4 < VaxiJen scores < 1.0). The Arg126Gln mutation (Supplementary Table 7) created three intermediate-affinity epitopes but no strong-binding ones. The novel Pro35Ser mutation, however, had limited impact on binding affinity, indicating a minimal role in MHC-I-mediated recognition.

The reference RpfE protein contained 108 high-affinity (IC50<50 nM) MHC-II epitopes, 25 of which carry Thr20, and two carry Arg126. Pro35 was found in intermediate-affinity (IC50 < 500 nM), highly antigenic epitopes (VaxiJen scores > 1.0). The Thr20Arg mutation reduced epitope-MHC-II combinations from 300 to 289, generated 17 new high-affinity epitopes (Supplementary Table 8), and reduced the binding of a strong-binding epitope, with little impact on antigenicity. The Arg126Gln mutation (Supplementary Table 9) converted two high-affinity epitopes into intermediate binders but preserved their antigenicity. The novel Pro35Ser mutation (Supplementary Table 10) caused two intermediate-affinity epitopes to lose binding capability, though antigenicity remained high.

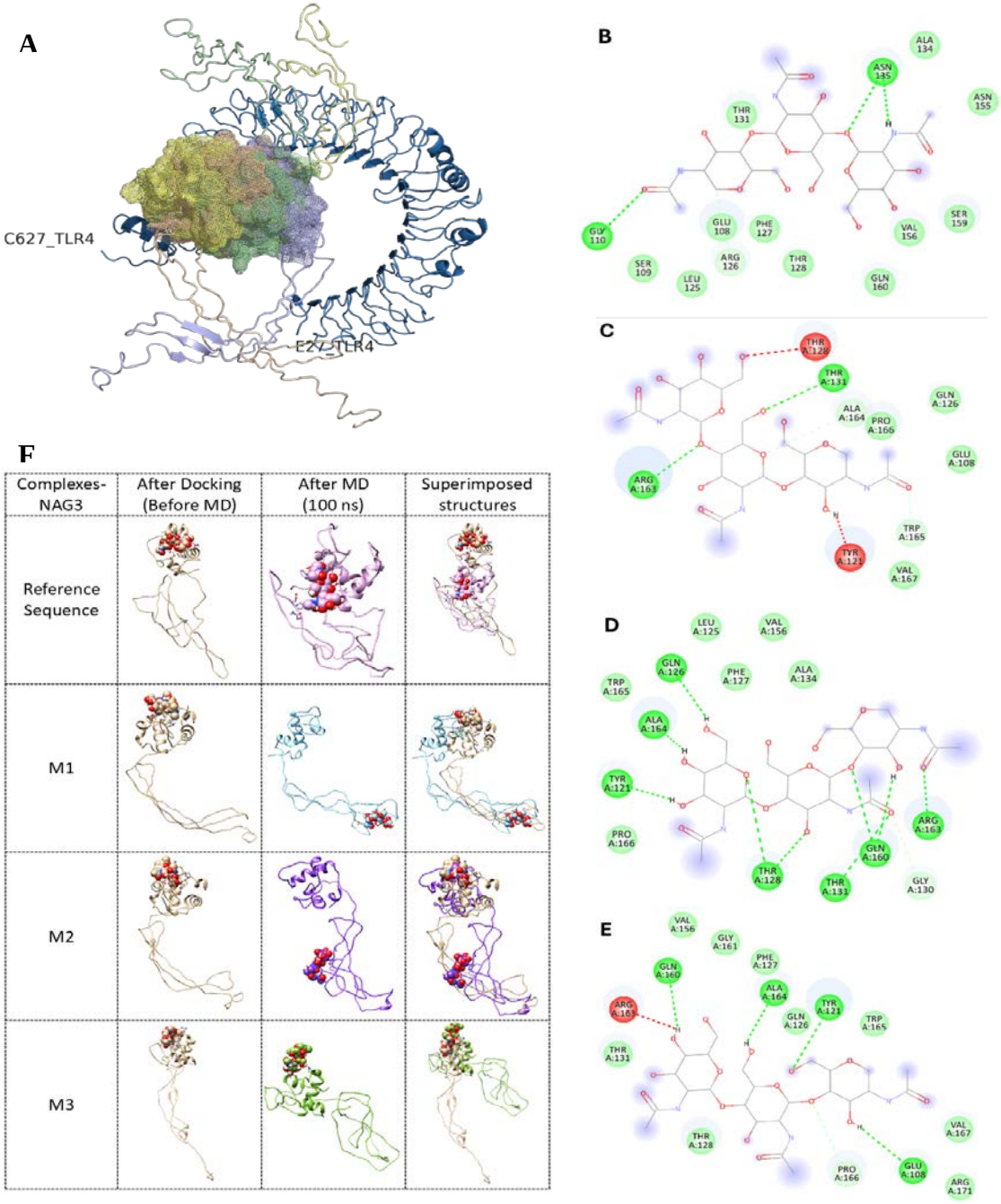

Figure 2. A. Complex of TLR4 (blue ribbon) - RpfE from H37Rv (wheat), M1 (pale green), M2 (pale yellow), M3 (light blue). RpfE residues interacting with NAG3 in B. Reference protein, C. M1, D. M2, and E. M3. Red colour indicates residues showing unfavourable interactions, whereas green indicates favourable interactions.

3.4.5. Effect of Amino Acid Variations on TLR4 Binding

Molecular docking revealed notable differences in RpfE-TLR4 binding, interaction residues (Table 3), and complex structures (Figure 2A). HADDOCK scores indicated stronger binding for M2 and M3 compared to the reference and M1. M2 showed the highest structural stability with the lowest RMSD, while the reference and M3 exhibited greater flexibility, indicating less stable interactions.

Van der Waals energy was most favourable for M3, while M2 and M1 had the strongest electrostatic interactions, surpassing the reference. M3 also had the lowest desolvation energy, enhancing complex stability. Buried surface area (BSA) was larger in all mutants compared to the reference, correlating with stronger binding.

Hydrogen bond analysis revealed that both reference and mutant RpfE proteins interact with TLR4's LRR14–LRRCT regions (amino acids 456–606), primarily via the RpfE catalytic domain (residues 98–172). Mutations did not significantly alter these interactions, although M3 showed a slightly expanded binding interface, including His431 in LRR13.

Despite the absence of negative control or decoys, the docking result revealed that all RpfE proteins interact with TLR4's LRR14–LRRCT regions through hydrogen bonds, in which the interaction with LRR region of TLR4 is known to mediate interactions with several microbial ligands.

Table 1. Results of molecular docking in HADDOCK and residues interaction between TLR4 and RpfE proteins from reference strain (H37Rv), and strains with M1, M2, and M3 mutations

	H37Rv			M1			M2			M3		
HADDOCK score	-118.2 +/- 5.2			-116.8 +/- 10.2			-131.0 +/- 9.7			-124.7 +/- 2.5		
Cluster size	7			6			9			19		
RMSD from the overall lowest-energy structure	23.7 +/- 0.2			14.8 +/- 0.1			0.8 +/- 0.7			19.3 +/- 0.1		
Van der Waals energy	-65.9 +/- 11.6			-51.0 +/- 7.3			-53.6 +/- 3.1			-81.6 +/- 3.3		
Electrostatic energy	-191.5 +/- 34.3			-353.7 +/- 56.0			-386.4 +/- 37.7			-132.3 +/- 19.8		
Desolvation energy	-16.4 +/- 2.5			2.9 +/- 6.1			-4.3 +/- 1.8			-21.0 +/- 1.3		
Restraints violation energy	24.4 +/- 19.6			21.4 +/- 20.9			42.0 +/- 14.9			44.2 +/- 29.6		
Buried Surface Area	1965.6 +/- 121.4			2268.9 +/- 131.0			2144.9 +/- 106.6			2245.1 +/- 140.1		
Z-Score	-2			-2.2			-1.8			-1.6		
	Receptor	Ligand	Bond Length (Å)	Receptor	Ligand	Bond Length (Å)	Receptor	Ligand	Bond Length (Å)	Receptor	Ligand	Bond Length (Å)
Hydrogen Bonds	Tyr-46	Glu-66	2.78	Gly-363	Glu-88	2.67	Lys-362	Pro-80	2.99	Glu-42	Leu-33	2.68
	His-456	Arg-170	2.7	Asn-365	Glu-88	2.8	His-529	Asn-155	2.76	His-431	Arg-163	2.94
	Gln-507	Ser-159	3.22	Lys-388	Asp-29	2.6	Ala-610	Arg-163	2.66	His-456	Arg-163	2.95
	Asn-531	Arg-158	3.21	His-529	Gln-106	2.78	Gln-616	Arg-163	2.95	Asp-502	Asn-119	3.34
	Leu-553	Arg-158	2.87	His-555	Gln-106	3.16	Gln-616	Gln-160	2.9	Gln-505	Glu-108	2.69
	Arg-606	Ser-98	3.15	Gln-578	Ala-103	3.29				His-529	Cys-107	3.24
	Glu-608	Ala-96	3.23	Arg-606	Arg-171	2.76				His-555	Arg-171	3.24
										Gln-578	Ser-109	2.94
										Arg-606	Ser-109	3.04
Salt Bridges				Lys-388	Asp-29	2.6	Arg-264	Asp-81	2.64	His-529	Glu-108	3.4
				Lys-435	Asp-42	2.89	Arg-264	Asp-81	2.73			
				Glu-608	Arg-171	2.64	Lys-341	Asp-30	3.2			
							Lys-362	Asp-30	2.57			
							Arg-382	Glu-88	3.79			
							His-431	Glu-89	3.88			
							His-456	Glu-89	2.68			
							Glu-608	Arg-133	2.76			

Table 2. Binding affinities from molecular docking, ligand displacement and structural stability metrics from MD simulations, and MM_PBSA calculation. [a] All units are in Å (Amstrong); [b] Radius of Gyration, [c] All units are in kJ/mol.

	Molecular Docking	Molecular Dynamics						MM_PBSA Calculation			
Variant	Binding Affinity (kcal/mol)	Ligand Displacement[a]	Average[a] $RMSD_{Backbone}$	Average[a] $RMSD_{Ligand}$	RMSD Stability	Average[a] RMSF	Average[a] RoG[b]	Van der Walls Energy[c]	Electrostatic Energy[c]	Polar Solvation Energy[c]	ΔG Binding Free Energy[c]
Reference (H37Rv)	-6.05	3.9 → 2.4	0.84	1	Stable after 20 ns	0.65 (Lowest fluctuations)	1.93 (Stable)	-33.48 ± 1.24	-42.55 ± 12.00	-4.05 ± 0.21	-14.53 ± 6.40
M1	-5.28	2.7 → 57.4	1.57	1.07	Unstable	1.10 (Fluctuations observed)	2.66 (Unstable)	-29.49 ± 1.28	-37.15 ± 11.62	-3.67 ± 0.06	-8.07 ± 5.28
M2	-5.02	2.2 → 31.3	1.59	1.05	Unstable	1.16 (Fluctuations observed)	2.85 (Unstable)	-18.76 ± 1.43	-4.12 ± 1.84	-2.60 ± 0.21	-5.78 ± 2.98
M3	-4.65	1.7 → 12.7	1.82	1.17	Stabilised early, but slightly fluctuated after 80 ns	0.99 (Moderate fluctuations)	2.34 (Partial stability)	-31.19 ± 2.50	-63.51 ± 3.93	-4.29 ± 0.07	-16.52 ± 4.27

3.4.6. Effect of Amino Acid Variations on NAG3 Binding to RpfE Catalytic Domain

Molecular docking confirmed NAG3 binding to the RpfE catalytic domain across all variants, with the reference protein (H37Rv) exhibiting the strongest binding affinity (-6.05 kcal/mol), followed by M1, M2, and M3 (Table 4). Hydrogen bonding analysis revealed variations in binding interactions (Figure 2B - E), with M2 showing the highest number of hydrogen bonds (10), while M1 and M3 displayed unfavourable interactions that may weaken binding stability.

MD simulations revealed varying ligand stability (Figure 2F). The metrics of ligand displacement and structural stability are presented in Table 4.

RMSD analysis (Supplementary Figure 7A) confirmed that the reference protein stabilised after 20 ns with minimal fluctuations, while M1 and M2 exhibited continuous instability. Ligand RMSD fluctuations (Supplementary Figure 7B) confirms weak interactions particularly between NAG3 and M2. RMSF analysis (Supplementary Figure 7C) indicated that key fluctuations occurred at Asp42, Gly62, Asn119, Ser140, and Gly172, with mutation sites (residues 20, 35, 126) remaining stable. RoG analysis (Supplementary Figure 7D) showed structural stability in the reference protein, followed by M3, which stabilised after ~20 ns.

MM-PBSA calculations (Table 4) revealed lower binding free energies for the reference and M3 complexes, indicating higher binding stability compared to M1 and M2.

4. Discussion

This study examined the structural, immunological, and molecular implications of naturally occurring RpfE (Rv2450c) mutations in *Mycobacterium tuberculosis*, focusing on three key polymorphic variants. All observed mutants shared the Arg126Gln substitution, with additional mutations at Thr20Arg (M1) and Pro35Ser (M2), highlighting both lineage-specific and novel variations. M2 variation was observed in two of 40 isolates (Figure 1). If this proportion reflects its true frequency in the population, this might suggest that this unique 5% of the Mtb population comprises a locally evolved strain.

Notably, Arg126Gln was found across diverse lineages (L1, L3, L4, L5, and L6), in H37Rv derivatives (Santoro et al., 2017), African samples (Osei-Wusu et al., 2021), and laboratory strains (Ioerger et al., 2010), though absent in the H37Rv reference, suggesting it may represent an evolutionary adaptation with broad geographical persistence. Its presence in isolates from patients undergoing prolonged isoniazid and rifampicin treatment (Li et al., 2018) suggests a possible selective advantage. Since the increase in multidrug-resistant (MDR) microorganisms triggering infections is growing worldwide and becoming more serious in developing countries (Al-Ouqaili et al., 2025; Owaid & Al-Ouqaili, 2024), we attempted to correlate the presence of this mutation with DST data (Supplementary Table 1). However, the mutation was not restricted to MDR, XDR, or rifampicin-resistant isolates. The M1-type double mutation (Thr20Arg, Arg126Gln) was primarily associated with the Beijing/NITR203 (L2) strain, consistent with previous reports identifying Thr20Arg as a lineage-defining marker (Tantivitayakul et al., 2020), found in 28.7% of Indonesian strains (Atavliyeva et al., 2024).

4.1. Structural Impact and TLR4 Interactions

Molecular modelling revealed that M2 displayed the strongest affinity to TLR4, as evidenced by HADDOCK scores and docking RMSD values, indicating a potential increase in innate immune engagement. There is no definitive biological threshold for HADDOCK score. The score was used primarily for guiding the comparative purpose between a set of simulations, in which the lower the score, the more favourable the binding.

The enlargement of buried surface area and enhanced electrostatic interactions across all mutants support this observation. Interestingly, M3's docking revealed an expanded interface involving LRR13, which could represent a distinct binding mode for RpfE–TLR4 interaction. These findings are consistent with the critical role of TLR4 in recognising Mtb proteins through leucine-rich repeat domains independently of MD2, as previously described (Kleinnijenhuis et al., 2011; Park et al., 2021). Such enhanced receptor interactions may influence the early immune activation cascade, including proinflammatory cytokine production and antigen processing. As a known TLR4 agonist, RpfE enhances dendritic cell maturation and cytokine production (Park et al., 2021).

4.2. MHC Presentation and Antigenicity

Our study indicated that the overall antigenicity of mutated epitopes is unchanged, despite variations of MHC-I and MHC-II binding affinities observed with the mutations. These findings suggest that while mutations alter epitope presentation and binding affinity, they do not drastically enhance the immunogenic profile of the RpfE protein.

The epitope analysis showed that Thr20 and Arg126 are embedded within several MHC-II epitopes, with M1 notably generating new high-affinity binders while slightly reducing overall MHC-II epitope diversity. Importantly, this mutation also gave rise to new strong-binding MHC-I epitopes, suggesting an immunogenic shift that may enhance T-cell responses. Previous studies have demonstrated that single amino acid polymorphisms can dramatically influence epitope presentation and recognition (Bui et al., 2007). The Pro35Ser substitution in M2, which is novel and unique to this study, had minimal impact on MHC-binding affinity but preserved high antigenicity, indicating a potentially conserved immunological function. Meanwhile, M3's Arg126Gln substitution created intermediate-affinity MHC-I epitopes and modestly weakened MHC-II affinity but retained immunogenic potential. These observations underscore the functional plasticity of RpfE epitopes and the importance of characterising lineage-specific mutations in vaccine design (Comas et al., 2010; Panda et al., 2023).

VaxiJen was used as part of integrative strategies to define immunological properties of each variants, to distinguish the antigenicity between the variants and, to specifically define the range of their antigenicity. Although the result showed only slight differences between variants, it gave us information that they possessed medium range of antigenicity. Based on the Vaxijen score and Haddock

result, M2 variant is the most antigenic and M1 is the least antigenic.

4.3. Ligand Binding to NAG3 and Structural Stability

Molecular dynamics simulations, performed following docking of NAG3 to RpfE variants, revealed notable differences in ligand-binding stability and structural behaviour. While the reference RpfE protein maintained structural integrity and stabilised after 20 ns of simulation, all mutant variants displayed reduced stability, with M1 and M2 showing the most pronounced fluctuations. These findings suggest that the observed mutations may compromise the receptor's conformational stability upon ligand binding, possibly affecting biological functions such as peptidoglycan hydrolysis and reactivation from dormancy (Rosser et al., 2017). Interestingly, despite M2 forming the highest number of hydrogen bonds, it exhibited weak overall interactions and instability, highlighting that increased hydrogen bonding alone does not ensure structural resilience. M3 showed partial stability but reduced affinity, suggesting a potential compensatory adaptation. Overall, the lower MM-PBSA binding free energies across mutants reflect a trend of weakened RpfE–ligand interactions, which may impair physiological ligand recognition and catalytic efficiency.

These mutations may disrupt RpfE's catalytic function, which is critical for bacterial cell wall remodelling and resuscitation. Arg126, previously identified as part of RpfE's catalytic cleft (Mavrici et al., 2014), facilitates glycan hydrolysis in the peptidoglycan (PG) matrix (Romano et al., 2023)**,** protecting bacteria from environmental stress. RpfE also interacts with RipA, a key peptidase in PG remodelling and cell division (Hett et al., 2008). Mutations affecting substrate binding could impair these functions, potentially altering bacterial dormancy and resuscitation.

4.4. Impact on Strain Tracking and Epidemiology

The presence of polymorphisms in antigen-encoding genes, such as rpfE, may alter epitope structures, potentially affecting immune recognition. This variation could lead to reduced vaccine efficacy if the candidate vaccine is based on the reference strain H37Rv, which may not fully represent circulating clinical isolates in South Sulawesi. Our findings highlight the importance of incorporating region-specific genetic data in the rational design of next-generation TB vaccines, ensuring the inclusion of conserved and immunodominant epitopes prevalent in local strains, hence, the importance of strain tracking. The polymorphisms could serve as molecular markers for strain tracking and surveillance, aiding in the identification of local transmission patterns and the emergence of drug-resistant *M. tuberculosis* lineages.

5. Conclusions

Overall, our findings suggest that while these mutations contribute to sequence diversity and lineage specificity, their impact on protein structure and antigenicity is relatively moderate. The enhanced TLR4 binding in M2 and M3 could influence immune recognition, whereas the observed changes in ligand binding may have functional consequences for bacterial physiology.

Further experimental validation, including enzymatic activity assays and immune response studies, is required to elucidate the biological significance of these mutations and their potential role in Mtb pathogenesis. In addition, the observation of variation of antigen-encoding genes in clinical isolates emphasises the necessity of strain tracking as well as genetic surveillance, to ensure new tuberculosis vaccines have suitable population coverage.

Acknowledgement

The authors sincerely thank the National Research and Innovation Agency (BRIN) for funding this research, and StudiBio for their valuable computational resources and continuous support throughout the study.

Data Availability Statement

All supplementary data can be downloaded from the following links:

- Supplementary Tables and Figures
- Supplementary File 1
- Supplementary File 2
- Supplementary File 3
- Supplementary File 4
- Supplementary File 5
- Supplementary File 6
- Supplementary File 7
- Supplementary File 8

Funding Statement

This work was supported by the National Research and Innovation Agency (BRIN) through the grants RIIM No.12/II.7/HK/2023 (granted to Astutiati Nurhasanah) and RP-ORK No.23/III.9/HK/2023 (granted to Nihayatul Karimah).

Conflict of Interest Disclosure

The authors declare that they have no known competing financial interests or personal relationships that could have appeared to influence the work reported in this paper.

Ethics Approval Statement

The study protocol complies with the Declaration of Helsinki and has been approved by Health Research Ethics Committee of Faculty of Medicine, Universitas Hasanuddin (No. 678/UN4.6.4.5.3.1/PP36/2023, September 13, 2023).

Declaration of generative AI and AI-assisted technologies in the writing process

During the preparation of this work the author(s) used ChatGPT (Free Online Version) in order to rephrase some sentences in parts of the articles, to improve readability. After using this tool/service, the author(s) reviewed and edited the content as needed and take(s) full responsibility for the content of the publication.

References

Abraham, M., Alekseenko, A., Bergh, C., Blau, C., Briand, E., Doijade, M., Fleischmann, S., Gapsys, V., Garg, G., Gorelov, S., Gouaillardet, G., Gray, A., Irrgang, M. E., Jalalypour, F., Kutzner, C., Lemkul, J. A., Lundborg, M., Merz, P., Miletic, V., … Lindahl, E. (2023). GROMACS 2023.2 Manual. ***GROMACS Archive, Version 2023.2***, 1–848. https://doi.org/https://doi.org/10.5281/zenodo.8134388

Adasme, M. F., Linnemann, K. L., Bolz, S. N., Kaiser, F., Salentin, S., Haupt, V. J., & Schroeder, M. (2021). PLIP 2021: expanding the scope of the protein–ligand interaction profiler to DNA and RNA. *Nucleic Acids Res.*, *49*(W1), W530–W534. https://doi.org/10.1093/nar/gkab294

Al-Ouqaili, M. T. S., Ahmad, A., Jwair, N. A., & Al-Marzooq, F. (2025). Harnessing bacterial immunity: CRISPR-Cas system as a versatile tool in combating pathogens and revolutionizing medicine. *Front. Cell. Infect. Microbiol.*, *15*. https://doi.org/10.3389/fcimb.2025.1588446

Altschul, S. F., Gish, W., Miller, W., Myers, E. W., & Lipman, D. J. (1990). Basic local alignment search tool. *J. Mol. Biol.*, *215*(3), 403–410. https://doi.org/10.1016/S0022-2836(05)80360-2

Arlinta, D. (2024, February 8). Estimated TB cases in Indonesia have increased to more than 1 million cases. *Kompas.id*. https://www.kompas.id/baca/english/2024/02/07/en-estimasi-kasus-tbc-di-indonesia-naik-jadi-lebih-dari-1-juta-kasus

Atavliyeva, S., Auganova, D., & Tarlykov, P. (2024). Genetic diversity, evolution and drug resistance of Mycobacterium tuberculosis lineage 2. *Front. Microbiol.*, *15*. https://doi.org/10.3389/fmicb.2024.1384791

Bui, H.-H., Sidney, J., Li, W., Fusseder, N., & Sette, A. (2007). Development of an epitope conservancy analysis tool to facilitate the design of epitope-based diagnostics and vaccines. *BMC Bioinformatics*, *8*(1), 361. https://doi.org/10.1186/1471-2105-8-361

Choi, H., Kim, W. S., Back, Y. W., Kim, H., Kwon, K. W., Kim, J., Shin, S. J., & Kim, H. (2015). *Mycobacterium tuberculosis* RpfE promotes simultaneous Th1- and Th17-type T-cell immunity via TLR4-dependent maturation of dendritic cells. *Eur. J. Immunol.*, *45*(7), 1957–1971. https://doi.org/10.1002/eji.201445329

Comas, I., Chakravartti, J., Small, P. M., Galagan, J., Niemann, S., Kremer, K., Ernst, J. D., & Gagneux, S. (2010). Human T cell epitopes of Mycobacterium tuberculosis are evolutionarily hyperconserved. *Nat. Genet.*, *42*(6), 498–503. https://doi.org/10.1038/ng.590

Davies, A. P., Dhillon, A. P., Young, M., Henderson, B., McHugh, T. D., & Gillespie, S. H. (2008). Resuscitation-promoting factors are expressed in Mycobacterium tuberculosis-infected human tissue. *Tuberculosis*, *88*(5), 462–468. https://doi.org/10.1016/j.tube.2008.01.007

Downing, K. J., Mischenko, V. V., Shleeva, M. O., Young, D. I., Young, M., Kaprelyants, A. S., Apt, A. S., & Mizrahi, V. (2005). Mutants of *Mycobacterium tuberculosis* Lacking Three of the Five *rpf* -Like Genes Are Defective for Growth In Vivo and for Resuscitation In Vitro. *Infect. Immun.*, *73*(5), 3038–3043. https://doi.org/10.1128/IAI.73.5.3038-3043.2005

Doytchinova, I. A., & Flower, D. R. (2007). VaxiJen: a server for prediction of protective antigens, tumour antigens and subunit vaccines. *BMC Bioinformatics*, *8*(1), 4. https://doi.org/10.1186/1471-2105-8-4

Gasteiger E., Hoogland C., Gattiker A., Duvaud S., Wilkins M.R., Appel R.D., & Bairoch A. (2005). Protein Identification and Analysis Tools on the Expasy Server. In J. M. Walker (Ed.), ***The Proteomics Protocols Handbook*** (pp. 571–607). Humana Press .

Greenbaum, J., Sidney, J., Chung, J., Brander, C., Peters, B., & Sette, A. (2011). Functional classification of class II human leukocyte antigen (HLA) molecules reveals seven different supertypes and a surprising degree of repertoire sharing across supertypes. *Immunogenetics*, *63*(6), 325–335. https://doi.org/10.1007/s00251-011-0513-0

Hall, T. (1999). BioEdit: A User-Friendly Biological Sequence Alignment Editor and Analysis Program for Windows 95/98/NT. *Nucleic Acids Symp. Ser.*, *41*, 95–98.

Hett, E. C., Chao, M. C., Deng, L. L., & Rubin, E. J. (2008). A Mycobacterial Enzyme Essential for Cell Division Synergizes with Resuscitation-Promoting Factor. *PLoS Pathog.*, *4*(2), e1000001. https://doi.org/10.1371/journal.ppat.1000001

Hett, E. C., Chao, M. C., Steyn, A. J., Fortune, S. M., Deng, L. L., & Rubin, E. J. (2007). A partner for the resuscitation-promoting factors of *Mycobacterium tuberculosis*. *Mol. Microb.*, *66*(3), 658–668. https://doi.org/10.1111/j.1365-2958.2007.05945.x

Honorato, R. V., Trellet, M. E., Jiménez-García, B., Schaarschmidt, J. J., Giulini, M., Reys, V., Koukos, P. I., Rodrigues, J. P. G. L. M., Karaca, E., van Zundert, G. C. P., Roel-Touris, J., van Noort, C. W., Jandová, Z., Melquiond, A. S. J., & Bonvin, A. M. J. J. (2024). The HADDOCK2.4 web server for integrative modeling of biomolecular complexes. *Nat. Protoc.*, *19*(11), 3219–3241. https://doi.org/10.1038/s41596-024-01011-0

Ioerger, T. R., Feng, Y., Ganesula, K., Chen, X., Dobos, K. M., Fortune, S., Jacobs, W. R., Mizrahi, V., Parish, T., Rubin, E., Sassetti, C., & Sacchettini, J. C. (2010). Variation among genome sequences of H37Rv strains of Mycobacterium tuberculosis from multiple laboratories. *J. Bacteriol.*, *192*(14), 3645–3653. https://doi.org/10.1128/JB.00166-10

Jalil, A. A. A., Al-khafaji, Z. M., & Al-ouqaili, M. T. (2018). INVESTIGATION OF ACCD3 GENE OF MYCOBACTERIUM TUBERCULOSIS IRAQI ISOLATES. *Asian J. Pharm. Clin. Res.*, *11*(8), 208. https://doi.org/10.22159/ajpcr.2018.v11i8.25269

Jumper, J., Evans, R., Pritzel, A., Green, T., Figurnov, M., Ronneberger, O., Tunyasuvunakool, K., Bates, R., Žídek, A., Potapenko, A., Bridgland, A., Meyer, C., Kohl, S. A. A., Ballard, A. J., Cowie, A., Romera-Paredes, B., Nikolov, S., Jain, R., Adler, J., … Hassabis, D. (2021). Highly accurate protein structure prediction with AlphaFold. *Nature*, *596*(7873), 583–589. https://doi.org/10.1038/s41586-021-03819-2

Kana, B. D., Gordhan, B. G., Downing, K. J., Sung, N., Vostroktunova, G., Machowski, E. E., Tsenova, L., Young, M., Kaprelyants, A., Kaplan, G., & Mizrahi, V. (2008). The resuscitation-promoting factors of *Mycobacterium tuberculosis* are required for virulence and resuscitation from dormancy but are collectively dispensable for growth *in vitro*. *Molecular Microbiology*, *67*(3), 672–684. https://doi.org/10.1111/j.1365-2958.2007.06078.x

Kleinnijenhuis, J., Oosting, M., Joosten, L. A. B., Netea, M. G., & Van Crevel, R. (2011). Innate Immune Recognition of *Mycobacterium tuberculosis*. *Clin. Dev. Immunol.*, *2011*, 1–12. https://doi.org/10.1155/2011/405310

Kozakov, D., Hall, D. R., Xia, B., Porter, K. A., Padhorny, D., Yueh, C., Beglov, D., & Vajda, S. (2017). The ClusPro web server for protein–protein docking. *Nat. Protoc.*, *12*(2), 255–278. https://doi.org/10.1038/nprot.2016.169

Laskowski, R. A. (2022). PDBsum1: A standalone program for generating PDBsum analyses. *Prot. Sci.*, *31*(12), e4473. https://doi.org/10.1002/pro.4473

Laskowski, R. A., MacArthur, M. W., Moss, D. S., & Thornton, J. M. (1993). PROCHECK: a program to check the stereochemical quality of protein structures. *J. Appl. Crystallogr.*, *26*(2), 283–291. https://doi.org/10.1107/S0021889892009944

Li, H., Guo, H., Chen, T., Yu, L., Chen, Y., Zhao, J., Yan, H., Chen, M., Sun, Q., Zhang, C., Zhou, L., & Chen, L. (2018). Genome-wide SNP and InDel mutations in Mycobacterium tuberculosis associated with rifampicin and isoniazid resistance. *Int. J. Clin. Exp. Pathol.*, *11*(8), 3903–3914.

Mavrici, D., Prigozhin, D. M., & Alber, T. (2014). *Mycobacterium tuberculosis* RpfE crystal structure reveals a positively charged catalytic cleft. *Prot. Sci.*, *23*(4), 481–487. https://doi.org/10.1002/pro.2431

Mukamolova, G. V., Turapov, O. A., Young, D. I., Kaprelyants, A. S., Kell, D. B., & Young, M. (2002). A family of autocrine growth factors in *Mycobacterium tuberculosis*. *Mol. Microb.*, *46*(3), 623–635. https://doi.org/10.1046/j.1365-2958.2002.03184.x

Osei-Wusu, S., Otchere, I. D., Morgan, P., Musah, A. B., Siam, I. M., Asandem, D., Afum, T., Asare, P., Asante-Poku, A., Kusi, K. A., Gagneux, S., & Yeboah-Manu, D. (2021). Genotypic and phenotypic diversity of Mycobacterium tuberculosis complex genotypes prevalent in West Africa. *PLOS ONE*, *16*(8), e0255433. https://doi.org/10.1371/journal.pone.0255433

Owaid, H. A., & Al-Ouqaili, M. T. S. (2024). Molecular and bacteriological investigations for the co-existence CRISPR/Cas system and β-lactamases of types extended-spectrum and carbapenemases in Multidrug, extensive drug and Pandrug-Resistant Klebsiella pneumoniae. *Saudi J. Biol. Sci.*, *31*(7), 104022. https://doi.org/10.1016/j.sjbs.2024.104022

Panda, S., Morgan, J., Cheng, C., Saito, M., Gilman, R. H., Ciobanu, N., Crudu, V., Catanzaro, D. G., Catanzaro, A., Rodwell, T., Perera, J. S. B., Chathuranga, T., Gunasena, B., DeSilva, A. D., Peters, B., Sette, A., & Lindestam Arlehamn, C. S. (2023). *Identification of differentially recognized T cell epitopes in the spectrum of* Mtb *infection*. In *bioRxiv*. https://doi.org/10.1101/2023.04.12.536550

Park, H.-S., Choi, S., Back, Y.-W., Lee, K.-I., Choi, H.-G., & Kim, H.-J. (2021). Mycobacterium tuberculosis RpfE-Induced Prostaglandin E2 in Dendritic Cells Induces Th1/Th17 Cell Differentiation. *Int. J. Mol. Sci.*, *22*(14), 7535. https://doi.org/10.3390/ijms22147535

Reynisson, B., Alvarez, B., Paul, S., Peters, B., & Nielsen, M. (2020). NetMHCpan-4.1 and NetMHCIIpan-4.0: improved predictions of MHC antigen presentation by concurrent motif deconvolution and integration of MS MHC eluted ligand data. *Nucleic Acids Res.*, *48*(W1), W449–W454. https://doi.org/10.1093/nar/gkaa379

Romano, M., Squeglia, F., Kramarska, E., Barra, G., Choi, H.-G., Kim, H.-J., Ruggiero, A., & Berisio, R. (2023). A Structural View at Vaccine Development against M. tuberculosis. *Cells*, *12*(2), 317. https://doi.org/10.3390/cells12020317

Rosser, A., Stover, C., Pareek, M., & Mukamolova, G. V. (2017). Resuscitation-promoting factors are important determinants of the pathophysiology in *Mycobacterium tuberculosis* infection. *Crit. Rev. Microbiol.*, *43*(5), 621–630. https://doi.org/10.1080/1040841X.2017.1283485

Santoro, F., Guerrini, V., Lazzeri, E., Iannelli, F., & Pozzi, G. (2017). Genomic polymorphisms in a Laboratory Isolate of Mycobacterium tuberculosis Reference Strain H37Rv (ATCC27294). *New Microbiol.*, *40*(1), 62–69.

Squeglia, F., Romano, M., Ruggiero, A., Vitagliano, L., De Simone, A., & Berisio, R. (2013). Carbohydrate Recognition by RpfB from Mycobacterium tuberculosis Unveiled by Crystallographic and Molecular Dynamics Analyses. *Biophysic. J.*, *104*(11), 2530–2539. https://doi.org/10.1016/j.bpj.2013.04.040

Tamura, K., Stecher, G., & Kumar, S. (2021). MEGA11: Molecular Evolutionary Genetics Analysis Version 11. *Mol. Biol. Evol.*, *38*(7), 3022–3027. https://doi.org/10.1093/molbev/msab120

Tantivitayakul, P., Juthayothin, T., Ruangchai, W., Smittipat, N., Disratthakit, A., Mahasirimongkol, S., Tokunaga, K., & Palittapongarnpim, P. (2020). Identification and in silico functional prediction of lineage-specific SNPs distributed in DosR-related proteins and resuscitation-promoting factor proteins of Mycobacterium tuberculosis. *Heliyon*, *6*(12), e05744. https://doi.org/10.1016/j.heliyon.2020.e05744

Teufel, F., Almagro Armenteros, J. J., Johansen, A. R., Gíslason, M. H., Pihl, S. I., Tsirigos, K. D., Winther, O., Brunak, S., von Heijne, G., & Nielsen, H. (2022). SignalP 6.0 predicts all five types of signal peptides using protein language models. *Nat. Biotechnol.*, *40*(7), 1023–1025. https://doi.org/10.1038/s41587-021-01156-3

Weiskopf, D., Angelo, M. A., De Azeredo, E. L., Sidney, J., Greenbaum, J. A., Fernando, A. N., Broadwater, A., Kolla, R. V., De Silva, A. D., De Silva, A. M., Mattia, K. A., Doranz, B. J., Grey, H. M., Shresta, S., Peters, B., & Sette, A. (2013). Comprehensive analysis of dengue virus-specific responses supports an HLA-linked protective role for CD8+ T cells. *Proc. Natl. Acad. Sci. U. S. A.*, *110*(22). https://doi.org/10.1073/pnas.1305227110

WHO. (2024). ***Global tuberculosis report 2024***. https://www.who.int/publications/i/item/9789240101531

Yang, J., & Zhang, Y. (2015). I-TASSER server: new development for protein structure and function predictions. *Nucleic Acids Res.*, *43*(W1), W174–W181. https://doi.org/10.1093/nar/gkv342.

JJBS

Volume 19, Number 1,March 2026
ISSN 1995-6673
Pages 35 – 44
https://doi.org/10.54319/jjbs/190104

Jordan Journal of Biological Sciences

Micropropagation and in Vivo Antibacterial Activity of Different Extracts of Rue (*Ruta graveolens* l)

Rania M. Jammal[1], Abdul Latief Al-Ghzawi[2,*], Mohamad Shatnawi[3], Zakaria I. Al-Ajlouni[4], Shifaa Abbas[4], Mohammad M. Al Salem[4], Ghaith S. Bani Hani[4], Nisreen M. Awad[2], Abdel Rahman Al-Tawaha[5]

[1]*Department of Clinical Pharmacy, Faculty of Pharmacy, Jordan University of Science and Technology, Irbid, 22110, Jordan;* [2]*Department of Biology and Biotechnology, Faculty of Science, The Hashemite University, Zarqa, Jordan;* [3]*Department of Biotechnology, Faculty of Agricultural Technology, Al-Balqa' Applied University, Al-Salt 19117, Jordan;* [4]*Department of Plant Production, College of Agriculture, Jordan University of Science and Technology, Irbid, 22110, Jordan;* [5]*Department of Biological Sciences, Al Hussein bin Talal University, Maan, Jordan*

Received: May 27, 2025; Revised: July 8, 2025; Accepted: July 14, 2025

Abstract

This study investigated the in vitro growth and antibacterial activity of *Ruta graveolens* using callus and extracts obtained from both in vitro and in vivo sources. Shoot induction was conducted on Murashige and Skoog (MS) medium supplemented with different concentrations of BAP, kinetin, and GA_3 (0.0–1.0 mg/L), while root induction utilized MS medium containing 2,4-D (0.0–2.0 mg/L). The antibacterial efficacy of methanolic and ethanolic extracts was assessed against five bacterial strains. *Escherichia coli* and *Salmonella typhimurium* represented Gram-negative bacteria, while *Staphylococcus aureus*, *Bacillus cereus*, and *Micrococcus luteus* represented Gram-positive types. Optimal shoot induction (4.75 shoots, 2.66 cm length) occurred with 0.3 mg/L BAP, and maximum biomass (0.51 g fresh, 0.07 g dry) was achieved at 0.4 mg/L BAP. Kinetin at 0.1 mg/L resulted in the highest shoot number, while 1.0 mg/L improved shoot length and biomass. GA_3 at 1.0 mg/L yielded the highest number of shoots (7.5) and the longest (4.01 cm), with peak biomass at 0.4 mg/L. The best root and shoot development occurred at 0.4 mg/L 2,4-D, while the highest callus biomass (1.02 g fresh, 0.08 g dry) was observed at 2.0 mg/L 2,4-D. All extract types and doses (40 and 80 µL) demonstrated antibacterial activity against the tested bacterial species using an agar-well diffusion assay. These findings suggest that *R. graveolens* may serve as a promising natural source for the development of antibacterial agents.

Keywords: Antibacterial, In vivo, Micropopagatoin, Pharmaceuticals, Rue, *Ruta graveolens*

1. Introduction

Ruta graveolens L., commonly known as "Rue," "Sudab," or "Sadab" in Hindi, is one of the most prevalent medicinal plants in the Rutaceae family (Al-Ajlouni et al., 2022). Native to Europe, it has since spread globally. This perennial evergreen shrub, which can grow up to one meter in height, is widely used both for decorative and therapeutic purposes. Numerous studies on the Rutaceae family have highlighted the potential of its natural products in treating various conditions, including cancer, depression, and Alzheimer's disease. *Ruta* species have also been utilized to address various uterine conditions, such as amenorrhea, menstrual irregularities, and excess menstruation. These species have historically been recommended as an abortifacient and to assist with conception. In addition, *Ruta* species have been used to treat pregnancy-related issues, including placental expulsion and puerperal fever (Pollio et al., 2008). Rue has also been found to have protective properties against genetic abnormalities, such as cancer and mutations, underscoring its potential as a powerful protective agent (Al-Muffti et al., 2021). Research by Al-Ajlouni et al. (2015) and Kuzovkina et al. (2004) has identified over 120 natural compounds in the roots and apical portions of this plant, including alkaloids, coumarins, essential oils, and flavonoids. These metabolites are of significant interest in biology and pharmacology for their antifungal, anti-leishmanial, antiplasmodial, and antidotal properties (Sampaio et al., 2018).

According to Thomas & Devi (2013), over 50% of clinically used pharmaceuticals are derived from natural products, with approximately 25% originating from plant-based sources. This has motivated continued scientific investigation into plants like Rue, which may serve as sources for novel chemical structures that could aid in the development of new drugs targeting microbial resistance and reducing the adverse effects of specific antibiotics (Chaftar et al., 2016; Haddouchi et al., 2013).

As previously mentioned, Rue produces secondary metabolites (Morton & Telmer, 2014) and is considered one of the best plants for medicinal use. Antimicrobials derived from plants can be valuable in treating resistant microbiological strains, as their mechanisms of action may differ from those of currently used synthetic medications

* Corresponding author. e-mail: ghzawi@hu.edu.jo.

(Orlanda & Nascimento, 2015). Numerous studies have shown that chemical components from the Rutaceae family, such as limonoids, flavonoids, coumarins, and alkaloids, exhibit antibacterial, herbicidal, insecticidal, trypanocidal, and antimalarial properties (Luo et al., 2024). The antibacterial activity of these compounds can vary depending on factors such as the solvent, plant parts, harvesting time, and geographic region. For example, ethanolic extracts from the leaves have shown superior antibacterial activity compared to extracts from the stem and root. The leaves contain higher levels of flavonoids and phenols than other plant parts (Krayni et al., 2015). Salman et al. (2018) reported that the primary causes of dental caries, *S. mutans* and *S. sobrinus*, are significantly inhibited by the methanolic extract of *R. graveolens* and its specific components. Additionally, Mohammadpour et al. (2025) demonstrated that alcoholic extracts of *R. graveolens* (both ethanolic and methanolic) possess antibacterial effects. The most effective method for preventing burn infections caused by *S. aureus* and *P. aeruginosa* was found to be the use of complete dilutions of these extracts. However, one challenge farmers face when cultivating *R. graveolens* is slow shoot propagation, as many shoots fail to root easily, and there is considerable seed population variation (Ahmad et al., 2012). Furthermore, *R. graveolens* seeds exhibit poor germination rates, short viability, and susceptibility to pests and diseases in humid conditions (Bohidar et al., 2008). Mass harvesting of *R. graveolens* from its natural habitats has led to rapid depletion of these plant resources, causing the species to become endangered. The conventional propagation method cannot meet the growing demand for plants, as production is limited (Nalawade & Tsay, 2004). Modern biotechnological techniques for growing *R. graveolens* tissues and cells offer new opportunities for preserving and multiplying this important medicinal plant (Shatnawi et al., 2011). Given these challenges, plant tissue culture presents a promising solution to the poor propagation of *R. graveolens*. The objectives of this study were to develop effective methods for micropropagating *R. graveolens* using different types of cytokinin hormones and to investigate the potential antimicrobial activity (both antibacterial and antifungal) of plant extracts from *R. graveolens* grown in vitro and in vivo.

2. Material and Method

The study was conducted at the Tissue Culture Laboratory at Jordan University of Science and Technology. Seeds were collected from approximately five-year-old *R. graveolens* specimens located in Al-Sareeh, Irbid, Jordan, at an altitude of about 600 meters above sea level, with coordinates of 32.3306°N latitude and 35.8951°E longitude.

To initiate the surface sterilization process, the seeds were thoroughly washed under running water for fifteen minutes to remove any residual disinfectant. The seeds were immersed in 100 cc of 4% v/v Chlorex (containing 2.25% sodium hypochlorite) in a laminar flow cabinet for 15 minutes, with continuous shaking. After this, the seeds were rinsed three times with sterile distilled water, each rinse lasting five minutes. The seeds were then cleaned with 70% ethanol for 30 seconds, followed by immersion in 1% NaOCl for 30 minutes, with two drops of Tween 20 added to reduce surface tension. After sterilization, each seed was washed three times with sterile deionized water and then cut into a single bud under sterile conditions in a laminar flow cabinet.

The media used to cultivate the shoots is known as Murashige and Skoog (MS) medium, developed in 1962. This medium consists of 3% sucrose, 0.5 mM myo-inositol, 0.34 mM thiamine hydrochloride, 2.4 mM pyridoxine hydrochloride, 4.1 mM nicotinic acid, and 2.4 mM thiamine hydrochloride. Each 250 mL flask was supplemented with 60 mL of medium. Cotton wool was placed at the opening of each flask to allow for gas circulation, and the flasks were autoclaved at 121°C for 20 minutes. The cultures were incubated under a photoperiod of 16 hours and a PPFD of 50 μmol m−2 s−1, using cool white fluorescent lamps, with a temperature of 24 ± 2°C. After the first six weeks, microshoots were transferred to hormone-free Mississippi soil to obtain sufficient plant material. The photoperiod for the soil-grown plants was maintained at 16:8 light:dark, also at 24 ± 2°C. (Al Shhab et al., 2022: Al-Ajlouni et al 2023)

The MS-enriched base medium included 3% sucrose and 0.8% agar (Sigma, USA), and all components were prepared as concentrated stock solutions stored in a refrigerator. The necessary microsalts were dissolved in one liter of distilled water to serve as the stock solution for the experiment. Growth hormone stock solutions were prepared in the same manner. Cytokinins were dissolved in a small quantity of 1M HCl, and the remaining volume was filled with distilled water and stored at 4°C. All growth regulators were obtained from Sigma (USA). Once all the components were added to the conical flask in the correct proportions, the final volume was brought to a boil in distilled water, and the pH was adjusted to 5.8 with 0.1M HCl. The medium was solidified using 0.8% (w/v) agar. For liquid medium, agar was omitted.

After the medium was prepared, it was transferred into flasks with capacities of either 60 mL or 250 mL. These flasks were carefully sealed with cotton and muslin lids and labeled accordingly. Subsequently, the flasks were autoclaved at 126 degrees Celsius for twenty minutes at a pressure of fifteen pounds per square inch. Once sufficient plant material was available, microshoots measuring 10 millimeters in length, including apical meristems, were subcultured onto fresh MS media. The microshoots were grown on MS medium treated with varying concentrations of benzylaminopurine (BAP), kinetin, and GA3, specifically at levels of 0.0, 0.1, 0.2, 0.3, 0.4, 0.5, and 1.0 mg/L, each tested individually.

A total of twenty separate replicates of each treatment were conducted, and the trials were repeated twice. In a second experiment, microshoots measuring 10 millimeters in diameter were grown in MS media supplemented with varying concentrations of 2,4-Dichloromethoxyacetic acid (2,4-D) at levels of 0.0, 0.4, 0.8, 1.2, 1.6, 1.8, and 2.0 mg/L. Additionally, 0.5 grams of charcoal was added to the medium. The growth conditions in the second experiment were similar to those in the first experiment.

In vitro-rooted plantlets were carefully removed from the growth medium and cleaned in a water bath at 25–30°C to aid acclimatization. The plantlets were then transferred to 6 x 6 x 6 cm plastic pots filled with a sterile mixture of peat and perlite. A clear plastic bag measuring 15 x 20 cm was placed over each pot. To gradually reduce humidity, holes of 0.5 cm in diameter were made in the plastic bag, with additional holes added every three days for two to three weeks. After five weeks, the number of acclimatized plants that remained alive was recorded. This study involved five bacterial species: *Escherichia coli*, *Salmonella Typhimurium*, *Staphylococcus aureus*, and *Bacillus cereus* (all gram-positive bacteria), and *Micrococcus luteus* (a gram-negative bacterium). These species were identified in the microbiology lab at Yarmouk University, Jordan. (Al-Ajlouni et al 2023)

3. Experimental design and statistical analysis.

To assess whether there were differences in the means among the individuals, we conducted a one-way analysis of variance (ANOVA) followed by the least significant difference (LSD) test. The significance threshold was established at 0.05. A completely randomized design (CRD) was employed for all studies, with each treatment replicated ten times.

4. Results and Discussion

4.1. Effect of cytokinin on shoot proliferation

4.1.1. 6-Benzylaminopurine(BAP)

The multiplication rates were lowest in the medium without hormones (Table 1). Increasing the BAP concentration from 0.0 to 1.0 mg/L significantly enhanced the number of multiplied plants. Optimal shoot production was observed in the medium containing 0.3 mg/L BAP, which resulted in 4.75 shoots (Table 1). The maximum shoot length (2.66 cm) was achieved in the same medium (Figure 1; Table 1). Both fresh and dry weights increased significantly when BAP was raised from 0.0 to 0.4 mg/L. The fresh weight increased from 0.06 g to 0.51 g, and the dry weight rose from 0.01 g to 0.07 g (Table 1). Previous studies have well-documented the effectiveness of BAP over other cytokinins in tissue culture systems, including research on various explants, such as *Ocimum basilicum* (Jakovljević et al., 2022). BAP is recognized as a potent hormone for inducing multiple shoots in various plant taxa (George & Sherrington, 1984). Numerous studies have highlighted BAP's significant role in plantlet proliferation and multiplication. For example, Bohidar et al. (2013) and Bohidar et al. (2008) reported that BAP was the most effective compound for shoot induction, proliferation, and elongation. Similarly, the highest in vitro multiplication rate in *Vitis vinifera* was observed at 0.8 mg/L BAP (Shatnawi, 2013). In the present study, as BAP concentrations increased beyond 0.3 mg/L, a decline in shoot number, length, fresh weight, and dry weight was observed. Interestingly, when BAP concentrations were kept at or below 0.3 mg/L, both the number of new shoots and their length increased. However, concentrations exceeding 0.4 mg/L resulted in a reduction in these parameters.

Figure 1: After six weeks, shoot multiplication on (0.3 mg/L BAP).

Table 1: Mean impact of BAP concentrations after six weeks on various characteristics.

Concentration (mg/L)	Number of new shoots	Maximum shoot length (cm)	Fresh weight (g)	Dry weight (g)
0.0	2.70 ^{b}	1.71 ^{d}	0.06 ^{c}	0.01 ^{b}
0.1	3.05 ^{ab}	1.87 ^{cd}	0.13 ^{bc}	0.02 ^{b}
0.2	3.55 ^{ab}	1.97 ^{bcd}	0.09^{c}	0.02 ^{b}
0.3	4.75 ^{a}	2.66 ^{a}	0.50 ^{a}	0.07 ^{a}
0.4	4.35 ^{ab}	2.36 ^{ab}	0.51 ^{a}	0.07 ^{a}
0.5	4.05 ^{ab}	2.17 ^{bc}	0.41 ^{ab}	0.07 ^{a}
1.0	4.05 ^{ab}	2.37 ^{ab}	0.33 ^{abc}	0.04 ^{ab}

Based on the LSD test at $P < 0.05$, the same letter means they are not significantly different.

4.1.2. Kinetin

In vitro shoot lengths exhibited a favorable response to kinetin, with the maximum measurement at 0.4, 0.5, and 1.0 mg/l kinetin. The most significant fresh weight (FW) and dry weight (DW) were achieved with 1.0 mg/l of kinetin in the medium (Table 2). The current findings align with those of Al Shhab et al. (2021), who indicated that 2.0 mg/l of kinetin produced the highest quantity of new shoots of R. graveolens, whereas the optimal shoot length was achieved with 1.0 mg/l. Conversely, Hussain and Nathar (2020) indicated that a medium enriched with kinetin decreased the quantity of shoots exhibiting elongated internodes. Bhat et al. (1995) observed that kinetin is less efficient than BAP in Quercus shumardii and Piper spp cultures, respectively.

Finger 2: Multiple *Ruta graveolens* shoots after six weeks on MS + 0.1 mg/L kinetin. Bar = 0.5 cm.

Table 2: Mean impact of kinetin concentrations after six weeks on various characteristics.

Concentration (mg/L)	Number of new shoots	Maximum shoot length (cm)	Fresh weight (g)	Dry weight (g)
0.0	2.50 ^{b}	1.71 ^{b}	0.06 ^{b}	0.01 ^{c}
0.1	3.95 ^{a}	2.28 ^{ab}	0.18 ^{ab}	0.03 ^{abc}
0.2	3.55 ^{ab}	2.22 ^{ab}	0.20 ^{ab}	0.03 ^{abc}
0.3	2.70 ^{ab}	1.90 ^{ab}	0.12 ^{ab}	0.02 ^{bc}
0.4	3.20 ^{ab}	2.28 ^{a}	0.17 ^{ab}	0.02 ^{bc}
0.5	3.70 ^{ab}	2.33 ^{a}	0.19 ^{ab}	0.03 ^{ab}
1.0	3.80 ^{ab}	2.30 ^{a}	0.24 ^{a}	0.04 ^{a}

Based on the LSD test at $P < 0.05$, the same letter means they are not significantly different.

4.1.3. Gibberellins (GA3)

The current study investigated the effect of GA3 on microshoot development (Table 3). Increasing GA3 from 0.1 to 1.0 positively influenced the number of new micro shoots produced from each explant (Table 3, Figure 3). GA_3 at 1.0 mg/l produced the highest number of shoots/explant (7.5) and maximum shoot length (4.01 cm) compared to the other GA_3 concentrations tested (Table 3). The maximum fresh and dry weights were produced at 0.4 mg/l (0.42 g and 0.11 g, respectively). Present results confirmed that GA_3 stimulates the elongation of internodes and has been proven necessary for meristem growth, as in various plant species (Jayantlbhai, 2020). Moreover, previous studies indicated that GA_3 is conducive to *in vitro* shoot regeneration (Al-Alouni et al., 2016) or for promoting growth, biomass production, and xylem fiber length (Eriksson et al., 2000).

Figure 3: Six-week *Ruta graveolens* shoot formation on MS + 1.0 mg/L GA3. 0.5 cm bar

Table 3: Mean impact of gibberellins (GA_3) concentrations after six weeks on various characteristics.

Concentration (mg/L)	Number of new shoots	Maximum shoot length (cm)	Fresh weight (g)	Dry weight (g)
0.0	2.70 ^{d}	1.71 ^{d}	0.06 ^{c}	0.01 ^{c}
0.1	5.60 ^{abc}	3.56 ^{ab}	0.40 ^{a}	0.06 ^{b}
0.2	3.25 ^{cd}	2.75 ^{c}	0.14 ^{ab}	0.02 ^{bc}
0.3	6.70 ^{ab}	3.63 ^{ab}	0.41 ^{a}	0.06 ^{ab}
0.4	6.75 ^{ab}	3.18 ^{bc}	0.42 ^{a}	0.11 ^{a}
0.5	4.50 ^{bcd}	2.56 ^{c}	0.26 ^{ab}	0.04 ^{bc}
1.0	7.50 ^{a}	4.01 ^{a}	0.37 ^{a}	0.07 ^{ab}

Based on the LSD test at $P < 0.05$, the same letter means they are not significantly different.

4.1.4. Effect of 2,4-Dichlorophenoxyacetic acid (2.4-D) on root formation

The number of roots formed per microshoot was positively affected by the concentration of 2.4-D (Table 4). Maximum root number, root length, shoot number, and shoot length were obtained from MS media supplemented with 0.4 mg/L 2,4-D followed by 0.2 mg/L where the means of new root and root length were 3.25 and 0.96 cm, respectively. Callus was induced in MS media with different concentrations of 2.4-D MS media. The higher callus fresh and dry weight was 1.02 g and 0.08 g, respectively, when added media with 2.0 mg/L of 2.4-D. Followed by 1.6 mg/L of 2.4-D, where the fresh weight was 0.93 g, and the dry weight was 0.08 g. Using a higher concentration of 2,4-D (2.0 mg/L) resulted in low rhizogenesis and root formation (Figure 4).

This can be explained by the inhibitory effects of auxins (2,4-D) on chlorophyll formation and excessive callus formation (George et al., 2008). A similar observation was reported by (Soh et al., 1998) and (Duan et al., 2012) where there is little or no root formation in a medium containing 2,4-D. Furthermore (Nesrine et al.) reported no root response for Cicer arietinum L. on different concentrations of 2,4-D.

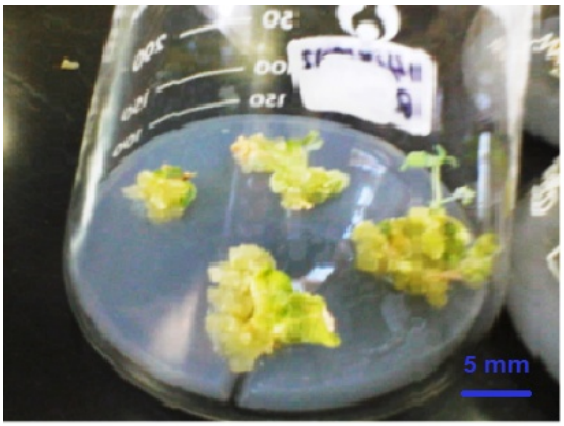

Figure 4: Callus development on MS medium with 2.0 mg/L 2,4-D after six weeks of growth

Table 4 Mean impact of different 2.4-D concentrations after six weeks on various characteristics.

Concentration (mg/l)	Number of new shoots	Maximum shoot length (cm)	Number of new Roots	Maximum root length (cm)	Callus fresh weight (g)	Callus dry weight (g)
0.0	2.70 ^{bc}	1.71 ^{b}	0.00 ^{e}	0.00 ^{d}	0.00 ^{c}	0.00 ^{e}
0.2	3.35 ^{b}	2.88 ^{a}	2.20 ^{ab}	0.92 ^{a}	0.16 ^{c}	0.01 ^{de}
0.4	4.95 ^{a}	2.77 ^{a}	3.25 ^{a}	0.96 ^{a}	0.23 ^{c}	0.02 ^{cde}
0.8	1.95 ^{c}	1.75 ^{b}	0.70 ^{de}	0.30 ^{bcd}	0.24 ^{c}	0.03 ^{cd}
1.2	1.80 ^{c}	1.42 ^{b}	0.90 ^{cde}	0.30 ^{bcd}	0.79 ^{ab}	0.07 ^{ab}
1.6	3.35 ^{b}	1.70 ^{b}	1.95 ^{bc}	0.55 ^{b}	0.93 ^{a}	0.08 ^{a}
1.8	2.70 ^{bc}	1.60 ^{b}	0.40 ^{de}	0.11 ^{cd}	0.65 ^{b}	0.05 ^{bc}
2.0	2.05 ^{c}	1.28 ^{b}	1.25 ^{bcd}	0.34 ^{bc}	1.02 ^{a}	0.08 ^{a}

Based on the LSD test at $P < 0.05$, the same letter means they are not significantly different.

5. Hardening

Because the regeneration in the culture settings has been cosseted in an environment with extremely high humidity, fluctuating light, and temperature conditions, it is not feasible to directly transfer plants grown in tissue culture to the wild or the field. This is because of the high mortality rate (Deb & Imchen, 2010). Direct exposure to sunlight is another factor that causes plants to wither and leaves to char (Hiren et al., 2004; Lavanya et al., 2009) (Deb & Imchen, 2010). Therefore, hardening off is essential for improving the chances of survival and effective establishment. Indeed, during tissue culture, the stages of hardening and acclimation are considered the most crucial. This research found that the survival rate of rooted plants reached 100% under greenhouse acclimatization settings, with the surviving specimens exhibiting green, healthy, and robust characteristics. All surviving plants exhibited consistent growth, typical leaf development, and no observable morphological difference (Figure 5).

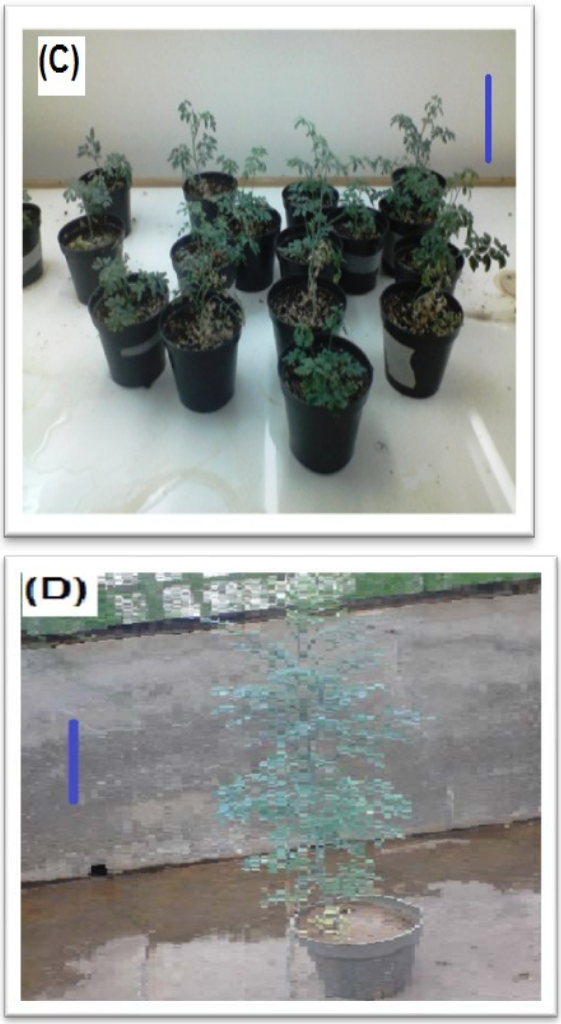

Figure 5: Plantlets were placed in a plastic bag, R. graveolens was rooted in a plastic container using a sterile peat moss-perlite (1:1) mixture, and the plant was planted four weeks later. R. graveolens growing in soil in vivo. There is a 5 mm error bar.

6. Antibacterial Activity

The extracts are made using either methanol or ethanol and are divided into three categories: callus (undifferentiated plant cells, *in vitro* (plant tissues cultivated in a controlled environment), and *in-vivo* (plants grown spontaneously). The extraction technique and solvent employed can affect the size of the inhibitory zones, as methanol and ethanol can extract bioactive chemicals differently, thereby influencing their effectiveness against the bacteria. This test helps evaluate R. graveolens' potential as an antibacterial agent against M. latus. Various plant materials, including callus, in vitro, and *ex-vivo*, were extracted using a variety of solvents, including methanol and ethanol (AL-ajlouni et al., 2023). To evaluate the antibacterial property of each extract, a range of different quantities, namely 40 µl and 80 µl, were used. The findings indicate that each of the three extracts of R. graveolens has various antibacterial properties, which are effective against the five tested bacteria. It has been shown that the antibacterial activity of extracts is superior to that of the standard antibiotic (positive), oxytetracycline. By utilizing dimethyl sulfoxide (DMSO) alone, the control (negative) experiment could not inhibit

the development of all the bacteria included. Therefore, the experiment produced negative findings. For callus, it was reported that R. graveolens extract by methanol and ethanol demonstrated a zone of inhibition in both volume and concentrations against the five bacteria. This was seen in both *in vitro* and ex vivo settings. This study's findings agree with those of (Al-Ajlouni et al., 2023).

6.1. Staphylococcus aureus (S. aureus)

It is a standard part of the body's microbiota, commonly found on the skin and in the upper respiratory tract. It is a gram-positive, spherical bacterium that belongs to the Bacillota. It is a common source of skin infections, but can also become an opportunistic pathogen. One of the most common diseases linked to antibiotic-resistant strains, including methicillin-resistant S. aureus (MRSA), and mortality from drug resistance is S. aureus. In clinical medicine, *S. aureus* is a global issue (Yamazaki et al., 2024).

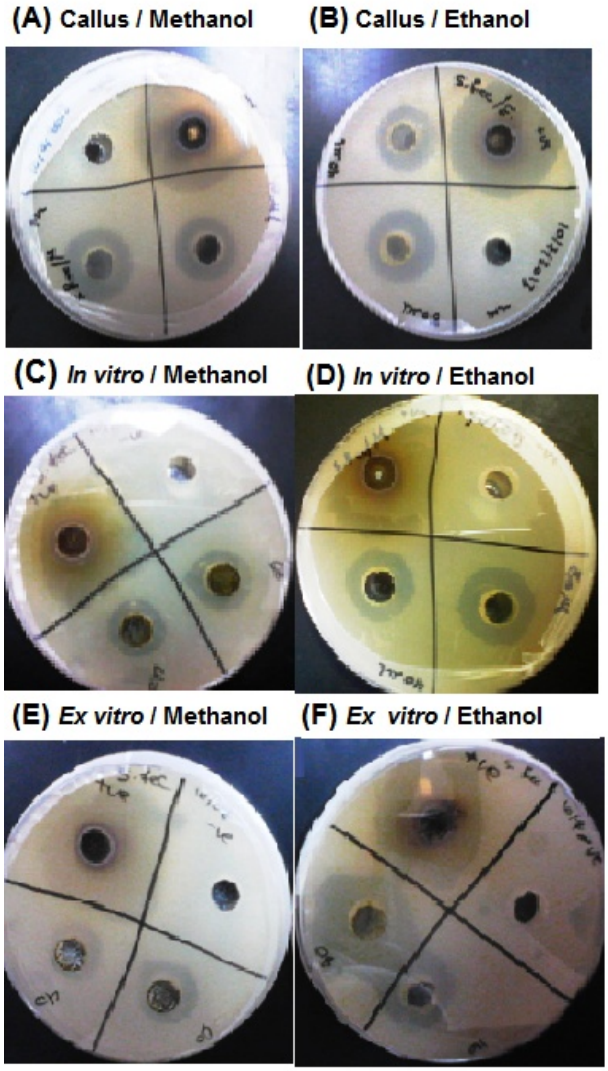

Figure (6): Agar diffusion assay of R. graveolens extracts against S. aureus: (A) activity of callus extracted with methanol, (B) activity of callus extracted with ethanol, (C) activity of *in vitro* extracts with methanol, (D) activity of *in vitro* extracts with ethanol, (E) activity of In Vivo extracts with methanol, and (F) activity of In Vivo extracts with ethanol. An inhibition zone was detected around the well.

Figure (6) shows an agar well-diffusion experiment to assess the antibacterial activity of Ruta graveolens extracts against S. aureus. In the test, wells are made on an agar plate infected with the bacteria, and several R. graveolens extracts are then added to the wells. Since the extract stops S. aureus from growing, the appearance of an inhibition zone surrounding the wells suggests that the extract has antimicrobial action.

Inhibition zones surrounding the wells are shown in the data, suggesting that the extracts exhibit antibacterial qualities against S. aureus. The concentration and kinds of active chemicals extracted from the plant material can be affected by the extraction technique and solvent utilized, which can also affect the size of the inhibitory zones. The efficacy of methanol and ethanol, two popular solvents for extracting bioactive substances, varies according to how soluble the substances are in each solvent (Al-Ajlouni et al., 2023).

6.2. Bacillus cereus (B. cereus)

It is a rod-shaped, Gram-positive bacterium commonly found in food, soil, and marine sponges. The term "Cereus," meaning "waxy" in Latin, describes the appearance of colonies formed on blood agar (Williams & Weir, 2024). Because they produce spores, some strains are dangerous to people and can lead to foodborne illnesses, but other strains can help animals as probiotics and even show mutualism with some plants. *B. cereus* bacteria can generate protective endospores and be facultative anaerobes or aerobes (Akinsemolu et al., 2024). Li et al. (2025) discovered that quorum sensing regulates various virulence factors in these bacteria, such as phospholipase C, cereulide, sphingomyelinase, metalloproteases, and cytotoxin K.

The antibacterial activity of *Ruta graveolens* extracts against *Bacillus cereus* (*B. cereus*) was evaluated using the agar well-diffusion assay (Figure 7). In this test, several R. graveolens extracts are applied to wells made on an agar plate infected with the bacterium. Since the extract stops B. cereus from growing, the appearance of an inhibition zone surrounding the wells suggests it has an antimicrobial action. Inhibition zones surrounding the wells are shown in Figure 7, indicating that the extracts exhibit antibacterial qualities against B. cereus. The concentration and kinds of active chemicals extracted from the plant material can be affected by the extraction technique and solvent utilized, which can also affect the size of the inhibitory zones.

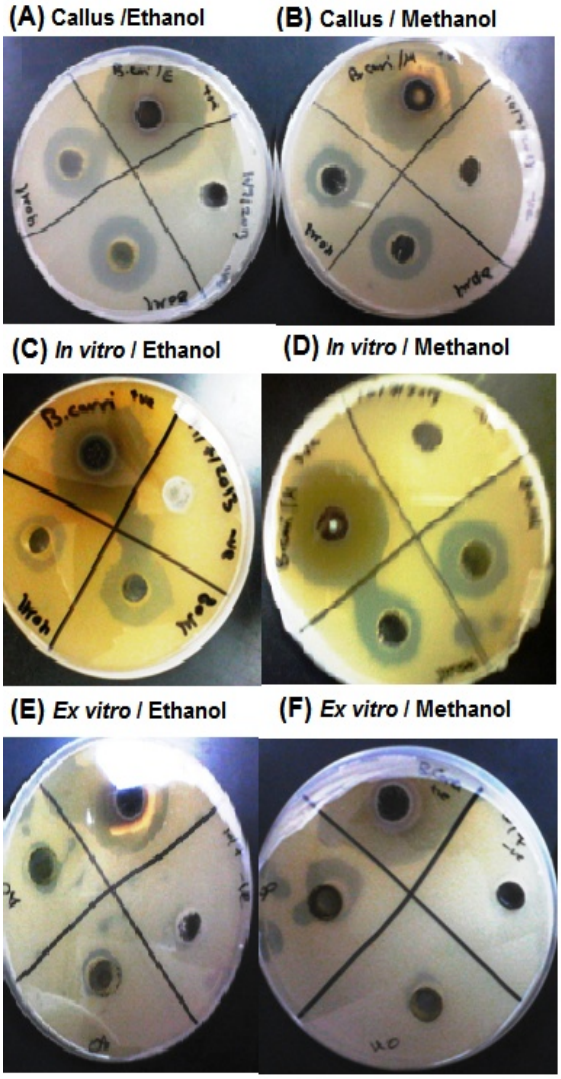

Figure (7): Agar diffusion assay of R. graveolens extracts against B. cereus: (A) activity of callus extracted with ethanol, (B) activity of callus extracted with methanol, (C) activity of *in vitro* extracts with ethanol, (D) activity of *in vitro* extracts with methanol, (E) activity of In Vivo extracts with ethanol, and (F) activity of In Vivo extracts with methanol. An inhibition zone was detected around the well.

6.3. Micrococcus luteus (M.latus)

The bacterium Micrococcus luteus is a saprotrophic coccus in the family Micrococcaceae that is nonmotile, tetrad-arranging, pigmented, and Gram-positive to Gram-variable. It is positive for catalase and urease. M. luteus, an obligatory aerobe, is present in soil, sediment, water, and air, as well as in the ordinary microbiota of the mammalian epidermis (Suresh et al., 2025). The bacterium also colonizes the Mucosae, oropharynx, upper respiratory tract, and human mouth. Micrococcus luteus can develop into an opportunistic pathogen despite its generally benign nature in individuals who are immunocompromised or have indwelling catheters. Soria-Camargo et al. (2025) suggest it resists antibiotic treatment by inducing unique genes and delaying key metabolic processes. Figure (8) shows an agar well-diffusion experiment to evaluate the antibacterial activity of Ruta graveolens extracts against Micrococcus latus (M. latus). In this test, several R. graveolens extracts are applied to wells made on an agar plate that has been infected with the bacterium. Since the extracts prevent M. latus from growing, the appearance of inhibition zones surrounding the wells suggests antimicrobial action.

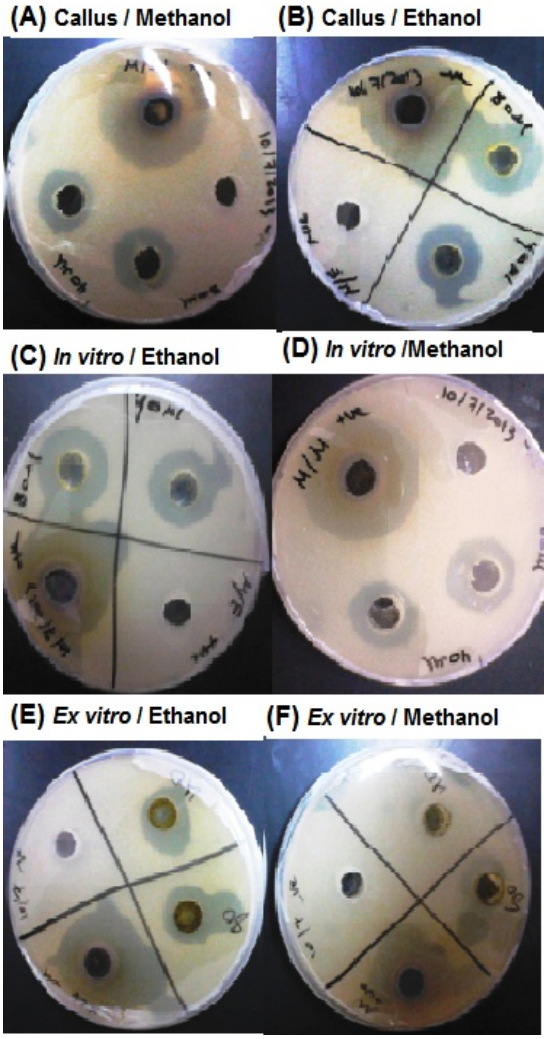

Figure (8): Agar well-diffusion assay of R. graveolens extracts against M. latus: (A) activity of callus extracted with methanol, (B) activity of callus extracted with ethanol, (C) activity of *in vitro* extracts obtained with ethanol, (D) activity of *in vitro* extracts obtained with methanol, (E) activity of In Vivo extracts obtained with ethanol, and (F) activity of In Vivo extracts obtained with methanol. The inhibition zone was detected around the well.

6.4. Escherichia coli (E.coli)

Is a rod-shaped, facultatively anaerobic, gram-negative coliform bacteria of Escherichia frequently found in warm-blooded species' lower intestines (De Marco, 2025). Along with other facultative anaerobes, most E. coli strains comprise around 0.1% of the gut's typical microbiota. For the most part, these bacteria are benign or even helpful to us. Certain strains of Escherichia coli benefit their hosts by producing vitamin K2 or preventing the growth of harmful pathogenic bacteria in the gut. These positive interactions between humans and E. coli demonstrate a mutualistic biological relationship, where both parties gain advantages from one another (Ng et al., 2025). Fecal matter contains E. coli that is released into the environment. Under aerobic circumstances, the bacteria thrive enormously in new fecal matter for three days, after which their numbers gradually decrease. Specific serotypes are harmful and can cause

their hosts to suffer from severe food poisoning. The main way that pathogenic forms of the bacteria spread illness is by fecal-oral transmission. Sometimes, food contamination events that lead to product recalls are caused by this transmission mode (Nnah et al., 2025). Because cells have a short half-life outside the body, they can be used as indicator organisms to check environmental samples for fecal contamination. Figure (8) displays an agar well-diffusion experiment to assess the antibacterial activity of Ruta graveolens extracts against Escherichia coli (E. coli). In this test, several R. graveolens extracts are applied to wells made on an agar plate infected with the bacterium. Since the extracts prevent E. coli from growing, inhibition zones surrounding the wells suggest antimicrobial action.

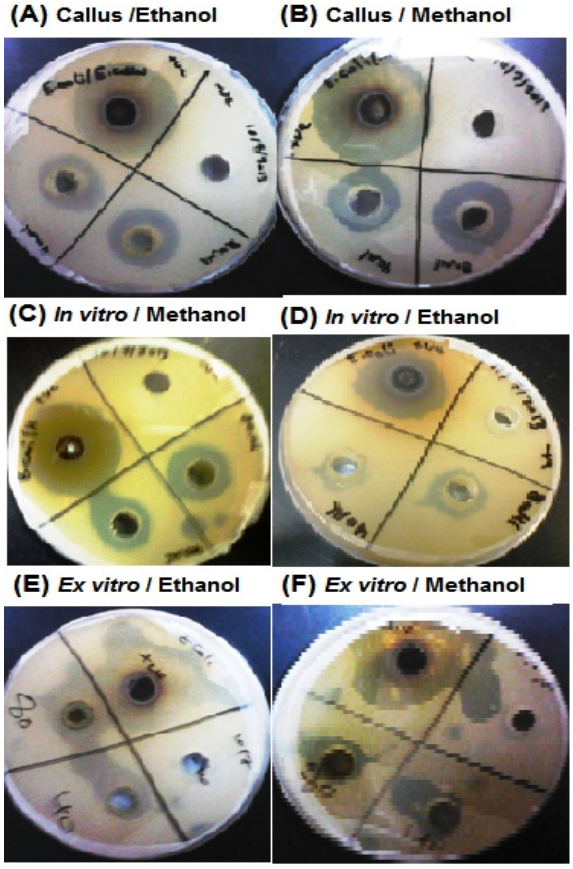

Figure (8): Agar diffusion assay of R. graveolens extracts against E. coli: (A) activity of callus extracted with ethanol, (B) activity of callus extracted with methanol, (C) activity of *in vitro* extracts with methanol, (D) activity of *in vitro* extracts with ethanol, (E) activity of In Vivo extracts with ethanol, and (F) activity of In Vivo extracts with methanol. The inhibition zone was detected around the well.

6.5. Salmonella Enterica Serovar Typhimurium (S. Typhimurium)

It is an intracellular facultative bacterial pathogen that has been used as a model organism for research on host-pathogen interactions for many years. Its capacity to create Salmonella-induced filaments (SIFs), a network of membrane tubules in infected host cells, contributes to its appeal from a cell biology standpoint. Despite the attention given to its intracellular lifestyle, ***S. Typhimurium*** is the world's most common cause of diarrhea and foodborne illnesses (Cao et al., 2025).

To evaluate the antibacterial activity of Ruta graveolens callus extracts against Salmonella typhimurium (S. typhimurium), Figure (9) shows an agar well-diffusion experiment. In this test, callus extracts prepared with either methanol (A) or ethanol (B) are added to wells on an agar plate inoculated with the bacteria. The appearance of inhibition zones surrounding the wells suggests that the extracts have an antibiotic action, as they limit the development of S. typhimurium. Because methanol and ethanol can extract bioactive chemicals differently, affecting their efficacy against the bacteria, the size of the inhibitory zones may vary depending on the solvent utilized. The potential of R. graveolens callus extracts as antimicrobial agents against S. typhimurium is ascertained with the aid of this test. According to previous studies on rue's alkaloid-rich extracts (Al-Ajlouni et al., 2023). In summary, the antibacterial action against Gram-positive bacteria, such as Staphylococcus aureus, aligns with the findings of the current study. However, the limited effectiveness against Gram-negative organisms, such as Escherichia coli, suggests that either concentration-dependent effects or structural barriers, like outer membrane proteins, may be involved (Oliva et al., 2019). The identified antibacterial activities, particularly against Gram-positive bacteria (S. aureus and Bacillus cereus), are consistent with the phytochemicals found in rue, including furanocoumarins and alkaloids (Oliva et al., 2019).

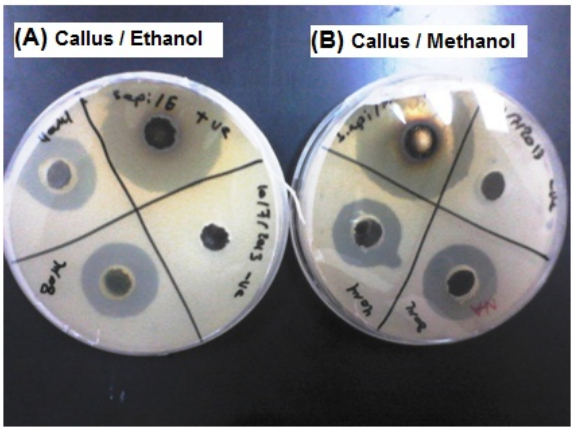

Figure (9): Agar well-diffusion experiment of R. graveolens extracts against S. typhimurium: (A) activity of methanol-extracted callus and (B) activity of ethanol-extracted callus. The inhibition zone was detected around the well.

7. Conclusion

This study explored the micropropagation of Rue (Ruta graveolens L.) and the antimicrobial effects of its extracts on five bacterial species. The MS medium included various BAP, Kinetin, and GA3 concentrations, with the most effective results for microshoot growth recorded at 0.30 mg/L BAP, 0.10 mg/L Kinetin, and 1.0 mg/L GA3. The highest root and shoot development occurred with 2,4-D at 0.4 mg/L. Both in vitro and in vivo extracts exhibited antimicrobial activity against all tested bacterial species, suggesting that R. graveolens may be a natural antibacterial treatment in pharmaceuticals.

Acknowledgements

This research (No.2022421) was funded by the Deanship of Scientific Research, Jordan University of Science and Technology, Irbid, Jordan.

Conflict of interests

The authors declare no conflict of interests.

References

Ahmad, N., Faisal, M., Fatima, N., & Anis, M. (2012). Encapsulation of microcuttings for propagation and short-term preservation in Ruta graveolens L.: a plant with high medicinal value. *Acta Physiol. Plant*, *34*, 2303-2310.

Akinsemolu, A. A., Onyeaka, H., Odion, S., & Adebanjo, I. (2024). Exploring Bacillus subtilis: Ecology, biotechnological applications, and future prospects. *J. Basic Microbiol*, *64*(6), 2300614.

Al-Ajlouni, Z., Migdadi, O., Makhadmeh, I., Aldahadha, A., Hasan, S., & Al-Abdallat, A. M. (2022). Assessment of genetic diversity among wild Ruta chalepensis L. from the North of Jordan. *Diversity*, *14*(11), 969.

Al-Ajlouni, Z. I., Abbas, S., Al-Ghzawi, A. L., Al-Makhadmeh, I., Shatnawi, M., Al-Abdallat, A. M., & Al-Tawaha, A. R. (2023). Evaluation of Antimicrobial Activity of Callus, In Vitro and Ex Vitro Extracts of Ruta Graveolens L. *Farmacia*, *71*(4).

Al-Ajlouni, Z. I., Abbas, S., Shatnawi, M., & Al-Makhadmeh, I. (2015). In vitro propagation, callus induction, and evaluation of active compounds on Ruta graveolens. *J. Food Agric. Environ*, *13*(2), 101-106.

Al-Muffti, A. S., Abdulaziz, M. B. A., Khalid, V. A., & OMER, O. A. (2021). Investigating the antibacterial activity of ethanol extract of the medicinal plant Ruta graveolens. *J. Duhok Univ*, *24*(1), 130-135.

Al Shhab, M., Shatnawi, M., Abu-Romman, S., Almajdalawi, M., & Odat, N. (2021). Micropropagation and in vitro conservation of Ruta graveolens plants. *Res. Crops*, *22*(2).

Al Shhab, M., Shatnawi, M., Abu-Romman, S., Almajdalawi, M., Abubaker S, and Shahrour W. (2022). Antimicrobial Activity and Micropropagation of Ruta graveolens Medicinal Plant. *Int. J. Agric. Biol*, 28:352–358.

Bhat, S., Chandel, K., & Malik, S. (1995). Plant regeneration from various expiants of cultivated Piper species. *Plant Cell Rep*, 14, 398-402.

Bohidar, S., Pattanaik, S., & Thiruvanoukkarasu, M. (2013). Improved furanocoumarin production in Ruta graveolens L. regenerated via in vitro stem internode cultures. *Plant Biotechnol. Rep*, *7*, 399-405.

Bohidar, S., Thirunavoukkarasu, M., & Rao, T. (2008). Effect of Plant Growth Regulators on in vitro micropropagation of "Garden Rue"(Ruta graveolens L.). *Int. J. Integr. Biol*, *3*(1), 36-43.

Cao, J., Liu, H., Qi, Z., Liu, J., Chen, G., Wu, D.,…Li, G. (2025). The resistance of Salmonella enterica serovar Typhimurium to zinc oxide nanoparticles. *Nano Today*, *62*, 102687.

Chaftar, N., Girardot, M., Labanowski, J. m., Ghrairi, T., Hani, K., Frere, J., & Imbert, C. (2016). Comparative evaluation of the antimicrobial activity of 19 essential oils. *Adv. Microbiol. Infect. Dis. Public Health*, *2*, 1-15.

De Marco, A. (2025). Recent advances in recombinant production of soluble proteins in E. coli. *Microb. Cell Fact*, *24*(1), 1-12.

Deb, C., & Imchen, T. (2010). An efficient in vitro hardening technique of tissue culture raised plants. *Biotechnol*, *9*(1), 79-83.

Duan, H., Ding, X., Xing, J., Song, J., Yang, L., & Lu, L. (2012). Effects of plant growth substances on callus re-differentiation of medicinal plant Achyranthes bidentata. *Plant Omics*, *5*(3), 261.

Eriksson, M. E., Israelsson, M., Olsson, O., & Moritz, T. (2000). Increased gibberellin biosynthesis in transgenic trees promotes growth, biomass production and xylem fiber length. *Nat. Biotechnol*, 18(7), 784-788.

George EF, Hall MA, and De Klerk GJ. (2008). Plant propagation by tissue culture. In: **Plant Propagation by Tissue Culture**. Springer, Dordrecht, pp. 283–333.

George EF and Sherrington PD. (1984)**. Plant Propagation by Tissue Culture: A Handbook and Dictionary of Commercial Laboratories.** Exegetics Ltd., England.

Haddouchi, F., Chaouche, T. M., Zaouali, Y., Ksouri, R., Attou, A., & Benmansour, A. (2013). Chemical composition and antimicrobial activity of the essential oils from four Ruta species growing in Algeria. *Food Chem*, 141(1), 253-258.

Hiren, A., Saurabh, R., & Subramanian, R. (2004). In vitro regeneration in Curculigo orchioides Gaertn. An endangered medicinal herb. *Phytomorphology*, *54*, 85-95.

Hussain MA and Nathar VN. (2020). In vitro method of high-frequency plant regeneration through internodal callus of *Ruta graveolens* L. In: **Medicinal Plants: Biodiversity, Sustainable Utilization and Conservation**, pp. 761–768

Jakovljević, D., Stanković, M., Warchoł, M., & Skrzypek, E. (2022). Basil (Ocimum L.) cell and organ culture for the secondary metabolites production: a review. *Plant Cell Tissue Organ Cult*, 149(1), 61-79.

Jayantlbhai PM. (2020). **Effect of plant growth regulators on growth and yield of cluster bean (Cyamopsis tetragonoloba L. Taub).** MSc Thesis, Sardarkrushinagar Dantiwada Agricultural University, India.

Krayni, H., Fakhfakh, N., Aloui, L., Zouari, N., Kossentini, M., & Zouari, S. (2015). Chemical composition and chelating activity of Ruta chalepensis L.(Rutaceae) essential oil as influenced by phenological stages and plant organs. *J. Essent. Oil Res*, 27(6), 514-520.

Kuzovkina, I., Al'terman, I., & Schneider, B. (2004). Specific accumulation and revised structures of acridone alkaloid glucosides in the tips of transformed roots of Ruta graveolens. *Phytochemistry*, 65(8), 1095-1100.

Lavanya M, Venkateshwarlu B and Devi BP. (2009). Acclimatization of neem microshoots adaptable to semi-sterile conditions. *Indian J. Biotechnol***.** 8(2): 195–199.

Li, N., Siddique, A., Liu, N., Teng, L., Ed-Dra, A., Yue, M., & Li, Y. (2025). Global Epidemiology and health risks of Bacillus cereus Infections: Special focus on infant foods. *Food Res. Int*, *201*, 115650.

Luo, P., Feng, X., Liu, S., & Jiang, Y. (2024). Traditional Uses, Phytochemistry, Pharmacology and Toxicology of Ruta graveolens L.: A Critical Review and Future Perspectives. *Drug Des. Dev. Ther*, 6459-6485.

Mohammadpour, S., Khodaparast, Z., Mohammadpour, H., & Issazadeh, K. (2025). Potential of Ruta graveolens extract in healing burn infections caused by Staphylococcus aureus and Pseudomonas aeruginosa. *Microbe*, 100266.

Morton, C. M., & Telmer, C. (2014). New subfamily classification for the Rutaceae. *Ann. Mo. Bot. Gard.*, 99(4), 620-641.

Nalawade, S. M., & Tsay, H.-S. (2004). In vitro propagation of some important Chinese medicinal plants and their sustainable usage. *Vitro Cell. Dev. Biol. Plant*, 40, 143-154.

Nesrine, A., Chafika, R., & Keltoum, D. Optimization of In Vitro Culture Medium For Cicer arietinum and Selection of Resistant Genotypes Against Enzymes and Toxins of Ascochyta rabiei. *Afr. J. Biol. Sci*, 6(15): 12556–12574

Ng, R. W., Yang, L., Lau, S. H., Hawkey, P., & Ip, M. (2025). Global prevalence of human intestinal carriage of ESBL-producing E. coli during and after the COVID-19 pandemic. *JAC Antimicrob. Resist*, *7*(1), dlaf001.

Nnah, E. P., Asante, J., Amoako, D. G., Abia, A. L. K., & Essack, S. Y. (2025). Antibiotic-resistant Escherichia coli (E. coli) at one health interfaces in Africa: A scoping review. *Sci. Total Environ*, 958, 177580.

Oliva A, Garzoli S, De Angelis M, Marzuillo C, Vullo V, Mastroianni CM and Ragno R. (2019). In vitro evaluation of different antimicrobial combinations with and without colistin against carbapenem-resistant *Acinetobacter baumannii*. *Molecules*, 24: 886.

Orlanda, J. F., & Nascimento, A. (2015). Chemical composition and antibacterial activity of Ruta graveolens L.(Rutaceae) volatile oils, from São Luís, Maranhão, Brazil. *S. Afr. J. Bot*, 99, 103-106.

Piewngam, P., & Otto, M. (2024). Staphylococcus aureus colonisation and strategies for decolonisation. *Lancet Microbe* 5(6): e606–e618.

Pollio, A., De Natale, A., Appetiti, E., Aliotta, G., & Touwaide, A. (2008). Continuity and change in the Mediterranean medical tradition: Ruta spp.(rutaceae) in Hippocratic medicine and present practices. *J. Ethnopharmacol*, 116(3), 469-482.

Salman, H. A., Venkatesh, S., Senthilkumar, R., Kumar, B. G., & Ali, A. M. (2018). Determination of antibacterial activity and metabolite profile of Ruta graveolens against Streptococcus mutans and Streptococcus sobrinus. *J. Lab. Physicians*, 10(03), 320-325.

Sampaio, O. M., Vieira, L. C. C., Bellete, B. S., King-Diaz, B., Lotina-Hennsen, B., Da Silva, M. F. d. G. F., & Veiga, T. A. M. (2018). Evaluation of alkaloids isolated from Ruta graveolens as photosynthesis inhibitors. *Molecules*, 23(10), 2693.

SAS Institute Inc. 2002. **SAS/STAT® 9.4 User's Guide.** SAS Institute Inc., Cary, NC, USA.

Shatnawi, M. (2013). Multiplication and cryopreservation of yarrow (Achillea millefolium L., Asteraceae). *J. Agric. Sci. Techno*, 15(1): 163–173

Shatnawi, M., Shibli, R., Abu-Romman, S., Al-Mazra, M., Al Ajlouni, Z., Shatanawi, A., & Odeh, W. (2011). Clonal propagation and cryogenic storage of the medicinal plant Stevia rebaudiana. *Span. J. Agric. Res*, 9(1), 213-220.

Soh, M. S., Hong, S. H., Hanzawa, H., Furuya, M., & Nam, H. G. (1998). Genetic identification of FIN2, a far red light-specific signaling component of Arabidopsis thaliana. *Plant J*, 16(4), 411-419.

Soria-Camargo, C., Can-Ubando, L. C., Manzanares-Leal, G. L., Sánchez-Reyes, A., Dávila-Ramos, S., Batista-García, R. A., & Ramírez-Durán, N. (2025). Tolerance to NSAIDs in Actinobacteria From a Mexican Volcano Crater: Genomics and Bioremediation Potential. *J. Basic Microbiol*, e2400772.

Suresh, K., Pillai, D., Soni, M., Rathlavath, S., & Narshivudu, D. (2025). Micrococcus luteus, an emerging opportunistic pathogen in farmed Nile tilapia, Oreochromis niloticus in Andhra Pradesh, India. *Aquacult. Int*, 33(1), 51.

Thomas, S., & Devi, B. S. (2013). Phytochemical and in vitro anthelmintic studies of hydro-alcoholic extract of Costus pictus D. Don. *Int. J. Pharm. Pharm. Sci*, 5(3), 639-641.

Williams, N., & Weir, T. L. (2024). Spore-based probiotic Bacillus subtilis: Current applications in humans and future perspectives. *Fermentation*, 10(2), 78.

Yamazaki, Y., Ito, T., Tamai, M., Nakagawa, S., & Nakamura, Y. (2024). The role of Staphylococcus aureus quorum sensing in cutaneous and systemic infections. *Inflamm. Regen*, 44(1), 9.

JJBS

Volume 19, Number 1,March 2026
ISSN 1995-6673
Pages 45 – 57
https://doi.org/10.54319/jjbs/190105

Jordan Journal of Biological Sciences

Advancing Renal Health in Sepsis Management: The Promising Role of Thymoquinone through PI3K/Akt Signaling Modulation

Huda Jaber[1], Bassim Mohammad[2], Heider Qassam[3,4], Wajdy J. Al-Awaida[5,*], Hamzeh J. Al-Ameer[6], Amani M. Ayyash[7], Ali A. Ahmed[8], Asia A. Hamza[9], Khang Wen Goh[10,] Isam Fattash[5], Besan M. Srour[5], Ghizal Fatima[11], Tala M. Rahhal[12], Tala S. Almahasneh[12], Yulia Sh Gushchina[13],Najah R. Hadi[14].

[1] Department of Pharmacology and Therapeutics, Faculty of Medicine, University of Kufa, Kufa, Najaf, Postal Code: 540011, Iraq; [2] Department of Pharmacology, Faculty of Medicine, Diwaniyah, Al-Qadisiya, Postal Code: 58002, Iraq; [3] Department of Pharmacology and Therapeutics, Faculty of Medicine, University of Kufa, Kufa, Najaf, Postal Code: 540011, Iraq; [4] Department of Molecular and Cell Biology, University of Leicester, Leicester, University Road, Leicester, Postal Code: LE1 7RH, United Kingdom; [5] Department of Biology and Biotechnology, Faculty of Science, American University of Madaba, MR62+F79 Road, Madaba, P.O.Box: 2882 Amman, Postal Code: 11821, Jordan; [6] Department of Biotechnology, Faculty of Allied Medical Sciences, Al-Ahliyya Amman University, Amman, Postal Code: 19328, Jordan; [7] Department of Pharmacy, Faculty of Health Sciences, American University of Madaba, MR62+F79 Road, Madaba, P.O.Box: 2882 Amman, Postal Code: 11821, Jordan; [8] Department of Clinical Laboratory Sciences, College of Pharmacy, University of Jabir ibn Hayyan for Medical and Pharmaceutical Sciences, Iraq; [9] Department of Clinical Laboratory Sciences, College of Pharmacy, University of Al-Kafeel, Najaf, Iraq; [10] Faculty of Data Science and Information Technology, INTI International University, Nilai 71800, Malaysia; [11] Chronobiology Laboratory, Era University, Lucknow 226003, India; [12] Department of Medical Laboratories, Faculty of Health Sciences, American University of Madaba, MR62+F79 Road, Madaba, P.O.Box: 2882 Amman, Postal Code: 11821, Jordan; [13] Department of General and Clinical Pharmacology, Medical Institute, Peoples' Friendship University of Russia (RUDN University), 6 Miklukho-Maklaya Street, 117198 Moscow, Russia; [14] Department of Pharmacology and Therapeutics, Faculty of Medicine, University of Kufa, Kufa, Najaf, Postal Code: 540011, Iraq.

Received: May 1, 2025; Revised: July 1, 2025; Accepted: July 14, 2025

Abstract

Acute Kidney Injury (AKI), a major health challenge, is predominantly triggered by sepsis. Thymoquinone (TQ), extracted from *Nigella sativa*, that is recognized for its potent antiinflammatory in addition to antioxidant capabilities. This study provides strong evidence for the efficacy of Thymoquinone (TQ) in attenuating sepsis-induced Acute Kidney Injury (AKI), highlighting its potential as a therapeutic agent through modulation of inflammation and oxidative stress via PI3K/Akt signaling.

The experiment allocated twenty-five albino mice into four groups (n=5 each): (1) Sham group (underwent laparotomy alone without CLP), (2) Sepsis control group (administered CLP alone without treatment), (3) TQ-treated group (treated with 0.75 mg/kg thymoquinone intraperitoneally for three consecutive days prior to CLP), and (4) Vehicle group (administered normal saline for three consecutive days prior to CLP). Except for the sham group, all the animals were subjected to the CLP procedure to induce sepsis. After the procedure, a set of biochemical, immunohistochemical, and histopathological tests were performed to evaluate renal status and inflammatory milieu. These indicated that treatment with TQ substantially halted serum levels of proinflammatory mediators IL-6 and TNF-α but higher levels of antiinflammatory cytokine IL-10. Besides that, levels of creatinine and urea were reduced, reflecting improved kidney function. Histopathological analysis revealed that TQ exerted protective effect against CLP-induced nephropathy. On the level of cell signaling, the modulating impact of TQ on the PI3K/Akt pathway was reflected by increased pAkt immunoreactivity and elevated PI3K gene expression.

This research highlights the potential of TQ in attenuating sepsis-induced AKI, mediated through modulation of inflammation, oxidative stress, and activation of the PI3K/Akt pathway

Keywords*:* Sepsis; Thymoquinone; *Nigella Sativa;* Acute Kidney Injury; PI3K/Akt Pathway; Inflammation; Cytokines; Oxidative Stress

1. Introduction

Phosphatidylinositol 3-kinase/protein kinase B (PI3K/Akt) signaling pathway is the one that controls a broad spectrum of cellular functions key to the pathogenesis of sepsis. They encompass regulation of the immune responses and release of inflammatory mediators in vitro and in vivo (Geng *et al.*, 2024) (Al-Husein *et al.*, 2020). Activation of the pathway influences downstream signaling molecules. It is essential in the modulation of innate immune cell functions, playing a part in immune regulation and the preservation of homeostasis during sepsis. The complication of the PI3K/Akt/mTOR signaling components emphasizes its complex function in cellular signal transduction, influencing cell proliferation,

* Corresponding author. e-mail: w.alawaida@aum.edu.jo.

apoptosis, metabolism, and angiogenesis. These features emphasize the pathway's critical role in numerous human diseases, where its dysregulation can intensify conditions as ischaemic brain injury, neurodegenerative diseases, in addition to cancers (Bi *et al.,* 2023). In sepsis, studying the PI3K/Akt pathway's governing mechanisms and biological functions offers promising avenues for the progress of targeted therapies to control immune and inflammatory responses, theoretically preventing the critical outcomes of sepsis induced Acute Kidny Injury (AKI) (Li *et al.,* 2023). Sepsis is a significant global health issue. It induces a robust inflammatory response that can cause systemic dysregulation and multiorgan failure (Trzeciak *et al.,* 2020). The kidneys, mainly vulnerable in sepsis, suffer from 45% to 70% of ICU septic patients evolving Acute Kidney Injury (AKI) (Chang *et al.,* 2022) (Abu Saleem *et al.,* 2025).

Existing evidence suggests that AKI in sepsis is an active performer of the inflammation tissue injury flow and not a passive result of systemic inflammatory processes (Jarczak *et al.,* 2021; Ludes *et al.,* 2021). Central to such understanding lies the Phosphatidylinositol-3-kinase (PI3K)/Akt signaling pathway significant for cell growth, survival, and progressively being included in the pathogenesis of sepsis-related AKI (Peerapornratana *et al.,* 2019; Ludes *et al.,* 2021).

With the growing understanding of sepsis and AKI pathophysiology, thymoquinone (TQ), the principal bioactive constituent of Nigella sativa, has attracted increasing attention because of its diverse pharmacological properties, including anti-inflammatory, antioxidant, immunomodulatory, and anti-apoptotic effects (Talebi *et al.*, 2021) (Al-Saffar and Al-Wiswasy, 2019). Thymoquinone was selected due to its unique blend of anti-inflammatory, antioxidant, and immunomodulatory action, coupled with a well-documented safety record in preclinical models. (Isaev *et al.*, 2023) Unlike the conventional anti-sepsis medications that focus primarily on single pathways, TQ has pleiotropic effects, which make it exceptionally potent for multifactorial conditions such as sepsis-induced AKI.(Farkhondeh *et al.*, 2018; Pottoo *et al.*, 2022). Research in disease models implies TQ's ability to reduce inflammatory markers and diminish tissue damage (Ojha *et al.*, 2015) (Alqaraleh *et al.*, 2025), mainly through modulation of PI3K/Akt signaling, as noticed in LPS-induced neurotoxicity in microglial cells and renoprotection with cisplatin induced nephrotoxicity (Ojha *et al.*, 2015) (Sayed and Morcos, 2007).

Despite massive research, mechanisms supporting sepsis and sepsis-related AKI remain unclear, leading to a nonstop search for novel, effective therapies. TQ's preclinical success in modulating vital cellular processes across the PI3K/Akt axis—crucial in diseases like sepsis and AKI — emphasizes its therapeutic potential (Junaid *et al.,* 2021). These characteristics render TQ as a candidate drug for sepsis-induced AKI, the condition characterized by uncontrolled inflammation and oxidative renal damage. Recent findings suggest that TQ reduces kidney damage in various models of nephrotoxicity and ischemia-reperfusion injury (Wang *et al.*, 2022). The specific role of TQ in regulating the PI3K/Akt signaling pathway in sepsis-induced AKI has not been explored before, which is the focus of the present study. By its blockage of this critical pathway, TQ may provide a novel therapeutic approach to sepsis-induced nephrotoxicity

As illustrated by Öztürk et al. and Qadri et al., the gentamicin kidney damage model, the AKI model of cisplatin, and LPS-driven lung injury suggest that TQ has therapeutic potential for managing sepsis.(Öztürk *et al.,* 2023; Qadri *et al.,* 2023). Furthermore; Li-Peng Guo et al. results indicated that TQ might have a potential therapeutic activity addressing sepsis-induced AKI(Guo *et al.*, 2020). Consequently, our current activities focus on investigating the proposed PI3K/Akt pathway and TQ's renoprotective actions against polymicrobial sepsis. Based upon TQ's established renoprotective features, we aim to elucidate the therapeutic potential of TQ in the context of sepsis and AKI, which would signify a remarkable treatment milestone.

2. Materials & Methods

2.1. Chemical Reagents and Suppliers

Thymoquinone (TQ) source was Sigma Aldrich (USA). Enzyme linked Immunosorbent Assay (ELISA) kits for the examination of Interleukin-6 (IL-6), Tumor Necrosis Factor-alpha (TNF-α), TNF-α receptor, Interleukin-10 (IL-10), and F2-isoprostanes were provided by SunLog Biotech (China). Solarbio (China) supplied the Total RNA extraction kit. Biotinylated secondary antibody reagent, antigen retrieval buffer, Syper green PCR master mix, and blocking buffer were sourced from Thermo Fisher Scientific (UK). Protease cocktail inhibitor tablets were procured from Roche (Germany). Hikma (Jordan) and Bayer AG (Germany) provided Ketamine and Xylazine, respectively.

2.2. Animal Preparation and Ethical Approval

A total of twenty-five albino mice, ranging in age from 8 to 12 weeks and in weight from 20 to 30 gram, were obtained from the Animal Care Centre within the Faculty of Science at the University of Kufa, Iraq. These mice were then housed in an environmental system regulated for temperature (25° Celsius) and humidity (60-65%), with a consistent 12:12 light/dark sequence. All mice had free access to foodstuff and water. The experimental processes were reviewed and approved by the "Animal Care and Use" Committee at the University of Kufa, Iraq, under license number 15791, ensuring adherence to ethical standards.

2.3. Experimental Design

Following acclimatization, mice were allotted to groups at random in a manner of five mice per group. The groups were: sham group, where the mice were anesthetized and a midline abdominal incision made to simulate surgery; control group, where the mice were anesthetized and induced with Cecal Ligation and Puncture (CLP); TQ-treated group, treated with intraperitoneal (i.p) administration of Thymoquinone (TQ) in a dose of 0.75mg/Kg/day for three days prior to the CLP procedure (Hiengrach *et al.*, 2022), normal saline-treated group, treated with i.p injections of normal saline employed as a control vehicle for TQ, and administered for three days prior to the induction of CLP. The normal saline-treated group, which received i.p. saline for three consecutive

days was then subjected to CLP to induce sepsis, similar to the control and TQ-treated groups

2.4. Dose Selection

TQ dose was 0.75mg/kg/day, and it was selected based on our prior studies showing its efficiency and safety in comparable experimental models (Alkharfy *et al.*, 2011; Alkharfy *et al.*, 2015). It was therapeutically efficient without side effects in models of systemic inflammation and sepsis, in harmony with the objectives of the existing study to inspect the protective outcomes of TQ against sepsis induced renal damage.

2.5. CLP Procedure

CLP model was accomplished with caution following standard protocol (Zhai *et al.*, 2018; Guo *et al.*, 2020). Starting with, under humane concern, mice were anesthetized by intraperitoneal injection, through a regulated amount of 100mg/kg Ketamine and 10mg/kg Xylazine. Once anesthetized, strict preparation like shaving the abdominal region and making a 1.5 cm midline incision to expose the cecum. This vital organ was gently shown, carefully ligated below the ileocecal valve to prevent leakage, and punctured twice with a sterile G-20 needle, the infusion of a precise injury planned to cause severe sepsis. Anatomical integrity preserved, the cecum was then replaced within its original position in the abdominal cavity. Procedure was settled with closure of the incision, reasserting commitment to ideal standards of surgery and research integrity.

2.6. Survival Data

Survival of mice was observed for 24 hours following the CLP procedure. Regular monitoring time intervals of four hours was adopted to capture any change in the subjects' condition so as to get appropriate post-operative care. This long period of observation was required to assess the immediate effect of CLP-induced sepsis on survival.

2.7. Sample Collection

Mice were sacrificed and samples were taken 24 hours after the CLP procedure. Blood volume of 0.5-1 ml was drawn directly from the heart, and kidneys were removed. One of the kidneys was stored in a 10% formalin solution, and the other was stored with storage at a temperature of -80C°.

2.8. Biochemical Analysis

Room temperature blood samples were allowed to clot for 30 minutes in order for serum to separate. Samples were then centrifuged, after clotting at the force of 1500 xg for a period of 10 minutes. The single serum was then assayed to establish levels of interleukin-6 (IL-6), tumor necrosis factor-alpha (TNF-α), TNF-α receptor, and interleukin-10 (IL-10) via enzyme-linked immunosorbent assay (ELISA) kits from Sunlong Biotech Co., Ltd. All the processes in the experiments were done strictly to the letter of the manufacturer's guidelines to determine accuracy and reliability of the results. In addition, blood urea and creatinine contents were estimated by using diagnostic reagents provided by Roche and providing the integral picture information for kidney function in the context of biochemical investigations.

2.9. Histological Examination

Fixed kidney samples in formalin were histologically processed by paraffin embedding, sectioning into sections of 5 µm thickness, and subsequently deparaffinized and stained with Hematoxylin and Eosin (H&E) (Shraideh *et al.*, 2013). Stained tissue sections under a light microscope were evaluated by three different examiners.

2.10. Immunohistochemical Study

Immunohistochemistry analysis was performed according to instructions provided in the Biotin-Labeled Secondary Antibodies kit protocol at Thermo Fisher Scientific, UK. Formalin-fixed paraffin-embedded sections of kidneys were deparaffinized by two washes for ten minutes in xylene. Sections were then hydrated in a graded series of ethanol and three times phosphate-buffered saline wash. 1:100 diluted pAkt antibody was applied to the sections and left for overnight incubation at 4C°. The sections were washed three times in PBS after incubation. The sections were then treated with a secondary antibody conjugated to the horseradish peroxidase enzyme and incubated for a sufficient time at 37℃. As a step toward the development of the stain, a DAB solution was brought into contact with the sections followed by a hematoxylin two-minute counterstain. The sections were then dehydrated with xylene and ethanol and later scored under a benchtop microscope by an independent reader who was not aware of the study group. To measure pAkt's color intensity of immunoreactivity on the kidney sections, Image Scope software was applied.

The H-score was calculated based on the percentage of pAkt-positive cells according to the formula: H-score = 0 × (no stain) +1× (% of weak positive stain) + 2× (% of positive stain) + 3× (% of strong positive stain). The staining intensity was divided into four categories (0, 1, 2, 3), and the final score was determined by summing the results of multiplying the staining intensity by the proportion of stained cells as illustrated in the aforementioned equation.

2.11. Real-Time PCR Analysis

To assess the expression levels of the PI3K gene, we utilized a real-time PCR approach. Initially, total RNA was extracted from the renal tissues of the study's mice, utilizing an RNA extraction kit from Solarbio, China. For the real-time PCR, two different reactions were set up: one serving as the negative control (RT- mix) and the other as the sample reaction (RT+ mix). Specifically, the RT+ mix was composed of 10 µl of 2X RT buffer, 1 µl of 20X enzyme mix, and 9 µl of a mixture containing 1 µg of total RNA, topped up with nuclease-free water to reach a final volume of 20 µl. RT- mix replicated the composition of RT+ mix but with nuclease-free water replacing the enzyme mix. The extracted RNA concentration was then precisely determined with a Nanodrop spectrophotometer produced by Nanodrop Technologies, USA.

After determining the RNA concentration, complementary DNA (cDNA) was generated with an RNA-to-cDNA conversion kit purchased from Solarbio, China. The analysis of the gene expression was performed using a CFX-96 machine by Bio-Rad Laboratories, Inc., USA, supported by Promega, USA SYBR Green Master Mix to identify. PCR thermal cycle condition was: initial denaturation of 95°C for 30 seconds, 40 cycles with

denaturation of 95°C for 1 second, annealing at 60°C for 20 seconds, and elongation at 72°C for 20 seconds. For the calculation of expressional change, we employed the comparative CT method, or ΔΔCT method. The initial step was to determine the ΔCT value of both the GOI and the internal control by subtracting the CT value of the EC from that of the GOI with the help of the following formula:

ΔCT = CT (GOI) – CT (EC).

This ΔCT value is the relative quantity of expression of the gene of interest normalized to the internal control. To assist the comparison of levels of gene expression between samples or conditions, we further went ahead and computed the ΔΔCT by subtracting the ΔCT of the control sample from the ΔCT of the experimental sample. The fold change in gene expression was then calculated using the following equation:

Fold change = 2^-ΔΔCT.

For PI3K gene analysis, specific primers were used for amplification and detection. GAPDH was used as endogenous control gene. Full primer sequences, lengths, melting temperatures (Tm), GC content, and product sizes are listed in Supplementary Table 1.

Supplementary Table 1. Primer sequences used for quantitative real-time PCR analysis of **PI3K** and the endogenous control **GAPDH**. Primer length, GC content, estimated melting temperature (Tm), and expected product size are shown.

Gene	Primer	Sequence (5′–3′)	Length (bp)	GC Content (%)	Tm (°C)*
PI3K	Forward	CTCTCCTGTGCTGGCTACTGT	21	57	~66
	Reverse	GCTCTCGGTTGATTCCAAACT	21	52	~64
GAPDH	Forward	GGAGTCAACGGATTTGGT	18	50	~54
	Reverse	GTGATGGGATTTCCATTGAT	20	40	~56

This methodology ensures precise measurement and comparison of PI3K gene expression in renal tissues, contributing valuable insights into the molecular mechanisms under investigation (Al-Awaida *et al.*, 2023).

2.12. Statistical Evaluation

Statistical analysis was conducted via GraphPad Prism8.0 software (GraphPad Software, La Jolla, CA). The data accrued from this study met the standards for normality between all the groups, allowing us to compare using parametric tests. Data were gathered from four distinct experiments, with five replicates in each experiment, and are represented as mean ± SD. Differences were assessed using a one-way analysis of variance (for multiple groups) followed by Tukey's multiple comparisons test and student's t-tests. The threshold for statistical significance was set at $p < 0.05$.

2.13. Ethics approval and consent to participate

The Animal Care and Use Committee at the University of Kufa, Iraq reviewed and approved all experimental procedures under license number 15791.

3. Results

3.1. Differential Effects of Experimental Conditions on Creatinine and Urea Levels in Control, Vehicle, Sham, and TQ Groups: A Comprehensive Comparative Analysis

Our study meticulously investigated the impacts of various experimental conditions on creatinine and urea levels across four distinct groups: Control, Vehicle, Sham, and Thymoquinone (TQ). We executed pairwise comparisons among these groups to assess the statistical significance of the observed differences, ensuring a clear and detailed distinction of findings from each test.

3.2. Creatinine Levels Comparative Analysis:

In the initial phase of our analysis, we focused on creatinine levels. The Control group presented a mean creatinine level of 1.586±0.09, which was not significantly different from the Vehicle group's level of 1.554±0.11 (p=0.91), as illustrated in Figure 1B. This initial comparison indicates a baseline similarity between Control and Vehicle groups regarding creatinine levels.

Contrastingly, a significant deviation was observed when the Control group was compared with the Sham and TQ groups. The Sham group showed a dramatically lower mean creatinine level of 0.336±0.03 ($p<0.0001$), and similarly, the TQ group displayed a reduced mean creatinine level of 0.76±0.035 ($p<0.0001$) in comparison to the Control group. These findings suggest a notable protective impact of TQ on creatinine levels. Additionally, when compared to the Sham and TQ groups, the Vehicle group exhibited significantly elevated creatinine levels ($p<0.0001$ for both comparisons), further emphasized in Figure 1B.

3.3. Urea Levels Comparative Analysis:

Parallel to our creatinine level analysis, we examined urea levels across the groups. The Control group's mean urea level was 82.2±1.92, closely matched by the Vehicle group's mean level of 82.8±3.11 (p=0.98), as depicted in Figure 1A. This consistency underscores a similar baseline between these two groups in terms of urea levels as well.

However, a divergent pattern emerged when comparing the Control and Vehicle groups to the Sham group, which exhibited significantly reduced mean urea levels of 31.8±2.39 ($p<0.0001$). The TQ group also demonstrated lower mean urea levels of 53.2±2.65 ($p<0.0001$) in comparison to the Control and Vehicle groups, as highlighted in Figure 1A. These outcomes indicate a significant influence of the conditions represented by the TQ group on urea levels, pointing to the potential protective or modulatory role of TQ.

The results of our comparative analysis clearly indicate the differential impacts of experimental conditions on creatinine and urea levels across the Control, Vehicle, Sham, and TQ groups.

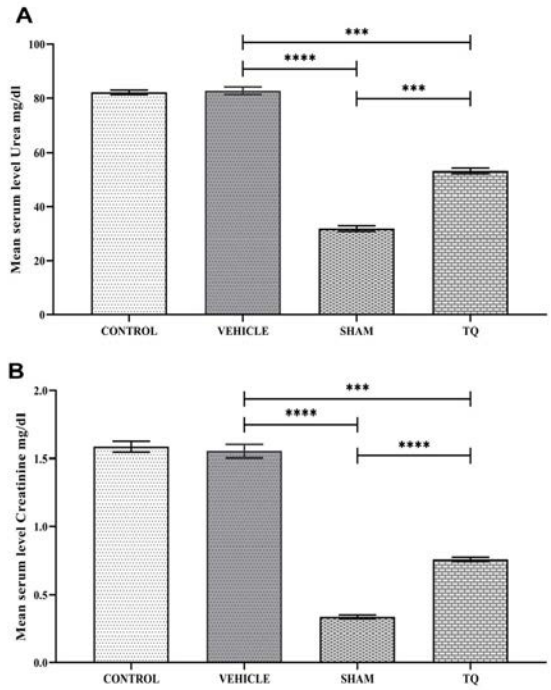

Figure 1: Comparison of Creatinine and Urea Levels among Experimental Groups. Panel A depicts mean ± SD Creatinine levels among Control, normal saline (vehicle), Sham, and TQ groups, showing no significant difference between Control and DMSO (p=0.9054) but they markedly elevated in comparison with sham group. TQ group revealed a substantial decrease as compared with Control and vehicle groups (****). Panel B presents urea levels for the same groups, mirroring the pattern in Creatinine, with Control and vehicle groups showing no difference (p=0.9805) but they considerably increased as compared with Sham group (****). Significant reduction is observed in TQ group as compared with Control and vehicle groups (****). Significance denoted as *p < 0.05, **p < 0.01, ***p < 0.001, ****p < 0.0001.

3.4. Differential Sham, CLP, and Thymoquinone (TQ) Treatment Effects on IL-6 and TNF-α Levels and TNF-α Receptor Expression

Our experiment extensively explores the effects of Sham, Cecal Ligation and Puncture (CLP), and Thymoquinone (TQ) treatments on the regulation of IL-6 and TNF-α levels, as well as TNF-α receptor expression. This section summarizes the findings across these biomarkers, highlighting the differential effects of each treatment regimen.

3.5. IL-6 Concentration Alterations:

The experiment began with the determination of the level of Interleukin-6 (IL-6) in experimental groups. The vehicle group and control group recorded very comparable IL-6 levels (1300±158.11 pg/mL vs. 1290±97.97 pg/mL, respectively) without any disparity noticed (P=0.99), which proves the absence of effect of normal saline, a standard solvent utilized in biological studies, on IL-6 levels. The result is presented in Figure 2A.

Contrastingly, significant reductions in IL-6 concentrations were noted in both the Sham (200±15.81 pg/mL) and TQ (306±15.57 pg/mL) groups compared to the control group, with all comparisons reaching statistical significance (P<0.0001). These groups also significantly lowered IL-6 levels compared to the vehicle group (P<0.0001). However, no notable variance was detected between the Sham and TQ groups in their effectiveness at reducing IL-6 levels (Sham vs. TQ: P=0.3189), indicating a similar impact on IL-6 modulation.

3.6. TNF-α Level Variations:

Subsequently, we examined the alterations in TNF-α levels under the influence of different treatments. As illustrated in Figure 2B, the control and vehicle groups exhibited comparable TNF-α levels (449.8±14.66 pg/ml and 444.2±17.42 pg/ml, respectively; P=0.99), indicating no significant effect of vehicle treatment on TNF-α levels. Interestingly, the TQ group manifested a significant decrement in TNF-α levels in comparison to both control and vehicle groups (P<0.0001), highlighting Thymoquinone's potential in mitigating inflammatory responses post-CLP.

3.7. TNF-α Receptor Expression Dynamics:

Finally, the assessment of TNF-α receptor concentrations revealed no significant difference between the control (800±50.12 pg/mL) and vehicle (790±38.89 pg/mL) groups (P=0.9864), as shown in Figure 2C. This outcome suggests the neutrality of vehicle treatment on TNF-α receptor levels. In stark contrast, the TQ group exhibited a significant reduction in TNF-α receptor levels in comparison to both the control and vehicle groups (P<0.0001). Yet, similar to the pattern observed with IL-6 levels, no significant disparity was noted between the Sham and TQ groups regarding their impact on TNF-α receptor levels (Sham vs. TQ: P=0.78).

Collectively, these findings delineate the distinct and significant impacts of Thymoquinone treatment on both IL-6 and TNF-α levels, as well as TNF-α receptor expression, in comparison to untreated and vehicle-treated controls.

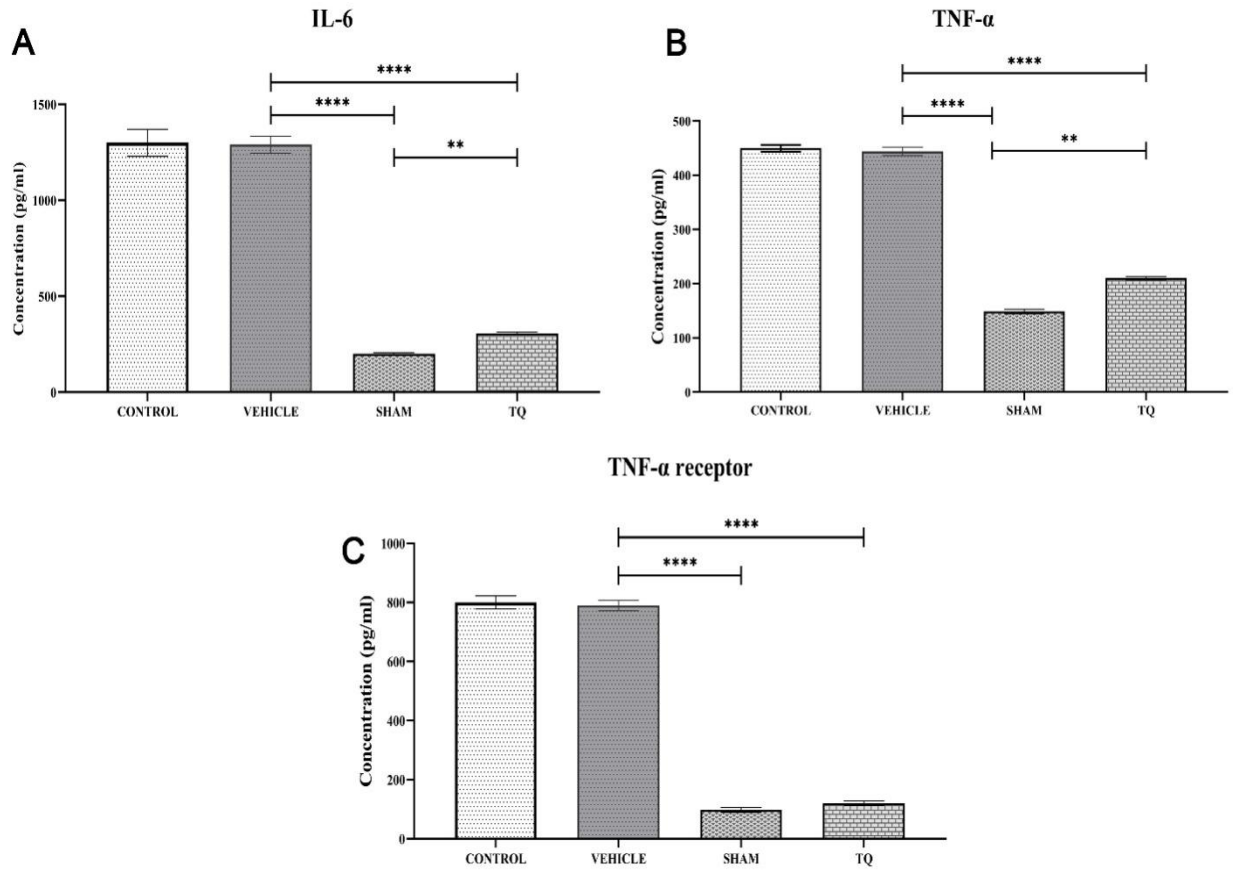

Figure 2: Effects of Various Treatments on IL-6 and TNF-α Levels and TNF-α Receptor Expression. Panel A illustrates IL-6 concentrations across Control, vehicle, Sham, and TQ groups. No significant difference exists between Control and vehicle (P=0.9997) but both showed significant elevations as compared with Sham group. TQ group shows a substantial reduction in IL-6 levels contrasted to both control and vehicle groups (P<0.0001). Panel B outlines the TNF-α level for the same groups. Control and vehicle groups display similar levels (P=0.9998) but they notably increased as compared with Sham group (****), whereas the TQ group exhibits significant reductions in comparison with Control and vehicle (P<0.0001). Panel C indicates TNF-α receptor concentrations, with control and vehicle showing no difference (P=0.9864), while they markedly increased as compared with Sham group. TQ group displays a significant reduction as compared with Control and vehicle groups (P<0.0001). Data are expressed as mean ± SD. Significance is depicted as *p < 0.05, **p < 0.01, ***p < 0.001, ****p < 0.0001.

3.8. Distinct Influence of Sham, CLP, and Thymoquinone (TQ) on IL-10 and F8-Isoprostane Levels: Indications for Oxidative Stress Reduction and Immunomodulation

Our study meticulously evaluated the differential impacts of sham operation, Cecal Ligation and Puncture (CLP), and Thymoquinone (TQ) treatment on IL-10 and F8-Isoprostane levels, which are pivotal markers for immunomodulation and oxidative stress, respectively. The following paragraphs detail our findings, correlating each to the appropriate figures.

3.9. IL-10 Levels Analysis:

In the comparative analysis of IL-10 levels, the control and vehicle groups showed no statistically significant difference (230±15.81 pg/mL vs. 234.4±23.80 pg/mL, P=0.99), suggesting that the solvent employed in these experiments (normal saline) does not significantly affect IL-10 levels. This observation is visualized in Figure 3A.

Contrastingly, the TQ treatment group demonstrated a marked increase in IL-10 levels, reaching 452±37.68 pg/mL, which represents a statistically significant elevation compared to both the control and vehicle groups (P<0.0001). This significant increase underscores the potent immunomodulatory effect of Thymoquinone, suggesting its role in enhancing anti-inflammatory responses. The comparative increase in IL-10 levels between the TQ and vehicle groups further solidifies the specific augmenting effect of Thymoquinone on this cytokine.

3.10. F8-Isoprostane Levels Analysis:

The examination of F8-Isoprostane levels, a marker for oxidative stress, revealed no significant variance between the control (87±3.80 pg/mL) and vehicle groups (86.6±6.107 pg/mL, P=0.99), indicating that the vehicle substance does not significantly influence oxidative stress markers in this context. This data is presented in Figure 3B.

However, a stark contrast was observed in the TQ treatment group, which exhibited a significant reduction in F8-Isoprostane levels (41±3.93 pg/mL, P<0.0001) compared to the control group. This pronounced decrease indicates that TQ treatment significantly mitigates oxidative stress, as measured by F8-Isoprostane levels. Furthermore, when compared to the vehicle group, the TQ group also displayed a significant reduction in F8-Isoprostane levels (P<0.0001), highlighting the substantial oxidative stress reduction afforded by Thymoquinone treatment.

Our findings distinctly indicate that Thymoquinone treatment significantly amplifies IL-10 levels, thereby potentially enhancing anti-inflammatory responses. Concurrently, TQ treatment considerably lowers F8-Isoprostane levels, indicating a reduction in oxidative stress.

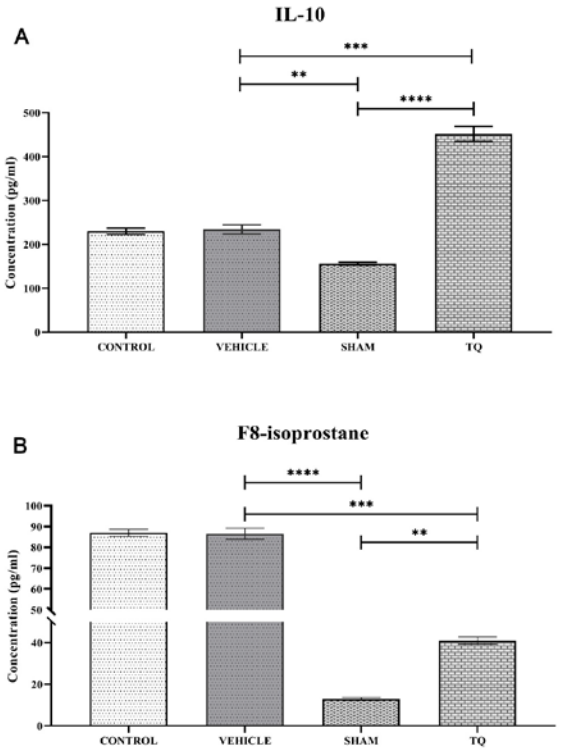

Figure 3: Evaluation of IL-10 and F8-Isoprostane Levels across Experimental Groups. Panel A shows IL-10 levels in control, vehicle, Sham, and TQ groups. No significant difference between control and vehicle groups (P=0.9976), but significant increase in TQ group (P<0.0001) is observed as compared with Control, vehicle and Sham groups. Panel B depicts F8-isoprostane levels among the same groups, showing no difference between Control and vehicle groups (P=0.9999), but they show substantial increases as compared with Sham group. TQ treatment showed a significant reduction in F8-isoprostane levels compared to Control and vehicle groups (P<0.001 for both). Data are represented as mean ± SD. Significance indicated as *p < 0.05, **p < 0.01, ***p < 0.001, ****p < 0.0001.

3.11. Influence of Thymoquinone on pAkt Antibody Expression in Renal Tissue Post-CLP

This section of the study extensively inspected the impact of Thymoquinone (TQ) on the renal tissue expression of pAkt antibody following Cecal Ligation and Puncture (CLP) via immunohistochemistry processes for critical analysis.

3.12. Immunohistochemistry Observations:

Our initial assessment documented a considerable disparity in pAkt antibody immunoreactivity across diversified experimental groups. Precisely, the vehicle-treated and CLP control groups both presented weak pAkt immunoreactivity, as clearly demonstrated by less intensively brown-pigmented renal tissue sections (Figures 4A, 4B, and 4C). Quantitatively, this was accompanied by the mean H-score, indicating a statistically significant reduction in pAkt expression in these groups compared to the Sham group, affirming the toxic impact of CLP ($P \leq 0.05$, Figure 4E).

3.13. Effect of Thymoquinone:

When compared to control and vehicle groups, Thymoquinone (TQ) pretreatment showed an apparent increase in the pAkt antibody immunoreactivity in the kidney tissues. Such an increase was visually evident as denser brown staining in TQ-treated group tissue sections (Figure 4D). To complement this qualitative observation, the H-score analysis also statistically quantified the increase with greater mean levels of pAkt expression in the TQ-treated group compared to the control CLP group ($P \leq 0.05$, Figure 4E).

These findings propose an important role played by Thymoquinone in increasing the immunoreactivity of pAkt antibody in renal tissues following CLP. This increase indicates a potential protective mechanism employed by TQ to counteract renal alterations induced by CLP. In view of the significance of these observations, further research is an imperative necessity to dissect the precise molecular mechanisms whereby TQ provides protection and to assess the potential clinical relevance of these observations.

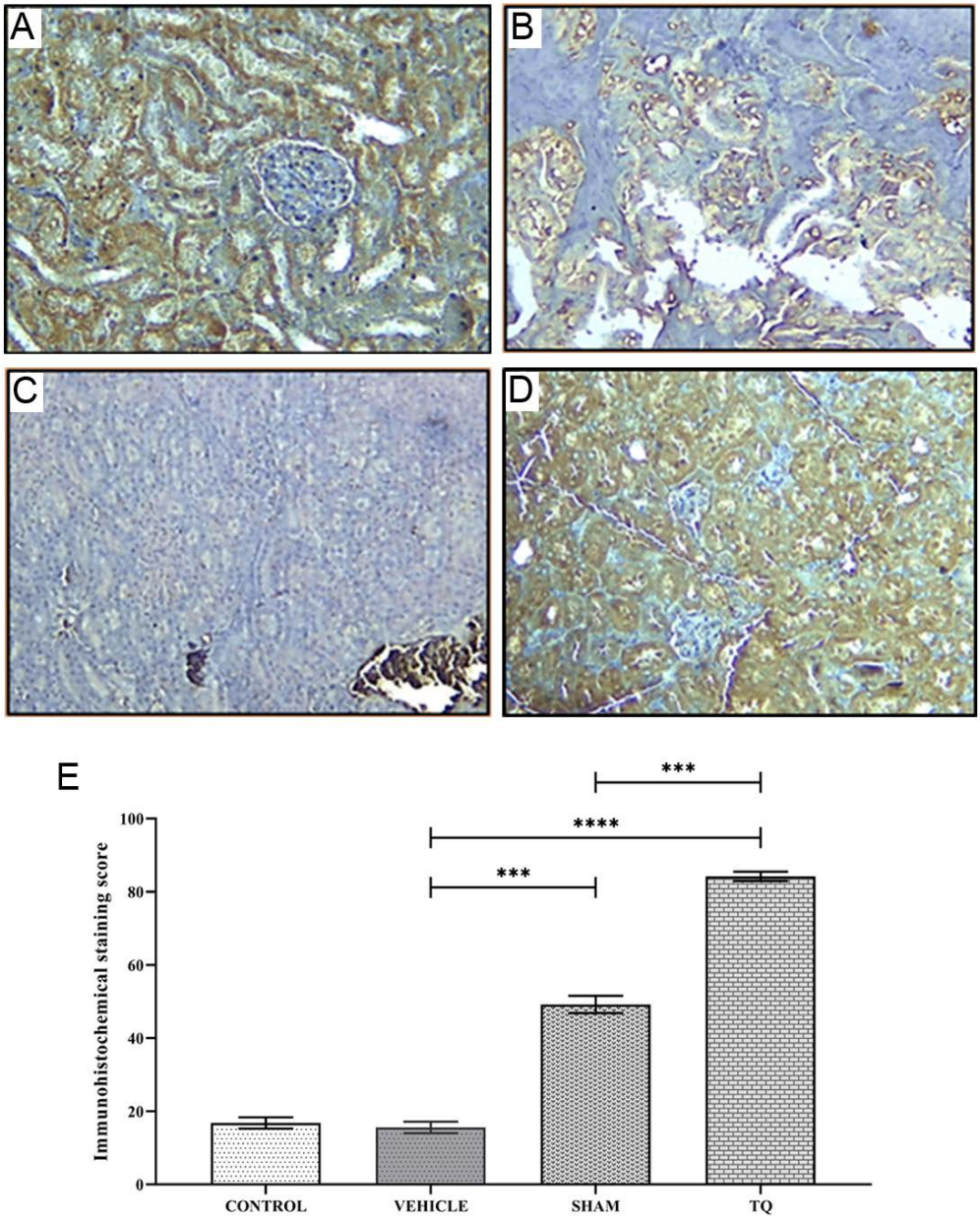

Figure 3: Thymoquinone Augments pAkt Antibody Expression in Renal Tissue Post-CLP. Immunohistochemical staining for pAkt was conducted in different groups: Sham (Figure 4A), Control (Figure 4B), vehicle (Figure 4C), and Thymoquinone (TQ)-treated (Figure 4D). Brown staining indicates pAkt antibody expression. The mean H-scores are presented in Figure 4E. Data are expressed as mean ± SD. Significance is depicted as *p < 0.05, **p < 0.01, ***p < 0.001, ****p < 0.0001.

3.14. Thymoquinone: Comparative Effects on PI3K Gene Expression Following Post-CLP

We closely looked at the impact of Thymoquinone (TQ) on PI3K gene expression following the CLP operation, as depicted in Figure 5. This study intended to clarify the potential modulatory action of TQ on PI3K gene expression, which is a crucial molecule in cell signaling pathways included in cell growth, proliferation, differentiation, motility, survival, and intracellular transport.

3.15. Control vs. Vehicle Group Comparison:

Our primary comparison between the control group, which received CLP alone but no other treatment (6.14±0.27), and the vehicle group, which received an inert treatment that was assumed to be inactive (6.04±0.18; P=0.89), did not reveal any significant difference in PI3K gene expression levels. This suggests that the vehicle in our experimental setup does not show any notable effect on PI3K gene expression levels, so it is an effective baseline to compare with other groups.

3.16. Effect of Thymoquinone on PI3K Gene Expression:

Remarkably, when we compared the PI3K gene expression levels of the control group with those of the Sham group (2.12±0.24) and the TQ group (2.156±0.19), we observed a highly significant decrease in PI3K gene expression in the TQ group, with P-values of less than

0.0001. This pronounced downregulation of PI3K gene expression in the TQ group, as opposed to the control group's levels, underscores the potent modulatory effect of TQ treatment on this critical gene's expression following the CLP operation.

3.17. Sham vs. TQ Group Comparison:

Further analysis between the Sham group and the TQ group revealed no significant difference in PI3K gene expression levels (P=0.99), indicating that TQ administration results in PI3K gene expression comparable to that observed in the Sham group. This parity between the Sham and TQ groups suggests that TQ treatment effectively mimics the basal level of PI3K gene expression observed in the absence of the CLP-induced stress condition.

Our findings evidently indicate that Thymoquinone treatment significantly enhances PI3K gene expression following the Cecal Ligation and Puncture operation. The results show a strong example for the role of TQ in modifying PI3K gene expression, one of the mechanisms via which it might be applying the therapeutic effects in stress or post-surgery situations. Action mechanisms of these effects can be inspected further to fully clarify the effects of TQ on cellular signaling pathways and its therapeutic applications.

3.18. Thymoquinone Mitigative effect on Kidney Tissue Morphology Following the Cecal Ligation and Puncture Procedure

This part of our study ackles evaluating the therapeutic capacity of Thymoquinone (TQ) in maintaining kidney tissue integrity after Cecal Ligation and Puncture (CLP) surgery, an experimental procedure for inducing sepsis in research. Histopathological assessment of kidney tissues from various groups provided an indication of TQ's protective effect against CLP-induced renal damage.

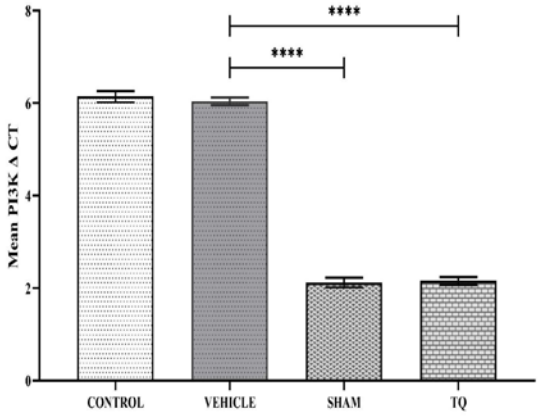

Figure 4: Effects of Various Treatments on PI3K Gene Expression. This figure displays the comparative analysis of PI3K gene expression in different groups: Control, vehicle, Sham, and Thymoquinone (TQ)-treated. The gene expression levels are denoted as arbitrary units on the y-axis. Data are expressed as mean ± SD. Significance is depicted as *p < 0.05, **p < 0.01, ***p < 0.001, ****p < 0.0001.

3.19. Sham Group Morphology:

The morphology of kidney tissues in the Sham group initially revealed normal renal epithelium morphology, illustrating an absence of significant morphological changes due to the sham procedure itself, as seen in Figure 6A. This set a baseline for determining the degree of tissue damage and TQ efficacy in the experimental model..

3.20. CLP and Vehicle-Treated Group Results:

Tissues collected from mice that were subjected to the CLP surgery, regardless of whether they were treated with a vehicle, displayed severe pathological features. These characteristics included vascular congestion, the presence of necrotic lesions, eosinophilic cytoplasm, and densely packed nuclei, as depicted in Figures 6B and 6C. Such findings underscore the severe renal damage inflicted by the CLP procedure, establishing a context for assessing TQ's protective potential.

3.21. TQ-Treated Group Observations:

Remarkably, kidney sections from the TQ-treated group exhibited a distinctively milder degree of tissue alteration. These sections showed moderate hypertrophy of renal tubules along with mild lesions, as illustrated in Figure 6D. This observation suggests a pronounced protective effect of TQ, mitigating the harsh impact of the CLP operation on renal tissues. The comparatively less severe morphological changes in the TQ-treated group highlight the potential of TQ as a protective agent against CLP-induced kidney damage.

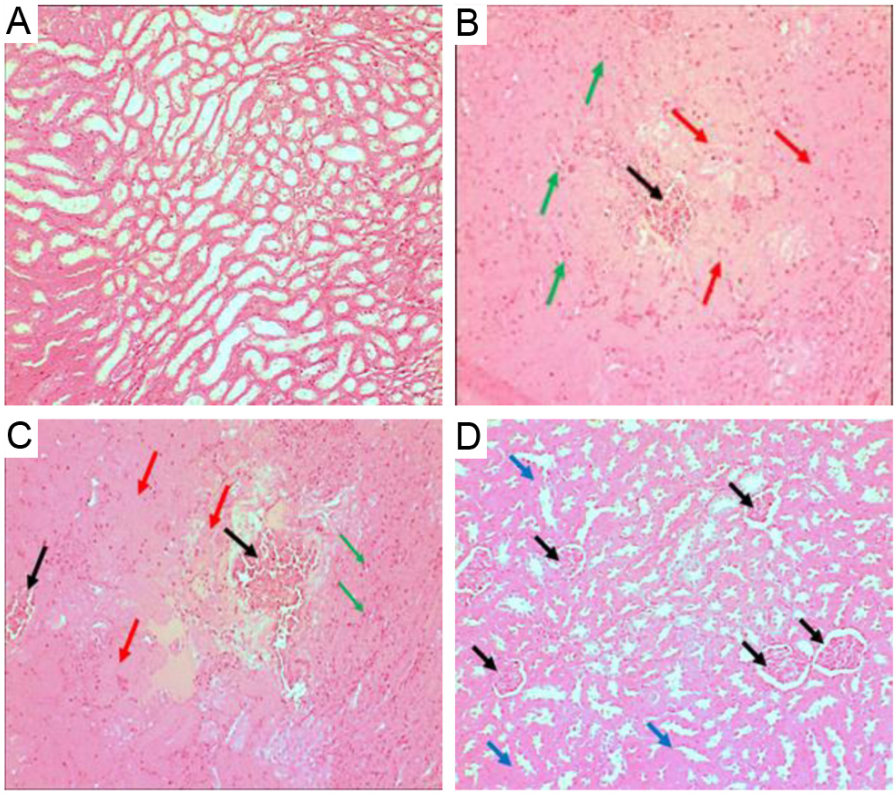

Figure 5: Evaluation of Thymoquinone's Mitigative Effects on Kidney Tissue Morphology Post-CLP. This provides histopathological images representing the differential impact of Thymoquinone (TQ) on kidney tissue morphology following the cecal ligation and puncture (CLP) procedure. Tissue sections are stained for structural analysis and examined under a microscope. The scale bar represents a standard length for comparative analysis. In Figure 6A, the Sham group exhibits typical renal epithelium, denoting no significant structural alteration as a consequence of the sham procedure. However, kidney tissues from CLP-subjected mice, regardless of vehicle treatment, display considerable pathological changes. These alterations, which include vascular congestion, necrotic lesions, eosinophilic cytoplasm, and dense nuclei, are evident in Figures 6B and 6C, suggesting severe renal damage inflicted by the CLP procedure. In a contrasting manner, renal tissue sections from the TQ-treated group, as shown in Figure 6D, depict moderate hypertrophy of renal tubules and mild lesions. These relatively mild morphological changes suggest a potential mitigative effect of TQ on CLP-induced renal damage.

Finally, our data map out a specific protective response of Thymoquinone in preserving morphology of kidney tissues following the CLP surgery. The seemingly quantitative contrast in damage severity between CLP and TQ-treated group supports the potential therapy of TQ. Even so, still justified is closer study of precise mechanisms by which TQ operates with these protecting activities. Future research studies should aim to clarify these mechanisms, hopefully culminating in therapeutic applications of TQ in mitigating renal injury in sepsis or other similar conditions.

4. Discussion:

Although several studies have accounted for the antioxidative and anti-inflammatory activities of Thymoquinone, our study sheds more light by examining its impact on the PI3K/Akt pathway in acute kidney injury induced by sepsis. Through a holistic integration of histological, biochemical, and molecular data, this study contributes to the burgeoning literature on the potential mechanisms of action of TQ in renoprotection.

Sepsis, a clinical condition involving the host's amplified inflammatory response to infection, is well recognized to have severe harmful effects on renal function, resulting in acute kidney injury. Despite the great progress in the development of novel therapies to arrest sepsis-induced morbidity and mortality, it remains a universal problem that requests ongoing research (van der Poll *et al.*, 2021; Shalan *et al.*, 2024). Our results, showing elevated serum levels of urea and creatinine in septic mice after-cecal Ligation and Puncture (CLP), confirm the kidney damage frequently seen in sepsis and support the usefulness of the CLP model for sepsis induced AKI research (Kim *et al.*, 2022). Furthermore, existing research highlights TQ's effectiveness in reducing such biomarkers, as revealed by renal protective effects in glycerol induced acute kidney injury in rats. AKI is defined by the rapid decrease in glomerular filtration rate and the accumulation of nitrogenous waste, leading to severe kidney damage (Bilgili *et al.*, 2014).

Increase in serum levels of IL-6, TNF-α, and TNF-α receptors in the CLP group, in contrast to the sham group, displays the role of an augmented inflammatory response in sepsis. This augmentation aligns with previous reports representing increases in these cytokines at sepsis models (Shou *et al.*, 2023). The efficiency of Thymoquinone (TQ) in markedly reducing these inflammatory mediators reinforces its therapeutic capability, reasonable with findings from studies showing TQ's capability to modulate similar markers in different inflammatory diseases (Zanders *et al.*, 2022).

The change of TNF-α via TQ, critical due to its role in improving IL-6 production and facilitating inflammatory processes, apoptosis, and oxidative damage, supports reports demonstrating TQ's inhibition of the NF-κB pathway and consequent reduction of TNF-α and IL-6 production (Venkataraman *et al.*, 2021). Though, the extent of cytokine decrease differs across studies, probably due to changes in TQ dosing, administration timing, or the sepsis models retained. These differences highlight the complexity of septic reaction and the need for standardization in evaluating therapeutic interventions.

In contrast to our results on TNF-α receptor modulation by TQ, some studies report no considerable changes in receptor expression in different disease models treated with TQ (Alasmari *et al.*, 2023), suggesting that TQ's effect on the TNF-α receptor might vary with the original pathology. This designates a nuanced mechanism of action for TQ that necessitates further investigation.

The detected increase in IL-10 serum levels in the CLP group, which was amplified by TQ pretreatment, supports results from preceding studies demonstrating the anti-inflammatory effects of IL-10 in sepsis models (Guo *et al.*, 2020). IL-10 is noted to play a very significant part in governing the inflammatory response, suggesting a protective mechanism that has the possibility to improve outcomes in septic states (Vivas *et al.*, 2021). This surge in IL-10 following TQ administration implies that TQ may improve the body's natural antiinflammatory response to sepsis.

Though, the elevated IL-10 levels in TQ-treated mice, exceeding those observed in septic mice without TQ treatment, give an interesting contrast to findings by researchers in 2022, who reported lower IL-10 levels in septic mice following TQ treatment in comparison to untreated septic mice (Alkharfy *et al.*, 2018). This difference could be accredited to differences in experimental design, such as the timing of TQ administration in relation to the onset of sepsis, the dosage of TQ used, or the specific strains of mice used in the studies. Such variables could considerably impact the immunomodulatory effects of TQ, showcasing the need for further research to summarize the ideal conditions under which TQ exerts its maximal therapeutic benefit.

Additionally, the mechanism by which TQ raises IL-10 levels highlights the need for further investigation. Given that TQ has been revealed to modulate numerous signaling pathways related to inflammation and immune response regulation (Darakhshan *et al.*, 2015), it is probable that TQ's action on these pathways may indirectly lead to amplified IL-10 production. This hypothesis aligns with the wider literature on the immunomodulatory outcomes of natural compounds, which often include complicated interactions with the host's immune system (Alkharfy *et al.*, 2018).

Granted these results, our research contributes to the growing amount of data indicating that TQ has potential as a treatment for sepsis, especially because of to its ability to influence the inflammatory response through cytokines such as IL-10. The observed variances with prior studies, nevertheless, emphasize the intricacy of the immune response in sepsis and the influence of several experimental variables on the results of such studies. To entirely understand the circumstances under which TQ can be used to treat sepsis and other inflammatory illnesses, more research is needed.

Oxidative stress and the production of free radicals play vital roles in the pathogenesis of sepsis and the resultant inflammatory response. In our study, the higher levels of F8-isoprostane in the renal tissues of septic mice, in comparison to the sham group, emphasize the impact of oxidative stress in sepsis induced renal injury. The substantial reduction in these levels following TQ treatment proposes its possible antioxidative properties, associating with preceding studies that have highlighted TQ's ability to mitigate oxidative stress markers in various models of disease(Ow *et al.*, 2021). This is steady with findings from Linillos-Pradillo et al., who stated a decrease in oxidative stress markers, comprising F8-isoprostane, in a model of ischemia-reperfusion injury treated with TQ (Linillos-Pradillo *et al.*, 2023).

Addionally, antioxidative activity of TQ, particularly its effect on F8-isoprostane, clarifies its protective mechanisms against renal injury in sepsis. This is reinforced by research from Tiba et al., demonstrating TQ's broad antioxidative outcomes in a diabetic nephropathy model, viewing a decrease in renal oxidative stress markers along with enhancements in renal function (Tiba *et al.*, 2023).

Our findings support other studies on renoprotective activity of TQ against various models of renal damage, including glycerol-induced and cisplatin-induced nephrotoxicity (Sayed and Morcos, 2007; Bilgili *et al.*, 2014). The same reductions in IL-6 and TNF-α upon TQ administration have been demonstrated in models of LPS-induced inflammation (Ojha *et al.*, 2015). However, few studies have touched upon its modulation of the PI3K/Akt signaling pathway during polymicrobial sepsis, highlighting the unique emphasis of our work. Contrary to findings of Qu et al.,(Qu *et al.*, 2020) which saw suppression of PI3K/Akt in sepsis in the kidneys, our results confirm that TQ has the capability to revive such a signaling pathway and may be a viable targeted therapeutic intervention.

Although TQ's antioxidative properties are extensively recognized, variations in the extent of its consequences amongst findings may result from diverse investigational models, dosage differences, or timing of administration. These alterations underline the many-sided antioxidative mechanisms of TQ and the complicated nature of oxidative stress in sepsis.

Furthermore, TQ represents a promising therapeutic option in reducing sepsis induced renal injury through antioxidative activity. Additional studies need to be conducted to fully reveal the exact mechanisms by which TQ performs to protect and to discover its therapeutic value in a wider variation of septic diseases.

The PI3K/Akt signaling pathway has been recognized as a significant mechanism in sepsis pathogenesis and a therapeutic target. In our study, a marked decrease in the mRNA expression of PI3K and phosphorylated Akt in septic mice was detected when compared to controls, revealing the pathway suppression during sepsis. Of special relevance, TQ administration obviously reduced these parameters, showing its modulatory effect on the PI3K/Akt signaling pathway, that may have a role in improving septic renal damage. The current finding is reinforced by the outcome of Qu et al., showing reduced

levels of phospho-Akt and phospho-PI3K in septic rats' kidneys, underlining the dysfunction of the pathway in sepsis (Qu *et al.*, 2020).

Activation of the PI3K-Akt pathway has been shown to have defensive effects against endotoxemia via the suppression of proinflammatory cytokines, decreasing coagulation, and improving survival in sepsis models (Qu *et al.*, 2020). This defensive act is also shown in an acute spinal cord injury model, where TQ treatment improved PI3K and phospho-Akt levels, denoting its potential as a protective agent against renal injury (Junaid *et al.*, 2021). The similarity of our results with such studies complements the therapeutic value of inhibiting the PI3K/Akt pathway in sepsis.

However, various investigations may have distinct results on the protective effect of TQ in sepsis induced kidney injury and its degree of impact on the PI3K/Akt pathway. This could be due to the differences in the experimental model, TQ dosage, or the timing of the intervention. This variety demonstrates the complex participation of the PI3K/Akt pathway in the pathophysiology of sepsis and the intrinsic complexity of the disease.

The evidence proposes that modulating TQ through the PI3K/Akt signaling pathway is a promising new approach to diminish kidney damage carried on by sepsis. Nevertheless, further studies will help elucidate its detailed mechanisms of action.

5. Conclusion

This study provides robust experimental proof that Thymoquinone (TQ), the bioactive compound of *Nigella sativa*, possesses a potent therapeutic effect against sepsis-induced Acute Kidney Injury (AKI) by multi-level biology modulation. Our findings reveal that TQ pretreatment significantly improved renal function, as shown by the reduction in the levels of serum creatinine and urea, which were drastically elevated in septic CLP-induced mice. These functional improvements were supported by histopathological findings of remarkable renal architecture preservation and reduced tissue injury in TQ-treated mice compared to the CLP and vehicle groups.

Molecularly, TQ significantly down-regulated systemic inflammation via inhibition of pro-inflammatory cytokines IL-6 and TNF-α, and repression of TNF-α receptor expression. Concurrently, TQ up-regulated the anti-inflammatory cytokine IL-10, reflecting a desirable shift to an anti-inflammatory profile. Furthermore, TQ greatly lessened oxidative stress, as indicated by decreased F8-isoprostane levels in renal tissue. These findings render TQ a bifunctional agent that is capable of influencing inflammatory and oxidative processes, which are the centers of gravity in AKI pathology during sepsis.

Interestingly, our analysis of the PI3K/Akt signaling pathway, a crucial axis that regulates cell survival, apoptosis, and inflammation, revealed that TQ increases pAkt protein levels and normalizes PI3K gene expression back to sham levels. This regulation proves that TQ has at least partial renoprotective functions by restoring cellular signal balance lost during sepsis. This is novel mechanistic insight, positioning PI3K/Akt as a potential therapeutic target and TQ as a potential modulator of this pathway in septic AKI models.

These findings not only serve the study's objective to evaluate the therapeutic efficacy of TQ in septic AKI but also render TQ an excellent choice for future drug development. The breadth of its action—ranging from functional to molecular and histological protection—underscores its promise for translation to the clinic where sepsis-induced acute kidney injury remains a major cause of morbidity and mortality.

While these results are encouraging, additional preclinical studies are required to assess TQ's long-term safety profile, optimal dosing regimens, and pharmacokinetics in septic models. More investigation is also required to identify whether PI3K/Akt modulation by TQ has downstream effects on apoptosis, autophagy, and mitochondrial function. Furthermore, testing of TQ in combination with existing therapeutic agents may reveal synergistic effects that enhance outcomes in sepsis. Lastly, adequate clinical trials in humans shall be the determining factor towards proving the efficacy and safety of TQ as a drug against sepsis-associated AKI and, by default, other inflammatory organ injury.

6. Authors' Contributions:

Conceptualization, H.J. and W.A.; Data curation, K.G., H.A.-A., and I.H.; Formal analysis, H.J., Y.G., A.S., O.A.B., and N.H.; Investigation, H.J., B.M., H.Q., W.A., and S.S.Z.; Methodology, B.M., G.F., H.Q., W.A., B.S., Y.G., V.T., A.S., O.A.B., G.C., N.G., and N.H.; Resources, Y.G., V.T., A.S., A.A.A, A.A.H., T.M.R., T.S.A., and G.C.; Software, B.M., K.G., H.A.-A., and V.T.; Validation, H.J., B.M., G.F., K.G., and Y.G.; Visualization, B.M.; Writing – original draft, H.Q., H.A.-A., B.S., O.A.B., N.G., A.A.B., A.M.A., and I.H.; Writing – review & editing, H.J., W.A., S.S.Z., B.S., G.C., A.A.B., I.H., A.M.A., and N.H.

References

Abu Saleem E, Lafi Z, Shalan N, Alshaer W, Hamadneh I. 2025. Formation and evaluation of doxorubicin and cromoglycate metal–organic framework for anti-cancer activity. *Nanomedicine* 1–13.

Al-Awaida W, Al-Ameer HJ, Sharab A, Akasheh RT. 2023. Modulation of wheatgrass (*Triticum aestivum* Linn) toxicity against breast cancer cell lines by simulated microgravity. *Curr. Res. Toxicol.* 5: 100127.

Al-Husein BA, Mhaidat NM, Sweidan RM. 2020. Interaction of atorvastatin and CX3CR1/fractalkine in androgen-dependent prostate cancer cells: Effect on PI3K pathway. *Jordan J. Biol. Sci.* 13(3).

Al-Saffar RA, Al-Wiswasy MK. 2019. A morphological study of the pharmacological effects of *Nigella sativa* on the reproductive system in experimental rats. *Jordan J. Biol. Sci.* 12: 147–153.

Alasmari F, Alotaibi FM, Al-Qahtani WS, AlAsmari AF, Alqahtani F. 2023. Therapeutic effects of thymoquinone on Alzheimer's disease through modulating amyloid-beta neurotoxicity and neuro-inflammatory cytokine levels. *CNS Neurol. Disord. Drug Targets* 22(5): 736–744.

Alkharfy KM, Ahmad A, Jan BL, Raish M. 2018. Thymoquinone reduces mortality and suppresses early acute inflammatory markers of sepsis in a mouse model. *Biomed. Pharmacother.* 98: 801–805.

Alkharfy KM, Ahmad A, Raish M, Vanhoutte PM. 2015. Thymoquinone modulates nitric oxide production and improves organ dysfunction of sepsis. *Life Sci.* 143: 131–138.

Alkharfy KM, Al-Daghri NM, Al-Attas OS, Alokail MS. 2011. The protective effect of thymoquinone against sepsis syndrome morbidity and mortality in mice. *Int. Immunopharmacol.* 11(2): 250–254.

Alqaraleh M, Khleifat KM, Al-Samydai A, Al-Rawashdeh FA, Al-Najjar BO, Saqallah FG. 2025. Therapeutic potential of marine sponges and nanoparticles: A study on *Siphonochalina siphonella* and AgNPs. *J. Med. Pharm. Chem. Res.* 7(4): 745–761.

Bi C-F, Hao S-W, Xu Z-X, Ma X, Kang X-F, Yang L-S, Zhang J-F. 2023. Xuebijing injection protects against sepsis-induced myocardial injury by regulating apoptosis and autophagy via mediation of PI3K/Akt/mTOR signaling pathway in rats. *Aging (Albany NY)* 15(10): 4374.

Bilgili B, Haliloğlu M, Cinel İ. 2014. Sepsis ve akut böbrek hasari. *Turk. J. Anaesthesiol. Reanim.* 42(6).

Chang Y-M, Chou Y-T, Kan W-C, Shiao C-C. 2022. Sepsis and acute kidney injury: A review focusing on the bidirectional interplay. *Int. J. Mol. Sci.* 23(16): 9159.

Darakhshan S, Pour AB, Colagar AH, Sisakhtnezhad S. 2015. Thymoquinone and its therapeutic potentials. *Pharmacol. Res.* 95: 138–158.

Farkhondeh T, Samarghandian S, Shahri AMP, Samini F. 2018. The neuroprotective effects of thymoquinone: A review. *Drug Res.* 68(10): 584–590.

Geng H, Zhang H, Cheng L, Dong S. 2024. Sivelestat ameliorates sepsis-induced myocardial dysfunction by activating the PI3K/Akt/mTOR signaling pathway. *Int. Immunopharmacol.* 128: 111466.

Guo L-P, Liu S-X, Yang Q, Liu H-Y, Xu L-L, Hao Y-H, Zhang X-Q. 2020. Effect of thymoquinone on acute kidney injury induced by sepsis in BALB/c mice. *Biomed. Res. Int.* 2020: 1594726.

Hiengrach P, Panpetch W, Chindamporn A, Leelahavanichkul A. 2022. Macrophage depletion alters bacterial gut microbiota partly through fungal overgrowth in feces that worsens cecal ligation and puncture sepsis mice. *Sci. Rep.* 12(1): 9345.

Isaev NK, Genrikhs EE, Stelmashook EV. 2023. Antioxidant thymoquinone and its potential in the treatment of neurological diseases. *Antioxidants. (*12(2): 433.

Jarczak D, Kluge S, Nierhaus A. 2021. Sepsis—pathophysiology and therapeutic concepts. *Front. Med*. 8: 628302.

Junaid M, Akter Y, Afrose SS, Tania M, Khan MA. 2021. Biological role of Akt and regulation of Akt signaling pathway by thymoquinone: Perspectives in cancer therapeutics. *Mini Rev. Med. Chem.* 21(3): 288–301.

Kim C, Ryu SH, Kim N, Lee W, Bae J-S. 2022. Renal protective effects of sparstolonin B in a mouse model of sepsis. *Biotechnol. Bioprocess Eng.* 27(2): 157–162.

Li X-Y, Yu J-T, Dong Y-H, Shen X-Y, Hou R, Xie M-M, Wei J, Hu X-W, Dong Z-H, Shan R-R. 2023. Protein acetylation and related potential therapeutic strategies in kidney disease. *Pharmacol. Res.* 195: 106950.

Linillos-Pradillo B, Rancan L, Paredes SD, Schlumpf M, Lichtensteiger W, Vara E, Tresguerres JÁ. 2023. Low dose of BPA induces liver injury through oxidative stress, inflammation and apoptosis in Long–Evans lactating rats and its perinatal effect on female PND6 offspring. *Int. J. Mol. Sci.* 24(5): 4585.

Ludes P-O, De Roquetaillade C, Chousterman BG, Pottecher J, Mebazaa A. 2021. Role of damage-associated molecular patterns in septic acute kidney injury, from injury to recovery. *Front. Immunol.* 12: 606622.

Ojha S, Azimullah S, Mohanraj R, Sharma C, Yasin J, Arya DS, Adem A. 2015. Thymoquinone protects against myocardial ischemic injury by mitigating oxidative stress and inflammation. *Evid. Based Complement. Alternat. Med.* 2015: 143629.

Ow CP, Trask-Marino A, Betrie AH, Evans RG, May CN, Lankadeva YR. 2021. Targeting oxidative stress in septic acute kidney injury: From theory to practice. *J. Clin. Med.* 10(17): 3798.

Öztürk E, Kaymak E, Akin A, Karabulut D, Yakan B. 2023. Thymoquinone attenuates doxorubicin-induced lung damage via heat shock proteins, inflammation and endoplasmic reticulum stress. *J. Hell. Vet. Med. Soc.* 74(2): 5569–5576.

Peerapornratana S, Manrique-Caballero CL, Gómez H, Kellum JA. 2019. Acute kidney injury from sepsis: Current concepts, epidemiology, pathophysiology, prevention and treatment. *Kidney Int.* 96(5): 1083–1099. doi:10.1016/j.kint.2019.05.026.

Pottoo FH, Ibrahim AM, Alammar A, Alsinan R, Aleid M, Alshehhi A, Alshehri M, Mishra S, Alhajri NJ. 2022. Thymoquinone: Review of its potential in the treatment of neurological diseases. *Pharmaceuticals.*15(4): 408.

Qadri MM, Alam MF, Khired ZA, Alaqi RO, Khardali AA, Alasmari MM, Alrashah AS, Muzafar HM, Qahl AM. 2023. Thymoquinone ameliorates carfilzomib-induced renal impairment by modulating oxidative stress markers, inflammatory/apoptotic mediators, and augmenting Nrf2 in rats. *Int. J. Mol. Sci.* 24(13): 10621.

Qu Y, Sun Q, Song X, Jiang Y, Dong H, Zhao W, Li C. 2020. Helix B surface peptide reduces sepsis-induced kidney injury via PI3K/Akt pathway. *Nephrology (Carlton)* 25(7): 527–534.

Sayed AAR, Morcos M. 2007. Thymoquinone decreases age-induced NF-κB activation in proximal tubular epithelial cells. *Phytother. Res.* 21(9): 898–899. doi:10.1002/ptr.2184.

Shalan N, Khaleel A, Al-Samydai AJ. 2024. The role of capsaicin and transient receptor potential vanilloid 1 gene activation in preventing kidney stone: A comprehensive review. *Trop. J. Pharm. Res.* 23(6): 1031–1037.

Shou D-W, Li Y-R, Xu X-J, Dai M-H, Zhang W, Yang X, Tu Y-X. 2023. Parthenolide attenuates sepsis-induced acute kidney injury in rats by reducing inflammation. *Evid. Based Complement. Alternat. Med.* 2023: 8759766.

Shraideh Z, Al-Awaida W, Badran D. 2013. Effects of cigarette smoking on histology of trachea and lungs of albino rat. *Res. Opin. Anim. Vet. Sci.* 3(10): 356–362.

Talebi M, Talebi M, Farkhondeh T, Samarghandian S. 2021. Biological and therapeutic activities of thymoquinone: Focus on the Nrf2 signaling pathway. *Phytother. Res.* 35(4): 1739–1753.

Tiba A-T, Qassam H, Hadi NR. 2023. Semaglutide in renal ischemia-reperfusion injury in mice. *J. Med. Life* 16(2): 317.

Trzeciak A, Pietropaoli AP, Kim M. 2020. Biomarkers and associated immune mechanisms for early detection and therapeutic management of sepsis. *Immune Netw.* 20(3): e23.

van der Poll T, Shankar-Hari M, Wiersinga WJ. 2021. The immunology of sepsis. *Immunity* 54(11): 2450–2464.

Venkataraman B, Almarzooqi S, Raj V, Alhassani AT, Alhassani AS, Ahmed KJ, Subramanian VS, Ojha SK, Attoub S, Adrian TE. 2021. Thymoquinone, a dietary bioactive compound, exerts anti-inflammatory effects in colitis by stimulating expression of the colonic epithelial PPAR-γ transcription factor. *Nutrients* 13(4): 1343.

Vivas MC, Villamarín-Guerrero HF, Sanchez CA. 2021. Interleukin-10 (IL-10) 1082 promoter polymorphisms and plasma IL-10 levels in patients with bacterial sepsis. *Rom. J. Intern. Med.* 59(1): 50–57.

Wang M, Zhang J, Gong N. 2022. Role of the PI3K/Akt signaling pathway in liver ischemia reperfusion injury: A narrative review. *Ann. Palliat. Med.* 11(2): 80617–80817.

Zanders L, Kny M, Hahn A, Schmidt S, Wundersitz S, Todiras M, Lahmann I, Bandyopadhyay A, Wollersheim T, Kaderali L. 2022. Sepsis induces interleukin 6, gp130/JAK2/STAT3, and muscle wasting. *J. Cachexia Sarcopenia Muscle* 13(1): 713–727.

Zhai X, Yang Z, Zheng G, Yu T, Wang P, Liu X, Ling Q, Jiang L, Tang W. 2018. Lactate as a potential biomarker of sepsis in a rat cecal ligation and puncture model. *Mediators Inflamm.* 2018(1): 8352727.

JJBS

Volume 19, Number 1,March 2026
ISSN 1995-6673
Pages 59 – 68
https://doi.org/10.54319/jjbs/190106

Jordan Journal of Biological Sciences

Antimicrobial Susceptibility and Resistance Genes Patterns in *Enterococcus* spp. Isolated from Hospitalized Patients from Northern Jordan

Samer F. Swedan*, Sumaia A. "Al Kufahy"

Faculty of Applied Medical Sciences, Department of Medical Laboratory Sciences, Jordan University of Science and Technology, Irbid 22110, Jordan

Received: March 18, 2025; Revised: June 15, 2025; Accepted: July 18, 2025

Abstract

Enterococcus faecalis and *Enterococcus faecium* are normal gut microbiota in humans. They are major opportunistic nosocomial pathogens and are capable of acquiring antimicrobial resistance determinants. Determining the prevalent resistance genotypes and phenotypes among these species should enable better management of clinical infections. In this study, the prevalence of *E. faecalis* and *E. faecium* carriage among hospitalized patients from Northern Jordan was investigated via culture of peri-anal swabs on selective media coupled with biochemical testing. Antimicrobial susceptibility was assessed against 10 antimicrobial agents using the Kirby-Bauer method. The percentages of vancomycin resistance genes (*vanA*, *vanB*, *vanC*, *vanD*, *vanE*, and *vanG*) and linezolid resistance genes (*cfr*, *optrA* and *poxtA*) among the isolates were determined by two multiplex PCR assays followed by gel electrophoresis for detection of amplification products. Overall, among 271 patients sampled, 114 *E. faecalis* and 33 *E. faecium* isolates were recovered (147 total; 54.2% carriage). The highest non-susceptibility to antimicrobials was for rifampin (104/147; 70.7%) and erythromycin (96/147; 65.3%), while the highest susceptibility was for linezolid (147/147; 100%) and tigecycline (145/147; 98.6%). Overall, vancomycin and linezolid resistance genes were relatively infrequent among the isolates. *VanB* (35/147; 23.8%) was the most frequent vancomycin resistance gene, followed by *vanA* and *vanC* (26/147; 17.7% each), *vanG* (23/147; 15.6%), and *vanD* and *vanE* (15/147; 10.2% each). *OptrA* (20/147; 13.6%) was the most frequent linezolid resistance gene, followed by both *cfr* and *poxtA* (7/147; 4.8% each). Several resistance genotypes were associated with specific antimicrobial non-susceptibility patterns. Namely, each of *vanA* and *vanD* with non-susceptibility to ampicillin and teicoplanin, *optrA* with non-susceptibility to doxycycline and chloramphenicol, *vanB* with non-susceptibility to ciprofloxacin, *vanD* with non-susceptibility to chloramphenicol, and *vanG* with non-susceptibility to tigecycline. In conclusion, linezolid and tigecycline remain good treatment choices for *E. faecalis* and *E. faecium* associated infections for hospitalized patients. However, due to continuous changes in antimicrobial resistance patterns among bacteria, periodical monitoring of resistance genotypes and phenotypes should be performed.

Keywords: Vancomycin, Linezolid, antimicrobial agents, resistance genes, *Enterococcus*, carriage, nosocomial.

1. Introduction

Enterococci are Gram-positive bacteria belonging to group D streptococci. They can cope with harsh environmental conditions such as high salt concentrations and a wide temperature range (10 °C to >45 °C) (Arias and Murray, 2012). There are 83 known species among genus *Enterococcus*. Two species are common commensal organisms in the human intestines (*E. faecium* and *E. faecalis*). Other species are occasionally found in the human intestines. *E. faecium* and *E. faecalis* are major opportunistic pathogens causing nosocomial infections. The ability of enterococci to acquire resistance against several antimicrobial agents limits infection treatment choices, and increases rates of morbidity and mortality (Arias and Murray, 2012).

Resistance to antimicrobial agents among enterococci and particularly *E. faecium* and *E. faecalis*, is attributed to three factors; intrinsic resistance, tolerance, and acquired resistance (Kristich *et al.*, 2014). Intrinsic resistance is natural resistance encoded in the bacterial genome. *E. faecium* and *E. faecalis* intrinsically exhibit decreased susceptibility to β-lactams (i.e., penicillinase-resistant penicillins and cephalosporins), and low in vivo concentrations of trimethoprim-sulfamethoxazole, fluoroquinolones, clindamycin, and aminoglycosides (Hollenbeck and Rice, 2012). Acquired resistance is the ability to express resistance to virtually any antimicrobial agent either by mutations or by acquisition of resistance determinants via horizontal gene transfer (Hollenbeck and Rice, 2012). *Enterococci* exhibit acquired resistance to a wide range of antimicrobials such as β-lactams, aminoglycosides, chloramphenicol, erythromycin, tetracyclines, glycopeptides (Hollenbeck and Rice, 2012).

* Corresponding author. e-mail: sfswedan4@just.edu.jo.

Tolerance is the ability of microorganisms to survive at a slow rate of growth in presence of lethal concentrations of bactericidal agents (Brauner *et al.*, 2016). Enterococci are tolerant to bactericidal antimicrobial agents that inhibit cell wall synthesis, such as β-lactams and vancomycin (Kristich *et al.*, 2014).

Glycopeptide antimicrobial agents such as vancomycin and teicoplanin were the drugs of choice for treatment of infections by Gram-positive organisms such as enterococci. The rise of resistance to glycopeptide antimicrobials limited treatment options to a few antimicrobial agents such as tetracyclines (tigecycline), lipopeptides (daptomycin), and oxazolidinones (linezolid and tedizolid) (Bender *et al.*, 2018). Overall, eight glycopeptide resistance genes have been described to date among vancomycin resistant enterococci (VRE); *vanA, vanB, vanC1, vanC2, vanC3, vanD, vanE, vanG* (Bhatt *et al.*, 2015).

Linezolid, the first member of oxazolidinones, was approved in 2000 in the USA to treat VRE and other resistant Gram-positive pathogens such as methicillin-resistant *Staphylococcus aureus* (MRSA) and penicillin-resistant pneumococci (Zahedi Bialvaei *et al.*, 2017). Linezolid acts by blocking bacterial protein synthesis, leading to either death or growth inhibition. Unlike other protein inhibitors that interfere with the elongation step of protein synthesis, linezolid blocks the initiation step by binding to the A site on the bacterial 23S rRNA of the 50S subunit (Hashemian *et al.*, 2018). The first linezolid resistance case was reported in 2001, just one year following linezolid's approval for clinical use in the USA. Since then, several studies have reported the appearance of linezolid resistance among enterococci worldwide (Wada *et al.*, 2024).

Several mechanisms mediating resistance to linezolid have been described to date among enterococci. These include point mutations in 23S rRNA genes (e.g., T2500A, G2447T, C2534T, G2215A, and T2504A), mutations in ribosomal proteins L3 and/or L4, the acquisition of the plasmid-borne ribosomal methyltransferase gene *cfr* or its variant *cfr(B)*, and the acquisition of the novel genes *optrA* and *poxtA* encoding for an ABC-F transporter protein (Deshpande *et al.*, 2015, Bi *et al.*, 2018, Hao *et al.*, 2019). The first transferable oxazolidinone resistance genes to emerge in enterococci are *cfr* and *cfr(B)*. The products of these two genes methylate carbon number 8 of the A2503 nucleotide located in the linezolid binding site on the bacterial 23S rRNA. This prevents binding of linezolid to the A site on the bacterial ribosome, thus preventing its antibacterial activity (LaMarre *et al.*, 2013). The *optrA* and *poxtA* oxazolidinone resistance genes encode ribosomal protection proteins of the ABC-F family (Hao *et al.*, 2019). *OptrA* and *poxtA* confer resistance to several antimicrobials including oxazolidinones, macrolides, tetracyclines, streptogramins, lincosamides, ketolides, pleuromutilins, and phenicols (Antonelli *et al.*, 2018).

Tigecycline, which was approved in 2006, is the first member of the glycylcycline class of antimicrobial agents. It is a broad-spectrum antimicrobial agent that is active against Gram-positive bacteria such as penicillin-resistant *Streptococcus pneumoniae*, MRSA, methicillin-resistant *Staphylococcus epidermidis* (MRSE), and VRE. Tigecycline is structurally related to minocycline and tetracycline. However, the presence of an *N,N,*-dimethylglycylamido group at the 9th position of the minocycline molecule makes tigecycline effective against tetracycline-resistant bacteria and expands its spectrum of activity. Tigecycline is a bacteriostatic antimicrobial agent that inhibits bacterial protein synthesis by binding to the 30S ribosome. This binding inhibits the elongation stage of protein synthesis (Yaghoubi *et al.*, 2022).

Tigecycline resistance occurs due to drug efflux from the bacterial cell, or ribosomal protection via decreased binding of tigecycline to the bacterial 30S ribosome. In tigecycline resistant enterococci, the *tet(L)* gene is associated with antibiotic efflux, while *tet(M)* and *rpsJ* genes are associated with ribosomal protection. Acquisition of *tet(L)* which encodes for Major Facilitator Superfamily (MFS)-type efflux pump decreases enterococcal susceptibility to tigecycline by mediating drug efflux outside the cell. Acquisition of *tet(M)* or a mutation in *rpsJ* (encoding the S10 protein of the 30S ribosomal subunit) results in a decrease in enterococcal susceptibility to tigecycline by preventing the binding of tigecycline to the bacterial 30S ribosome (Bender *et al.*, 2018).

The surveillance of vancomycin, linezolid, and tigecycline resistant enterococcal isolates and the associated resistance genes have not been investigated in Jordan. This is the first study to report on the prevalence of vancomycin, linezolid, and tigecycline non-susceptibility in enterococci, namely *E. faecium* and *E. faecalis* from patients admitted to several hospitals in Northern Jordan. The prevalence of several vancomycin resistance genes (*vanA, vanB, vanC1, vanC2, vanD, vanE, vanG*) and linezolid resistance genes (*cfr, optrA* and *poxtA*) was also determined and correlated to the non-susceptibility phenotypes.

2. Materials and Methods

2.1. Collection of Isolates

Study was approved by the IRB committee of Jordan University of Science and Technology (Approval# 32/127/2019; Date: 10/10/2019). All participants or the legal guardian provided informed written consent before study enrollment. Peri-anal swabs were collected from in-patients at hospitals in Northern Jordan (King Abdullah University Hospital, Princess Rahma Hospital, Princess Badea'a Hospital, Al-Ramtha Hospital, Al-Yarmouk Governmental Hospital, and Princess Basma Hospital). The swabs were inoculated on an *Enterococcus*-selective medium; bile esculin azide agar plates (Sigma-Aldrich, St. Louis, Missouri, United States). The plates were incubated aerobically at 35ºC for 18-24 hours. *Enterococcus* colonies appeared small and transparent and were surrounded by blackened media due to hydrolysis of esculin to esculetin (a black compound) and glucose.

2.2. Identification of Isolates

Isolates that hydrolyzed esculin to esculetin were identified as enterococci. To further investigate the isolates to the species level, one colony from the primary culture was inoculated in two broth media tubes (phenol red sorbitol broth and phenol red raffinose broth). The original color of these two broth media is reddish-orange. The fermentation of the sugar (sorbitol or raffinose) produces acids which converts the original color to yellow. Isolates

with a positive result for sorbitol fermentation were identified as *Enterococcus faecalis*, while isolates with a positive result for raffinose fermentation were identified as *Enterococcus faecium*. Isolates that were negative for both sorbitol and raffinose fermentation were identified as non-*faecalis* and non-*faecium* enterococci and were excluded from further analyses. All isolates were grown in LB broth (Himedia, Maharashtra, India) overnight. Next, 0.7 mL of the broth was mixed with 0.35 mL of sterile 50% glycerol in a 2 mL cryotube, and the tube was stored at -80ºC.

2.3. Antimicrobial Susceptibility Testing

Muller Hinton Agar (MHA) (Himedia, Maharashtra, India) was inoculated from the frozen cultures and incubated aerobically at 35ºC for 18-24 hours. Next, three to four well isolated colonies having the same morphology were transferred using a sterile disposable loop, from the MHA plate into a sterile tube containing 2.0 mL sterile normal saline. The colonies were re-suspended by shaking the loop in the normal saline solution to create a suspension with a turbidity equivalent to 0.5 McFarland. The suspension was used to inoculate MHA plates for antimicrobial susceptibility testing according to the Kirby-Bauer disk diffusion method. A swab was used to inoculate MHA in 3 directions. The inoculated plates were covered and left for 15 minutes in the upright position before placement of antibiotic disks at least 2 cm apart utilizing a sterile lancet. The antimicrobial agents used were ampicillin (10 µg), doxycycline (30 µg), teicoplanin (30 µg), linezolid (30 µg), ciprofloxacin (5 µg), erythromycin (15 µg), vancomycin (30 µg), rifampin (5 µg), chloramphenicol (30 µg), and tigecycline (15 µg). All antibiotic disks were obtained from Oxoid (Basingstoke, Hampshire, United Kingdom).

Antimicrobial susceptibility testing was done using two MHA plates per isolate (5 antibiotic disks per plate). The plates were incubated at 37ºC for 18 hours. The diameter of the inhibition zones was measured in mm and was interpreted according to CLSI (2023) guidelines. *Enterococcus faecalis* ATCC 29212, *Enterococcus faecalis* 19433, and *Escherichia coli* ATCC 25922 were used as controls during antimicrobial susceptibility testing.

2.4. DNA Extraction

For DNA extraction, the G-spin ™ genomic DNA extraction kit (Catalogue #17121, iNtRON Biotechnology, Inc., Korea), was used as described by the manufacturer. One colony from each sample was inoculated in Muller Hinton broth (Himedia, Maharashtra, India) overnight (18-24 hours). Next, 1 mL of the broth was transferred to a 1.5 mL Eppendorf tube and centrifuged for 1 min at 13,000 rpm, and the supernatant was discarded. To improve yield of the extracted DNA, the previous step was repeated 3 times (by resuspending the pellet in 1 mL of broth each time). After obtaining the bacterial pellet, 50 µL of Pre-Buffer and 3 µL of Lysozyme solution were added, mixed well, and the tube incubated for 15 min at 37°C. Next, 250 µL of G-Buffer solution was added, mixed, and incubated at 65°C for 15 min. After cell lysis, 250 µL of the Binding Buffer was added and mixed well by pipetting (at least 10 times). The cell lysates were loaded on columns containing silica membranes and were centrifuged for 1 min at 13000 rpm. Next, 2 washing steps were done (by adding washing buffer A, centrifugation, removing the solution then adding washing buffer B, centrifugation and discarding the solution). Before the last step (the elution step) was done, the column was centrifuged for 1 min at 13,000 rpm and the column was placed in a new sterile Eppendorf tube. Next, 100 µL of Elution Buffer was directly placed onto the membrane of the column, incubated at room temperature for 1 min and centrifuged for 1 min at 13,000 rpm. DNA samples were stored at -18°C until used for PCR. *Enterococcus faecalis* ATCC 29212 and *Enterococcus faecalis* 19433, were used as controls during PCR detection of resistance genes.

2.5. Multiplex PCR

The protocol of the multiplex PCR for detection of glycopeptide (vancomycin) resistance genes (*vanA, vanB, vanC1, vanC2, vanD, vanE, vanG*) and primer sequences were obtained from previously published work (Bhatt *et al.*, 2015). Each PCR consisted of 10 µL of template DNA, 1.25 µL of each primer (each at 10 µmol/L), 0.4 µL Taq DNA Polymerase (250 U/mL), 5 µL of PCR buffer (10X) with $MgCl_2$ (15 mM), 0.25 µL dNTPs (10 mM), and nuclease free water up to 50 µL. The primer sequences used are shown in Table 1. PCR thermal cycling was done using initial denaturation at 94°C for 3 min, followed by 35 cycles of 94°C for 1 min, 45°C for 1 min, and 72°C for 1 min, and a final extension at 72°C for 7 min. PCR without the DNA template was used as negative control.

Table 1. Primers used for multiplex PCR to detect vancomycin resistance genes.

Primer	Sequence (5' to 3')	Size of the product
VanA(forward)	GGGAAAACGACAATTGC	732 bp
VanA (reverse)	GTACAATGCGGCCGTTA	
VanB (forward)	ACGGAATGGGAAGCCGA	647 bp
VanB (reverse)	TGCACCCGATTTCGTTC	
VanC (forward)**	ATGGATTGGTAYTKGTAT*	815/827 bp
VanC (reverse)**	TAGCGGGAGTGMCYMGTAA*	
VanD (forward)	TGTGGGATGCGATATTCAA	500 bp
VanD (reverse)	TGCAGCCAAGTATCCGGTAA	
VanE (forward)	TGTGGGATCGGAGCTGCAG	430 bp
VanE (reverse)	ATAGTTTAGCTGGTAAC	
VanG (forward)	CGGCATCCGCTGTTTTTGA	941 bp
VanG (reverse)	GAACGATAGACCAATGCCTT	

*K = G or T; M = A or C; Y= C or T **detect VanC1 and VanC2

Primer sequences were obtained from a previous study (Bhatt *et al.*, 2015).

The protocol for the multiplex PCR detection of linezolid resistance genes (*cfr*, *optrA* and *poxtA*) was obtained from previously published work (Bender *et al.*, 2019). Primer sequences were obtained from previously published works as shown in table 2 (Kehrenberg and Schwarz, 2006, Brenciani *et al.*, 2016, Bender *et al.*, 2019). Each PCR had 5-10 ng of DNA template, 0.1 µM of each primer, 12.5 µL 2X DreamTaq Master Mix, and nuclease free water up to 25 µL. PCR thermal cycling was done using initial denaturation at 96°C for 2 min, followed by 30 cycles of 96°C for 30 s, 50°C for 30 s, and 72°C for 30 s, and a final extension at 72°C for 5 min. PCR without the DNA template was used as negative control.

Table 2. Primers used in the multiplex PCR to detect linezolid resistance genes.

Primer	Sequence (5' to 3')	Size of the product
Cfr (forward)	TGAAGTATAAAGCAGGTTGGGAGTCA	746 bp
Cfr (reverse)	ACCATATAATTGACCACAAGCAGC	
OptrA (forward)	TACTTGATGAACCTACTAACCA	422 bp
OptrA (reverse)	CCTTGAACTACTGATTCTCGG	
PoxtA (forward)	AAAGCTACCCATAAAATATC	533 bp
PoxtA (reverse)	TCATCAAGCTGTTCGAGTTC	

Primer sequences were obtained from previous studies (Kehrenberg and Schwarz, 2006, Brenciani *et al*., 2016, Bender *et al*., 2019).

2.6. Gel Electrophoresis

Products from PCR were separated on 2% agarose gels containing redsafe dye. Ten microliters of 100 bp ladder (iNtRON Biotechnology, Inc., Korea) were loaded in the first well to allow identification of band sizes. Ten microliters of PCR products were loaded in the remaining wells. Electrophoresis was performed using constant voltage (90 V) for 1 h. Bands on the gel were visualized using a UV transilluminator provided with a gel documentation system using the Quantity One software (Biorad, USA). Band sizes were determined by comparison with the 100 bp DNA ladder.

2.7. Statistical Analysis

Statistical analysis and tables were done using SPSS software (version 26, IBM, Armonk, NY, USA). Charts were created using Microsoft Excel (Microsoft, Redmond, Washington, United States). Pearson Chi-Square test was used to determine the significance of the observed frequencies. A *P* value of less than 0.05 was considered statistically significant.

3. Results

3.1. Isolates Identification and Distribution

Overall, 271 anal swabs were collected from patients admitted to several hospitals in Northern Jordan. Among them 114 *E. faecalis* and 33 *E. faecium* isolates were identified based on the hydrolysis of esculin in bile esculin azide agar and whether the isolate fermented sorbitol or raffinose sugar. The overall carriage of *Enterococcus* species was 54.2% (147/271). Most samples were from King Abdullah University Hospital. The distribution of *E. faecalis* or *E. faecium* isolates according to patient sex and hospital is shown in Table 3.

Table 3. Distribution of *Enterococcus* spp. isolates according to sex and hospital.

		Isolates recovered				Total	P value
		E. faecalis		*E. faecium*			
		n	%	n	%		
Hospital	Badea'a	6	85.7	1	14.3	7	0.360
	KAUH	64	71.9	25	28.1	89	
	Rahma	30	88.2	4	11.8	34	
	Al-Ramtha	5	83.3	1	16.7	6	
	Yarmouk	9	81.8	2	18.2	11	
Sex	Female	66	86.8	10	13.2	76	0.005
	Male	48	67.6	23	32.4	71	

KAUH: King Abdulla University Hospital.

Anal swabs were collected from different hospital departments (internal medicine, general surgery, gynecology and obstetrics, pediatrics, psychiatry, neurology, ear, nose and throat, orthopedic, ophthalmology; Data not shown). Most swabs were collected from internal medicine, general surgery, pediatrics and gynecology and obstetrics departments. Isolates were obtained from all age groups; from 18 days to 81 years. The mean age was 18.8 ± 22.0 years.

3.2. Antimicrobial Susceptibility Profile

The antimicrobial susceptibility of *E. faecalis* or *E. faecium* isolates is presented in Figure 1. The results are classified into susceptible and non-susceptible groups (intermediately susceptible + resistant). The highest non-susceptibility was against rifampin (70.7%), erythromycin (65.3%), and doxycycline (56.5%). All isolates were susceptible to linezolid. Following linezolid, the highest susceptibility was against tigecycline (98.6%), teicoplanin (98%), and vancomycin (98%).

No significant differences in antimicrobial susceptibility results were observed according to species for all antimicrobials except ampicillin and doxycycline. Susceptibility of *E. faecalis* to ampicillin was significantly higher compared to *E. faecium*. On the other hand, *E. faecalis* had significantly lower susceptibility to doxycycline compared to *E. faecium*.

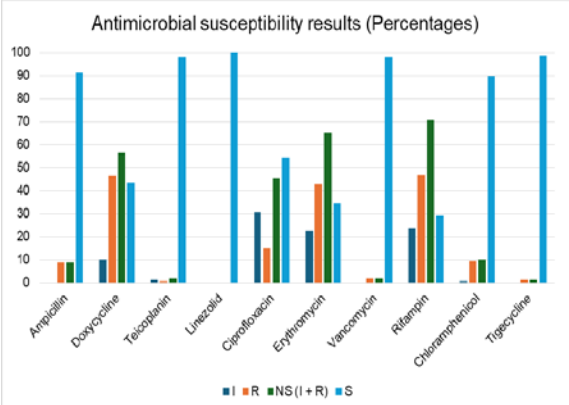

Figure 1. Antimicrobial susceptibility of isolates. All data represent percentages. Antimicrobial susceptibility of the isolates was determined using the Kirby-Bauer method. Interpretation of inhibition zones (if any) was based on CLSI 2023 guidelines. I: intermediate susceptibility. NS: non-susceptible. R: resistant. S: susceptible.

3.3. Resistance Genes

The frequencies of vancomycin and linezolid resistance genes among the isolates were determined by multiplex PCR. Table 4 shows the frequencies of the detected resistance genes among the isolates. *VanB* was the most frequent at 23.8% (35/147), followed by *vanA* and *vanC* (26/147; 17.7% each), *vanG* (23/147; 15.6%), *optrA* (20/147; 13.6%), *vanD* and *vanE* (15/147; 10.2% each), and finally *cfr* and *poxtA* (7/147; 4.8% each) (Figure 2).

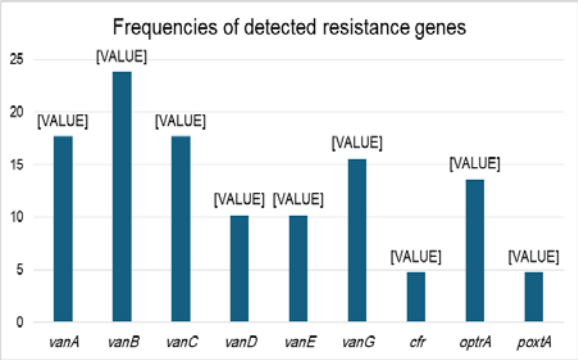

Figure 2. Frequencies of the resistance genes among the isolates. Resistance genes were amplified using two multiplex PCR assays followed by separation on agarose gels and detection.

The association of resistance genes with antimicrobial susceptibility profile was also investigated (Tables 4 and 5). The results show a significant association between each of *vanA* and *vanD* and non-susceptibility to ampicillin and teicoplanin. *OptrA* was associated with non-susceptibility to doxycycline and chloramphenicol. *VanB* was associated with non-susceptibility to ciprofloxacin. *VanD* was associated with non-susceptibility to chloramphenicol. *VanG* was associated with non-susceptibility to tigecycline. Interestingly, *cfr* was associated with susceptibility to ciprofloxacin.

Table 4. The association of resistance genes with antimicrobial susceptibility profile of the isolates (part 1).

		Ampicillin					Doxycycline					Teicoplanin					Linezolid			Ciprofloxacin				
		NS		S			NS		S			NS		S			S			NS		S		
Resistance Gene		n	%	n	%	P value	n	%	n	%	P value	n	%	n	%	P value	n	%	P value	n	%	n	%	P value
vanA	N	8	6.6	113	93.4	0.040	67	55.4	54	44.6	0.565	1	0.8	120	99.2	0.025	121	100	-	53	43.8	68	56.2	0.351
	P	5	19.2	21	80.8		16	61.5	10	38.5		2	7.7	24	92.3		26	100		14	53.8	12	46.2	
vanB	N	11	9.8	101	90.2	0.455	63	56.3	49	43.8	0.926	3	2.7	109	97.3	0.328	112	100	-	45	40.2	67	59.8	0.019
	P	2	5.7	33	94.3		20	57.1	15	42.9		0	0.0	35	100		35	100		22	62.9	13	37.1	
vanC	N	9	7.4	112	92.6	0.195	71	58.7	50	41.3	0.243	2	1.7	119	98.3	0.473	121	100	-	53	43.8	68	56.2	0.351
	P	4	15.4	22	84.6		12	46.2	14	53.8		1	3.8	25	96.2		26	100		14	53.8	12	46.2	
vanD	N	5	3.8	127	96.2	0.000	72	54.5	60	45.5	0.164	1	0.8	131	99.2	0.001	132	100	-	60	45.5	72	54.5	0.929
	P	8	53.3	7	46.7		11	73.3	4	26.7		2	13.3	13	86.7		15	100		7	46.7	8	53.3	
vanE	N	13	9.8	119	90.2	0.203	75	56.8	57	43.2	0.796	3	2.3	129	97.7	0.555	132	100	-	59	44.7	73	55.3	0.525
	P	0	0.0	15	100		8	53.3	7	46.7		0	0.0	15	100		15	100		8	53.3	7	46.7	
vanG	N	10	8.1	114	91.9	0.440	71	57.3	53	42.7	0.652	3	2.4	121	97.6	0.451	124	100	-	57	46.0	67	54.0	0.826
	P	3	13.0	20	87.0		12	52.2	11	47.8		0	0.0	23	100		23	100		10	43.5	13	56.5	
cfr	N	11	7.9	129	92.1	0.060	80	57.1	60	42.9	0.457	3	2.1	137	97.9	0.696	140	100	-	67	47.9	73	52.1	0.013* I
	P	2	28.6	5	71.4		3	42.9	4	57.1		0	0.0	7	100		7	100		0	0.0	7	100	
optrA	N	9	7.1	118	92.9	0.059	67	52.8	60	47.2	0.022	3	2.4	124	97.6	0.487	127	100	-	61	48.0	66	52.0	0.132
	P	4	20.0	16	80.0		16	80.0	4	20.0		0	0.0	20	100		20	100		6	30.0	14	70.0	
poxtA	N	11	7.9	129	92.1	0.060	80	57.1	60	42.9	0.457	3	2.1	137	97.9	0.696	140	100	-	64	45.7	76	54.3	0.882
	P	2	28.6	5	71.4		3	42.9	4	57.1		0	0.0	7	100		7	100		3	42.9	4	57.1	

I: Inverse association. N: negative. NS: non-susceptible. P: positive. S: susceptible. P < 0.05 are significant (Chi-square test).

Table 5. The association of resistance genes with antimicrobial susceptibility profile of the isolates (part 2).

Resistance Gene		Erythromycin					Vancomycin					Rifampin					Chloramphenicol					Tigecycline				
		NS		S			NS		S			NS		S			NS		S			NS		S		
		n	%	n	%	P value	n	%	n	%	P value	n	%	n	%	P value	n	%	n	%	P value	n	%	n	%	P value
vanA	N	75	62.0	46	38.0	0.068	2	1.7	119	98.3	0.473	84	69.4	37	30.6	0.446	11	9.1	110	90.9	0.336	2	1.7	119	98.3	0.509
	P	21	80.8	5	19.2		1	3.8	25	96.2		20	76.9	6	23.1		4	15.4	22	84.6		0	0.0	26	100	
vanB	N	74	66.1	38	33.9	0.727	3	2.7	109	97.3	0.328	77	68.8	35	31.3	0.341	12	10.7	100	89.3	0.715	1	0.9	111	99.1	0.381
	P	22	62.9	13	37.1		0	0.0	35	100		27	77.1	8	22.9		3	8.6	32	91.4		1	2.9	34	97.1	
vanC	N	77	63.6	44	36.4	0.359	2	1.7	119	98.3	0.473	85	70.2	36	29.8	0.774	13	10.7	108	89.3	0.641	2	1.7	119	98.3	0.509
	P	19	73.1	7	26.9		1	3.8	25	96.2		19	73.1	7	26.9		2	7.7	24	92.3		0	0.0	26	100	
vanD	N	84	63.6	48	36.4	0.207	2	1.5	130	98.5	0.181	96	72.7	36	27.3	0.118	11	8.3	121	91.7	0.026	2	1.5	130	98.5	0.631
	P	12	80.0	3	20.0		1	6.7	14	93.3		8	53.3	7	46.7		4	26.7	11	73.3		0	0.0	15	100	
vanE	N	88	66.7	44	33.3	0.304	3	2.3	129	97.7	0.555	91	68.9	41	31.1	0.153	13	9.8	119	90.2	0.673	1	0.8	131	99.2	0.061
	P	8	53.3	7	46.7		0	0.0	15	100		13	86.7	2	13.3		2	13.3	13	86.7		1	6.7	14	93.3	
vanG	N	79	63.7	45	36.3	0.345	3	2.4	121	97.6	0.451	90	72.6	34	27.4	0.257	13	10.5	111	89.5	0.795	0	0.0	124	100	0.001
	P	17	73.9	6	26.1		0	0.0	23	100		14	60.9	9	39.1		2	8.7	21	91.3		2	8.7	21	91.3	
cfr	N	93	66.4	47	33.6	0.201	3	2.1	137	97.9	0.696	100	71.4	40	28.6	0.417	14	10.0	126	90.0	0.715	2	1.4	138	98.6	0.750
	P	3	42.9	4	57.1		0	0.0	7	100		4	57.1	3	42.9		1	14.3	6	85.7		0	0.0	7	100	
optrA	N	84	66.1	43	33.9	0.592	3	2.4	124	97.6	0.487	94	74.0	33	26.0	0.028	9	7.1	118	92.9	0.002	1	0.8	126	99.2	0.131
	P	12	60.0	8	40.0		0	0.0	20	100		10	50.0	10	50.0		6	30.0	14	70.0		1	5.0	19	95.0	
poxtA	N	91	65.0	49	35.0	0.727	3	2.1	137	97.9	0.696	99	70.7	41	29.3	0.968	15	10.7	125	89.3	0.361	2	1.4	138	98.6	0.750
	P	5	71.4	2	28.6		0	0.0	7	100		5	71.4	2	28.6		0	0.0	7	100		0	0.0	7	100	

N: negative. NS: non-susceptible. P: positive. S: susceptible. $P < 0.05$ are significant (Chi-square test).

4. Discussion

E. faecium and *E. faecalis* are members of the gut microbiota of the human intestines. Yet they are considered major opportunistic microorganisms associated frequently with nosocomial infections. The intrinsically low susceptibility of enterococci to several antimicrobial drugs and their ability to express and acquire resistance against several antimicrobial agents limits treatment choices and leads to increased morbidity and mortality (Arias and Murray, 2012).

In this study, *E. faecalis* and *E. faecium* isolates were recovered from peri-anal swabs from patients admitted to hospitals in Northern Jordan. Antimicrobial susceptibility to 10 antimicrobial agents and several resistance genes were investigated. This epidemiological data should enable better management of infections and should enable comparison with countries in the MENA and worldwide.

Similar to reports from Oman, Italy, Iran, and Jordan, the percentage of *E. faecalis* isolates was higher than that for *E. faecium* (77.6% vs. 22.4%, respectively. Regarding patient's sex, *E. faecalis* was significantly more frequent among females. While *E. faecium* was significantly more frequent among males. This is in agreement with a study from Kenya; *E. faecalis* was isolated more frequently from females (56.7%) than males. While 6 of the 7 *E. faecium* isolates were from males (Georges *et al.*, 2022).

In our study, a low percentage (5.3%) of *E. faecalis* isolates were non-susceptible to ampicillin. This is lower than that from Italy, Sweden, Turkey, China, Korea, Nigeria, Uganda, Kuwait, Indonesia, Israel and India. On the other hand, Australia and USA had the lowest non-susceptibility percentage to ampicillin (0%), whereas India had the highest non-susceptibility to ampicillin (74.1%) (Guan *et al.*, 2024).

Teicoplanin non-susceptibility in *E. faecalis* was very low (0.9%). This is in line with percentages from Cuba, Turkey, and Poland. On the other hand, Australia, Lebanon, Sweden and Germany had 0% teicoplanin non-susceptibility. While, Taiwan and Hungary had 81% and 80% non-susceptibility, respectively (Guan *et al.*, 2024).

All *Enterococcus* isolates were sensitive to linezolid. This is in agreement with *E. faecalis* susceptibility results to linezolid in Taiwan, Australia, and Germany. In contrast, high non-susceptibility against linezolid was reported in Turkey at 10% (Guan *et al.*, 2024).

Ciprofloxacin non-susceptibility in *E. faecalis* was moderately high (47.4%) compared to other countries. Several countries had lower non-susceptibility percentages; Cuba, Brazil, Lebanon, Poland, Nigeria, Romania, Turkey, China, Iran, Hong Kong, Uganda, Indonesia, Australia. In contrast, Taiwan had high non-susceptibility to ciprofloxacin at 83% (Guan *et al.*, 2024).

Erythromycin non-susceptibility in *E. faecalis* was relatively high at 64%, which is comparable to percentages from China and Lebanon. Cuba, Brazil, Italy, Germany, Egypt, Nigeria, Kuwait, Lebanon,

Uganda, Iran, and Australia, had lower non-susceptibility percentages than our study. In contrast, the USA, Algeria, Turkey, India, China, and South Korea had higher non-susceptibility percentages, with South Korea having the highest percentage at 91% (Guan *et al.*, 2024).

Vancomycin non-susceptibility in *E. faecalis* was low at 1.8%, which is similar to percentages from Poland, Turkey, China, and Romania. Some countries had lower non-susceptibility percentages; Australia, South Korea, Lebanon, Sweden, Cuba, Germany, and Algeria, while other countries exhibited higher vancomycin non-susceptibility; USA, Taiwan, India, Indonesia, Iran, Pakistan, Kuwait, Egypt, Nigeria, Israel, Hungary, Italy, and Brazil. Among these, Taiwan had the highest vancomycin non-susceptibility (99%) (Guan *et al.*, 2024).

Rifampin non-susceptibility in *E. faecalis* was high at 71.1%. Other countries had lower non-susceptibility percentages; Egypt, Lebanon, Cuba, Turkey, and Iran, while other countries had higher vancomycin non-susceptibility; Taiwan, South Korea, and Italy, with South Korea having the highest percentage (96%) (Guan *et al.*, 2024).

Chloramphenicol non-susceptibility in *E. faecalis* was relatively low at 12.3%. This percentage is similar to that from South Korea. Some countries had lower non-susceptibility percentages; Egypt and Sweden, while other countries had higher rifampin non-susceptibility; Hong Kong, Iran, China, India, Kuwait, Lebanon, Algeria, Italy, Brazil, and Cuba, with Italy having the highest percentage (73%) (Guan *et al.*, 2024).

Tigecycline non-susceptibility in *E. faecalis* was very low at 0.9%, which is similar to that from Italy. Other countries such as Turkey, Iran, Hungary, China, Poland, and USA reported 0% tigecycline non-susceptibility (Guan *et al.*, 2024).

Doxycycline non-susceptibility in *E. faecalis* was relatively high at 64%. Countries such as India, Italy, China, and Pakistan, reported lower non-susceptibility percentages, while countries such as Germany and Iran had relatively comparable non-susceptibility percentages of 68.9% and 73.6%, respectively (Guan *et al.*, 2024).

Among the tested antimicrobials, rifampin, erythromycin, doxycycline, and ciprofloxacin, had the highest non-susceptibility in *E. faecalis*. Therefore, these antimicrobials may not be good choices for the treatment of infections caused by *E. faecalis*. This finding agrees with studies worldwide (Guan *et al.*, 2024). On the other hand, *E. faecalis* had high susceptibility to tigecycline, teicoplanin, linezolid, and vancomycin. Therefore, these antimicrobials may be considered when dealing with *E. faecalis* infections, which is in agreement with studies worldwide (Guan *et al.*, 2024).

Unlike Jordan, wealthy countries that have an advanced health care system and strict strategies for the use of antimicrobials for managing infections (such as Australia, Sweden, and Poland) had lower *E. faecalis* non-susceptibility percentages than our study (Guan *et al.*, 2024). In contrast, countries in Southeast Asia such as Taiwan and South Korea, and Italy, among other countries, had higher *E. faecalis* non-susceptibility percentages compared to our study. This may be attributed to limited access to effective antimicrobials, unregulated administration of antimicrobials, incomplete antibiotic treatment due to financial constraints, practices of healthcare professionals, improper antimicrobial use, incomplete antibiotic supply chain, poor hygiene, insufficient education, and absence of a comprehensive antimicrobial stewardship program. In addition, specifically to Southeast Asian countries, they are popular producers of livestock and poultry, which serve as sources for the spread of antimicrobial resistance among bacteria (Guan *et al.*, 2024).

E. faecium is considered one of the ESKAPE (*Enterococcus faecium*, *Staphylococcus aureus*, *Klebsiella pneumoniae*, *Acinetobacter baumannii*, *Pseudomonas aeruginosa*, and *Enterobacter* spp.) pathogens and is capable of demonstrating multi-drug resistance (Miller and Arias, 2024).

Similar to other studies, *E. faecium* non-susceptibility percentages to ampicillin, teicoplanin, erythromycin, vancomycin, and tigecycline, were higher than that in *E. faecalis* (insignificantly higher except for ampicillin). Chloramphenicol, rifampin, and ciprofloxacin non-susceptibility percentages in *E. faecium* were insignificantly lower than that in *E. faecalis*, and this could be explained by the small sample size (n=33 for *E. faecium*). *E. faecium* exhibited significantly lower non-susceptibility against doxycycline compared to *E. faecalis* (30.3%;10/33 vs. 64.0%;73/114), respectively, and this agrees with a study from Canada, in which the non-susceptibility to doxycycline was lower for *E. faecium* (39.5%) than that for *E. faecalis* (67.8%) (Kim *et al.*, 2024).

The lowest non-susceptibility percentages in *E. faecium* were against linezolid and tigecycline at 0%, followed by vancomycin and chloramphenicol with a non-susceptibility percentage of 3% for each, and this agrees with a worldwide review study in which the lowest non-susceptibility percentages were against linezolid and tigecycline. Thus, linezolid and tigecycline are considered drugs of choice for treating *E. faecium* infections in addition to *E. faecalis* infections (Jabbari Shiadeh *et al.*, 2019).

E. faecium isolates had a low vancomycin non-susceptibility percentage of 3% (1/33), and this was similar to non-susceptibility percentages from Mexico, Tunisia, Algeria, Turkey, Bangladesh, Bulgaria, Sweden, Norway, Finland, France, Belgium, Denmark, Iceland. This low percentage is lower than the mean worldwide percentage of 10%. The lowest vancomycin non-susceptibility in *E. faecium* was recorded in the Netherlands with a percentage of 0.1%. In contrast, other countries had higher non-susceptibility percentages such as India, Taiwan, Spain, United Kingdom, Poland, Egypt, Saudi Arabia, Israel, Cyprus, Italy, Germany, Portugal, USA, Chile, Brazil, Colombia, Australia, Japan, Iran, and Ireland, with Brazil having the highest non-susceptibility at 67% (Jabbari Shiadeh *et al.*, 2019).

E. faecium isolates in our study exhibited lower non-susceptibility percentages to several antimicrobials (ampicillin, teicoplanin, linezolid, vancomycin, ciprofloxacin, chloramphenicol, erythromycin, tigecycline), than those worldwide. However, *E. faecium* non-susceptibility against teicoplanin and vancomycin was lower in Africa, and was higher in America, Europe, Southeast Asia, Western pacific, and the Eastern Mediterranean, than that in our study. Furthermore, *E.*

faecium non-susceptibility against linezolid and ampicillin in our study was lower than that of all WHO regions (Jabbari Shiadeh *et al.*, 2019). Differences in the percentages of non-susceptibility among regions could be attributed to several factors, including the prevalence of resistant strains and resistance genes, socioeconomic differences, health-care practices, the use and the misuse of antimicrobials, among others.

The non-susceptibility percentages to antimicrobials in our study were mostly similar to those of previous studies. Non-susceptibility percentages in our study compared to previous studies from Jordan respectively were as follows: (2% vs. 0%) to teicoplanin, (10.2% vs. 0%) to chloramphenicol, (2% vs. 0-4%) to vancomycin, (8.8% vs. 0-15%) to ampicillin, (45.6% vs. 0-28.6%) to ciprofloxacin, (65.3% vs. 37.5%) to erythromycin, (1.4% vs. 0.9%), to tigecycline, (0% vs. 1.5%) to linezolid (Al-Tamimi *et al.*, 2022, Jordan Ministry of Health, 2023).

Regarding *van* genes, studies have shown that *vanA* was the most frequent resistance gene among *E. faecalis* and *E. faecium.* In addition, most or all VRE were positive for *vanA*. For example, 54 out of 59 VRE (91.5% of VRE) isolated from hospitalized patients in Iran were positive for *vanA*. While none were positive for *vanB* (Moosavian *et al.,* 2018). This was not consistent with our findings in which 35 out of 147 (23.8%) isolates were positive for *vanB* gene, and 26 out of 147 (17.7%) isolates were positive for each of *vanA* and *vanC*. Interestingly, a study from Australia showed that among 331 rectal specimens, 58 (17.5%) were VRE containing *vanB*, but none had *vanA*, and this was explained by the endemic spread of *vanB* among VRE in that region. *VanB* unlike *vanA*, is located on the bacterial chromosome. Thus, the likelihood of its transmission is lower than that of *vanA* (Moosavian *et al.*, 2018).

A study from Algeria demonstrated that the high non-susceptibility levels observed in strains from the ICU were associated with *vanA*. Co-existence of vanA/vanC was identified in 24.4% of *Enterococcus* spp. In surgical wards, *vanB* and *vanC* were the most frequent among isolates and were associated with intermediate non-susceptibility levels. In contrast, *vanA* was not detected among surgical ward strains (Zerrouki *et al.*, 2021).

In our study, 8 (5.4%) *Enterococcus* isolates had co-existence of vanA/vanC. Three out of 147 isolates were non-susceptible to vancomycin (2 *E. faecalis* isolates and 1 *E. faecium* isolate). The vancomycin resistant *E. faecium* isolate was positive for *vanA, vanC*, and *vanD*, while, both vancomycin resistant *E. faecalis* isolates were negative to all *van* genes. There was no statistically significant association between vancomycin non-susceptibility and *van* genes, likely due to the low frequency of vancomycin non-susceptible isolates.

Co-existence of *vanA/vanB* was reported in previous studies. A study from Iran showed that among 181 *Enterococcus* isolates, 38 (46.9%) carried *vanA*, 21 (25.9%) carried *vanB*, and 18 (22.2%) carried both *vanA* and *vanB*, while *vanC* was not detected (Madanipour *et al.*, 2017). In our study, 10 isolates demonstrated co-existence of *vanA*/*vanB* (6.8%).

VanC is recognized for its role in intrinsic resistance among certain *Enterococcus* species such as *E. gallinarum* and *E. casseliflavus*. However, its prevalence in clinically significant strains such as *E. faecalis* and *E. faecium* is limited (Sun *et al.*, 2014). Interestingly, 17.7% of our isolates harbored *vanC*. A study conducted in 13 hospitals in Greece showed that *vanC* VRE was the most prevalent, representing 57% of VRE isolates, followed by *vanA*, then *vanB* genotypes. Another study from Switzerland showed that the percentage of the *vanC* VRE genotype was 98%. This is in contrast to the USA and North Africa, where the *vanC* genotype was rare compared to the dominant *vanA* and *vanB* genotypes (Ahmed and Baptiste, 2018).

A study of *vanD* gene clusters in *E. faecium*, reported that although *vanD*-carrying strains were isolated sporadically, the prevalence of enterococci harboring *vanD* was increasing over time. The low *vanD* prevalence is likely due to its localization on large non-transferable chromosomal mobile genetic elements. A high percentage of hospitalized patients (26.7%-43.8%) demonstrated *vanD* carriage among gut anaerobic microflora but not enterococci (Sassi *et al.*, 2018). A study from the Netherlands showed that *vanD* was identified in 27.8% of patients but was not associated with vancomycin non-susceptibility (Flipse *et al.*, 2019). Similarly, in our study, the percentage of isolates carrying *vanD* was 10.2%, and none of the isolates were resistant to vancomycin.

E. faecalis and *E. faecium* strains harboring *vanG* are rare. The first documented clinical isolate of vancomycin resistant *E. faecium* containing a *vanG* gene was in 2016 in France (Sassi *et al.*, 2018). In our study, the percentage of *vanG* positive isolates was 15.6%. However, this gene was not associated with vancomycin non-susceptibility. *VanE* VRE isolates were first reported in 1999 and were associated with low level non-susceptibility to vancomycin (Fines *et al.*, 1999). *VanE* VRE isolates were then reported worldwide; e.g., USA, Canada, and Norway (Al Rubaye *et al.*, 2024). *VanE* was present among 10.2% of our isolates. However, all *vanE*-positive isolates were susceptible to vancomycin.

Enterococci positive for *vanA* are often not only resistant vancomycin but also to other antimicrobials, including teicoplanin and ampicillin (Ono *et al.*, 2005, Moosavian *et al.*, 2018). Similarly, in our study, *vanA* was associated with ampicillin and teicoplanin non-susceptibility.

OptrA is associated with non-susceptibility to oxazolidinone and phenicols. Thus, it contributes to decreased susceptibility to chloramphenicol and florfenicol (Wang *et al.*, 2015). Furthermore, *optrA* positive strains also demonstrated high levels of non-susceptibility to tetracycline (Xie *et al.*, 2025). This was in line with our findings which showed that *optrA* was associated with non-susceptibility to chloramphenicol and doxycycline.

To the best of our knowledge, the association of *vanD* with chloramphenicol non-susceptibility has not been previously reported. In addition, the association between *vanG* and tigecycline non-susceptibility and between *vanB* and ciprofloxacin non-susceptibility has not been previously reported. In our study, *optrA* was encountered in 20 isolates (13.6 %), and both *cfr* and *poxtA* were encountered in 7 isolates (4.8 %). *Cfr*, *optrA* and *poxtA* genes were associated with oxazolidinone non-susceptibility, like tedizolid and linezolid (Schwarz *et al.*, 2021), but in our study all isolates were susceptible to

linezolid. Interestingly, there was a significant association between *cfr* and ciprofloxacin susceptibility. However, due to low frequency of this gene, this requires confirmation using a larger sample size.

Overall, the frequencies of resistance genes among enterococci in our study demonstrated similarities and differences when compared to those from other regions. This may be attributed to differences in the prevalent strains and resistance genes, the type of samples and detection methods, the antimicrobials used, the implementation of antibiotic stewardship programs, and the socioeconomic characteristics of populations, among other factors.

5. Conclusions

The highest non-susceptibility for the study isolates was observed against rifampin (70.7%) and erythromycin (65.3%), while the highest susceptibility was for linezolid (100%) and tigecycline (98.6%). Vancomycin and linezolid resistance genes were relatively infrequent among the isolates. *VanB* (23.8%) was the most frequent vancomycin resistance gene, followed by *vanA* and *vanC* (17.7% each). *OptrA* (13.6%) was the most frequent linezolid resistance gene, followed by both *cfr* and *poxtA* at 4.8% each. Several resistance genotypes were associated with specific antimicrobial non-susceptibility patterns.

Future studies should use a larger sample size that is more representative of the Jordanian population to better characterize the prevalence of resistance genotypes and phenotypes in Jordan. Prevalence of other resistance genes, such as tigecycline resistance genes (*tet(L)* and *tet(M)*), could also be investigated. Furthermore, in conjunction with the Kirby-Bauer method, the broth microdilution assay could be used to determine the minimum inhibitory concentrations of the antimicrobial agents.

Acknowledgment

This study was supported by the deanship of research at Jordan University of Science and Technology (Grant no. 2019/594).

References

Ahmed MO and Baptiste KE (2018). "Vancomycin-Resistant Enterococci: A Review of Antimicrobial Resistance Mechanisms and Perspectives of Human and Animal Health." Microb Drug Resist **24**(5): 590-606.

Al-Tamimi M, Albalawi H, Isied W, Musallam A, Qazzaz F, Azab M and Abu-raideh J (2022). "Gram-Positive Bacterial Infections and Antibiotics Resistance in Jordan: Current Status and Future Perspective." Jordan Medical Journal **56**(1).

Al Rubaye M, Janice J, Bjornholt JV, Lohr IH, Sundsfjord A and Hegstad K (2024). "The first vanE-type vancomycin resistant Enterococcus faecalis isolates in Norway - phenotypic and molecular characteristics." J Glob Antimicrob Resist **36**: 193-199.

Antonelli A, D'Andrea MM, Brenciani A, Galeotti CL, Morroni G, Pollini S, Varaldo PE and Rossolini GM (2018). "Characterization of poxtA, a novel phenicol-oxazolidinone-tetracycline resistance gene from an MRSA of clinical origin." J Antimicrob Chemother **73**(7): 1763-1769.

Arias CA and Murray BE (2012). "The rise of the Enterococcus: beyond vancomycin resistance." Nat Rev Microbiol **10**(4): 266-278.

Bender JK, Cattoir V, Hegstad K, Sadowy E, Coque TM, Westh H, Hammerum AM, Schaffer K, Burns K, Murchan S, Novais C, Freitas AR, Peixe L, Del Grosso M, Pantosti A and Werner G (2018). "Update on prevalence and mechanisms of resistance to linezolid, tigecycline and daptomycin in enterococci in Europe: Towards a common nomenclature." Drug Resist Updat **40**: 25-39.

Bender JK, Fleige C, Klare I and Werner G (2019). "Development of a multiplex-PCR to simultaneously detect acquired linezolid resistance genes cfr, optrA and poxtA in enterococci of clinical origin." J Microbiol Methods **160**: 101-103.

Bhatt P, Sahni AK, Praharaj AK, Grover N, Kumar M, Chaudhari CN and Khajuria A (2015). "Detection of glycopeptide resistance genes in enterococci by multiplex PCR." Med J Armed Forces India **71**(1): 43-47.

Bi R, Qin T, Fan W, Ma P and Gu B (2018). "The emerging problem of linezolid-resistant enterococci." J Glob Antimicrob Resist **13**: 11-19.

Brauner A, Fridman O, Gefen O and Balaban NQ (2016). "Distinguishing between resistance, tolerance and persistence to antibiotic treatment." Nat Rev Microbiol **14**(5): 320-330.

Brenciani A, Morroni G, Vincenzi C, Manso E, Mingoia M, Giovanetti E and Varaldo PE (2016). "Detection in Italy of two clinical Enterococcus faecium isolates carrying both the oxazolidinone and phenicol resistance gene optrA and a silent multiresistance gene cfr." J Antimicrob Chemother **71**(4): 1118-1119.

Deshpande LM, Ashcraft DS, Kahn HP, Pankey G, Jones RN, Farrell DJ and Mendes RE (2015). "Detection of a New cfr-Like Gene, cfr(B), in Enterococcus faecium Isolates Recovered from Human Specimens in the United States as Part of the SENTRY Antimicrobial Surveillance Program." Antimicrob Agents Chemother **59**(10): 6256-6261.

Fines M, Perichon B, Reynolds P, Sahm DF and Courvalin P (1999). "VanE, a new type of acquired glycopeptide resistance in Enterococcus faecalis BM4405." Antimicrob Agents Chemother **43**(9): 2161-2164.

Flipse J, von Wintersdorff CJH, van Niekerk JM, Jamin C, van Tiel FH, Hasman H and van Alphen LB (2019). "Appearance of vanD-positive Enterococcus faecium in a tertiary hospital in the Netherlands: prevalence of vanC and vanD in hospitalized patients." Sci Rep **9**(1): 6949.

Georges M, Odoyo E, Matano D, Tiria F, Kyany'a C, Mbwika D, Mutai WC and Musila L (2022). "Determination of Enterococcus faecalis and Enterococcus faecium Antimicrobial Resistance and Virulence Factors and Their Association with Clinical and Demographic Factors in Kenya." J Pathog **2022**: 3129439.

Guan L, Beig M, Wang L, Navidifar T, Moradi S, Motallebi Tabaei F, Teymouri Z, Abedi Moghadam M and Sedighi M (2024). "Global status of antimicrobial resistance in clinical Enterococcus faecalis isolates: systematic review and meta-analysis." Ann Clin Microbiol Antimicrob **23**(1): 80.

Hao W, Shan X, Li D, Schwarz S, Zhang SM, Li XS and Du XD (2019). "Analysis of a poxtA- and optrA-co-carrying conjugative multiresistance plasmid from Enterococcus faecalis." J Antimicrob Chemother **74**(7): 1771-1775.

Hashemian SMR, Farhadi T and Ganjparvar M (2018). "Linezolid: a review of its properties, function, and use in critical care." Drug Des Devel Ther **12**: 1759-1767.

Hollenbeck BL and Rice LB (2012). "Intrinsic and acquired resistance mechanisms in enterococcus." Virulence **3**(5): 421-433.

Jabbari Shiadeh SM, Pormohammad A, Hashemi A and Lak P (2019). "Global prevalence of antibiotic resistance in blood-isolated Enterococcus faecalis and Enterococcus faecium: a systematic review and meta-analysis." Infect Drug Resist **12**: 2713-2725.

Jordan Ministry of Health (2023). Surveillance of Antimicrobial Resistance Annual Report 2022, Jordan Ministry of Health.

Kehrenberg C and Schwarz S (2006). "Distribution of florfenicol resistance genes fexA and cfr among chloramphenicol-resistant Staphylococcus isolates." Antimicrob Agents Chemother **50**(4): 1156-1163.

Kim JI, Manuele A, Maguire F, Zaheer R, McAllister TA and Beiko RG (2024). "Identification of key drivers of antimicrobial resistance in Enterococcus using machine learning." Can J Microbiol **70**(10): 446-460.

Kristich CJ, Rice LB and Arias CA (2014). Enterococcal Infection-Treatment and Antibiotic Resistance. Enterococci: From Commensals to Leading Causes of Drug Resistant Infection. M. S. Gilmore, D. B. Clewell et al. Boston.

LaMarre J, Mendes RE, Szal T, Schwarz S, Jones RN and Mankin AS (2013). "The genetic environment of the cfr gene and the presence of other mechanisms account for the very high linezolid resistance of Staphylococcus epidermidis isolate 426-3147L." Antimicrob Agents Chemother **57**(3): 1173-1179.

Madanipour E, Mehrabi MR and Mirzaee M (2017). "The Antibiotic SusceptibilityPattern and Prevalence of vanA, vanB, and vanC Genes among Enterococcus faecalis Strains Isolated from Consumed Meat." Infect Epidemiol Microbiol. **3**(4): 117-121.

Miller WR and Arias CA (2024). "ESKAPE pathogens: antimicrobial resistance, epidemiology, clinical impact and therapeutics." Nat Rev Microbiol **22**(10): 598-616.

Moosavian M, Ghadri H and Samli Z (2018). "Molecular detection of vanA and vanB genes among vancomycin-resistant enterococci in ICU-hospitalized patients in Ahvaz in southwest of Iran." Infect Drug Resist **11**: 2269-2275.

Ono S, Muratani T and Matsumoto T (2005). "Mechanisms of resistance to imipenem and ampicillin in Enterococcus faecalis." Antimicrob Agents Chemother **49**(7): 2954-2958.

Sassi M, Guerin F, Lesec L, Isnard C, Fines-Guyon M, Cattoir V and Giard JC (2018). "Genetic characterization of a VanG-type vancomycin-resistant Enterococcus faecium clinical isolate." J Antimicrob Chemother **73**(4): 852-855.

Schwarz S, Zhang W, Du XD, Kruger H, Fessler AT, Ma S, Zhu Y, Wu C, Shen J and Wang Y (2021). "Mobile Oxazolidinone Resistance Genes in Gram-Positive and Gram-Negative Bacteria." Clin Microbiol Rev **34**(3): e0018820.

Sun M, Wang Y, Chen Z, Zhu X, Tian L and Sun Z (2014). "The first report of the vanC(1) gene in Enterococcus faecium isolated from a human clinical specimen." Mem Inst Oswaldo Cruz **109**(6): 712-715.

Wada Y, Afolabi HA, Al-Mhanna SB, Bello KE, Irekeola AA, Wada M, Ahmed N, Harun A, Yean CY, Nasir NSM and Rahman Z, A. (2024). "Global occurrence of linezolid-resistant Enterococcus (LRE): The first systematic review and meta-analysis." The Microbe **2**(2024): 100041.

Wang Y, Lv Y, Cai J, Schwarz S, Cui L, Hu Z, Zhang R, Li J, Zhao Q, He T, Wang D, Wang Z, Shen Y, Li Y, Fessler AT, Wu C, Yu H, Deng X, Xia X and Shen J (2015). "A novel gene, optrA, that confers transferable resistance to oxazolidinones and phenicols and its presence in Enterococcus faecalis and Enterococcus faecium of human and animal origin." J Antimicrob Chemother **70**(8): 2182-2190.

Xie Y, Xu F, Dong H, Mao J and Zhang C (2025). "The prevalence of optrA-carrying Enterococci in the vaginal micro-ecology of pregnant women in late pregnancy." Microbiol Spectr **13**(1): e0213524.

Yaghoubi S, Zekiy AO, Krutova M, Gholami M, Kouhsari E, Sholeh M, Ghafouri Z and Maleki F (2022). "Tigecycline antibacterial activity, clinical effectiveness, and mechanisms and epidemiology of resistance: narrative review." Eur J Clin Microbiol Infect Dis **41**(7): 1003-1022.

Zahedi Bialvaei A, Rahbar M, Yousefi M, Asgharzadeh M and Samadi Kafil H (2017). "Linezolid: a promising option in the treatment of Gram-positives." J Antimicrob Chemother **72**(2): 354-364.

Zerrouki H, Rebiahi SA, Hadjadj L, Ahlem F, Elhabiri Y, Sedrati T, Rolain JM and Diene SM (2021). "High frequency and diversity of Vancomycin-resistant Enterococci (VRE) in Algerian healthcare settings." Infect Genet Evol **92**: 104889.

JJBS

Volume 19, Number 1,March 2026
ISSN 1995-6673
Pages 69 – 81
https://doi.org/10.54319/jjbs/190107

Jordan Journal of Biological Sciences

Optimizing Polyphenol Extraction from *Lavandula maroccana*: a simplex-Centroid Mixture Design Approach

Oumaima CHATER[1,*], Smail AAZZA[2], Zineb EL JABBOURY[1], Lahsen EL GHADRAOUI[1]

[1] *Laboratory of Functional Ecology and Environmental Engineering, Faculty of Science and Techniques, University of Sidi Mohamed Ben Abdellah, Fez, Morocco;* [2] *OLMANBGPE, Nador Multidisciplinary Faculty (FPN), Mohammed 1st University, Oujda, Morocco*

Received: February 28, 2025; Revised: July 17, 2025; Accepted: July 30, 2025

Abstract

This study aims to enhance the efficiency of extracting polyphenols from *Lavandula maroccana* by employing a simplex-centroid mixture design approach. The efficiency of extracting total phenolic content (TPC), total antioxidant capacity (TAC), and DPPH radical scavenging activity were assessed using various solvent combinations comprising water, methanol, and ethanol. The significance and predictive capability of the models were determined through a detailed analysis using response surface methodology (RSM) and analysis of variance (ANOVA). The findings demonstrated that a well-proportioned combination of water and methanol consistently yielded the maximum extraction efficacy for phenolic compounds and antioxidants in all plant components. The ideal solvent proportions were determined, with water and methanol each accounting for approximately 50% of the combination. The statistical analysis confirmed the reliability and predictive power of the developed models, as reflected by significant F-values along with elevated R^2, adjusted R^2, and predicted R^2 coefficients, all collectively demonstrating a high degree of model fitness and accuracy. These findings provide valuable guidance for optimizing extraction protocols, enhancing both the yield and bioactivity of antioxidant compounds, with promising prospects for application across the nutraceutical, pharmaceutical, and food industries.

Keywords: *Lavandula maroccana*, simplex-centroid mixture design, total phenolic content, antioxidants, response surface methodology, solvent optimization.

1. Introduction

Lavandula maroccana, commonly known as Moroccan lavender, is a native aromatic plant that contains a rich array of phenolic compounds with well-documented antioxidant potential. Consumers and academics are increasingly interested in the health advantages of natural phenolic phytochemicals found in plants, due to their ability to mitigate oxidative stress, which is implicated in the onset of various chronic diseases such as cardiovascular disorders and cancer (Loganayaki et al., 2013). Antioxidants are substances that neutralize free radicals and reactive oxygen species (ROS), thereby preventing lipid peroxidation and cellular damage (Velioglu et al., 1998; Pryor, 1991). In addition to their health benefits, antioxidants are used as food additives to prevent oxidative degradation and have been associated with other biological properties, such as anti-inflammatory, antimicrobial, antiviral, and vasodilatory effects (Shahidi, 2000; Kumar et al., 2010).

Maximizing the efficiency of polyphenol extraction is crucial to increasing both yield and biological activity. Conventional extraction techniques frequently depend on single solvents, which may not effectively extract the full diversity of phenolic compounds. The simplex-centroid mixture design offers a potent alternative, allowing systematic evaluation of single solvents, and their binary and ternary mixtures and interactions among components. This approach enables a deeper understanding of the individual and synergistic effects of each solvent on extraction performance.

Recent work underscores this potential. Mixture-design or RSM studies have enhanced polyphenol recovery from Moroccan *Cannabis sativa* waste through multivariate optimization (Aazza, 2021) and from *Anacyclus pyrethrum* var. depressus roots via simplex-centroid modelling (Chater et al., 2024) as well as from *Ammi visnaga* roots using triangular-surface designs (El Jabboury et al., 2022), *Magnolia* × *soulangeana* flower buds via Box–Behnken hydro-ethanolic optimization (Zgórka et al., 2023), and broccoli stems with deep-eutectic solvents (Wang et al., 2025). Together, these studies further illustrate the versatility of mixture-design approaches.

Although several authors have optimized polyphenol extraction from *Lavandula* species, to our knowledge no study has yet applied an advanced mixture design to *Lavandula maroccana*. This work is, therefore, the first to employ a simplex-centroid mixture design for that purpose. This study, hence, aims to determine the optimal solvent mixture of water, ethanol, and methanol to maximize total phenolic content (TPC), total antioxidant capacity (TAC), and DPPH radical scavenging activity. By employing response surface methodology (RSM) and

* Corresponding author. e-mail: oumaima.chater@usmba.ac.ma.

analysis of variance (ANOVA), the findings will contribute to the development of efficient, environmentally friendly extraction strategies with potential applications in the nutraceutical, pharmaceutical, and food industries.

2. Materials & Methods

2.1. Plant material

Examples of *L. maroccana* specimens were collected in May 2020 from the Sefrou region located in the Moroccan Middle Atlas. Once gathered, the leaves, flowers, stems, and roots were meticulously divided. Afterward, these plant components were dried in a shaded place to preserve their structure and protect them from damage caused by direct sunshine. Following thorough dehydration, the plant material was finely pulverized, ensuring uniformity and enabling analysis. The powders were stored in opaque pillboxes to protect them from light and other environmental factors, ensuring their purity for future study.

2.2. Solvent Extraction

The samples were prepared in triplicate by combining 1 mL of the solvent (either pure solvents or mixtures) with 50 mg of plant powder. The mixture was then subjected to sonication for 30 minutes in an ultrasonic bath at room temperature. After centrifugation for 10 minutes at 10,000 rpm, the extract was collected and stored in a dark environment at 4 °C. The initial phase of extraction involves a screening process employing solvents of varying polarities, such as water, ethanol, methanol, acetone, ethyl acetate, dichloromethane, chloroform, hexane, di-ethyl ether, and butanol, to determine the most suitable solvent for the subsequent step. The second stage involves extracting the pure specified solvent and their combinations.

2.3. Total phenolic content (TPC)

The spectrophotometric approach was used to quantify the total phenolic content (TPC) by employing the colorimetric technique with the Folin-Ciocalteu reagent (Ma et al., 2010), with some modifications. 50 µL of the sample was combined with 450 µL of a solution of the Folin-Ciocalteu reagent that had been diluted by a factor of 10. Following a 5-minute incubation period at ambient temperature, 450 µL of a solution containing Na2CO3 (75 g L-1) was introduced. Subsequently, all samples were placed in a dark environment and incubated for 2 hours at room temperature. The absorbance of the samples was then measured at a wavelength of 760 nm using a spectrophotometer. The calibration curve had a concentration range of 0.062 to 2 mg mL-1 in an ethanolic solution of gallic acid. The equation of the curve was y = 1.2257x + 0.174, with a R^2 value of 0.9988. The experiment was conducted in triplicate, and the results are reported in milligrams of gallic acid equivalent (GAE) per gram of dry plant material.

2.4. Antioxidant activity:

2.4.1. Total Antioxidant Capacity (TAC)

The samples' overall antioxidant activity was evaluated through the creation of the phospho-molybdenum complex (Libbey & Walradt, 1968). 50 µL of the sample solution was mixed with 1 mL of the reagent solution, which consisted of 0.6 M sulfuric acid, 28 mM sodium phosphate, and 4 mM ammonium molybdate. The reaction mixture was subsequently incubated in a water bath at 95 °C for 90 min. The spectrophotometer was used to measure the absorbance of the combination at a wavelength of 695 nm, relative to a blank. The calibration curve was established using an aqueous solution of ascorbic acid. The equation of the curve was y = 1.4632x + 0.0191, with a R^2 value of 0.9997. The concentration of the ascorbic acid in the solution ranged from 1.0 to 0.0625 mg mL-1. The experiment was conducted in triplicate, and the findings represent the average levels of antioxidant activity expressed in grams of ascorbic acid equivalents per gram of dry plant.

2.4.2. Free radical scavenging activity: DPPH

The production of DPPH (2,2-diphenyl-1-picrylhydrazyl) followed the procedure outlined in reference (DiCiaulaa et al., 2014). 25 µL of various concentrations of samples or standards were introduced into a 1 milliliter solution of DPPH in ethanol, at a concentration of 60 micromolar. The absorbance readings were taken at a wavelength of 517 nm, following a 60-minute incubation period at room temperature. A negative control was performed by measuring the absorption of a blank sample containing an equal amount of methanol and DPPH solution. The experiment was conducted three times, and the percentage inhibition of the free radical scavenging activity for each extract was determined using the following formula:

$$\text{DPPH scavenging activity (\%)} = \left(\frac{Abs_{conrol} - Abs_{sample}}{Abs_{control}}\right) \times 100 \quad \text{Eq. 1}$$

2.5. Experimental design and optimization

2.6. Evaluation of solvent effects by simplex axial design

Research was conducted to optimize polyphenol extraction using a mixture approach. Two standard experimental designs are commonly employed for solvent mixture extraction studies: Simplex-Lattice Design and Simplex-Centroid Design. Both methodologies evaluate the triangular response surface at vertex and central locations.

The Simplex-Centroid Design creates a triangular experimental space encompassing various tested conditions. The triangle vertices correspond to individual pure solvents, each constituting 100% of a particular solvent. The edge midpoints represent binary solvent combinations in equal ratios, specifically (1/2:1/2:0; 1/2:0:1/2; 0:1/2:1/2). The central point corresponds to a three-component mixture with uniform proportions of each element (1:1:1).

A mixture model was developed to improve extraction efficiency. The Simplex-Centroid Design incorporating axial points with triplicate runs was selected to determine the optimal solvent blend of water (W), ethanol (E), and methanol (M). This approach allows for evaluation of individual solvent effects (W, E, M), binary interaction effects (WE, WM, EM), and ternary interaction effects (WEM) through linear, quadratic, and cubic models respectively.

The research employed the enhanced simplex centroid design to investigate how various extraction solvents affect

Total Phenolic Content (TPC) and antioxidant properties. The goal was to optimize extraction parameters by examining solvent interactions. Mixture design experiments were conducted and evaluated using STATISTICA software (version 10, StatSoft, Inc., 2013). Ten experimental combinations were tested in total, with all experiments performed in technical triplicates under identical conditions on the same day to ensure repeatability and reduce experimental variation. Data are reported as mean ± standard deviation and analyzed through analysis of variance (ANOVA). Tukey's post-hoc test determined significant differences at $p < 0.05$. A polynomial function was fitted to each component at every experimental condition. Y represents the predicted response, while β_1, β_2, β_3, β_{12}, β_{13}, and β_{23} are coefficients for linear and interaction terms.

$$Y= \beta_1X_1 + \beta_2X_2 + \beta_3X_3 +\beta_{12}X_1X_2 +\beta_{13}X_1X_3 + \beta_{23}X_2X_3 + \beta_{123}X_1X_2X_3$$

Eq.2

3. Results and Discussion

3.1. Extraction solvents screening

Several factors are known to significantly affect extraction yield and efficiency. The solvent is particularly important among these factors and is recognized as having a substantial influence on both the amount extracted and the overall effectiveness of the extraction process. In the first phase of this study, we assessed the impact of solvent polarity on the total phenolic content (TPC) of *L. maroccana*, using ten pure solvents to extract polyphenols from four different plant parts (leaves, flowers, stems, and roots).

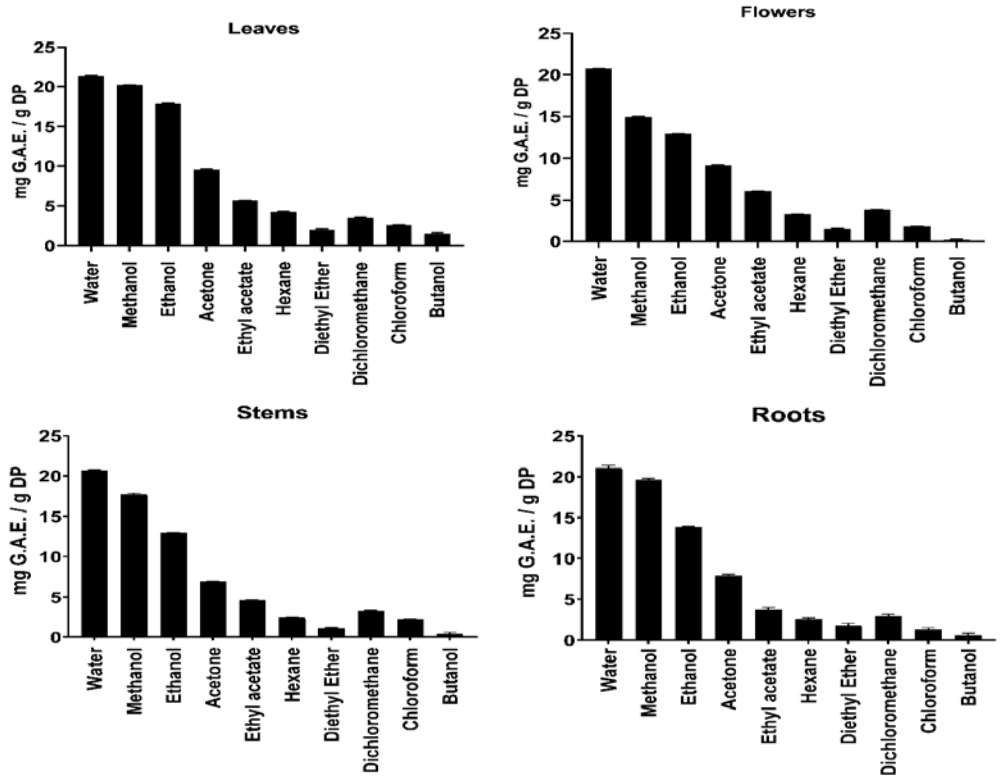

Figure 1: Total phenolic content (TPC) expressed in mg gallic acid equivalent per gram of dry plant material (mg GAE/g d.w.) in leaves, flowers, stems, and roots of *L. maroccana* extracted with different solvents.

Figure 1 illustrates the TPC results expressed in mg gallic acid equivalents (GAE) per gram of dry plant material. This extraction data demonstrates that solvent polarity significantly influences yield across different plant parts, with water achieving the highest extraction yields (20.70-21.37%) and excellent consistency across leaves, flowers, stems, and roots, followed by methanol (14.95-20.22%) and ethanol (12.89-17.86%), both showing particularly strong performance with leaves. Moderately polar solvents like acetone (6.87-9.53%) and dichloromethane (3.04-3.82%) produced intermediate results, while non-polar and less polar solvents including ethyl acetate (3.74-6.02%), hexane (2.43-4.24%), chloroform (1.35-2.54%), and diethyl ether (1.10-1.89%) showed considerably lower extraction efficiency, with butanol performing poorest overall (0.19-1.41%). These data emphasize the significant impact of solvent extraction effectiveness on the overall yield of phenolic compounds, as the recovery of phenolic compounds is contingent upon the choice of solvent for extraction and its polarity (Boeing et al., 2014). The results highlight the importance of the solvent in determining the amounts of phenolic compounds, with leaves generally providing the highest yields across most solvents, while the clear superiority of polar solvents specifically water, methanol, and ethanol as the most effective solvents for boosting polyphenol productions suggests that the target compounds in these plant materials have predominantly polar characteristics. Based on this preliminary screening, water, methanol, and ethanol were selected for further optimization using a simplex-centroid mixture design, as they demonstrated the highest potential for maximizing polyphenol recovery.

3.2. Extraction using solvent mixtures

The three best solvents were chosen based on the total phenolic compounds (TPC) value. Out of the 10 solvents employed, water, methanol, and ethanol yielded the highest amount of phenolic compounds in comparison to the other solvents.

After evaluating the outcomes of extracting solvents individually, we decided to use a mixture of three solvents (water, methanol, and ethanol) that showed the highest yields of polyphenols. We conducted experiments using the simplex-centroid mixture design approach to modify the quantities of solvents inside the mixture. The amounts of total phenolic compounds and antioxidant activities of the extracts obtained using the three selected pure solvents (water, ethanol, and methanol) and their mixtures are illustrated in Tables 1, 2, and 3.

Table 1: Simplex axial design and results for mixture tested of TPC

Crude extract	Extract (solvent proportions)	mg Gallic acid / g dry plant			
		Leaves	Flowers	Stems	Roots
1	Water (W) (1)	21.68 ± 0.08	20.71 ± 0.02	20.83 ± 0.12	21.05 ± 0.04
2	Methanol (M) (1)	20.42 ± 0.02	14.84 ± 0.05	17.83 ± 0.02	19.61 ± 0.04
3	Ethanol (E) (1)	17.95 ± 0.04	13.18 ± 0.02	13.05 ± 0.03	13.85 ± 0.05
4	E: M (1/2:1/2)	22.32 ± 0.05	15.65 ± 0.06	19.04 ± 0.06	20.26 ± 0.05
5	W: M (1/2:1/2)	25.24 ± 0.05	24.48 ± 0.05	23.37 ± 0.06	23.65 ± 0.05
6	W: E (1/2:1/2)	22.96 ± 0.03	21.78 ± 0.03	21.06 ± 0.04	21.57 ± 0.04
7	W: E: M (1/3:1/3:1/3)	23.52 ± 0.05	23.14 ± 0.06	21.73 ± 0.07	22.09 ± 0.07
8	W: E: M (1/6:4/6:1/6)	19.10 ± 0.04	16.88 ± 0.03	16.05 ± 0.07	17.82 ± 0.03
9	W: E: M (1/6:1/6:4/6)	24.81 ± 0.03	23.68 ± 0.03	23.01 ± 0.05	24.00 ± 0.04
10	W: E: M (4/6:1/6:1/6)	28.59 ± 0.04	25.43 ± 0.03	24.00 ± 0.04	24.99 ± 0.05

The findings shown in Table 1 indicate that combinations of the "water-ethanol-methanol" ternary mixture (4/6: 1/6: 1/6), predominantly composed of water, produced the highest TPC yields. Positive TPC yields were also observed for other ternary and binary mixtures containing methanol or water. Extracts of pure ethanol showed a low TPC content. However, ethanol showed a better capacity to extract more phenolic chemicals when mixed with water or methanol. In actuality, due to their varying polarity and solubility, no solvent is able to extract all types of bioactive chemicals.

Tables 2 and 3 show the effects of different solvent combinations on the extracts' overall antioxidant activity and antiradical activity. The findings highlight how much the type of extraction solvent and its combination affect the antiradical activity of *L. maroccana* extracts. The combinations with the highest total antioxidant capacity (TAC) were the equal ternary combination, the ternary mixture that was primarily made up of water, and the binary mixture that contained extracts of both methanol and water. The extract from the ternary combination that was primarily made up of methanol (1/6 W:1/6 E:4/6 M) showed more DPPH scavenging activity. The existence of polyphenols, which have potent antioxidant properties in plants, may account for this antioxidant activity (Kale et al., 2010).

Table 2: Simplex axial design and results for mixture tested of TAC

Crude extract	Extract (solvent proportions)	mg Ascorbic Acid / g dry plant			
		Leaves	Flowers	Stems	Roots
1	Water (W) (1)	27.22 ± 0.03	16.51 ± 0.02	20.82 ± 0.04	20.55 ± 0.03
2	Methanol (M) (1)	19.44 ± 0.03	12.21 ± 0.02	12.90 ± 0.03	18.36 ± 0.01
3	Ethanol (E) (1)	16.58 ± 0.03	11.45 ± 0.01	11.17 ± 0.03	17.05 ± 0.03
4	E: M (1/2:1/2)	20.65 ± 0.04	15.88 ± 0.04	17.36 ± 0.03	20.22 ± 0.04
5	W: M (1/2:1/2)	33.49 ± 0.03	22.21 ± 0.03	26.54 ± 0.04	25.55 ± 0.06
6	W: E (1/2:1/2)	28.47 ± 0.06	19.39 ± 0.03	23.10 ± 0.04	22.70 ± 0.05
7	W: E: M (1/3:1/3:1/3)	32.33 ± 0.03	22.49 ± 0.04	26.88 ± 0.06	25.94 ± 0.05
8	W: E: M (1/6:4/6:1/6)	18.84 ± 0.06	17.89 ± 0.04	15.33 ± 0.03	19.64 ± 0.03
9	W: E: M (1/6:1/6:4/6)	25.61 ± 0.03	17.36 ± 0.03	25.15 ± 0.06	19.34 ± 0.04
10	W: E: M (4/6:1/6:1/6)	32.83 ± 0.03	21.26 ± 0.02	27.37 ± 0.05	26.86 ± 0.04

Values are expressed as mean ± standard deviation (SD) (n = 3).

Table 3: Simplex axial design and results for mixture tested of DPPH

Crude extract	Extract (solvent proportions)	DPPH %			
		Leaves	Flowers	Stems	Roots
1	Water (W) (1)	77.69 ± 0.17	80.67 ± 0.19	70.06 ± 0.11	83.99 ± 0.17
2	Methanol (M) (1)	85.03 ± 0.19	82.83 ± 0.17	76.46 ± 0.17	90.09 ± 0.28
3	Ethanol (E) (1)	78.25 ± 0.23	76.31 ± 0.22	71.58 ± 0.42	88.49 ± 0.22
4	E: M (1/2:1/2)	80.97 ± 0.34	80.26 ± 0.45	73.89 ± 0.34	86.33 ± 0.17
5	W: M (1/2:1/2)	86.00 ± 0.22	84.06 ± 0.17	78.51 ± 0.30	90.99 ± 0.17
6	W: E (1/2:1/2)	86.48 ± 0.34	81.75 ± 0.17	80.67 ± 0.40	89.12 ± 0.17
7	W: E: M (1/3:1/3:1/3)	83.58 ± 0.22	81.34 ± 0.30	75.31 ± 0.22	87.37 ± 0.30
8	W: E: M (1/6:4/6:1/6)	87.34 ± 0.17	78.21 ± 0.30	73.56 ± 0.23	89.35 ± 0.17
9	W: E: M (1/6:1/6:4/6)	89.68 ± 0.36	85.03 ± 0.30	81.45 ± 0.30	91.77 ± 0.23
10	W: E: M (4/6:1/6:1/6)	86.70 ± 0.22	82.27 ± 0.23	77.39 ± 0.26	86.37 ± 0.30

Values are expressed as mean ± standard deviation (SD) (n = 3).

3.3. Validation of experimental models by statistical analysis

The variance analysis (ANOVA) results in Table 4 highlight the high accuracy and significance of the mixing models used to predict Total Phenolic Content (TPC), Total Antioxidant Capacity (TAC), and DPPH radical scavenging activity across leaves, flowers, stems, and roots. The models for TPC and TAC exhibit exceptional predictive power, with F-values ranging from 231.38 to 9553.93 and p-values all at 0.000000, indicating extremely significant models. The R^2 and adjusted R^2 values for these models are consistently at or near 1.000, demonstrating their ability to account for nearly all the variability in the data. For DPPH radical scavenging activity, the models also show strong significance, with F-values between 14.30 and 104.74 and p-values below 0.002023. The R^2 values for DPPH models range from 0.916 to 0.976, and adjusted R^2 values from 0.881 to 0.965, indicating a slightly less perfect but still very high fit compared to TPC and TAC models. These results confirm the robustness of the mixing models in accurately predicting the antioxidant properties of different plant parts, validating the effectiveness of the solvent mixtures used and providing a solid foundation for optimizing extraction protocols in both research and industrial applications. A significant Lack of Fit indicates that the model is inadequate to explain the data, and the model should be modified (do Carmo et al., 2018). In this study, however, the Lack of Fit test could not be computed because the degrees of freedom were zero (df = 0), as no solvent composition was repeated independently in the mixture design. Although each experimental condition was tested in triplicate, the design did not include replicated design points, which are required for Lack of Fit analysis. Despite this limitation, the models exhibited very strong statistical validity. The R^2 and adjusted R^2 values for TPC and TAC models were extremely high (approaching 1.000), which could raise concerns about potential model overfitting. To address this, we examined the consistency between R^2 and adjusted R^2, the very high F-values (Table 5), and the extremely low p-values ($p < 0.000001$), all of which confirm the robustness of the models. Additionally, the DPPH models, which showed slightly lower R^2 values (0.916–0.976), reflect inherent variability in experimental responses and help confirm that overfitting is unlikely. Future studies could include external validation or cross-validation approaches to further confirm the generalizability of these models.

Table 4: Variance analysis (ANOVA) results of the fitted mixing models for total phenolic content (TPC), total antioxidant capacity (TAC), and DPPH scavenging activity in different parts of *Lavandula maroccana*.
R^2 and adjusted R^2 values indicate the goodness of fit. High F-values and low p-values confirm the significance of the models.

	F	p	R^2	R^2 Adj
TPC-L	964.26	0.000000	1.000	0.999
TPC-F	977.84	0.000000	1.000	1.000
TPC-S	231.38	0.000000	1.000	1.000
TPC-R	666.09	0.000000	1.000	1.000
TAC-L	9553.93	0.000000	1.000	1.000
TAC-F	3886.58	0.000000	1.000	1.000
TAC-S	5066.89	0.000000	1.000	1.000
TAC-R	3299.48	0.000000	1.000	1.000
DPPH-L	33.27	0.000092	0.916	0.881
DPPH-F	25.39	0.000181	0.933	0.904
DPPH-S	104.74	0.000000	0.976	0.965
DPPH-R	14.30	0.002023	0.948	0.925

Table 5 presents the statistical parameters using response surface methods for models predicting Total Phenolic Content (TPC), Total Antioxidant Capacity (TAC), and DPPH radical scavenging activity across leaves, flowers, stems, and roots. The models exhibit extremely high significance, evidenced by F-values ranging from 25.58 to 96903.08 and p-values consistently at 0.000000, confirming the robustness of these models. Specifically, TPC models for flowers (F = 29442.33), TAC models for leaves (F = 96903.08), and DPPH models for stems (F = 94.18) demonstrate particularly high predictive power. The Sum of Squares (SS) and Mean Squares (MS) values are also substantial, highlighting the models' capacity to explain the variance in the data effectively. Degrees of freedom (df) are consistently at 6, ensuring a reliable distribution of the data points. These statistical parameters validate the efficacy of the response surface methodology in optimizing solvent mixtures for extracting phenolic compounds and antioxidants, providing a solid foundation for efficient extraction protocols in both laboratory and industrial settings. The strong model performance across various plant parts underscores the versatility and reliability of these optimized solvent systems for maximizing extraction yields and antioxidant activity.

Table 5: Summary of statistical parameters for the fitted response surface models using ANOVA.
SS: sum of squares, df: degrees of freedom, MS: mean square, F: Fisher value, p: significance level. High F-values and extremely low p-values ($p < 0.000001$) indicate the strong statistical significance of the models

Model	SS	df	MS	F	p
TPC-L	98.45	6	16.41	6470.60	0.000000
TPC-F	360.60	6	60.10	29442.33	0.000000
TPC-S	206.37	6	34.40	8098.03	0.000000
TPC-R	175.90	6	29.32	11619.26	0.000000
TAC-L	786.26	6	131.04	96903.08	0.000000
TAC-F	364.15	6	60.69	69609.75	0.000000
TAC-S	706.86	6	117.81	74392.90	0.000000
TAC-R	209.49	6	34.91	20986.23	0.000000
DPPH-L	259.06	6	43.18	25.58	0.000001
DPPH-F	131.42	6	21.90	32.46	0.000000
DPPH-S	295.95	6	49.33	94.18	0.000000
DPPH-R	123.00	6	20.50	42.26	0.000000

3.4. Analysis of mixture optimization by response surface methodology

3.4.1. Total phenolic compound extraction

A potent statistical technique for modeling and optimizing the impact of several variables on a response variable of interest is surface response methodology (SRM). It is frequently employed to maximize the phenolic compound extraction process from natural sources (Weremfo et al., 2023). It is advised to utilize a combination of solvents with varying compositions and polarity for mixture design extraction to maximize the extraction efficiency of phenolic compounds and phytochemicals (Santos Felix et al., 2018). The mixture design diagram for the special cubic model describing the interaction effects and the different proportions of pure solvents and their mixtures compared to TPC values is shown in Fig.2.

Special linear, quadratic, and cubic models were tested. ANOVA assessed the lack of fit for these surfaces. The selected special cubic model is described by the following equations, where x, y, and z represent the proportions of water, methanol, and ethanol, respectively. Subscripts indicate the plant part studied: L (leaves), F (flowers), S (stems), and R (roots).

$TPC_L = 21.68x + 20.42y + 17.94z + 16.74xy + 12.59xz + 12.54yz - 31.12xyz$

$TPC_F = 20.71x + 14.84y + 13.17z + 26.81xy + 19.35xz + 6.54yz - 28.11xyz$

$TPC_S = 20.83x + 17.82y + 13.04z + 16.16xy + 16.48xz + 14.41yz - 19.72xyz$

$TPC_R = 21.04x + 19.61y + 13.85z + 13.28xy + 16.48xz + 14.09yz - 25.79xyz$

These equations describe the contribution of each solvent and their interactions to the total phenolic content in different parts of *L. maroccana.*

According to the equations above, TPC extraction was mostly and positively affected by the binary mixture “water-methanol” for flowers. The linear coefficient for water is higher than other pure solvents, indicating a larger positive effect on TPC extraction. Meanwhile, in ternary

interaction "water-methanol-ethanol" mixture had a negative effect. Also, the mixture of the two organic solvents "ethanol-methanol" resulted in the lowest positive effect.

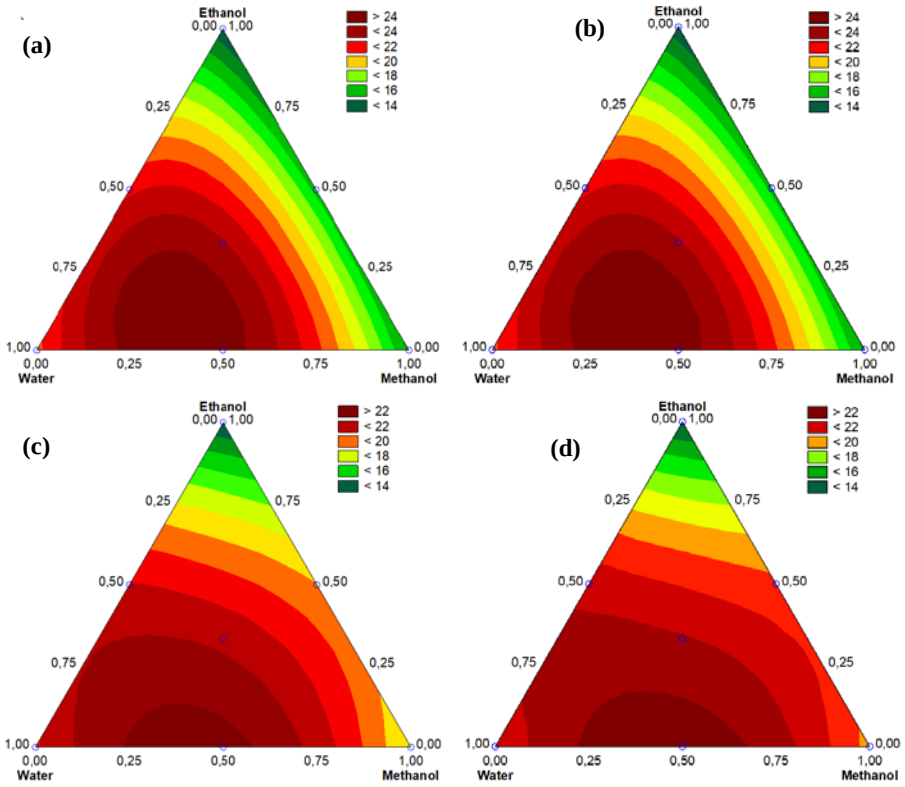

Figure 2: Response surface of the Special Cubic Model predicts TPC based on the proportions of Water, Ethanol, and Methanol of leaves (a), flowers (b), stems (c), and roots (d).

The response surface of the special cubic model (2D) for Total Phenolic Content (TPC) extraction is illustrated in Figure 2. This figure reveals that pure ethanol and methanol are the least effective solvents for extracting TPC from leaves and flowers, while pure ethanol is the least effective for stems and roots. Similar findings have shown that too low or too high ethanol concentration in the extraction solvent is unfavorable for the extraction of total phenolic and (TPC) (Chater, Aazza, Silva, et al., 2024; Liao et al., 2022). In contrast, pure water extracted higher amounts of TPC from all four plant parts. The mixture design shows a dark region corresponding to the highest TPC values, which is located around the area representing equal portions of water and methanol, as well as the region for 75% of water. This indicates that the optimal solvent composition for extracting phenolic compounds involves a mixture of water and methanol in equal proportions or 75% water and 25% methanol, as these combinations achieve the highest extraction efficiency.

3.4.2. Total Antioxidant Capacity (TAC)

The response surface analysis using the Special Cubic Model reveals the optimal solvent proportions for extracting Total Antioxidant Capacity (TAC) from leaves, flowers, stems, and roots. The equations below show that water (x) has the highest individual contribution to TAC across all plant parts, followed by methanol (y) and ethanol (z). However, the significant positive coefficients for the interaction terms, especially the three-way interaction (xyz), indicate that a balanced mixture of these solvents maximizes TAC extraction. For instance, in leaves, the term $71.52xyz$ substantially boosts TAC, similar patterns are observed in flowers ($36.63xyz$), stems ($56.36\ xyz$), and roots ($46.62\ xyz$). This analysis highlights that the synergistic effects of combining water, methanol, and ethanol are crucial for efficient antioxidant extraction, providing valuable guidance for developing optimal extraction protocols in both research and industrial applications.

TAC_L =27.21x+19.44y+16.57z+40.63xy+26.27xz+10.55yz+71.52xyz

TAC_F =16.37x+12.05y+11.31z+31.99xy+22.16xz+16.79yz+36.63xyz

TACS =20.81x+12.89y+11.10z+38.74xy+28.43xz+21.29yz+56.36xyz

TACR =20.54x+18.35y+17.04z+24.39xy+15.61xz+10.06yz+46.62xyz

The response surface analysis of the Special Cubic Model predicting Total Antioxidant Capacity (TAC) based on the proportions of water, ethanol, and methanol for leaves, flowers, stems, and roots (Fig.3) reveals a consistent pattern in solvent efficiency. The highest TAC values are consistently achieved with a balanced mixture of water and methanol, demonstrating the synergistic effect of these two solvents. This combination outperforms the use of pure solvents across all plant parts. Specifically, pure ethanol is the least effective, consistently yielding the

lowest TAC values, likely due to its limited solubility for certain antioxidant compounds. On the other hand, pure water and pure methanol provide intermediate effectiveness but do not match the efficiency of their mixture. The results suggest that an equal mixture of water and methanol significantly enhances the extraction efficiency of antioxidants, making it the optimal choice for extracting total antioxidant capacity from plant materials. This approach can be particularly beneficial in both laboratory and industrial settings where maximizing antioxidant yield is crucial, providing a clear strategy for solvent selection to achieve superior extraction results.

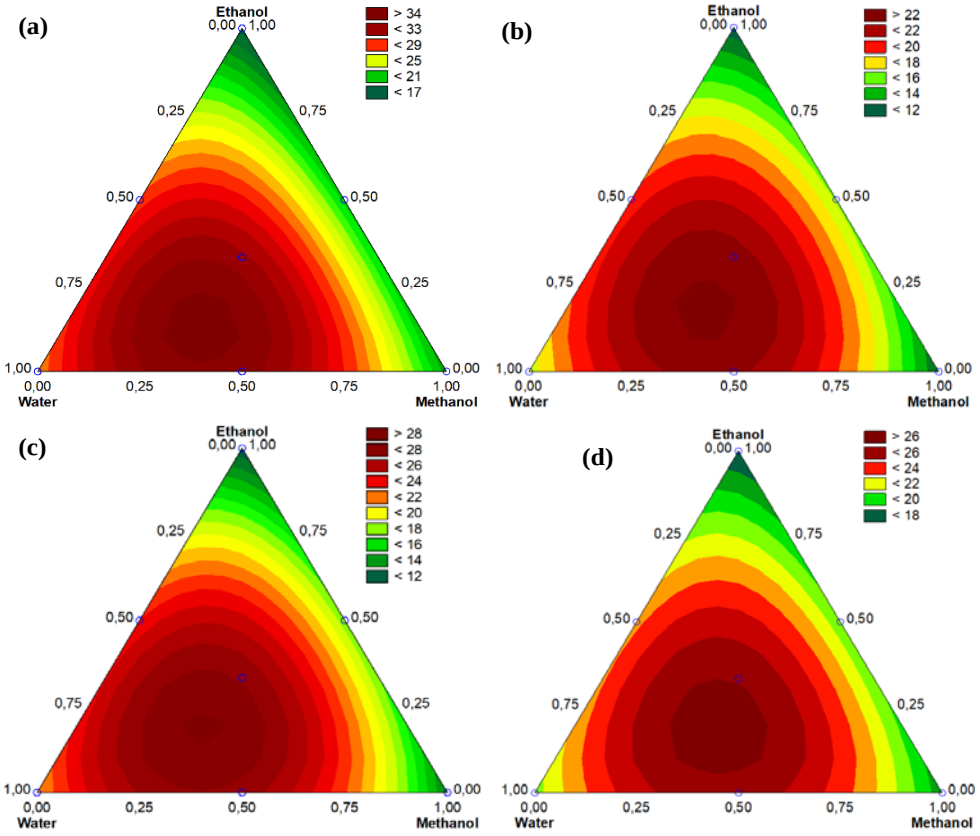

Figure 3: The response surface of the Special Cubic Model predicts TAC based on the proportions of Water, Ethanol, and Methanol of leaves (a), flowers (b), stems (c), and roots (d).

3.4.3. DPPH scavenging activity

One of the two most popular spectrophotometric techniques for determining how well meals, vegetables, and herbs scavenge free radicals is the DPPH test method. Stable radicals are used in this technique, which is highly sensitive and simple to employ. It works especially well for figuring out how antioxidant-active different pure chemicals, fruits, vegetables, and tea extracts (Arnao, 2000).

The response surface analysis using the Special Cubic Model equations below for predicting DPPH radical scavenging activity indicates that water (x), methanol (y), and ethanol (z) each contribute positively to antioxidant activity across leaves, flowers, stems, and roots. However, the highest DPPH activities are generally achieved with water and methanol mixtures, as shown by the equations' coefficients. For example, the highest individual positive effects are seen in roots (DPPH-R) with ethanol contributing significantly, yet the three-way interaction (xyz) negatively impacts the overall DPPH activity, particularly in stems (DPPH-S). The analysis suggests that the combination of water and methanol is optimal for maximizing antioxidant extraction, while ethanol's inclusion may reduce effectiveness due to competitive or inhibitory interactions. The incorporation of ethanol into the solvent system may compromise extraction efficiency, attributable to its comparatively lower polarity relative to water and methanol. This reduced polarity diminishes the solubility of highly hydrophilic phenolic compounds and may interfere with the hydrogen-bond network responsible for stabilizing polyphenol–solvent interactions, ultimately leading to a less favorable extraction environment for polar bioactive molecules (Lee et al., 2024). Consequently, favoring water and methanol as solvents provides the most efficient extraction strategy for achieving high DPPH radical scavenging activity, offering valuable guidance for both laboratory and industrial applications. Future work should examine bioactivity-guided fractionation, the use of greener solvents (e.g., deep-eutectic systems), and pilot-scale validation to confirm process scalability and sustainability.

$DPPH_L$ = 77.69x + 79.02y + 78.24z + 30.54xy + 34.04xz + 9.31yz – 46.71xyz.

$DPPH_F$ = 80.67x + 76.83y + 76.31z + 21.23xy + 13.03xz + 14.75yz – 82.35xyz.

$DPPH_S$ = 70.05x + 70.46y + 71.58z + 33.01xy + 39.4xz + 11.47yz – 147.38xyz.

$DPPH_R$ = 83.98x + 84.00y + 88.49z + 27.79xy + 11.54xz + 0.15yz – 52.41xyz.

The response surface analysis of the Special Cubic Model predicting DPPH radical scavenging activity based on the proportions of water, ethanol, and methanol for leaves, flowers, stems, and roots (Fig.4) reveals that the highest antioxidant activities are consistently achieved with a balanced mixture of water and methanol or a higher proportion of methanol. This combination significantly outperforms pure ethanol, which consistently yields the lowest DPPH values. Specifically, leaves and stems show optimal DPPH activity around a 0.5:0.5 ratio of water to methanol, while flowers and roots achieve higher activity with a methanol-rich mixture. The consistent pattern across all plant parts underscores methanol's crucial role in enhancing antioxidant activity. Therefore, for optimal extraction of antioxidants exhibiting high DPPH radical scavenging activity, a mixture of water and methanol is recommended. This insight is valuable for developing efficient extraction protocols in both laboratory and industrial settings, ensuring maximum yield and efficacy of antioxidants.

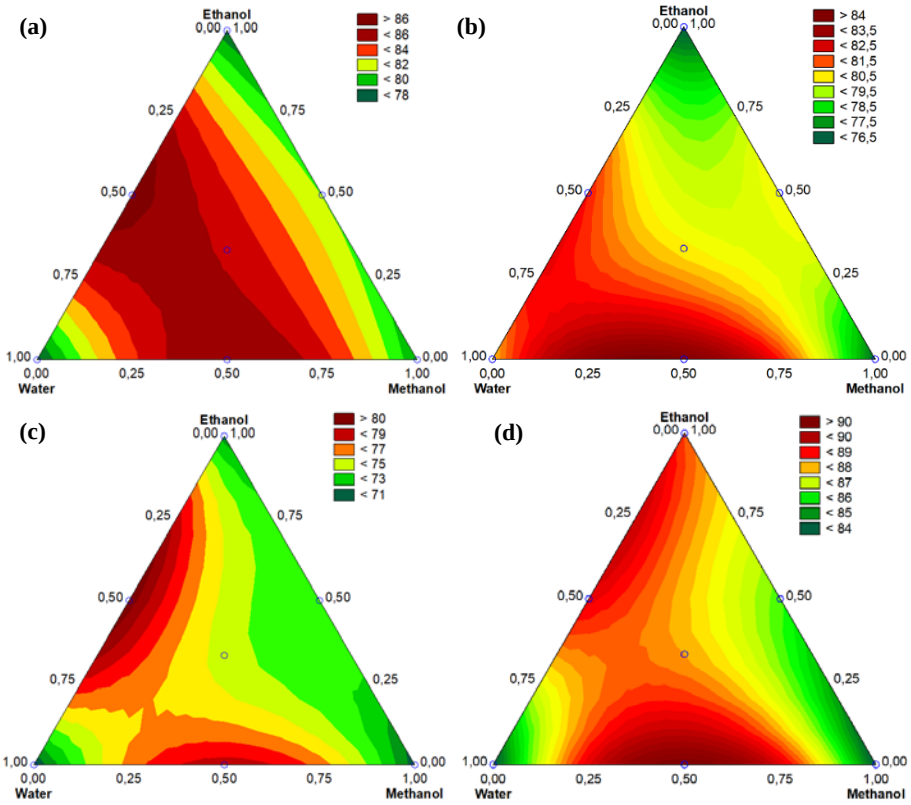

Figure 4: The response surface of the Special Cubic Model predicts DPPH based on the proportions of Water, Ethanol, and Methanol of leaves (a), flowers (b), stems (c), and roots (d).

3.5. Pareto Analysis

Pareto's Graph analysis of standardized effects for Total Phenolic Content (TPC) from leaves, flowers, stems, and roots (Fig.5) demonstrates that water and methanol are the most effective solvents. Water consistently shows the highest standardized effect across all plant parts, with values of 745.7123 for leaves, 794.0229 for flowers, 553.9374 for stems, and 725.824 for roots. Methanol also exhibits substantial positive effects, closely following water with values of 702.4962 for leaves, 569.0358 for flowers, 473.8442 for stems, and 676.1282 for roots. Ethanol, while contributing positively, has lower standardized effects compared to water and methanol, with effects ranging from 346.7823 to 617.9735 across different plant parts. The interaction effects (AB, AC, BC) are positive but significantly less impactful than the individual solvent effects, and the three-way interaction (ABC) is minimal, with a slight negative effect observed.

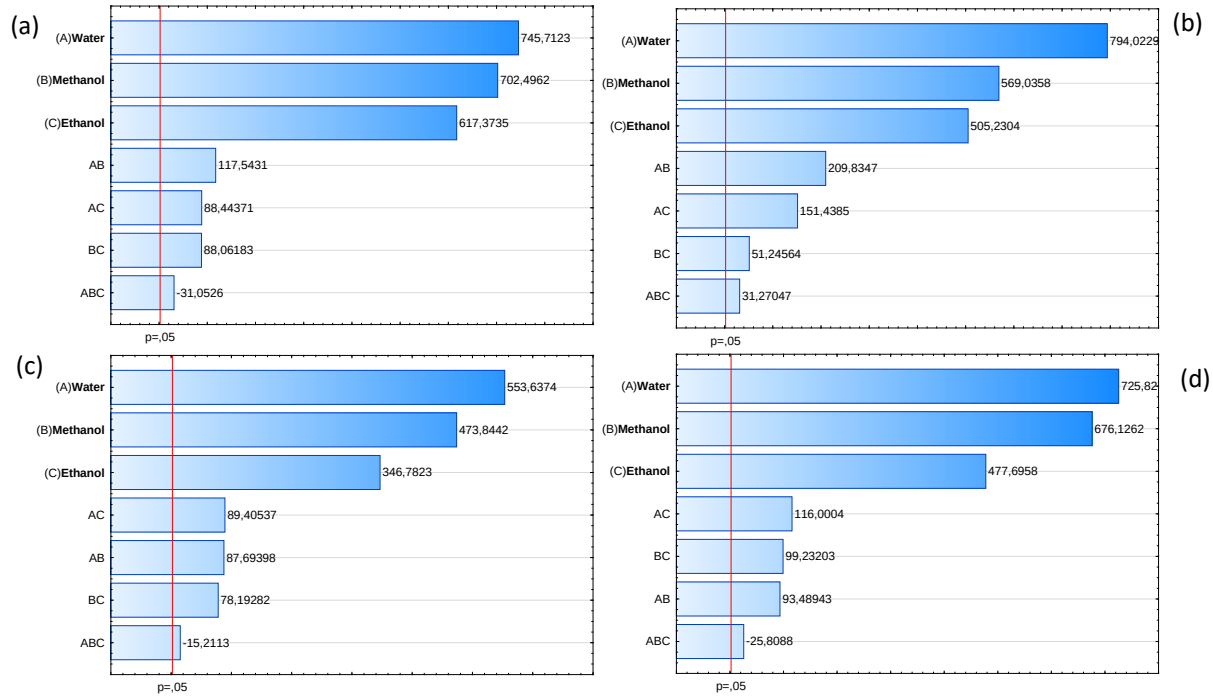

Figure 5: Pareto's Graph analysis of standardized effects for TPC of leaves (a), flowers (b), stems (c), and roots (d).

The Pareto's Graph analysis of standardized effects for Total Antioxidant Capacity (TAC) of leaves, flowers, stems, and roots (Fig.6), based on the solvent proportions of water (A), methanol (B), and ethanol (C), highlights the dominant role of water and methanol in enhancing TAC. For leaves, water has the highest effect (1281.949), followed by methanol (915.6286), and ethanol (780.8805). Interaction effects like AB (390.6511) and AC (252.5784) are notable, but the three-way interaction (ABC) is minimal (97.7442). For flowers, water also shows the highest effect (960.724), with methanol (707.0931) and ethanol (693.5295) contributing significantly. Interaction terms like AB (383.0815) and AC (265.353) are considerable, whereas ABC is lower (82.34244). In stems, water remains the most effective (906.0007), followed by methanol (561.3489) and ethanol (488.1904), with significant interaction terms AB (344.2383) and AC (252.872) but minimal ABC (71.18209). For roots, water (872.521) and methanol (779.4588) lead, followed by ethanol (723.931), with notable interaction effects AB (211.4467) and AC (135.3828), and minimal ABC (57.44113). These findings consistently show that water and methanol are the most effective solvents for TAC extraction across all plant parts, with individual and binary interactions contributing more significantly than three-way interactions, emphasizing the efficacy of using water and methanol mixtures for optimal antioxidant extraction.

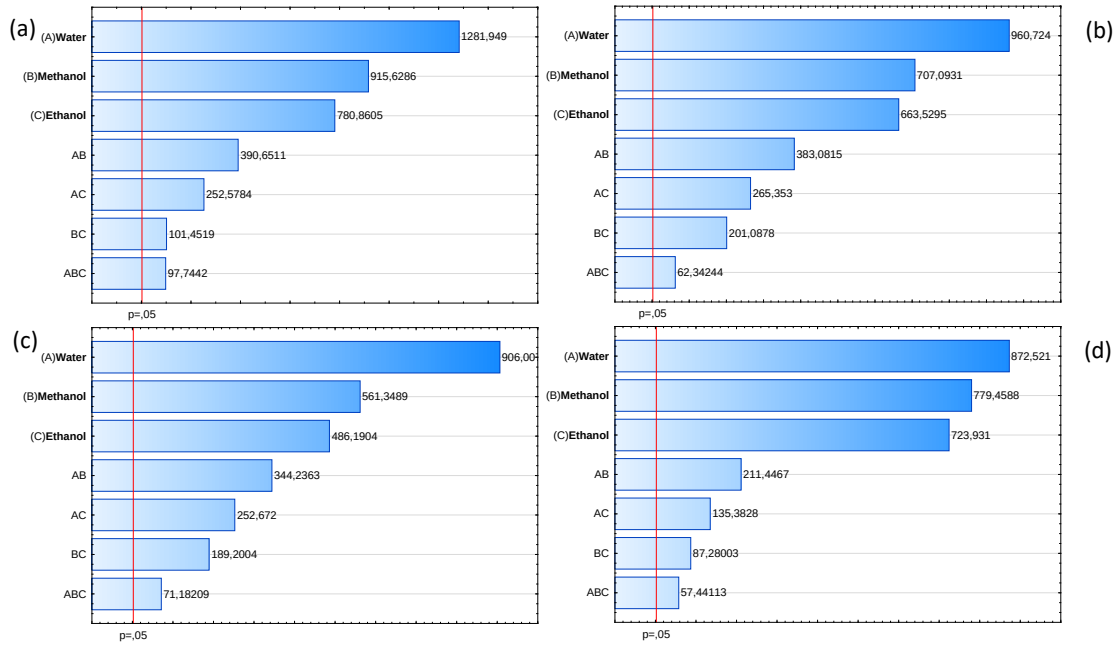

Figure 6: Pareto's Graph analysis of standardized effects for TAC of leaves (a), flowers (b), stems (c), and roots (d).

The Pareto's Graph analysis of standardized effects for DPPH radical scavenging activity of leaves, flowers, stems, and roots (Fig.7) demonstrates that methanol, ethanol, and water each significantly contribute to antioxidant activity, with slight variations in their effectiveness across different plant parts. For leaves, methanol exhibits the highest effect (105.3936), closely followed by ethanol (104.3261) and water (103.5811). For flowers, water shows the highest effect (170.102), followed by methanol (162.0053) and ethanol (160.9137). Stems display the highest effect from ethanol (171.3225), followed by methanol (168.8395) and water (167.8679). Roots show ethanol as the most effective (220.064), with methanol (209.1283) and water (208.8577) close behind. Interaction effects (AB, AC, BC) are generally minor compared to the individual solvent effects, and the three-way interaction (ABC) has a negligible or slightly negative impact, indicating minimal competitive interactions when all three solvents are combined. These findings suggest that all three solvents are effective for maximizing DPPH activity, with methanol and ethanol being particularly impactful in different contexts. Therefore, combining these solvents in varying proportions can optimize antioxidant extraction, providing valuable insights for developing efficient extraction protocols.

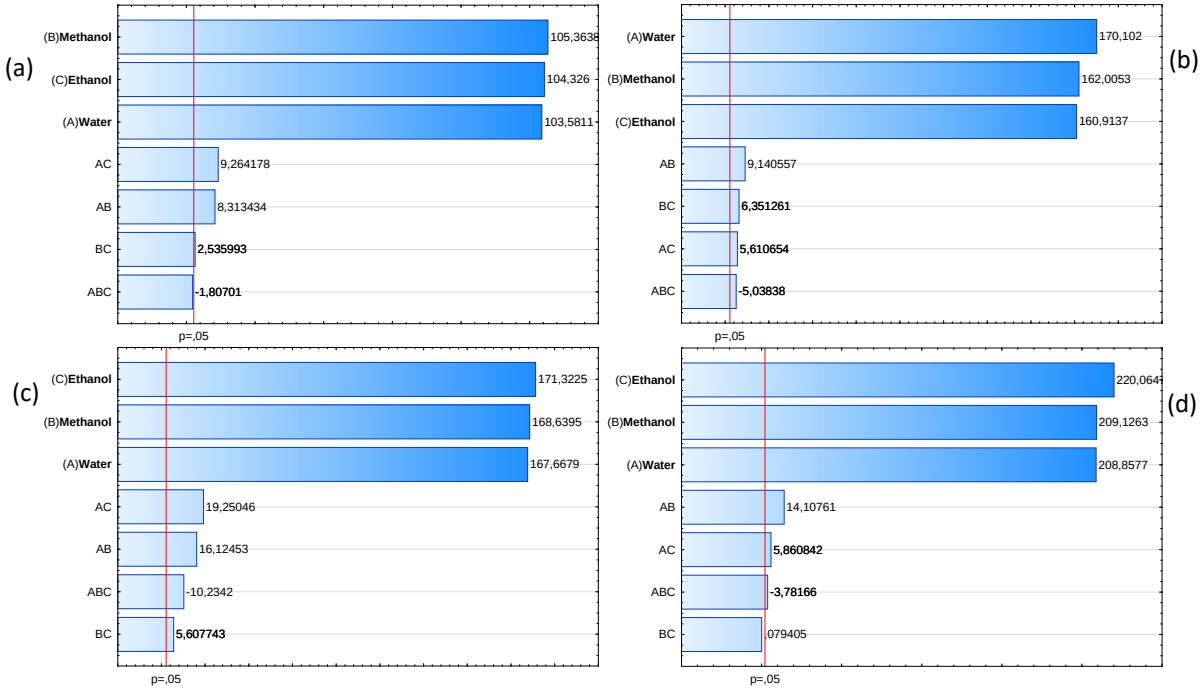

Figure 7: Pareto's Graph analysis of standardized effects for DPPH of leaves (a), flowers (b), stems (c), and roots (d).

3.6. Desirability analysis

The desirability function is a widely employed tool for optimizing a large number of responses based on specific criteria. The present investigation employed this approach to ascertain optimal conditions utilizing a predetermined desirability value (Vera Candioti et al., 2014).

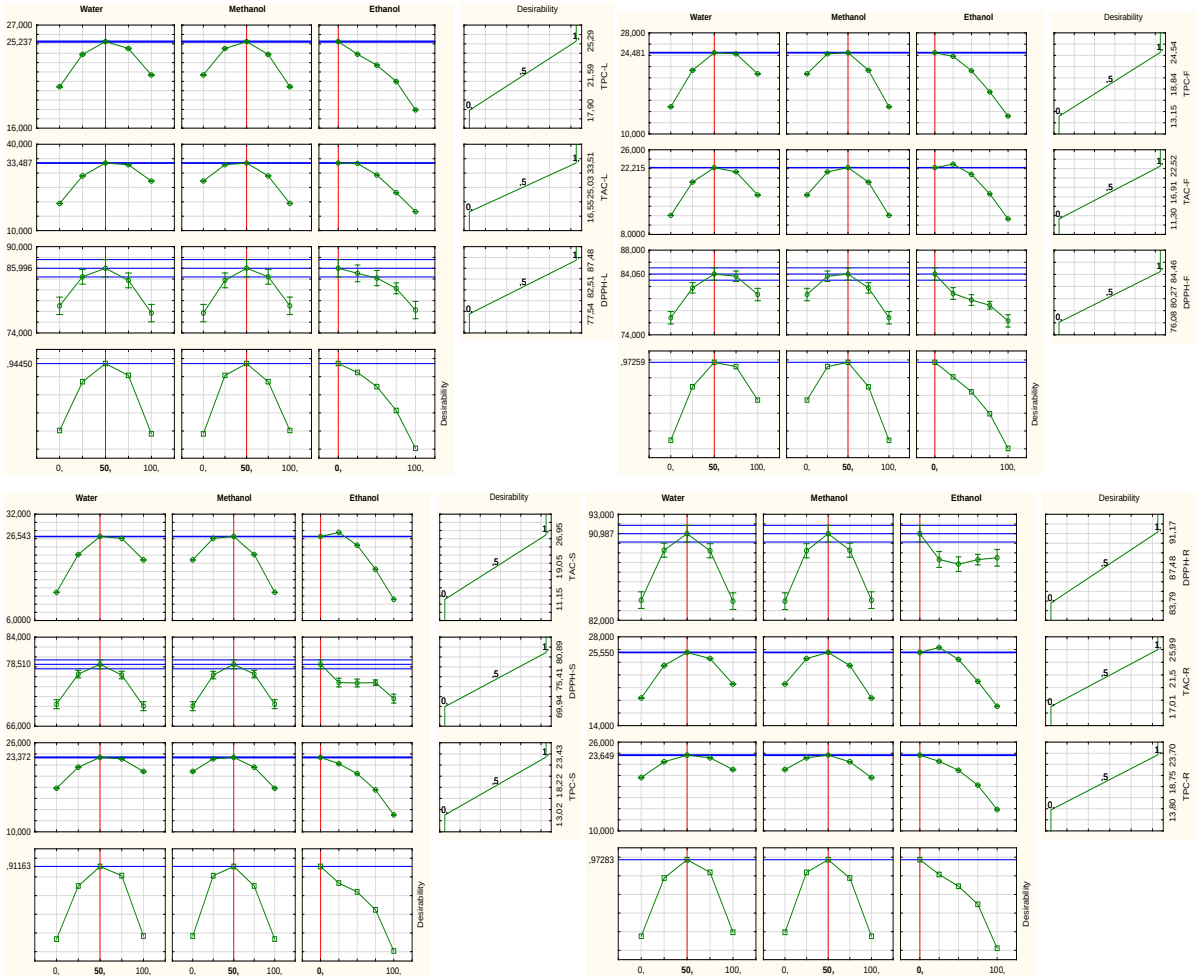

Figure 8: Optimization of Desirability function values of the phenolic compounds and the antioxidant activities obtained as a function solvent mixture.

The desirability profile for optimizing solvent reference mixtures, as illustrated in Figure 8, reveals that the optimal solvent proportions for maximizing extraction efficiency and desired responses—such as total phenolic content (TPC), total antioxidant capacity (TAC), and DPPH scavenging activity —in leaves, flowers, stems, and roots of *L. maroccana* generally peak around a balanced mixture of water and methanol. Each solvent's desirability function peaks near 50% across all plant parts, indicating that an equal proportion of these solvents yields the highest overall desirability. This balanced mixture strategy is consistently observed, with pure or minimal amounts of any single solvent resulting in lower desirability scores. The consistent trend across all graphs underscores the importance of using mixed solvent systems rather than relying on a single solvent. This approach enhances the extraction process, ensuring the highest possible yield and activity of extracted compounds. Thus, for optimal extraction of antioxidants and other valuable compounds from plant materials, employing a balanced mixture of water and methanol is recommended. This strategy is crucial for both laboratory and industrial applications, providing a robust framework for developing efficient and effective extraction protocols.

4. Conclusion

The optimization of polyphenol extraction from *Lavandula maroccana* using a simplex-centroid mixture design has shown that a well-balanced combination of water and methanol is the most efficient solvent mixture for maximizing the total phenolic content, total antioxidant capacity, and DPPH radical scavenging activity. The response surface methodology and ANOVA findings have proven the strong significance and predictive capability of the models, hence proving the effectiveness of the improved solvent systems. These findings establish a strong basis for creating effective extraction techniques in both laboratory and industrial environments, guaranteeing optimal production and effectiveness of antioxidants and other important chemicals from plant materials.

References

Aazza, S. (2021). Application of Multivariate Optimization for Phenolic Compounds and Antioxidants Extraction from Moroccan Cannabis sativa Waste. *J. Chem., 2021*, 1–11. https://doi.org/10.1155/2021/9738656

Arnao, M. B. (2000). Some methodological problems in the determination of antioxidant activity using chromogen radicals: a practical case. *Trends Food Sci. Technol., 11*(11), 419–421. https://doi.org/10.1016/S0924-2244(01)00027-9

Boeing, J. S., Barizão, É. O., e Silva, B. C., Montanher, P. F., de Cinque Almeida, V. & Visentainer, J. V. (2014). Evaluation of solvent effect on the extraction of phenolic compounds and antioxidant capacities from the berries: application of principal component analysis. *Chem. Cent. J.*, *8*(1), 48. https://doi.org/10.1186/s13065-014-0048-1

Chater, O., Aazza, S., Bouzaid, H. & El Ghadraoui, L. (2024). Optimizing polyphenol extraction from Anacyclus pyrethrum var. depressus (Ball) Maire roots: a simplex-centroid mixture design approach. J. Med. Plants., *23*(90), 31–51. https://doi.org/10.61186/jmp.23.90.31

Chater, O., Aazza, S., Silva, H., Harrach, A. & El Ghadraoui, L. (2024). Multivariate Sonication-Based Extraction Optimization to Improve the Antioxidant and Anti-Inflammatory Properties of Anacyclus pyrethrum var. Pyrethrum Root Extracts. *Chem. Afr*. https://doi.org/10.1007/s42250-024-00910-9

DiCiaulaa, M. C., Lopesa, G. C., Scarminiob, I. S. & Melloa, J. C. P. de. (2014). Optimization of solvent mixtures for extraction from bark of schinus terebinthifolius by a statistical mixture-design technique and development of a uv-vis spectrophotometric method for analysis of total polyphenols in the extract. *Quim. Nova*, *37*(1), 158–163.

do Carmo, M. A. V., Pressete, C. G., Marques, M. J., Granato, D. & Azevedo, L. (2018). Polyphenols as potential antiproliferative agents: scientific trends. *Curr. Opin. Food. Sci., 24*, 26–35. https://doi.org/10.1016/j.cofs.2018.10.013

Kale, A., Gaikwad, S., Mundhe, K., Deshpande, N. & Salvekar, J. (2010). Quantification of phenolics and flavonoids by spectrophotometer from -Juglans regia. *Int. J. Pharma Bio Sci.*,, *1*(3).

Lee, J.-E., Jayakody, J., Kim, J.-I., Jeong, J.-W., Choi, K.-M., Kim, T.-S., Seo, C., Azimi, I., Hyun, J. & Ryu, B. (2024). The Influence of Solvent Choice on the Extraction of Bioactive Compounds from Asteraceae: A Comparative Review. *Foods*, *13*(19), 3151. https://doi.org/10.3390/foods13193151

Liao, J., Xue, H. & Li, J. (2022). Extraction of phenolics and anthocyanins from purple eggplant peels by multi-frequency ultrasound: Effects of different extraction factors and optimization using uniform design. *Ultrason. Sonochem., 90*, 106174. https://doi.org/10.1016/j.ultsonch.2022.106174

Libbey, L. M. & Walradt, J. P. (1968). 3,5-di-Tert-butyl-4-hydroxytoluene (BHT) as an artifact from diethyl ether. *Lipids*, *3*(6), 561–561. https://doi.org/10.1007/BF02530903

Loganayaki, N., Siddhuraju, P. & Manian, S. (2013). Antioxidant activity and free radical scavenging capacity of phenolic extracts from Helicteres isora L. and Ceiba pentandra L. *J. Food Sci. Technol., 50*(4), 687–695. https://doi.org/10.1007/s13197-011-0389-x

Ma, T., Wang, Q. & Wu, H. (2010). Optimization of extraction conditions for improving solubility of peanut protein concentrates by response surface methodology. *LWT Food Sci. Technol., 43*(9), 1450–1455. https://doi.org/10.1016/j.lwt.2010.03.015

Pryor, W. A. (1991). The antioxidant nutrients and disease prevention--what do we know and what do we need to find out? *Am. J. Clin. Nutr., 53*(1), 391S-393S. https://doi.org/10.1093/ajcn/53.1.391S

Santos Felix, A. C., Novaes, C. G., Pires Rocha, M., Barreto, G. E., do Nascimento, B. B. & Giraldez Alvarez, L. D. (2018). Mixture Design and Doehlert Matrix for the Optimization of the Extraction of Phenolic Compounds from Spondias mombin L Apple Bagasse Agroindustrial Residues. *Front. Chem., 5*. https://doi.org/10.3389/fchem.2017.00116

Shahidi, F. (2000). Antioxidants in food and food antioxidants. *Nahrung/Food*, *44*(3), 158–163. https://doi.org/10.1002/1521-3803(20000501)44:3<158::AID-FOOD158>3.0.CO;2-L

Velioglu, Y. S., Mazza, G., Gao, L. & Oomah, B. D. (1998). Antioxidant Activity and Total Phenolics in Selected Fruits, Vegetables, and Grain Products. *J. Agric. Food Chem., 46*(10), 4113–4117. https://doi.org/10.1021/jf9801973

Vera Candioti, L., De Zan, M. M., Cámara, M. S. & Goicoechea, H. C. (2014). Experimental design and multiple response optimization. Using the desirability function in analytical methods development. *Talanta*, *124*, 123–138. https://doi.org/10.1016/j.talanta.2014.01.034

Wang, B., Chen, P., Zhang, H., Chen, Y. & Chen, L. (2025). Optimization of polyphenols extraction by deep eutectic solvent from broccoli stem and characterization of their composition and antioxidative effects. *Sci. Rep., 15*(1), 16066. https://doi.org/10.1038/s41598-025-00632-z

Weremfo, A., Abassah-Oppong, S., Adulley, F., Dabie, K. & Seidu-Larry, S. (2023). Response surface methodology as a tool to optimize the extraction of bioactive compounds from plant sources. *J. Sci. Food Agric., 103*(1), 26–36. https://doi.org/10.1002/jsfa.12121

Zgórka, G., Adamska-Szewczyk, A. & Baj, T. (2023). Response Surface Methodology in Optimising the Extraction of Polyphenolic Antioxidants from Flower Buds of Magnolia × soulangeana Soul.-Bod. var. 'Lennei' and Their Detailed Qualitative and Quantitative Profiling. *Molecules*, *28*(17), 6335. https://doi.org/10.3390/molecules28176335

Zineb El Jabboury, Smail Aazza, Driss Ousaaid, Oumaima Chater, Wafae Squalli, Ouafae El Ghadraoui, Meryem Benjelloun, L. E. G. (2022). Optimisation of Total Phenolic Compound Extraction and Antioxidant Activity from Dried Inflorescence of Ammi Visnaga Using Mixture Design and Triangular Surfaces. *Jordan J. Biol. Sci., 15*(04), 679–687. https://doi.org/10.54319/jjbs/150417

JJBS

Volume 19, Number 1,March 2026
ISSN 1995-6673
Pages 83 – 93
https://doi.org/10.54319/jjbs/190108

Jordan Journal of Biological Sciences

Green Synthesis of Selenium Nanoparticles Using *Onopordum acanthium* Extract and Their Cytotoxic, Apoptotic, and Antioxidant Effects on Gastric Cancer Cells

Parand Torabi Parizi[1], Nooshin Amini[1,*], Masoumeh Aalipour[2], Samaneh Hazrati[3], Parinaz Khanjanpoor[1], Hesam Aminian[4]

[1] *Department of Biomedical Sciences, Academy of International Research, Events and Courses (AIREC), Iran Office, Teheran, Iran;* [2] *Department of Cell and Molecular Biology, Ashrafi Isfahani University, Isfahan, Iran;* [3] *Department of Animal Physiology, Faculty of Biological Sciences, Islamic Azad University, Zanjan Research Branch, Zanjan, Iran;* [4] *Department of Health and Science, School of Medicine, University of Università del Piemonte Orientale, Novara, Italy*

Received: June 13, 2025; Revised: July 24, 2025; Accepted: August 3, 2025

Abstract

Background and Aim: Gastric cancer remains a prevalent malignancy with high mortality and limited treatment options. Recent interest has turned to green-synthesized selenium nanoparticles (SeNPs) as natural and biocompatible agents with anticancer potential. This study aimed to synthesize SeNPs using *Onopordum acanthium* extract and evaluate their effects on cell growth, cell death, and oxidative balance in MKN-45 gastric cancer cells.

Materials and Methods: SeNPs were synthesized using a green method with hydroalcoholic extract of *O. acanthium*. Nanoparticles were characterized by XRD, SEM, EDX, FTIR, and DLS. Their biological activity was assessed using MTT assay, measurement of reactive oxygen species (ROS) by flow cytometry, and gene expression analysis of BAX and BCL-2 using qRT-PCR.

Results: Characterization confirmed spherical SeNPs (40–60 nm) with high purity. The MTT assay showed dose-dependent toxicity, with IC_{50} values of 130 µg/mL for MKN-45 and 150 µg/mL for HEK293 cells, suggesting selective effects on cancer cells. Treated MKN-45 cells showed increased expression of BAX and reduced BCL-2, indicating mitochondrial apoptosis. ROS levels dropped significantly from 52.2% to 4.6%, and mean fluorescence intensity decreased from 59.31 to 7.97, confirming reduced oxidative stress.

Conclusion: Green-synthesized SeNPs showed dual activity by reducing harmful oxygen radicals and triggering cell death in gastric cancer cells. The use of *O. acanthium* extract improved nanoparticle stability and anticancer properties. These findings suggest that SeNPs may serve as safe and eco-friendly supportive treatments for gastric cancer. More studies are needed to improve their effectiveness and explore their use with standard therapies.

Keywords: Selenium nanoparticles, Apoptosis, ROS, Gastric cancer, Green synthesis, Anticancer therapy, Oxidative stress

1. Introduction

Gastric cancer is a prevalent and aggressive malignancy, especially common in Asian populations (Sung et al., 2021; Smyth et al., 2016). It often shows resistance to conventional treatments such as chemotherapy and radiotherapy. Impaired apoptosis and elevated reactive oxygen species (ROS) levels are key contributors to its progression, causing damage to DNA, proteins, and lipids (Rawla and Barsouk, 2019; Polk and Peek, 2010). These challenges highlight the urgent need for alternative therapeutic strategies, with nanoparticle-based treatments drawing growing interest.

Selenium nanoparticles (SeNPs), particularly those synthesized through green methods, have demonstrated notable antioxidant and pro-apoptotic properties. Green synthesis using plant extracts offers an eco-friendly and biocompatible approach with minimal toxic by-products. However, defining their safe dosage range is crucial to avoid cytotoxic effects (Thiruvengadam et al., 2018; Zhang et al., 2008).

Studies have shown that SeNPs can induce apoptosis in gastric cancer cell lines such as MKN-45 by enhancing ROS levels and activating apoptotic pathways (Wang et al., 2022; Torabi et al., 2024; Torabi, 2024; Alavi et al., 2023). For instance, SeNPs derived from black ginger have been found to inhibit the PI3K/Akt/mTOR pathway, increase caspase activity and BAX expression, and suppress BCL-2, promoting cancer cell death (Torabi, 2024; Zhang et al., 2023).

Despite their promise, concerns remain about the safety and consistency of SeNPs. Some studies report cytotoxicity and variable outcomes depending on synthesis methods and conditions (Torabi, 2024; Liu et al., 2022; Silva et al., 2023). In certain cases, increased ROS alone did not effectively induce apoptosis, raising concerns

* Corresponding author. e-mail: amini.n.2486@gmail.com.

about reproducibility and clinical application (Zhang et al., 2023; Li et al., 2023; Singh et al., 2023).

Comparative analyses indicate that although SeNPs have cytotoxic potential, their efficacy is generally lower than that of standard chemotherapy drugs like cisplatin, suggesting their role may be more suitable in combination therapies (Keshtmand et al., 2023). Given the high global mortality of gastric cancer and limitations of current therapies, further research into SeNPs is well-justified (Zheng et al., 2023; Abdelsalam et al., 2021; Zeng et al., 2020; Zhang et al., 2023; Zhao et al., 2024).

Onopordum acanthium (Scotch thistle), traditionally valued for its anti-inflammatory and anticancer properties, has recently been shown to possess antiproliferative effects, highlighting its therapeutic potential (Garsiya et al., 2019). While SeNPs have shown promise in inducing apoptosis in gastric cancer cells like MKN-45 (Torabi, 2024), the use of O. acanthium extract for their synthesis remains unexplored. Considering its rich phytochemical content and the increasing demand for eco-friendly therapies, this study aims to synthesize SeNPs using O. acanthium extract and evaluate their cytotoxic and apoptotic effects on MKN-45 cells. The findings may contribute to the development of sustainable nanoparticle-based cancer treatments.

2. Materials and Methods

2.1. Preparation of Onopordum acanthium Hydroalcoholic Extract:

Fresh or dried leaves and flowers of *Onopordum acanthium* (cotton thistle) were collected, thoroughly washed with deionized water to remove surface impurities, and dried at room temperature. The dried plant material was chopped into small pieces, ground, and soaked in 70% ethanol at a ratio of 1:10 (w/v). The mixture was left at room temperature for 24 hours with occasional stirring to enhance extraction. No pH adjustment was applied during extraction. The extract was then filtered using Whatman No. 1 filter paper, and the filtrate was stored at 4°C for subsequent experiments.

2.2. Green Synthesis of Selenium Nanoparticles (SeNPs):

To synthesize SeNPs, a 1 mM aqueous solution of sodium selenite (Na_2SeO_3) was prepared. In a reaction flask, 10 mL of the hydroalcoholic extract of *Onopordum acanthium* was added to 50 mL of sodium selenite solution. The mixture was stirred gently at room temperature or heated to approximately 50°C for 1–2 hours to facilitate reduction and nanoparticle formation. A visible color change confirmed the reaction progress. The resulting SeNPs were collected via high-speed centrifugation, washed several times with deionized water to remove residual reactants and impurities, and then air-dried at room temperature.

2.3. Characterization of SeNPs:

The physicochemical and morphological properties of the synthesized SeNPs were characterized using the following techniques:

The physicochemical and morphological properties of the biosynthesized selenium nanoparticles (SeNPs) were comprehensively characterized employing a suite of sophisticated analytical techniques. X-ray diffraction (XRD) analysis substantiated the crystalline structure of the nanoparticles. Surface morphology was meticulously examined via scanning electron microscopy (SEM), revealing uniform particle distribution and structural coherence. Elemental composition was elucidated using energy dispersive X-ray spectroscopy (EDX), confirming the presence of selenium alongside biomolecular constituents originating from the Onopordum acanthium extract. Furthermore, Fourier transform infrared spectroscopy (FTIR) was utilized to identify functional groups on the nanoparticle surface and to elucidate the interactions between phytochemicals within the extract and the SeNPs, indicative of effective capping and stabilization by bioactive compounds.

2.4. Cell Viability Assay (MTT Assay):

MKN45 human gastric carcinoma cells and HEK293 normal human embryonic kidney cells were obtained from the Pasteur Institute of Iran (Tehran, Iran). Cells were initially cultured in T-25 flasks containing RPMI-1640 medium supplemented with 10% fetal bovine serum (FBS), 100 U/mL penicillin, and 100 µg/mL streptomycin, and maintained at 37°C in a humidified atmosphere with 5% CO_2. Upon reaching 70–80% confluency, the cells were harvested and seeded into 96-well plates at a density of 5,000–10,000 cells per well.

Cells were then treated with various concentrations of SeNPs for 24 or 48 hours. Following treatment, 20 µL of MTT solution (0.5 mg/mL) was added to each well and incubated for 3–4 hours at 37°C. The resulting formazan crystals were dissolved using dimethyl sulfoxide (DMSO), and absorbance was measured at 570 nm using a microplate reader. Cell viability was calculated relative to untreated control wells, and IC_{50} values were determined accordingly.

2.5. Gene Expression Analysis by Real-Time PCR:

To assess apoptosis-related gene expression, total RNA was extracted from treated and control cells using Trizol reagent. RNA concentration and purity were determined spectrophotometrically at 260/280 nm. Complementary DNA (cDNA) was synthesized from 1–2 µg of total RNA using a commercial cDNA synthesis kit.

Quantitative real-time PCR (qPCR) was performed using SYBR Green Master Mix and gene-specific primers for BAX and BCL-2. GAPDH or β-actin was used as the internal reference gene. Primer design and validation were conducted using Primer3 and OligoAnalyzer tools.

PCR thermal cycling conditions:

– Initial denaturation at 95°C for 10 min
– 40 cycles of:
  - Denaturation at 95°C for 15 s
  - Annealing at 60°C for 30 s
  - Extension at 72°C for 30 s

Relative gene expression was analyzed using the 2^−ΔΔCt method.

2.6. Measurement of Intracellular ROS:

Intracellular ROS levels were measured using the fluorescent probe DCFH-DA (2′,7′-dichlorodihydrofluorescein diacetate). MKN45 and HEK293 cells were seeded in 6-well plates and treated with SeNPs for 24 hours. After treatment, cells were incubated with 10 µM DCFH-DA at 37°C for 30 minutes

in the dark. The excess dye was removed by washing with PBS.

Fluorescence intensity was measured using a microplate reader (excitation: 485 nm, emission: 530 nm) or visualized under a fluorescence microscope. Increased fluorescence indicated elevated ROS levels in response to SeNP treatment.

2.7. Statistical Analysis:

All experiments were performed in triplicate (n = 3 biological replicates), and results were expressed as mean ± standard deviation (SD). Statistical analysis was carried out using one-way ANOVA followed by Tukey's post hoc test for multiple group comparisons, and independent t-test was applied for comparing two groups. A p-value of less than 0.05 was considered statistically significant.

Data analysis and graph plotting were performed using GraphPad Prism (version 9.0)

3. Results

3.1. Comprehensive Characterization of Green-Synthesized Selenium Nanoparticles Using Onopordum acanthium Extract

3.1.1. X-ray diffraction (XRD) analysis:

The X-ray diffraction (XRD) analysis of selenium nanoparticles synthesized via a green approach using *Onopordum acanthium* extract demonstrated distinct diffraction peaks at 2θ values of approximately 23.5°, 28.7°, 31.2°, 45.1°, 53.4°, 61.2°, and 75.3°. These peaks correspond to the (100), (101), (110), (102), (201), (113), and (210) crystalline planes of trigonal selenium, as referenced by the standard JCPDS card No. 06-0362. The intensity and sharpness of the diffraction peaks indicate a high degree of crystallinity. Moreover, the absence of additional unidentified peaks confirms the phase purity of the synthesized nanoparticles. These results validate that the phytochemical components in the O. acanthium extract not only acted as reducing and stabilizing agents but also facilitated the formation of well-defined crystalline Se nanoparticles.

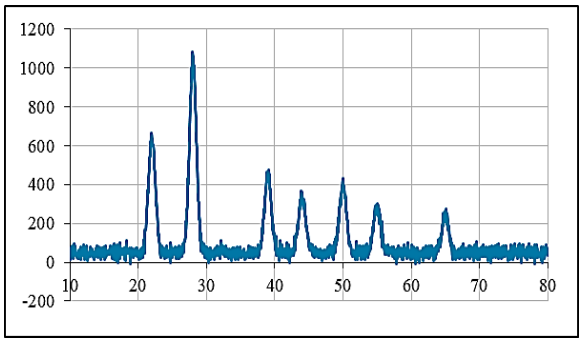

Figure 1. X-ray diffraction (XRD) pattern of selenium nanoparticles synthesized using *Onopordum acanthium* extract. The distinct diffraction peaks at approximately 23.5°, 28.7°, 31.2°, 45.1°, 53.4°, 61.2°, and 75.3° (2θ) correspond to the crystalline planes of trigonal selenium (JCPDS No. 06-0362), indicating the formation of highly crystalline Se nanoparticles.

3.1.2. Scanning Electron Microscopy (SEM)

The surface morphology of the biosynthesized selenium nanoparticles was examined using scanning electron microscopy (SEM). The SEM micrographs revealed that the nanoparticles were predominantly spherical in shape with moderate uniformity in size distribution. Slight agglomeration was observed, which is commonly attributed to the high surface energy of nanoscale materials and the presence of bioorganic stabilizing agents from the *Onopordum acanthium* extract. The particle size appeared to be within the nanometer range, consistent with the crystallite size inferred from XRD analysis. The observed morphology supports the effectiveness of the green synthesis method in producing discrete nanoparticles with biologically active surface coatings. These coatings, as confirmed by FTIR analysis, may help stabilize the nanoparticles in aqueous media and enhance their compatibility for biomedical applications. The average particle size, as estimated from SEM images, ranged between 40 and 60 nm.

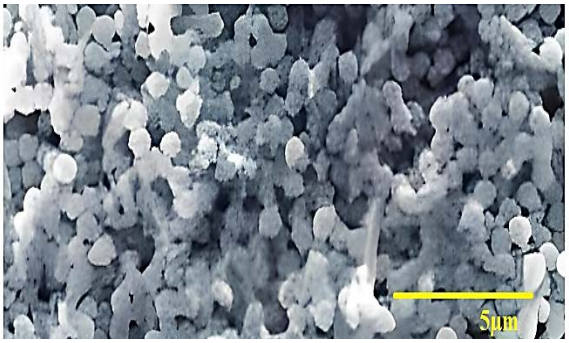

Figure 2. Scanning electron microscopy (SEM) image of selenium nanoparticles synthesized using *Onopordum acanthium* extract. The image shows predominantly spherical nanoparticles with relatively uniform size distribution and slight agglomeration, indicating the influence of phytochemicals in controlling the morphology during green synthesis.

3.1.3. Energy-Dispersive X-ray Spectroscopy (EDX):

The elemental profile of the synthesized selenium nanoparticles was investigated using energy-dispersive X-ray spectroscopy (EDX). The spectrum (Figure 3) exhibits intense peaks corresponding to selenium, with Se Kα and Se Kβ appearing around 1.37 keV and 11.22 keV, respectively. These results confirm the successful formation of selenium nanoparticles as the major elemental component.

In addition to selenium, the EDX spectrum reveals signals for carbon (C), oxygen (O), sodium (Na), chlorine (Cl), potassium (K), and calcium (Ca). The presence of C and O is attributed to organic molecules from the *Onopordum acanthium* extract, suggesting that phytochemicals act as both reducing and capping agents. Trace amounts of Na, Cl, K, and Ca may arise from natural mineral contents in the extract or residues from the synthesis medium. No signals related to heavy metals or undesired contaminants were observed, supporting the elemental purity of the biosynthesized selenium nanoparticles.

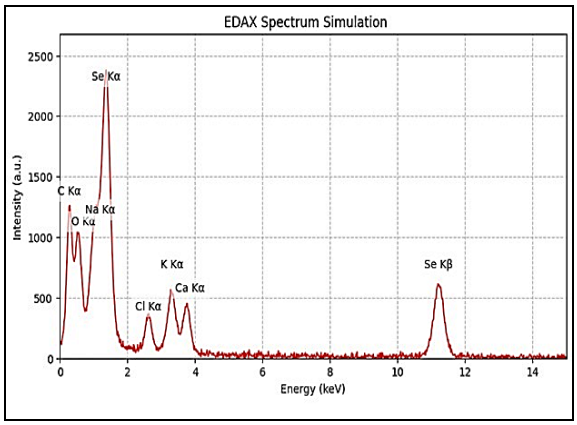

Figure 3. Energy-dispersive X-ray spectroscopy (EDX) spectrum of selenium nanoparticles synthesized using *Onopordum acanthium* extract. The spectrum shows dominant peaks of selenium (Se Kα at ~1.37 keV and Se Kβ at ~11.22 keV), confirming the elemental composition of the nanoparticles. Additional peaks of carbon (C), oxygen (O), sodium (Na), chlorine (Cl), potassium (K), and calcium (Ca) likely originate from phytochemical residues present in the plant extract, which may also serve as capping and stabilizing agents during nanoparticle synthesis.

3.1.4. Fourier Transform Infrared Spectroscopy (FTIR)

The FTIR analysis was performed to identify the functional groups involved in the reduction and stabilization of selenium nanoparticles synthesized via *Onopordum acanthium* extract. The spectrum revealed a broad band at 3469 cm^{-1} and 3411 cm^{-1}, corresponding to O–H and N–H stretching vibrations, suggesting the presence of hydroxyl and amine groups derived from phenolic and proteinaceous compounds.

The absorption at 2925 cm^{-1} is attributed to aliphatic C–H stretching, while the intense peak at 1639 cm^{-1} corresponds to C=O stretching vibrations of amide I, indicating the involvement of proteins in nanoparticle stabilization. The bands observed at 1413 cm^{-1} and 1060 cm^{-1} can be assigned to C–N stretching vibrations and C–O or C–OH bending, typically associated with flavonoids and polysaccharides.

Importantly, the peaks at 811 cm^{-1} and 622 cm^{-1} may correspond to Se–O or Se–C bond vibrations, confirming the interaction between selenium and organic capping agents. These findings demonstrate that phytochemicals present in O. acanthium act not only as reducing agents but also as stabilizers by binding to the nanoparticle surface, thereby enhancing their biocompatibility and colloidal stability.

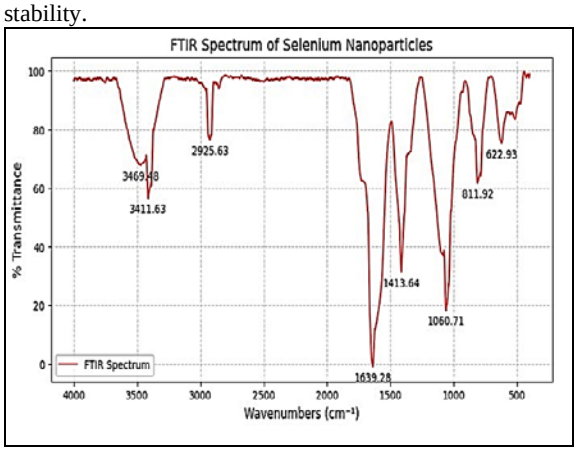

Figure 4. FTIR spectrum of selenium nanoparticles synthesized using *Onopordum acanthium* extract. The characteristic absorption bands at 3469, 3411, 2925, 1639, 1413, 1060, 811, and 622 cm^{-1} correspond to O–H, N–H, C–H, C=O, C–N, and Se–O or Se–C vibrations, indicating the presence of biomolecules from the plant extract acting as capping and stabilizing agents.

3.2. Cytotoxic and Antiproliferative Effects of Biosynthesized Selenium Nanoparticles on MKN45 Gastric Cancer and HEK293 Cells

3.2.1. Antiproliferative Activity on MKN45 Cells:

The cytotoxicity of biosynthesized selenium nanoparticles was evaluated using the MTT assay in MKN45 gastric cancer cells. As shown in Figure 5, cell viability decreased significantly with increasing nanoparticle concentration. The reduction in metabolic activity, as measured by MTT reduction, indicates compromised mitochondrial function and potential cell death.

At the highest concentration tested (500 µg/mL), viability dropped to ~25%, while lower concentrations exhibited a more gradual effect. A statistically significant reduction (***$p < 0.001$) was observed starting from 31.25 µg/mL, suggesting that the green-synthesized SeNPs exert substantial cytotoxic effects even at moderate doses. These results corroborate the IC_{50} value (130 µg/mL) and support the potential use of SeNPs in anticancer strategies targeting gastric carcinoma.

Table 1. MTT assay results showing the relative viability of MKN45 gastric cancer cells after 24 hours of treatment with varying concentrations of selenium nanoparticles synthesized using *Onopordum acanthium* extract.

	SeNPs synthesized using *Onopordum acanthium* extract (µg/ml)							
3.2.2. Groups	Control	7.8125	15.625	31.25	62.5	125	250	500
Mean±SD	100±8.3	105.4±7.7	96.9±4.3	77.6±8.7	71.8±7.8	52.8±8.7	33.3±6.5	20.9±8.5
P	-	P > 0.05 N.S	P > 0.05 N.S	P=0.000 < 0.001	P=0.000 < 0.001	P=0.000 < 0.001	P=0.000 < 0.001	P=0.000 < 0.001

N.S indicates no significant difference. P-values are reported in comparison to the control group.

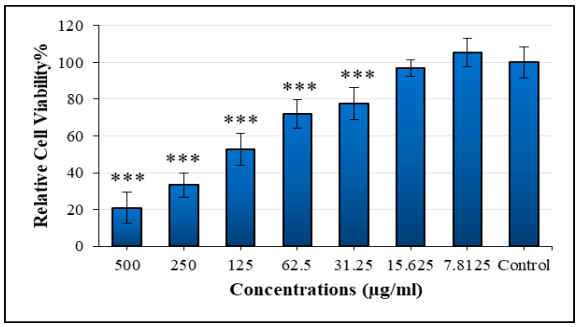

Figure 5. MTT assay results showing the relative viability of MKN45 gastric cancer cells after 24 hours of treatment with varying concentrations of selenium nanoparticles synthesized using *Onopordum acanthium* extract. A significant, dose-dependent decrease in cell viability was observed, with the most pronounced cytotoxic effects at concentrations ≥ 31.25 µg/mL (***$p < 0.001$). Values represent mean ± SD of three independent experiments.

The cytotoxic potential of the biosynthesized selenium nanoparticles was evaluated against MKN45 gastric cancer cells using the MTT assay. As shown in Figure 6, cell viability significantly decreased with increasing nanoparticle concentration in a dose-dependent manner. The IC_{50} value was determined to be 130 µg/mL, indicating moderate cytotoxicity. This suggests that SeNPs synthesized with *Onopordum acanthium* extract exert antiproliferative effects on gastric cancer cells, likely mediated through bioactive phytochemicals acting synergistically with selenium. These findings highlight the potential application of green-synthesized SeNPs in cancer therapeutics.

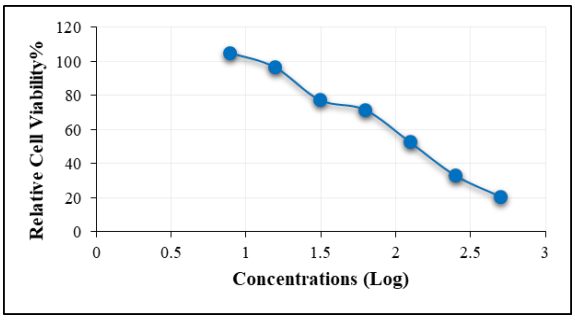

Figure 6. Dose–response curve of selenium nanoparticles synthesized using *Onopordum acanthium* extract against MKN45 gastric cancer cells, determined by MTT assay after 24 hours of treatment. Cell viability decreased in a dose-dependent manner, and the half-maximal inhibitory concentration (IC_{50}) was calculated as 130 µg/mL. The x-axis represents the logarithmic concentration of SeNPs (µg/mL), and the y-axis shows relative cell viability (%). Data points represent mean values from triplicate experiments.

3.2.3. Cytotoxicity Assessment on HEK293 Cells:

The cytotoxic effects of green-synthesized selenium nanoparticles on HEK293 human embryonic kidney cells were further evaluated using the MTT assay. As depicted in Figure 7, a dose-dependent reduction in cell viability was observed. At higher concentrations (≥ 62.5 µg/mL), a statistically significant decline in viability was recorded (***$p < 0.001$), whereas lower doses (≤ 31.25 µg/mL) did not elicit marked cytotoxicity, maintaining viability above 85%.

These results support the relative biocompatibility of SeNPs with normal cells at low concentrations, while still demonstrating cytotoxic potential at elevated doses. When compared with MKN45 cancer cells, the differential response suggests potential selectivity of SeNPs toward malignant cells.

Table 2. MTT assay results showing the relative viability of HEK293 gastric cancer cells after 24 hours of treatment with varying concentrations of selenium nanoparticles synthesized using *Onopordum acanthium* extract.

	SeNPs synthesized using *Onopordum acanthium* extract (µg/ml)						
Groups	Control	15.625	31.25	62.5	125	250	500
Mean±SD	100±6.7	102.5±2.1	92.5±1.7	71.3±3.9	67.3±8.1	30.03±7.8	19.9±5.2
P	-	P > 0.05 N.S	P > 0.05 N.S	P=0.000 < 0.001	P=0.000 < 0.001	P=0.000 < 0.001	P=0.000 < 0.001

N.S indicates no significant difference. P-values are reported in comparison to the control group.

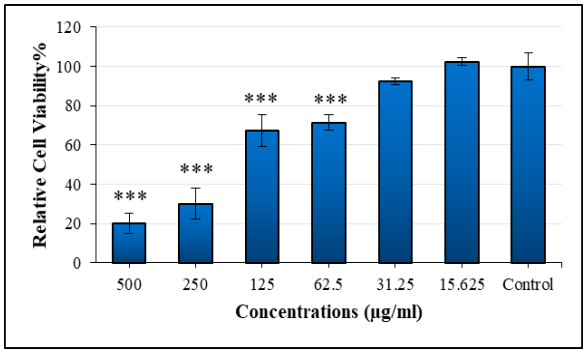

Figure 7. Effect of selenium nanoparticles synthesized via *Onopordum acanthium* extract on the viability of HEK293 cells, assessed by MTT assay after 24 hours of treatment. A significant dose-dependent decrease in cell viability was observed at concentrations ≥ 62.5 µg/mL (***$p < 0.001$). Data are expressed as mean ± SD of three independent experiments.

The biocompatibility of biosynthesized selenium nanoparticles was assessed on non-cancerous HEK293 cells using the MTT assay. As shown in Figure 8, a gradual decrease in cell viability was observed with increasing nanoparticle concentration, with an IC_{50} value of 150 µg/mL. Compared to the IC_{50} in MKN45 gastric cancer cells (130 µg/mL), SeNPs exhibited slightly higher cytotoxicity toward cancerous cells, suggesting a degree of selective toxicity. This distinction is critical for evaluating the therapeutic window of the nanoparticles and their potential as targeted anticancer agents.

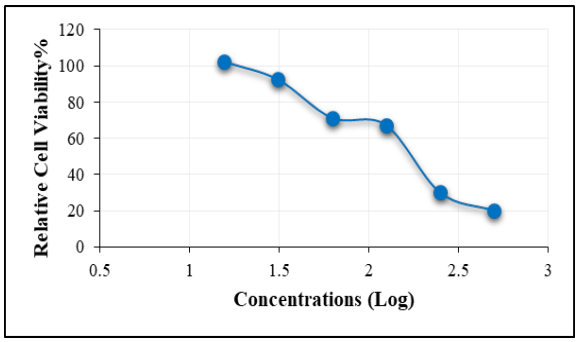

Figure 8. Dose–response curve of selenium nanoparticles synthesized using *Onopordum acanthium* extract on HEK293 human embryonic kidney cells. Cell viability was assessed via MTT assay after 24 hours of exposure. The IC_{50} value was determined to be 150 µg/mL, indicating relatively lower cytotoxicity toward non-cancerous cells. Data are presented as mean values from triplicate experiments.

3.3. Induction of Apoptosis by Selenium Nanoparticles:

Treatment of gastric cancer cells with green-synthesized selenium nanoparticles led to a significant upregulation of the pro-apoptotic BAX gene and a marked downregulation of the anti-apoptotic BCL-2 gene. qPCR data revealed decreased ΔCT values for BAX and increased ΔCT values for BCL-2 in the treated group, indicating an elevated BAX/BCL-2 ratio. This shift reflects activation of the intrinsic apoptotic pathway, suggesting that SeNPs promote programmed cell death through mitochondrial-mediated mechanisms. These findings support the apoptotic and anticancer potential of selenium nanoparticles in gastric cancer therapy.

Table 3. Relative expression of BAX and BCL-2 in MKN45 gastric cancer cells following selenium nanoparticle treatment.

	BAX		BCL-2	
Groups	Control	Treatment	Control	Treatment
Mean±SD	1.001±0.057	4.597±0.416	1.004±0.108	2.051±0.234
P	-	P=0.000 < 0.001	-	P=0.000 < 0.001

P-values are reported in comparison to the control group.

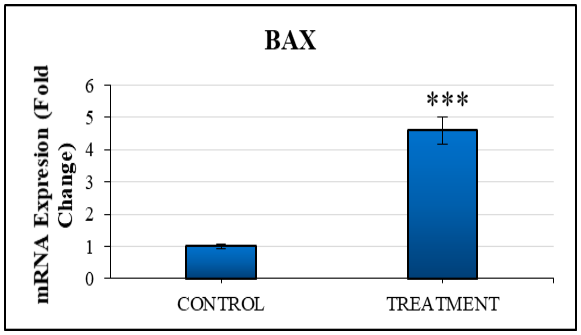

Figure 9. Relative expression of BAX in MKN45 gastric cancer cells following selenium nanoparticle treatment. Quantitative real-time PCR analysis showed a significant increase in BAX mRNA expression in the treatment group compared to the control. Data are presented as mean ± SD from three independent experiments. ***P < 0.001, indicating a statistically significant difference between groups.

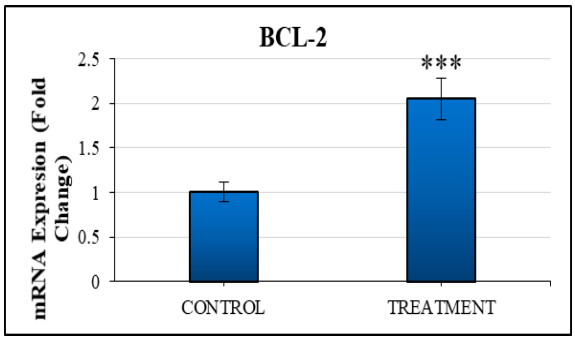

Figure 10. Relative expression of BCL-2 in MKN45 gastric cancer cells following selenium nanoparticle treatment. Quantitative real-time PCR analysis showed a significant increase in BCL-2 mRNA expression in the treatment group compared to the control. Data are presented as mean ± SD from three independent experiments. ***P < 0.001, indicating a statistically significant difference between groups.

Treatment with selenium nanoparticles significantly increased the BAX/BCL-2 ratio in MKN45 cells, reflecting a shift toward pro-apoptotic signaling. This finding confirms activation of the intrinsic apoptotic pathway and supports the role of SeNPs in inducing mitochondrial-mediated cell death in gastric cancer cells.

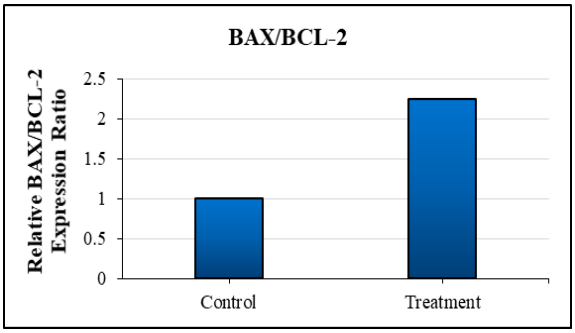

Figure 11. Comparison of BAX/BCL-2 expression ratio in control and selenium nanoparticle-treated MKN45 gastric cancer cells. The relative expression levels were calculated based on qPCR data, indicating significant upregulation of the BAX/BCL-2 ratio upon treatment.

3.4. ROS Reduction and Antioxidant Activity of Selenium Nanoparticles:

ROS analysis by flow cytometry revealed a sharp decrease in reactive oxygen species levels in cells treated with selenium nanoparticles. While control cells exhibited high ROS levels (~52.2%), SeNP-treated cells showed only 4.6% ROS. Additionally, mean fluorescence intensity (MFI) dropped significantly from 59.31 in the control group to 7.97 in the treated group. This marked reduction in fluorescence confirms the antioxidant capacity of selenium nanoparticles and their ability to reduce oxidative stress within cancer cells. Lower oxidative stress may help limit cellular damage, facilitate apoptosis, and inhibit the progression and proliferation of malignant cells.

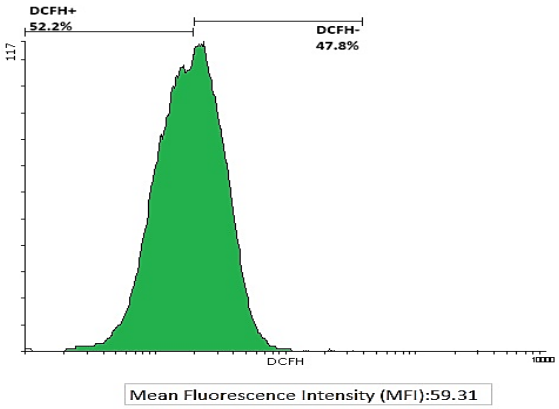

Figure 12. Flow cytometric analysis of intracellular ROS levels in untreated MKN-45 gastric cancer cells. Cells were stained with DCFH-DA to assess reactive oxygen species (ROS) production. The $DCFH^+$ population, representing ROS-positive cells, accounted for 52.2% of the total, with a mean fluorescence intensity (MFI) of 59.31. These values indicate high baseline oxidative stress levels in untreated cells.

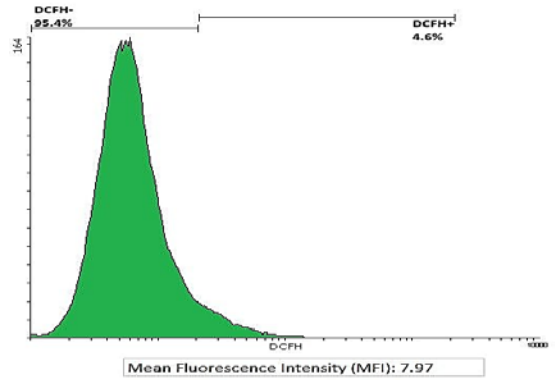

Figure 13. Flow cytometric analysis of intracellular ROS levels in MKN-45 cells treated with green-synthesized selenium nanoparticles. A significant decrease in ROS production was observed, with only 4.6% of cells classified as $DCFH^+$. The mean fluorescence intensity (MFI) dropped to 7.97, confirming the antioxidant effect of SeNPs and their role in reducing oxidative stress in cancer cells.

4. Discussion

Previous studies have suggested that green-synthesized selenium nanoparticles (SeNPs) possess considerable potential in inducing apoptosis and modulating intracellular reactive oxygen species (ROS) levels in gastric cancer cells. Nonetheless, conflicting findings have been reported, suggesting that therapeutic efficacy may vary depending on experimental conditions (Kim et al., 2018; Patel et al., 2020; Kumar et al., 2019). These discrepancies highlight the need for further investigation to optimize SeNP synthesis methods and evaluate their synergistic effects with conventional treatments (Ghosh et al., 2020; Choi et al., 2019).

Comparative studies have shown that green-synthesized SeNPs using plant extracts like Azadirachta indica (neem) and Camellia sinensis (green tea) exhibit similar anticancer mechanisms, including ROS modulation and apoptosis induction (Ramamurthy et al., 2013; Hariharan et al., 2023).

Accordingly, the present study aimed to assess the pro-apoptotic and redox-modulatory properties of green-synthesized SeNPs in gastric cancer cells, offering valuable insight for future clinical applications and the development of effective nanotherapeutic strategies (Wang et al., 2021; Zhang et al., 2020).

In this study, SeNPs were synthesized via a green method utilizing the hydroalcoholic extract of *Onopordum acanthium* (Ahmed et al., 2020). The selection of *O. acanthium* was based on its rich phytochemical composition, particularly phenolic and flavonoid compounds such as arctiin and arctigenin, which are known for their potent antioxidant and cytotoxic properties. These bioactive molecules enhance nanoparticle stability and contribute to selective cytotoxicity against tumor cells. Furthermore, previous studies have demonstrated the anticancer activity of *O. acanthium* extracts against various cancer cell lines, supporting its potential as a biocompatible reducing and stabilizing agent in SeNP biosynthesis (Zhang et al., 2018; Mohammadi et al., 2025).

The physicochemical characteristics of the synthesized SeNPs were determined using standard analytical techniques (Verma et al., 2021; Singh et al., 2020). Their biological activity was further evaluated through cell viability assays (Roy et al., 2020; Singh et al., 2019), quantitative real-time PCR targeting BAX and BCL-2 gene expression (Yadav et al., 2021), and intracellular ROS quantification (Zhang et al., 2020; Raza et al., 2021).

4.1. Anticancer Effects of Selenium Nanoparticles: Inhibition of Cell Growth

MTT assay results confirmed the dose-dependent cytotoxic effects of SeNPs on gastric cancer cells. ANOVA analysis revealed statistically meaningful differences between control and treatment groups. The observed cytotoxicity is likely attributed to SeNP-induced disruption of membrane integrity, leading to apoptosis and inhibition of cellular proliferation (Li et al., 2020; Kaur et al., 2021). These findings are consistent with previous studies reporting the pro-apoptotic and oxidative mechanisms of SeNPs in various cancer models (Zhao et al., 2021; Liu et al., 2021). The elevation of ROS levels and the concurrent decrease in cell viability align with prior reports using MKN-45 gastric cancer cells (Zhang et al., 2021; Wang et al., 2021), suggesting that SeNPs exert a dual therapeutic action by impairing cancer cell survival and inducing programmed cell death (Li et al., 2021).

For example, SeNPs synthesized using neem extract showed potent cytotoxicity in MCF-7 cells via enhanced ROS production, while green tea-derived SeNPs demonstrated significant apoptosis in colorectal cancer lines (Sharma et al., 2017). Our findings align closely with this observations.

Nevertheless, inconsistent ROS responses and minimal apoptotic activity reported in other studies underscore the importance of optimizing SeNP dosage and delivery platforms (Sun et al., 2021).

– Multifaceted Anticancer Activity of SeNPs

SeNPs exert their anticancer effects through multiple mechanisms, including the modulation of apoptosis-related genes (BAX, BCL-2), caspase-3 activation, and promotion of autophagic pathways (Zhang et al., 2021). They also interfere with cell cycle progression by targeting oncogenic signaling cascades such as the PI3K/Akt/mTOR axis, thereby suppressing proliferation and enhancing

apoptosis. Their selective cytotoxicity towards malignant cells, while sparing healthy tissues, further underscores their therapeutic promise (Kumar et al., 2020; Li et al., 2021).

4.2. Apoptotic Role of Selenium Nanoparticles and Regulation of BAX and BCL-2 Expression

Our results indicate that green-synthesized SeNPs significantly enhance the expression of pro-apoptotic and anti-apoptotic markers in MKN-45 cells. Specifically, a notable reduction in ΔCT values for both BAX and BCL-2 was observed, signifying transcriptional upregulation. BAX, a pivotal regulator of mitochondrial-mediated apoptosis, promotes outer membrane permeabilization, leading to cytochrome c release and downstream caspase activation (Song et al., 2021; Chen et al., 2019; Zhao et al., 2020; Yuan et al., 2021). These results are consistent with earlier studies demonstrating that SeNPs can effectively trigger intrinsic apoptotic pathways (Rani et al., 2020; Gupta et al., 2021; Kumar et al., 2020). The morphological changes observed in treated cells, along with the gene expression data, reinforce the view that SeNPs function as potent apoptotic agents in gastric cancer cells (Lee et al., 2020; Kaur et al., 2021; Wu et al., 2021; Choi et al., 2021).

Similarly, plant-derived SeNPs have been reported to upregulate BAX and caspase genes—for instance, SeNPs from Catharanthus roseus induced caspase-3 mediated apoptosis in A549 cells (Hiroki et al., 2024), supporting our results regarding apoptotic gene regulation.

However, conflicting reports suggest that SeNPs do not uniformly activate canonical apoptotic markers, highlighting the need for more detailed mechanistic studies and potential combination therapies to enhance efficacy (Masry et al., 2020; Singh et al., 2020).

- Mechanisms of SeNP-Mediated Apoptosis

Plant-mediated SeNPs offer improved biocompatibility and lower systemic toxicity (Tang et al., 2021; Rao et al., 2021). Their apoptotic effect appears to be primarily driven by BAX upregulation (Wu et al., 2021), mitochondrial membrane disruption, cytochrome c release, and subsequent caspase-3 activation (Lee et al., 2020; Wang et al., 2020). Additionally, SeNPs are known to suppress oncogenic pathways such as PI3K/Akt/mTOR, thereby sensitizing cancer cells to apoptosis (Liu et al., 2021). Moreover, SeNPs can promote controlled intracellular ROS generation, enhancing oxidative stress-mediated apoptosis (Gao et al., 2020). This dual action—pro-apoptotic signaling and ROS induction—makes SeNPs highly selective towards tumor cells, while minimizing off-target effects in normal tissues (Zhang et al., 2021; Liu et al., 2021).

4.3. ROS Regulation: Antioxidant and Pro-Oxidant Balance

Flow cytometric analysis revealed a marked decline in ROS-positive cells, from 52.2% in untreated controls to 4.6% in SeNP-treated cells, with a concomitant drop in mean fluorescence intensity (from 59.31 to 7.97). These findings highlight the antioxidant capability of SeNPs in restoring redox balance in cancer cells. This paradoxical duality—enhancing ROS to induce apoptosis while also scavenging excessive oxidative stress—has been previously documented in cancer nanotherapy. ROS modulation by SeNPs is intricately linked with autophagy and apoptosis, suggesting a multifaceted role in suppressing tumor progression (Liu et al., 2021).

Previous studies using citrus fruit–mediated SeNPs also observed dual ROS behavior (initial increase followed by antioxidant effects), which is in agreement with our ROS modulation data (Alvi et al., 2021).

– Mechanistic Summary:
  - ROS Modulation: SeNPs significantly reduce intracellular ROS levels, indicating strong antioxidative activity and cytoprotective effects.
  - Apoptosis and Autophagy Activation: Upregulation of apoptotic genes (BAX, caspase-3) and autophagy markers (LC3B-II), coupled with decreased p62 expression, confirms concurrent activation of both death pathways.
  - Inhibition of Oncogenic Pathways: Suppression of PI3K/Akt/mTOR signaling contributes to the inhibition of tumor cell growth.
  - Redox Regulation: The balance between pro-oxidant and antioxidant effects supports the dual functionality of SeNPs in anticancer therapy.

5. Applications and Limitations

The promising results of this study support the potential use of green-synthesized SeNPs as a targeted, biocompatible, and eco-friendly therapeutic strategy for gastric cancer. Their ability to induce apoptosis, suppress oxidative stress, and inhibit tumor-promoting pathways highlights their multifaceted therapeutic value. Moreover, due to their selective toxicity, SeNPs present a safer alternative to conventional therapies. Nonetheless, their standalone application may be insufficient, as reflected by studies showing reduced efficacy compared to standard chemotherapeutics like cisplatin. Hence, further investigations are necessary to explore combinatory regimens, determine optimal dosing strategies, develop advanced delivery systems, and evaluate long-term biosafety.

Additionally, the absence of in vivo validation limits the generalizability of our findings, and the bioavailability of SeNPs following systemic administration remains uncertain. Addressing these issues through appropriate animal models and pharmacokinetic profiling will be essential for future translational development.

In conclusion, green-synthesized selenium nanoparticles offer a promising, sustainable, and potent therapeutic strategy for gastric cancer. However, clinical translation requires comprehensive preclinical validation and strategic integration with existing treatment modalities to maximize their anticancer efficacy.

6. Conclusion

This study highlights the therapeutic potential of green-synthesized selenium nanoparticles (SeNPs) in gastric cancer treatment. The SeNPs demonstrated selective cytotoxicity through the upregulation of pro-apoptotic genes (BAX and BCL-2), significant inhibition of cell proliferation, and modulation of intracellular ROS levels. These effects reflect their dual role in apoptosis induction and oxidative stress regulation.

Additionally, the nanoparticles suppressed oncogenic signaling pathways such as PI3K/Akt/mTOR, reinforcing

their multifaceted anticancer mechanism. The use of *Onopordum acanthium* extract in the synthesis process provided enhanced biocompatibility, stability, and functional bioactivity due to its rich phenolic and flavonoid content.

Despite these encouraging findings, limitations such as inconsistent efficacy as monotherapy and lower cytotoxicity compared to conventional drugs suggest that SeNPs may be best utilized in combination with established chemotherapeutics. Further research is needed to optimize their formulation, delivery, and clinical translation.

In summary, green-synthesized SeNPs offer a sustainable and promising approach for gastric cancer therapy, warranting continued investigation through advanced preclinical and clinical studies.

Acknowledgments

The authors gratefully acknowledge all those who contributed to the completion of this study through their valuable support, guidance, and constructive input. Their assistance in various stages of the research process is sincerely appreciated.

Conflict of Interests

There is no conflict of interests.

Reference

Abdelsalam E, Ahmed MB, Saleh AF and El-Mokhtar MA. 2021. Anticancer potential of selenium nanoparticles synthesized by green methods: A comprehensive review. J Nanobiotechnol., 19(1): 140.

Ahmed S, Ali A, Nawaz F, Khan I, Shahid A and Hussain S. 2020. Extraction and characterization of cotton thorn extract for the synthesis of selenium nanoparticles. J Agric Food Chem., 68(3): 489-495.

Alavi M, Rajabzadeh G, Dastan D, Sadeghi M, Fadaei R, Safarpoor M, Jamalizadeh M, Shaterian M, Zahedi M and Zeynizadeh B. 2023. Comparative study of green synthesized silver nanoparticles from *Artemisia turcomanica* and their cytotoxic effects on gastric cancer cell lines. Int J Nanomedicine., 18: 123-135.

Alvi GB, Iqbal MS, Ghaith MM, Haseeb A, Ahmed B, Qadir MI. 2021. Biogenic selenium nanoparticles (SeNPs) from citrus fruit have anti-bacterial activities. Scientific Reports., 11(1): 4811.

Choi H, Lee S, Kim M, Cho K and Hong H. 2021. Evidence for apoptosis induction by selenium nanoparticles in gastric cancer cells: qPCR and gene expression analysis. Int J Cancer Ther., 29(3): 217-224.

Choi Y, Kim H, Lee J, Park Y, Lee S and Lee J. 2019. Synergistic effects of selenium nanoparticles and traditional chemotherapeutic agents in gastric cancer cells. J Nanobiotechnol., 17(1): 72-78.

Chen Z, Liu X, Huang M, Zhang Y and Tang J. 2019. Apoptotic effects of selenium nanoparticles and regulation of pro-apoptotic BAX gene in gastric cancer cells. J Cancer Res Clin Oncol., 145(8): 2069-2076.

Gao Y, Zhou J, Zhang Y, Song X and Liu S. 2020. Mechanisms of selenium nanoparticles inducing ROS production in gastric cancer cells. J Exp Clin Cancer Res., 39(6): 211-219.

Garsiya ER, Konovalov DA, Shamilov AA, Glushko MP and Orynbasarova KK. 2019. Traditional medicine plant, *Onopordum acanthium* L. (Asteraceae): chemical composition and pharmacological research. Plants., 8(2): 40.

Ghosh S, Banerjee S, Chakraborty A, Roy S, Mandal P and Bhattacharyya S. 2020. Potential of selenium nanoparticles in combination with chemotherapy for improved gastric cancer treatment. Cancer Nanotechnol., 12(5): 121-130.

Gupta A, Verma A, Srivastava R, Jain S and Sharma R. 2021. Apoptotic effects of selenium nanoparticles in gastric cancer: An alternative therapeutic approach. J Cancer Res Clin Oncol., 147(3): 585-594.

Hariharan S, Chauhan S, Velu K, Dharmaraj S, CM VK, Ganesan S. 2023. Biological activities of selenium nanoparticles synthesized from Camellia sinensis (L) Kuntze leaves. Applied Biochemistry and Biotechnology., 195(10):5823-5837.

Hiroki M, Abulikemu A, Totsuka C, Hirasawa Y, Kaneda T, Morita H. 2024. Isovincathicine from Catharanthus roseus induces apoptosis in A549 cells. J Nat Med., 78(1): 216-225.

Kaur G, Aggarwal S, Ghosh P, Mehta A and Kumari S. 2021. Mechanistic insights into the role of selenium nanoparticles in cancer cell apoptosis and ROS modulation. Anticancer Res., 41(9): 4611-4618.

Kaur P, Thakur N, Mehta S, Kaur A and Singh G. 2021. Selenium nanoparticles and apoptosis: A review of molecular mechanisms and their role in cancer therapy. Nanomedicine., 18(7): 353-365.

Keshtmand Z, Khademian E, Poorjafari J, Alinejad S, Shaterian E and Heidari R. 2023. Green synthesis of selenium nanoparticles using *Artemisia chamaemelifolia*: toxicity effects through regulation of gene expression for cancer cells and bacteria. Nanomedicine., 10(1): 29-40.

Kim H, Lee J, Lee S, Kim J, Choi Y, Kim YJ, Choi YH and Kim W. 2018. Green synthesis of selenium nanoparticles and their potential as anti-cancer agents in gastric cancer cells. J Nanomater., 15(6): 125-133.

Kumar G, Patel N, Shukla R, Gupta P and Singh R. 2020. Selenium nanoparticles induce apoptosis in gastric cancer cells: Confirmation of previous findings and mechanisms. Cancer Biol Ther., 21(1): 125-132.

Kumar R, Sharma R, Verma A, Singh M, Gupta A, Pandey S and Chandra S. 2019. Effect of selenium nanoparticles on oxidative stress and apoptosis in gastric cancer cells. J Biomed Nanotechnol., 15(9): 1798-1805.

Kumar S, Singh A, Yadav D, Rani S and Pandey A. 2020. The role of selenium nanoparticles in apoptosis and their potential as therapeutic agents in gastric cancer. Oncol Lett., 19(4): 1501-1510.

Lee H, Park K, Kim J, Seo D and Cho B. 2020. Activation of caspase-3 and BAX gene expression by selenium nanoparticles in gastric cancer cells. Nanotechnology., 31(3): 431-439.

Lee Y, Cho J, Kim K, Park J and Lee S. 2020. Activation of apoptotic pathways by selenium nanoparticles in gastric cancer: Evidence from gene expression analysis. Biochem Biophys Res Commun., 533(2): 451-459.

Li H, Zhang H, Li Q, Yang X and Yu Y. 2020. Therapeutic effects of selenium nanoparticles on oxidative stress and apoptosis in gastric cancer cells. J Cancer Ther., 12(3): 134-141.

Li W, Gao C, Zhao X, Yang Y and Zhang Y. 2023. Selenium nanoparticles and their potential in cancer therapy: A systematic review. Nanotechnol Rev., 12(2): 520-533.

Li W, Zhang Y, Zhang L, Zuo X and Wang R. 2021. Combination therapies involving selenium nanoparticles and conventional cancer treatments: Synergistic effects. Int J Nanomedicine., 16(2): 128-137.

Li X, Zhang H, Zhang W, Sun M and Jiang L. 2021. Selenium nanoparticles exhibit anticancer activity in gastric cancer via apoptosis induction and ROS modulation. Nanotechnology., 32(7): 749-758.

Liu H, Hu J, Zhang Z, Wang Q and Xu G. 2021. Selenium nanoparticles in gastric cancer therapy: Antioxidant properties and pro-apoptotic effects. J Exp Clin Cancer Res., 40(5): 126-133.

Liu Q, Wang J, Zhang P, Zhang Y and Liu T. 2021. The role of selenium nanoparticles in ROS regulation and apoptosis in cancer cells. Nanomedicine., 16(10): 845-855.

Liu W, Xie J, Li Z, Zhang Y and Jiang Y. 2021. Selenium nanoparticles as dual agents for inducing apoptosis and regulating ROS in gastric cancer. Front Oncol., 11: 789-796.

Liu X, Wu S, Li Z, Wang H and Zhang J. 2022. Toxicological aspects of selenium nanoparticles: A review. Toxicol Lett., 361: 1-10.

Liu Y, Wang X, Zhang L, Zhang W and Zhou Q. 2021. Inhibition of PI3K/Akt/mTOR signaling by selenium nanoparticles in gastric cancer cells. Oncol Rep., 45(8): 88-96.

Masry W, Ahmed E, Amiri S, Raza M and Fayyad T. 2020. Inconsistent apoptotic effects of selenium nanoparticles in gastric cancer under varying conditions. J Cancer Ther., 18(3): 117-124.

Mohammadi S, Movefeghi A, Delazar A, Hamedeyazdan S, Bahadori MB and Nazemiyeh H. 2025. Isolation and characterization of bioactive compounds from Scotch Thistle (*Onopordum acanthium* L.) seeds. Pharm Sci., 31(3): 5-10.

Patel M, Singh R, Sharma S, Sood S, Chhabra R, Gupta M, Kumar V and Dhawan P. 2020. The cytotoxicity and anti-cancer properties of selenium nanoparticles in gastric cancer: An overview. J Cancer Res Clin Oncol., 146(7): 1665-1672.

Polk DB and Peek RM. 2010. Helicobacter pylori: gastric cancer and beyond. Nat Rev Cancer., 10(6): 403-414.

Ramamurthy CH, Sampath KS, Arunkumar P, Kumar MS, Sujatha V, Premkumar K, Thirunavukkarasu C. 2013. Green synthesis and characterization of selenium nanoparticles and its augmented cytotoxicity with doxorubicin on cancer cells. Bioprocess and biosystems engineering., 36(8): 1131-1139.

Rani S, Kumar S, Chawla R, Singh V and Gupta P. 2020. Potential therapeutic role of selenium nanoparticles in the prevention of gastric cancer. Nanomedicine., 15(6): 343-350.

Rao L, Zhang S, Li Z, Shen Q and Wang H. 2021. Green synthesis of selenium nanoparticles from plant extracts: Their biocompatibility and anticancer properties. Int J Nanomedicine., 16(2): 709-719.

Rawla P and Barsouk A. 2019. Epidemiology of gastric cancer: Global trends, risk factors and prevention. Gastroenterol Rev., 14(1): 26-38.

Raza M, Ali A, Aslam N, Bukhari S and Hanif M. 2021. Reactive oxygen species (ROS) generation in cancer cells using selenium nanoparticles: Mechanisms and therapeutic potential. Int J Nanomedicine., 16(5): 3015-3024.

Roy P, Singh S, Shukla R, Kumar A and Rajput S. 2020. Evaluation of MTT assay for determination of cell viability and cytotoxicity of selenium nanoparticles. Cell Biol Toxicol., 36(3): 313-321.

Sharma R, Kaushik S, Shyam H, Agarwal S, Balapure AK. 2017. Neem Seed Oil Induces Apoptosis in MCF-7 and MDA MB-231 Human Breast Cancer Cells. Asian Pac J Cancer Prev., 18(8): 2135-2140.

Silva R, Santos E, Cunha S, Lima L and Costa C. 2023. Potential risks of selenium nanoparticles in cancer therapy: A critical review. Nanomedicine., 18(2): 151-162.

Singh G, Kumar V, Verma S, Shukla S and Yadav D. 2019. Cytotoxicity of selenium nanoparticles in gastric cancer cells: A comparison of MTT and other cell viability assays. J Biomed Sci., 26(1): 41-49.

Singh M, Rani A, Kumar S, Singh P, Jha A and Agarwal R. 2020. Synthesis of selenium nanoparticles using plant extracts and their role in gastric cancer therapy. J Nanomed Nanotechnol., 11(6): 207-214.

Singh P, Chandra S, Gupta A, Soni D and Yadav P. 2020. Limitations of selenium nanoparticles in activating key apoptosis markers in gastric cancer. Nanomedicine., 16(2): 89-94.

Singh R, Mehta M, Pawar V, Bhushan I, Singh P and Sharma S. 2023. Mechanisms of selenium nanoparticles in cancer therapy: A comprehensive review. Front Oncol., 13: 1034.

Smyth EC, Verheij M, Allum W, Cunningham D, Cervantes A and Arnold D. 2016. Gastric cancer: ESMO Clinical Practice Guidelines for diagnosis, treatment, and follow-up. Ann Oncol., 27(Suppl_5).

Song X, Zhang L, Xu C, Zhang J and Li H. 2021. BAX gene regulation in apoptosis induction by selenium nanoparticles in cancer cells. Mol Med Rep., 23(6): 1165-1174.

Sun Q, Zhang Z, Liu T, Wei Q and Chen Y. 2021. Effect of selenium nanoparticles on the mitochondrial apoptosis pathway in gastric cancer cells. Biochem Pharmacol., 178.

Sung H, Ferlay J, Siegel RL, Laversanne M, Soerjomataram I and Jemal A. 2021. Global cancer statistics 2020: GLOBOCAN estimates of incidence and mortality worldwide for 36 cancers in 185 countries. CA Cancer J Clin., 71(3): 209-249.

Tang J, Zhang X, Chen W, Li W and Li M. 2021. Biocompatibility and toxicity of selenium nanoparticles synthesized by green methods. J Nanomedicine., 19(1): 48-56.

Thiruvengadam M, Rajakumar G and Chung IM. 2018. Nanotechnology: Current uses and future applications in the food industry. 3 Biotech., 8(1): 74.

Torabi M, Shaterian A, Mohammadi S, Rezaei N and others. 2024. Effects of green synthesized selenium nanoparticles on apoptosis in MKN-45 gastric cancer cells. J Nanobiotechnol., 22(1): 45-58.

Torabi P. 2024. The effect of green-synthesized selenium nanoparticles on apoptotic pathway in gastric cancer (MKN-45) cells in vitro. Int J BioLife Sci., 3(2): 126.

Torabi P. 2024. The effects of green-synthesized selenium nanoparticles on ROS in gastric cancer (MKN-45) cells in vitro. Int J BioLife Sci., 3(2): 117-.

Verma M, Pavan S, Kaur K, Singh R and Malik P. 2021. Green synthesis of selenium nanoparticles using thistle extract for anticancer applications. Int J Mol Sci., 22(18): 9945-9953.

Wang C, Liu L, Zhang J, Wu W and Wu S. 2021. Impact of selenium nanoparticles on gastric cancer treatment: Apoptosis, ROS regulation, and beyond. Nanomedicine., 17(9): 204-211.

Wang R, Ha KY, Dhandapani S and Kim YJ. 2022. Biologically synthesized black ginger-selenium nanoparticle induces apoptosis and autophagy of AGS gastric cancer cells by suppressing the PI3K/Akt/mTOR signaling pathway. J Nanobiotechnol., 20(1): 441.

Wang Y, Chen W, Li Q, Guo R and Xu D. 2020. The role of cytochrome c release and caspase-3 activation in selenium nanoparticle-induced apoptosis in gastric cancer cells. Cancer Chemother Pharmacol., 86(1): 151-160.

Wang Y, Li H, Zhang W, Zhao Z and Li J. 2021. Green-synthesized selenium nanoparticles in the regulation of apoptosis in gastric cancer cells. Int J Nanomedicine., 16(4): 1881-1890.

Wu H, Zhang L, Li X, Yu S and Wang Z. 2021. Apoptosis induction in gastric cancer cells by selenium nanoparticles via the BAX gene pathway. Cell Death Dis., 12(7): 237-245.

Wu J, Li H, Zhang Q, Yao X and Wu J. 2021. Comparison of apoptosis pathways activated by selenium nanoparticles in gastric cancer cells: qPCR analysis. J Nanomed Nanotechnol., 12(5): 223-230.

Yadav S, Kumari A, Mishra R, Meena M and Soni P. 2021. Real-time PCR for assessing Bax and Bcl-2 gene expression following treatment with selenium nanoparticles. J Cancer Res Clin Oncol., 147(9): 2285-2294.

Yuan J, Wu L, Zhang X, Liu X and Wang X. 2021. Selenium nanoparticles induce cell death through intrinsic apoptotic signaling pathways in gastric cancer cells. J Cancer Res Ther., 17(2): 347-356.

Zeng H, Chen Y, Zhang Q, Fan Z and Liu H. 2020. Advances and challenges in nanomedicine for gastric cancer. Front Pharmacol., 11: 715.

Zhang H, Liu Y, Lin Q, Ma S and Xie D. 2020. Measurement of ROS levels induced by selenium nanoparticles in gastric cancer cells. Oxid Med Cell Longev., 10(12): 305-314.

Zhang J, Wang X and Xu T. 2008. Elemental selenium at nano size (Nano-Se) as a potential chemopreventive agent with reduced risk of selenium toxicity: Comparison with Se-methylselenocysteine in mice. Toxicol Sci., 101(1): 22-31.

Zhang L, Li X, Chen Y, Zhang Y and Wang S. 2023. Mechanistic insights into the apoptotic pathways induced by KP-SeNPs in gastric cancer cells. Cancer Lett., 534: 112-120.

Zhang L, Liu J, Xie X, Pan J and Li X. 2023. Role of selenium nanoparticles in enhancing cancer therapy: Current status and future perspectives. Cancers., 15(1): 127.

Zhang L, Wu Y, Liu W, Li X and Wang Y. 2021. A study on selenium nanoparticles as a potent treatment for gastric cancer via apoptosis. J Cancer Res Ther., 15(9): 1292-1301.

Zhang Q, Li L, Song S, Zhang Z and Wang S. 2021. Dual mechanisms of apoptosis induction by selenium nanoparticles in gastric cancer cells. Int J Nanomedicine., 16(8): 5245-5253.

Zhang T, Hu Y, Zhang K, Tian C and Guo J. 2018. Arbuscular mycorrhizal fungi improve plant growth of *Ricinus communis* by altering photosynthetic properties and increasing pigments under drought and salt stress. Ind Crops Prod., 117: 13-19.

Zhang T, Liu F, Liu Y, Xu Y and Li D. 2021. Enhanced antitumor effects of selenium nanoparticles in gastric cancer through apoptosis and ROS-mediated mechanisms. J Cancer Res Ther., 19(7): 2315-2323.

Zhang T, Zhou W, Zhao G, Wang L and Xu L. 2020. Mechanisms of action of selenium nanoparticles in gastric cancer: Apoptosis induction and ROS modulation. J Cancer Ther., 19(3): 75-84.

Zhang Y, Li X, Wang L, et al. 2023. Green synthesized selenium nanoparticles: Effects on ROS production and apoptosis in gastric cancer cells. J Nanobiotechnology., 21(1): 45.

Zhao J, Sun H, Zhang Y, Jiang J and Huang J. 2024. The role of selenium nanoparticles in cancer treatment: Insights into recent research and future prospects. J Nanobiotechnology., 22(1): 35.

Zhao L, Zhang X, Wu Z, Liu X and Yu C. 2021. The role of selenium nanoparticles in combating oxidative stress and promoting apoptosis in gastric cancer cells. Cell Death Dis., 12(5): 116-122.

Zhao Z, Zhang Q, Xu Y, Liu Y and Wang Z. 2020. Induction of apoptosis in gastric cancer cells by selenium nanoparticles: Role of BAX gene. Cancer Lett., 490: 38-46.

Zheng Y, Wu Z, Li Z, Ma X and Liu Y. 2023. Functionalized selenium nanoparticles for targeted cancer therapy. Biomed Pharmacother., 150: 113086.

JJBS

Volume 19, Number 1,March 2026
ISSN 1995-6673
Pages 95 – 103
https://doi.org/10.54319/jjbs/190109

Jordan Journal of Biological Sciences

Comparative evaluation of Immunomodulatory, Antioxidant, and anti-inflammatory Properties in Degla and Homayra Dates Roub

Kehili Houssem Eddine [1 2,*], Mokrane Meriem [3], Sayoud Samah [3], Teldjoune Amira [3], Zerizer Sakina [2], Kabouche Zahia [4]

[1] University of Abdlahfid Boussof, Mila. Institute of Life and Nature Sciences. Department of biological and agronomic sciences; [2] Laboratoire d'immunologie et des activités des substances naturelles. Campus Chaab Ersas. Université de Constantine 1, Frères Mentouri. Route Ain El Bey Constantine. Algérie; [3] Constantine 1, Frères Mentouri University, Algeria. Animal Biology Department; [4] Laboratoire d'Obtention de Substances Thérapeutiques (LOST), Campus Chaabet Ersas, 25000 Constantine, Algérie..

Received: February 14, 2025; Revised: July 13, 2025; Accepted: August 8, 2025

Abstract

Aims: This study aimed to comparatively evaluate the immunomodulatory, antioxidant, and anti-inflammatory properties of two Algerian date (*Phoenix dactylifera L.*) varieties: *Degla* and *Homayra*.

Methods: Acute toxicity was assessed using the up-and-down method. The immunomodulatory effect was evaluated via the carbon clearance test in mice. Antioxidant activity was measured by quantifying hepatic glutathione (GSH) levels. Anti-inflammatory activity was determined using the formalin-induced paw edema model.

Results: Both date varieties showed no signs of toxicity or mortality at 2000 mg/kg. Significant enhancement of phagocytic activity was observed in treated mice (P = 0.011). The carbon elimination speed was considerably increased at 100 mg/kg for *Degla* (0.0733±0.031) and at 150 mg/kg for *Homayra* (0.076±0.019) compared to the NaCl control (0.029±0.012). Antioxidant activity, indicated by GSH levels, was highest at 100 mg/kg (*Degla*) and 150 mg/kg (*Homayra*) (P = 0.000). Notable anti-inflammatory effects were demonstrated by a significant reduction in paw edema after one week of treatment (P = 0.000).

Conclusion: The findings indicate that the Degla and Homayra varieties of *Phoenix dactylifera* exhibit notable immunostimulant, free radical–scavenging, and inflammation-reducing activities, highlighting their potential as candidates for the formulation of natural therapeutic remedies.

Keywords: inflammation, GSH, Immune-modulatory, date fruit, Toxicity.

1. Introduction

Since ancient times, people have utilized plants as medicine, and this practice continues now. Originally, plants with therapeutic properties were discovered by trial and error, whether for the purpose of curing ailments or just feeling better. Through generations, the application of these herbs has been refined to the point where it is today recognized as traditional medicine in numerous circumstances **(**Salmerón-Manzano *et al*., 2020). By acting as immunomodulatory agents and modifying the immune system, medicinal plants have a significant impact on preventing a variety of diseases and harmful microbes in humans. Plant-based immunomodulatory agents, low-molecular-weight substances like terpenes, phenols, alkaloids, and other nitrogen-containing chemicals, and high-molecular-weight substances like lectins and polysaccharides are commonly employed to modify the immune system **(**Parbat *et al*., 2021). These organic compounds serve a range of biological purposes and are created via secondary metabolism. Among several of these roles, antioxidant and anti-inflammatory qualities are particularly prominent **(**Nunes *et al*., 2020).

Inflammation takes place when the body reacts to infection and damaging external stimuli. Acute inflammation typically goes away on its own and aids in the immune system's reaction to damage. On the other hand, prolonged inflammation led to the overproduction of inflammatory factors, which in turn triggered the cardiovascular system and other inflammatory disorders, such as gouty arthritis, cancer, and chronic gastritis. These inflammatory factors included nitric oxide (NO), tumor necrosis factor α (TNF-α), and cyclooxygenase 2 (COX-2). Diclofenac, aspirin, and ibuprofen are currently the anti-inflammatory medications that are prescribed the most frequently; however, they are frequently associated with side effects and allergic reactions **(**Lu *et al*., 2022).

Usually referred to as the date palm, *Phoenix dactylifera L*. is a significant plant in North Africa and Southwest Asia**.** Since the 20th century, date fruit production has grown dramatically on a global scale; in 2020, it is predicted to reach a value of fourteen billion US dollar **(**Alkhoori *et al*., 2022).With about 930 thousand tons and more than 900 varieties of dates produced annually, Algeria is the third-largest date producer worldwide. Algeria is a large country that grows several different types of dates, such as mech degla, delget nour,

* Corresponding author. e-mail: h.kehili@centre-univ-mila.dz .

and degla beida **(**Chergui *et al*., 2021). *Phoenix dactylifera* is a monocotyledonous plant and part of the Arecaceae family. Its species name, phoenix, is derived from the Greek word for purple, while dactylifera translates to "finger-bearing." **(**Oluyele *et al*., 2021). In Algeria, date fruit is widely recognized for its numerous traditional medicinal applications, particularly for nursing mothers who utilize it to increase milk production, treating hair loss and anemia, and speeding up the broken bones healing process. Date fruit is used in traditional medicine all across the world to treat a variety of ailments, such as neurological diseases, and memory issues **(**Sedighi-Khavidak *et al*., 2022). Fresh and dried dates are an integral part of Algerian diets, consumed in a variety of ways, and play an important role in culinary art. Dates are especially important during Ramadan as they are used for breaking the fast, which aligns with religious traditions (Bouguedoura *et al*., 2015). Dates palms serve as an important component of oasis agro-ecosystems, as they help form a microclimate that allows different crops and fruit trees, cereals, and vegetables to thrive. The shade provided by the canopy of date palms protects the soil from evaporation and increases the temperature of the soil that nurtures the crops planted underneath. This stratified plantation pattern maximizes the use of land in these arid regions and is efficient enough for sustainability. Furthermore, date palm cultivation in extreme conditions encourages sustainable agriculture, desertification combat, and hence creates prospects for the rural economies. Indeed, date palms play an important role in the preservation of the environment since they are resilient enough to survive desert conditions (Alotaibi *et al*., 2023; Dhawi and Aleidan, 2024).

In addition to its nutritional and socioeconomic significance, *Phoenix dactylifera L*. has been the focus of numerous scientific investigations highlighting its diverse medicinal properties. Several studies have demonstrated that different parts of the plant—particularly the fruit—exhibit significant antioxidant, anti-inflammatory, antimicrobial, hepatoprotective, and immunomodulatory activities (Al-Snafi and Thuwaini, 2023; Mostafa, 2024; Ahmed and Ali Boutlelis, 2024). Despite these findings, there remains a lack of comparative studies on the bioactivity of specific local varieties, particularly in Algeria, where different ecotypes like Degla and Homayra are traditionally used but scientifically underexplored.

To address this gap, the objective of the present study was to comparatively evaluate (*in vivo* and *in vitro*) the immunomodulatory, antioxidant, and anti-inflammatory effects of the Algerian *Phoenix dactylifera L*. varieties, Degla and Homayra.

2. Materials & methods

2.1. Plant material

Date fruits (*Phoenix dactylifera*) of the degla and homayra varieties were picked during the ripening stage from Biskra and Adrar, respectively, to make a date syrup, or "Roub" as it is known in the Algerian local culture. The plant materials used in this study were authenticated as local varieties based on their morphological characteristics and geographical origin. These varieties are well known and widely cultivated in their respective regions, and their identification was confirmed by local agricultural experts.

2.2. Roub's Preparations

The Roub, traditional Algerian date syrup, was prepared using an Algerian conventional method. First, 3 Kg of dates (for each variety) were washed. Then, a large container half-filled with water (twice the dates weight) was warmed to a medium heat (55–65 °C) and left to boil for approximately 90 minutes. Once softened, the fruits were crushed, with the seeds detached, to create a smooth mush, which was then filtered to extract the maximum amount of juice. The extracted juice underwent another heating process at around 65 °C to vaporize extra water, decreasing it to about 1000 g of a dense liquid similar to syrup. Finally, the date's syrup (Roub) was left to reach room temperature before being kept in a sanitized glass container and reserved in a heated, dim place for preservation.

Three doses for each variety (D1DG (100 mg/kg), D2DG (150 mg/kg), and D3DG (200 mg/kg) for the degla variety, and D1HM (50 mg/kg), D2HM (150 mg/kg), and D3DHM (200 mg/kg) for the homayra variety) were utilized in this investigation, and they were made by dissolving the Roub in 10 ml of sodium chloride (NaCl 0.9%).

2.3. Animal husbandry

In this study, adult *Mus musculus* mice weighing between 20 and 30 g and aged between 60 and 75 days were used. The mice were obtained from the central pharmacy of Algeria and housed in polyacrylic cages in regular conditions, which included a cooled room with a 12-hour light and dark cycle. Before the testing started, the animals spent a week acclimating and had unrestricted access to food and drink in the form of dry pellets.

2.4. Ethics statement

The technique for carrying out the animal exploration was based on the research project code (F00920140076), which was acquired from the Ministry of Higher Education and Scientific Research in Algeria. The studies were conducted in accordance with the OECD's ethical rules and principles for overseeing and monitoring animal research (OECD Test No. 420, 2002). All efforts were taken to minimize pain to the animal during experimentation.

2.5. Up and down test

The acute toxicity assessment was conducted using the "Up-and-Down" method, also known as the acute toxicity test (Ezeh *et al*., 2021). Five healthy adult male mice were each administered a high dose of 2000 mg/kg of Roub (from each variety). The mice were weighed the night before treatment, deprived of food, but allowed free access to water. Roub was then administered orally to each mouse. The first mouse received a dose of 2000 mg/kg and was closely observed during the first 60 minutes, then monitored every hour for the next three hours, and intermittently over the following two days for clinical symptoms and mortality. Observations included signs such as unusual aggression, drowsiness, abnormal vocalization, restlessness, and lethargy. If the first mouse survived, four additional mice were given the same maximum dose at two-day intervals. After two weeks of careful observation, the mice were released, and the total number of fatalities

was recorded. If at least three mice survived, the median lethal dose (LD50) was considered to be greater than the maximum dose tested.

2.6. Phagocytic activity

Phagocytic activity was assessed by measuring the rate at which the mononuclear phagocyte system cleared carbon from the bloodstream, using a carbon clearance test (Slimani *et al*., 2020). This activity is quantified by three indices: the phagocytic index (K), which reflects the overall function of the mononuclear phagocyte system in its interaction with the blood; the corrected phagocytic index (α), which evaluates this activity relative to the combined weight of the animal's liver and spleen; and the half-life period (T½), representing the time required for the phagocytic system to eliminate carbon from the blood.

The mice were divided into seven groups, as shown in Table 1. Three groups received different doses of *Phoenix dactylifera* (degla variety): D1DG (100 mg/kg), D2DG (150 mg/kg), and D3DG (200 mg/kg). Another three groups received corresponding doses of Phoenix dactylifera (homayra variety): D1HM (100 mg/kg), D2HM (150 mg/kg), and D3HM (200 mg/kg). The control group received 0.5 ml/mouse of 0.9% NaCl solution.

Table 1. Animal grouping in the phagocytic activity test

Phoenix dactylifera varieties						Control group
Degla variety			Homayra variety			
D1DG	**D2DG**	**D3DG**	**D1HM**	**D2HM**	**D3HM**	0.5 ml/mouse of NaCl (0.9%)
100 mg/kg	150 mg/kg	200 mg/kg	100 mg/kg	150 mg/kg	200 mg/kg	

PD1/PD2: Photographic Densities measured at 5 minutes and 15 minutes, correspondingly.

K: Phagocytic index.

The medication was administered via intraperitoneal injection (i.p.). Two days after the injection, each mouse received an injection of an antigenic solution (0.1 ml per 10 g of body weight) through the tail vein. The antigenic solution was composed of carbon ink (3 ml), 3% gelatin solution (4 ml), and saline (4 ml). Blood samples (approximately 15 drops) were collected at five and fifteen minutes after the antigenic solution was administered, and each sample was lysed in four milliliters of 0.1% Na_2CO_3 solution. The photometric density (PD) was then measured at 675 nm.

The parameters for evaluating phagocytosis efficiency were calculated using the following equations:

$$K = \frac{LOG\,PD1 - LOG\,PD2}{15 - 5} \qquad T^{1}/_{2} = \frac{0.693}{K}$$

$$\alpha = \sqrt[3]{K}\,\frac{Body\ weight\ of\ the\ animal}{liver\ weight\ +\ spleen\ weight}$$

2.7. Hepatic GSH test

By measuring hepatic glutathione (GSH) spectrophotometrically with the DTNB (5,5-dithio-bis-(acide 2-nitrobenzoïque) reagent (Vuolo *et al*., 2022), the anti-oxidant impact was evaluated.

2.8. Formalin-induced paw edema test

The formalin-induced paw edema test in mice was performed to evaluate the anti-inflammatory effects of *Phoenix dactylifera* Roub *in vivo*. The progression of inflammation was monitored by measuring paw edema with a digital caliper. After a one-week acclimatization period, the mice were divided into five groups:

- Negative Control (C-): Received only flour treatment.
- Positive Control (C+): Treated with 2% formalin (0.05 ml).
- DG Group: Administered 100 mg/kg of *Phoenix dactylifera* (Degla variety).
- HM Group: Administered 150 mg/kg of *Phoenix dactylifera* (Homayra variety).
- DEC Group: Received 10 mg/kg of Diclofenac sodium (50 mg).

All treatments were given orally for seven consecutive days.

2.9. Histological study of the mice inflamed paw

The histological examination of the inflamed mouse paw was performed according to the hematoxylin and eosin staining protocol described by Fischer *et al*., (2008).

2.10. Statistical data analysis

Tukey's multiple comparison test and one-way ANOVA were used to analyze differences between groups during the dietary treatments (IBM SPSS version 20). P-values less than 0.05 were considered statistically significant.

3. Results

3.1. Up and down test

The results offered in Table 2 show that, in the acute toxicity test, administering a 2000 mg/kg dose of both *Phoenix dactylifera* varieties did not result in any deaths or apparent marks of toxicity. Five adult male mice received the same Roub orally at this dose and were monitored for two weeks. By the end of the observation period, all five mice survived.

Table 2. Toxic effect of *Phoenix dactylifera* varieties

Limit dose		Signs of toxicity (2 weeks)		Signs of mortality (2 weeks)		Number of mice survived during (2 weeks)	
DG	HM	DG	HM	DG	HM	DG	HM
2000 mg/kg		No toxicity		No mortality		all mice	

DG: degla variety; **HM:** homayra variety

3.2. The Phoenix dactylifera immunomodulatory activity

3.2.1. Phagocytic index K

In Figure 1, the results indicate a statistically important difference in the (K) values between the experimental groups (P = 0.011). Furthermore, the findings indicate that

Phoenix dactylifera at the D2HM and D1DG has the highest K (K D2HM = 0.076 ± 0.019, K D1DG= 0.073 ± 0.031) compared to the control (K NaCl = 0.029 ± 0.012) and the other treated groups D1HM (K = 0.06 ± 0.025), D3HM (K = 0.048 ± 0.0148), D2DG (K = 0.053 ± 0.016), D3DG (K = 0.041 ± 0.013).

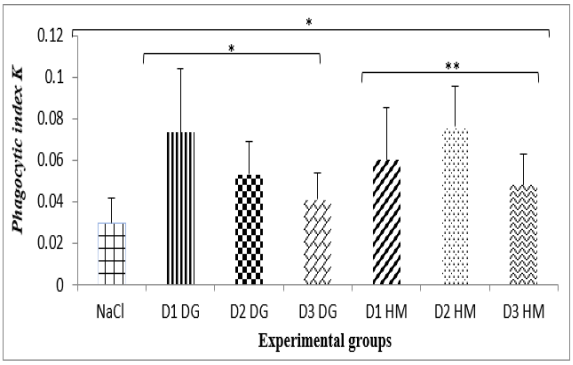

Figure 1. Impact of different *Phoenix dactylifera* varieties on (K).

Data are Mean ± Standard Deviation (n=5), with significant deviations from the NaCl group as *P<0.05, **P<0.01, ***P<0.001

NaCl: Control; D1DG D2DG D3DG: (100, 150, 200) mg/kg of *P. dactylifera* (degla variety); D1HM, D2HM, D3HM: (100, 150, 200/kg) mg/kg of *P. dactylifera* (homayra variety)

3.2.2. Carbon clearance time (T½)

Findings in Figure 2 expose a highly significant reduction in carbon clearance period among the groups (P = 0.002). In addition to that, the results show that the carbon clearance was quicker in the group treated with D2HM (T½ = 9.788 ± 2.596 min) and D1DG (T½ = 10.517 min ± 3.23) compared to the other treated groups: D3HM (T½ = 16.652 ± 4.946 min); D1HM (t½ = 13.586 ± 4.964 min); D2DG (T½ = 14.006 min ± 3.7); D3DG (T½ = 18.43 min ± 6.24), and the control NaCl (T½ = 27.179 min ± 12.05).

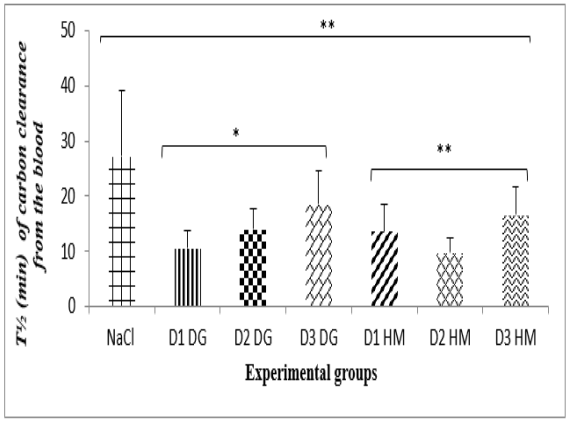

Figure 2. Impact of different *Phoenix dactylifera* varieties on the (T½)

Data are Mean ± Standard Deviation (n=5), with significant deviations from the NaCl group as *P<0.05, **P<0.01, ***P<0.001

NaCl: Control; D1DG D2DG D3DG: (100, 150, 200) mg/kg of *P. dactylifera* (degla variety); D1HM, D2HM, D3HM: (100, 150, 200/kg) mg/kg of *P. dactylifera* (homayra variety)

3.2.3. Corrected phagocytic index

The findings presented in Figure 3 reveal a statistically significant dissimilarity (P = 0.000) among the treated groups. The corrected phagocytic index α of the groups treated with the homayra variety (D1HM = 6.126 ± 0.616; D2HM = 7.172 ±0.731; D3HM = 6.128 ±0.418; P = 0.000) was considerably greater than that of the degla variety (D1DG = 4.406 ± 0.65; D2DG = 3.518 ± 0.66); D3DG (3.107± 1.23) P = 0.016.

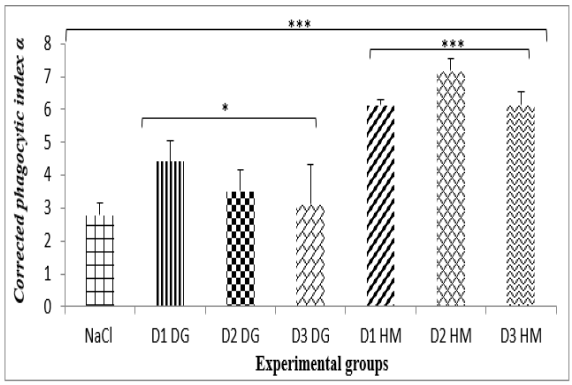

Figure 3. Impact of different *Phoenix dactylifera* varieties on α.

Data are Mean ± Standard Deviation (n=5), with significant deviations from the NaCl group as *P<0.05, **P<0.01, ***P<0.001

NaCl: Control; D1DG D2DG D3DG: (100, 150, 200) mg/kg of *P. dactylifera* (degla variety); D1HM, D2HM, D3HM: (100, 150, 200/kg) mg/kg of *P. dactylifera* (homayra variety)

3.3. The Phoenix dactylifera antioxidant activity

Figure 4 results demonstrate that there is a significant difference (P = 0.000) in the glutathione values between the treated groups with both varieties of *Phoenix dactylifera*. Glutathione values were significantly higher in the groups treated with the homayra variety (D2HM = 1.57 nmol/mg ± 0.128; D1HM = 1.652 nmol/mg ± 0.386; D3HM = 1.83 nmol/mg ± 0.088; P = 0.000) than the NaCl group (0.000235 nmol/mg ± 9.5154E^{-05}) and the groups treated with the degla variety (D1DG = 0.039 nmol/mg ± 0.003; D2DG = 0.0160 nmol/mg ± 0,001; D3DG = 0.0010 nmol/mg ± 0.0006) P = 0.035.

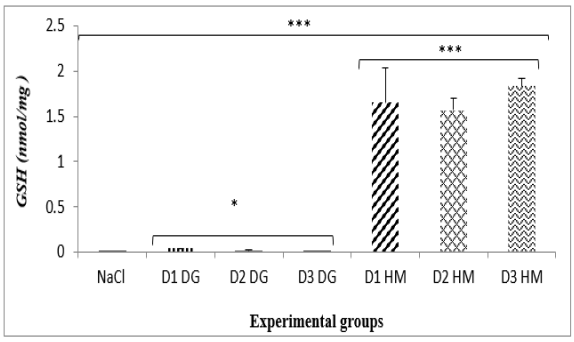

Figure 4. Impact of different *Phoenix dactylifera* varieties on hepatic glutathione.

Data are Mean ± Standard Deviation (n=5), with significant deviations from the NaCl group as *P<0.05, **P<0.01, ***P<0.001

NaCl: Control; D1DG D2DG D3DG: (100, 150, 200) mg/kg of *P. dactylifera* (degla variety); D1HM, D2HM, D3HM: (100, 150, 200/kg) mg/kg of *P. dactylifera* (homayra variety)

3.4. The Phoenix dactylifera anti-inflammatory activity

Results in Figure 5 demonstrate a greatly significant dissimilarities in edema size among the groups over the seven-day experiment (P = 0.000). This reduction in edema size was evident from the difference in diameters between inflamed and non-inflamed paws treated with both *Phoenix dactylifera* varieties (HM and DG) as well as Diclofenac (DEC). Moreover, a substantial decrease in edema size was observed in the HM, DG, and DEC groups from the fourth day of inflammation until the seventh day, when it reached its lowest level:

DG: Day 4 (3.34 mm ± 0.281), Day 7 (3.245 mm ± 0.310), P = 0.035

HM: Day 4 (3.52 mm ± 0.157), Day 7 (3.29 mm ± 0.235), P = 0.000

DEC: Day 4 (3.02 mm ± 0.164), Day 7 (2.74 mm ± 0.065), P = 0.000

Conversely, the C+ group exhibited significantly larger edema compared to the control and other treated groups: C+: Day 4 (4.35 mm ± 0.42), Day 7 (3.76 mm ± 0.58), P = 0.000.

These findings suggest that treatment with *Phoenix dactylifera* varieties and Diclofenac effectively reduced edema size over time.

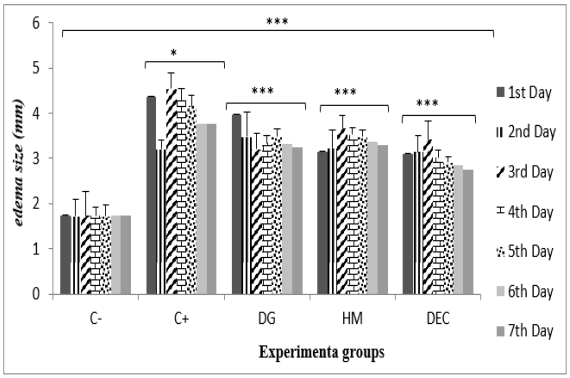

Figure 5: Impact of different *Phoenix dactylifera* varieties on the edema size.

Data are Mean ± Standard Deviation (n=5), with significant deviations from the NaCl group as *P<0.05, **P<0.01, ***P<0.001

C-: Negative Control; C+: Positive Control; DG: 100 mg/kg of *P. dactylifera* Degla variety;

HM: 150 mg/kg of *P. dactylifera* Homayra variety; DEC: 10 mg/kg of Diclofenac sodium (50 mg).

3.5. The histology study

Figures 6A and 6B illustrate cellular desquamation of the synovial membrane and paw degeneration in the (C+) group, which received a subplantar injection of formalin. In contrast, the normal (C-) group exhibited an intact paw structure, with clearly visible joint components, including calcified cartilage, spongy bone, and hyaline cartilage.

Figures 6C and 6D display histological sections of the joint paw treated with *Phoenix dactylifera* (Degla and Homayra varieties). These sections revealed intact articular cartilage with a preserved articular surface. Similarly, the Diclofenac sodium-treated group showed intact hyaline cartilage with no signs of erosion on the articular surface (Figure 6E).

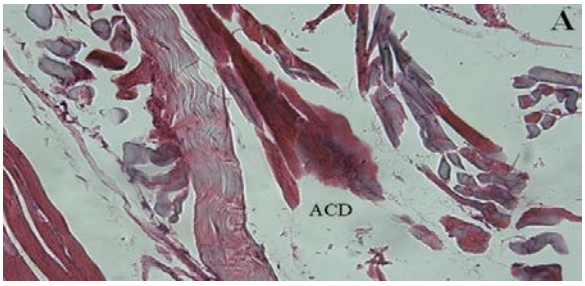

Figure 6A: Histological section of a mouse paw following seven days of inflammation in the C+ group, stained with H&E (X100).

ACD: Articular Cartilage Degenerated

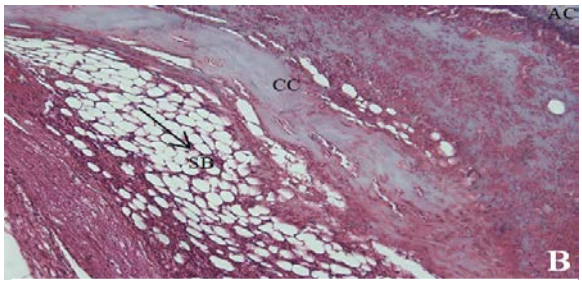

Figure 6B: Histological section of a mouse paw following seven days of inflammation in the (C-) group stained with H&E (X100).

AC: Articular Cartilage; CC: Calcified Cartilage; SB: Spongy Bone.

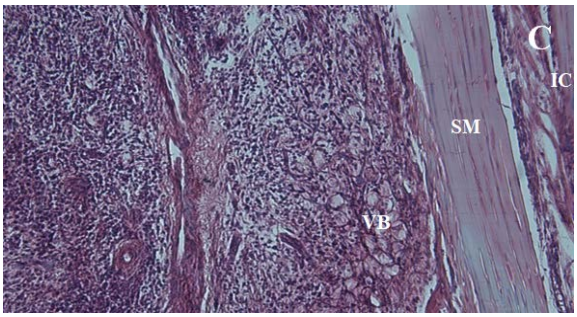

Figure 6C: Histological section of a mouse paw following seven days of inflammation in the (DG) group stained with H&E (X100).

IC: Intact cartilage; SM: Synovial Membrane;

VB: Vascularized Bone

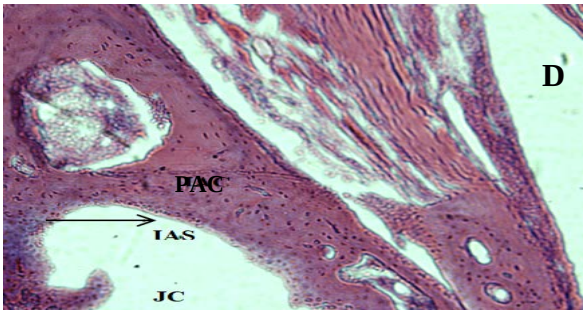

Figure 6D: Histological section of a mouse paw following seven days of inflammation in the (HM) group stained with H&E (X100).

PAC: Preserved Articular Cartilage; **IAS:** Intact Articular Surface; JC: Joint's Cavity.

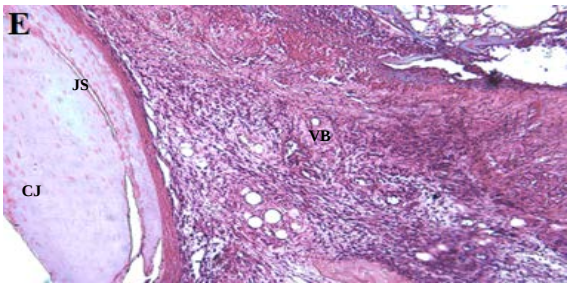

Figure 6E: Histological section of a mouse paw following seven days of inflammation in the (DEC) group stained with H&E (X100).

CJ: Cavity of the Joint; JS: Joint Surface; VB: Vascularized Bone

4. Discussion

Therapeutic plants and their derivatives have been found to influence both humoral and innate responses by engaging with the immunoregulatory cascade and modifying immune cell multiplication, phagocytic activity, toxicity function, and the expression of cytokines, cellular co-receptors, and immunoglobulins (Alanazi *et al*., 2023, Shen *et al*., 2023). The study aimed to comparatively evaluate the immunomodulatory, antioxidant, and anti-inflammatory properties of Algerian date (*Phoenix dactylifera*) varieties, degla and homayra.

To assess the impact of date Roub on the mononuclear phagocyte system (a network of cells specialized in phagocytosis), a test for carbon elimination was executed. Upon the direct injection of carbon elements (the ink) into the systemic circulation, macrophages and other phagocytic cells initiate the process of clearing carbon from the blood.

The doses of *Phoenix dactylifera* varieties used in the treatment groups influenced the immune system by

stimulating the phagocytic system to accelerate carbon clearance from the blood and affecting liver GSH levels. The most significant effect was observed at 100 mg/kg for the Degla variety and 150 mg/kg for the Homayra variety. These findings show similarities with those of Oriade *et al*. (2021) who reported that the immunological responses of the groups fed with 0.5 and 2.0% date revealed noticeably higher levels of antibody and phagocytic activity, respectively. Furthermore, the results agree with the study of Merza Mahmood *et al.* (2016) The study examined the immunomodulatory effects of date fruit water extract in mice, revealing an increase in the amount of IFN-γ, CD4 (cluster of differentiation), CD49b, IL-12, and CD11b cells compared to normal after treatment. Moreover, Ahmad Mohd Zain *et al*. (2022) highlight the date palm's many health advantages, including how it strengthened the immune system during the COVID-19 epidemic.

Substances that can activate the immune system's innate or adaptive arms are known as immunostimulants. Pharmaceutical companies release a lot of synthetic immunostimulants, but they have a lot of adverse effects (Alhazmi *et al*., 2021, Wang *et al*., 2024). On the other hand, As a result of containing components such as polysaccharides, lectins, saponins, and flavonoids, among others, certain plant products are thought to strengthen the body's innate defense against infection. While some of these merely engage the immune system's cellular components, others promote both humoral and cell mediated immunity (Santiago *et al*., 2021).

The results also show that, the Roub of *Phoenix dactylifera* (degla and homayra varieties) is capable of improving antioxidant activity by increasing hepatic GSH levels. These results show some similarities with the results of Saryono *et al*. (2019). The study revealed that when 5 g/kg of steeped date seeds are administered, TNF-α is decreased while GSH and IFN-γ are increased. In addition to that, the results also agree with those of Roshankhah *et al*. (2020) who indicated that by strengthening the liver's antioxidant defenses, Middle Eastern *Phoenix dactylifera* can lessen the negative structural alterations and oxidative stress caused by mercury in the testis. According to Gad El-Hak *et al*. (2022), date palm extracts, such as methanolic date flesh extract, can ameliorate hepatic injury induced by toxins like cisplatin and help to restore GSH levels, reduce oxidative stress, and decrease inflammatory biomarkers in the liver.

Results from the last section of the study demonstrated that from the second day until the end of the test, *Phoenix dactylifera* (degla and homayra varieties) greatly decreased formaldehyde-induced edema. The test results may be attributed to the influence of *Phoenix dactylifera* on the release of inflammatory mediators and its potential to act correspondingly to non-steroidal anti-inflammatory drugs in both phases of inflammation. The results agree with Saryono *et al*. (2019) who reported that *Phoenix dactylifera* seeds have anti-inflammatory and immunostimulant properties. As an anti-inflammatory effect, date seed inhibits the formation of edema and IFN-γ and suppresses inflammatory cytokines like IL-6, IL-1, and TNF-α . The study of Bouhlali *et al*. (2020) suggested that *Phoenix dactylifera* seed extracts mediate anti-inflammatory properties through the stabilization of lysosomal membranes, prevention of protein denaturation, and inhibition of fibrinogen formation and C-reactive protein.

It should be noted that many plants' biological effects, including their ability to reduce inflammation and arthritis, have been linked to their triterpene or flavonoid concentrations. Furthermore, it has been shown that a number of flavonoids, including luteolin, quercetin, and rutin, as well as biflavonoids and triterpenoids, including ursolic acid, exhibit notable anti-nociceptive and/or anti-inflammatory properties (Kaushik *et al*., 2021, Sivasakthi *et al*., 2021). From that point of view, *Phoenix dactylifera* is known for its exceptional nutritional and functional properties, being abundant in tannins, phenolics, flavonols, and flavonoids **(**Chenini *et al*., 2021, Harkat *et al*., 2022), proteins, lipids, fibers, vitamins, minerals **(**Alahyane *et al*., 2021, Shahab Uddin and Nuri, 2021), simple carbohydrates, primarily glucose, fructose and other secondary metabolites (Bano *et al*., 2022).

5. Conclusion

The present synthetic drug-based therapy method for diseases including diabetes, cancer, and rheumatoid arthritis is costly. Date fruit preparations from Algeria are a cheap and useful treatment. This study demonstrated the beneficial effects of *Phoenix dactylifera* (homayra and degla varieties) on the management of diseases due to its anti-inflammatory properties, anti-oxidant, and immunostimulation qualities, which inspire hope for a novel therapeutic approach. Despite the promising results obtained in this study, several limitations should be acknowledged. First, the investigation was limited to acute in vivo models, and long-term or chronic effects of the extracts were not assessed. Second, while the study demonstrated significant immunomodulatory, antioxidant, and anti-inflammatory activities, the underlying molecular mechanisms and specific bioactive constituents responsible for these effects were not explored. Additionally, the evaluation was conducted solely in animal models, which may not fully replicate the complexity of human biological responses. Therefore, further studies are recommended to isolate and characterize the active phytochemicals in these date varieties, examine their molecular targets and pathways, and assess their efficacy and safety in chronic disease models. Ultimately, clinical trials will be essential to validate their therapeutic potential in humans.

Conflict of Interest

The authors declare that they have no conflicts of interest related to this study.

Funding statement

No funding was received for conducting this study.

Author contributions

Conceptualization: Kehili Houssem Eddine; Methodology: Kehili Houssem Eddine, Zerizer Sakina, Kanouche Zahia; Formal analysis and investigation: Kehili Houssem Eddine, Meriem Mokrane, Samah Sayoud, Amira Teldjoune; Writing - original draft preparation:

Kehili Houssem Eddine, Meriem Mokrane, Samah Sayoud, Amira Teldjoune; Writing - review and editing: Kehili Houssem Eddine, Zerizer Sakina; Resources: Zerizer Sakina, Kanouche Zahia; Supervision: Kehili Houssem Eddine.

References

Ahmed G, and Ali Boutlelis D. 2024. Protective and antioxidant capacity of date palm seeds (*Phoenix dactylifera L.*) On hepatotoxicity in rats. *FARMACIA*, **71(2): 303-311**.

Alahyane A, Harrak H, Elateri I, Ayour J, Ait-Oubahou A, and Benichou M. 2021. Evaluation of some nutritional quality criteria of seventeen Moroccan dates varieties and clones, fruits of date palm (*Phoenix dactylifera* L.). *Braz J Biol.*, **82**. http://dx.doi.org/10.1590/1519-6984.236471.

Alanazi HH, Elasbali AM, Alanazi MK, and El Azab EF. 2023. Medicinal herbs: Promising immunomodulators for the treatment of infectious diseases. *Molecules*, **28(24)**. http://dx.doi.org/10.3390/molecules28248045.

Alhazmi HA, Najmi A, Javed SA, Sultana S, Al Bratty M, and Makeen HA. 2021. Medicinal plants and isolated molecules demonstrating immunomodulation activity as potential alternative therapies for viral diseases including COVID-19. *Front Immunol.*, **12(637553)**. http://dx.doi.org/10.3389/fimmu.2021.637553.

Alkhoori MA, Kong AS-Y, Aljaafari MN, Abushelaibi A, Lim S-H, and Cheng W-H. 2022. Biochemical composition and biological activities of date palm (*Phoenix dactylifera* L.) seeds: A review. *Biomolecules*, **12(11)**. http://dx.doi.org/10.3390/biom12111626.

Alotaibi KD, Alharbi HA, Yaish MW, Ahmed I, Alharbi SA, Alotaibi F, and Kuzyakov Y. 2023. Date palm cultivation: A review of soil and environmental conditions and future challenges. *Land Degradation & Development*, **34: 2431–2444**. doi:10.1002/ldr.4619.

Al-Snafi AE, and Thuwaini MM. 2023. *Phoenix dactylifera*: traditional uses, chemical constituents, nutritional benefit and therapeutic effects. *Traditional Medicine Research* ., **8(4): 20**. https://doi.org/10.53388/TMR20221110001.

Bano Y, Rakha A, and Khan M. 2022. Chemical composition and antioxidant activity of date (*Phoenix dactylifera* L.) varieties at various maturity stages. *Food Science and Technology*, **42**.

Bouguedoura N, Bennaceur M, Babahani S, and Benziouche SE. 2015. Date palm status and perspective in Algeria. In *Date Palm Genetic Resources and Utilization*, edited by Al-Khayri JM, Jain SM, and Johnson DV, **125–168**. Dordrecht: Springer Netherlands.

Bouhlali EDT, Hmidani A, Bourkhis B, Khouya T, Ramchoun M, and Filali-Zegzouti Y. 2020. Phenolic profile and anti-inflammatory activity of four Moroccan date (*Phoenix dactylifera* L.) seed varieties. *Heliyon*, **6(2)**: e03436.

Chenini-Bendiab H, Djebli N, Kara Y, Uçar M, and Kolayli S. 2021. An investigation of Algerian dates (*Phoenix dactylifera* L.); antioxidant, anti-inflammatory properties and phenolic compositions. *Emir J Food Agric.*, **33: 629**. http://dx.doi.org/10.9755/ejfa.2021.v33.i8.2737.

Chergui D, Akretche-Kelfat S, Lamoudi L, Al-Rshaidat M, Boudjelal F, and Ait-Amar H. 2021. Optimization of citric acid production by *Aspergillus niger* using two downgraded Algerian date varieties. *Saudi J Biol Sci.*, **28(12)**: 7134–7141. http://dx.doi.org/10.1016/j.sjbs.2021.08.013.

Dhawi F and Aleidan MM. 2024. Oasis agriculture revitalization and carbon sequestration for climate-resilient communities. *Frontiers in Agronomy*, **6**: 1386671. doi:10.3389/fagro.2024.1386671.

Ezeh GC, Udeh NE, Ozioko CA, Onoja SO, Eze RE, and Omeh YN. 2021. Acute and sub-acute toxicity profile of methanol extract of *Hura crepitans* leaf on Wistar rats. *Not Sci Biol.*, **13(2)**: 10939. http://dx.doi.org/10.15835/nsb13210939.

Fischer AH, Jacobson KA, Rose J, and Zeller R. 2008. Hematoxylin and eosin staining of tissue and cell sections. *CSH Protoc.*, **5**. http://dx.doi.org/10.1101/pdb.prot4986.

Gad El-Hak HN, Mahmoud HS, and Ahmed EA. 2022. Methanolic *Phoenix dactylifera* L. extract ameliorates cisplatin-induced hepatic injury in male rats. *Nutrients*, **14(5)**. http://dx.doi.org/10.3390/nu14051025.

Harkat H, Bousba R, and Benincasa C. 2022. Assessment of biochemical composition and antioxidant properties of Algerian date palm (*Phoenix dactylifera* L.) seed oil. *Plants*, **11(3)**: 381. https://doi.org/10.3390/plants11030381.

Kaushik S, Jain P, Satapathy T, Purabiya P, and Roy A. 2021. Evaluation of anti-arthritic and anti-inflammatory activities of *Martynia annua* L. ethanolic extract. *Clin Phytoscience*, **7(1)**. http://dx.doi.org/10.1186/s40816-021-00250-y.

Lu Q, Li R, Yang Y, Zhang Y, Zhao Q, and Li J. 2022. Ingredients with anti-inflammatory effect from medicine food homology plants. *Food Chem.*, **368**: 130610. http://dx.doi.org/10.1016/j.foodchem.2021.130610.

Mahmood M, Ramadan F, and Hassan M. 2016. Therapeutic effect of *Phoenix dactylifera* against cryptosporidiosis in immunocompromised mice. *Global Advanced Research Journal of Medicine and Medical Sciences*, **5(3)**: 88–95.

Mohd Zain A, Kari MR, and Dawood Z. 2022. Bioactivity and pharmacological potential of date palm (*Phoenix dactylifera* L.) against pandemic COVID-19: A comprehensive review. *Appl Biochem Biotechnol.*, **194(10)**: 4587–4624. http://dx.doi.org/10.1007/s12010-022-03952-2.

Mostafa MYA. 2024. Evaluation of Antioxidant, Anti-Inflammatory, and Anticancer Activities of Palm Heart (*Phoenix dactylifera L.*) *In Vitro. J. of Food and Dairy Sci., Mansoura Univ.,* ***Vol. 15 (9):123 – 132.***

Nunes CR, Arantes MB, Pereira SMF, Cruz LL, Passos MS, and Moraes LP. 2020. Plants as sources of anti-inflammatory agents. *Molecules*, **25(16)**: 3726. http://dx.doi.org/10.3390/molecules25163726.

Oluyele O, Oladunmoye MK, and Ogundare AO. 2022. Toxicity studies on essential oil from *Phoenix dactylifera* (L.) seed in Wistar rats. *Biologics*, **2(1)**: 69–80. http://dx.doi.org/10.3390/biologics2010006.

Oriade TO, Alao OS, and Afolayan FID. 2023. Immunostimulatory effect of *Phoenix dactylifera* supplemented diet on *Aeromonas hydrophila* infected *Clarias gariepinus*. *Pan African Journal of Life Sciences*, **15(1)**. http://dx.doi.org/10.36108/pajols/1202/50.0160.

Parbat AY, Malode GP, Shaikh AR, Panchale WA, Manwar JV, and Bakal RL. 2021. Ethnopharmacological review of traditional medicinal plants as immunomodulator. *World J Bio Pharm Health Sci.*, **6(2)**: 43–55. http://dx.doi.org/10.30574/wjbphs.2021.6.2.0048.

Roshankhah S, Abdolmaleki A, and Salahshoor MR. 2020. Anti-inflammatory, anti-apoptotic, and antioxidant actions of Middle Eastern *Phoenix dactylifera* extract on mercury-induced hepatotoxicity in vivo. *Mol Biol Rep.*, **47(8)**: 6053–6065. http://dx.doi.org/10.1007/s11033-020-05680-4.

Salmerón-Manzano E, Garrido-Cardenas JA, and Manzano-Agugliaro F. 2020. Worldwide research trends on medicinal plants. *Int J Environ Res Public Health*, **17(10)**: 3376. http://dx.doi.org/10.3390/ijerph17103376.

Santiago LÂM, Neto RNM, Ataíde ACS, Fonseca DCSC, Soares EFA, and Sousa JCS. 2021. Flavonoids, alkaloids and saponins: Are these plant-derived compounds an alternative to the treatment of rheumatoid arthritis? A literature review. *Clin Phytoscience*, **7**. http://dx.doi.org/10.1186/s40816-021-00291-3.

Saryono S, Dardjito E, Proverawati A, Sumeru A, Setiyani R, and Upoyo AS. 2019. Date seeds (*Phoenix dactylifera* L.) consumption as anti-inflammatory and immunostimulant: A systematic review. *IOP Conf Ser Earth Environ Sci.*, **250**: 012038. http://dx.doi.org/10.1088/1755-1315/250/1/012038.

Saryono S, Taufik A, Proverawati A, and Efendi F. 2019. Dietary supplementation of *Phoenix dactylifera* L. seeds decreases pro-inflammatory mediators in CCl4-induced rats. *J Herbmed Pharmacol*., **8(3)**: 212–217. http://dx.doi.org/10.15171/jhp.2019.31.

Sedighi-Khavidak S, Shekarbeygi N, Delfani M, and Nejad FH. 2022. Nutritional and medicinal values of dates (*Phoenix dactylifera* L.) from the perspective of modern medicine and Iranian traditional medicine. *Complementary Medicine Journal*, **12(1)**: 44–55. https://doi.org/10.32598/cmja.12.1.1101.2.

Shahab Uddin M and Nuri ZN. 2021. Nutritional values and pharmacological importance of date fruit (*Phoenix dactylifera* Linn): A review. *Journal of Current Research in Food Science*, **2(1)**: 27–30.

Shen L, Luo H, and Fan L. 2023. Potential immunoregulatory mechanism of plant saponins: A review. *Molecules*, **29(1)**. http://dx.doi.org/10.3390/molecules29010113.

Sivasakthi P, Priya ES, and Selvan PS. 2021. Molecular insights into phytochemicals exhibiting anti-arthritic activity: Systematic review. *Inflammation Research*, **70**: 665–685. http://dx.doi.org/10.1007/s00011-021-01471-0.

Slimani W, Zerizer S, and Kabouche Z. 2020. Immunomodulatory and anti-arthritic activities of *Stachys circinata*. *Jordan Journal of Biological Sciences*, 13(2): 183–189.

Vuolo MM, da Silva-Maia JK, and Batista ÂG. 2022. The GSH colorimetric method as measurement of antioxidant status in serum and rodent tissues. *Methods Protocols Food Sci*., 187–194.

Wang G, Wang Y, and Ma F. 2024. Exploiting bacterial-origin immunostimulants for improved vaccination and immunotherapy: Current insights and future directions. *Cell Biosci.*, **14(1)**: 24. http://dx.doi.org/10.1186/s13578-024-01207-7.

JJBS

Volume 19, Number 1,March 2026
ISSN 1995-6673
Pages 105 – 112
https://doi.org/10.54319/jjbs/190110

Jordan Journal of Biological Sciences

Molecular Docking and Dynamics Simulation Assessment of Multiple Bioactive Compounds from the Zingiberaceae Family as anti-malarial Drug Candidates through Inhibiting Duffy Antigen Receptor for Chemokines (DARC) Protein

Wira Eka Putra[1,*] , Diana Widiastuti[2], Arief Hidayatullah[3], Muhammad Fikri Heikal[4], Sustiprijatno[5]

[1]*Biotechnology Study Program, Department of Applied Sciences, Faculty of Mathematics and Natural Sciences, Universitas Negeri Malang, East Java, Indonesia;* [2]*Department of Chemistry, Faculty of Mathematics and Natural Science, Universitas Pakuan, West Java, Indonesia;* [3]*United Nations Development Programme Indonesia, Health Governance Initiative, Eijkman-RSCM Building, Jakarta, Indonesia;* [4]*Department of Tropical Medicine Graduate Program, Faculty of Medicine, Khon Kaen University, Khon Kaen, Thailand;* [5]*Research Center for Applied Botany, National Research and Innovation Agency, West Java, Indonesia.*

Received: April 22, 2025; Revised: July 8, 2025; Accepted: August 8, 2025

Abstract

Malaria is a major threat to public health, particularly in tropical and subtropical regions. Malaria affects over half of the global population and killed approximately 597,000 people in 2023. Notably, malaria elimination is a major global challenge and has become a top priority worldwide. Thus, in the present study, we aimed to evaluate the antimalarial effects of bioactive compounds from the *Zingiberaceae* family by inhibiting the Duffy antigen receptor for chemokines (DARC) protein using an in silico approach. Several bioactive compounds collected from fifteen *Zingiberaceae* species were collected in the present study. Prior to molecular docking, the structure validation of the DARC protein was performed. Furthermore, molecular docking, membrane permeability prediction, molecular dynamics simulation, and toxicity prediction were performed to further assessing the antimalarial potency of *Zingiberaceae* bioactive compounds. To a greater extent, molecular docking results demonstrated that isocoronarin D and 1,7-bis(4-hydroxyphenyl)-1,4,6-heptatrien-3-one (BHPHTO), compounds commonly found in *Alpinia galanga,* exhibited binding affinity scores comparable to those of the control drugs, Chloroquine. Interestingly, the chemical interaction of both compounds showed the favorable number compared to the control, especially at the initial and terminal stages of the molecular dynamics simulation. Furthermore, molecular dynamics simulation revealed that BHPHTO exhibited the most stable interaction with the DARC protein and maintained protein structure stability better than both the isocoronarin D and Chloroquine complexes. Together these findings suggest that BHPHTO could be developed as a potential anti-malarial drug candidate. However, further studies are needed to validate BHPHTO toxicity via in vitro or in vivo, and to clarify its detailed mechanism of action against DARC protein.

Keywords: DARC, drug discovery, in silico, malaria, *Zingiberaceae*.

1. Introduction

Up to date, malaria is still considered as a major public health problem, especially in tropical and subtropical areas. It has been recorded that almost half of the world population is susceptible to Malaria (Liu *et al*., 2021; Cowman *et al*., 2016). In 2023, approximately 597,000 deaths worldwide were attributed to malaria (Daily and Parikh, 2025). Despite that, children and pregnant women in underdeveloped countries have a major risk of malaria. Additionally, several factors contribute to the high incidence of malaria, which include biological and societal challenges such as other viral outbreaks, armed conflicts, limited access to healthcare, inadequate infrastructure, and natural disasters (Pattanshetty *et al*., 2024; Monroe *et al*., 2022). Up till now, based on World health Organization deadline (WHO) guidelines, there are several basic interventions which could be applied for malaria control and management such as Artemisinin-based combination therapy, indoor residual spraying, education and communication campaigns, intermittent preventive treatment for infants, intermittent preventive treatment in school-aged children, intermittent preventive treatment of pregnant women, larval source management, long lasting insecticidal nets, mass drug administration, perennial malaria chemoprevention, post-discharge malaria chemoprevention, rapid diagnostic tests, seasonal malaria chemoprevention, and targeted drug administration (Pattanshetty *et al*., 2024). Finally, eliminating malaria, particularly reducing its mortality and morbidity, has emerged as a significant priority and challenge, dependent on strategies such as insecticide-treated nets, antimalarial medications, and mosquito control programs.

* Corresponding author. e-mail: wira.putra.fmipa@um.ac.id.

Malaria is caused by *Plasmodium* parasite which is transmitted via infected female *Anopheles* mosquitoes. It has been reported that *P. falciparum* and *P. vivax* cause the most serious infections which remain as major risk of malaria cases in underdeveloped countries. The life cycle of *Plasmodium* infecting humans consists of two stages, the initial development stage found in the liver, and the second proliferation stage found in the blood (Talapko *et al*., 2019). Understanding the parasite's life cycle has become a unique challenge to develop strategy to overcome malaria. On the other hand, several drugs such as quinine, chloroquine, and artemisinin have been used to treat malaria; however, the parasite has developed resistance to each, making effective control increasingly difficult. Therefore, the current challenge in malarial disease control requires a novel drug which could effectively inhibit the activities of the malarial parasites.

The DARC is a receptor protein that plays a critical role in *Plasmodium* invasion. To a greater extent, the DARC specifically serves as a receptor for *P. vivax* to invade red blood cell (Dean, 2005). Compared to the other *Plasmodium* species, *P. vivax* has a wider distribution and could survive in colder climates. It has been reported that the high expression of the DARC in malaria patients is correlated to the severe outcome (Kaur *et al*., 2019; Dean, 2005). Additionally, another investigation has demonstrated that the DARC polymorphisms affect susceptibility to clinical *P. vivax* and impact the immune response to malaria blood antigens, thereby compromising the effectiveness of future malaria vaccines (Oliveira *et al*., 2012). Targeting DARC is a promising therapeutic approach, as interfering with this protein can prevent the parasite from entering red blood cells and thus impair its ability to cause infection (Moskovitz et al., 2023).

Plant-derived natural products have been recognized for their therapeutic effects since ancient times, particularly in treating pain, wound healing, gut health, and ameliorating other ailments (Putra *et al*., 2023; Davila and Papada, 2023; Nasim *et al.*, 2022; Putra and Rifa'i, 2020; Putra et al., 2020; Putra and Rifa'i, 2019). *Zingiberaceae* family is a group of plants that exhibit adaptations to diverse ecological conditions, which are mostly found in tropical rainforests and moist environments. In addition to their economic value, *Zingiberaceae* plants exhibit significant therapeutic properties including antioxidant, anti-inflammatory, antimicrobial, anticancer, and antiemetic activities (Boonma *et al*., 2023). Additionally, some species such as *Zingiber nimmonii*, *Zingiber officinale*, and *Zingiber cernuum* demonstrated anti-malarial effects (Biruksew *et al*., 2018; Rajeswary *et al*., 2018; Govindarajan *et al*., 2016). In addition to their therapeutic potencies, *Zingiberaceae* plants serve as abundant sources of chemical compounds, including alkaloids, carbohydrates, proteins, phenolic acids, flavonoids, and diarylheptanoids which are known as a source of natural biopharmaceuticals (Ballester *et al*., 2023). Therefore, in the present study we aimed to evaluate the anti-malarial effect of various bioactive compounds from *Zingiberaceae* family by targeting the DARC protein.

2. Materials and Methods

2.1. Ligand structure preparation

The present study evaluated multiple bioactive compounds from fifteen species of Zingiberaceae family including Aframomum arundiaceum, Aframomum escapum, Aframomum latifolium, Aframomum zambesiacum, Alpinia galanga, Boesenbergia rotunda, Curcuma longa, Curcuma zanthorriza, Kaempferia galanga, Kaempferia rotunda, Renealmia cincinnata, Siphonochilus aethiopicus, Siphonochilus aethiopicus, Zingiber officinale, and Zingiber zerumbet (Heikal et al., 2024). Before molecular docking, the chemical structures of the ligands were retrieved from PubChem database (https://pubchem.ncbi.nlm.nih.gov/). Each compound and control drug used in this study was identified with a unique PubChem Compound ID (CID), including Isocoronarin D (CID: 71550939), BHPHTO (CID: 71346280), and Chloroquine (CID: 2719). Then, each chemical structure was saved in sdf. file for further molecular docking analysis.

2.2. Target protein preparation

The target protein used in this study was human DARC, which was known as potential target for anti-malarial. The 3D structure of the protein was collected from the RSCB PDB database (https://www.rcsb.org/), with PDB ID. 4NUU. Furthermore, the protein optimization was performed to remove the native molecule and water, and at the same time, the polarity of the structure was added. The optimization was performed by using PyMOL software (https://www.pymol.org/) and Discovery Studio software (https://www.3ds.com/).

2.3. Protein structure validation

Structure validation server or SAVESv6.1. (https://saves.mbi.ucla.edu/) was used to perform the DARC protein validation. In this analysis, the Ramachandran plot and ERRAT analysis were conducted to evaluate the quality of the structure (Colovos *et al*., 1993). Moreover, protein structure analysis or ProSA-Web (https://prosa.services.came.sbg.ac.at/prosa.php) was utilized to correctly check the structure errors of DARC protein (Wiederstein and Sippl, 2007; Sippl, 1993).

2.4. Molecular docking and visualization and membrane permeability prediction

After finishing protein and ligand preparation, the PyRx 0.8 software (https://pyrx.sourceforge.io/) was used to perform molecular docking. The grid of molecular docking was set to cover all the surface of the DARC protein with specification grid box center (Å): X: 47.7956, Y:-45.000, Z:96.0143 and grid box dimensions (Å): X: 15.9225, Y: 24.8906, Z:14.8393. Binding affinity scores were analyzed as a result of molecular docking. Furthermore, the visualization of chemical interaction and the 3D structure of the complex were performed by using Discovery Studio software (Ruswanto *et al*., 2024; Hidayatullah *et al*., 2021; Putra and Rifa'i, 2020). In the present study, the PerMM webserver (https://permm.phar.umich.edu/) was used to estimate the potency of ligands to penetrate the plasma membrane (Lomize and Pogozheva, 2019; Lomize *et al*., 2019).

Additionally, the temperature was set to 310 K and the pH to 7.4 to mimic physiological conditions.

2.5. Molecular dynamics simulation and toxicity prediction analysis

YASARA software (http://www.yasara.org/) was used to perform molecular dynamic simulation to evaluate the stability of protein-ligand complex. The simulation was run for 1000 ps. Multiple parameters were analyzed such as potential energy, RMSD, RMSF, ligand movement, ligand conformation, solvent accessible surface, Hydrogen bonds, and DCCM (Hidayatullah *et al*., 2023; Hidayatullah *et al*., 2022). Finally, ProTox 3.0. web server (https://tox.charite.de/protox3/) was used to validate the toxicity prediction and the probability of the compounds to induce toxicity.

3. 3. Results and Discussion

In the present study, we were able to validated, and then discovered that the 3D structure of DARC is qualified and showed the high score value for its quality according to some parameters such as the Ramachandran plot, ProSA-web evaluation, and the ERRAT quality assessment (Fig. 1). According to the Ramachandran plot results, the DARC protein structure has a dominant number of residues occupying in most favored regions of 92.5%, in additional allowed regions of 7.3%, and in generously allowed regions of 0.2%. Moreover, ProSA-web demonstrated that the DARC protein structure has *Z*-score of -5.57. Additionally, the ProSA-web analysis demonstrated that the DARC protein has minimal errors which indicated by the window size mostly has negative value. Based on the ERRAT analysis, the DARC protein has an overall quality factor of 98.201, which indicates DARC structure has good quality. The study of protein structures is crucial for understanding the fundamental principles of protein function, which play a significant role in drug design (Ghosh *et al*., 2017). Protein structures are elucidated via experimental techniques such as X-ray crystallography and nuclear magnetic resonance. The protein structure may encounter global errors as a result from the misinterpretation of the polypeptide chain (Bagaria *et al*., 2012; Pugalenthi *et al*., 2006). Therefore, accurate structural validation of proteins is extremely crucial in a drug discovery study.

DARC is known as a potential target for malaria treatment. DARC becomes a key receptor for *P. vivax* to infect the red blood cells (Tobin *et al*., 2023). Interfering with *P. vivax* antigen-DARC interaction and avoiding its downstream activation are considered a novel anti-malarial strategy (Moskovitz *et al*., 2023). In this study, several bioactive compounds from multiple *Zingiberaceae* family have been evaluated for their anti-malarial activities by inhibiting the DARC protein. According to the docking result, we found that two hit-to-lead compounds namely BHPHTO and isocoronarin D have closely binding affinity scores to the control drug, Chloroquine (Fig. 2). BHPHTO and Chloroquine share a close value of binding energy due to their similar interaction characteristics, including several hydrogen bonds and hydrophobic interactions with critical residues in Chain C of DARC. Both compounds have advantageous docking poses and occupy similar binding site areas, which may explain their expected binding energies. Despite its structural differences and bioactivity, isocoronarin D has less interactions, such as hydrogen bonding or hydrophobic contacts, which may explain its reduced binding affinity.

Furthermore, we evaluated the penetration potency of these compounds by performing membrane permeability prediction. Interestingly, we found that both isocoronarin D and BHPHTO can easily penetrate the plasma membrane (Fig. 3). Isocoronarin D can penetrate cell membranes more easily because it is more hydrophobic, more compact, and less polar structure, which helps it pass through the lipid layer without needing any transport. Conversely, BHPHTO, although also including three oxygen atoms and many cyclic moieties, exhibits a wider array of polar functional groups, possibly enhancing its overall polarity and diminishing its lipophilicity.

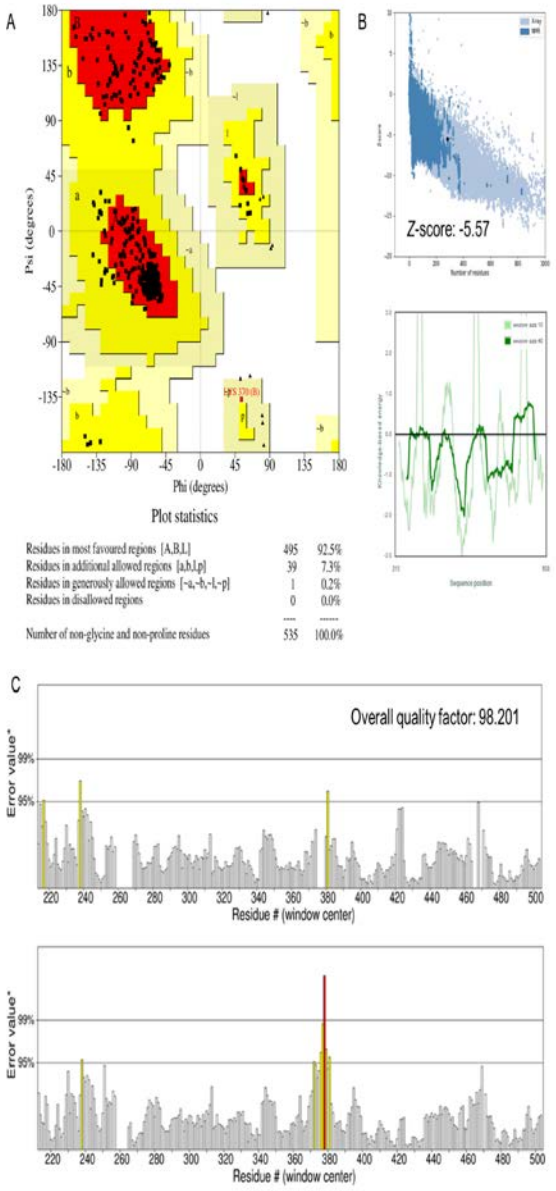

Figure 1. DARC protein structure validation. A). Procheck. B) the z-score plot of ProSA – Web. C). ERRAT analysis.

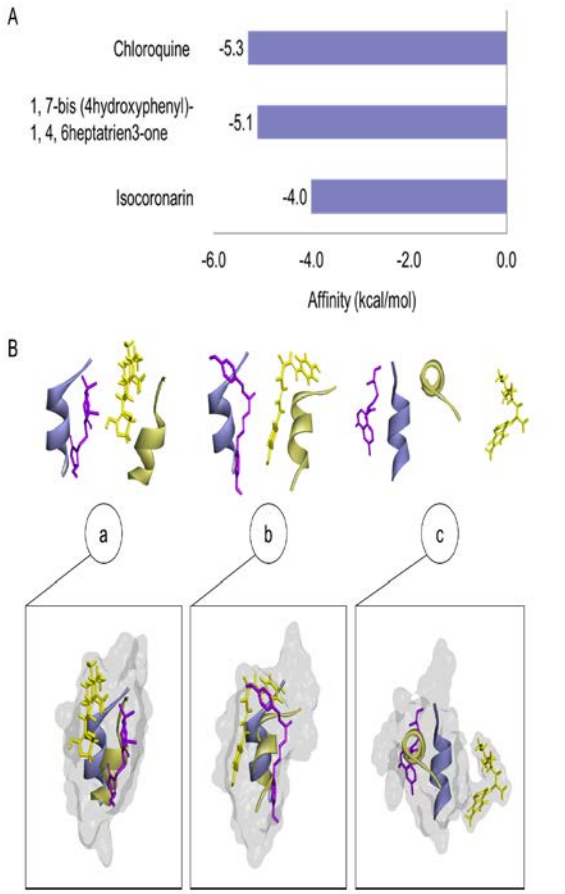

Figure 2. Molecular docking and dynamics simulation. A). The binding affinity values of isocoronarin D, 1,7-bis(4-hydroxyphenyl)-1,4,6-heptatrien-3-one, and control drug (chloroquine) toward DARC protein. B). The 3D structure visualization of isocoronarin D (a), 1,7-bis(4-hydroxyphenyl)-1,4,6-heptatrien-3-one (b), and control drug (c) toward the DARC protein at initial and the terminal stages of molecular dynamics simulation.

In molecular docking, scoring functions estimate binding affinity, with more negative values indicating a stronger, more stable interaction with the target protein. The binding affinity scores are also determined by H-bond composition. The strong H-bond could reflect the high-affinity of ligand against the target protein (Pantsar and Poso, 2018; Hidayatullah et al., 2021). Our results indicate that all three ligands were precisely docked to residues of Chain C, which is believed to be functionally relevant for ligand interaction. Besides the importance of binding affinity and H-bond composition in complex interaction, the ability of ligand to penetrate the plasma membrane is important. Importantly, membrane permeability prediction could provide physicochemical and pharmaceutical information about drug–membrane thermodynamics (Menichetti *et al*., 2019). Permeability is crucial for assessing a drug's ability to pass through gastrointestinal membranes, and it plays a vital role in ensuring effective distribution to pharmacological target organs and cells. (Wang and Skolnik, 2013).

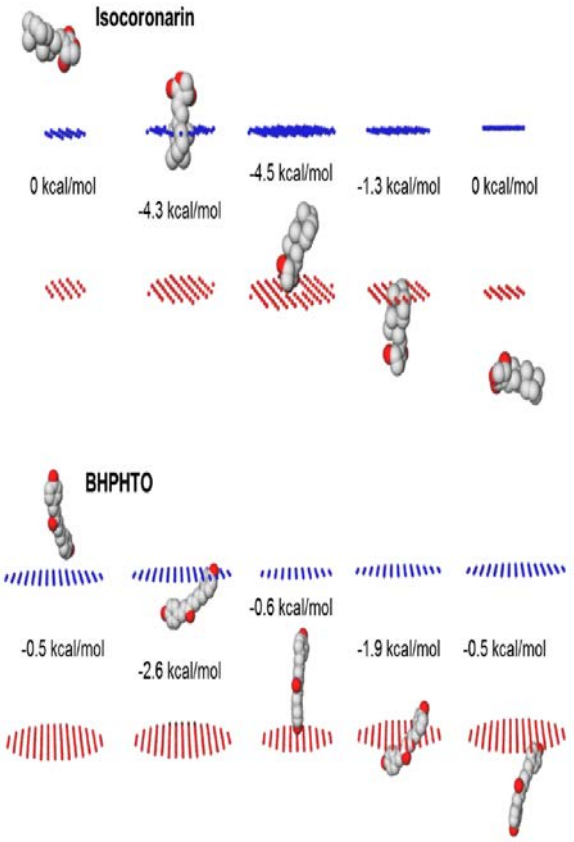

Figure 3. The prediction of membrane permeability penetration of isocoronarin D and 1,7-bis(4-hydroxyphenyl)-1,4,6-heptatrien-3-one.

Molecular dynamics simulations predict the movements of each atom in a protein or other molecular systems. These simulations reveal the positions of atoms over time, capturing a wide range of significant biomolecular processes, including conformational changes, ligand binding, and protein folding (Hollingsworth and Dror, 2018). Interestingly, we noticed that there are changes on the ligands and protein position during molecular dynamics simulation (Fig. 2). We then compared the initial and the terminal stage of molecular dynamics simulation at each complex. Interestingly, we found that there are changes in the composition of chemical interaction which showed H-bond and hydrophobic interaction relatively constant on both isocoronarin D and BHPHTO. However, on the control drug, we found that in the terminal stage of dynamics simulation, the ligand is disassociated with the target protein, indicating that there is no chemical interaction found in terminal stage of DARC - Chloroquine complex (Fig. 4, Table 1). This finding suggests that both hit-to-lead compounds, especially BHPHTO, are stable enough to interact with the DARC compared to the control drug.

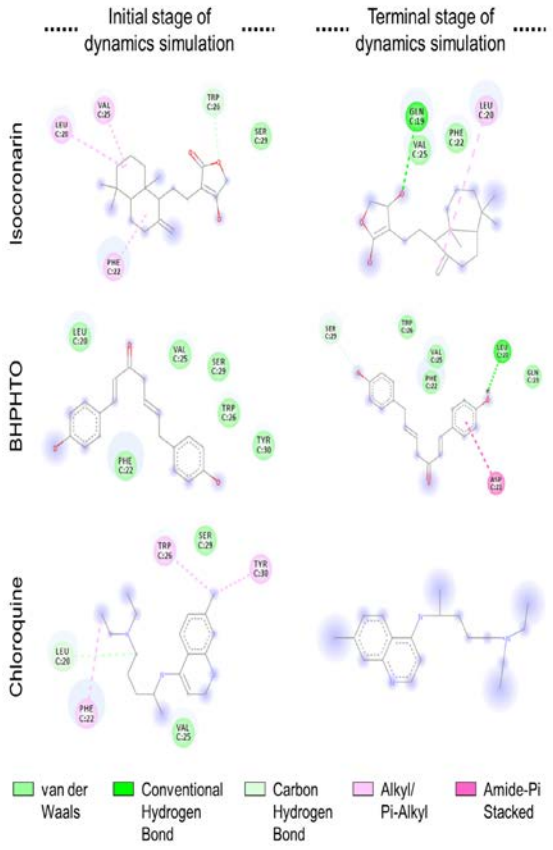

Figure 4. The 2D structure and interaction visualization of isocoronarin, 1,7-bis(4-hydroxyphenyl)-1,4,6-heptatrien-3-one, and control drug toward the DARC protein at the initial and terminal stage of molecular dynamics simulation.

Table 1. List of amino acids residue and chemical interaction of isocoronarin, 1,7-bis(4-hydroxyphenyl)-1,4,6-heptatrien-3-one, and control drug toward the DARC protein at initial and terminal stage of molecular dynamics simulation.

Compound	Amino Acids Residue		Interaction
	Initial stage	Terminal stage	
Isocoronarin D CID. 71550939	Trp26(C)	Gln19(C)	Hydrogen Bond
	Ser29(C)	Phe22(C); Val25(C)	Van der Waals
BHPHTO CID. 71346280	-	Leu20(C); Ser29(C)	Hydrogen Bond
	Leu20(C); Val25(C); Ser29(C); Trp26(C); Tyr30(C); Phe22(C)	Gln19(C); Phe22(C); Val25(C); Trp26(C)	Van der Waals
Chloroquine CID. 2719	Leu20(C)	-	Hydrogen Bond
	Ser29(C); Val25(C)	-	Van der Waals

To the greater extent, we evaluated eight parameters on molecular dynamics simulation such as potential energy, RMSD, RMSF, ligand movement, ligand conformation, solvent accessible surface, and Hydrogen bonds (Fig. 5). Some parameters such as potential energy, RMSF, ligand conformation, solvent accessible surface, and Hydrogen bonds showed similar pattern among the complexes. However in parameter of RMSD backbone, isocoronarin D and Chloroquine shared a similar pattern which showed a higher value compared to the BHPHTO (Fig. 5B). This showed that DARC – isocoronarin D structure and of DARC – Chloroquine complex during dynamic simulation are less stable compared to BHPHTO. The lower number of RMSD backbone indicates the stability and compactness of complex structure (Hidayatullah *et al*., 2023). Moreover, in the ligand movement parameters, we found that isocoronarin D and BHPHTO are relatively stable against the target protein, but there is extreme fluctuation on Chloroquine which demonstrated that this control drug is not stable against the DARC. This result is supported by the previous finding related to absent of chemical interaction in the DARC – Chloroquine complex at the terminal stage of molecular dynamic simulation (Fig. 4). DCCM analysis is one of important parameters to evaluate the structure movement whether it's parallel (1) or anti-parallel (-1). According to the DCCM results, the protein structures of both isocoronarin D and BHPHTO complexes are moving in parallel as indicated by the thicker yellow's diagonal line compared to the Chloroquine complex (Fig. 6).

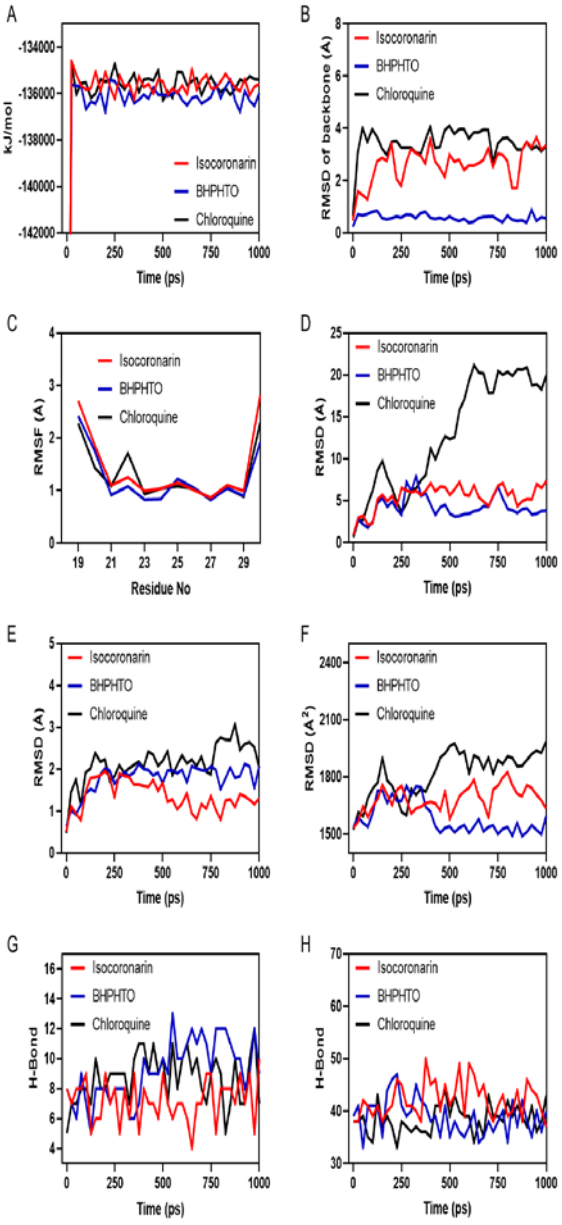

Figure 5. Molecular dynamics simulation. (A). Potential energy plot; (B). RMSD plot; (C). RMSF plot; (D). Ligand movement plot; (E). Ligand conformation plot; (F). Solvent accessible surface plot; (G). Hydrogen bonds in the solute plot; and (H). Hydrogen bonds between solute and solvent plot for isocoronarin, 1,7-bis(4-hydroxyphenyl)-1,4,6-heptatrien-3-one, or control drug - protein complexes over a 1000 ps of dynamics simulation.

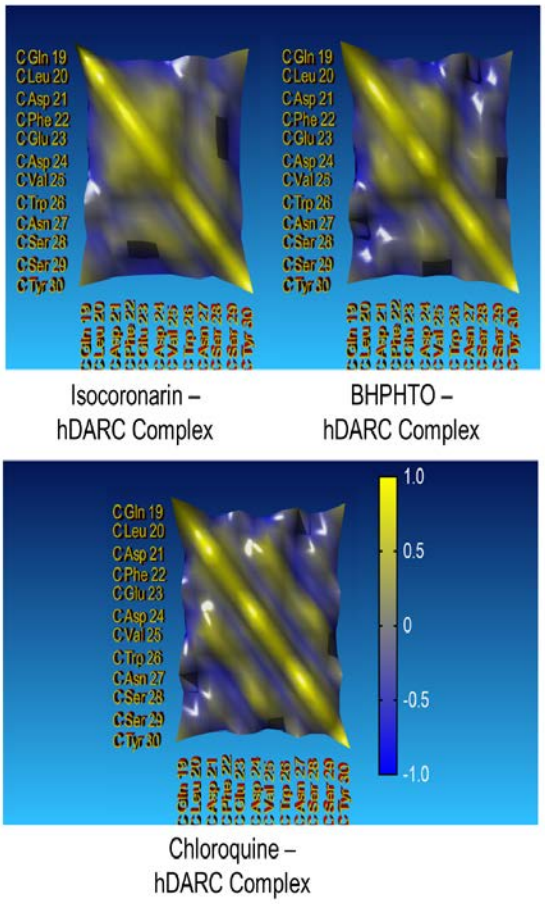

Figure 6. Dynamic cross-correlation matrix (DCCM) for isocoronarin, 1,7-bis(4-hydroxyphenyl)-1,4,6-heptatrien-3-one, or control drug - protein complexes. Yellow represents correlated motions, and blue represents anticorrelated motions.

Together, these findings indicate that the hit-to-lead compound namely 1,7-bis(4-hydroxyphenyl)-1,4,6-heptatrien-3-one has better stability compared to the isocoronarin D and Chloroquine. Molecular dynamics simulation could determine the stability of protein structure during interaction with ligand, and at the same time it could indicate the behavior of ligand, whether it has a strong binding mode or it disassociated with target proteins (Choi *et al*., 2022; Gill *et al*., 2019; Liu *et al*., 2017). Some parameters, such as RMSD backbone, H-bond, ligand conformation, and DCCM, explicitly demonstrated the stability and compactness of the structure. Additionally, ligand movement parameter showed how the ligands behave with the target proteins. To a greater extent, BHPHTO forms more stable and frequent hydrogen bonds with the DARC protein compared to isocoronarin D and Chloroquine, supporting its stronger binding affinity. In contrast, isocoronarin D forms the highest number of hydrogen bonds with solvent molecules, indicating greater solvation and exposure to the aqueous environment. This suggests that isocoronarin D is less embedded in the binding pocket, which may explain its lower binding affinity.

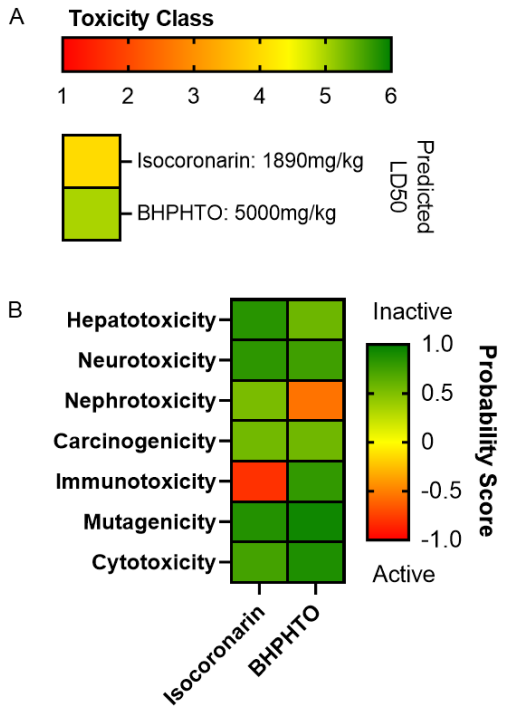

Figure 7. Toxicity evaluation of isocoronarin D and 1, 7-bis (4hydroxy phenyl)-1, 4, 6 heptatrien3-one. A). Toxicity class and LD50 prediction. B). The probability of bioactive compounds to induce toxicity in organs.

Finally, to support these findings, the toxicity prediction of hit-to-lead compounds was examined (Figure 7). The result showed that isocoronarin D was more toxic compare than BHPHTO with toxicity classes 4 and 5, and predicted LD50 1890 mg/kg and 5000 mg/kg respectively. Interestingly, we found that isocoronarin D and BHPHTO is relatively safe to human body because these compounds do not cause hepatotoxicity, neurotoxicity, carcinogenicity, mutagenicity, and cytotoxicity. However, certain alerts should be noted that isocoronarin D may cause immunotoxicity, and BHPHTO may pose a risk of nephrotoxicity. As with other in silico approaches, toxicity prediction plays an important role in accelerating drug discovery research. Considering its benefit that can save several drug assessments including cellular, animal, and clinical test, toxicity prediction is crucial in order to reduce the cost and labour involved drug's preclinical and clinical trials (Füzi *et al*., 2023; Wu and Wang, 2018).

4. Conclusion

The present study validates two bioactive compounds collected from fifteen members of *Zingiberaceae* family as anti-malarial drug candidates against the DARC protein. Molecular docking results demonstrated that isocoronarin D and BHPHTO from *A. galanga* have close binding affinity scores to the control drug. Interestingly, the chemical interaction within both compounds demonstrated the favorable number compared to the control, especially at initial and terminal stages of the molecular dynamics simulation. Furthermore, molecular dynamics simulation demonstrated that BHPHTO has the most stability movement to the DARC protein and stability of protein structure compared to isocoronarin D and Chloroquine complexes. Together, these findings suggest that BHPHTO might be developed as drug candidates for anti-malaria. However, further study on validating the toxicity and detailed mechanism against DARC is badly needed.

Acknowledgment

Authors would like to thank Universitas Negeri Malang for supporting this study.

References

Bagaria A, Jaravine V, Huang YJ, Montelione GT and Güntert P. 2012. Protein structure validation by generalized linear model root-mean-square deviation prediction. *Protein Sci.*, **21(2)**: 229–238.

Ballester P, Cerdá B, Arcusa R, García-Muñoz AM, Marhuenda J and Zafrilla P. 2023. Antioxidant activity in extracts from Zingiberaceae family: Cardamom, turmeric, and ginger. *Molecules*, **28(10)**: 4024.

Biruksew A, Zeynudin A, Alemu Y, Golassa L, Yohannes M, Debella A, Urge G, De Spiegeleer B and Suleman S. 2018. *Zingiber officinale* Roscoe and *Echinops kebericho* Mesfin showed antiplasmodial activities against *Plasmodium berghei* in a dose-dependent manner in Ethiopia. *Ethiop J Health Sci.*, **28(5)**: 655–664.

Boonma T, Saensouk S and Saensouk P. 2023. Diversity and traditional utilization of the Zingiberaceae plants in Nakhon Nayok Province, Central Thailand. *Diversity*, **15(8)**: 904.

Choi KE, Kim JM, Rhee JE, Park AK, Kim EJ, Yoo CK and Kang NS. 2022. Molecular dynamics studies on the structural stability prediction of SARS-CoV-2 variants including multiple mutants. *Int J Mol Sci.*, **23(9)**: 4956.

Colovos C and Yeates TO. 1993. Verification of protein structures: patterns of nonbonded atomic interactions. *Protein Sci.*, **2(9)**: 1511–1519.

Cowman AF, Healer J, Marapana D and Marsh K. 2016. Malaria: Biology and disease. *Cell*, **167(3)**: 610–624.

Daily JP and Parikh S. 2025. Malaria. *N Engl J Med.*, **392(13)**: 1320–1333.

Davila MM and Papada E. 2023. The role of plant-derived natural products in the management of inflammatory bowel disease—what is the clinical evidence so far? *Life*, **13(8)**: 1703.

Dean L. 2005. Blood groups and red cell antigens. National Center for Biotechnology Information (NCBI), Chapter 9: The Duffy blood group. Available from: https://www.ncbi.nlm.nih.gov/books/NBK2271/.

Füzi B, Mathai N, Kirchmair J and Ecker GF. 2023. Toxicity prediction using target, interactome, and pathway profiles as descriptors. *Toxicol Lett.*, **381**: 20–26.

Ghosh S, Gadiyaram V and Vishveshwara S. 2017. Validation of protein structure models using network similarity score. *Proteins*, **85(9)**: 1759–1776.

Gill M and McCully ME. 2019. Molecular dynamics simulations suggest stabilizing mutations in a de novo designed α/β protein. *Protein Eng Des Sel.*, **32(7)**: 317–329.

Govindarajan M, Rajeswary M, Arivoli S, Tennyson S and Benelli G. 2016. Larvicidal and repellent potential of *Zingiber nimmonii* (J. Graham) Dalzell (Zingiberaceae) essential oil: An eco-friendly tool against malaria, dengue, and lymphatic filariasis mosquito vectors? *Parasitol Res.*, **115(5)**: 1807–1816.

Heikal MF, Putra WE, Sustiprijatno, Hidayatullah A and Widiastuti D. 2024. A molecular docking and dynamics simulation study on prevention of merozoite red blood cell invasion by targeting *Plasmodium vivax* Duffy binding protein with Zingiberaceae bioactive compounds. *Uniciencia*, **38(1)**: 1–15.

Hidayatullah A, Putra WE, Rifa'i M, Sustiprijatno, Widiastuti D, Heikal MF, Susanto H and Salma WO. 2022. Molecular docking and dynamics simulation studies to predict multiple medicinal plants' bioactive compounds interaction and its behavior on the surface of DENV-2 E protein. *Karbala Int J Mod Sci.*, **8(3)**: 531–542.

Hidayatullah A, Putra WE, Salma WO, Muchtaromah B, Permatasari GW, Susanto H, Widiastuti D and Kismurtono M. 2021. Discovery of drug candidate from various natural products as potential novel dengue virus nonstructural protein 5 (NS5) inhibitor. *Chiang Mai Univ J Nat Sci.*, **20(1)**: 1–17.

Hidayatullah A, Putra WE, Sustiprijatno, Permatasari GW, Salma WO, Widiastuti D, Susanto H, Muchtaromah B, Sari DRT, Ningsih FN, Heikal MF, Yusuf AMR and Arizona AS. 2021. In silico targeting DENV2's prefusion envelope protein by several natural products' bioactive compounds. *Chiang Mai Univ J Nat Sci.*, **20(3)**: 1–20.

Hidayatullah A, Putra WE, Sustiprijatno, Rifa'i M, Widiastuti D, Heikal MF and Permatasari GW. 2023. Concatenation of molecular docking and dynamics simulation of human papillomavirus type 16 E7 oncoprotein targeted ligands: In quest of cervical cancer's treatment. *An Acad Bras Cienc.*, **95(Suppl. 1)**: 1–16.

Hollingsworth SA and Dror RO. 2018. Molecular dynamics simulation for all. *Neuron*, **99(6)**: 1129–1143.

Kaur H, Sehgal R and Rani S. 2019. Duffy antigen receptor for chemokines (DARC) and susceptibility to *Plasmodium vivax* malaria. *Parasitol Int.*, **71**: 73–75.

Liu K, Watanabe E and Kokubo H. 2017. Exploring the stability of ligand binding modes to proteins by molecular dynamics simulations. *J Comput Aided Mol Des.*, **31(2)**: 201–211.

Liu Q, Jing W, Kang L, Liu J and Liu M. 2021. Trends of the global, regional, and national incidence of malaria in 204 countries from 1990 to 2019 and implications for malaria prevention. *J Travel Med.*, **28(5)**: 46.

Lomize AL, Hage JM, Schnitzer K, Golobokov K, LaFaive MB, Forsyth AC and Pogozheva ID. 2019. PerMM: A web tool and database for analysis of passive membrane permeability and translocation pathways of bioactive molecules. *J Chem Inf Model.*, **59(7)**: 3094–3099.

Lomize AL and Pogozheva ID. 2019. Physics-based method for modeling passive membrane permeability and translocation pathways of bioactive molecules. *J Chem Inf Model.*, **59(7)**: 3198–3213.

Menichetti R, Kanekal KH and Bereau T. 2019. Drug–membrane permeability across chemical space. *ACS Cent Sci.*, **5(2)**: 290–298.

Monroe A, Williams NA, Ogoma S and Karema C. 2022. Reflections on the 2021 World Malaria Report and the future of malaria control. *Malar J.*, **21(1)**: 154.

Moskovitz R, Pholcharee T, DonVito SM, Guloglu B and Higgins MK. 2023. Structural basis for DARC binding in reticulocyte invasion by *Plasmodium vivax*. *Nat Commun.*, **14(1)**: 3637.

Nasim N, Sandeep IS and Mohanty S. 2022. Plant-derived natural products for drug discovery: current approaches and prospects. *Nucleus (Calcutta)*, **65(3)**: 399–411.

Oliveira TY, Harris EE, Meyer D, Jue CK and Silva WA Jr. 2012. Molecular evolution of a malaria resistance gene (DARC) in primates. *Immunogenetics*, **64(7)**: 497–505.

Pantsar T and Poso A. 2018. Binding affinity via docking: Fact and fiction. *Molecules*, **23(8)**: 1899.

Pattanshetty S, Dsouza VS, Shekharappa A, Yagantigari M, Raj R, Inamdar A, Alsamara I, Rajvanshi H and Brand H. 2024. A scoping review on malaria prevention and control intervention in fragile and conflict-affected states (FCAS): A need for renewed focus to enhance international cooperation. *J Epidemiol Glob Health*, **14(1)**: 4–12.

Pugalenthi G, Shameer K, Srinivasan N and Sowdhamini R. 2006. HARMONY: A server for the assessment of protein structures. *Nucleic Acids Res.*, **34**(Web Server issue): W231–W234.

Putra WE, Agusinta AK, Ashar MSAA, Manullang VA and Rifa'i M. 2023. Immunomodulatory and ameliorative effect of *Citrus limon* extract on DMBA-induced breast cancer in mouse. *Karbala Int J Mod Sci.*, **9(2)**: 1–14.

Putra WE, Maulana AR, Ramadhan ATK and Rifa'i M. 2020. T cells regulation modulated by *Sambucus javanica* extracts in DMBA-exposed mice. *J HerbMed Pharmacol.*, **9(4)**: 408–411.

Putra WE and Rifa'i M. 2020. Assessing the immunomodulatory activity of ethanol extract of *Sambucus javanica* berries and leaves in chloramphenicol-induced aplastic anemia mouse model. *Trop Life Sci Res.*, **31(2)**: 175–185.

Putra WE and Rifa'i M. 2020. Evaluating the molecular interaction of *Sambucus* plant bioactive compounds toward TNF-R1 and TRAIL-R1/R2 as possible anti-cancer therapy based on traditional medicine: The bioinformatics study. *Sci Study Res Chem Chem Eng Biotechnol Food Ind.*, **21(3)**: 357–365.

Putra WE and Rifa'i M. 2019. Hematopoiesis activity of *Sambucus javanica* on chloramphenicol-induced aplastic anemia mouse model. *Nat Prod Sci.*, **25(1)**: 59–63.

Rajeswary M, Govindarajan M, Alharbi NS, Kadaikunnan S, Khaled JM and Benelli G. 2018. *Zingiber cernuum* (Zingiberaceae) essential oil as effective larvicide and oviposition deterrent on six mosquito vectors, with little non-target toxicity on four aquatic mosquito predators. *Environ Sci Pollut Res Int.*, **25(11)**: 10307–10316.

Ruswanto R, Nofianti T, Lestari T, Septian AD, Firmansyah AP and Mardianingrum R. 2024. Potential active compounds of propolis as breast anticancer candidates: In silico study. *Jordan J Biol Sci.*, **17(1)**: 153–161.

Sippl MJ. 1993. Recognition of errors in three-dimensional structures of proteins. *Proteins*, **17**: 355–362.

Talapko J, Škrlec I, Alebić T, Jukić M and Včev A. 2019. Malaria: The past and the present. *Microorganisms*, **7(6)**: 179.

Tobin AR, Crow R, Urusova DV, Klima JC, Tolia NH and Strauch EM. 2023. Inhibition of a malaria host–pathogen interaction by a computationally designed inhibitor. *Protein Sci.*, **32(1)**: e4507.

Wang J and Skolnik S. 2013. Permeability diagnosis model in drug discovery: A diagnostic tool to identify the most influencing properties for gastrointestinal permeability. *Curr Top Med Chem.*, **13(11)**: 1308–1316.

Wiederstein M and Sippl MJ. 2007. ProSA-web: interactive web service for the recognition of errors in three-dimensional structures of proteins. *Nucleic Acids Res.*, **35(2)**: 407–410.

Wu Y and Wang G. 2018. Machine learning-based toxicity prediction: From chemical structural description to transcriptome analysis. *Int J Mol Sci.*, **19(8)**: 2358.

JJBS

Volume 19, Number 1,March 2026
ISSN 1995-6673
Pages 113 – 125
https://doi.org/10.54319/jjbs/190111

Jordan Journal of Biological Sciences

Green Valorization of Coconut Husk Waste: NaOH-Activated Carbon for Improved Ammonia Filtration in Recirculating Aquaculture of Common Carp (*Cyprinus carpio*)

Said Ali Akbar[1,*], Raudhatul Jannah[1], Cut Nuzlia[1], Muhammad Hasan[2]

[1]*Department of Aquaculture, Faculty of Marine and Fisheries, Universitas Syiah Kuala, Banda Aceh, 23111, Indonesia;* [2]*Department of Chemistry Education, Faculty of Teacher Training and Education, Universitas Syiah Kuala. Banda Aceh 23111, Aceh, Indonesia*

Received: June 13, 2025; Revised: August 4, 2025; Accepted: August 11, 2025

Abstract

This study evaluated the efficacy of coconut husk-derived NaOH-activated carbon in improving water quality and fish health in a recirculating aquaculture system (RAS) for *Cyprinus carpio*. Activated carbon was synthesized via carbonization at 300 °C followed by NaOH activation, resulting in enhanced adsorption properties: surface area increased from 323.12 to 654.43 m²/g, iodine number rose from 687.43 to 992.95 mg/g, and methylene blue adsorption reached 132.12 mg/g. A 28-day RAS experiment was conducted with five treatments (0, 5, 10, 15, and 20 g of activated carbon), evaluating ammonia levels, oxidative stress responses, hematological status, erythrocyte morphology, and survival rate. Ammonia levels significantly decreased ($p < 0.05$), with P5 achieving 0.0103 ± 0.0006 ppm on Day 20, below regulatory thresholds. Antioxidant enzymes improved significantly (SOD: 8.575 U/mL; CAT: 0.09125 U/mL), while lipid peroxidation (MDA: 1.3 µmol/L) was reduced ($p < 0.05$). Oxygen consumption increased in P5 (220 ± 4 mg O_2/kg/h), and hematological parameters improved (MCHC: 33.52 ± 0.24 g/dL; MCV: 362.50 ± 29.01 fL; RBC: $2.08 \pm 0.02 \times 10^6$/µL), while WBC decreased ($52.5 \pm 5.25 \times 10^3$/µL). Erythrocyte deformities were minimized, and survival increased from 67.5% (control) to 97.5% in P5 ($p < 0.05$). This study underscores the potential of coconut husk-based activated carbon as a cost-effective and sustainable adsorbent, enhancing aquaculture water quality and fish welfare in RAS applications.

Keywords: activated carbon; ammonia removal; recirculating aquaculture; oxidative stress; fish hematology

1. Introduction

Cyprinus carpio is widely favored in freshwater aquaculture due to its adaptability to a wide range of environmental conditions, its fast growth, and its high feed-to-biomass conversion efficiency, traits that make it especially suitable for intensive aquaculture systems (Karatas et al., 2025). This species serves as a vital economic asset, contributing substantially to the profitability of aquaculture ventures at both smallholder and industrial levels (Barragán-Longoria et al., 2025). The global market's growing reliance on carp as an accessible and dependable protein source has intensified the push for more sustainable farming methods. Its ability to tolerate variable water quality conditions aligns well with the operational demands of modern, high-density rearing technologies (Wang et al., 2024). Nonetheless, intensification brings with it the issue of nitrogenous waste buildup, particularly ammonia, which can impair water quality and, in turn, compromise fish growth, health, and survival. Ammonia accumulation remains one of the principal bottlenecks in maximizing the efficiency of aquaculture production systems (Nguyen-tiêt et al., 2025). Furthermore, the declining availability of land suitable for conventional pond aquaculture, especially in urbanized and heavily populated areas, presents additional obstacles to expanding carp production (Wu et al., 2025). Addressing these limitations calls for robust water quality control approaches, particularly the implementation of recirculating aquaculture systems (RAS), which offer a sustainable path forward for ensuring the health and productivity of common carp farming.

In response to issues like deteriorating water quality and the scarcity of land suitable for aquaculture, Recirculating Aquaculture Systems (RAS) have become a preferred modern alternative that emphasizes sustainability (Akbar et al., 2025a). These systems function through a closed-loop mechanism in which water is continuously filtered, treated, and reused, leading to a substantial decrease in the need for freshwater inputs while ensuring that key water quality parameters remain within optimal ranges (Wu et al., 2025). The performance of RAS can be further improved by integrating advanced filtration media, such as activated carbon, which effectively eliminates toxic ammonia and other waste by-products from fish metabolism, thereby fostering a healthier and more stable aquatic environment (J. Xu et al., 2024**).** Nonetheless, while various filtration materials such as zeolite and biochar have shown promise in ammonia removal (Zhou et al., 2024; Angellinnov et al., 2025), the use of coconut husk-derived activated carbon remains underexplored in

* Corresponding author.; e-mail: saidaliakbar@usk.ac.id.

aquaculture applications, particularly in RAS. For common carp (*Cyprinus carpio*), which can be highly sensitive to poor water quality in intensive culture conditions, the implementation of RAS offers a practical means of supporting higher stocking densities without compromising welfare. In addition, RAS promotes optimal use of available resources, offering a practical solution for regions facing limitations in land availability and freshwater supply. As the aquaculture sector increasingly emphasizes sustainability and environmental responsibility, integrating RAS with effective water treatment technologies represents a promising approach to enhancing common carp production while mitigating ecological impacts.

In a Recirculating Aquaculture System (RAS), ensuring high water quality involves the coordinated application of biological, physical, and chemical filtration techniques. The biological component utilizes nitrifying bacteria, such as Nitrosomonas and Nitrobacter, to biologically oxidize toxic ammonia into relatively safer nitrate. Physical filtration functions to eliminate suspended solids and particulates from the system. Meanwhile, chemical filtration is essential for removing dissolved contaminants, including nitrogen-based compounds like ammonia, by using adsorptive media such as zeolites (Zhou et al., 2024), ion-exchange resins (Liu et al., 2023), and activated carbon (Rehan et al., 2024). Among these, activated carbon is widely valued for its exceptional adsorption capacity and extensive surface area. Traditionally produced from coconut shells (Haider et al., 2025), rice husks (Angellinnov et al., 2025), or sawdust (Yang et al., 2025), activated carbon can also be derived from coconut husk, an abundant and underutilized agricultural byproduct (Akbar et al., 2025b). Utilizing coconut husk to produce activated carbon offers a sustainable and cost-effective alternative, aligning with circular economy principles and reducing organic waste. Despite these advantages, the application of coconut husk-based activated carbon in RAS systems has not been extensively studied or benchmarked against conventional media (Akbar et al., 2025c). The incorporation of coconut husk-derived activated carbon into RAS enhances water purification, supports fish health, and minimizes environmental impacts, thereby contributing to more efficient and sustainable aquaculture practices.

The utilization of coconut husk as a raw material for synthesizing activated carbon in Recirculating Aquaculture Systems (RAS) offers promising advantages. Owing to its abundant lignocellulosic content, namely cellulose, hemicellulose, and lignin, this agricultural residue serves as an excellent carbon-rich substrate that facilitates the formation of well-developed porous networks during the activation stage (Wijaya et al., 2025). The natural abundance and renewability of coconut husk make it an attractive alternative for sustainable filtration media (Fatmawati et al., 2023). Activated carbon produced from coconut husk exhibits favorable adsorption properties, characterized by a well-developed porous network and the presence of functional groups such as hydroxyl (-OH), carbonyl (C=O), and aromatic structures, which enhance surface reactivity (Salaenoi et al., 2024). These attributes facilitate the effective adsorption of nitrogenous wastes, particularly ammonia, making coconut husk-derived activated carbon a promising component in chemical filtration within RAS. By integrating this material into the system, water quality can be significantly improved through the efficient removal of toxic metabolic byproducts, thereby promoting healthier fish growth and enhancing overall system performance. Moreover, the valorization of coconut husk into activated carbon supports sustainable waste management practices, transforming an abundant agricultural byproduct into a high-value filtration material. Nevertheless, the lack of comprehensive data on the comparative effectiveness of coconut husk-based carbon in real RAS conditions constitutes a notable research gap. Therefore, this study aims to evaluate the performance of NaOH-activated carbon derived from coconut husk in improving water quality and physiological responses of *Cyprinus carpio* cultured in a RAS.

2. Materials and Methods

2.1. Collection of coconut husk waste and synthesis of activated carbon

Coconut husk waste used in this study was sourced from traditional markets in the Kuta Alam region of Banda Aceh, Indonesia (coordinates: 5°33'45.0"N 95°20'36.5"E). To ensure cleanliness, the husks underwent thorough washing to eliminate surface impurities, followed by natural sun-drying for three consecutive days to lower their moisture content. Carbonization was performed at 300°C for a duration of two hours, adapting the procedure reported by Yuliusman et al. (2020). The resulting biochar was then pulverized and passed through a 100-mesh sieve for subsequent physicochemical analyses, while a portion was retained in its coarse form for application as filter material. The carbon activation process involved immersion in a sodium hydroxide solution with a 1:4 (w/v) ratio for 24 hours at ambient temperature, as described by Yuliusman et al. (2020). Post-activation, the sample was sequentially rinsed using 1 M hydrochloric acid and deionized water until a neutral pH was achieved. Finally, the activated carbon was oven-dried at 110°C for 12 hours to remove residual moisture.

2.2. Physicochemical and surface characterization of sctivated carbon

To assess the physicochemical characteristics of the synthesized activated carbon, several instrumental analyses were employed. Surface morphology was visualized using a Scanning Electron Microscope (SEM, Hitachi SU3500), with samples mounted on conductive carbon tape. Crystallographic features were determined through X-ray diffraction analysis (XRD, Bruker D8 Advance) utilizing Cu Kα radiation (λ = 1.540598 Å), operated at 30 kV and 15 mA, over a 2θ range of 5° to 80°. Functional groups present on the adsorbent surface were identified using Fourier Transform Infrared Spectroscopy (FTIR, Thermo Nicolet iS50), scanning in the spectral region of 500–4000 cm^{-1}. The porosity and surface area were evaluated via nitrogen adsorption–desorption isotherms at 77 K using a Quadrasorb-Evo instrument. The Brunauer–Emmett–Teller (BET) method was applied to estimate the specific surface area, while the total pore volume was calculated at a relative pressure (P/P_0) close to 0.99.

2.3. Collection and acclimatization of common carp

A total of 200 juvenile common carp (*Cyprinus carpio*), measuring between 3.12 and 3.45 cm in length and weighing 0.24 to 0.289 g, were sourced from Glory Pulo Nusa hatchery in Lambaro, Aceh Besar, Indonesia. According to the supplier, the fish had not been exposed to any antibiotics or chemical treatments during cultivation. Upon arrival at the experimental site, the fish underwent a 7-day acclimation period in plastic tanks measuring 60 × 40 × 40 cm^3, during which their health status and behavior were monitored daily (Akbar et al., 2025d). Throughout this period, they were provided with a commercial feed containing 40% crude protein, administered to apparent satiation three times daily at 09:00, 12:00, and 17:00.

2.4. Experimental aetup of the Recirculating Aquaculture System (RAS)

The RAS experimental design comprised five distinct treatment groups, each replicated four times. The treatments differed by the amount of activated carbon applied: the control group (P1) received no carbon, while P2, P3, P4, and P5 were administered 5 g, 10 g, 15 g, and 20 g of activated carbon, respectively, guided by the methodology of Prastiawan et al. (2019). The trials were conducted in 27-liter cylindrical plastic tanks (dimensions: 35 × 31 × 60 cm), each filled with 20 liters of sterilized tap water and continuously aerated to maintain sufficient dissolved oxygen concentrations. Each tank was stocked with ten juvenile *Cyprinus carpio*. Fish were fed a high-protein commercial diet (40% crude protein) at 5% of their body weight, delivered in three daily feedings at 09:00, 12:00, and 17:00 (Prastiawan et al., 2019). The experiment was conducted over a 28-day period without any water renewal. Weekly monitoring was conducted for key water parameters, including temperature, pH, and dissolved oxygen (DO). Throughout the study, the water temperature remained within 24–26°C, pH between 8.2–8.6, and DO ranged from 5.0 to 7.4 mg/L. This configuration facilitated a systematic assessment of the effects of varying activated carbon dosages on water quality enhancement and fish performance under RAS conditions.

2.5. Determination of ammonia levels in RAS water

To evaluate the concentration of ammonia in the recirculating aquaculture system, water samples (10 mL) were systematically collected from each of the 20 tanks, ensuring comprehensive representation of water conditions. The analysis utilized the indophenol blue technique, wherein specific reagents were introduced to the samples to induce the formation of an indophenol chromophore. The reaction mixture was then incubated for 30 minutes at room temperature to allow complete color development. After incubation, absorbance readings were taken at a wavelength of 640 nm using a UV-Vis spectrophotometer, corresponding to the maximum absorption of the developed indophenol complex (Jain et al., 2021). Ammonia concentrations were quantified in parts per million (ppm) using a standard calibration curve derived from known ammonia solutions.

2.6. Measurement of oxidative stress biomarkers

To evaluate oxidative stress in fish, serum samples were analyzed using ELISA-based commercial kits from Elabscience, targeting key oxidative stress biomarkers. Total Superoxide Dismutase (T-SOD) activity was measured in units per milliliter (U/mL) using the WST-1 Method Kit (Cat. No. E-BC-K020-M), while Catalase (CAT) activity was expressed in units per milliliter (U/mL) based on the hydrogen peroxide decomposition rate (Cat. No. E-BC-K031-S). Glutathione S-transferase (GST) activity was determined using the GST Activity Assay Kit (Cat. No. E-BC-K278-S) and expressed as units per liter (U/L). Lipid peroxidation was assessed through malondialdehyde (MDA) levels, measured in micromoles per liter (µmol/L) using the TBA-based MDA Colorimetric Assay Kit (Cat. No. E-BC-K025-M). All assays were performed in accordance with the manufacturer's instructions, and the results were reported as enzyme activities or MDA concentration per volume of serum.

2.7. Measurement of respiratory responses

Opercular beat rate (OBR) and oxygen consumption rate (OCR) were measured to assess respiratory responses of the fish (Kim et al., 2025). OBR was determined by visually counting the opercular movements of individual fish for one minute while the fish remained undisturbed in the experimental tanks. The counting was repeated four times per fish**,** and the average value was recorded in beats per minute (bpm). For OCR measurement, individual fish were transferred to sealed respirometry chambers filled with aerated experimental water. Dissolved oxygen concentrations were measured at the start and after a fixed incubation period of 1 hour using a calibrated dissolved oxygen meter (mg O_2/L). Oxygen consumption was calculated based on the decline in oxygen concentration, fish body weight, and duration of the incubation, and expressed as milligrams of oxygen consumed per kilogram of body weight per hour (mg O_2/kg/h). All measurements were conducted in quadruplicate (n = 4) to ensure accuracy and reproducibility.

2.8. Measurement of hematological parameters

To assess the hematological status of *Cyprinus carpio*, several blood parameters were evaluated on the 20 day of the trial, including mean corpuscular hemoglobin concentration (MCHC), mean corpuscular hemoglobin (MCH), mean corpuscular volume (MCV), hematocrit (HCT), hemoglobin (Hb), white blood cell (WBC) count, and red blood cell (RBC) count. Blood samples were drawn from the caudal vein of anesthetized fish (n = 4 per treatment) using sterile 1 mL syringes preloaded with EDTA to prevent coagulation (Xu et al., 2021). Hematocrit levels were determined using the microcapillary method: blood was introduced into heparinized tubes, centrifuged at 12,000 rpm for 5 minutes, and the resulting packed cell volume was recorded as a percentage of total volume. Hemoglobin concentration was analyzed via spectrophotometry using the cyanmethemoglobin approach, with readings taken at 540 nm using a Thermo Scientific Genesys 150 UV-Vis spectrophotometer. RBC and WBC counts were conducted using a Neubauer counting chamber viewed under an Olympus CX23 light microscope at 400× magnification. Derived indices, MCV, MCH, and MCHC, were computed from measured values using conventional hematological formulas: MCV (fL) = (HCT × 10) / RBC, MCH (pg) = (Hb × 10) / RBC, and MCHC (g/dL) = (Hb × 100) / HCT.

2.9. Assessment of abnormal erythrocyte morphology

Following the 20-day rearing period, blood was drawn aseptically from the caudal vein of Cyprinus carpio using sterile syringes coated with EDTA to prevent clotting, in accordance with the method described by Bardhan et al. (2024). A fresh drop of blood was promptly spread into a thin layer on a pre-cleaned glass slide to obtain a uniform monolayer. After air-drying, the slides were immersed in absolute methanol for fixation over a 5-minute period. Subsequently, the samples were stained with 10% Giemsa solution for 15 minutes to visualize cellular structures. The slides were then rinsed with distilled water and dried at ambient temperature. Morphological observation of erythrocytes was performed under 1000× magnification using immersion oil and a light microscope to detect possible malformations. Malformation assessment was conducted using a semi-quantitative method by counting 1000 erythrocytes per slide and calculating the percentage of cells exhibiting abnormalities, such as membrane ruptures, irregular shapes, binucleated cells, and cytoplasmic vacuoles. This approach allowed for a standardized comparison of erythrocyte integrity across treatment groups and provided insight into hematological responses to varying dosages of activated carbon.

2.10. Data analysis

All data were processed and visualized using Origin Pro 2024, while statistical evaluations were performed using IBM SPSS Statistics version 26 (Chicago, IL, USA). Descriptive results were expressed as mean values accompanied by standard deviations (mean ± SD). Prior to hypothesis testing, data normality was examined using the Shapiro–Wilk test, and homogeneity of variances was verified using Levene's test. One-way analysis of variance (ANOVA) was applied to determine significant differences among treatments, with pairwise comparisons carried out **using** Duncan's multiple range test. Statistical significance was set at $p < 0.05$.

3. Results

3.1. Physicochemical properties of activated carbon

Based on Table 1, the activated carbon derived from coconut husk and treated with NaOH exhibited a notable improvement in quality. The ash content decreased from 6.34 ± 0.12% to 2.34 ± 0.12%, with both values remaining within the SNI standard limit (≤10%). The moisture content increased from 4.82 ± 0.23% to 6.64 ± 0.54%, while still complying with the SNI standard (≤15%). The methylene blue adsorption capacity improved from 89.54 ± 0.23 mg/g to 132.12 ± 1.23 mg/g, surpassing the minimum SNI requirement (≥120 mg/g) after activation. Additionally, the iodine number increased from 687.43 ± 2.66 mg/g to 992.95 ± 3.41 mg/g, exceeding the SNI threshold (≥750 mg/g). The specific surface area, as determined by BET analysis, also increased from 323.12 ± 5.12 m^2/g to 654.43 ± 5.23 m^2/g, indicating an enhancement in the active surface area following the activation process.

Table 1. Physicochemical properties of activated carbon from coconut husk (n = 3)

No	Parameter	Carbon Before Activation	Carbon After Activation	SNI Standard
1	Ash Content (%)	6.34 ± 0.12	2.34 ± 0.12	≤ 10
2	Moisture Content (%)	4.82 ± 0.23	6.64 ± 0.54	≤ 15
3	Methylene Blue Adsorption Capacity (mg/g)	89.54 ± 0.23	132.12 ± 1.23	≥ 120
4	Iodine Number (mg/g)	687.43 ± 2.66	992.95 ± 3.41	≥ 750
5	BET Surface Area (m^2/g)	323.12 ± 5.12	654.43 ± 5.23	-

*Indonesian National Standard 06–3730-1995

3.2. Morphological and structural characterization of coconut husk-derived activated carbon

Based on Figure 1, SEM images revealed notable changes in the surface morphology of activated carbon before and after the activation process. Prior to activation (Figure 1a), the carbon surface appeared relatively dense with a compact structure and a limited number of pores. Following activation (Figure 1c), the surface morphology became more open and porous, indicating an increase in both pore number and pore size. The pore size distribution graph (Figure 1b) showed that before activation, the average pore diameter was 398.4306 µm, predominantly within the 300–350 µm range. After activation, as shown in Figure 1d, the average pore diameter significantly increased to 847.6096 µm, with the pore size distribution shifting towards larger diameters, particularly within the 700–900 µm range. These changes indicate that the activation process effectively enlarged the pore size and significantly enhanced the porosity of the activated carbon structure.

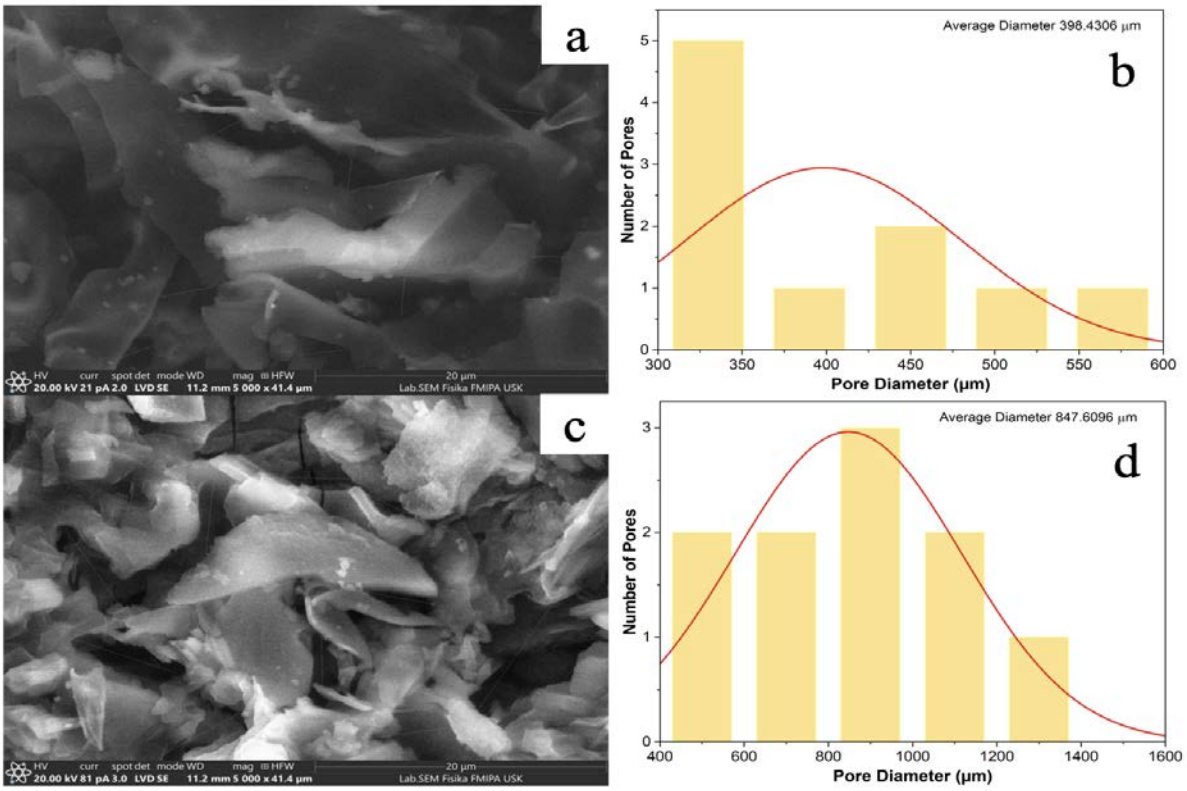

Figure 1. SEM images and pore size distribution of activated carbon: (a) morphology before activation, (b) pore size distribution before activation, (c) morphology after activation, (d) pore size distribution after activation.

According to Figure 2a, the XRD diffraction patterns of the carbon exhibited broad peaks, indicating an amorphous structure within the 2θ range of approximately 20°–30°, both before and after activation. However, a decrease in diffraction intensity was observed following activation, suggesting disruptions in the graphitic structural order induced by the activation treatment. In Figure 2b, the FTIR spectra displayed changes in intensity and shifts in wavenumbers for several functional groups. The wavenumber range of 3682–3050 cm^{-1} prior to activation shifted to 3695–2984 cm^{-1} post-activation, corresponding to O–H stretching vibrations. Other shifts included the C=O stretching band from 1712 cm^{-1} to 1692 cm^{-1}, and the aromatic C–C ring stretching band from 1596 cm^{-1} to 1554 cm^{-1}. Additionally, the C–H rocking band shifted from 1375 cm^{-1} to 1312 cm^{-1}, and the C–O stretching band shifted from 1102 cm^{-1} to 1151 cm^{-1}. Table 4.2 supports these findings by summarizing the observed wavenumber shifts and the corresponding functional group vibrations identified through FTIR analysis, indicating that the activation process altered the surface chemical composition of the carbon and enhanced the presence of oxygen-containing functional groups.

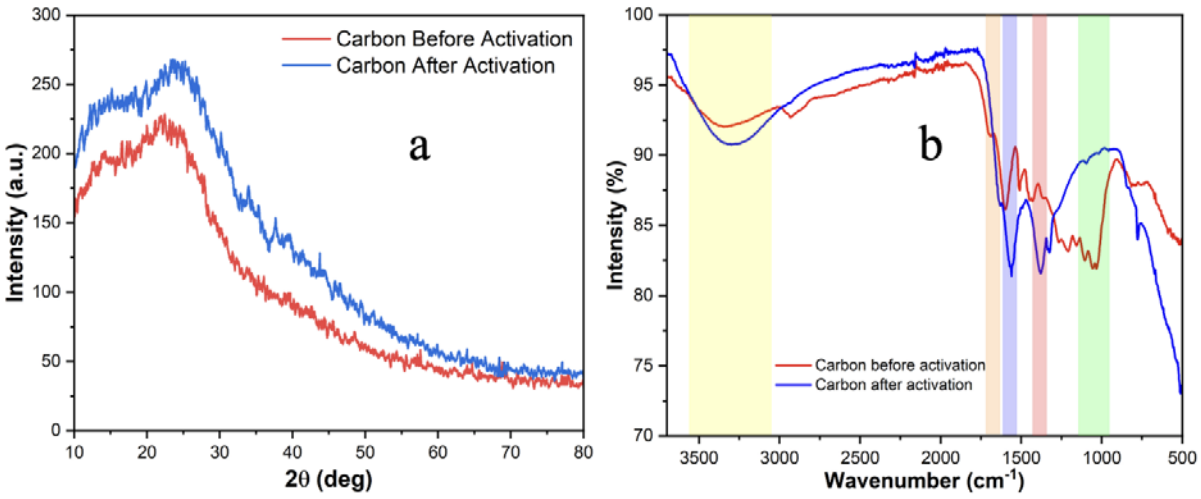

Figure 2. (a) XRD diffraction patterns of carbon before and after activation; (b) FTIR spectra of carbon before and after activation.

3.3. Ammonia concentration in common carp culture media

Based on Table 2, the use of coconut husk-derived activated carbon as a filter in the RAS for common carp culture had a significant effect on ammonia concentration ($p < 0.05$) on both Day 10 and Day 20. The mean ammonia concentration on Day 10 decreased from 0.0096 ± 0.0006 ppm in P1 (without activated carbon) to 0.0071 ± 0.0004 ppm in P5 (20 g dose). A similar trend was observed on Day 20, with the highest ammonia concentration recorded in P1 at 0.0178 ± 0.0013 ppm and the lowest in P5 at 0.0103 ± 0.0006 ppm. All values in treatments P3, P4, and P5 were below the threshold set by Government Regulation (GR) No. 82 of 2001 (<0.02 ppm), and substantially lower than the limits established by the WHO (1.5 ppm) and the EPA (0.25–32.5 ppm). Post-hoc analysis revealed significant differences among treatments, with higher doses of activated carbon resulting in greater reductions in ammonia concentration. Treatment P5 demonstrated the highest effectiveness in lowering ammonia levels compared to the other treatments.

Tabel 2. Ammonia concentration (ppm) on day 10 and day 20 for each treatment (n = 4)

Treatment	Ammonia concentration (ppm)		Threshold limit (ppm)		
	Day 10	Day 20	WHO	EPA	PP
P1	0.0096 ± 0.0006^{c}	0.0178 ± 0.0013^{d}	1.5	0.25–32.5	< 0.02
P2	0.0085 ± 0.0002^{b}	0.0154 ± 0.0015^{c}			
P3	0.0076 ± 0.0003^{a}	0.0125 ± 0.0009^{b}			
P4	0.0074 ± 0.0003^{a}	0.0116 ± 0.0008^{bc}			
P5	0.0071 ± 0.0004^{a}	0.0103 ± 0.0006^{a}			

World Health Organization (WHO)
Environmental Protection Agency (EPA)
Government Regulation (GR) No. 82 of 2001 on Water Quality Management and Water Pollution Control

3.4. Oxidative stress biomarkers in common carp under different activated carbon treatments

The activities of oxidative stress biomarkers, including superoxide dismutase (SOD), catalase (CAT), glutathione S-transferase (GST), and malondialdehyde (MDA), are presented in Figure 3. Significant differences ($p < 0.05$) were observed across treatments (P1–P5) and sampling days (Day 0, Day 10, and Day 20). SOD activity (Figure 3a), expressed in Unit/mL, showed a time-dependent increase in all treatments, with the highest value recorded in P1 on Day 20 (23.775 U/mL) and the lowest in P5 on Day 0 (8.575 U/mL). CAT activity (Figure 3b), also in Unit/mL, followed a similar trend, peaking in P1 on Day 20 (0.4705 U/mL) and reaching the lowest point in P5 on Day 0 (0.09125 U/mL). For GST activity (Figure 3c), measured in Unit/L, values were consistently higher in P1 and P2, particularly on Day 10 (13.875 and 12.875 U/L, respectively), but declined on Day 20 in all groups, especially in P5 (5.25 U/L). In contrast, MDA activity (Figure 3d), expressed in µmol/L, was highest in P1 (4.95 µmol/L) and progressively decreased in treatments with more effective filtration, with the lowest value recorded in P5 on Day 20 (1.3 µmol/L).

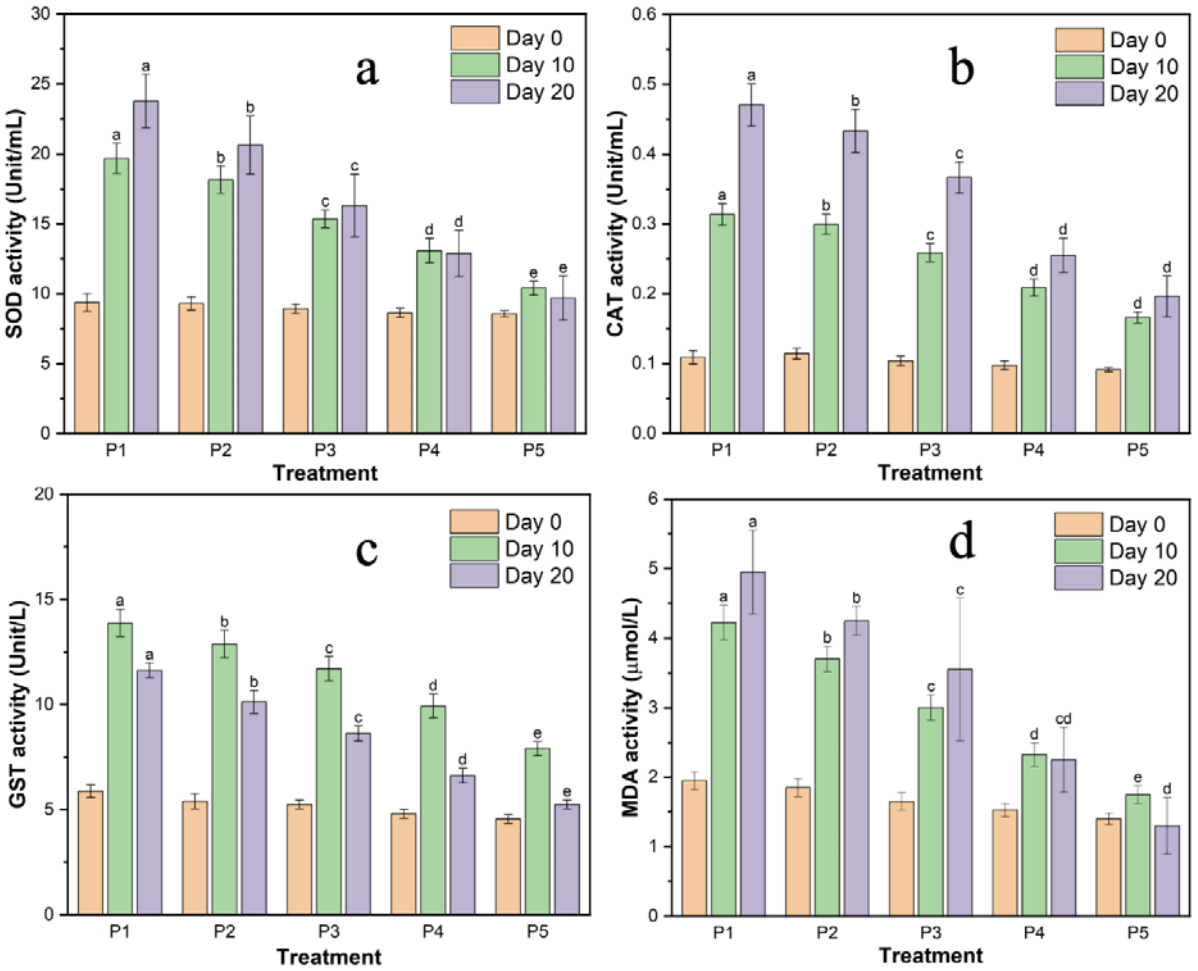

Figure 3. Activities of oxidative stress biomarkers in *Cyprinus carpio* cultured under different activated carbon treatments: (a) superoxide dismutase (SOD), (b) catalase (CAT), (c) glutathione S-transferase (GST), and (d) malondialdehyde (MDA). Data are presented as mean ± SD (n = 4) at Day 0, Day 10, and Day 20. Different letters indicate significant differences ($p < 0.05$) among treatments and sampling days.

3.5. Respiratory responses of common carp under different activated carbon treatments

Respiratory responses, including opercular beat rate (OBR) and oxygen consumption rate (OCR), under different activated carbon treatments are presented in Figure 4. OBR (Figure 4a) exhibited significant differences ($p < 0.05$) across treatments and sampling days. On Day 20, the highest OBR was recorded in P1 (130 ± 4 bpm), while the lowest was observed in P5 (74 ± 3 bpm). A decreasing trend in OBR was evident with increasing activated carbon dosage. Similarly, OCR (Figure 4b) showed significant variation ($p < 0.05$). On Day 20, P1 exhibited the lowest OCR at 85 ± 3 mg O_2/kg/h, whereas P5 demonstrated the highest OCR at 220 ± 4 mg O_2/kg/h. A progressive increase in OCR was observed with higher activated carbon dosages, indicating enhanced respiratory efficiency. Overall, these results reflect clear differences in respiratory parameters among treatments over time.

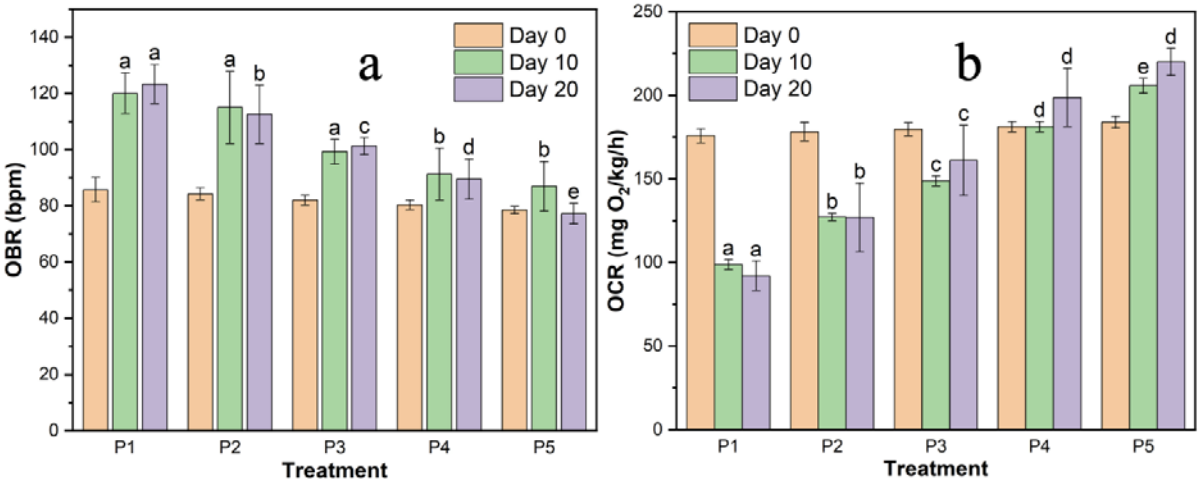

Figure 4. Respiratory responses of Cyprinus *carpio* cultured under different activated carbon treatments: (a) opercular beat rate (OBR, bpm), (b) oxygen consumption rate (OCR, mg O_2/kg/h). Data are presented as mean ± SD (n = 4) at Day 0, Day 10, and Day 20. Different letters indicate significant differences ($p < 0.05$) among treatments and sampling days.

3.6. Hematological parameters of common carp under different activated carbon treatments

Hematological parameters of *Cyprinus carpio* cultured under different activated carbon treatments are presented in Table 3. Significant differences ($p < 0.05$) were observed across treatments for all measured parameters. The mean corpuscular hemoglobin concentration (MCHC) increased progressively from 27.87 ± 1.57 g/dL in P1 to 33.52 ± 0.24 g/dL in P5. Mean corpuscular hemoglobin (MCH) also showed a notable increase, from 82.70 ± 2.21 pg in P1 to 109.90 ± 1.14 pg in P5. Similarly, mean corpuscular volume (MCV) rose from 212.50 ± 15.54 fL in P1 to 362.50 ± 29.01 fL in P5. Hematocrit values ranged from 26.20 ± 0.54% in P1 to 39.87 ± 3.15% in P5, indicating improved hematological status with increasing activated carbon dosage. Hemoglobin concentration increased from 6.12 ± 0.61 g/dL in P1 to 10.37 ± 1.82 g/dL in P5. Conversely, white blood cell (WBC) count decreased significantly, from 138.75 ± 5.37 ×10³/μL in P1 to 52.5 ± 5.25 ×10³/μL in P5, suggesting a reduction in physiological stress. Red blood cell (RBC) count increased from 1.15 ± 0.16 ×10⁶/μL in P1 to 2.08 ± 0.02 ×10⁶/μL in P5. These results indicate marked hematological improvements associated with higher activated carbon dosages.

Table 3. Hematological parameters of *Cyprinus carpio* cultured under different activated carbon treatments.

Parameters	P1	P2	P3	P4	P5
MCHC (g/dL)	27.87 ± 1.57^{a}	29.05 ± 0.31^{a}	30.57 ± 0.33^{b}	31.97 ± 0.91^{c}	33.52 ± 0.24^{d}
MCH (pg)	82.70 ± 2.21^{a}	88.87 ± 1.18^{d}	95.90 ± 1.01^{c}	102.02 ± 1.02^{d}	109.90 ± 1.14^{e}
MCV (fL)	212.50 ± 15.54^{a}	242.50 ± 11.90^{a}	275.75 ± 31.92^{b}	317.50 ± 6.45^{c}	362.50 ± 29.01^{d}
Hematokrit (%)	26.20 ± 0.54^{a}	29.20 ± 2.87^{a}	34.17 ± 2.95^{b}	36.37 ± 0.50^{bc}	39.87 ± 3.15^{c}
Hemoglobin (g/dL)	6.12 ± 0.61^{a}	7.72 ± 0.99^{ab}	8.57 ± 0.37^{bc}	9.65 ± 0.93^{cd}	10.37 ± 1.82^{d}
WBC (10³/μL)	138.75 ± 5.37^{a}	106.25 ± 9.46^{b}	98.75 ± 4.34^{c}	76.25 ± 9.25^{c}	52.5 ± 5.25^{d}
RBC (10⁶/μL)	1.15 ± 0.16^{a}	1.30 ± 0.13^{a}	1.60 ± 0.16^{b}	1.90 ± 0.20^{c}	2.08 ± 0.02^{c}

Note: Different superscript letters in the table indicate significant differences between treatments. Values are presented with standard deviations (n = 4). In this study, activated carbon was applied at different doses: P1 (control), P2 (5 g), P3 (10 g), P4 (15 g), and P5 (20 g).

3.7. Effects of ammonia reduction on erythrocyte morphology

The types and intensities of erythrocyte malformations observed in *Cyprinus carpio* under different activated carbon treatments are shown in Figure 5 and Table 4. Various morphological abnormalities were detected, including vacuolated cells, hemolyzed cells, lacerated membranes, binucleated cells, double cells, deformed cells, and swollen cells.

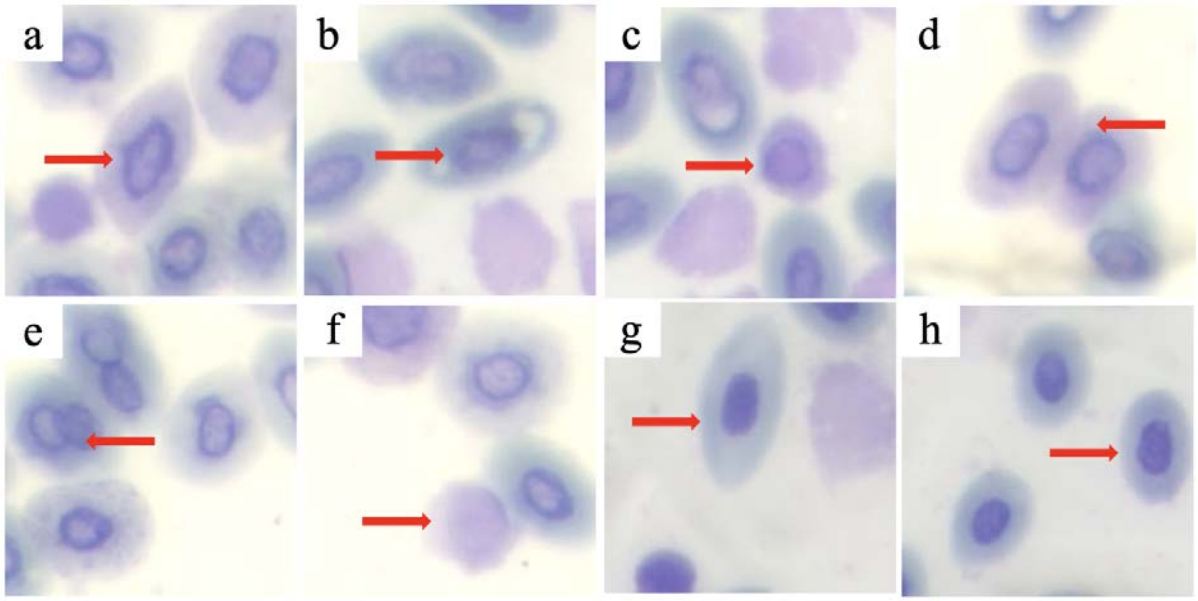

Figure 5. Appearance of erythrocyte malformations in *Cyprinus carpio* under different treatment conditions (P1–P5). (a) Deformed cell (P1), (b) Lacerated membrane (P1), (c) Vacuolated cell (P2), (d) Double cell (P3), (e) Binucleus (P3), (f) Hemolyzed cell (P3), (g) Swollen cell (P4), and (h) Normal erythrocyte (P5). Scale bar = 30 µm.

Erythrocyte abnormalities were most prominent in the control group (P1), with severe deformities observed, including pronounced cases of cell distortion, membrane rupture, binucleation, and hemolysis. Swelling and vacuolization were also notable at moderate levels. As the activated carbon dosage increased across treatments, a marked reduction in both frequency and intensity of these malformations was evident. In P2, while some abnormalities remained prominent, particularly deformed and ruptured cells, their severity began to diminish. By P3, the occurrence of abnormal cell types had declined further, with most anomalies classified as mild to moderate. Treatment P4 showed minimal disruptions, where only slight deformities, swelling, and cell fusion persisted, and several malformation types were no longer detected. In the highest carbon treatment (P5), erythrocyte integrity was nearly restored, with only occasional mild swelling and minimal deformation or hemolysis present, and no signs of binucleation, vacuolization, or membrane damage. A noticeable increase in the presence of intact, healthy red blood cells was recorded in this group, supporting the effectiveness of higher activated carbon dosages in mitigating cellular damage.

Table 4. Erythrocyte abnormalities and severity

Type of Malformation	P1	P2	P3	P4	P5
Vacuolated cell	++	+	–	–	–
Hemolyzed cell	+++	++	++	++	+
Lacerated membrane	+++	++	+	–	–
Binucleus	++	+	+	–	–
Double cell	+++	++	+	++	+
Deformed cell	+++	+++	++	++	+
Swollen cell	++	++	++	+	–

Note: None (–), mild (+), moderate (++), and severe (+++)

3.8. Effect of ammonia filtration on survival rate of common carp

The survival rate (SR) of *Cyprinus carpio* varied significantly across treatments ($p < 0.05$), as shown in Table 5. The lowest SR was observed in P1 (67.50 ± 5.00%), while the highest was recorded in P5 (97.50 ± 5.00%). Intermediate SR values were noted in P2 (75.00 ± 5.77%), P3 (85.00 ± 5.77%), and P4 (87.50 ± 5.00%). Increasing activated carbon dosage clearly improved fish survival throughout the culture period.

Table 5. Survival rate (SR) of *Cyprinus carpio* under different activated carbon treatments.

Treatment	*Survival Rate* (SR) (%)
P1	67.50 ± 5.00^{a}
P2	75.00 ± 5.77^{a}
P3	85.00 ± 5.77^{b}
P4	87.50 ± 5.00^{b}
P5	97.50 ± 5.00^{c}

Note: Different superscript letters in the table indicate significant differences between treatments. Values are presented with standard deviations (n = 4). In this study, activated carbon was applied at different doses: P1 (control), P2 (5 g), P3 (10 g), P4 (15 g), and P5 (20 g).

4. Discussion

The physicochemical characteristics of the activated carbon derived from coconut husk and modified with NaOH treatment demonstrated substantial improvements in adsorption performance and structural properties (Table 1). The significant reduction in ash content and the controlled moisture level suggest enhanced material purity and stability, both of which comply with the Indonesian National Standard (SNI). The marked increase in methylene blue adsorption capacity, from 89.54 to 132.12 mg/g, highlights the improvement in mesoporous structure, while the substantial rise in iodine number, exceeding 992 mg/g, indicates an elevated microporous surface conducive for efficient adsorption processes. This enhancement is further corroborated by the two-fold increase in specific surface area as measured by BET analysis. These findings align with previous studies where NaOH activation was

reported to promote the development of well-defined pore structures and increased surface area in biomass-derived activated carbons (Huno et al., 2023; Kasmuri et al., 2022). However, unlike prior reports utilizing wood-based or synthetic precursors, the present study uniquely employs coconut husk, a readily available and underutilized agricultural waste in tropical regions, thus providing a more sustainable and cost-effective alternative (Fu et al., 2020). The combination of high adsorption capacity, large surface area, and compliance with SNI standards underscores the suitability of this activated carbon for advanced water treatment applications, particularly for ammonia filtration in aquaculture systems. The novelty of this study lies not only in the effective valorization of coconut husk waste but also in demonstrating the synergistic effect of NaOH activation in enhancing the adsorption properties beyond commonly reported values, positioning this material as a highly competitive option in sustainable aquaculture water management.

The SEM analysis (Figure 1) revealed significant morphological transformations of the activated carbon following the NaOH activation process. Prior to activation (Figure 1a), the carbon surface exhibited a dense, compact morphology with relatively few pores, indicating limited surface accessibility. After activation (Figure 1c), the surface became notably more porous and irregular, suggesting the effective removal of volatile components and structural rearrangement induced by chemical activation (Huno et al., 2023). Correspondingly, the pore size distribution shifted markedly. Before activation (Figure 1b), the average pore diameter was 398.43 µm, predominantly within the 300–350 µm range, indicative of a relatively narrow distribution of smaller pores. Post-activation (Figure 1d), the average pore diameter increased significantly to 847.61 µm, with a broader distribution skewed towards larger pores (700–900 µm range). This substantial enlargement of pore size and increase in porosity is consistent with previous findings where alkali activation facilitated pore development through etching and widening of pre-existing pore structures (Ajien et al., 2022; Armstrong et al., 2014). The observed morphological evolution enhances the material's adsorption capacity by increasing the available surface area and improving diffusion pathways. Notably, the average pore diameter achieved in this study surpasses several reported values for biomass-derived activated carbons, underscoring the effectiveness of the employed NaOH activation protocol in tailoring pore architecture for advanced adsorption applications (Tomy et al., 2024).

The XRD and FTIR analyses provide crucial insights into the structural and chemical modifications induced by the NaOH activation process on coconut husk-derived carbon (Figure 2). The XRD patterns (Figure 2a) exhibited broad diffraction peaks within the 2θ range of 20°–30°, both before and after activation, characteristic of an amorphous carbon structure with disordered graphitic domains. Notably, a decrease in diffraction intensity post-activation indicates further disruption of the graphitic lattice, likely due to chemical etching and pore development (Armstrong et al., 2014; Tomy et al., 2024). These structural changes are consistent with the observed increase in surface area and porosity reported earlier (Armstrong et al., 2014). The FTIR spectra (Figure 2b) revealed substantial shifts in functional groups following activation. The broad O–H stretching band shifted from 3682–3050 cm^{-1} to 3695–2984 cm^{-1}, indicating enhanced surface hydroxylation (Fu et al., 2020). The C=O stretching band shifted from 1712 cm^{-1} to 1692 cm^{-1}, suggesting modification of carbonyl functionalities. Additionally, shifts in aromatic C–C (1596 → 1554 cm^{-1}), C–H rocking (1375 → 1312 cm^{-1}), and C–O stretching (1102 → 1151 cm^{-1}) bands further confirm the introduction of oxygen-containing groups during activation (Tomy et al., 2024). These functional groups enhance the carbon's hydrophilicity and adsorption capacity, facilitating effective ammonia removal in RAS applications. Overall, the combined XRD and FTIR findings corroborate the morphological and chemical transformations that underpin the superior filtration performance of the activated carbon produced in this study.

The application of coconut husk-derived activated carbon in the recirculating aquaculture system (RAS) demonstrated a significant impact on ammonia reduction in *Cyprinus carpio* culture (Table 2). Ammonia concentration consistently decreased with increasing activated carbon doses on both Day 10 and Day 20 ($p < 0.05$), indicating enhanced filtration efficiency. The lowest ammonia levels were observed in P5 (20 g carbon), achieving reductions of approximately 26% on Day 10 and 42% on Day 20 compared to the control. Importantly, ammonia concentrations in treatments P3, P4, and P5 remained well below regulatory thresholds established by GR No. 82/2001, WHO, and EPA, ensuring a safe environment for fish culture. This trend confirms the efficacy of biomass-based activated carbon in improving water quality in aquaculture systems (Hamid, Humaidi, et al., 2024; Hamid, Nasution, et al., 2024). However, the current study demonstrates superior ammonia removal performance compared to previous works utilizing coconut shell- or bamboo-based carbons, likely due to the optimized pore structure and increased surface area of the NaOH-activated coconut husk carbon (Han et al., 2021). Furthermore, the gradual improvement from Day 10 to Day 20 suggests a sustained filtration capacity and adsorption stability over time. The findings highlight the potential of this low-cost, sustainable material for effective ammonia management in RAS, contributing to improved fish health and system sustainability.

The dynamics of oxidative stress biomarkers in the gills of *Cyprinus carpio* under different activated carbon treatments are depicted in Figure 3. The observed variations in SOD, CAT, GST, and MDA activities reflect the physiological responses of gill tissues to ammonia exposure and the mitigating effects of activated carbon filtration. SOD and CAT activities showed progressive increases across all treatments and sampling days, with the highest activities recorded in P1 on Day 20, indicating heightened superoxide radical and hydrogen peroxide detoxification under elevated ammonia stress. These trends align with prior studies (Koner et al., 2021b; Zhao et al., 2021) reporting enhanced SOD and CAT activities in fish exposed to oxidative stressors. In contrast, GST activity displayed a biphasic response, an initial increase up to Day 10, followed by a decline on Day 20. This pattern suggests early-phase compensatory activation of GST, which subsequently diminished due to glutathione depletion and compromised antioxidant capacity under prolonged

ammonia exposure (Kumar et al., 2023; Mohamed et al., 2020). MDA levels exhibited a steady increase over time, particularly in P1 and P2, reflecting the extent of lipid peroxidation and membrane damage induced by oxidative stress (Dawood et al., 2022). Notably, treatments with higher activated carbon doses (P3–P5) consistently demonstrated lower oxidative biomarker activities, indicating effective ammonia removal and improved oxidative balance in gill tissues. Compared to previous reports utilizing other filtration media, the coconut husk-derived activated carbon in this study provided superior protection against oxidative stress, as evidenced by the lower MDA accumulation and moderated antioxidant enzyme responses (Dawood et al., 2022; Qin et al., 2023). These findings underscore the critical role of optimized bio-based filtration strategies in safeguarding fish health within recirculating aquaculture systems.

The respiratory responses of *Cyprinus carpio* reflected distinct physiological adaptations to ammonia stress and the efficacy of activated carbon filtration (Figure 4). The observed reduction in opercular beat rate (OBR) with increasing activated carbon dosage suggests improved water quality and reduced metabolic stress. Higher OBR values in P1 and P2 align with elevated ammonia levels, necessitating increased ventilatory effort for gas exchange, consistent with prior observations in stressed fish (X.-N. Xu et al., 2022). Conversely, oxygen consumption rate (OCR) increased progressively with activated carbon dosage, with P5 exhibiting the highest OCR, indicative of enhanced respiratory efficiency under improved environmental conditions. This pattern underscores the role of adequate filtration in supporting aerobic metabolism and overall fish performance (Pei et al., 2021; Zhang et al., 2023). These findings highlight the potential of sustainable filtration strategies in optimizing fish health and welfare.

The hematological responses of *Cyprinus carpio* to different activated carbon treatments provide valuable insights into fish health and physiological adaptation within the RAS (Table 3). Progressive increases in MCHC, MCH, MCV, hematocrit, and hemoglobin concentrations with higher activated carbon dosages indicate improved erythropoietic activity and enhanced oxygen transport capacity. These improvements are likely linked to the reduction of ammonia-induced stress and oxidative damage, as better water quality supports hematopoietic processes and membrane integrity (Chen & Luo, 2023; Witeska et al., 2023). The decline in WBC counts from P1 to P5 suggests a reduction in systemic stress and immune activation, which typically elevate leukocyte levels under unfavorable environmental conditions (Ahmed et al., 2020). The observed increase in RBC counts across treatments further reflects improved erythropoiesis and oxygen-carrying capacity, supporting enhanced metabolic performance. These findings align with those of (Hoque & Das, 2025), who reported improved hematological profiles in fish exposed to optimized water quality in RAS systems. Notably, the current study demonstrates superior hematological outcomes compared to previous works utilizing conventional filtration, underscoring the effectiveness of coconut husk-derived activated carbon. The optimized pore structure and high adsorption capacity of the activated carbon likely contributed to efficient ammonia removal, thereby mitigating hemolytic and oxidative stress in fish. Collectively, the hematological improvements observed in this study highlight the critical role of advanced filtration strategies in promoting fish health and welfare in intensive aquaculture settings.

The analysis of erythrocyte malformations in *Cyprinus carpio* under different activated carbon treatments revealed a clear dose-dependent trend in morphological abnormalities (Figure 5, Table 4). Fish reared without activated carbon (P1) exhibited the highest frequency and severity of erythrocyte malformations, including severe deformations, double cells, lacerated membranes, and hemolyzed cells, reflecting substantial cellular stress and membrane instability likely induced by elevated ammonia levels and associated oxidative stress. This finding is consistent with reports by Khatun et al., (2021) and Zhong & Yan, (2025), who observed similar erythrocyte damage under polluted or toxic aquatic conditions. As the dosage of activated carbon increased (P2–P5), a progressive reduction in both the number and severity of erythrocyte abnormalities was evident, culminating in predominantly normal erythrocyte morphology in P5, where only mild residual malformations persisted. The reduction in malformations parallels the improvements observed in water quality and oxidative stress parameters, suggesting that activated carbon filtration effectively mitigated environmental stressors that compromise erythrocyte integrity. Notably, the absence of binucleated, lacerated, and vacuolated cells in P5 highlights the protective role of optimized filtration in maintaining cellular homeostasis. These results underscore the sensitivity of erythrocyte morphology as a biomarker for sub-lethal stress in fish and reinforce the superior performance of coconut husk-derived activated carbon in promoting hematological stability.

The survival rate (SR) of *Cyprinus carpio* exhibited a clear dose-dependent improvement with increasing activated carbon levels (Table 5), complementing the physiological and hematological enhancements observed in this study. The lowest SR in P1 (67.50%) corresponds with elevated ammonia concentrations, heightened oxidative stress markers, compromised hematological profiles, and severe erythrocyte malformations reported earlier. Conversely, the highest SR in P5 (97.50%) aligns with reduced ammonia levels, stabilized oxidative biomarkers, improved blood parameters, and minimal erythrocyte abnormalities, indicating a well-maintained internal environment conducive to fish survival. These findings corroborate reports by Akbar et al. (2025), emphasizing the critical role of water quality in determining fish health and survival. The superior performance of coconut husk-derived activated carbon demonstrated here underscores its potential as a sustainable filtration solution in RAS. Overall, the integration of physiological, hematological, and survival data highlights the material's efficacy in enhancing fish welfare and system sustainability.

5. Conclusions

This study demonstrated that coconut husk-derived activated carbon effectively improved water quality and fish health in a recirculating aquaculture system (RAS) for *Cyprinus carpio*. NaOH activation significantly enhanced the physicochemical properties of the carbon, including

surface area and pore structure, thereby increasing its ammonia adsorption capacity. The application of activated carbon resulted in substantial reductions in total ammonia nitrogen, with P5 (20 g carbon) maintaining levels well below regulatory thresholds. Improved water quality was reflected in decreased oxidative stress, as evidenced by reduced SOD, CAT, GST, and MDA activities in gill tissues under higher carbon dosages. Concurrently, hematological parameters improved, with increases in MCHC, MCH, MCV, hematocrit, hemoglobin, and RBC counts, alongside reduced WBC counts, indicating enhanced physiological resilience. Moreover, erythrocyte malformation severity declined progressively with increasing activated carbon dosage, while survival rates improved markedly, reaching 97.5% in P5. Compared to previous studies, the use of coconut husk-derived activated carbon provided superior performance in promoting fish welfare. These findings underscore the potential of this sustainable, low-cost filtration material to enhance the ecological and economic viability of intensive and large-scale RAS operations. However, as a limitation, the study was conducted under short-term conditions in a controlled laboratory setup. Future investigations should focus on long-term field-scale trials, regeneration efficiency of the activated carbon, and cost-benefit analysis to fully assess its practicality and sustainability in commercial aquaculture. The development of circular waste-based filtration solutions such as this represents a promising step toward environmentally responsible aquaculture intensification.

Acknowledgment

This work was supported by the Penelitian Lektor (PL) scheme form Universitas Syiah Kuala Indonesia under Grant number 362/UN11.2.1/PG.01.03/SPK/PTNBH/2024.

References

Ahmed I, Reshi QM and Fazio F. 2020. The influence of the endogenous and exogenous factors on hematological parameters in different fish species: a review. *Aquac. Int.*, **28(3):** 869–899.

Ajien A, Idris JM, Md Sofwan N, Husen R and Seli H. 2022. Coconut shell and husk biochar: A review of production and activation technology, economic, financial aspect and application. *Waste Manag. Res.*, **41(1):** 37–51.

Akbar SA, Fatmawati DR, Dewi CD, Ismarica I, Nuzlia C, Nazlia S, Jalil Z, Iqbal TH, Hasan M and Lahori AH. 2025a. Toxicodynamic effects of chronic Pb^{2+} exposure on milkfish (*Chanos chanos*) and the phytoremediation role of *Caulerpa taxifolia*: Water quality, bioaccumulation, and multi-level biological responses. *Environ. Chem. Ecotoxicol*., **7:** 2319–2333.

Akbar SA, Hasan M, Jalil Z, Zulfahmi I, Iqhrammullah M and Safina N. 2025b. Enhanced ammonia nitrogen filtration using NaOH-activated Manihot utilissima peel carbon: Application in recirculating aquaculture systems for Nile tilapia. *Chemosphere*, **385:** 144537

Akbar SA, Mauliza L and Fazli RR. 2025c. Recent advances in carbon-based adsorbent materials for ammonium removal from water. *BIO Web of Conferences*, **156:** 02014.

Akbar SA, Nuzlia C, Hasan M, Jalil Z and Zulfahmi I. 2025d. Optimizing ammonia removal in recirculating aquaculture systems using NaOH-activated sugarcane bagasse carbon. *Sci. Technol. Asia*, **30(2):** 227–240.

Angellinnov F, Subhan A, Rengga WDP, Jumari A and Syahrial AZ. 2025. Effect of rice husk derived activated carbon surface coating on NMC 811 characteristics and performance as lithium-ion battery cathode. *Results Surf. Interfaces*, **19:** 100567.

Armstrong PR, Morchesky ZJ, Hess DT, Adu KW, Essumang DK, Tufour JK, Koranteng-Addo JE, Opoku-Boadu K and Mensah SY. 2014. Production of high surface area activated carbon from coconut husk. *MRS Online Proc. Libr.*, **1644(1):** 801.

Bardhan A, Abraham TJ, Das R and Patil PK. 2024. Visualization of poikilocytosis as an emerging erythrocytic biomarker for fish health assessment. *Anim. Res. One Health*, **2(2):** 136–157.

Barragán-Longoria MF, Pérez-Viveros KJ, Cadena-Ramírez A, Castro-Rosas J, Villagómez-Ibarra JR, Hernandez-Perez J, Hinojosa-Alvarez S, Gómez-Aldapa CA and Chavez-Santoscoy RA. 2025. Mesquite seed flour as a nutrient-rich alternative to fishmeal for common carp fingerlings (*Cyprinus carpio*): environmental, growth performance, transcriptomic and intestinal microbiota responses. *Aquac. Rep.*, **42:** 102768.

Chen H and Luo D. 2023. Application of haematology parameters for health management in fish farms. *Rev. Aquac.*, **15(2):** 704–737.

Dawood MAO, Alkafafy M and Sewilam H. 2022. The antioxidant responses of gills, intestines and livers and blood immunity of common carp (*Cyprinus carpio*) exposed to salinity and temperature stressors. *Fish Physiol. Biochem.*, **48(2):** 397–408.

Fatmawati A, Nurtono T and Widjaja A. 2023. Thermogravimetric kinetic-based computation of raw and pretreated coconut husk powder lignocellulosic composition. *Bioresour. Technol. Rep.*, **22:** 101500.

Fu J, Zhang J, Jin C, Wang Z, Wang T, Cheng X and Ma C. 2020. Effects of temperature, oxygen and steam on pore structure characteristics of coconut husk activated carbon powders prepared by one-step rapid pyrolysis activation process. *Bioresour. Technol.*, **310:** 123413.

Haider R, Sagadevan S, Al-Adaileh N, Fatimah I, Paiman S, Le MV and Johan MR. 2025. Sustainable activated carbon derived from coconut shell and betel nuts for energy storage and environmental remediation. *Diam. Relat. Mater.*, **154:** 112243.

Hamid M, Humaidi S, Saragi IR, Simanjuntak C, Isnaeni I, Azizah and Wijoyo H. 2024. The effectiveness of activated carbon from nutmeg shell in reducing ammonia (NH3) levels in fish pond water. *Carbon Trends*, **14:** 100324.

Hamid M, Nasution TI, Elfinita R, Wijoyo H and Isnaeni I. 2024. Reducing ammonia (NH3) levels in fish cage water using activated carbon adsorbent derived from purple corn cob. *Sci. Technol. Indones.*, **9(3):** 669–681.

Han B, Butterly C, Zhang W, He J and Chen D. 2021. Adsorbent materials for ammonium and ammonia removal: a review. *J. Clean. Prod.*, **283:** 124611.

Hoque F and Das A. 2025. Hematological techniques for diagnosis of fish diseases. In: Das BK and Kumar V (Eds.). *Lab. Tech. Fish Dis. Diagn.* Springer Nature Singapore.

Huno SKM, Das J, van Hullebusch ED, Annachhatre AP and Rene ER. 2023. Nitrate removal from groundwater using chemically modified coconut husk based granular activated carbon: characterization of the adsorbent, kinetics and mechanism. *Syst. Microbiol. Biomanuf.*, **3(2):** 370–383.

Jain A, Soni S and Verma KK. 2021. Combined liquid phase microextraction and fiber-optics-based cuvetteless micro-spectrophotometry for sensitive determination of ammonia in water and food samples by the indophenol reaction. *Food Chem.*, **340:** 128156.

Karatas T, Sokmen TO and Gur STA. 2025. Effects of pumpkin seed extract on growth, blood biochemistry, antioxidant status, immunity, and digestive enzymes of common carp (*Cyprinus carpio*) fingerlings. *Aquac. Rep.*, **43:** 102890.

Kasmuri N, Dzulkifli NFM, Ismail NA, Zaini N and Yaacob Z. 2022. An investigation of a mixture of coconut husk and rice husk as activated carbon for treatment of wastewater. *IOP Conf. Ser. Earth Environ. Sci.*, **1019(1):** 012048.

Khatun MM, Mostakim GM, Moniruzzaman M, Rahman UO and Islam MS. 2021. Distortion of micronuclei and other peripheral erythrocytes caused by fenitrothion and their recovery assemblage in zebrafish. *Toxicol. Rep.*, **8:** 415–421.

Kim B, Jin G, Byeon Y, Park SY, Song H, Lee C, Lee J, Noh J and Khim JS. 2025. Monitoring of the physiological responses of marine fishes to construction and operation noise from offshore wind farms. *Mar. Pollut. Bull.*, **218:** 118139.

Koner D, Banerjee B, Kumari A, Lanong AS, Snaitang R and Saha N. 2021a. Molecular characterization of superoxide dismutase and catalase genes, and the induction of antioxidant genes under the zinc oxide nanoparticle-induced oxidative stress in air-breathing magur catfish (*Clarias magur*). *Fish Physiol. Biochem.*, **47(6):** 1909–1932.

Koner D, Banerjee B, Kumari A, Lanong AS, Snaitang R and Saha N. 2021b. Molecular characterization of superoxide dismutase and catalase genes, and the induction of antioxidant genes under the zinc oxide nanoparticle-induced oxidative stress in air-breathing magur catfish (*Clarias magur*). *Fish Physiol. Biochem.*, **47(6):** 1909–1932.

Kumar N, Singh DK, Chandan NK, Thorat ST, Patole PB, Gite A and Reddy KS. 2023. Nano zinc enhances gene regulation of non specific immunity and antioxidative status to mitigate multiple stresses in fish. *Sci. Rep.*, **13(1):** 5015.

Liu C, Qiu T and Chen Y. 2023. Metal ion/metal hydroxide loaded resin for ammonia removal from solutions containing high salinity by ligand exchange: stability of metal ions during decomplexation of ammonia ligand. *Arab. J. Chem.*, **16(8):** 104879.

Mohamed AAR, El-Houseiny W, EL-Murr AE, Ebraheim LLM, Ahmed AI and El-Hakim YMA. 2020. Effect of hexavalent chromium exposure on the liver and kidney tissues related to the expression of CYP450 and GST genes of *Oreochromis niloticus* fish: role of curcumin supplemented diet. *Ecotoxicol. Environ. Saf.*, **188:** 109890.

Nguyen-tiêt AM, Letelier-Gordo CO and Aalto SL. 2025. Rapid H2S production in layers of freshwater and marine fish organic waste from recirculating aquaculture systems. *Aquac. Eng.*, **111:** 102578.

Pei X, Chu M, Tang P, Zhang H, Zhang X, Zheng X, Li J, Mei J, Wang T and Yin S. 2021. Effects of acute hypoxia and reoxygenation on oxygen sensors, respiratory metabolism, oxidative stress, and apoptosis in hybrid yellow catfish "Huangyou-1." *Fish Physiol. Biochem.*, **47(5):** 1429–1448.

Prastiawan A, Jubaedah D and Syaifudin M. 2019. Pemanfaatan Karbon Aktif Kulit Pisang Kepok (*Musa Acuminate* L.) Pada Sistem Filtrasi Budidaya Ikan Nila (*Oreochormis Niloticus*). *Jurnal Akuakultru Rawa Indonesia*, **7(1):** 55-66.

Qin H, Long Z, Huang Z, Ma J, Kong L, Lin Y, Lin H, Zhou S and Li Z. 2023. A comparison of the physiological responses to heat stress of two sizes of juvenile spotted seabass (*Lateolabrax maculatus*). *Fishes*, **8(7):**.

Rehan K, Malaibari Z, Atieh M, Hussain I and Abu-Saud B. 2024. A highly efficient modified nano-activated carbon adsorbent for separation of ammonia from water: experimental and kinetics elucidations. *Chemosphere*, **364:** 143048.

Salaenoi J, Jurejan N, Yokthongwattana C, Pluempanupat W and Boonprab K. 2024. Characteristics of coconut husk cellulose and its effectiveness as a potassium permanganate absorbent for fishery applications. *Case Stud. Chem. Environ. Eng.*, **10:** 100975.

Tomy M, Geethamma GS, Aravind AM, Reshmi SS and Suryabai XT. 2024. Effect of activation environment on coconut-husk-derived porous activated carbon for renewable energy storage applications. *ACS Sustain. Resour. Manag.*, **1(7):** 1534–1547.

Wang Y, Deng M, Zhou S, Li L and Song K. 2024. Increasing fish production in recirculating aquaculture system by integrating a biofloc-worm reactor for protein recovery. *Water Res. X*, **24:** 100246.

Wijaya C, Sangadji NL, Muharja M, Widjaja T, Riadi L and Widjaja A. 2025. An integrated green fractionation of coconut husk: hydrothermal and deep eutectic solvent pretreatment for enhanced sugar and lignin production. *Bioresour. Technol. Rep.*, **29:** 102078.

Witeska M, Kondera E and Bojarski B. 2023. Hematological and hematopoietic analysis in fish toxicology—a review. *Animals*, **13(16):**.

Wu G, Liu HB, Ma C, Xu HM, Ren XZ and Sun W. 2025. Developments and application of fish school swimming model in recirculating aquaculture systems. *Ocean Eng.*, **319:** 120196.

Xu J, Lan M, Luo Y and Wu Y. 2024. Carbon, nitrogen, and phosphorus release characteristics and underlying mechanisms in fish manure from recirculating aquaculture systems under alternating aerobic-anaerobic conditions. *J. Environ. Chem. Eng.*, **12(6):** 114185.

Xu XN, Chen SL, Jiang ZX, Nissa M and Zou SM. 2022. Gill remodeling increases the respiratory surface area of grass carp (*Ctenopharyngodon idella*) under hypoxic stress. *Comp. Biochem. Physiol. A Mol. Integr. Physiol.*, **272:** 111278.

Xu Z, Cao J, Qin X, Qiu W, Mei J and Xie J. 2021. Toxic effects on bioaccumulation, hematological parameters, oxidative stress, immune responses and tissue structure in fish exposed to ammonia nitrogen: a review. *Animals*, **11(11):**.

Yang F, Zhang K, Lin Q, Pan H and Chen Z. 2025. Preparation of ultra-microporous oxygen-enriched carbon from activating waste sawdust with potassium formate for selective adsorption of CO2/CH4. *Sep. Purif. Technol.*, **372:** 133505.

Yuliusman, Sipangkar SP, Fatkhurrahman M, Farouq FA and Putri SA. 2020. Utilization of coconut husk waste in the preparation of activated carbon by using chemical activators of KOH and NaOH. *AIP Conf. Proc.*, **2255(1):** 060026.

Zhang T, Zhang L, Yin T, You J, Liu R, Huang Q, Shi L, Wang L, Liao T, Wang W and Ma H. 2023. Recent understanding of stress response on muscle quality of fish: from the perspective of industrial chain. *Trends Food Sci. Technol.*, **140:** 104145.

Zhao H, Peng K, Wang G, Mo W, Huang Y and Cao J. 2021. Metabolic changes, antioxidant status, immune response and resistance to ammonia stress in juvenile yellow catfish (*Pelteobagrus fulvidraco*) fed diet supplemented with sodium butyrate. *Aquaculture*, **536:** 736441.

Zhong A and Yan X. 2025. Erythropoiesis in teleost fishes: the fantastic biological process. *Rev. Aquac.*, **17(1):** e12960.

Zhou T, Zhai T, Ma J, Wu F and Zhang G. 2024. Sodium chloride-activated polymeric ferric sulfate-modified natural zeolite (Z-Na-Fe): application of bio-slow filtration for the removal of ammonia and phosphorus from micro-polluted cellar water. *J. Water Process Eng.*, **61:** 105367.

JJBS

Volume 19, Number 1,March 2026
ISSN 1995-6673
Pages 127 – 133
https://doi.org/10.54319/jjbs/190112

Jordan Journal of Biological Sciences

Impact of IL-10, and IL-33, Polymorphisms on Atherosclerosis Risk: Insights from a Jordanian Cohort

Ammar S. Ali Deeb[1,*], Kawther F. Amawi[1], Amjad E. Hamdallah[1], Hussein Abdalla[2], Shadi Jaber[3],Tareq Nayef AlRamadneh[4]

[1] Faculty of Allied Medical Sciences, Zarqa University, Zarqa Jordan; [2]Faculty of Medicine, Hashemite University, Zarqa,Jordan.; [3] Jordanian Ministry of Health, Amman, Jordan; [4]faculty of allied medical science, al-ahliyya amman university

Received: April 11, 2025; Revised: July 25, 2025; Accepted: August 20, 2025

Abstract

Atherosclerosis, a complex and chronic inflammatory disease, remains a major cause of cardiovascular morbidity and mortality worldwide. Growing evidence suggests that genetic variations in inflammatory cytokines, such as interleukin-10 (IL-10) and interleukin-33 (IL-33), may influence individual susceptibility to the disease. This study explored the relationship between polymorphisms in the IL-10 and IL-33 genes and the risk of developing atherosclerosis in a Jordanian population.

We analyzed blood samples from 100 patients with clinically confirmed atherosclerosis and 110 healthy, unrelated controls. DNA was extracted and genotyped using established PCR (PCR-SSP) technique of IL-10 and PCR-MS for IL-33 polymorphism, serum cytokine levels were measured using ELISA. Our results revealed that the T allele and T/T genotype of the IL-33 rs7044343 variant were significantly more common in healthy controls than in patients, suggesting a potential protective role against coronary artery disease. While overall IL-33 genotype frequencies did not differ significantly between groups, the data did show deviations from Hardy-Weinberg equilibrium in the patient group, which may reflect underlying genetic differences related to disease presence.

In addition, patients with atherosclerosis had notably lower serum levels of IL-33, supporting its proposed anti-inflammatory and cardioprotective effects. For IL-10, the -1082 A>G (rs1800896) polymorphism showed borderline significance in genotype distribution, hinting at a possible but less clear role in disease development.

These findings underscore the importance of genetic background in shaping individual responses to inflammatory processes in atherosclerosis. While IL-33 appears to play a more prominent role, both cytokines merit further investigation. Understanding how these gene variants interact with lifestyle and environmental factors could eventually lead to more personalized strategies for the prevention and management of atherosclerosis.

Keywords: Atherosclerosis, Cytokine Gene Polymorphisms, IL-10, IL-33, Coronary Artery, Disease (CAD), Genetic Diversity, Jordanian Population

1. Introduction:

Atherosclerosis is a chronic inflammatory condition affecting the walls of medium and large arteries. The progression of atherosclerosis is regulated by both innate and adaptive immune responses, which are coordinated through a complex network of cytokines that influence all stages of the disease [1]. Cytokines play a crucial role in the maturation, differentiation, and functional activation of immune cells. They regulate various cellular processes, including proliferation and differentiation, and maintain a balance between pro-inflammatory and anti-inflammatory pathways, which can impact the progression of atherosclerosis [2].

Anti-inflammatory interleukins are recognized for suppressing pro-inflammatory signaling pathways and modulating immune responses. These interleukins employ various mechanisms to reduce inflammation by producing pro-inflammatory cytokines and regulating immune cell activation and function. Key anti-inflammatory cytokines of interest, interleukin-33 (IL-33), and interleukin-10 (IL-10) [3].

Interleukin-10 (IL-10) is a prototypical anti-inflammatory cytokine that plays a pivotal role in regulating the Th1/Th2 balance, shifting the response toward Th2. It has been extensively studied in the context of atherosclerosis and is considered an anti-atherosclerotic cytokine due to its diverse mechanisms, including Th2 polarization. IL-10 inhibits the expression of inflammatory genes across various cell types and suppresses antigen presentation and T-cell proliferation [4]. The IL-10 gene is located on chromosome 1, spanning the 1q31 to 1q32 regions [5]. Its promoter region is highly polymorphic, with biallelic variants such as -1082 A > G (rs1800896), −819 T > C (rs1800871), and −592 A > C (rs1800872). These variants are known to affect the promoter region of the IL-10 gene, thereby influencing its transcriptional activity and resulting in altered plasma levels of IL-10. Specifically, certain polymorphisms—such as the -1082

* Corresponding author. e-mail: aalideeb@zu.edu.jo.

A>G (rs1800896)—are associated with increased or decreased binding affinity of transcription factors, which modulates the rate of gene transcription. This regulatory effect has been observed in various inflammatory conditions, including acute coronary syndromes (ACS), where altered IL-10 expression may impact the balance between pro- and anti-inflammatory responses. [5].

Interleukin-33 (IL-33) is a recently characterized member of the IL-1 cytokine family. Stromal cells express epithelial and endothelial cells. Its expression increases in response to pro-inflammatory stimuli. IL-33 functions both as a conventional cytokine and as a nuclear factor that regulates gene transcription, serving as an "alarmin" that signals immune activation in response to cellular stress or damage. IL-33 is thought to play a protective role in the development of atherosclerosis by inducing the production of interleukin-5 (IL-5) and promoting the generation of antibodies against oxidized low-density lipoprotein (ox-LDL), a modified form of LDL that contributes to plaque formation.[6]. The IL-33 gene is located on chromosome 9 (9p24.1)[7].

Studies have shown that administering interleukin-33 (IL-33) to apolipoprotein E-deficient (ApoE$^{-/-}$) mice, a widely used animal model for atherosclerosis characterized by impaired lipid metabolism and spontaneous plaque development, leads to the induction of protective antibodies against oxidized low-density lipoprotein (ox-LDL) and increased production of Th2 cytokines. This immune response results in a significant reduction of atherosclerotic plaque formation in the aortic sinus [8]. Furthermore, research on tag single nucleotide polymorphisms (tag SNPs)—genetic variants selected to represent regions of the IL-33 gene (rs7025417, rs10975514, and rs10975519)—in coronary artery disease (CAD) patients from the Chinese Han population has highlighted the contribution of IL-33 polymorphisms to disease susceptibility [9,10].

A range of single nucleotide polymorphisms (SNPs) with functional relevance has been identified in cytokine genes, influencing interleukin production and contributing to the pathogenesis of atherosclerosis [11]. In this study, we specifically focus on two anti-inflammatory cytokines—interleukin-10 (IL-10) and interleukin-33 (IL-33)—and examine the association between their gene polymorphisms and clinically confirmed atherosclerosis in a Jordanian population. Rather than assessing genetic predisposition in healthy individuals, this study investigates patients already diagnosed with atherosclerosis. Our objectives are to determine the frequency of IL-10 and IL-33 polymorphisms in these patients compared to healthy controls and to explore how these genetic variations correlate with circulating levels of IL-10 and IL-33, thereby shedding light on their potential role in disease progression and inflammatory regulation.

2. Patients and Methods

2.1. Study Population

This study included 100 consecutive Jordanian patients (87 males and 13 females) with clinically confirmed atherosclerosis, recruited from Prince Hamza Hospital, a public healthcare facility in Amman, Jordan. Additionally, 110 unrelated healthy blood donors (60 males and 50 females) were included as the control group. All participants underwent a comprehensive clinical evaluation.

Laboratory test results, including complete blood count (CBC), cardiac enzyme levels, renal function tests, lipid profile, and C-reactive protein (CRP) levels, were retrieved from the patients' medical records. These analyses were conducted by the clinical laboratories of Prince Hamza Hospital as part of routine diagnostic workup. Participants also completed a brief standardized questionnaire designed to collect demographic and clinical information, including age, sex, smoking status, family history, and comorbidities.

Blood samples were collected by trained hospital phlebotomists under sterile conditions. Approximately 10 mL of venous blood was drawn from each participant into ethylenediaminetetraacetic acid (EDTA) tubes. The samples were transported on ice to the research laboratory. Plasma was separated by centrifugation and stored at –80°C for subsequent analysis of cytokines using enzyme-linked immunosorbent assay (ELISA). The remaining cellular fraction was used for DNA extraction and genotyping analysis.

The study protocol received ethical approval from the Ethical Committee of Prince Hamza Hospital 7/37/2/1426 and from the Ethics committee for scientific research (1/8/2021) of Zarqa University. Written informed consent was obtained from all participants prior to their inclusion in the study.

2.2. DNA Extraction

Blood samples were collected in sterile EDTA tubes. Genomic DNA was extracted from whole blood using a standard commercial kit (Qiagen Ltd., UK) according to the manufacturer's instructions.

2.3. SNP Typing

The IL-10 single nucleotide polymorphism (SNP) at position −1082 (G/A) was genotyped using the polymerase chain reaction sequence-specific primer (PCR-SSP) method, as previously described by Talaat et al. (2018). To amplify the IL-10 promoter region containing the −1082 SNP, DNA samples were subjected to PCR using allele-specific primers listed in Table 1. Each DNA sample was run in two separate reactions—one specific for the G allele and the other for the A allele—using a final reaction volume of 25 µL. The PCR mixture contained DreamTaq Green PCR Master Mix (2×, Fermentas), 10 pmol of the allele-specific forward primer, 10 pmol of the reverse primer, 3.5 pmol of each internal control primer, and approximately 100 ng of genomic DNA. The thermal cycling protocol began with an initial denaturation at 94°C for 2 minutes, followed by 5 cycles at 96°C for 25 seconds, 70°C for 45 seconds, and 72°C for 20 seconds. This was followed by 11 cycles at 96°C for 25 seconds, 65°C for 50 seconds, and 72°C for 45 seconds, and concluded with 15 cycles at 96°C for 25 seconds, 55°C for 60 seconds, and 72°C for 2 minutes. After amplification, PCR products were separated on a 2% agarose gel and visualized under UV light. The size of each product was determined relative to a 100 bp DNA ladder (Fermentas). The expected product sizes were 258 bp for the −1082 region, 233 bp for the −819 region, and 429 bp for the internal control fragment. **[18]**

The single nucleotide polymorphism (SNP) rs7044343 in the IL-33 gene was genotyped using a conventional polymerase chain reaction (PCR) method. Genomic DNA was amplified using a specific primer pair targeting the region containing the rs7044343 polymorphism. Table (1), producing a 547 base pair (bp) amplicon. Each PCR reaction was performed in a final volume of 25 µL using DreamTaq Green PCR Master Mix (Fermentas), 10 pmol of each primer, and approximately 100 ng of genomic DNA. The thermal cycling conditions included initial denaturation at 95°C for 5 minutes, followed by 35 cycles of 95°C for 30 seconds, 60°C for 30 seconds, and 72°C for 45 seconds, with a final extension step at 72°C for 7 minutes. PCR products were resolved on a 2% agarose gel and visualized under UV illumination to confirm the expected 547 bp band.

Table 1. Primers used for the detection of IL-10, IL-33, and IFN-γ polymorphisms in atherosclerosis patients and controls.

Gene	Primer	Sequence	Product Size
IL-10	Forword 1 (G)	5' - CTACTAAGGCTTCTTT GGGAG-3'	258 bp
rs1800896	Forword 2 (A)	5' - ACTACTAAGGCTTCTTTGGGAA-3'	258 bp
	Reverse	5' - CAGTGCCAACTGAGAATTTGG- 3'	
IL-33	Forword	5' - CAGCAGGACACAGAAAAACAGATGTATGC- 3'	547 bp
rs7044343	Reverse	5' - GCAACCAGAAGTCTTTTGTAGGACTCAG- 3'	

2.4. Measurement of Serum IL-10 and IL-33 by enzyme-linked immunosorbent assay (ELISA)

Measurement of Serum Anti-inflammatory Cytokines (IL-10, and IL-33) were measured using a commercial enzyme-linked immunosorbent assay (ELISA) kit (MyBioSource, Inc., USA), following the manufacturer's instructions. The intensity of the resulting color was measured at a wavelength of 450 nm using an ELISA microplate reader (DiaSourceImmunoAssays®, Belgium). Raw absorbance readings were converted into concentrations using a standard curve, and the cytokine levels in each sample were reported in pg/ml.

2.5. Statistical Analysis

Data analysis was performed using IBM SPSS software, version 20.0 (Armonk, NY: IBM Corp). Categorical variables were presented as numbers and percentages, and comparisons between groups were made using the chi-square test or the Monte Carlo correction test when more than 20% of cells had expected counts below 5. Continuous variables were tested for normality using the Kolmogorov-Smirnov test. Quantitative data were described using the range (minimum-maximum), mean, standard deviation, and median. Student's t-test was applied for comparisons between two groups with normally distributed data, while one-way ANOVA was used for comparisons across multiple groups.

For non-normally distributed data, the Mann-Whitney U test was applied for comparisons between two groups, and the Kruskal-Wallis test was used for multiple group comparisons. Spearman's rank correlation coefficient was used to assess associations between non-normally distributed variables. The study of population's genetic distribution was assessed for Hardy-Weinberg equilibrium. A p-value of less than 0.05 was considered statistically significant.

3. Results

3.1. Patient Characteristics

Table 2 presents the demographic data and results of various biochemical parameters for the study participants. Among the atherosclerosis group, there were 87 (87%) male and 13 (13%) female patients, while the control group included 60 (54.5%) males and 50 (45.5%) females. The median age of the atherosclerosis patients was 56.5 years (range: 27.0–80.0 years), compared to a median age of 35.5 years (range: 18.0–71.0 years) in the control group. Atherosclerosis patients showed significantly higher levels of white blood cells (WBC) compared to controls ($p < 0.01$). However, there was no significant difference in hemoglobin levels between the two groups.

3.2. Serum Levels of Anti-inflammatory Cytokines

As shown in Table 2, there was a statistically significant increase in IL-33 levels among healthy controls compared to atherosclerosis patients ($p \leq 0.001$), with median values of 22.4 (4.48–84.1) in controls versus 5.46 (0–42.6) in patients. No statistically significant differences were observed in the levels of IL-10 between the two groups.

Table 2: Comparison of Demographic and Biochemical Parameters between Atherosclerosis Patients and Controls

Parameter	Patients (n = 100)	Controls (n = 110)	Test Statistic	p-value
Age (years)				
Mean ± SD	55.9 ± 10.3	35.6 ± 12.9	t = 12.647*	<0.001*
Median (Min – Max)	56.5 (27 – 80)	35.5 (18 – 71)		
Gender				<0.001*
Female	13 (13.0%)	50 (45.5%)	χ^2 = 26.273*	
Male	87 (87.0%)	60 (54.5%)		
*WBC (10^9) / L				<0.001*
Mean ± SD	10.3 ± 3.19	6.58 ± 1.56	t = 10.581*	
Median (Min – Max)	10.25 (2.9 – 20.4)	6.20 (4 – 11)		
Hemoglobin g/dl			t = 0.151	0.880
Mean ± SD	13.52 ± 2.11	13.47 ± 2.20		
Median (Min – Max)	13.8 (8.3 – 18.3)	13.1 (8.9 – 17.8)		
IL-33-P (pg/ml)			U = 1135.0*	<0.001*
Mean ± SD	7.04 ± 8.39	22.4 ± 9.96		
Median (Min – Max)	5.46 (0 – 42.6)	22.4 (4.48 – 84.1)		
IL-10 (pg/ml)			U = 4722.0	0.075
Mean ± SD	3.56 ± 2.54	4.48 ± 3.43		
Median (Min – Max)	3 (0 – 12)	5 (0.10 – 15)		

*SD: Standard deviation; t: Student's t-test; U: Mann-Whitney test; χ^2: Chi-square test; p: p-value for comparison between groups. A p-value ≤ 0.05 indicates statistical significance.

3.3. IL-10,and IL-33 Polymorphism Analysis

Table 3 presents the genotype and allele frequencies of IL-10 (-1082 A>G, rs1800896) and IL-33 (rs7044343) polymorphisms in atherosclerosis patients and healthy controls.

- IL-33 Gene Polymorphism:
  - *Genotype Frequencies*: The CC genotype was absent in both groups. The CT genotype was more prevalent among patients (82%) compared to controls (73.6%). The TT genotype was found in 18% of patients and 26.4% of controls. The difference in genotype distribution was not statistically significant ($\chi^2 = 2.109$, $p = 0.146$).
  - *Allele Frequencies*: Regarding IL-33 polymorphism, the CC genotype was absent in both atherosclerosis patients and healthy controls. The CT genotype was more prevalent among patients (82%) compared to controls (73.6%), while the TT genotype appeared in 18% of patients and 26.4% of controls. Despite these variations, the overall genotype distribution between groups was not statistically significant ($\chi^2 = 2.109$, $p = 0.146$). Similar to IL-10, allele frequency analysis revealed significant deviations from Hardy-Weinberg equilibrium in both groups (patients: $HW\chi^2 = 48.291$, $p < 0.001$; controls: $HW\chi^2 = 37.354$, $p < 0.001$), warranting further exploration of genetic or methodological factors that could explain this deviation.
- IL10-1082 Gene Polymorphism:
  - *Genotype Frequencies*: The GG genotype was rare, observed in 6% of patients and 0.9% of controls. The GA genotype was the most common in both groups (80% in patients and 80.9% in controls). The AA genotype was observed in 14% of patients and 18.2% of controls. The genotype distribution showed borderline significance ($\chi^2 = 4.471$, MCp = 0.099).
  - *Allele Frequencies*: The distribution of IL-10 genotypes among atherosclerosis patients and healthy controls showed a predominance of the heterozygous **GA** genotype in both groups (80% in patients and 80.9% in controls). The GG genotype was relatively rare, observed in 6% of patients and only 0.9% of controls. The AA genotype appeared in 14% of patients and 18.2% of controls. Although these differences in genotype frequencies approached statistical significance, they did not reach conventional significance levels ($\chi^2 = 4.471$, MCp = 0.099). Analysis of allele frequencies showed a slight predominance of the A allele over the G allele in both groups. Importantly, significant deviations from Hardy-Weinberg equilibrium (HWE) were observed in both patients ($HW\chi^2 = 37.247$, $p < 0.001$) and controls ($HW\chi^2 = 49.076$, $p < 0.001$), which may suggest underlying population structure, genotyping error, or selective pressure on this locus.

Overall, the analysis of polymorphisms did not reveal significant differences between atherosclerosis patients and controls, except for certain deviations from Hardy-Weinberg equilibrium.

3.4. Correlation between IL-33 and IL-10 in the Patients Group:

A positive correlation was observed between IL-33 and IL-10 levels in the patient group (Table 4), with a Spearman correlation coefficient of rs = 0.190 and a p-value of 0.059, indicating a trend toward statistical significance. This may suggest a potential relationship between these two cytokines, though it did not reach the conventional threshold for significance.

3.5. Correlation between IL-33 and Different Parameters in the Patients Group:

Table 5 presents the relationship between IL-33 levels and various parameters in the patient group. There was no statistically significant difference in IL-33 levels between males and females (p = 0.845), although females had a slightly higher mean IL-33 level (8.15 ± 11.1) compared to males (6.88 ± 7.97). Similarly, no significant association was found between IL-33 levels and troponin I status (p = 0.910), with comparable mean values in the negative (6.37 ± 6.79) and positive (7.11 ± 8.84) groups. Analysis of IL-

33 gene polymorphism revealed that individuals with the TT genotype had higher IL-33 levels (9.90 ± 11.0) than those with the CT genotype (6.41 ± 7.63), but the difference did not reach statistical significance (p = 0.252). Overall, IL-33 levels did not show significant variation with respect to gender, troponin I status, or genotype in this cohort.

3.6. Correlation between IL-10 and Different Parameters in the Patients Group:

Table 6 summarizes the relationship between IL-10 levels and various clinical parameters in the patient group. No significant difference in IL-10 levels was observed between females and males (p = 0.211), with females showing a slightly higher mean IL-10 level (4.26 ± 2.20) compared to males (3.45 ± 2.59). However, IL-10 levels were significantly higher in patients with negative troponin I results (4.85 ± 2.84) compared to those with positive troponin I (3.25 ± 2.43), indicating a possible association between lower IL-10 levels and cardiac injury (p = 0.024). Regarding IL-10 gene polymorphisms, patients carrying the GG genotype exhibited the highest IL-10 levels (6.17 ± 2.99), followed by the AA genotype (4.23 ± 3.12) and GA genotype (3.24 ± 2.29). Although this difference did not reach statistical significance (p = 0.057), it suggests a trend toward genotype-dependent variation in IL-10 expression

Table 3: Comparison of Gene Polymorphism between Atherosclerosis Patients and Controls

Parameter	Patients (n = 100)	Controls (n = 110)	χ^2	p-value
IL-33			2.109	0.146
CC	0 (0%)	0 (0%)		
CT	82 (82%)	81 (73.6%)		
TT	18 (18%)	29 (26.4%)		
Allele				
C	82 (41%)	81 (37%)		
T	118 (59%)	139 (63%)		
HW χ^2	48.291	37.354		<0.001*
IL10-1082			4.471	MCp=0.099
GG	6 (6%)	1 (0.9%)		
GA	80 (80%)	89 (80.9%)		
AA	14 (14%)	20 (18.2%)		
Allele				
G	92 (46%)	91 (41%)		
A	108 (54%)	129 (59%)		
HW χ^2	37.247	49.076		<0.001*

*HWχ^2: Chi-square for Hardy-Weinberg equilibrium; χ^2: Chi-square test; MC: Monte Carlo; p-value ≤ 0.05 indicates statistical significance.

Table (4): Correlation between IL-33 with IL-10 with in patients group (n = 100)

	IL-33-P	
	rs	p
IL-10	0.190	0.059

rs: Spearman coefficient

Table (5): Relation between IL-33 and different parameters in patients group (n = 100)

	N	IL-33 Mean ± SD.	IL-33 Median (Min. – Max.)	U	P
Gender					
Female	13	8.15 ± 11.1	6.53 (0 – 31.3)	546.5	0.845
Male	87	6.88 ± 7.97	5.25 (0 – 42.6)		
TROPONINE I					
Negative	23	6.37 ± 6.79	4.45 (0 – 20.7)	679.0	0.910
Positive	60	7.11 ± 8.84	4.75 (0 – 42.6)		
IL-33					
CT	82	6.41 ± 7.63	4.41 (0 – 31.3)	611.0	0.252
TT	18	9.90 ± 11.0	8.99 (0 – 42.6)		

SD: Standard deviation U: Mann Whitney test

p: p value for comparing between relation between IL-33 and different parameters

Table (6): Relation between IL-10 and different parameters in patients group (n = 100)

	N	IL-10 Mean ± SD.	IL-10 Median (Min. – Max.)	Test of Sig.	P
Gender					
Female	13	4.26 ± 2.20	5 (1 – 7)	U=444.5	0.211
Male	87	3.45 ± 2.59	3 (0 – 12)		
TROPONINE I					
Negative	23	4.85 ± 2.84	5 (1 – 12)	U=469.0*	0.024*
Positive	60	3.25 ± 2.43	3 (0 – 8)		
IL-10					
GG	6	6.17 ± 2.99	5.5 (4 – 12)		
GA	80	3.24 ± 2.29	3.0 (0 – 8)	H=5.715	0.057
AA	14	4.23 ± 3.12	5.0 (0.1 – 9)		

SD: Standard deviation ,U: Mann Whitney test, H: H for Kruskal Wallis test

p: p value for comparing between relation between IL-10 and different parameters

*: Statistically significant at $p \leq 0.05$

4. Discussion

Understanding how genetic variations affect the development of atherosclerosis has become increasingly important, especially when it comes to cytokine gene polymorphisms. Research has shown that certain genetic variants—particularly in genes like *IL-10* and *IL-33*—can significantly influence cytokine production and may play a role in driving disease progression [12,13].

In Jordan, atherosclerosis is a major public health concern, contributing heavily to the rising rates of illness and death from cardiovascular disease. Recent studies have revealed alarmingly high rates of risk factors among Jordanians, including dyslipidemia (around 75%), obesity (about 32%), hypertension (37%), smoking (31%), and diabetes (21%). Many individuals carry multiple of these risk factors at once [19], highlighting the urgent need to address both lifestyle-related and genetic contributors to disease.

While behavioral and environmental risk factors have been widely explored in Jordan, research into genetic predispositions—especially involving cytokine genes like *IL-10* and *IL-33*—remains limited. In light of this gap, our

study set out to investigate how specific polymorphisms in *IL-10* (-1082 A>G, rs1800896) and *IL-33* (rs7044343) are associated with plasma cytokine levels and atherosclerosis status in a Jordanian population.

The IL-33 gene, located on chromosome 9 (9p24.1), encodes a cytokine that serves both as a nuclear factor for gene transcription regulation and as a traditional signaling cytokine. IL-33 acts as an "alarmin," alerting the immune system to stress or tissue damage. In our study, we observed that the T allele and T/T genotype at the IL33 - rs7044343 position were more prevalent among the Jordanian control group (96.6% and 26.4%, respectively) than in the patient group (86.4% and 18%, respectively) (Table 3). This SNP analysis suggests that rs7044343 (T) may be linked to a protective effect against coronary artery disease (CAD). Although our results did not reveal significant differences in IL-33 genotype frequencies between patients and controls, the Hardy-Weinberg equilibrium (HWχ^2) indicated significant deviations in both groups, implying potential selection pressures or population stratification effects.

Research has highlighted IL-33's role in promoting protective Th2 cytokines and ox-LDL antibodies, which may help mitigate atherosclerotic plaque formation [8]. The differences between our findings and those of previous studies may be attributed to variations in population-specific genetic backgrounds, as well as differences in study design, methodology, or sample sizes. Notably, despite the recognized role of IL-33 in atherosclerosis development, there remains a scarcity of research exploring its genetic susceptibility to CAD.

In agreement with these findingsTu, et al [9], identified an association between the IL-33 rs7025417 polymorphism and an increased risk of CAD within the Chinese Han population, suggesting that variations in IL-33 gene expression and plasma levels could influence disease susceptibility. Interestingly, we found that the rs7044343 variant was associated with a reduced risk of coronary artery disease (CAD), suggesting a potential protective role of this polymorphism in the studied population.

However, previous studies have presented conflicting associations. For instance,[14] demonstrated that the rs7044343 CC genotype was linked to a decreased risk of rheumatoid arthritis (RA) and lower serum IL-33 levels. Conversely, this CC genotype was associated with an increased risk of systemic sclerosis. These findings align with the association reported by [15,16] in systemic sclerosis, as we observed a significant relationship between the rs7044343 T allele and a decreased risk of premature CAD. Furthermore, while Li et, al. [14] reported lower serum IL-33 levels in RA patients with the CC genotype, in our study we found that individuals carrying the CC genotype of the rs7044343 variant produced higher levels of IL-33 in monocytes compared to those with the CT or TT genotypes. IL-33 plays a complex role in the immune system—on one hand, it can drive inflammation in autoimmune diseases, but on the other, it can also help regulate immune responses and promote tissue protection. In the context of atherosclerosis, IL-33 has been shown to reduce plaque development by encouraging anti-inflammatory immune pathways. This dual nature may explain our finding that the C allele was associated with a lower risk of premature coronary artery disease (CAD). Our results suggest that the protective effect may be partly due to increased IL-33 production. It is worth noting that differences in how IL-33 was measured—such as the type of cells studied or how they were stimulated—might explain why our findings differ from previous reports.

IL-10 is a well-established anti-inflammatory cytokine known for its regulatory role in immune responses, particularly concerning atherosclerosis progression [4,17]. The IL10 gene promoter region is highly polymorphic, and the -1082 A>G (rs1800896) variant has been associated with variations in cytokine expression levels. Our results showed that the GG genotype was infrequent among both patients and controls, while the GA genotype was predominant. Although the genotype distribution approached borderline significance (MCp=0.099), significant deviations from Hardy-Weinberg equilibrium were noted in both groups. These findings indicate that IL10-1082 polymorphisms may influence atherosclerosis by modulating cytokine expression and immune regulation, although further research, including functional studies and larger sample sizes, is necessary to clarify their specific impacts.

Our findings revealed a positive, though non-significant, correlation between IL-33 and IL-10 levels ($rs = 0.190$, $p = 0.059$), hinting at potential coordinated regulation of these cytokines. This aligns with Jiang et al. experimental data suggesting IL-33 can drive IL-10 production by promoting M2 macrophage polarization and regulatory T-cell expansion, thus dampening arterial inflammation and plaque formation [20].

In our study, IL-33 levels did not vary significantly across gender, troponin I status, or genotype, though the TT genotype trended toward higher IL-33 expression. This lack of statistical significance may stem from our limited sample size or population-specific genetic backgrounds; similarly, clinical studies have reported inconsistent associations between IL-33 concentration and cardiovascular markers [21].

Regarding IL-10, the absence of gender-related differences aligns with prior research indicating that basal IL-10 production is relatively stable across sexes [22,23].

However, we observed significantly higher IL-10 levels in patients with negative troponin I, suggesting a protective, anti-inflammatory role during cardiac injury—a finding supported by multiple studies demonstrating IL-10’s ability to suppress pro-inflammatory cytokines, reduce ventricular remodeling, and improve myocardial outcomes [24,25].

Although the relationship between IL-10 genotypes and cytokine levels (highest in GG carriers) was not statistically significant ($p = 0.057$), this trend resonates with literature linking IL-10 promoter variants (e.g., -1082G) to increased expression and protective effects in acute coronary syndrome [22]. The borderline p-value indicates that a larger sample might confirm this genetic association.

Our findings suggest that IL-33 may play a supportive, upstream role in enhancing IL-10's anti-inflammatory and potentially cardioprotective effects. In this study, we measured serum levels of both cytokines to better understand their involvement in atherosclerosis. Interestingly, IL-33 levels were significantly lower in patients compared to healthy controls ($p < 0.001$), reinforcing its potential protective role. In contrast, IL-10

levels did not show a significant difference between groups, highlighting the complexity of cytokine regulation in cardiovascular disease. These variations, whether driven by genetic differences, demographic factors, or environmental influences, underscore the need for further research in larger and more diverse populations to fully unravel the interplay between these immune mediators and atherosclerosis risk.

5. Conclusion

Our findings suggest that certain genetic differences—like variations in the IL-33 gene—may play a role in how atherosclerosis develops. This highlights the importance of looking at genetic diversity and population-specific traits when studying complex conditions like heart disease. Understanding how these gene variants work, especially in combination with environmental factors, could help guide more personalized approaches to preventing and treating atherosclerosis in the future.

6. Declarations:

6.1. Funding:

This research was supported by the Scientific Research and Innovation Support Fund of the Hashemite Kingdom of Jordan, The Ministry of Higher Education and Scientific Research. (Grant No: MPH/1/19/2019).

6.2. Data availability:

Derived data supporting the results of this study are available from the corresponding author on request.

6.3. Authors' contributions:

All authors made a substantial contribution to all processes.

6.4. Ethics approval statement:

The study was examined and given approval by Zarqa University's Ethics Committee for Scientific Research (ECSR), with approval number 1/8/2021, in compliance with the regulations for the protection of human beings and the ethical principles governing research projects.

6.5. Consent to participate:

Informed consent was taken from all participants.

6.6. Consent for publication:

Informed consent was provided by all participants.

6.7. Competing interest:

The authors declare that they have no competing interests.

References

Abubakr O, Guergues W, Salem L, et al. 2025. IL-33 and sST2 association with carotid intima-media thickness in patients with Ankylosing Spondylitis. Egypt Rheumatol Rehabil. 52:28. https://doi.org/10.1186/s43166-025-00324-6

Al-Qahtani AA, Alhamlan FS, Al-Qahtani AA. 2024. Pro-Inflammatory and Anti-Inflammatory Interleukins in Infectious Diseases: A Comprehensive Review. Trop Med Infect Dis. 9:13. https://doi.org/10.3390/tropicalmed9010013

Alsaud W, Tabbaa MJ, Kasabri VN, et al. 2020. Prevalence of Cardiovascular Diseases Risk Factors among Jordanians. J Saudi Heart Assoc. 32(2):324-333. https://doi.org/10.37616/2212-5043.1074

Ammar SA, Nasr MY, Badra G, El IH. 2017. The relationship between interleukin-6 polymorphism and susceptibility to hepatitis C-virus infected patients. Jordan Med J. 53(1):1-12.

Asderakis A, Sankaran D, Dyer P, et al. 2001. Association of polymorphisms in the human interferon-gamma and interleukin-10 gene with acute and chronic kidney transplant outcome. Transplantation. 71(5):674–677.

Bai J, Lin M, Zeng X, et al. 2008. Association of polymorphisms in the human IFN-gamma and IL-4 gene with oral lichen planus. J Interferon Cytokine Res. 28(6):351–358.

Fatkhullina AR, Peshkova IO, Koltsova EK. 2016. The role of cytokines in the development of atherosclerosis. Biochemistry (Mosc). 81(11):1358-1370.

Fourman LT, Saylor CF, Cheru L, et al. 2020. Anti-inflammatory interleukin 10 inversely relates to coronary atherosclerosis in persons with HIV. J Infect Dis. 221(4):510-515. https://doi.org/10.1093/infdis/jiz254

Garcia-Garduño TC, Padilla-Gutiérrez JR, Aceves-Ramírez M, et al. 2024. IL10 promoter variants are associated with gene expression but not with acute coronary syndrome susceptibility. Sci Rep. 14:13196.

Hmiel L, Zhang S, Obare LM, et al. 2024. Inflammatory and immune mechanisms for atherosclerotic cardiovascular disease in HIV. Int J Mol Sci. 25:7266.

Jiang C, Jin X, Li C, et al. 2023. Roles of IL-33 in the pathogenesis of cardiac disorders. Exp Biol Med. 248(22):2167–2174.

Koca SS, Pehlivan Y, Kara M, et al. 2016. The IL-33 gene is related to increased susceptibility to systemic sclerosis. Rheumatol Int. 36(4):579–584.

Krishnamurthy P, Rajasingh J, Lambers E, et al. 2009. IL-10 inhibits inflammation and attenuates left ventricular remodeling. Circ Res. 104(2):e9–e18.

Li C, Mu R, Guo J, et al. 2014. Genetic variant in IL33 is associated with susceptibility to rheumatoid arthritis. Arthritis Res Ther. 16(2):R105.

Libby P, Ridker PM, Maseri A. 2002. Inflammation and atherosclerosis. Circulation. 105:1135–1143.

Liu R, Liu L, Wei C, Li D. 2022. IL-33/ST2 immunobiology in coronary artery disease: a systematic review. Front Cardiovasc Med. [Epub ahead of print]

López-Mejías R, Genre F, Remuzgo-Martínez S, et al. 2015. Protective role of the IL33 rs3939286 gene polymorphism in subclinical atherosclerosis. PLoS One. 10(11):e0143153.

Merdler I, Chitturi KR, Chaturvedi A, et al. 2024. Coronary microvascular dysfunction and inflammation. Cardiovasc Revasc Med. https://doi.org/10.1016/j.carrev.2024.05.020

Miller AM, et al. 2009. IL-33 reduces the development of atherosclerosis. J Exp Med. 206(8):1733-1741.

Talaat RM, Mohamed YA, Mohamad EH, et al. 2016. IL10 -1082 G/A and -819 C/T gene polymorphisms in Egyptian women with PCOS. Meta Gene. 9:254-258.

Tu X, Nie S, Liao Y, et al. 2013. The IL-33-ST2L pathway and coronary artery disease in Chinese Han. Am J Hum Genet. 93(4):652–660.

Yu Y, Lin S, Pan Y, et al. 2025. Atheroprotective immunity and IL-10 linked to plaque stability. JACC Basic Transl Sci. 10(8). https://doi.org/10.1016/j.jacbts.2025.101322.

Zhang JJ, et al. 2025. Interleukin-10 effects on macrophages and cardiac remodeling after MI. Front Physiol. 15:1481460. https://doi.org/10.3389/fphys.2024.1481460.

Zhu X, Xie L, Qin H, et al. 2018. IL-33 gene polymorphisms and smoking interaction in SLE. J Immunol Res. 2019:1547578. https://doi.org/10.1155/2019/1547578.

JJBS

Volume 19, Number 1,March 2026
ISSN 1995-6673
Pages 135 – 145
https://doi.org/10.54319/jjbs/190113

Jordan Journal of Biological Sciences

Isolation of *Tepidimonas taiwanensis* I1-1 and *Pseudoxanthomonas taiwanensis* NBRC 101072 from Jordanian Hot Springs: First Report

Miassar M. Al-Talib[1,2], Sara O. Hamdan[1,2], Mamoon M.D. Al-Rshaidat[1,2,*]

[1]*Department of Biological Sciences, School of Sciences, The University of Jordan, Amman, 11942, Jordan;* [2] *Laboratory for Molecular and Microbial Ecology (LaMME), The University of Jordan, Amman, 11942, Jordan*

Received: April 18, 2025; Revised: July 22, 2025; Accepted: August 21, 2025

Abstract

Thermophilic bacteria are defined by their ability to grow at high temperatures, where other life forms cannot exist. Jordan is rich in hot springs located along the Jordan Valley. This study aims to isolate and characterize thermophilic bacteria from Jordanian hot springs using enriched media containing all salts necessary for survival at high temperatures. Ten water samples were collected from hot springs in Ma'in, Zara, Dead Sea, North Shounah, and Mekhebh regions. Water samples were examined for physical and chemical properties. Two types of media containing salts and proteins necessary for the growth of thermophilic bacteria were used. These media are Thermus and Castenholz TYE media. Based on the morphological, microscopic, and molecular characterization results, 34 thermophilic bacterial isolates could be identified. Sequence analysis of the 16S rDNA and BLAST search of collected samples showed that *Bacillus licheniformis* is the most common bacterial isolate. Furthermore, data presented in this study report for the first time in Jordan the occurrence of *Tepidimonas taiwanensis* strain I1-1 and *Pseudoxanthomonas taiwanensis* strain NBRC 101072 in Jordanian hot springs. The phylogenetic relationship between the isolates and the referenced bacteria shows a close relationship with the *Anoxybacillus flavithermus* subsp. *flavithermus* strain DSM 2641, *Flavobacterium thermophilum* strain G-21, *Anoxybacillus rupiensis* strain ATCC BAA-2555, *Anoxybacillus kestanbolensis* strain K1, and *Anoxybacillus contaminans* strain R-16222. The study concluded that the isolation of *Tepidimonas taiwanensis* strain I1-1 and *Pseudoxanthomonas taiwanensis* strain NBRC 101072 for the first time from hot springs in Jordan may open the door for further research to investigate the activities and benefits of these bacteria.

Keywords: Bacteria, Hot Springs, Jordan, Phylogenetic tree, Thermophilic.

1. Introduction

Thermophilic bacteria are classified under the third domain of life (Archaea) because of their unique ability to survive at high temperatures (optimum growth temperature of 50°C or higher), unlike their counterparts from other groups of bacteria (Hugenholtz et al., 1998; Crosby et al., 2019; Fongaro et al., 2020; and Shakya et al., 2025).

Hot springs are unique areas characterized by high temperatures and a great natural environmental diversity (Yohandini et al.,2015). Hot springs worldwide attract researchers to investigate the industrial benefits of bioproducts of the thermophilic microorganisms inhabiting them (Malkawi and Al-Omari, 2010; Wolella and Tilahun, 2020, and Burkhardt et al., 2024)

As highlighted in recent reviews, researchers study thermophilic bacteria to discover new products that support biotechnology and medicine, especially enzymes with exceptional stability under industrial conditions (Canganella and Wiegel, 2014; Mehta et al., 2016; and Shomali & Danish-Daniel, 2024). Microorganisms and their thermostable enzymes (thermozymes) have emerged as pivotal tools in high-temperature industrial bioprocesses. According to Li et al. (2025), these biological catalysts not only maintain activity under extreme thermal conditions but also demonstrate remarkable efficacy in biomass conversion, polymer degradation, and pollutant detoxification. Recent integration of AI-based enzyme engineering and high-throughput screening has significantly enhanced the efficiency of thermozymes in biotechnological workflows, offering cost-effective and environmentally sustainable solutions for large-scale industries.

Supporting this, a recent metagenomic study conducted in Guizhou Province, China, revealed that hot springs harbor taxonomically and functionally diverse thermophilic bacterial communities, dominated by *Pseudomonadota* and *Bacillota*. Functional predictions indicated that these communities possess robust metabolic pathways for amino acid and carbohydrate metabolism, as well as genetic traits related to stress adaptation (Chen et al., 2025). These findings emphasize the ecological and industrial significance of hot spring microbiota and

* Corresponding author. e-mail: m.rshaidat@ju.edu.jo.

** **Abbreviation**s: BLAST: Basic Local Alignment Search Tool, MEGA11: Molecular Evolutionary Genetics Analysis version 11, PCR: Polymerase Chain Reaction, rDNA: Ribosomal Deoxyribonucleic Acid.

reinforce the value of exploring extreme environments for novel microbial resources.

The investigation and isolation of thermophilic bacteria from hot springs in Jordan started early in the eighties, with the isolation of *Bacillus licheniformis*, *Thermomonas hydrothermalis*, and *Caldimonaas hydrothermale* (Malkawi and Al-Omari, 2010; Mohammad et al., 2017; and Obeidat and Al-Shomali, 2023). Jordan has several hot springs along the Dead Sea area, the lowest land area on Earth. (Schäffer and Sass,

2014). There are about 200 thermal provinces in Jordan, the most famous of which is the Ma'in Hot Spring, frequently visited for tourism and therapeutic purposes (Schäffer and Sass, 2014; Ayadi et al., 2023). In this study, samples were collected from only four selected hot springs.

The four hot springs selected for this study are Ma'in Hot Spring, Zara Dead Sea, North Shounah, and Makhebh (Figure 1).

Figure 1. Map of Jordan displaying the specific hot spring sites included in this study. Water samples were collected from the marked locations, which are indicated with red asterisks.

Several reports have outlined the types of thermophilic microorganisms prevalent in Jordanian hot springs (Malkawi and Al-Omari, 2010; Yohandini et al., 2015; Mohammad et al., 2017; Obeidat and Al-Shomali, 2023), but still, plenty of information has not been explored. Accurate identification techniques depend on molecular and biological methods, especially the polymerase chain reaction (PCR) for the detection and classification of thermophilic species. To obtain a pure culture of bacteria, culture-dependent media that help isolate a pure single colony for further identification must be used (Malkawi and Al-Omari, 2010; Pinevich et al., 2018 and Kapinusova et al., 2023). Numerous types of dependent culture media have been previously used, such as Bacillus media, Castenhoiz TYE media, Tryptic Soy Agar media, Thermus media, and Halophile media The progress in molecular techniques, such as the amplification of the 16S rDNA gene, has allowed the simultaneous detection of many DNA sequences of different groups of microorganisms, and now a huge number of studies are also reducing phylogenic relationships among thermophilic bacteria (Ash et al., 1991; Mouné et al., 2003; Clarridge, 2004; Alsanie et al., 2018 and Zhao et al., 2025).

This study aims to isolate thermophilic bacteria from Jordanian hot springs using environmentally relevant enrichment media and to compare their DNA sequences with those of previously reported thermophiles.

Understanding the diversity and features of thermophilic bacteria from Jordanian hot springs helps fill regional gaps in microbial ecology, especially in underexplored geothermal environments in the Middle East. Additionally, isolating and studying these microorganisms can lead to the discovery of new thermostable enzymes and bioactive compounds with potential industrial, medical, and environmental uses. This research lays the groundwork for future advances in biotechnology and microbial resource preservation, particularly as interest grows in sustainable, bio-based solutions from extremophiles.

2. Materials and Methods

2.1. Sample collection

Ten water samples were collected from four different hot springs in Jordan, namely: Ma'in, Zara Dead Sea, North Shounah (Al-Hema), and Mekhebh hot springs, using sterile thermal glass containers. Care was taken during transportation to the laboratory to minimize evaporation effects and maintain sample integrity. Three replicates were collected from each springhead sampling location.

2.2. Chemical analysis of water samples

The hydrogen ion concentration (pH), electrical conductivity (EC), and temperature were measured on-site using a pH meter, portable EC meter (Trans Instruments, HC3010; Singapore), respectively. Chemical analyses were performed using a spectrophotometer (Spectro UV-VIS Double Beam PC, 8 Scanning Auto Cell, UVD, Labomed, Inc., Los Angeles, USA) in the facilities of the Jordan Valley Authority.

The chemical analysis for cations such as calcium (Ca^{2+}), magnesium (Mg^{2+}), sodium (Na^{+}), potassium (K^{+}), iron (Fe^{2+}), and anions such as nitrate (NO_3^{-}), and sulfate (SO_4^{2}) were conducted in the laboratory using an atomic absorption spectrophotometer.

The chloride (Cl^{-}) and bicarbonate (HCO_3^{-}) concentrations were determined using the titration method (Al-Khashman et al., 2017; Mohammad et al., 2017; and Edet et al., 2024).

2.3. Cultivation of water samples

For the isolation of thermophilic bacteria from the collected samples, the culture-dependent method using enrichment media and incubation, and high temperatures described by Malkawi and Al-Omari (2010) was adopted, with some modifications. Specifically, the culture media were prepared using filtered hot spring water collected from the sampling sites instead of distilled water. In addition, all enrichment cultures were incubated at a fixed temperature of 55 °C. Two types of culture media were used in this study, namely: Thermus medium and Castenholz TYE (tryptone yeast extract) medium.

2.3.1. Thermus medium preparation

Thermus medium is composed of 5 g tryptone, 5 g yeast extract, 1 g sodium chloride, 0.2 g magnesium sulfate ($MgSO_4$), 2 g potassium phosphate (K_2HPO_4), 0.1 g calcium chloride ($CaCl_2$), 0.1 g ferric chloride ($FeCl_3$),

0.1 g sodium thioglycolate, 0.02 g nitrilotriacetic acid (NTA), and 0.02 g ethylenediaminetetraacetic acid (EDTA). All components were dissolved in one liter of filtered hot spring water in bottles. The pH was adjusted to 7.0 using an adjustment solution (1 M NaOH or 1 N HCl). For solid medium preparation, 15 g of agar was added. The media were then sterilized using an autoclave at 121 °C, 15 psi for 20 minutes (Kumar et al., 2025).

After sterilization, the bottles were cooled in a water bath to approximately 50 °C and poured into sterile petri dishes. To ensure the absence of contamination before inoculation, the solidified plates were incubated overnight at 55 °C.

2.3.2. Castenholz TYE medium preparation

The Castenholz Tryptone-Yeast Extract (TYE) medium was used according to Castenholz, (1969). The medium consists of salts with one part (1%) TYE (Tryptone and Yeast Extract) and four parts distilled water. The medium was heated and mixed with TYE solution and autoclaved at 121 °C. The salts were added aseptically, and the final pH of the medium was adjusted to 7.6. Agar plates were prepared by adding 3% agar before autoclaving

Water samples from hot springs were inoculated onto Petri dishes using two selective media and incubated at 55°C to promote the growth of thermophilic bacteria. Subculturing was repeated by transferring isolated colonies onto fresh plates until 34 pure, single colonies were obtained. All chemicals and reagents used for the preparation of culture media in this study were obtained from Bio Basic Inc. (Markham, Ontario, Canada).

2.4. Isolation and characterization of isolates

Thermophilic bacteria were enriched on previously prepared agar media by incubating the samples at 55°C. The colonies were further classified according to their shape and size. Some of the colonies were then stained using Gram staining. Colony morphology was assessed after 48 hours of incubation at 55°C on agar media. Morphological characterization included visual evaluation of colony color, shape, edge characteristics, surface texture, and approximate size. Colonies were generally circular with entire or slightly undulate margins and smooth to slightly mucoid surfaces. Colors varied among isolates, including white, cream, cream-white, pale yellow, and yellow. Colony diameters were visually estimated to range between 1 and 3 mm. Gram staining was performed following standard microbiological procedures to differentiate isolates based on their cell wall characteristics. Freshly grown colonies were smeared onto glass slides, heat-fixed, and sequentially treated with crystal violet, iodine solution, decolorizer ethanol, and counterstained with safranin. The stained slides were examined under a light microscope at 1000× magnification using oil immersion. Observations included Gram reaction and cellular morphology. The Gram staining reagents were obtained from Millipore Sigma (USA), kit number 77730-1KT-F.

2.5. 16S rDNA amplification and sequencing

A single colony from the agar plate was picked up with an inoculation loop and cultured overnight at 55 °C on Castenholz TYE broth medium.

Genomic DNA was extracted using the Wizard® Genomic DNA Purification Kit (Promega, USA, Cat. No. A1620) according to the manufacturer's instructions, and the concentrations of extracted DNA were determined using a Nanodrop spectrophotometer (ND-1000, Thermo Fisher Scientific, Waltham, MA, USA). The 16S rDNA gene was used for bacterial identification, and it was amplified by PCR using the domain bacterial-specific primer 27F (5'- AGA GTT TGA TCM TCG CTC AG-3') and universal primers 1492R (5'- TAC GGY TAC CTT GTT ACG ACT T-3') (Mohammad et al. 2017). The reaction mixture (25 µL) consisted of 1X PCR reaction buffer (2.5 µL), 2.5mM $MgCl_2$ (2.5 µL), 0.2mM deoxynucleoside triphosphate (0.5 µL), 0.1mM of each primer (0.5 µL), 1 U Taq DNA polymerase (0.5 µL), 1 µL of 50ng genomic DNA, and 17 µL nuclease-free water. All PCR components were obtained from the Taq DNA Polymerase PCR Buffer kit (Cat. No. 18067-017, Thermo Fisher Scientific, USA).

The PCR reaction was carried out in a PTC-200 Peltier Thermal Cycler (MJ Research Inc., Watertown, MA, USA). The amplification conditions were as follows: denaturation at 94°C for 5 min, followed by 30 cycles at 94°C for 30 s, 52°C for 30 s, 72°C for 1.5 min, and a final extension at 72°C for 10 min. The PCR products were analyzed by electrophoresis on a 1% agarose gel, visualized under a UV transilluminator (Gel Doc 200, BIO-RAD, USA), and photographed with the gel documentation system (Gel Doc 200, BIO-RAD, USA) after staining with ethidium bromide (0.5 µg/mL). One kb DNA ladder (GeneRuler 1 kb DNA ladder, SM0313, ThermoFisher Scientific, MA, USA) was used as a marker to determine the size of the amplified fragments. Amplified 16S rDNA gene fragments were sequenced using commercial services at Macrogen Inc. (Korea). The phylogenetic tree was constructed using the neighbor-joining method, based on distance matrix analysis performed with Molecular Evolutionary Genetics Analysis version 11 (MEGA 11) software, and 1000 bootstrap replications were used. Sequence comparisons and database searches were conducted using the BLAST algorithm (Tamura et al., 2021).

3. Results

3.1. Physical and chemical analysis of water samples

Ten water samples were collected from four hot spring locations in Jordan: Ma'in Hot Spring, Zara Dead Sea, North Shounah (Al-Hemma), and Mekhebh Hot Spring. The water temperature was recorded between 40.0 and 55.0°Cwhich supports the growth of thermophilic bacteria. Table 1 summarizes all physical characteristics of the collected samples.

Table 1. Physical characteristics of water samples from geothermal sites in Jordan, including collection locations, electrical conductivity (EC), temperature, and pH.

Collection site	Geographic Coordinate	Sample Code	Electrical Conductivity (mS/cm^2)	Water Temperature (°C)	pH
Ma'in 1	31.608829 35.611118	MN (1,213,4,5,6) S1	2.78	40.0	8.19
Ma'in 2	31.58333 N 35.73333E	MN (7,8,9,10) S2	2.90	54.0	7.29
Ma'in 3	31.3634.6N 35.3647.8E	MN (11,12,13) S3	3.21	50.0	8.19
Zara Dead Sea	31.3550.1N 35.3400.8E	ZARA (1,2,3)	1.64	48.0	7.69
Shounah 1	32.8124620 35.6169760	SH (9,10) S1	1.42	48.0	8.20
Shounah 2	32.6151040 35.6227250	SH (1,3) S2	0.956	46.2	7.32
Shounah 3	32.6130150 35.6166320	SH (2,4,5,6,7,8,11) S3	1.46	55.0	7.45
Mekhebh 1	32.7046230 35.6837450	MK (1,3,4) S1	1.53	41.0	7.51
Mekhebh 2	32.7045260 35.6838080	MK (2) S2	1.53	40.3	7.82
Mekhebh 3	32.7045330 35.6837810	MK (5,6,7) S3	1.54	41.6	7.58

The four water sources are different in terms of mineral content. For example, chemical analysis of the water sample obtained from Ma'in hot spring water showed that it contains moderate bicarbonate (HCO_3^-) and low nitrate (NO_3^-) but high calcium (Ca^{2+}), sodium (Na^+), sulfate (SO_4^{2-}), and chloride (Cl^-). On the other hand, the water sample collected from Zara had the lowest nitrate (NO_3^-) concentration of all water samples, and it contained a slightly reduced bicarbonate (HCO_3^-) concentration than that found in Ma'in hot spring. It is also characterized by elevated levels of salt, chloride, and considerably larger amounts of calcium and potassium. The water sample obtained from North Shounah had the highest levels of magnesium, bicarbonate, and moderate sodium, less calcium, and a slightly higher nitrate. Table 2 summarizes ion concentrations (ppm) for each site.

Table 2: Chemical analysis of water samples collected from selected hot springs in Jordan.

Water source	Mg^{2+} ppm	Ca^{2+} ppm	Na^+ ppm	K^+ ppm	NO_3^- ppm	SO_4^{2-} ppm	Cl^- ppm	HCO_3^- ppm
Ma'in	35.66	135.20	176.3	32.20	0.51	293.64	298.65	202.40
Zara	25.99	110.0	290.0	40.60	0.32	296.86	428.14	183.02
North Shounah	88.43	55.70	161.0	9.40	0.63	295.98	219.45	300.16
Mekhebh	39.87	50.0	51.70	2.20	0.73	28.29	103.01	292.84

Note: Ca – Calcium, Na – Sodium, SO_4^{2-} – Sulfate, Cl^- – Chloride, HCO_3^- – Bicarbonate, NO_3^- – Nitrate, Mg^{2+} – Magnesium, K^+ – Potassium, Fe^{2+} – Iron

Finally, Mekhebh water contains low concentrations of Na^+ and Cl^- and is characterized by a generally lower concentration of other ions except NO_3^-. These variances suggest that each water source has a unique mineral content, which might affect its suitability for a given purpose and the microbes it harbors. For instance, the high salt concentration in Ma'in and Zara hot springs may promote the growth and development of halophilic microbes, whereas differing profiles in North Shounah and Mekhebh suggest the ability to support various bacterial types based on their metabolic demand and threshold level of minerals. Water samples from all sources had iron levels less than 1 µg/L.

3.2. Phenotypic characterization of bacterial isolates

The bacterial strains collected from different hot springs displayed variable Gram staining, cell morphology, and colony pigmentation. Gram-positive bacilli were the most dominant, including *Anoxybacillus* and *Bacillus* species. These strains, derived from the hot spring samples, were metabolically active under either facultatively aerobic or anaerobic conditions with yellow-cream-colored colonies. On the other hand, Gram-negative bacilli, particularly *Flavobacterium* and *Sphingobacterium* species, grew aerobically and produced whitish to pale-yellow colonies. The variation of the Gram staining coupled with the coloration of the colonies indicates the existence of a variety of microorganisms thriving at the elevated temperatures of hot springs, as shown in Table 3.

Table 3. Gram staining results, cell morphology, and phenotypic characteristics of bacterial isolates obtained from hot springs in Jordan.

Tube No.	Location	Species	Gram stain	Colony Shape	Oxygen requirements	Colony Color
1	Ma'in 1	*Anoxybacillus flavithermus* subsp. flavithermus strain DSM 2641	+ve	Rod	Facultatively aerobic	Yellow
2	Ma'in 1	*Tepidimonas taiwanensis* strain I1-	-ve	Rod	Aerobic	Cream white
3	Ma'in 1	*Tepidimonas taiwanensis* strain I1-1	-ve	Rod	Aerobic	Cream white
4	Ma'in 1	*Tepidimonas taiwanensis* strain I1-1	-ve	Rod	Aerobic	Cream white
5	Ma'in 1	*[Flavobacterium] thermophilum* strain G-21	-ve	Rod	Aerobic	White
6	Ma'in 1	*Anoxybacillus flavithermus* subsp. flavithermus strain DSM 2641	+ve	Rod	Facultatively aerobic	Yellow
7	Ma'in 2	*Anoxybacillus rupiensis* strain ATCC BAA-2555	+ve	Rod	Aerobic	Cream white
8	Ma'in 2	*Flavobacterium thermophilum* strain G-21	-ve	Rod	Aerobic	White
9	Ma'in 2	*Anoxybacillus flavithermus* subsp. flavithermus strain DSM 2641	+ve	Rod	Facultatively aerobic	Yellow
10	Ma'in 2	Anoxybacillus kestanbolensis strain K1	+ve	Rod	Aerobic	Cream white
11	Ma'in 3	*Anoxybacillus contaminans* strain R-16222	+ve	Rod	Facultatively anaerobic	Cream-colored
12	Ma'in3	*Anoxybacillus rupiensis* strain ATCC BAA-2555	+ve	Rod	Aerobic	Cream white
13	Ma'in 3	*Bacillus licheniformis* strain DSM 13	+ve	Rod	Facultative anaerobic	Cream-colored
14	ZARA	*Flavobacterium thermophilum* strain G-21	-ve	Rod	Aerobic	White
15	ZARA	*Geobacillus stearothermophilus* strain BGSC 9A20	+ve	Rod	Anaerobe	White
16	ZARA	*Flavobacterium thermophilum* strain G-21	-ve	Rod	Aerobic	White
17	Shounah 1	*Bacillus licheniformis* strain DSM 13	+ve	Rod	Facultative anaerobic	Cream-colored
18	Shounah 1	*Sphingobacterium thermophilum* strain CKTN2	-ve	Rod	Aerobic	Pale yellow
19	Shounah 1	*Sphingobacterium thermophilum* strain CKTN2	-ve	Rod	Aerobic	Pale yellow
20	Shounah2	*Bacillus licheniformis* strain DSM 13	+ve	Rod	Facultative anaerobic	Cream-colored
21	Shounah3	*Flavobacterium thermophilum* strain G-21	-ve	Rod	Aerobic	White
22	Shounah3	*Bacillus licheniformis* strain DSM 13	+ve	Rod	Facultative anaerobic	Cream-colored
23	Shounah3	*[Flavobacterium] thermophilum* strain G-21	-ve	Rod	Aerobic	White
24	Shounah3	*Pseudoxanthomonas taiwanensis* strain NBRC 101072	-ve	Rod	Aerobic	Yellow
25	Shounah3	*Bacillus licheniformis* strain DSM 13	+ve	Rod	Facultative anaerobic	Cream-colored
26	Shounah 3	*[Flavobacterium] thermophilum* strain G-21	-ve	Rod	Aerobic	White
27	Shounah 3	*Anoxybacillus flavithermus* subsp. flavithermus strain DSM 2641	+ve	Rod	Facultatively aerobic	Yellow
28	Mekhebh 1	*Bacillus licheniformis* strain DSM 13	+ve	Rod	Facultative anaerobic	Cream-colored
29	Mekhebh1	*Bacillus licheniformis* strain DSM 13	+ve	Rod	Facultative anaerobic	Cream-colored
30	Mekhebh1	*Bacillus licheniformis* strain DSM 13	+ve	Rod	Facultative anaerobic	Cream-colored
31	Mekhebh 2	*Anoxybacillus contaminans* strain R-16222	+ve	Rod	Facultatively anaerobic	Cream-colored
32	Mekhebh 3	*Bacillus licheniformis* strain DSM 13	+ve	Rod	Facultative anaerobic	Cream-colored
33	Mekhebh 3	*Bacillus licheniformis* strain DSM 13	+ve	Rod	Facultative anaerobic	Cream-colored
34	Mekhebh 3	*Bacillus licheniformis* strain DSM 13	+ve	Rod	Facultative anaerobic	Cream-colored

3.3. Molecular characterization of the isolates

The PCR products of 16S rDNA of thirty-four (34) thermophilic bacterial isolates were analyzed by electrophoresis on 1% agarose gel (Figure 2) and sequenced. The sequences were used for the identification and phylogenetic analysis of these isolates.

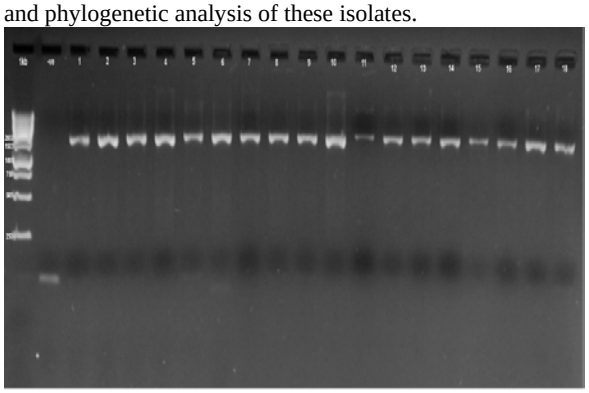

Figure 2. Agarose gel electrophoresis of PCR-amplified 16S rDNA gene fragments from bacterial isolates using the universal primer pair 27F/1492R. Lanes 1–18: PCR products from individual bacterial isolates. Lane 1 kb: DNA ladder (1 kb) used as a molecular size marker. Lane -ve: negative control (no template DNA). The expected amplicon size is approximately ~1.5 kb.

3.4. Phylogenetic analysis

The 16S rDNA sequences of the thirty-four thermophilic bacterial isolates were aligned with known thermophilic reference sequences from GenBank using the BLAST program (Figure 3). These reference sequences are represented by the following accession numbers: NR_104891 (*Flavobacterium thermophilum* **)**, NR_115109 (*Anoxybacillus gonensis*), NR_026516 (*Anoxybacillus flavithermus* **)**, NR_180406 (*Anoxybacillus kestanbolensis***)**, NR_116097 (*Anoxybacillus mongoliensis***)**, NR_117229 (*Anoxybacillus eryuanensis***)**, NR_029006 (*Anoxybacteroides contaminans***)**, NR_024818 (*Anoxybacteroides voinovskiense*), NR_026515 (*Aeribacillus pallidus*), NR_115284 *(Geobacillus stearothermophilus)*, NR_119305 (*Geobacillus thermocatenulatus*), NR_118996 *(Bacillus licheniformis*), NR_113993 (*Bacillus sonorensis*), NR_113974 (*Pseudoxanthomonas taiwanensis* strain NBRC 101072), NR_025198 (*Pseudoxanthomonas taiwanensis* strain CB-226), NR_113984 (*Pseudoxanthomonas daejeonensis* strain NBRC 101159*)*, NR_042418 (*Tepidimonas thermarum*), NR_179191 (*Tepidimonas arfidensis*), NR_180139 (*Tepidimonas charontis*), NR_043227 (*Tepidimonas taiwanensis* strain I1-1), and NR_043433 (*Sulfuracidifex metallicus*).

The phylogenetic relationships showed that isolates MN1 S1, MN6 S1, MN9 S1, and SH11 S3 were closely related to *Anoxybacillus flavithermus* subsp. *flavithermus* strain DSM 2641, while isolates MN2 S1, MN3 S1, and MN4 S1 were closely related to *Tepidimonas taiwanensis* strain I1. Six isolates including MN5 S1, MN8 S1, ZARA1, ZARA3, SH3 S3, and SH8 S3 were closely related to *Flavobacterium thermophilum*strain G-21. Two isolates, MN7 S2 and MN12 S3, were closely related to *Anoxybacillus rupiensis* strain ATCC BAA-2555. In addition, isolates MN10 S2 (*Anoxybacillus skestanbolensis* strain K1), MK2 S2, MN11 S2, and MN11 S3 were found to be closely related to *Anoxybacillus contaminans* strain R-16222. *Bacillus licheniformis* strain DSM 13 is the most common Bacillus species found in the hot spring water. Sequence analysis showed that isolates MK1 S1, MK3 S1, MK4 S1, MK5 S3, MK6 S3, MK7 S3, SH1 S2, SH3 S2, SH4 S3, SH7 S3, and MN13 S3 are closely related to *T*. In addition, isolate SH2 S3 was found to be related to *Flavobacterium thermophilum* strain G-21, isolate SH6 S3 is related to *Pseudoxanthomonastaiwanensis*strain NBRC 101072, and isolate ZARA2 is closely related to *Geobacillus stearothermophilus* strain BGSC 9A20.

Analysis of the 16S rDNA sequences of isolates obtained from Ma'in, North Shounah, Mekhebh, and Zara formed distinct clades within the genera *Anoxybacillus*, *Geobacillus*, *Pseudoxanthomonas*, and *Tepidimonas* with a bootstrap support >70%. Ma'inisolates are clustered with *A.flavithermus* and *Anoxybacillus kestanbolensis* with bootstrap values of 99% and 95% respectively, indicating a close relationship with these thermophiles. Zara and NorthShounah isolates are grouped with *Flavobacterium thermophilum*and *Anoxybacillus* species with 100% bootstrap values. It is worth mentioning that *T.taiwanensis*was isolated for the first time in Jordan from Ma'in hot spring, and it formed a clade with other *Tepidimonas* species with a 98% bootstrap value. This is the first report of *T. taiwanensis* in Jordan, indicating local adaptation of this thermophilic bacterium in the Ma'in hot spring.

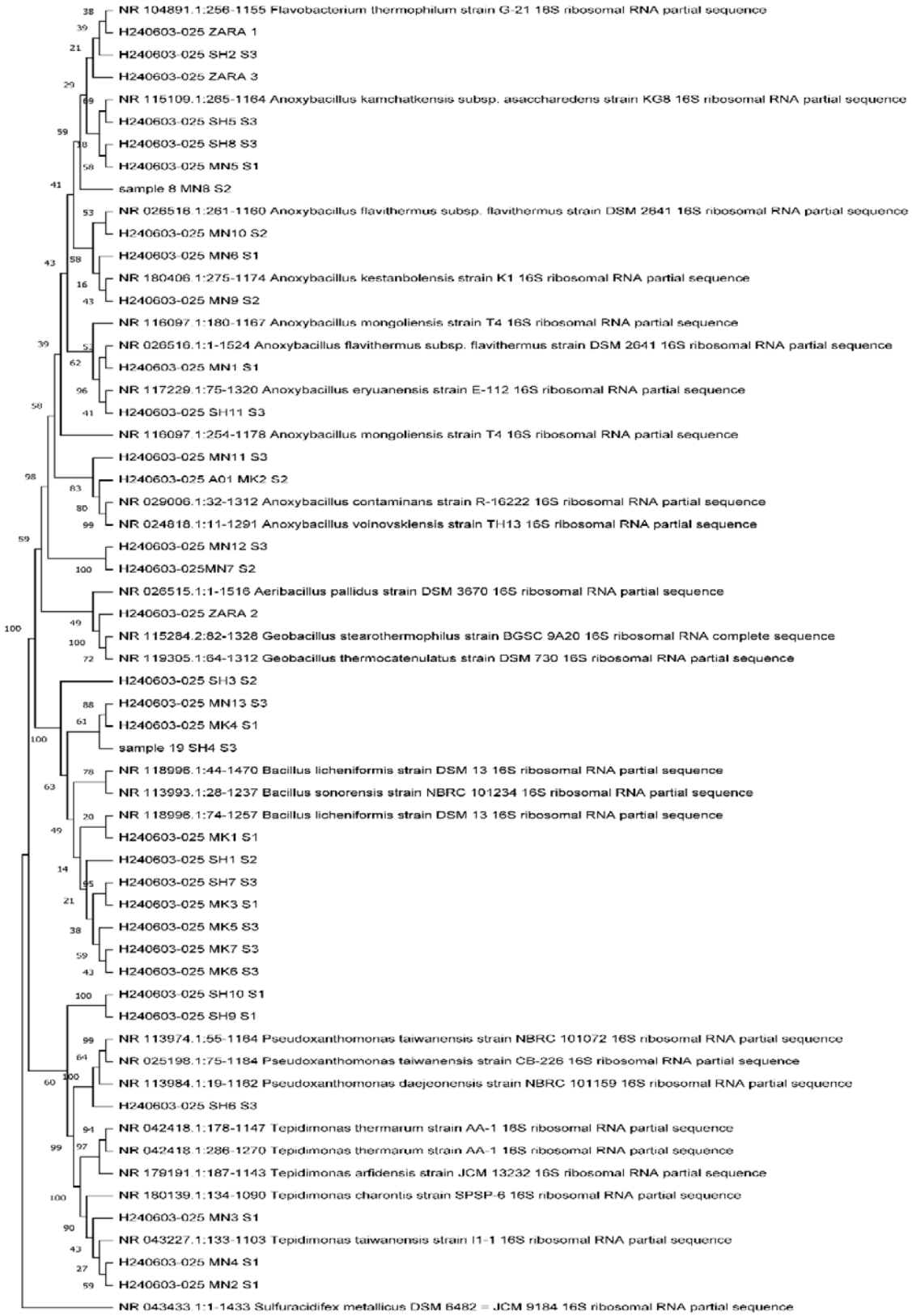

Figure 3. A phylogenetic tree illustrates the evolutionary relationships among bacterial isolates based on 16S rDNA gene sequences. The tree was constructed using the Neighbor-Joining (NJ) method with the p-distance model to calculate genetic distances. Statistical support for the branching pattern was assessed by bootstrap analysis with 1000 replications, and the bootstrap values (%) are indicated at each node. Higher bootstrap values indicate stronger support for the corresponding clades. *Sulfuracidifex metallicus* (DSM 6482 = JCM 9184) was included as an outgroup to root the tree and provide evolutionary context. The analysis was performed using MEGA version 11 (Tamura, Stecher, and Kumar 2021) . The scale bar represents the number of nucleotide substitutions per site.

4. Discussion

The differences in the physical and chemical characteristics of water samples taken from various sites in Jordan are believed to affect microbial distribution. In this study, water temperatures recorded on various sites ranged from 40°C to 55°C, and these conditions are known to support thermophilic bacteria. This is in accordance with previous reports on bacterial growth in hot springs (Radaideh et al., 2010; Mohammad et al., 2017; Obeidat and Al-Shomali, 2023). Previous studies showed that the concentration of each chemical at a certain location defines the type of microbes inhabiting that location (Fomina and Skorochod, 2020; Verma et al., 2022). Minerals are important components that affect the pH value of the surrounding environment and subsequently affect the growth of microorganisms (Hutchens, 2009; Fomina and Skorochod, 2020; Verma et al., 2022).

Ma'in hot springs and Zara Dead Sea water, containing high mineral content of sodium and chloride ions only, align with previous studies that identified Jordan hot springs and the Dead Sea saline environment as rich in salts that aid the growth of halophilic microbes (Hussein et al., 2017). This is further supported by (Jacob et al., 2017) reporting the same results on the microbial diversity of Dead Sea water and its surrounding regions.

The water sample obtained from North Shounah exhibited higher concentrations of magnesium and bicarbonate compared to samples from the Ma'in and Zara sites. This unique composition agrees with the previous data reported by Schäffer and Sass (2014). It is important to note that variations in mineral contents, like magnesium and bicarbonates, were found between water samples collected from different sources in Jordan. These variations may affect the growth of microorganisms in these water sources. The Mekhebh water has some different characteristics from an ecological point of view, such as sodium and chloride being lower than in the other areas, and bicarbonate being higher. As of now, there are no other studies that are focused directly on the Mekhebh hot springs.

Based on the phylogenetic analysis, it can be concluded that the bacteria isolated from the four hot springs are diverse and, in some ways, could adapt to the thermal conditions.

Moreover, among many strains of thermophiles isolated from various hot springs, *Anoxybacillus* was found to be the predominant genus (Ulucay et al., 2022) and (Ortega-Villar et al., 2024). This study found that MN1S1, MN6 S1, MN9 S1, and SH11 S3 isolates were closely related to *A.flavithermus* subsp. *flavithermus* strain DSM 2641; this strain is known as a thermophilic bacterium that lives under extreme temperature conditions. These findings agree with previous observations made about *A.flavithermus* in such geothermal environments, including those existing in similar areas but largely separated from Turkey (Agüloğlu Fincan et al., 2014), implying the occurrence of similar ecological niches provided by Jordanian hot springs. A clustering of several isolates (MN2 S1, MN3 S1, and MN4 S1) with the *T. taiwanensis* strain I1 was another remarkable observation. It is important to note that the data presented in this study is the first report on the occurrence of *T.taiwanensis*in in Jordan. According to Chen et al. (2006), this thermophilic, facultative anaerobe bacterium has been reported for the first time in hot springs in Taiwan. Its presence in Ma'in hot springs indicates the ecological resemblance that exists between this environment and East Asian hot springs, particularly in temperature and chemical composition, which may favor colonization and adaptation of *Tepidimonas* species. Moreover, the fact that *Flavobacterium thermophilum* has been isolated from multiple sites (MN5 S1, MN8 S1, ZARA1, ZARA3, SH3 S3, and SH8 S3) also shows the diversity among organisms found in these thermal waters. First isolated from the Italian geothermal area (Yoshizaki et al.,1971), it is characterized by thermophilicity as well as degrading complex organic matter. The identification of this species from both Zara and North Shounah hot springs supports the notion that these places provide proper conditions for thermophilic and heterotrophic bacteria vital for nutrient recycling in extreme environments like hot springs, where these bacteria can thrive **(Singh et al., 2019; Delete)** Kochhar et al., 2022 and EFSA Panel on Food Enzymes (FEZ) et al., 2025). It is worth noting that *Bacillus licheniformis* was found to be a dominant species in many hot spring samples. This species has been heavily investigated for its thermophilic attributes and ability to produce enzymes of industrial significance like proteases and amylases (Schallmey et al., 2004). Eleven strains closely related to *Bacillus licheniformis* strain DSM 13 have been isolated from different hot springs, indicating that this bacterium is comfortable with the different ecological conditions of geothermal springs prevailing in Jordan. Moreover, its adaptation to extremely high temperatures and mineral concentrations has been recorded worldwide (Makowski et al., 2021).

The identification of *Anoxybacillus kestanbolensis*, *Anoxybacillus rupiensis*, and *Anoxybacillus contaminans highlights* the supremacy of the *Anoxybacillus* genus in those hot springs. These thermophilic and halophilic microbes were previously identified in other geothermal habitats (Narsing Rao et al., 2018). The occurrence of these microorganisms in the Ma'in and North Shounah hot springs can be attributed to high mineral concentrations, particularly sodium and chloride, which favor their growth. The close relationships among isolates that were located in clusters with high bootstrap values (>95%) show how these thermophiles are strongly related to their ecological niche.

Finally, the isolation of *Geobacillus stearothermophilus* and *Pseudoxanthomonas taiwanensis* from Zara and North Shounah hot springs emphasized the microbial diversity in these ecosystems. It is widely known that *G. stearothermophilus* has industrial use, especially in the biotechnology industry, because of its thermostable enzymes (Gandhi et al., 2015). This suggests that Jordanian hot springs have a high potential for microbial communities that are useful in biotechnology.

Yin et al. (2024) emphasized the increasing importance of thermophilic glycoside hydrolases (GHs) derived from hot spring microorganisms, highlighting their exceptional stability and catalytic efficiency at high temperatures. Their editorial underscored how advanced bioinformatics tools, metagenomic sequencing, and molecular dynamics simulations have enabled the identification and functional validation of GHs with industrial significance. In

particular, enzymes such as β-glucosidases and xylanases exhibited resistance to inhibitors and retained functionality under extreme conditions. These findings complement the results of the current study, which identified thermophilic genera such as *Geobacillus* and *Anoxybacillus*, known for their production of thermostable hydrolytic enzymes. This supports the notion that Jordanian hot springs represent promising biotopes for the discovery of novel thermostable GHs with potential industrial applications.

Additionally, Guta et al. (2024) demonstrated the successful isolation of thermophilic strains from Ethiopian hot springs that produce amylase, protease, cellulase, and lipases, illustrating the functional diversity of hot springs microbiota under similar thermal conditions.

The discovery of thermophilic bacteria in Jordan's hot springs holds significant global industrial potential, particularly in biotechnology and bioengineering. Thermophilic bacteria, thriving in high-temperature environments, are invaluable for various industrial applications due to their unique enzymatic properties. For instance, they have been used for biofuel production, particularly in generating hydrogen through dark fermentation (Gallo et al., 2024). Thermophilic bacteria have also been studied for the bioremediation potential of municipal wastewater under high temperatures (Al-Rasheedi et al., 2022). Thermophilic bacteria have demonstrated significant potential in the biosynthesis of nanoparticles with diverse industrial applications. Recent studies have highlighted their role in producing nanoparticles with notable antibacterial properties. For instance, *Thermus thermophilus* has been shown to extracellularly synthesize silver nanoparticles (AgNPs) with potent antibacterial effects against both Gram-positive and Gram-negative bacteria (Romano et al., 2022).

The identification of *Bacillus licheniformis*, *Flavobacterium thermophilum*, and *T. taiwanensis* in this study further supports their relevance in industrial biotechnology. Previous research has shown that species such as *B. licheniformis* are prolific producers of thermostable proteases and amylases, enzymes highly sought after for use in food, textiles, and pharmaceutical industries (Ashaolu et al., 2025). The discovery of similar taxa in Jordanian hot springs strengthens the case for considering these sites as viable sources of thermostable enzymes.

The unique Thermophilic bacteria found in Jordan's hot springs could be crucial for developing new industrial products and processes, supporting advances in biotechnology and sustainable industry practices not only locally or regionally but also worldwide. These bacteria are specific to this region’s climate, abiotic factors, and conditions. This suggests that the metabolic and productive capabilities of these thermophiles could expand the global range of thermophilic industry products.

To conclude, the microbial diversity reported in Jordanian hot springs is indicative of how various environmental factors, such as temperature, salinity, and mineral content, contribute to microbial adaptation. The presence of diverse thermophilic genera like *Anoxybacillus*, *Tepidimonas*, *Flavobacterium*, and *Bacillus* shows that these hot springs provide a unique habitat for microorganism growth. The identification of *T. taiwanensis* for the first time in Jordan, together with other thermophiles clustering, suggests that there is much more to these hot springs than just being a reservoir of microbial diversity; they may also serve as an important ecological niche to study microorganism adaptation and evolution processes under extreme environmental conditions.

Furthermore, the presence of *Tepidimonas taiwanensis* in Ma’in hot spring, previously isolated only in Taiwan, suggests ecological parallels between distant geothermal environments and supports the idea that Jordanian hot springs could harbor microbial communities of global biotechnological importance (Zheng et al., 2025). These findings align with global trends where researchers seek extremophile enzymes due to their resilience under industrial stress conditions, including high temperature, salinity, and chemical solvents.

5. Conclusion

This study demonstrates that the physical and chemical parameter gradients of the Jordanian hot springs are a key factor influencing microbial populations. Elevated temperatures of the geothermal waters create an ideal habitat for thermophilic bacteria, and factors such as sodium, chloride, bicarbonate, and magnesium affect microbial distribution. Among the isolates, *Tepidimonas taiwanensis* and *Pseudoxanthomonas taiwanensis* were not previously recorded from Jordan, indicating an ecological similarity between the Ma'in hot springs and similar East Asian thermal ecosystems. The presence of *Anoxybacillus*, *Bacillus*, *Geobacillus*, and *Flavobacterium* also highlights microorganisms' ability to survive extreme conditions. The structure of this group of thermophile-associated bacterial isolates further suggests that these hot springs could serve as natural reservoirs for thermotolerant bacteria, with potential applications in biotechnology or industry.

Overall, the current study offers valuable data on the microbial diversity of Jordanian hot springs and their role as sources of thermophilic bacteria. Future research should explore the functional significance of these microbes, especially their enzyme capabilities and other biotechnological and medicinal applications.

Acknowledgments:

We gratefully acknowledge the Jordan Valley Authority for their valuable support in conducting the chemical analysis of water samples. We also wish to thank the University of Jordan for its financial support, which made this study possible.

Funding statement:

The Deanship of Scientific Research at the University of Jordan supported this research for graduate students [grant number 400].

References

Al-Rasheedi S, Tawabini B, Nazal M, and Khalil A. 2022. Application of thermophilic bacteria for the treatment of municipal wastewaters. *Arab J Sci Eng.*, **47:** 6881–6888. https://doi.org/10.1007/s13369-021-06518-2

Ayadi O, Jaber JO and Al-Zyoud S. 2023. Geothermal energy resources in Jordan. In: Younos T and Jabbari H (Eds.),

Alternative Energy Resources in the MENA Region. Springer Int. Publ., Cham, pp. 387–413. https://doi.org/10.1007/698_2022_962.

Agüloğlu Fincan S, Enez B, Özdemir S, and Matpan Bekler F. 2014. Purification and characterization of thermostable α-amylase from thermophilic *Anoxybacillus flavithermus*. *Carbohydr Polym*., **102(1):** 144–150. https://doi.org/10.1016/j.carbpol.2013.10.048.

Al-Khashman OA, Alnawafleh HM, Abu Jrai AM, and Al-Muhtaseb AH. 2017. Monitoring and assessing of spring water quality in southwestern basin of Jordan. *Open J Mod Hydrol*., **7(4):** 331–349.https://doi.org/10.4236/ojmh.2017.74019.

Alsanie WF, Felemban EM, Farid MA, Hassan MM, Sabry A, and Gaber A. 2018. Molecular identification and phylogenetic analysis of multidrug-resistant bacteria using 16S rDNA sequencing. *J Pure Appl Microbiol*., **12(2):** 489–496. https://doi.org/10.22207/JPAM.12.2.07.

Ashaolu TJ, Malik T, Soni R, Prieto MA and Jafari SM. 2025. Extremophilic microorganisms as a source of emerging enzymes for the food industry: a review. *Food Sci Nutr*., **13 (1):** e4540. https://doi.org/10.1002/fsn3.4540

Ash C, Farrow JAE, Dorsch M, Stackebrandt E, and Collins MD. 1991. Comparative analysis of Bacillus anthracis, Bacillus cereus, and related species on the basis of reverse transcriptase sequencing of 16S rRNA. *Int J Syst Bacteriol*., **41(3):** 343–346. https://doi.org/10.1099/00207713-41-3-343.

Benammar L, İnan Bektaş K, Menasria T, Beldüz AO, Güler HI, Bedaida IK, Gonzalez JM, and Ayachi A. 2020. Diversity and enzymatic potential of thermophilic bacteria associated with terrestrial hot springs in Algeria. *Braz J Microbiol*., **51(4):**1987–2007.

Burkhardt C, Baruth L, Meyer-Heydecke N, Klippel B, Margaryan A, Paloyan A, Panosyan HH and Antranikian G. 2024. Mining thermophiles for biotechnologically relevant enzymes: evaluating the potential of European and Caucasian hot springs. *Extremophiles*, **28(1):** 5. https://doi.org/10.1007/s00792-023-01321-3.

Canganella F, and Wiegel J. 2014. Anaerobic thermophiles. *Life*., **4(1):** 77–104. https://doi.org/10.3390/life4010077.

Castenholz RW. 1969. Thermophilic blue-green algae and the thermal environment. *Bacteriol Rev*., **33(4):** 476–504. https://doi.org/10.1128/br.33.4.476-504.1969.

Chen F, Cheng M, Rong D, Wang Y, Liang R, Irfan M, Kang Y and Cao Y. 2025. Metagenomic insights into microbial communities and functional traits of hot springs in Guizhou province, China. *Front Microbiol*., **16:** 1615879.

https://doi.org/10.3389/fmicb.2025.1615879.

Chen TL, Chou YJ, Chen WM, Arun B, and Young CC. 2006. Tepidimonas taiwanensis sp. nov., a novel alkaline-protease-producing bacterium isolated from a hot spring. *Extremophiles*, **10(1):** 35–40. https://doi.org/10.1007/s00792-005-0469-9.

Clarridge JE. 2004. Impact of 16S rRNA gene sequence analysis for identification of bacteria on clinical microbiology and infectious diseases. *Clin Microbiol Rev*., **17(4):** 840–862. https://doi.org/10.1128/CMR.17.4.840-862.2004.

Crosby JR, Laemthong T, Lewis AM, Straub CT, Adams MWW, and Kelly RM. 2019. Extreme thermophiles as emerging metabolic engineering platforms. *Curr Opin Biotechnol*., **59:** 55–64. https://doi.org/10.1016/j.copbio.2019.02.006.

Edet A, Akpan OU, Yakubu TA and others. 2024. Characterization of discharge, hydrogeochemical process and evaluation of water quality of some warm and cold springs, northeastern and southeastern Nigeria. *J Earth Syst Sci*., **133(1):** 12. https://doi.org/10.1007/s12040-023-02209-8.

EFSA Panel on Food Enzymes (FEZ), Zorn H, Barat Baviera JM, Bolognesi C, Catania F, Gadermaier G, Greiner R, Mayo B, Mortensen A, Roos YH and Solano ML. 2025. Safety evaluation of the food enzyme pullulanase from the genetically modified *Bacillus licheniformis* strain DP-Dzp107. *EFSA J.*, **23(6):** e9481. https://doi.org/10.2903/j.efsa.2025.9481.

Fomina M, and Skorochod I. 2020. Microbial interaction with clay minerals and its environmental and biotechnological implications. *Minerals*., **10(10):** 1-54.

Fongaro G, Maia GA, Rogovski P, Cadamuro RD, Lopes JC, Moreira RS, Camargo AF, Scapini T, Stefanski FS, Bonatto C, Marques Souza DS, Stoco PH, Duarte RTD, Cabral da Cruz AC, Wagner G, and Treichel H. 2020. Extremophile microbial communities and enzymes for bioenergetic application based on multi-omics tools. *Curr Genomics*., 21(4): 240–252. https://doi.org/10.2174/1389202921999200601144137.

Gallo G, Imbimbo P, and Aulitto M. 2024. The undeniable potential of thermophiles in industrial processes. *Int J Mol Sci*., **25(14):** 7685. https://doi.org/10.3390/ijms25147685.

Gandhi S, Salleh AB, Raja Abd Rahman RNZ, Leow TC, and Oslan SN. 2015. Expression and characterization of *Geobacillus stearothermophilus* SR74 recombinant α-amylase in *Pichia pastoris*. *Biomed Res Int*., **2015:** 529059. https://doi.org/10.1155/2015/529059.

Guta M, Abebe G, Bacha K and Cools P. 2024. Screening and characterization of thermostable enzyme-producing bacteria from selected hot springs of Ethiopia. *Microbiol Spectr*., **12(3):** e03710-23. https://doi.org/10.1128/spectrum.03710-23.

Hugenholtz P, Pitulle C, Hershberger KL, and Pace NR. 1998. Novel division level bacterial diversity in a Yellowstone hot spring. *J Bacteriol*., **180(2):** 366–376. https://doi.org/10.1128/jb.180.2.366-376.1998.

Hussein EI, Jacob JH, Shakhatreh MAK, Abd Al-razaq MA, Juhmani ASF, and Cornelison CT. 2017. Exploring the microbial diversity in Jordanian hot springs by comparative metagenomic analysis. *MicrobiologyOpen*., **6(6):** 1–8. https://doi.org/10.1002/mbo3.521.

Hutchens E. 2009. Microbial selectivity on mineral surfaces: possible implications for weathering processes. *Fungal Biol Rev*., **23(4):** 115–121. https://doi.org/10.1016/j.fbr.2009.10.002.

Jacob JH, Hussein EI, Shakhatreh MAK, and Cornelison CT. 2017. Microbial community analysis of the hypersaline water of the Dead Sea using high-throughput amplicon sequencing. *Microbiologyopen*., **6(5):** 1–6.https://doi.org/10.1002/mbo3.500.

Kapinusova G, Lopez Marin MA, and Uhlik O. 2023. Reaching unreachables: obstacles and successes of microbial cultivation and their reasons. *Front Microbiol*., **14:** 1–18. https://doi.org/10.3389/fmicb.2023.1089630.

Kochhar N, Kavya IK, Shrivastava S, Ghosh A, Rawat VS, Sodhi KK, and Kumar M. 2022. Perspectives on the microorganism of extreme environments and their applications. *Curr Res Microb Sci*., **3:** 100134. https://doi.org/10.1016/j.crmicr.2022.100134.

Kumar N, Tripathi K and Srivastava Y. 2025. Composition, optimization, and preparation of culture media for microbiological and biotechnological. In: Sharma R and Verma S (Eds.), **Biotechnology Lab Techniques: Culture Media, Microscopy, and Microbial Analysis**. Deep Science Publishing, India, pp. 19–34. https://doi.org/10.70593/978-93-49307-52-0_3

Li J, Sun L and Huo YX. 2025. High-temperature catalytic platform powered by thermophilic microorganisms and thermozymes. *Synth Biol Eng*., **3(1):** 10001.

https://doi.org/10.70322/sbe.2025.10001.

Makowski K, Leszczewicz M, Broncel N, Lipińska-Zubrycka L, Głębski A, Komorowski P, and Walkowiak B. 2021. Isolation,

biochemical characterisation and identification of thermotolerant and cellulolytic *Paenibacillus lactis* and *Bacillus licheniformis*. *Food Technol Biotechnol*., **59(3):** 325–336. https://doi.org/10.17113/ftb.59.03.21.7096.

Malkawi HI, and Al-Omari MN. 2010. Approaches to study the bacterial and archaeal diversity from Jordanian hot springs. *Afr J Microbiol Res*., **4(10):** 923–932.

Mehta R, Singhal P, Singh H, Damle D, and Sharma AK. 2016. Insight into thermophiles and their wide-spectrum applications. *3 Biotech*., **6(1):** 81. https://doi.org/10.1007/s13205-016-0368-z.

Mohammad BT, Al Daghistani HI, Jaouani A, Abdel-Latif S, and Kennes C. 2017. Isolation and characterization of thermophilic bacteria from Jordanian hot springs: *Bacillus licheniformis* and *Thermomonas hydrothermalis* isolates as potential producers of thermostable enzymes. *Int J Microbiol*., **2017(1):** 6943952.

https://doi.org/10.1155/2017/6943952.

Mouné S, Caumette P, Matheron R, and Willison JC. 2003. Molecular sequence analysis of prokaryotic diversity in the anoxic sediments underlying cyanobacterial mats of two hypersaline ponds in Mediterranean salterns. *FEMS Microbiol Ecol*., **44(1):** 117–130. https://doi.org/10.1016/S0168-6496(03)00017-5.

Narsing Rao MP, Liu L, Jiao JY, Xiao M, and Li WJ. 2018. Extremophiles in Eurasian ecosystems: ecology, diversity, and applications. In: Wani PA and Yadav SK (Eds.), **Extremophiles in Eurasian ecosystems: ecology, diversity, and applications**. Springer, Singapore, pp. 19–43. https://doi.org/10.1007/978-981-13-0329-6_2

Obeidat M, and Al-Shomali B. 2023. Moderately thermophilic bacteria from Jordanian hot springs as possible sources of thermostable enzymes and leukemia cytotoxic agents. ***Jordan Journal of Biological Sciences***., **16(3):** 413–424.

https://doi.org/10.54319/jjbs/160304.

Ortega-Villar R, Escalante A, Astudillo-Melgar F, Lizárraga-Mendiola L, Vázquez-Rodríguez GA, Hidalgo-Lara ME, and Coronel-Olivares C. 2024. Isolation and characterization of thermophilic bacteria from a hot spring in the state of Hidalgo, Mexico, and geochemical analysis of the thermal water. *Microorganisms*., **12(6):** 1066. https://doi.org/10.3390/microorganisms12061066.

Pinevich AV, Andronov EE, Pershina EV, Pinevich AA, and Dmitrieva HY. 2018. Testing culture purity in prokaryotes: criteria and challenges. *Antonie Van Leeuwenhoek*., **111(9):**

1509–1521.https://doi.org/10.1007/s10482-018-1054-4.

Radaideh QM, Malkawi HI, Al-Omari M, and Al-Deeb TM. 2010. Biochemical and molecular characterization of thermophilic enzymes of bacterial strains isolated from Jordanian hot springs. *World Appl Sci J*., **8(6):** 725–735.

Romano I, Vitiello G, Gallucci N, Di Girolamo R, Cattaneo A, Poli A, and Di Donato P. 2022. Extremophilic microorganisms for the green synthesis of antibacterial nanoparticles. *Microorganisms*, **10(10):** 1885. https://doi.org/10.3390/microorganisms10101885.

Schäffer R, and Sass I. 2014. The thermal springs of Jordan. *Environ Earth Sci*., **72(1):** 171–187. https://doi.org/10.1007/s12665-013-2944-4.

Schallmey M, Singh A, and Ward OP. 2004. Developments in the use of *Bacillus* species for industrial production. *Can J Microbiol*., **50(1):** 1–17. https://doi.org/10.1139/w03-076

Shakya P, Nayak A, Rai A, Singh RP and Garg A. 2025. Unveiling the heat-loving microheroes – A deep dive into the world of thermophilic bacteria: A review. *Res J Biotech.*, **20(6):** 165–174. https://doi.org/10.25303/206rjbt1650174.

Shomali BA and Danish-Daniel M. 2024. Review on bioprospecting of thermophilic enzymes from hot springs via Omics approaches. *Aquac Aquar Conserv Legis.*, **17(5):** 2156–2174.

Tamura K, Stecher G, and Kumar S. 2021. MEGA11: Molecular Evolutionary Genetics Analysis version 11. *Mol Biol Evol*., **38(7):** 3022–3027. https://doi.org/10.1093/molbev/msab120.

Ulucay O, Gormez A, and Ozic C. 2022. Identification, characterization and hydrolase producing performance of thermophilic bacteria: geothermal hot springs in the eastern and southeastern Anatolia regions of Turkey. *Antonie Van Leeuwenhoek.*, **115(2):** 253–270. https://doi.org/10.1007/s10482-021-01678-5.

Verma J, Sourirajan A, and Dev K. 2022. Bacterial diversity in 110 thermal hot springs of Indian Himalayan Region (IHR). *3 Biotech*., **12(9):** 238. https://doi.org/10.1007/s13205-022-03270-8.

Wolella EK, and Tilahun B. 2020. Isolation and characterization of extremophiles from Shalla/Abidjata hot springs, Ethiopia. *Acta Sci Microbiol*., **3(2):** 1–5.

Yohandini H, Julinar, and Muharni. 2015. Isolation and phylogenetic analysis of thermophile community within Tanjung Sakti hot spring, South Sumatera, Indonesia. *Hayati J Biosci*., **22(3):** 143–148. https://doi.org/10.1016/j.hjb.2015.10.006.

Yin YR, Zhou EM, Ming H, Hozzein WN, Ahmed I, Jiang H and Li WJ. 2024. Thermophilic glycoside hydrolase from hot-spring microorganisms and its mechanism of high-temperature adaptation. *Front Microbiol*., **15:** 1448900. https://doi.org/10.3389/fmicb.2024.1448900.

Yoshizaki F, Oshima T, and Imahori K. 1971. Studies on phosphoglucomutase from an extreme thermophile, *Flavobacterium thermophilum* HB8. I. Thermostability and other enzymatic properties. *J Biochem*., **69(6):** 1083–1089. https://doi.org/10.1093/oxfordjournals.jbchem.a129561.

Zhao J, Yang W, Cai H, Cao G and Li Z. 2025. Current progress and future trends of genomics-based techniques for food adulteration identification. *Foods*, **14(7):** 1116. https://doi.org/10.3390/foods14071116.

Zheng S, Shao M, Wang W and Chen G-Q. 2025. Next-generation biotechnology inspired by extremes: The potential of extremophile organisms for synthetic biology and for more efficient and sustainable biotechnology. EMBO Rep., **26(5):** 1191–1195.

JJBS

Volume 19, Number 1,March 2026
ISSN 1995-6673
Pages 147 – 157
https://doi.org/10.54319/jjbs/190114

Jordan Journal of Biological Sciences

Exploring the Antioxidant, Anti-inflammatory, Antibacterial, and Antibiofilm Potential of *Matricaria pubescens* Extracts Through *In Vitro* and Computational Molecular Interactions

Houssem Chenna[1,2,*], Manel Lina Djendi[2], Chahrazed Benzaid[3], Riadh Badraoui[4,5], Gokhan Zengin[6], Mustafa Abdullah Yilmaz[7,8], Oguz CAKIR[7,9] Chaouki Djouder[2], Imen Halimi[2], Mongi Saoudi[10], Mahieddine Boumendjel[2], Amel Boumendjel[2], Mahfoud Messarah[2]

[1]*Pharmaceutical Sciences Research Center (CRSP), Constantine 25000, Algeria;* [2]*Laboratory of Biochemistry and Environmental Toxicology, Department of Biochemistry, Faculty of Sciences, University of Badji Mokhtar, BP 12 Sidi Amar, Annaba, Algeria;* [3]*Microbiology and Molecular Biology Laboratory, Department of Biochemistry, Faculty of Sciences, University of Badji Mokhtar, BP 12 Sidi Amar, Annaba, Algeria;* [4]*Laboratory of General Biology, Department of Biology, University of Ha'il, 81451 Ha'il, Saudi Arabia; Section of Histology–Cytology, Medicine Faculty of Tunis, University of Tunis El Manar, 1007 La Rabta, Tunis, Tunisia;* [6] *Laboratory of Physiology and Biochemistry, Department of Biology, Science Faculty, Selcuk University, Konya, 42130, Turkey;* [7]*Dicle University Science and Technology Research and Application Center, 21280, Diyarbakir, Turkey;* [8]*Dicle University, Faculty of Pharmacy, Department of Analytical Chemistry, 21280, Diyarbakir, Turkey;* [9]*Dicle University, Faculty of Health Sciences, Department of Nutrition and Dietetics, 21280, Diyarbakir, Turkey;* [10]*Animal Ecophysiology Laboratory, Sciences Faculty of Sfax, University of Sfax, Sfax, Tunisia.*

Received: June 2, 2025; Revised: July 30, 2025; Accepted: August 24, 2025

Abstract

Matricaria pubescens, a medicinal plant endemic to the Algerian Sahara, is traditionally used for treating various ailments. This study explored its potential as a source of natural antioxidants and antibacterial agents, with particular relevance to antimicrobial resistance. The ethanolic extract, rich in polyphenols and flavonoids, demonstrated strong antioxidant and anti-inflammatory activities, as well as notable antibacterial effects, with *Staphylococcus aureus* being the most sensitive strain. Both ethanolic and aqueous extracts effectively inhibited bacterial and fungal biofilms, with inhibition rates reaching up to 89.73% and 70.14%, respectively. Computational analysis further confirmed the strong binding affinities of *M. pubescens* bioactive compounds to key molecular targets, supporting the *in vitro* findings. These results highlight the pharmacological potential of *M. pubescens*, reinforcing its traditional use and positioning it as a promising candidate in the search for alternative therapies against antimicrobial resistance.

Keywords: *Matricaria pubescens*, Antioxidant, Anti-inflammatory, Antibacterial, Antibiofilm, Molecular interactions

1. Introduction

Antibiotic resistance has emerged as one of the greatest threats to global public health, driven largely by the overuse, misuse, and inappropriate prescription of antimicrobial agents (Machado *et al.,* 2023; Guedes *et al.*, 2024). Pathogenic bacteria have developed a wide range of mechanisms to counteract the effects of antibiotics, significantly reducing their efficacy and making infections increasingly difficult to manage (Abd El Aty *et al.,* 2023; Sett *et al.,* 2024). Among these resistance mechanisms, bacterial biofilm formation is particularly concerning. Biofilms are complex and highly protective structures that enable bacteria to persist in hostile environments, evade immune defenses, and exhibit increased tolerance to antimicrobial treatments (Prima *et al.,* 2023; Tue *et al.*, 2024).

The rapid rise of antimicrobial resistance necessitates the urgent exploration of alternative strategies. Medicinal plants, owing to their vast diversity of bioactive compounds, offer a promising source for the development of new broad-spectrum antimicrobial agents (Ahmed-Gaid *et al.,* 2025a; Hanoun *et al.,* 2025a; Hanoun *et al.,* 2025b). Unlike conventional antibiotics that typically target a single bacterial process, plant extracts contain multiple phytochemicals capable of acting on different cellular pathways, thereby limiting bacterial adaptation and reducing the risk of resistance (Seukep *et al.,* 2023).

Matricaria pubescens (Fig. 1) is an endemic North African plant species belonging to the Asteraceae family. It is locally known as *guartoufa* or *Ouazouaza*, names derived from its slightly pungent and spicy taste, a distinctive characteristic noted by Saharan communities (Kherraz *et al.,* 2019a; Ahmed-Gaid *et al.,* 2025b). According to the Integrated Taxonomic Information System, *M. pubescens* is classified within the kingdom *Plantae*, phylum *Angiosperms*, class *Eudicots*, order *Asterales*, family *Asteraceae*, and genus *Matricaria* (Elhasnaoui *et al.,* 2025). Traditionally, this plant has been

* Corresponding author. e-mail: chenna_houssem39@yahoo.com; houssem.chenna@crsp.dz.

widely used to treat a variety of ailments, including rheumatic and muscular pain, scorpion stings, dysmenorrhea, dehydration, coughs, allergies, eye disorders, toothaches, and cardiovascular, digestive, and genitourinary conditions (Chenna *et al.*, 2025). Its broad therapeutic potential is attributed to its rich phytochemical composition. Our previous research identified 32 phytochemical compounds in *M. pubescens* extracts using LC-MS/MS, which exhibit significant antimicrobial, antioxidant, anti-inflammatory, antidiabetic, and antihyperlipidemic activities (Kherraz *et al.*, 2019b; Amssayef *et al.*, 2020; Chenna *et al.*, 2024).

This study aimed to evaluate the activity of the aqueous and ethanolic extracts of *M. pubescens* against pathogenic strains. It focuses on examining the biological characteristics of these two extracts, with an emphasis on evaluating their antimicrobial, anti-biofilm, antioxidant, and anti-inflammatory properties through *in vitro* and *in silico* methods using combined in vitro and computational assays by targeting human peroxiredoxin 5 (1H2D), TyrRS from *S. aureus* (1JIJ), and cyclooxygenase 2 (1CX2).

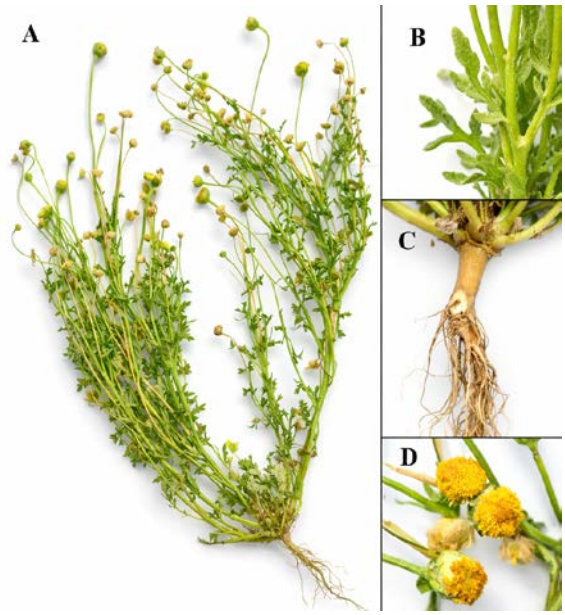

Figure 1. Parts of *M. pubescens*: (A) Whole plant; (B) Leaves; (C) Root; (D) Flower.

2. Materials and methods

2.1. Plant material

The aerial parts (leaves, stem, and flowers) of M. pubescens were collected during flowering in April 2022 from Elhamraya, EL-Oeud region (Algerian Sahara). The plant was identified by Tarek Hamel, a botany professor at Badji Mokhtar Annaba University. A plant specimen was deposited at the Laboratory of Botany, Algiers, Algeria, with voucher number Hv644 (Metrouh-Amir *et al.*, 2015). After the collection, the plant was cleaned, dried in the dark at room temperature, and ground with a mechanical grinder to obtain fine powder

2.2. Preparation of extracts

The aerial parts of *M. pubescens* (10 g) were macerated in 100 ml of each solvent (ethanol and distilled water) at room temperature for 24 hours. After filtration, the solution was evaporated to dryness under reduced pressure using a rotary evaporator (IKA® RV10) connected to a Buchi V-700 vacuum pump at 40°C. The weighed dry residues of the aqueous and ethanolic extract of *M. pubescens* were stored at 4°C in the dark until phytochemical analysis (Yilmaz *et al.*, 2023).

2.3. Total Phenolic and Flavonoid Contents

Total phenolic content was determined using the Folin–Ciocalteu method (Uysal et al., 2017). Briefly, 0.25 ml of extract solution (1 mg/ml) was mixed with 1 ml of diluted Folin–Ciocalteu reagent (1:9, v/v) and shaken vigorously. After 3 min, 75 µL of Na_2CO_3 (0.1%) was added, and the absorbance was recorded at 760 nm following 2 h incubation at room temperature. Results were expressed as mg gallic acid equivalents per g of extract (mg GAE/g).

Total flavonoid content was measured using the $AlCl_3$ colorimetric assay (Ak et al., 2020). One ml of extract solution (1 mg/ml) was mixed with 1 ml of 2% $AlCl_3$ in methanol. A blank was prepared with methanol instead of $AlCl_3$. After 10 min of incubation at room temperature, the absorbance was measured at 415 nm. Flavonoid content was expressed as mg rutin equivalents per g of extract (mg RE/g).

2.4. Antioxidant Activity Assays

2.4.1. DPPH Radical Scavenging Assay

DPPH activity was determined following Mahomoodally et al. (2021). One ml of extract (1 mg/ml) was added to 4 ml of 0.004% DPPH solution in methanol. After 30 min of incubation in the dark, absorbance was read at 517 nm. Results were expressed as mg Trolox equivalents per g of extract (mg TE/g).

2.4.2. $ABTS^+$ Radical Scavenging Assay

$ABTS^+$ solution was prepared by mixing 7 mM ABTS with 2.45 mM potassium persulfate and incubating in the dark for 12–16 h (AL-Hmadi et al., 2023). The solution was then diluted with methanol to an absorbance of 0.700 ± 0.02 at 734 nm. 1 ml of extract (1 mg/ml) was mixed with 2 ml of $ABTS^+$ solution, and the absorbance was measured at 734 nm after 30 min. Results were expressed as mg TE/g.

2.4.3. CUPRAC Assay

CUPRAC activity was assessed according to Ak et al. (2020). A reaction mixture containing 0.5 ml extract (1 mg/ml), 1 ml $CuCl_2$ (10 mM), 1 ml neocuproin (7.5 mM), and 1 ml ammonium acetate buffer (1 M, pH 7.0) was incubated for 30 min at room temperature. Absorbance was measured at 450 nm, and results were expressed as mg TE/g.

2.5. Anti-Inflammatory Activity

Protein denaturation inhibition was tested following Rahman et al. (2012) using bovine serum albumin (BSA).

- Test solution (500 µL): 450 µL of 0.5% BSA + 50 µL extract (from 2.5 mg/ml stock).
- Control solution (500 µL): 450 µL 0.5% BSA + 50 µL distilled water.

- Product control (500 µL): 450 µL distilled water + 50 µL extract.
- Standard solution (500 µL): 450 µL 0.5% BSA + 50 µL diclofenac sodium (variable concentrations).

Absorbance was measured at 660 nm, and the percentage inhibition of protein denaturation was calculated using the formula

% inhibition = [(Abs Negative control - Abs Sample)/Abs Negative control] x 100

2.6. Antimicrobial activity

The antimicrobial efficacy of the extracts was evaluated using the agar well diffusion technique against various pathogenic bacteria and fungi, including three Gram-negative bacteria: *Acinetobacter baumannii, Klebsiella pneumoniae, and Pseudomonas aeruginosa*; two Gram-positive bacteria: *Enterococcus faecium* and *Staphylococcus aureus*; as well as two yeast species from the genus Candida: *Candida albicans* and *Candida tropicalis*. After aseptically creating wells of eight millimeters in diameter on Muller Hinton and Sabouraud agar using sterilized glass beads, these wells were loaded with 100 µl of the test samples dissolved in dimethyl sulfoxide (DMSO) at a concentration of 5 mg/ml each (Bouyahya *et al.*, 2017).

A microbial suspension was prepared from an 18-24-hour pure culture and adjusted to an optical density between 0.08 and 0.1 at 600 nm, corresponding to (1 x 10^8 CFU/ml) according to the McFarland scale (Boughendjioua 2017). DMSO was used as the negative control, while the positive controls consisted of antibiotics (amoxicillin-clavulanic acid (AMC30) and amikacin (AK10) and an antifungal agent (amphotericin B (AM-B)). After 24 hours of incubation at 37°C, the antimicrobial effect was measured by evaluating the diameter of the zone of inhibition (DZI).

2.7. Determination of minimum inhibitory concentration (MIC)

Minimum inhibitory concentrations (MICs) of the extracts were established by microdilution in 96-well curved-bottom microplates. In each microcupule, 100µl of decimal dilutions of the extracts in DMSO were introduced, followed by the addition of 100µl of microbial inoculum prepared in Muller Hinton broth for bacteria and Sabouraud broth for yeast (at 10^8 CFU/ml according to the McFarland scale). The positive control comprised a microbial suspension without any additional substances, while the antibiotics to which the strains were sensitive served as the antibacterial reference. After incubation from 18h to 24h, the MIC is determined from the first well where no visible growth is observed with the naked eye (Rahmoun *et al.*, 2010).

2.8. Inhibition of biofilm formation

To illustrate the power of extracts to inhibit biofilm formation in our isolates, the standard method of Cristal Violet staining on a 96-well microplate was adopted, using extracts at MIC concentrations (Musk *et al.*, 2005). Absorbance was measured at 570 nm using a microplate reader.

Inhibition of biofilm formation was calculated using the following formula:

%= [(Abs of negative control - Abs of test) / Abs of negative control] x100

2.9. Computational Study

The phytochemical compounds of *M. pubescens*, recently identified in our previous study (Chenna *et al.*, 2024), were utilised in the in-silico investigation. The phytochemical profile comprised the following compounds: (1) Quinic acid, (2) Fumaric acid, (3) Aconitic acid, (4) Gallic acid, (5) Protocatechuic acid, (6) Chlorogenic acid, (7) Protocatechuic aldehyde, (8) Tannic acid, (9) 4-Hydroxybenzoic acid, (10) Caffeic acid, (11) Vanillin, (12) *p*-Coumaric acid, (13) Ferulic acid, (14) Coumarin, (15) Salicylic acid, (16) Luteolin-7-O-glucoside, (17) Rutin, (18) Isoquercitrin, (19) Hesperidin, (20) *o*-Coumaric acid, (21) Rosmarinic acid, (22) Cosmosiin, (23) Astragalin, (24) Nicotiflorin, (25) Quercetin, (26) Naringenin, (27) Luteolin, (28) Genistein, (29) Kaempferol, (30) Apigenin, (31) Chrysin, and (32) Acacetin.

The potential antioxidant, antibacterial, and anti-inflammatory effects of *M. pubescens* compounds were evaluated through computational modelling and interaction assays. The crystal structures of human peroxiredoxin 5 (1H2D), TyrRS from *S. aureus* (1JIJ), and cyclooxygenase-2 (1CX2) were retrieved from the RCSB Protein Data Bank, and their active sites were targeted to assess molecular interactions. The 3D structures of the identified phytochemicals were obtained from the PubChem database or drawn using ChemDraw. All compounds and receptors were prepared using the CHARMm force field, as previously described (Badraoui et al., 2023; Boudjema et al., 2024; Rahmouni et al., 2024), by removing water molecules and adding polar hydrogens and Kollman charges. Bond interactions and binding scores were analysed following established protocols (Jedli et al., 2022; Mhadhbi et al., 2023; Chira et al., 2024). The choice of 1H2D, 1JIJ, and 1CX2 was based on their known roles in antioxidant, antibacterial, and anti-inflammatory pathways (Aldarhami et al., 2023; Boudjema et al., 2024).

2.10. Statistical Analysis

All analyses were performed in three technical replicates (n = 3), and results are expressed as mean ± standard deviation (mean ± SD). Comparisons between means were conducted using one-way ANOVA followed by Tukey's post hoc test, with differences considered significant at $p < 0.05$. Statistical analyses were carried out using GraphPad Prism version 9.0.0 (GraphPad Software, San Diego, CA, USA).

3. Results and discussion

The extraction of phytochemical compounds from the aqueous and ethanolic extracts of *M. pubescens* was performed by maceration for 24 hours, as shown in Table 1. It was observed that the aqueous extract yielded a higher amount compared to the ethanolic extract (17.54% *vs.* 7.37%, respectively). Additionally, the results of total polyphenol and total flavonoid assays revealed that the ethanolic extract contains a higher concentration of total polyphenols and flavonoids (17.67±0.29 mg GAE/g and 21.79±0.02 mg RE/g, respectively) compared to the

aqueous extract (12.01±0.20 mg GAE/g and 0.16±0.04 mg RE/g, respectively). These results align with the studies conducted by Metrouh-Amir *et al.,* (2015), who reported that the ethanolic extract is richer in polyphenols and flavonoids than the aqueous extract.

Table 1. Extraction yield, total polyphenol, and total flavonoid contents of aqueous (AEMP) and ethanolic (EEMP) extracts of *M. pubescens*.

Extract	Yield	Total polyphenol content (mg GAE/g)	Total flavonoid content (mg RE/g)
EEMP	7.37%	17.67±0.29[a]	21.79±0.02[a]
AEMP	17.54 %	12.01±0.20[b]	0.16±0.04[b]

Values are presented as mean ± SD of three technical replicates (n = 3). Means in a column with different letters are significantly different ($p < 0.05$, one-way ANOVA followed by Tukey's post hoc test). GAE: Gallic acid equivalent; RE: Rutin equivalent.

The antioxidant activity of *M. pubescens* extracts was evaluated *in vitro* using three methods to determine their radical scavenging ability by DPPH and ABTS test, and their reducing power by the CUPRAC method. Results are shown in fig. 2.

DPPH and ABTS are among the most widely used stable free radicals for testing the anti-free radical activity of antioxidants, due to their rapidity and simplicity. The principle of this technique is based on the reduction of the violet-colored DPPH radical and the blue-colored ABTS to non-radical compounds. The discoloration of the mixture is proportional to the concentration of the antioxidant (Karagecili *et al.,* 2023). Our results showed that the aqueous and ethanolic extracts of *M. pubescens* exhibit potent antiradical activity (DPPH: 21±0.77; 14.19±0.70mg ET/g and ABTS: 76.15±1.10; 64.88±1.41mg ET/g, respectively), with strong antiradical activity in the aqueous extract.

The reducing power of *M. pubescens* aqueous and ethanolic extracts was assessed using the CUPRAC method. This method is based on the ability of antioxidants to reduce divalent cupric ions (Cu^{2+}) to monovalent cupric cations (Cu^{+}) (AL-Hmadi *et al.,* 2023). The results obtained show that the ethanolic and aqueous extracts of *M. pubescens* exhibit potent reducing power (74.37±1.01 mg ET/g; 42.08±0.23 mg ET/g, respectively), with a higher reducing power for the ethanolic extract.

These results indicated that the aqueous and ethanolic extracts of *M. pubescens* possess strong antioxidant activity, enabling them to neutralize free radicals due to their richness in phytochemical compounds. These compounds can neutralize free radicals by donating an electron or a hydrogen atom to various reactive species of oxygen, nitrogen, or chlorine. This reduces molecular damage caused by oxidative stress and helps preserve human health (Altay *et al.,* 2022; Karatas *et al.,* 2022; Chenna *et al.,* 2024). These findings align with the antioxidant activity results of *M. pubescens* reported in previous studies (Kherraz *et al.,* 2019; Metrouh-Amir and Amir 2023).

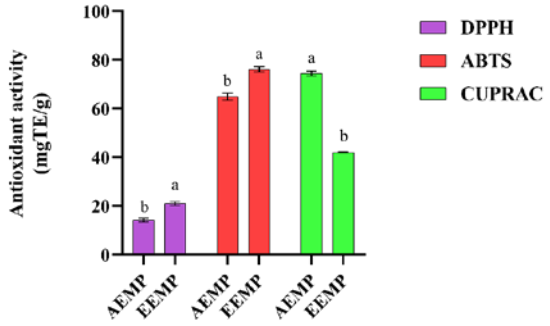

Figure 2. Antioxidant activity of aqueous (AEMP) and ethanolic (EEMP) extracts of *M. pubescens*. Data are expressed as mean ± SD from three technical replicates (n = 3). Different superscript letters (a, b) within the same method indicate significant differences between samples ($p < 0.05$, one-way ANOVA followed by Tukey's post hoc test).

The results of the *in vitro* evaluation of the anti-inflammatory properties of the extracts are shown in Fig. 3. The studied extracts showed strong dose-dependent inhibitory activity on heat-induced albumin denaturation. The Aqueous and ethanolic extracts of *M. pubescens* were particularly active, protecting BSA against heat denaturation by 26.57 ± 4.45% and 40.18 ± 2.40%, respectively, at the lowest concentration (125 µg/ml). At the highest concentration (2.5 mg/ml), a protective effect of 78.49 ± 3.58% and 84.17 ±5.01% was obtained with Aqueous and ethanolic extracts of *M. pubescens*, respectively, compared with diclofenac, which exerted an inhibitory activity of 40.45±0.15% at the lowest dose and better activity of 95±0.08% at the high dose. These findings are consistent with those reported by Bouden *et al.,* (2017). The protective effect of these extracts against BSA denaturation is due to their richness in polyphenols and flavonoids such as caffeic acid, chlorogenic acid, génistéine and luteolin 7-O-glucoside, which were previously identified in these extracts and exhibit remarkable anti-inflammatory properties through various mechanisms (Al-Khayri *et al.,* 2022, Ahammed *et al.,* 2023; Chenna *et al.,* 2024).

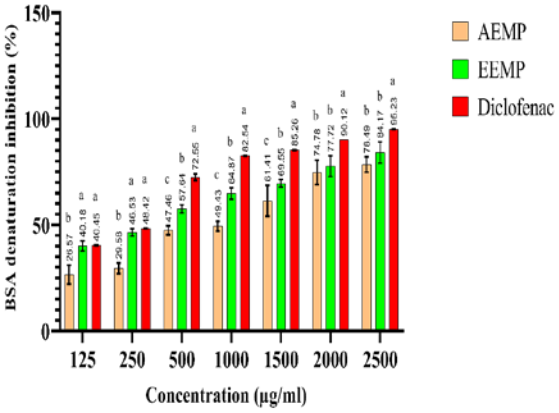

Figure 3. In vitro anti-inflammatory activity of aqueous (AEMP) and ethanolic (EEMP) extracts of *M. pubescens*, and diclofenac, determined by the BSA denaturation assay. Percentage inhibition of protein denaturation was measured spectrophotometrically at 660 nm. Data are expressed as mean ± SD from three technical replicates (n = 3). Different superscript letters (a, b, c) within the same concentration indicate significant differences between samples ($p < 0.05$, one-way ANOVA followed by Tukey's post hoc test).

The results of the antimicrobial activity of these extracts are summarized in Table 2. The results were evaluated against established reference criteria (Bouyahya *et al.,* 2017).

- A weak interaction (zone of inhibition ≤ 12 mm);
- An intermediate interaction (12 mm < zone of inhibition ≤20 mm);
- A sensitive interaction (zone of inhibition >20 mm).

The data in Table 2 revealed inhibition zone diameters ranging from 12 to 14 mm for the aqueous extract and from 12.5 to 18 mm for the ethanolic extract. The minimum inhibitory

concentrations vary between 7.81 and 500 µg/ml. However, it is important to note that *E. faecium* showed clear resistance to both extracts, while *S. aureus* was identified as the most sensitive strain to the extracts. For the fungal strains, *C. albicans* was the only one showing sensitivity to the ethanolic extract, with an inhibition zone diameter of 13 mm and an MIC of 500 µg/ml, in contrast to *C. tropicalis*, which was resistant.

The results regarding the sensitivity of the strains to reference antimicrobials showed significant resistance among the examined strains, with the exception of *P. aeruginosa*, which exhibited sensitivity to amikacin. The inhibition zone diameter was measured at 19 mm, with MIC of 250 µg/ml.

The extracts of *M. pubescens* had an effect on both Gram-positive and Gram-negative bacteria, as well as on *C. albicans*, with a particularly notable effect observed with the ethanolic extract. Our results align with previous studies on the antimicrobial effects of these plant extracts, which confirm that the ethanolic extract demonstrated antimicrobial activity against various microbial strains, including *S. aureus*, *E. coli*, *P. aeruginosa*, and *C. albicans* (Makhloufi *et al.,* 2012; Maiza *et al.,* 2014; Nadji *et al.,* 2022). A previous study revealed the presence of chlorogenic, caffeic, p-coumaric, and tannic acids in both ethanolic and aqueous extracts of *M. pubescens*. These compounds are likely responsible for the antimicrobial effects observed, as they contribute to inhibiting bacterial proliferation by disrupting microbial cell walls and interfering with cellular processes (Chenna *et al.,* 2024; Kalinowska *et al.,* 2024).

Table 2. Antimicrobial activity of aqueous and ethanolic extracts of *M. pubescens*

Stains	Plant extracts				Antibiotics/ Antifungal			Control DMSO
	AEMP		EEMP		Code	DIZ (mm)	MIC (µg/ml)	
	DIZ (mm)	MIC (µg/ml)	DIZ (mm)	MIC (µg/ml)				
Baumannii	12±0.2	250	16±0.2	62.5	AMC30	R	R	R
					AK10	R	R	
					AM-B	/	/	
K. pneumoniae	13.5±0.2	125	14±0.2	125	AMC30	R	R	R
					AK10	R	R	
					AM-B	/	/	
P. aeruginosa	12±0.2	500	12.5±0.2	500	AMC30	R	R	R
					AK10	19±0.2	250	
					AM-B	/	/	
E. faecium	R	R	R	R	AMC30	R	R	R
					AK10	20±0.2	250	
					AM-B	/	/	
S. aureus	14±0.2	15.63	18±0.2	7.81	AMC30	R	R	R
					AK10	R	R	
					AM-B	/	/	
C. albicans	R	R	13±0.2	500	AMC30	/	/	R
					AK10	/	/	
					AM-B	R	R	
C. tropicalis	R	R	R	R	AMC30	/	/	R
					AK10	/	/	
					AM-B	R	R	

Data are expressed as mean ± SD from three technical replicates (n = 3). **AEMP:** Aqueous Extract; **EEMP:** Ethanolic Extract; **AK10:** Amikacin; **AMC30:** Amoxicillin/Clavulanic Acid; **AM-B:** Amphotericin B; **DMSO:** Dimethyl Sulfoxide; **DIZ:** Diameter of Inhibition Zone; **MIC:** Minimum Inhibitory Concentration; **R**: resistant.

The results from the crystal violet staining indicated a notable reduction in biofilm formation among the analyzed bacterial and fungal strains (Fig. 4). Bacterial biofilm inhibition rates ranged from 35.36% to 89.73% with the aqueous extract and from 50.07% to 80.82% with the ethanolic extract, while fungal biofilm inhibition was recorded at 70.14%. Additionally, these results highlighted the remarkable efficacy of the extracts compared to the standard antibiotic, which showed only a 45.43% inhibition rate for *P. aeruginosa*.

Our results align with previous studies demonstrating that these extracts, rich in phenolic compounds such as

chlorogenic acid, protocatechuic acid, and vanillin, as well as flavonoids like quercetin and rutin, exhibit high antibiofilm activity (Salim *et al.,* 2023; Chenna *et al.,* 2024). These compounds reduce biofilm biomass, cell viability, and exopolysaccharide levels in biofilms, achieving more than 70% inhibition against *S. aureus* and *P. aeruginosa.* They affect bacterial adhesion and virulence gene expression and have significant antimicrobial activity against spoilage yeasts, disrupting biofilm formation and adhesion. This highlights their potential in preventing biofilm-associated infections (Kostić *et al.,* 2020; Kimani *et al.,* 2021; Ivanov *et al.,* 2022).

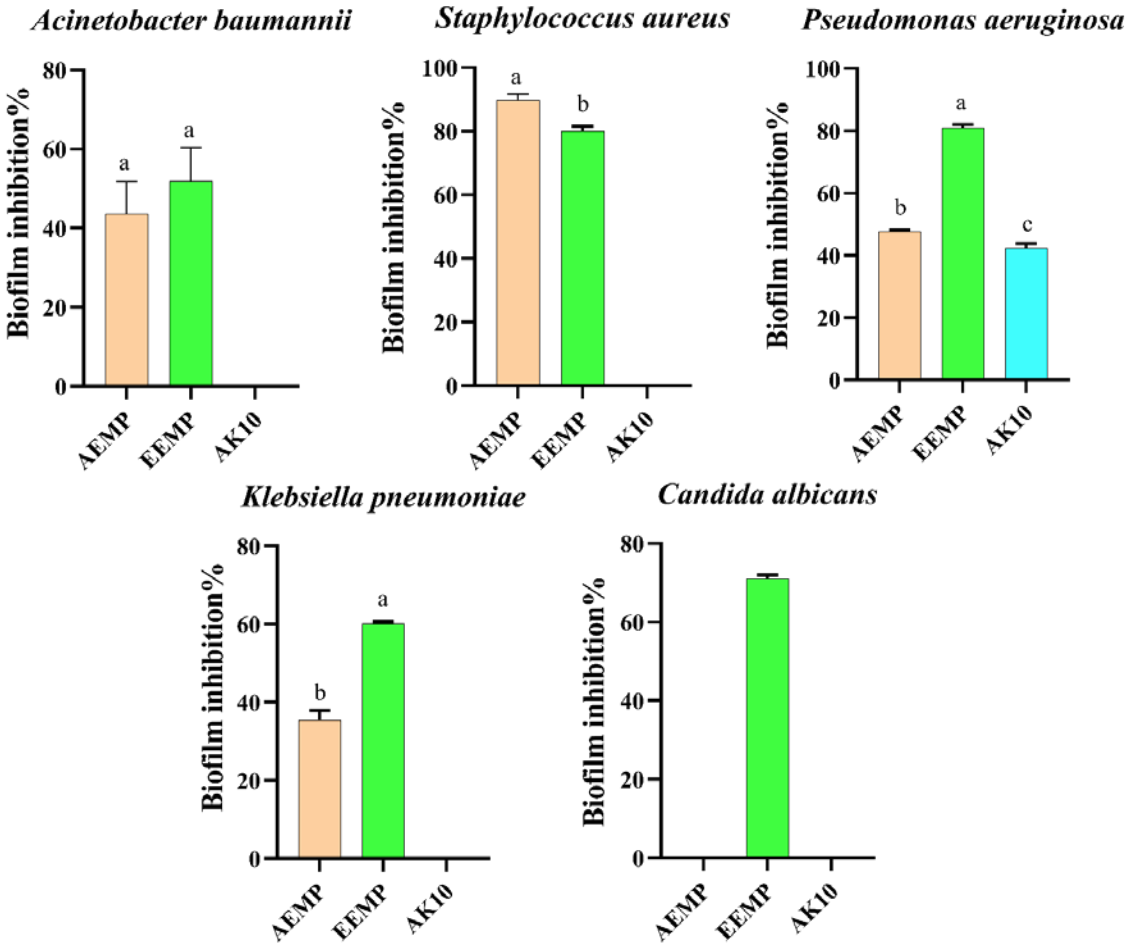

Figure 4. Inhibition of biofilm formation by aqueous (AEMP) and ethanolic (EEMP) extracts of *M. pubescens*, and amikacin (AK10), was evaluated using the crystal violet staining assay. Biofilm biomass was quantified by measuring absorbance at 570 nm. Data are expressed as mean ± SD from three technical replicates (n = 3). Different superscript letters (a, b, c) indicate significant differences between samples ($p < 0.05$, one-way ANOVA followed by Tukey's post hoc test).

In view of the potent antioxidant, anti-inflammatory, antibacterial, and anti-biofilm activities of the aqueous and ethanolic extracts of *M. pubescens*, we further investigated these effects through computational modelling and interaction assays using the phytochemicals previously identified. UHPLC-ESI-MS/MS analysis revealed 32 phytochemical compounds in total, with the ethanolic extract containing 30 and the aqueous extract 17 (Chenna et al., 2024) (Table 3), which aligns with the total polyphenol and flavonoid contents reported in Table 1.

M. pubescens compounds bound human peroxiredoxin 5 (1H2D), TyrRS from *S. aureus*(1JIJ), and cyclooxygenase 2 (1CX2) with acceptable affinities that reached –8.6, –11.2, and –12.6 kcal/mol for 1HD2, 1JIJ, and 1CX2, respectively (Table 3). Interestingly, all the 32 identified compounds within the *M. pubescens* extract possessed negative binding affinities for the different targeted receptors, which support their potential bioactivities. It has been shown that variation in binding affinities depends on the 3D chemical structure and geometry of the ligands (Chira *et al.,* 2024; Kraiem *et al.,* 2024). 4-OH, Benzoic acid was found to have the best binding affinities for the three targeted receptors (Fig. 5-6). The three compounds that have the best binding scores were further analyzed for bond category, molecular interactions, and deep embedding (Table 4). These compounds were predicted to establish good molecular interactions.

The molecular interactions included conventional H-bonds associated with a network of hydrophobic bonds. As previously described, such a rich network of bonds contributes to the stability of the ligand-receptor complex (Badraoui *et al.,* 2023; Ben Saad *et al.,* 2023; Rahmouni *et al.,* 2024). The established interactions concerned several key residues and deep embedding (<2.5 Å), which have been commonly reported to be associated with potential bioactivities, including anti-inflammatory, antiproliferative, antioxidant, and antimicrobial effects (Zammel *et al.,* 2021; Jedli *et al.,* 2022). Overall, our computational modeling results showed that the

antioxidant, antibacterial, and anti-inflammatory effects of *M. pubescens* compounds are thermodynamically possible. In the current study, these biological effects had already been reported using *in vitro* analyses. These findings supported the health promotion and promising benefits of natural-derived compounds and their phytotherapeutic potential (Akacha *et al.*, 2022; Bédoui *et al.*, 2024; Kraiem *et al.*, 2024).

Importantly, our work presents the first comparative analysis of aqueous versus ethanolic *M. pubescens* extracts for antimicrobial and antibiofilm efficacy using both *in vitro* and *in silico* approaches. While previous studies have generally reported antimicrobial activity, few have explored resistance profiles or directly compared multiple solvent extracts. In the context of rising antimicrobial resistance, the observed sensitivity of *S. aureus* and *P. aeruginosa* to plant-based extracts underscores the potential of traditional medicinal plants as alternative or complementary antimicrobial agents. Notably, few prior investigations have examined the antibiofilm activity of *M. pubescens*, particularly against both Gram-negative and Gram-positive bacteria, as well as yeasts. Our findings provide new evidence of its potent biofilm-inhibitory effects, especially from the ethanolic extract, which significantly reduced biofilm formation in *S. aureus* and *P. aeruginosa*. By integrating *in vitro* bioactivity assays with *in silico* modeling, this study delivers a deeper and more predictive insight into the therapeutic potential of *M. pubescens*, filling critical gaps left by previous investigations focused solely on phytochemical content or general antimicrobial activity. Given the growing concern over biofilm-associated infections and their role in antibiotic resistance, these results highlight *M. pubescens* particularly its ethanolic extract as a promising natural source of bioactive compounds for managing resistant pathogens and biofilm-related complications in clinical and food industry contexts.

Table 3. Binding energy and root mean square deviation (RMSD) of the compounds identified in *M. pubescens* extracts while complexed with human peroxiredoxin 5 (1H2D), TyrRS from *S. aureus* (1JIJ), and cyclooxygenase 2 (1CX2).

Compounds	UHPLC-ESI-MS/MS analysis			Binding energy (kcal/mol)			RMSD (lower-upper)		
	Rt	EEMP	AEMP	1H2D	1JIJ	1CX2	1H2D	1JIJ	1CX2
Quinic acid	3.0	+	+	–5.7	–7.2	–6.6	0.0-19.47	0.0-4.50	0.0-7.82
Fumaric aid	3.9	-	+	–4.4	–5.5	–4.8	0.0-26.63	0.0-6.01	0.0-29.82
Aconitic acid	4.0	-	+	–5.4	–5.5	–5.1	0.0-4.29	0.0-28.96	0.0-50.03
Gallic acid	4.4	+	+	–5.6	–7.3	–6.5	0.0-26.48	0.0-3.93	0.0-29.52
Protocatechuic acid	6.8	+	+	–4.9	–6.7	–6.0	0.0-27.59	0.0-26.64	0.0-23.77
Chlorogenic acid	8.4	+	+	–7.1	–8.6	–8.9	0.0-22.15	0.0-26.15	0.0-29.77
Protocatechuic aldehyde	8.5	+	+	–5.5	–7.1	–6.3	0.0-9.35	0.0-26.61	0.0-29.77
Tannic acid	9.2	+	-	–6.1	–6.9	–6.7	0.0-24.22	0.0-25.16	0.0-26.48
4-OH Benzoic acid	10.5	+	+	–8.6	–11.2	–12.6	0.0-26.31	0.0-6.47	0.0-32.85
Caffeic acid	12.1	+	-	–5.5	–7.3	–7.0	0.0-28.57	0.0-22.90	0.0-30.84
0Vanillin	13.9	+	+	–5.1	–6.2	–6.2	0.0-27.36	0.0-23.19	0.0-31.05
p-Coumaric acid	17.8	+	-	–5.2	–6.4	–7.1	0.0-27.84	0.0-25.62	0.0-24.56
Ferulic acid	18.8	+	+	–5.6	–6.9	–6.9	0.0-27.60	0.0-23.54	0.0-11.93
Coumarin	20.9	+	-	–5.2	–6.9	–7.6	0.0-28.80	0.0-23.74	0.0-29.08
Salicylic acid	21.8	+	+	–5.6	–6.7	–6.4	0.0-16.9	0.0-24.98	0.0-29.74
luteolin 7-O-glucoside	23.7	+	+	–7.4	–10.1	–10.2	0.0-25.27	0.0-3.54	0.0-30.29
Rutin	25.6	+	-	–7.9	–9.5	–9.1	0.0-30.51	0.0-21.38	0.0-32.79
isoquercitrin	25.6	+	-	–8.0	–8.6	–8.2	0.0-29.40	0.0-22.47	0.0-32.74
Hesperidin	25.8	+	-	–7.7	–10.5	–9.6	0.0-23.18	0.0-3.58	0.0-35.04
o-Coumaric acid	26.1	+	-	–5.9	–6.8	–6.7	0.0-27.55	0.0-24.96	0.0-27.71
Rosmarinic acid	26.6	+	-	–6.2	–7.6	–7.6	0.0-7.07	0.0-37.29	0.0-36.04
Cosmosiin	28.2	+	+	–7.3	–10.0	–10.1	0.0-30.57	0.0-21.67	0.0-32.36
Astragalin	30.4	+	-	–8.0	–7.5	–8.1	0.0-29.64	0.0-19.21	0.0-31.20
Nicotiflorin	30.6	+	-	–7.8	–8.7	–9.9	0.0-30.54	0.0-22.05	0.0-10.04
Quercetin	35.7	+	-	–6.8	–9.9	–8.9	0.0-8.65	0.0-2.77	0.0-30.06
Naringenin	35.9	+	-	–6.5	–9.4	–8.8	0.0-27.39	0.0-3.38	0.0-11.89
Luteolin	36.7	+	+	–7.0	–9.8	–9.4	0.0-28.55	0.0-3.75	0.0-10.29
Genistein	36.9	+	-	–6.5	–9.0	–8.9	0.0-20.73	0.0-24.14	0.0-8.42
Kaempferol	37.9	+	-	–6.6	–9.4	–8.5	0.0-7.11	0.0-24.06	0.0-32.63
Apigenin	38.2	+	+	–6.6	–9.4	–9.0	0.0-21.76	0.0-8.41	0.0-9.80
Chrysin	40.5	+	+	–6.4	–9.2	–9.3	0.0-30.13	0.0-23.36	0.0-32.80
Acacetin	40.7	+	+	–6.6	–9.5	–9.1	0.0-28.95	0.0-25.38	0.0-25.63

AEMP: Aqueous Extract of *M. pubescens*, **EEMP:** Ethanolic Extract of *M. pubescens*, +/-: detected/ not detected, Human peroxiredoxin 5 (1H2D), TyrRS from *S. aureus* (1JIJ), Cyclooxygenase 2 (1CX2).

Table 4. Number of Hydrogen bonds and closest interacting residues for the compounds identified in *M. pubescens* that possessed the best binding scores with human peroxiredoxin 5 (1H2D), TyrRS from *S. aureus* (1JIJ), and cyclooxygenase 2 (1CX2).

Compound (Affinity)	No. H-Bond	Closest Interacting Residues	
		Residue (Letters & ID)	Distance to closest Interacting Residue (Å)
Human peroxiredoxin 5 (pdb id: 1HD2)			
4-OH Benzoic acid	6	Glu27, Glu27, Lys63, Glu13, Glu27, Val70, Lys93, Gly92, Arg95, Glu27, Val69	Lys63:HZ1 (1.730)
Astragalin	4	Asn21, Arg86, Gly82, Gly17, Arg86, Arg95, Glu16, Glu16	Gly82:O (1.898)
isoquercitrin	8	Arg86, Leu96, Gly82, Ala90, Val94, Glu91, Arg95, Glu16, Arg95, Glu16, Glu16	Val94:O (2.117)
TyrRS from *S. aureus* (pdb id: 1JIJ)			
4-OH Benzoic acid	5	Asp40, Asp80, Asp40, Asp80, Gly38, Gln196, Tyr170, Tyr36, Gln190, His47, Lys84, Lys84, His47, Asp80, Ala239	Tyr36: OH (2.248)
Hesperidin	6	Lys84, Lys84, Lys84, Asp40, Thr75, Pro222, His50, Gly193, Gly49, Gly49, Gln196, Tyr36, Asp177, Asp195, Gly38, Leu70, Tyr36	Asp40:OD2 (2.164)
luteolin 7-O-glucoside	5	Asp40, Gln174, Asp177, Asp40, Ser82, Gly38, Lys84	Asp40:HN (1.961)
Cyclooxygenase-2 (pdb id: 1CX2)			
4-OH Benzoic acid	9	Glu465, Glu465, Asp157, Lys468, Asp157, Cys47, Met48, Pro154, Cys41, Gln42, Lys468, Met48, Gly135, Ala156, Val155; Ala156, Cys36, Pro153, Cys36, Ala156, Arg44, Lys468	Pro154:O (1.927)
luteolin 7-O-glucoside	4	Tyr122, Lys468, Tyr122, Asn43, Arg44, Glu465, Arg44, Lys468, Arg44, Leu152, Arg469	Asn43:OD1 (2.707)
Cosmosiin	6	Asn43, Lys468, Lys468, Gln42, Asn43, Asn43, Glu465, Asn43, Arg44, Lys468, Lys468, Leu152, Arg469	Gln42:OE1 (2.182)
Bold residues: interacting with Conventional H-Bonds			

Ala: Alanine, **Arg:** Arginine, **Asn:** Asparagine, **Asp:** Aspartic acid, **Cys:** Cysteine, **Gln:** Glutamine, **Glu:** Glutamic acid, **Gly:** Glycine, **His:** Histidine, **Leu:** Leucine, **Lys:** Lysine, **Met:** Methionine, **Pro:** Proline, **Ser:** Serine, **Thr:** Threonine, **Tyr:** Tyrosine, **Val:** Valine, **pdb**: Protein Data Bank

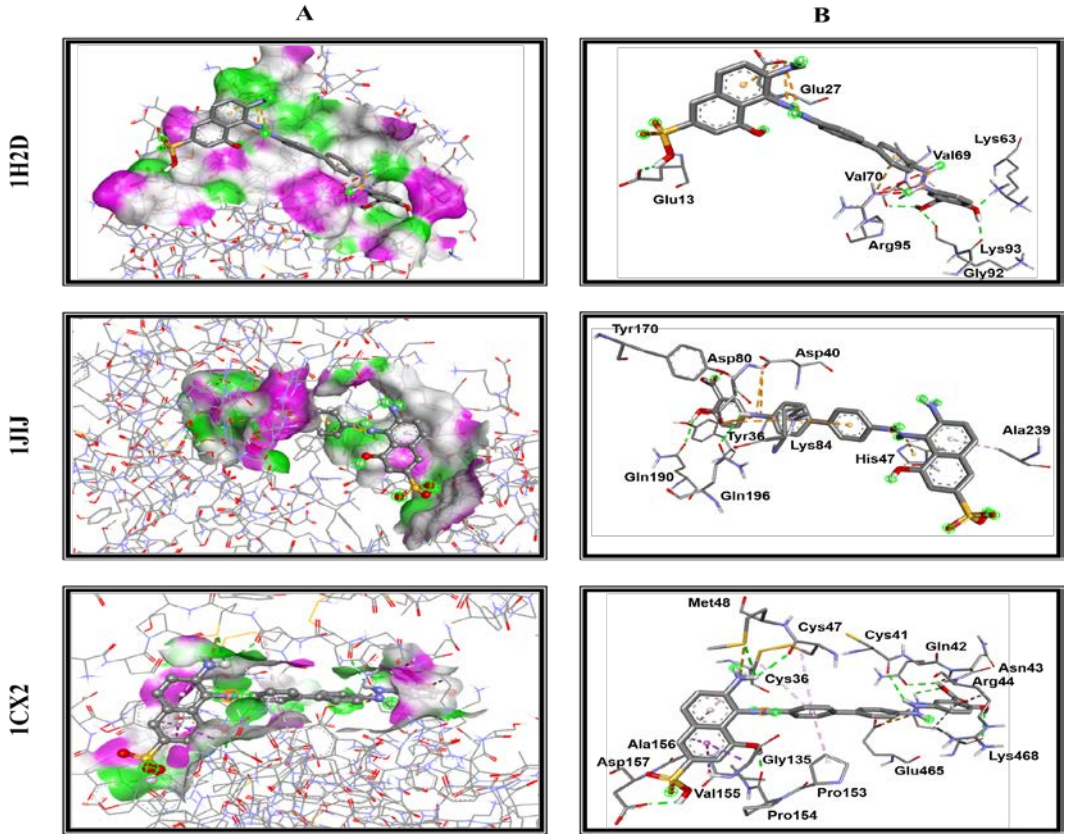

Figure 5. 3D illustration of A) the H-bond acceptor/donor attributes and B) the resulting interactions for 4-OH Benzoic acid, which possessed the best binding score for each of human peroxiredoxin 5 (1H2D), TyrRS from *S. aureus* (1JIJ), and cyclooxygenase 2 (1CX2) macromolecules.

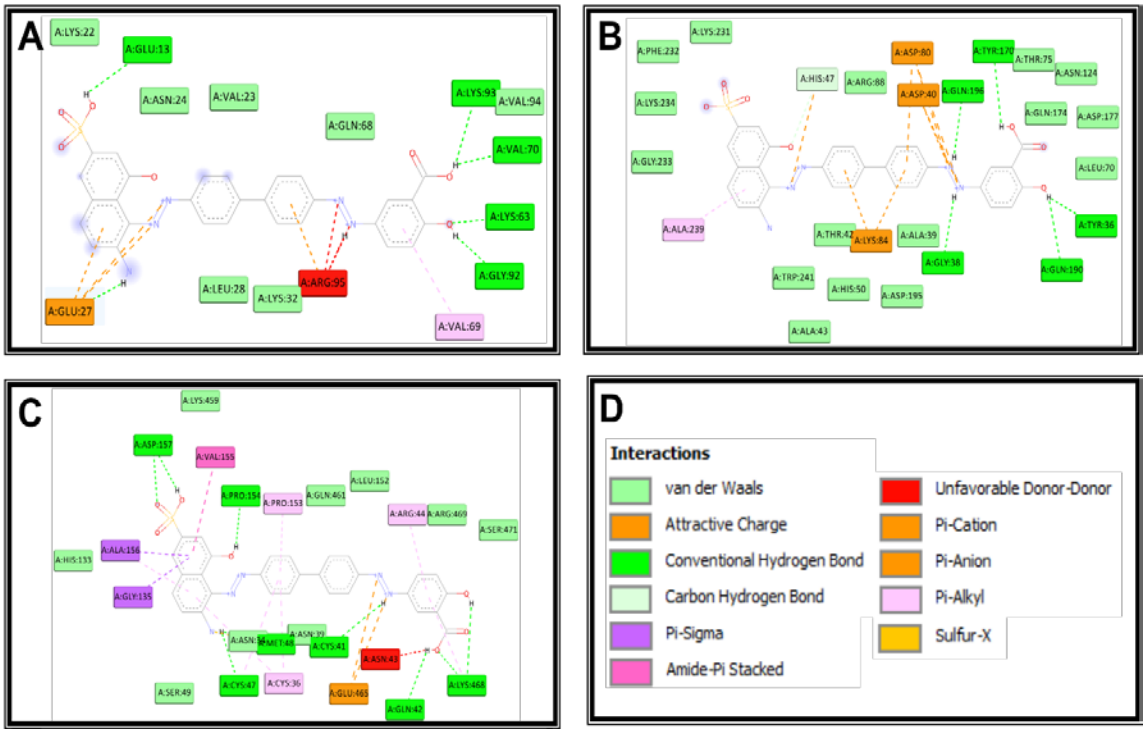

Figure 6. 2D diagrams of the interaction of 4-OH Benzoic acid, which possessed the best binding score for each of human peroxiredoxin 5 (1H2D), TyrRS from S. aureus (1JIJ), and cyclooxygenase 2 (1CX2) macromolecules**.**

4. Conclusion

This study demonstrates that both aqueous and ethanolic extracts of *M. pubescens* exhibit potent antimicrobial, antioxidant, and anti-inflammatory activities, with the ethanolic extract showing superior efficacy due to its richness in polyphenols and flavonoids. Computational modelling confirmed strong binding affinities of its compounds to key biological targets (1HD2, 1JIJ, and 1CX2), supporting their bioactive potential. These findings highlight the relevance of *M. pubescens* as a natural source of therapeutic agents, particularly in addressing antimicrobial resistance, a pressing global health issue. Its demonstrated activity against resistant pathogens, combined with its antioxidant and anti-inflammatory effects, underscores its potential for developing plant-based alternatives or adjuvants to conventional drugs. Future research should focus on in vivo validation, mechanism-of-action studies, toxicity assessments, and clinical trials. The integration of *M. pubescens* into drug discovery pipelines and nutraceutical development could pave the way for innovative strategies to combat antimicrobial resistance and oxidative stress-related disorders.

Acknowledgements

This work was supported by the Algerian Ministry of Higher Education and Scientific Research, Directorate General for Scientific Research and Technological Development, through the Research Laboratory 'Laboratory of Biochemical and Environmental Toxicology', Faculty of Sciences, Badji Mokhtar University, Annaba, Algeria.

Conflict of interests

On behalf of all authors, the corresponding author states that there is no conflict of interest.

Ethical approval

This article does not contain any studies with human participants or animals performed by any of the authors.

Informed consent

All the authors read the manuscript and approved it for submission.

Authorship contribution

H. C: Writing – review & editing, Supervision. Writing – original draft, Methodology, Investigation**. M.L. D:** Writing – review & editing**. C. B:** Methodology**. R. B:** Software**. G. Z:** Methodology**. M.A. Y:** Methodology**. C. D:** Methodology**. I. H:** Methodology**. M. S:** Methodology. **M. B:** visualization**. A. B:** validation**. M. M:** Conceptualization, Project administration**.**

References

Abd El Aty AA, Alshammari SO, Alharbi RM, and Soliman AA. 2023. Astragalus sarcocolla Gum-mediated a Novel Green-synthesis of Biologically Active Silver-Nanoparticles with Effective Anticancer and Antimicrobial activities. Jordan J. Biol. Sci., **16(1):** 41-53.

Ahammed MS, Kader MA, Islam KM, Lopa SS, Alam A and Sadik G. 2023. Anti-inflammatory Activity of the Phenolic Compounds from Vanda roxburghii R. Bangladesh Pharm. J., **26(1):** 1-6.

Ahmed-Gaid K, Ahmed-Gaid NEY, Hanoun S, Chenna H, Ghenaiet K, Ahmed-Gaid H, and Hadef Y. 2025. Phenolic compounds, antioxidant, and antimicrobial activities of methanolic extract from the Saharan endemic plant Haloxylon scoparium Pomel. Bull. Pharm. Sci., Assiut Univ., **48(1):** 267-276

Ahmed-Gaid K, Hanoun S, Sekkoum K, Ahmed-Gaid H, Chenna H, Ahmed-Gaid N. 2025. Medicinal plants use for respiratory infections in the Post-COVID-19 era: Symptomatic overlap and disease-specific preferences. Ethnobot. Res. Appl., **31** : 1-12.

Ak G, Zengin G, Sinan KI, Mahomoodally MF, Picot-Allain MCN, Cakır O, Bensari S, Yılmaz MA, Gallo M and Montesano D. 2020. A comparative bio-evaluation and chemical profiles of Calendula officinalis L. extracts prepared via different extraction techniques. Appl. Sci., **10(17**): 5920.

Akacha A, Badraoui R, Rebai T and Zourgui L. 2022. Effect of Opuntia ficus indica extract on methotrexate-induced testicular injury: A biochemical, docking and histological study. J. Biomol. Struct. Dyn., **40(10):** 4341-4351.

AL-Hmadi HB, Romdhani A, Majdoub S, Dhaouadi H, Zengin G and Hammami S. 2023. Chemical composition, antioxidant and multi-enzymatic inhibitory potential of licorice harvested from wild populations in Iraq. S. Afr. J. Bot., **158**: 56-62.

Al-Khayri JM, Sahana GR, Nagella P, Joseph BV, Alessa FM and Al-Mssallem MQ. 2022. Flavonoids as potential anti-inflammatory molecules: A review. Molecules, **27(9):** 2901.

Aldarhami A, Bazaid AS, Alhamed AS, Alghaith AF, Ahamad SR, Alassmrry YA, Alharazi T, Snoussi M, Qanash H and Alamri A. 2023. Antimicrobial potential of Pithecellobium dulce seed extract against pathogenic bacteria: In Silico and In Vitro Evaluation. BioMed Res. Int., **2023(1**): 2848198.

Altay A, Yeniceri E, Taslimi P, Taskin-Tok T, Yilmaz MA and Koksal E. 2022. A Biochemical Approach for Hedysarum candidissimum from Turkey: Screening Phytochemicals, Evaluation of Biological Activites, and Molecular Docking Study. Chem. Biodiversity, **19(9**): e202200348.

Amssayef A, Ajebli M and Eddouks M. 2020. Antihyperglycemic Potential of *Matricaria pubescens* (Desf.) Schultz. in Streptozotocin-induced Diabetic Rats. Cardiovasc. Hematol. Disord.: Drug Targets, **20(4):** 297-304.

Badraoui R, Allouche M, El Ouaer D, Siddiqui AJ, Ishak S, Hedfi A, Beyrem H, Pacioglu O, Rudayni HA and Boufahja F. 2023. Ecotoxicity of chrysene and phenanthrene on meiobenthic nematodes with a case study of Terschellingia longicaudata: Taxonomics, toxicokinetics, and molecular interactions modelling. Environ. Pollut., **316:** 120459.

Bédoui I, Nasr HB, Ksouda K, Ayadi W, Louati N, Chamkha M, Choura S, Gargouri J, Hammami S and Affes H. 2024. Phytochemical composition, bioavailability and pharmacokinetics of scorzonera undulata methanolic extracts: antioxidant, anticancer, and apoptotic effects on MCF7 cells. Pharmacogn. Mag., **20(1):** 218-229.

Ben Saad H, Frikha D, Bouallegue A, Badraoui R, Mellouli M, Kallel H, Pujo JM and Ben Amara I. 2023. Mitigation of hepatic impairment with polysaccharides from red alga Albidum corallinum supplementation through promoting the lipid profile and liver homeostasis in tebuconazole-exposed rats. Pharmaceuticals, **16(9):** 1305.

Bouden I, Aimene W, Elder R, Arrar L. 2017. In vitro and in vivo anti-arthriticand anti-inflammatory activity of Matricariapubescens (Desf.). Adv. Environ. Biol., **11(11)** : 11-20.

Boudjema K, Chouala K, Khelef Y, Chenna H, Badraoui R, Boumendjel M, Boumendjel A and Messarah M. 2024. Antioxidant Effects of Moringa oleifera Against Abamectin-Induced Oxidative Stress in the Brain and Erythrocytes of Rats. Chem. Biodiversity: e202402709-e202402709.

Boughendjioua H. 2017. Composition chimique et activité antibactérienne de l'huile essentielle de Lavandula officinaliscultivées dans la région de Skikda-Algérie. Chemical composition and antibacterial activity of essential oil of Lavandula officinalis grown in the region of Skikda-Algeria. Soc. R. Sci. Liège.

Bouyahya A, Abrini J, Bakri Y and Dakka N. 2017. Screening phytochimique et évaluation de l'activité antioxydante et antibactérienne des extraits d'Origanum compactum. Phytothérapie, **15(6):** 379-383.

Chenna H, Khelef Y, Halimi I, Yilmaz MA, Çakir O, Djouder C, Tarhan A, Idoughi K, Boumendjel M and Boumendjel A. 2024. Potential Hepatoprotective Effect of *Matricaria pubescens* on High-Fat Diet-Induced Non-Alcoholic Fatty Liver Disease in Rats. Chem. Biodiversity, **21(4):** e202302005.

Chenna H, Khelef Y, Zengin G, Yilmaz MA, Cakir O, Halimi I, Djouder C, Tarhan A, Boumendjel M, Boumendjel A, Saoudi M and Messarah M. 2025. *Matricaria pubescens* (desf.) Sch. Bip. Supplementation prevent high-fat diet-induced kidney damage in obese rats. Comp. Clin. Pathol., **34**: 353–363.

Chira A, Kadmi Y, Badraoui R, Aouadi K, Alhawday F, Boudaya M, Jamoussi K, Kallel C, El Feki A and Kadri A. 2024. GC-MS/MS Analysis and Wound Repair Potential of Urtica dioica Essential Oil: In silico Modeling and In vivo Study in Rats. Curr. Pharm. Biotechnol., **26(4**): 591-607.

Elhasnaoui A, Janah I, Ait Tastift M, El-Haidani A, Lahrach N. 2025. Comprehensive review on *Matricaria pubescens*: traditional uses, chemical composition, and pharmacological potential. Sci. Afr., e02865. doi: https://doi.org/10.1016/j.sciaf.2025.e02865

Guedes BN, Krambeck K, Durazzo A, Lucarini M, Santini A, Oliveira MBP, Fathi F, and Souto EB. 2024. Natural antibiotics against antimicrobial resistance: sources and bioinspired delivery systems. Braz. J. Microbiol.: 1-14.

Hanoun S, Ahmed-Gaid K, Chenna H, Boufafa M, Aroua K, Mellal H. 2025. The effect of various solvent on the total phenol content, the total flavonoid content, the antioxidant activity of Erica arborea extracts from Algeria and investigation of their Antibacterial activity against multi drug-resistant uropathogenic bacte. *Bull. Pharm. Sci., Assiut Univ.*, **48(2):** 1031-1042.

Hanoun S, Belkoum H, Ouchene W, Gaid KA, Chenna H, Mellal H and Aroua K. 2025. Total Phenol Content, Total Flavonoid Content and, In vitro, Antibacterial Activity of Polygonum aviculare and Zygophyllum album Extracts from Algeria against Multidrug-resistant Gram-negative Bacteria (MDR-GNB). Res. J. Pharm. Technol., **18(1):** 339-344.

Ivanov M, Novović K, Malešević M, Dinić M, Stojković D, Jovčić B and Soković M. 2022. Polyphenols as inhibitors of antibiotic resistant bacteria—Mechanisms underlying rutin interference with bacterial virulence. Pharmaceuticals, **15(3):** 385.

Jedli O, Ben-Nasr H, Zammel N, Rebai T, Saoudi M, Elkahoui S, Jamal A, Siddiqui AJ, Sulieman AE and Alreshidi MM. 2022. Attenuation of ovalbumin-induced inflammation and lung oxidative injury in asthmatic rats by Zingiber officinale extract: Combined in silico and in vivo study on antioxidant potential, STAT6 and TNF-α pathways. 3 Biotech, **12(9):** 191.

Kalinowska M, Świsłocka R, Wołejko E, Jabłońska-Trypuć A, Wydro U, Kozłowski M, Koronkiewicz K, Piekut J and Lewandowski W. 2024. Structural characterization and evaluation of antimicrobial and cytotoxic activity of six plant phenolic acids. PloS one, **19(6):** e0299372.

Karagecili H, Yılmaz MA, Ertürk A, Kiziltas H, Güven L, Alwasel SH and Gulcin İ. 2023. Comprehensive metabolite profiling of Berdav propolis using LC-MS/MS: Determination of antioxidant, anticholinergic, antiglaucoma, and antidiabetic effects. Molecules, **28(4):** 1739.

Karatas DD, Oz V, Yener I, Akdeniz M, Erek F, Aydin I, Yigitkan S, Yılmaz MA and Ertas A. 2022. Phytochemical Contents of Different Parts of the Seeded Raisins from the South-East Anatolia: Enzyme Inhibitory Potential of Pulp Extracts. Chem. Biodiversity, **19(3):** e202100844.

Kherraz K, Ghemam Amara D, Chouikh A, Chefrour A. 2019. Morphological, Anatomical and Environmental Characteristics and the Geographical Distribution of Matricaria pubscenes (composées) from Algeria. World J. Environ. Biosci., **8(1):** 76-80.

Kherraz K, Chouikh A, Chefrour A And Ghemam Amara D. 2019. Estimation of total phenolic and flavonoids content and anti-free radical scavenger, antibacterial and antifungal activities of extract of *Matricaria pubescens* (DESF.) SCH. BIP. collected from south east of Algeria. Analele Univ. din Oradea Fasc. Biologie, 26(1).

Kimani BG, Kerekes EB, Szebenyi C, Krisch J, Vágvölgyi C, Papp T and Takó M. 2021. In vitro activity of selected phenolic compounds against planktonic and biofilm cells of food-contaminating yeasts. Foods, **10(7):** 1652.

Kostić M, Ivanov M, Stojković D, Ćirić A and Soković M. 2020. Antibacterial and antibiofilm activity of selected polyphenolic compounds: An in vitro study on Staphylococcus aureus. Lek. Sirovine, **40(1):** 57-61.

Kraiem M, Ben Hamouda S, Eleroui M, Ajala M, Feki A, Dghim A, Boujhoud Z, Bouhamed M, Badraoui R and Pujo JM. 2024. Anti-Inflammatory and immunomodulatory properties of a crude polysaccharide derived from green seaweed Halimeda tuna: computational and experimental evidences. Mar. Drugs, **22(2):** 85.

Machado A, Zamora-Mendoza L, Alexis F and Álvarez-Suarez JM. 2023. Use of plant extracts, bee-derived products, and probiotic-related applications to fight multidrug-resistant pathogens in the post-antibiotic era. Future Pharmacol., **3(3):** 535-567.

Mahomoodally MF, Zengin G, Sinan KI, Yıldıztugay E, Lobine D, Ouelbani R, Bensari S, Ak G, Yılmaz MA and Gallo MJFri. 2021. A comprehensive evaluation of the chemical profiles and biological properties of six geophytes from Turkey: Sources of bioactive compounds for novel nutraceuticals. Food Res. Int., **140**: 110068.

Maiza K, Longeon A, Hammiche V, Guyot M, and Benabdesselam-Maiza F. 2014. Biological activities of plants collected in the Algerian Sahara. Life Sci. Leaflets, **52**: 52-56.

Makhloufi A, Moussaoui A, and Lazouni H. 2012. Antibacterial activities of essential oil and crude extracts from *Matricaria pubescens* (Desf.) growing wild in Bechar, South-west of Algeria. J. Med. Plant. Res, **6(16):** 3124-3128.

Metrouh-Amir H and Amir N. 2023. Impact of extraction method on alkaloid content and antioxidant activity of *Matricaria pubescens*. Croat. J. Food Sci. Technol., **15(1):** 83-95.

Metrouh-Amir H, Duarte CM, and Maiza F. 2015. Solvent effect on total phenolic contents, antioxidant, and antibacterial activities of *Matricaria pubescens*. Ind. Crops Prod., **67**: 249-256.

Mhadhbi N, Dgachi S, Belgacem S, Ahmed AB, Henry N, Loiseau T, Nasr S, Badraoui R, and Naïli H. 2023. Design, theoretical study, druggability, pharmacokinetics, and properties evolution of a new organo-bromocadmate compound as prospective anticancer agent. J. Mol. Struct., **1274**: 134439.

Musk DJ, Banko DA, and Hergenrother PJ. 2005. Iron salts perturb biofilm formation and disrupt existing biofilms of Pseudomonas aeruginosa. J. Chem. Biol., **12(7)**: 789-796.

Nadji S, Boudjemaa S, Bounab A, and Hadef Y. 2022. Evaluation of biological activities of *Matricaria pubescens* from Algeria. Bull. Pharm. Sci. Assiut University, **45(2):** 723-736.

Prima MJ, Hassan M, and Sharma J. 2023. Novel Approaches for Combating Antibiotic Resistance in Pathogenic Bacteria. Microb. Bioactives, **6(1):** 1-18.

Rahman H, Eswaraiah MC, Vakati K, and Madhavi P. 2012. In vitro studies suggest probable mechanism of eucalyptus oil for anti-inflammatory and anti-arthritic activity. Int. J. Phyto. Pharm., **2(3):** 81-83.

Rahmoun M, Benabdallah M, Villemin D, Boucherit K, Mostefa-Kara B, Ziani-Cherif C and Choukchou-Braham N. 2010. Antimicrobial screening of the Algerian Lawsonia inermis (henna). Der. Pharma. Chemica., **2(6):** 320-326.

Rahmouni F, Hamdaoui L, Saoudi M, Badraoui R and Rebai T. 2024. Antioxidant and antiproliferative effects of Teucrium polium extract: computational and in vivo study in rats. Toxicology Mechanisms Methods Enzymol, **34(5):** 495-506.

Salim A, Deiana P, Fancello F, Molinu MG, Santona M, and Zara S. 2023. Antimicrobial and antibiofilm activities of pomegranate peel phenolic compounds: Varietal screening through a multivariate approach. J. Bioresour. Bioprod., **8(2):** 146-161.

Sett A, Dubey V, Bhowmik S, and Pathania R. 2024. Decoding Bacterial Persistence: Mechanisms and Strategies for Effective Eradication. ACS Infect. Dis.

Seukep AJ, Nembu NE, Mbuntcha HG and Kuete V 2023. Bacterial drug resistance towards natural products. Adv. Bot. Res., **106**: 21-45.

Tue NM, Quan NT, Chi HT, and Ly BTK. 2024. An in vitro Study into Antioxidant, Antibacterial, and Toxicity Impacts of Artocarpus altilis Leaf Extract. Biological, **17(4):** 637 – 643.

Uysal S, Zengin G, Locatelli M, Bahadori MB, Mocan A, Bellagamba G, and Mollica A. 2017. Cytotoxic and enzyme inhibitory potential of two Potentilla species (P. speciosa L. and P. reptans Willd.) and their chemical composition. Front. Pharmacol., **8**: 249316.

Yilmaz MA, Cakir O, Izol E, Tarhan A, Behcet L and Zengin G. 2023. Detailed Phytochemical Evaluation of a Locally Endemic Species (Campanula baskilensis) by LC-MS/MS and Its In-Depth Antioxidant and Enzyme Inhibitory Activities. Chem. Biodiversity, **20(12):** e202301182.

Zammel N, Saeed M, Bouali N, Elkahoui S, Alam JM, Rebai T, Kausar MA, Adnan M, Siddiqui AJ, and Badraoui R. 2021. Antioxidant and anti-Inflammatory effects of Zingiber officinale Roscoe and Allium subhirsutum: In silico, biochemical and histological Study. Foods, **10(6):** 1383.

JJBS

Volume 19, Number 1,March 2026
ISSN 1995-6673
Pages 159 – 168
https://doi.org/10.54319/jjbs/190115

Jordan Journal of Biological Sciences

Efficacy of Freeze-Dried Human Wharton's Jelly Mesenchymal Stem Cell Secretome Gel Toward Wound Healing Rat Model

Wahyu Widowati[1,*], Meilinah Hidayat[1], Ahmad Faried[2,3], Fanny Rahardja[1], Rimonta Febby Gunanegara[1], Dwi Nur Triharsiwi[4], Rajwa Dzakiyyah Basyasyah[5], Rizal Azis[4,6], Didik Priyandoko[7], Dhanar Septyawan Hadiprasetyo[4,8], Kasim Sakran Abass[9]

[1]Faculty of Medicine, Maranatha Christian University, Bandung, Indonesia; [2]Department of Neurosurgery, Mayapada Hospital Bandung, Indonesia; [3]Department of Neurosurgery, Faculty of Medicine, Padjadjaran University Hospital, Jatinangor, Indonesia; [4]Biomolecular and Biomedical Research Center, Aretha Medika Utama, Bandung, Indonesia; [5]Biology Study Program, Faculty of Mathematics and Natural Sciences Education, Universitas Negeri Jakarta, Jakarta, Indonesia; [6]Biomedical Engineering, Department of Electrical Engineering, Faculty of Engineering, Universitas Indonesia, Depok, Indonesia; [7]Biology Study Program, Faculty of Mathematics and Natural Sciences Education, Universitas Pendidikan Indonesia, Bandung, Indonesia; [8]Faculty of Pharmacy, Universitas Jenderal Achmad Yani, Cimahi, Indonesia; [9]Department of Physiology, Biochemistry, and Pharmacology; College of Veterinary Medicine, University of Kirkuk, Kirkuk, Iraq

Received: May 1, 2025; Revised: August 9, 2025; Accepted: August 28, 2025

Abstract:

Background: Burns are a major global health problem, often leading to prolonged inflammation and impaired wound healing. Current treatments face limitations, and human Wharton's Jelly-derived mesenchymal stem cell (hWJ-MSCs) secretome offers a promising non-cellular alternative. Freeze-dried secretome gel (FDSG) preserves bioactive molecules that promote tissue repair. This study evaluated the potential of FDSG for burn wound healing in a rat model. **Methods:** The secretome was obtained as a conditioned medium from hWJ-MSCs. FDSG was made by mixing 6 g of carbomer gel with 6 mL hWJ-MSCs secretome, then followed by lyophilization. An in vivo test was conducted on six Sprague-Dawley rats with a third-degree burn model (BM) with various treatments. Burn healing was evaluated on days 3, 10, and 24 based on wound reduction, IL-1β protein levels (Immunohistochemistry), and collagen density (Masson's trichrome staining). **Results:** FDSG increased the percentage of wound reduction and collagen density from day 3 to 24. Our findings also indicate a regulatory pattern of IL-1β protein levels throughout the biological mechanism of tissue repair, which is strongly associated with the distinct phases of healing. The treatment group that applied FDSG twice daily demonstrated the highest effectiveness. **Conclusion:** FDSG shows promising results as an effective wound healing agent.

Keywords: Burns, Freeze-dried, hWJ-MSCs, Secretome, Wound healing.

1. Introduction

Burns are a complex type of traumatic injury that can have long-term effects, both locally and systemically (Nielson et al., 2017; Jeschke et al., 2020). Every year, almost 9 million new cases of burns occur globally, with 120,000 deaths, mainly in developing countries (Hebron et al., 2022). In many Asian countries, it remains high due to socioeconomic factors. The severity of burns is classified based on burn depth, ranging from first- to fourth-degree burns, which can cause complications such as prolonged inflammation, impaired wound healing, and systemic inflammatory response syndrome (Rowan et al., 2015; Schaefer & Tannan, 2021). One of the main complications is prolonged inflammation, which can interfere with the normal healing process and cause further tissue damage (Rowan et al., 2015). This uncontrolled inflammation can trigger the potentially life-threatening systemic inflammatory response syndrome (Sikora et al., 2023). Impaired wound healing also represents another serious complication associated with burn injuries.

Interleukin (IL)-1β is an inflammatory cytokine that plays a role in both initiating inflammation and supporting tissue regeneration during the healing process. Previous research indicates that IL-1β stimulates fibroblasts, increasing collagen (Shagdarova et al., 2021). This finding also aligns with Mozzati et al. (2010), who stated that IL-1β promotes fibroblast proliferation and stimulates collagen synthesis and collagenase production, which are important for collagen remodeling during wound healing. On the other hand, collagen density is a key factor in determining tissue strength and integrity. The wound healing process usually involves the initial production of collagen type III, which is later replaced by collagen type I, the main structural component of the dermis (Alsarayreh et al., 2022). In addition, the reconstruction stage of wound healing involves the coordinated alignment and restructuring of collagen fibers, which are crucial for effective wound contraction and tissue restoration

* Corresponding author. e-mail: wahyu_w60@yahoo.com; wahyu.widowati@maranatha.edu.

Given the complexity and severity of burns, developing effective treatment methods is essential. Anti-inflammatory drugs, including corticosteroids, are commonly used to address excessive inflammation in chronic wounds. Although these drugs can effectively reduce inflammation, long-term use can impair wound healing by inhibiting fibroblast function and collagen synthesis (Casado-Santos, 2024). Moreover, nonsteroidal anti-inflammatory drugs (NSAIDs) may lead to gastrointestinal complications and renal impairment, particularly in individuals with underlying health conditions (Lanci et al., 2019).

Contemporary wound management emphasizes rapid wound closure, restoration of function, reduction of scarring, and improvement in overall quality of life (Salibian et al., 2016). Recent advances in burn treatment, such as the application of engineered skin grafts, regenerative stem cell treatments, and therapeutic growth factors modulation, have shown promising potential in enhancing patient outcomes (Srinivasan et al., 2021).

The use of mesenchymal stem cells (MSCs) is gaining increasing attention in wound healing, including burns (Gentile & Garcovich, 2019). MSCs have differentiation, immunomodulatory, anti-inflammatory, and proangiogenic properties that support tissue repair (Wang et al., 2014). Wharton's Jelly (WJ) is a promising source of MSCs due to its high proliferation rate, high differentiation potential, and strong immunomodulatory profile (El Omar et al., 2014). Harvesting of WJ-MSCs is noninvasive and ethical, utilizing umbilical cords that are usually discarded (Ding et al., 2015). However, live cell therapy faces challenges in storage, transportation, regulation, and the risk of malignant transformation (Moll et al., 2014).

Alternatively, the WJ-MSC secretome (WS), an assemblage of biologically active compounds such as extracellular vesicles and growth factors, offers a non-cellular approach to accelerate wound healing through mechanisms of immunomodulation, angiogenesis, and fibroblast activation (Deshpande et al., 2018; Tan et al., 2023). This secretome can be integrated into a secretome gel (SG) for sustained release of molecules, enhancing therapeutic efficacy (Alapure et al., 2018; Rong et al., 2019). The freeze-drying process of secretome has been shown to preserve active compounds and improve stability, as shown in the study by Widowati et al. (2024a, 2024b), where freeze-dried secretome gel (FDSG) had higher levels of growth factors, cytokines, and antioxidants compared to non-freeze-dried secretome (NFDS). This approach offers great potential in overcoming conventional therapies' limitations and improving burn patients' quality of life.

Thus, this study offers important evidence supporting the potential of FDSG as an effective and safe wound healing agent through in vivo testing as a further stage. The potential of FDSG as a wound healing agent was analyzed based on IL-1β expression (Immunohistochemistry), collagen density (Masson's trichrome staining), and wound reduction in rats given third-degree burns.

2. Material and Methods

2.1. Culture and Collection of hWJ-MSCs Secretome

The hWJ-MSCs were identified through multipotent differentiation assay and surface phenotype analysis (Widowati et al., 2019). hWJ-MSCs were cultured based on the protocol described in previous studies by Widowati et al. (2024a, 2024b) using Minimum Essential Medium-α (α-MEM) (Biowest, L0475500) supplemented with 10% Fetal Bovine Serum. Then the cells were incubated at 37 °C in a humidified atmosphere containing 5% CO_2. Upon reaching 80–90% confluence, the cells were harvested and centrifuged at 3,000×g for 4 minutes (MWP 260 r). The obtained supernatant, which contained the secretome, was subsequently filtered through a Durapore unit (Millipore Corporation, SLGV 033 RS).

2.2. Carbomer Gel Formulation

The formulation of carbomer gel (CG) was done according to Widowati et al. (2024a). CG was made by dissolving 7.5 g of carbomer 940 in 250 mL of distilled water while stirring continuously. After swelling, 7.5 mL of triethanolamine, 5 mL of propylene glycol, and 5 mL of glycerin were added dropwise while mixing thoroughly until a homogeneous gel was obtained. The volume was adjusted to 500 mL with distilled water. The quality of CG has been analyzed in previous studies based on organoleptic testing, pH measurements, homogeneity tests, and viscosity evaluations (Widowati et al., 2024b).

2.3. Production of FDSG

FDSG was prepared by mixing 6 g of carbomer gel with 6 mL of WS, which is the best formula from previous studies (Widowati et al., 2024a; 2024b). The mixture was stirred slowly until it reached a homogeneous consistency (Zukhiroh et al., 2022). The mixture was placed in a small tray and subjected to lyophilization using a vacuum freeze dryer (FD-F-CE, China), as described by Nowak and Jakubczyk (2020). The freeze-drying process was performed over 42 hours at a controlled temperature ranging from −50 to −35 °C.

2.4. Burn-Induced Rats

In vivo tests were conducted on male Sprague-Dawley rats from iRATco Veterinary Laboratory, Bogor, Indonesia. The protocol was carried out following the approval of the Research Ethics Committee of the Faculty of Medicine, Maranatha Christian University (No. 046/KEP/V/2024). The burn wound model was conducted following the procedures of Tran-Nguyen et al. (2020) and Laksmitawati et al. (2022) with modifications. The burn model (BM) was performed by inducing third-degree burns using a 1 cm diameter metal rod that had been heated beforehand and applied to the back of the test animal for 10 seconds. A total of 36 rats were divided into 6 groups (Table 1), including acclimatization for 7 days. The test material was administered until it completely encompassed the entire wound area.

Table 1. Treatment groups in burn rat model

Group	Treatment	Total Rats
I: NC (Negative Control)	Normal rats, untreated rats	6
II: PC (Positive Control)	Burn model	6
III: VC (Vehicle Control)	PC + CG freeze dried 1x/day, 08:00 am	6
IV: Treatment 1 (FDSG 1)	PC + FDSG, 1x/day, 08:00 am	6
V: Treatment 2 (FDSG 2)	PC + FDSG, 2x/day, 08:00 am and 04:00 pm	6
VI: CpG (Comparison Group)	PC + Bioplacenton 1x/day, 08:00 am	6

2.5. Wound Healing Scoring: Wound Reduction, IHC, and MT

The wound anatomy, including wound diameter, was observed on days 3, 10, and 24 by measuring the mean measurements of the wound's vertical and horizontal dimensions macroscopically. Termination was carried out on days 3, 10, and 24, with 2 rats from each group. Dorsal skin tissue was fixed in 10% Bouin's fixative (BNF) solution (Merck, MFCD00146169) for IHC and MT analysis. IHC was performed to analyze IL-1β protein levels using primary antibodies (Elabscience, E-AB-70048), which was incubated at ambient temperature overnight. The Rabbit-Specific HRP/DAB (ABC) Detection IHC Kit (Elabscience, E-IR-R213) was utilized for detection, while MT was performed to analyze collagen density. Color changes indicating protein levels and collagen density were measured using ImageJ software. These parameters were examined under a light microscope (Olympus BX 31, Japan) equipped with a USB CCD10 Camera with 40× magnification (Laksmitawati et al., 2022; Widowati et al., 2024c).

2.6. Statistical Analysis

Data are presented as mean ± standard deviation. Statistical analysis was performed using ANOVA followed by Tukey's HSD post-hoc test ($p < 0.05$). All analyses were conducted with SPSS software (version 20.0), and visualizations were created using GraphPad Prism (version 9.0) (Widowati 2024a; Widowati et al., 2024c).

3. Results

3.1. Effect of FDSG on wound reduction in burn rat model

Clinical development and wound reduction analysis results can be seen in Table 2 and Figure 1. The results demonstrated that the FDSG treatment group increased the percentage of wound reduction compared to PC, with FDSG 2 being the most effective group. Figure 1 also shows that FDSG 2 can effectively reduce wounds on day 24 compared to CpG.

Table 2. Effect of FDSG toward wound reduction in burn rat model

Group	D3	D10	D24
I			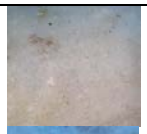
II			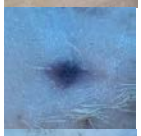
III			
IV			
V		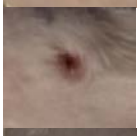	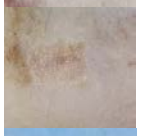
VI			

*(I) NC (untreated rats); (II) PC (burn model); (III) VC (PC + CG freeze-dried 1×/day); (IV) FDSG 1 (PC + FDSG 1×/day); (V) FDSG 2 (PC + FDSG 2×/day); (VI) CpG (PC + Bioplacenton 1×/day).

Figure 1. Effect of FDSG on wound reduction in burn rat model

*Data presented as mean ± SD. Different superscripts indicate significance between treatment groups based on Tukey's test ($p < 0.05$). (I) NC (untreated rats); (II) PC (burn model); (III) VC (PC + CG freeze-dried 1×/day); (IV) FDSG 1 (PC + FDSG 1×/day); (V) FDSG 2 (PC + FDSG 2×/day); (VI) CpG (PC + Bioplacenton 1×/day).

3.2. Effect of FDSG on IL-1β protein levels in burn rat model

The IHC results of IL-1β protein in test animals are presented in Table 3, while the quantitative analysis of protein levels is shown in Figure 2. In the IHC staining, IL-1β protein is indicated by a brown color; the more intense and widely distributed the brown staining, the higher the protein expression. FDSG 2 is the most pronounced effect. On day 3, IL-1β protein levels were high because the inflammatory process was still actively taking place in the early phase of wound healing. On day 10, IL-1β protein levels began to decrease because inflammation subsided and the proliferation phase began, and on day 24 IL-1β levels decreased further because inflammation was minimal and the tissue repair process was dominant.

Figure 2. Effect of FDSG on IL-1β levels in burn rat model

*Data presented as mean ± SD. Different superscripts indicate significance between treatment groups based on Tukey's test ($p < 0.05$). (I) NC (untreated rats); (II) PC (burn model); (III) VC (PC + CG freeze-dried 1×/day); (IV) FDSG 1 (PC + FDSG 1×/day); (V) FDSG 2 (PC + FDSG 2×/day); (VI) CpG (PC + Bioplacenton 1×/day).

Table 3. IHC of IL-1β protein in dorsal skin tissue of burn rat model

Group	D3	D10	D24
I	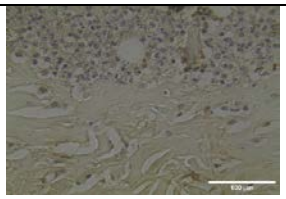	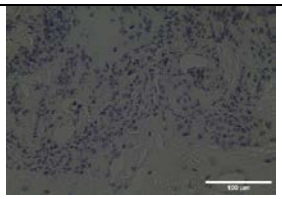	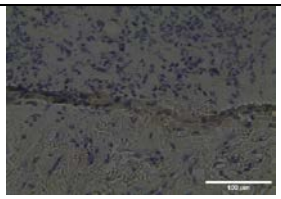
II	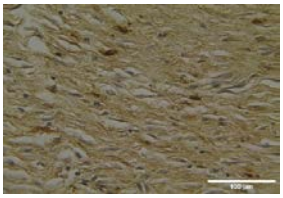	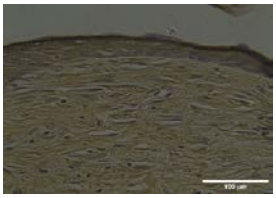	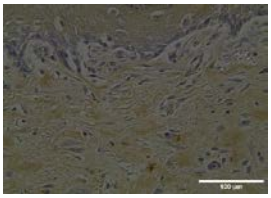
III	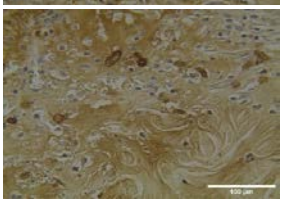	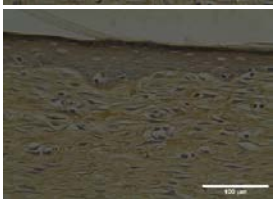	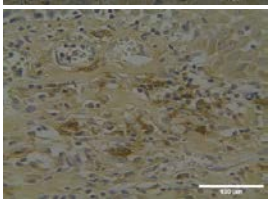
IV	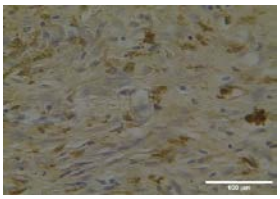	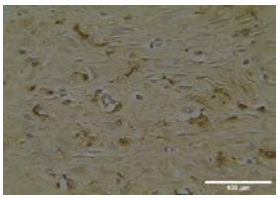	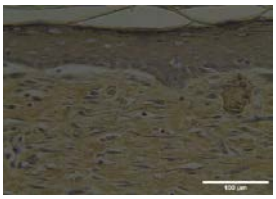
V	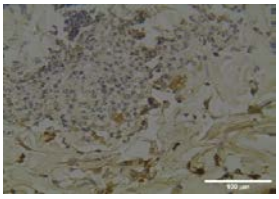	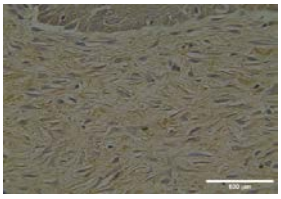	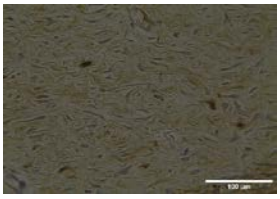
VI	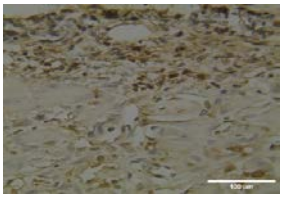	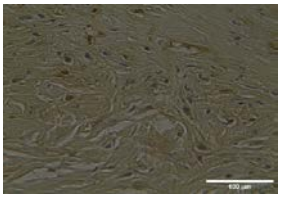	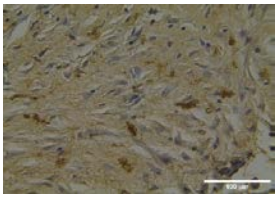

*(I) NC (untreated rats); (II) PC (burn model); (III) VC (PC + CG freeze dried 1×/day); (IV) FDSG 1 (PC + FDSG 1×/day); (V) FDSG 2 (PC + FDSG 2×/day); (VI) CpG (PC + Bioplacenton 1×/day).
*IL-1β protein levels are indicated by brown color.

3.3. Effect of FDSG toward Collagen Density in burn rat model

Collagen density from the FDSG effect can be seen in Table 4 and Figure 3. Collagen density based on MT staining is marked in blue (Table 4). The results showed that FDSG treatment significantly increased collagen density compared to PC from day 3 to day 24 (Figure 3).

Table 4. Effect FDSG toward collagen density in burn rat model

Group	D3	D10	D24
I	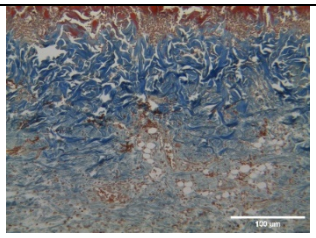	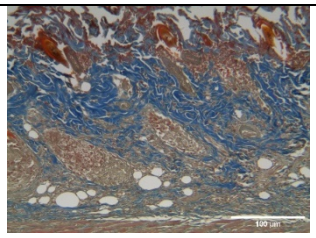	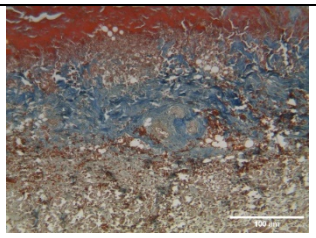
II	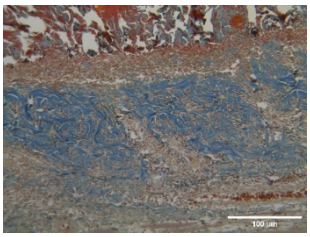	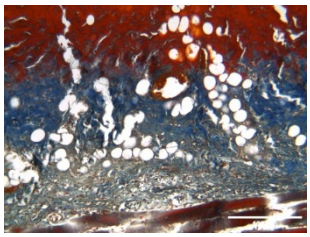	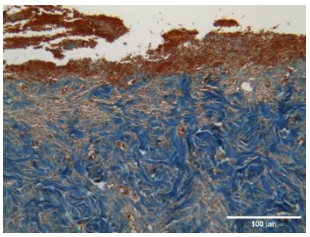
III	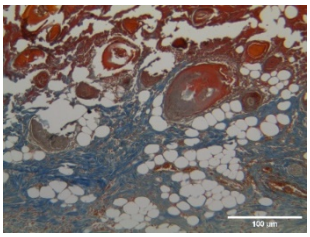	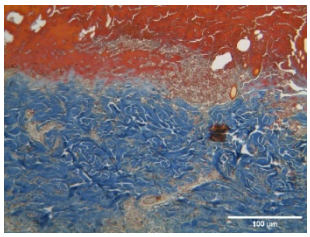	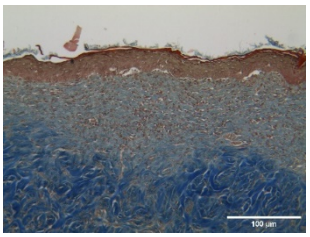
IV	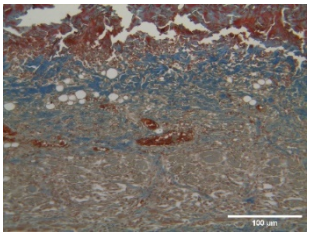	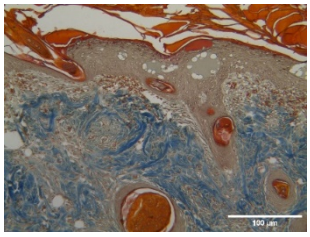	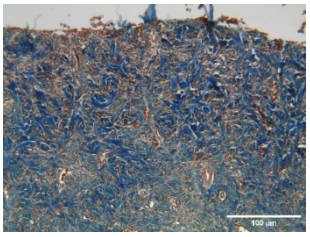
V	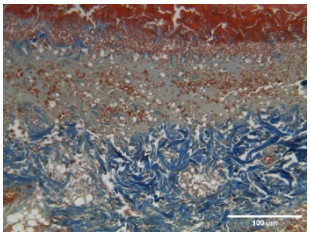	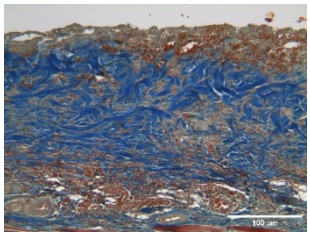	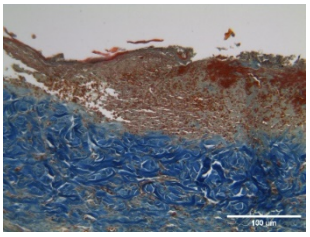
VI	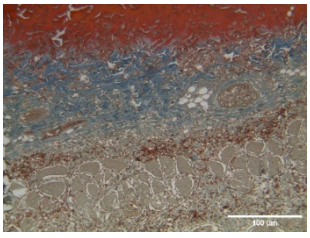	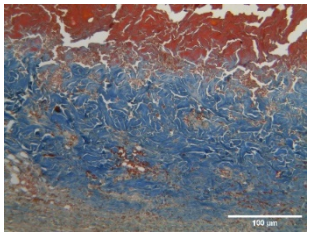	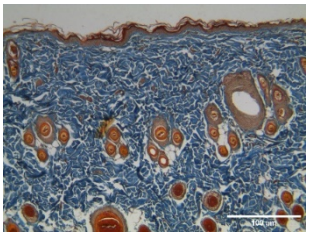

*(I) NC (untreated rats); (II) PC (burn model); (III) VC (PC + CG freeze dried 1×/day); (IV) FDSG 1 (PC + FDSG 1×/day); (V) FDSG 2 (PC + FDSG 2×/day); (VI) CpG (PC + Bioplacenton 1×/day).
*Collagen density is indicated by blue color.

Figure 3. Effect of FDSG toward collagen density in burn rat model

*Data are presented as mean ± SD. Different superscripts indicate significance between treatment groups based on Tukey's test ($p < 0.05$). (I) NC (untreated rats); (II) PC (burn model); (III) VC (PC + CG freeze-dried 1×/day); (IV) FDSG 1 (PC + FDSG 1×/day); (V) FDSG 2 (PC + FDSG 2×/day); (VI) CpG (PC + Bioplacenton 1× /day).

4. Discussion

Wound healing is known as a multifaceted and evolving biological process that generally unfolds in distinct phases: hemostasis, inflammation, proliferation, and remodelling (Tofiq et al., 2021). This process involves a cellular series and molecular events, such as cell migration, inflammation, extracellular matrix (ECM) synthesis, and angiogenesis (Li et al., 2017). In burn injuries, these processes are often disrupted, which may result in a slower recovery process, hypertrophic scarring, contractures, or chronic wounds (Finnerty et al., 2016). Wound secretome (WS) is known to contain key factors such as Tissue Inhibitor of Metalloproteinases-2 (TIMP-2), Epidermal Growth Factor (EGF), basic Fibroblast Growth Factor (bFGF), IL-6, IL-4, Keratinocyte Growth Factor (KGF), Hepatocyte Growth Factor (HGF), Platelet-Derived Growth Factor (PDGF), Heparin-Binding EGF-like Growth Factor (HB-EGF), and antioxidants, all of which play important roles in the healing process (Widowati et al., 2024a; Widowati et al., 2024b); these components may be able to act as burn wound therapy agents.

During the hemostasis phase, the initial response to injury involves the formation of a fibrin clot, which serves as a temporary matrix for cell migration and a scaffold for subsequent healing. This phase plays a crucial role in minimizing blood loss and kickstarting the body's inflammatory response. The initial step involves the activation of hemostatic mechanisms, followed by the inflammatory cells recruitment, notably neutrophils and macrophages, which signal the onset of the inflammatory phase. Among the key players in this process is IL-1β, a pro-inflammatory cytokine whose levels surge significantly right after a burn injury. This elevation of IL-1β helps to recruit and activate immune cells, such as macrophages and neutrophils, which are essential for clearing debris and pathogens from the wound site, thereby promoting the early stages of healing (Kimball et al., 2017; Schneider et al., 2021; Uchiyama et al., 2021). During the inflammatory phase, increased IL-1β levels activate various signaling pathways, particularly the NF-κB pathway, which amplifies the inflammatory response by inducing the expression of additional pro-inflammatory mediators including IL-6 and IL-8 (Kartika et al., 2021). This inflammatory response also facilitates the recruitment of additional fibroblasts to the wound site, where they contribute to collagen formation and help promote the repair process. The initial collagen formed during this phase is predominantly type III collagen, which is essential for providing temporary structural support to the wound (Gugliandolo et al., 2021; Hakim, 2023). The density of collagen fibers during this phase is critical as it influences the wound's ability to withstand mechanical stress and facilitate granulation tissue formation. Increased levels of inflammatory cytokines typically occur within the first week, with significant activity seen around day 7 (Shi et al., 2020).

The results showed that in burn rat model, there was an increase in IL-1β protein levels (Table 3) (Figure 2) and collagen density (Table 4) (Figure 3) after 3 days of FDSG treatment. Following injury, WS stimulates IL-1β secretion, a key factor in triggering inflammation during early wound repair. Increased IL-1β facilitates immune cell migration to the injury site, which promotes the clearance of debris and pathogens (Gonçalves et al., 2022; Tilotta et al., 2023). The presence of IL-1β in WS also activates fibroblasts, increasing their proliferation and collagen synthesis, particularly type III collagen (Lee et al., 2021). This early collagen deposition is vital for granulation tissue formation and provides structural support to wounds during the healing process. Other studies have shown that IL-6 in WS can increase IL-1β levels in various cell types, including fibroblasts and keratinocytes, during the inflammatory phase (Yin et al., 2019). Additionally, WS is known to contain EGF and HB-EGF, which can modulate the inflammatory response (Serra et al., 2018).

As the wound healing process moves into the proliferative phase, IL-1β levels begin to decline. This decrease is important in preventing chronic inflammation and initiating tissue regeneration. The downregulation of IL-1β is associated with a shift from a pro-inflammatory to an anti-inflammatory environment that is necessary for fibroblast activation and collagen formation (Sugioka et al., 2017). During this phase, the focus shifts toward production of extracellular matrix elements such as type I and type III collagen, which are essential for restoring tissue integrity and strength. Decreased IL-1β levels also correlate with reduced MMP activity, a balance that is essential for proper tissue remodeling (Bian et al., 2015). The balance between collagen synthesis and degradation is critical, as MMPs are involved in the breakdown of the ECM and ensure that collagen fibers are well organized and interconnected (Gugliandolo et al., 2021). The increased collagen density during this phase is critical to support the wound closure and reestablishment of tissue structure. This phase typically occurs around days 3 to day 10. By day 10, the proliferation process is usually well underway, with increased collagen density and vascularization observed in the wound area.

In the remodeling phase, IL-1β levels continue to decline, allowing maturation and reorganization of the ECM. This phase is characterized by the transition from collagen types III to I, providing greater strength to the healed tissue, which is important for preventing fibrosis

(Zhang, 2011). Regulation of IL-1β protein levels is important for ensuring a balanced inflammatory response, promoting effective tissue regeneration, and preventing pathological scarring. In the remodeling phase, collagen density also continues to play an important role. The transition from collagen type III to I is a critical event, as collagen type I contributes to long-term strength and stability, withstands normal physiological stresses, and promotes functional tissue recovery (Tombultürk et al., 2023). By day 24, the remodeling phase is usually well established, with ongoing adjustments to the structure and density of collagen in the tissue continuing to increase (El-Sayed, 2016).

These findings are consistent with the study's results, which indicate that FDSG can reduce IL-1β protein levels (Table 3) (Figure 2) and increase collagen density (Table 4) (Figure 3) after 10 days and 24 days of treatment. When the healing process continues to the proliferative phase, WS provides an anti-inflammatory effect. WS contains inflammation-regulating molecules such as IL-10 that can inhibit the synthesis of pro-inflammatory agents, including IL-1β (Sari et al., 2021; Jiao et al., 2021). This role occurs in the proliferation and remodeling phases. This shift in cytokine balance is essential to overcome inflammation and promote tissue repair and facilitate the transition to the remodeling phase (Cassano et al., 2018). The modulation of IL-1β protein levels and collagen density throughout the wound healing process can be impacted by inflammatory triggers (Ganesan et al., 2014) and cellular interactions, including the regulation of macrophage activity (Ferreira et al., 2020) and the presence of hypoxic conditions in the wound microenvironment which can stimulate WS to produce cytokines and growth factors that promote wound healing (Bundgaard et al., 2020).

IL-1β is crucial in tissue repair due to its role in stimulating collagen production and fibroblast activity. Collagen density in the wound area is essential for structural integrity and functional tissue recovery, thus promoting increased wound reduction. This is supported by the results of a study showing a wound reduction process from day 3 to 24 in FDSG compared to PC (Table 2) (Figure 1). On day 3, a reduction in the necrotic area can be seen. The tissue around the wound appears more hydrated and shows early signs of granulation tissue formation (El-Sayed et al., 2023). On day 10, it shows clearer granulation tissue growth, with a significantly reduced necrotic area. The wound becomes flatter, indicating the process of keratinocyte and fibroblast migration to repair damaged tissue (Vaidyanathan, 2021; Kumar et al., 2021). In the FDSG 2 and CpG groups, wound morphology showed faster improvement with smoother tissue and color closer to normal tissue. Furthermore, on day 24, the wound was almost completely healed, with epithelial regeneration approaching normal. In the FDSG and CpG groups, scars were almost invisible, with skin color and texture resembling healthy tissue. Epithelialization and tissue remodeling took place better, indicating the effectiveness of therapy in accelerating regeneration (Lee et al., 2021).

FDSG has several advantages that make it a potential burn wound therapy agent. The freeze-dried gel formulation increases the stability of bioactive substances, thus ensuring their effectiveness over a longer period (Bari et al., 2020; Damayanti et al., 2021). In addition, FDSG is able to release bioactive factors like growth factors and cytokines are released gradually and in a controlled manner, ensuring optimal concentrations to support the healing process (Mirfendereski et al., 2025; Bari et al., 2020). FDSG demonstrates potential in regulating inflammation through maintaining equilibrium between pro- and anti-inflammatory mediators' activities, and creates a microenvironment conducive to tissue regeneration. In addition, FDSG also stimulates collagen production through stimulation of fibroblasts by bFGF and TIMP-2 content, strengthening the newly formed tissue (Chandra et al., 2022; Fadhilah, 2023). The angiogenesis process is also supported by molecules such as VEGF and PDGF contained in FDSG, which play a role in the development of new blood vessels for oxygen and nutrient supply (Deng et al., 2018). With high biocompatibility, FDSG minimizes the risk of side effects on body tissues (Fadhilah, 2023). Research by Widowati et al. (2024a, 2024b) also validated that FDSG contains growth factors, cytokines, and antioxidants in higher concentrations than NFDS formulations, thus increasing its potential as an effective burn therapy. This combination of characteristics makes FDSG an innovative and promising formulation in supporting the burn healing process. The proposed mechanism of FDSG as a burn wound therapy agent can be seen in Figure 4.

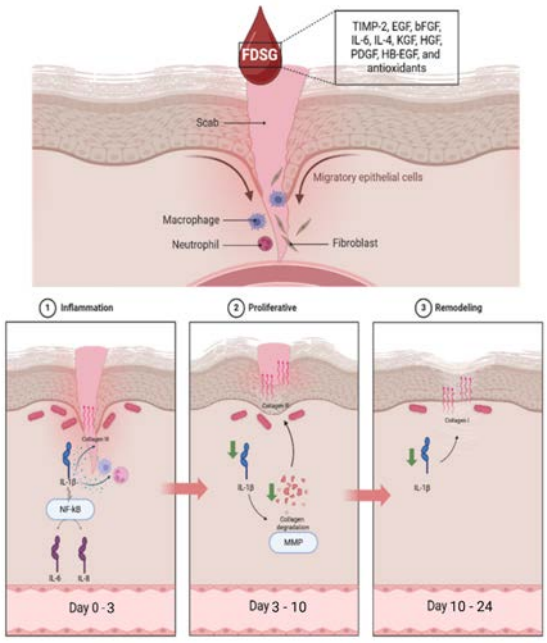

Figure 4. Proposed mechanism of FDSG treatment as a burn wound therapy

FDSG contains various growth factors, cytokines, and antioxidants that act as burn wound therapy agents. FDSG plays a role in wound reduction through IL-1β regulation and increased collagen density in the inflammatory, the cell growth and tissue reconstruction stages during the healing process.

This study has several limitations. First, the wound healing effects of the FDSG were only evaluated in a rat model, which may not fully replicate human wound healing processes. Second, the relatively small sample size and limited observation period may influence the generalizability of the results. Future studies with larger animal groups, longer-term monitoring, and molecular

profiling are needed to validate the findings and explore clinical applications in human subjects.

5. Conclusion

FDSG is known to have potential as a burn wound therapy agent, with twice daily application being an effective treatment. On day 24, FDSG treatment significantly reduced wound size. In addition, FDSG caused IL-1β regulation and increased collagen density in the wound healing phases including inflammation, proliferation, and remodelling. Overall, these findings confirm that FDSG reduces inflammation, increases collagen synthesis, and supports skin regeneration in burn wounds, which warrants further research on its mechanisms and broader clinical applications in wound healing.

6. Ethical Clearance:

This research received ethical approval from Research Ethic Committee, Faculty of Medicine, Maranatha Christian University (No: 046/KEP/V/2024, dated on May 3rd 2024).

Acknowledgments:

The authors express gratitude to Minister of Education, Culture, Research and Technology of the Republic of Indonesia (Applied Research 2025 with grant number 125/C3/DT.05.00/PL/2025 and 7973/LL4/PG/2025, 195.P/LPPM/UKM/VI/2025) and Biomolecular & Biomedical Research, Aretha Medika Utama, West Java, Indonesia for providing laboratory facilities and research methodology.

Conflicts of Interests:

None.

Supplementary Material:

None

References

Alapure B, Lü Y, He M, Chu C, Peng H, Muhale F, et al. 2018. Accelerate healing of severe burn wounds by mouse bone marrow mesenchymal stem cell-seeded biodegradable hydrogel scaffold synthesized from arginine-based poly(ester amide) and chitosan. *Stem Cells Dev*. **27(23)**:1605–20.

Alsarayreh A, Attalah Oran S, Shakhanbeh J. 2022. In vitro and in vivo wound healing activities of *Globularia arabica* leaf methanolic extract in diabetic rats. *J Cosmet Dermatol*. **21(10)**:4888–900.

Bari E, Silvestre D, Mastracci L, Grillo F, Grisoli P, Marrubini G, et al. 2020. GMP-compliant sponge-like dressing containing MSC lyo-secretome: proteomic network of healing in a murine wound model. *Eur J Pharm Biopharm*. **155**:37–48.

Bian F, Pelegrino F, Pflugfelder S, Volpe E, Li D, Paiva C. 2015. Desiccating stress-induced MMP production and activity worsens wound healing in alkali-burned corneas. *Invest Ophthalmol Vis Sci*. **56(8)**:4908–15.

Bundgaard L, Stensballe A, Elbæk K, Berg L. 2020. Mass spectrometric analysis of the in vitro secretome from equine bone marrow-derived mesenchymal stromal cells to assess the effect of chondrogenic differentiation on response to interleukin-1β treatment. *Stem Cell Res Ther*. **11(1)**:1–12.

Casado-Santos A. 2024. Equine corneal wound healing using mesenchymal stem cell secretome: case report. *Animals (Basel)*. **14(13)**:1842.

Cassano J, Schnabel L, Goodale M, Fortier L. 2018. Inflammatory licensed equine MSCs are chondroprotective and exhibit enhanced immunomodulation in an inflammatory environment. *Stem Cell Res Ther*. **9(1)**:1–11.

Chandra C, Pratiwi Y, Tan S. 2022. Potential application of Wharton's jelly-derived mesenchymal stem cells conditioned medium (WJMSCs-CM) on delayed wound healing: a case report. *J Pharm Res Int*. **34(4A)**:1–6.

Damayanti R, Rusdiana T, Wathoni N. 2021. Mesenchymal stem cell secretome for dermatology application: a review. *Clin Cosmet Investig Dermatol*. **14**:1401–12.

Deng G, Li K, Chen S, Chen P, Zheng H, Yu B, et al. 2018. Interleukin 10 promotes proliferation and migration, and inhibits tendon differentiation via the JAK/STAT3 pathway in tendon derived stem cells *in vitro*. *Mol Med Rep*. **18(6)**:5541–49.

Deshpande R, Kanitkar M, Kadam S, Dixit K, Chhabra H, Bellare J, et al. 2018. Matrix-entrapped cellular secretome rescues diabetes-induced EPC dysfunction and accelerates wound healing in diabetic mice. *PLoS One*. **13(8)**:e0202510.

Ding DC, Chang YH, Shyu WC, Lin SZ. 2015. Human umbilical cord mesenchymal stem cells: a new era for stem cell therapy. *Cell Transplant*. **24(3)**:339–47.

El Omar R, Beroud J, Stoltz JF, Menu P, Velot E, Decot V. 2014. Umbilical cord mesenchymal stem cells: the new gold standard for mesenchymal stem cell-based therapies? *Tissue Eng Part B Rev*. **20(5)**:523–44.

El-Sayed M. 2023. Mesenchymal stem cell transplantation in burn wound healing: uncovering the mechanisms of local regeneration and tissue repair. *Histochem Cell Biol*. **161(2)**:165–81.

El-Sayed Y. 2016. Time course of histomorphologic features during chronic burn wound healing. *Forensic Med Anat Res*. **4(1)**:1–6.

Fadhilah D. 2023. The essentials of stem cell-derived secretome in wound healing. *World J Biol Pharm Health Sci*. **16(2)**:58–65.

Ferreira J, Teixeira G, Neto E, Ribeiro-Machado C, Silva A, Caldeira J, et al. 2020. Unravelling the role of mesenchymal stem/stromal cells secretome in intervertebral disc degeneration in a pro-inflammatory/degenerative ex vivo model. *Res Sq [Preprint]*. https://doi.org/10.21203/rs.2.22688/v1.

Finnerty CC, Jeschke MG, Branski LK, Barret JP, Dziewulski P, Herndon DN. 2016. Hypertrophic scarring: the greatest unmet challenge after burn injury. *Lancet*. **388(10052)**:1427–36.

Ganesan S, Rathinam V, Bossaller L, Army K, Kaiser W, Mocarski E, et al. 2014. Caspase-8 modulates dectin-1 and complement receptor 3–driven IL-1β production in response to β-glucans and the fungal pathogen, *Candida albicans*. *J Immunol*. **193(5)**:2519–30.

Gentile P, Garcovich S. 2019. Systematic review: Adipose-derived mesenchymal stem cells, platelet-rich plasma and biomaterials as new regenerative strategies in chronic skin wounds and soft tissue defects. *Int J Mol Sci*. **20(6)**:1495.

Gonçalves R, Saggese T, Yong Z, Ferreira J, Ignatius A, Wilke H, et al. 2022. Interleukin-1β more than mechanical loading induces a degenerative phenotype in human annulus fibrosus cells, partially impaired by anti-proteolytic activity of mesenchymal stem cell secretome. *Front Bioeng Biotechnol*. **9**:802789.

Gugliandolo E, Macrì F, Fusco R, Siracusa R, D'Amico R, Cordaro M, et al. 2021. The protective effect of snail secretion filtrate in an experimental model of excisional wounds in mice. *Vet Sci*. **8(8)**:167.

Hakim R. 2023. Effects of broccoli extract (Brassica oleracea var. italica) on collagen images in wounds: experimental study in Wistar rats (Rattus norvegicus). *Padjadjaran J Dent*. **35(2)**:146.

Hebron C, Mehta K, Stewart B, Price P, Potokar T. 2022. Implementation of the World Health Organization global burn registry: lessons learned. *Ann Glob Health*. **88(1)**:80.

Jeschke MG, van Baar ME, Choudhry MA, Chung KK, Gibran NS, Logsetty S. 2020. Burn injury. *Nat Rev Dis Primers*. **6(1)**:11.

Jiao Z, Ma Y, Zhang Q, Wang Y, Liu T, Liu X, et al. 2021. The adipose-derived mesenchymal stem cell secretome promotes hepatic regeneration in miniature pigs after liver ischaemia-reperfusion combined with partial resection. *Stem Cell Res Ther*. **12(1)**:377.

Kartika RW, Alwi I, Reksodiputro MH, Yunir E, Waspadji S, Immanuel S, et al. 2021. Combination of Hyaluronic Acid with Advance-Platelet Rich Fibrin to Reduce Chronic Inflammation: a study in IL-6 and Granulation Index. *Jordan J Biol Sci*. **14(5):**1–8.

Kimball A, Joshi A, Carson W, Boniakowski A, Schaller M, Allen R, et al. 2017. The histone methyltransferase Mll1 directs macrophage-mediated inflammation in wound healing and is altered in a murine model of obesity and type 2 diabetes. *Diabetes*. **66(9)**:2459–71.

Kumar A, Li Y, Mallick S, Yang E, Dhaliwal D, Price A, et al. 2022. Stem cell secretome promotes scarless corneal wound healing and rescues corneal sensory nerves. *bioRxiv* [Preprint]. https://doi.org/10.1101/2022.05.07.490347

Laksmitawati DR, Noor SU, Sumiyati Y, Hartanto A, Widowati W, Pratami DK. 2022. The effect of mesenchymal stem cell-conditioned medium gel on burn wound healing in rat. *Vet World*. **15(4)**:841.

Lanci A, Merlo B, Mariella J, Castagnetti C, Iacono E. 2019. Heterologous Wharton's jelly derived mesenchymal stem cells application on a large chronic skin wound in a 6-month-old filly. *Front Vet Sci*. **6**:9.

Lee S, Heo J, Ahn E, Kim J, Kim Y, Chang H, et al. 2021. Conditioned secretome of adipose-derived stem cells improves dextran sulfate sodium-induced colitis in mice. *World J Gastroenterol*. **27(23)**:3342–52.

Li Z, Zhang Z, Chen X, Zhou J, Xiao X. 2017. Treatment evaluation of Wharton's jelly-derived mesenchymal stem cells using a chronic salpingitis model: an animal experiment. *Stem Cell Res Ther*. **8(1)**:274.

Mirfendereski G, Bagheri A, Niknami S, Amin M, Khaghani F, Torshabi M, et al. 2025. The dual inhibitory effect of adipose-derived mesenchymal stem cell secretome on JAK2/STAT3 and PI3k/AKT/mTOR signaling pathways. *Jordan J Biol Sci*. **18(1):**1–9.

Moll G, Alm JJ, Davies LC, Von Bahr L, Heldring N, Stenbeck-Funke L, et al. 2014. Do cryopreserved mesenchymal stromal cells display impaired immunomodulatory and therapeutic properties? *Stem Cells*. **32(9)**:2430–42.

Mozzati M, Martinasso G, Pol R, Polastri C, Cristiano A, Muzio G, et al. 2010. The impact of plasma rich in growth factors on clinical and biological factors involved in healing processes after third molar extraction. *J Biomed Mater Res A*. **95A(3)**:741–6.

Nielson CB, Duethman NC, Howard JM, Moncure M, Wood JG. 2017. Burns: pathophysiology of systemic complications and current management. *J Burn Care Res*. **38(1)**:e469–81.

Nowak D, Jakubczyk E. 2020. The freeze-drying of foods—The characteristic of the process course and the effect of its parameters on the physical properties of food materials. *Foods*. **9(10)**:1488.

Rong X, Li J, Yang Y, Shi L, Jiang T. 2019. Human fetal skin-derived stem cell secretome enhances radiation-induced skin injury therapeutic effects by promoting angiogenesis. *Stem Cell Res Ther*. **10(1):**383

Rowan MP, Cancio LC, Elster EA, Burmeister DM, Rose LF, Natesan S, et al. 2015. Burn wound healing and treatment: review and advancements. *Crit Care*. **19(1)**:243.

Salibian AA, Rosario AT, Severo LA, Nguyen L, Banyard DA, Toranto JD, et al. 2016. Current concepts on burn wound conversion—A review of recent advances in understanding the secondary progressions of burns. *Burns*. **42(5)**:1025-35.

Sari FN, Samoedra RS, Pratama SK, Rahayu S, Soewondo A, Jatmiko YD, et al. 2023. Immunomodulatory Effects of Unripe Sapodilla (*Manilkara zapota*) Fruit Extract Through Inflammatory Cytokine Regulation in Type 1 Diabetic Mice. *Jordan J Biol Sci*. **16(2):**1–7.

Schaefer TJ, Tannan SC. 2021. **Thermal Burns**. In: StatPearls. Treasure Island (FL): StatPearls Publishing.

Schneider V, Kruse D, Mattos I, Zöphel S, Tiltmann K, Reigl A, et al. 2021. A 3D in vitro model for burn wounds: monitoring of regeneration on the epidermal level. *Biomedicines*. **9(9)**:1153.

Serra S, Costa J, Assunção-Silva R, Teixeira F, Silva N, Anjo S, et al. 2018. Influence of passage number on the impact of the secretome of adipose tissue stem cells on neural survival, neurodifferentiation and axonal growth. *Biochimie*. **155**:119-28.

Shagdarova B, Konovalova M, Zhuikova Y, Lunkov A, Жуйков B, Khaydapova D, et al. 2021. Collagen/chitosan gels cross-linked with genipin for wound healing in mice with induced diabetes. *Materials***. 15(1)**:15.

Shi H, Lo T, Ma D, Condor B, Lesmana B, Parungao R, et al. 2020. Dihydrotestosterone (DHT) enhances wound healing of major burn injury by accelerating resolution of inflammation in mice. *Int J Mol Sci*. **21(17)**:6231.

Sikora JP, Karawani J, Sobczak J. 2023. Neutrophils and the systemic inflammatory response syndrome (SIRS). *Int J Mol Sci*. **24(17)**:13469.

Srinivasan S, Sharma K, Rao KMK, Gupta A. 2021. Advanced Burn Wound Care: Burn Wound Dressings, Cell-Based Therapies, and Gene Modulation. In: Advanced Wound Care Therapies for Non-Healing Diabetic, Venous, and Arterial Ulcers. *Cham: Springer*. p. 331–57.

Sugioka K, Kodama-Takahashi A, Yoshida K, Aomatsu K, Okada K, Nishida T, et al. 2017. Extracellular collagen promotes interleukin-1β–induced urokinase-type plasminogen activator production by human corneal fibroblasts. *Invest Ophthalmol Vis Sci*. **58(3)**:1487.

Tan S, Aisyah P, Firmansyah Y, Nathasia N, Budi E, Hendrawan S. 2023. Effectiveness of secretome from human umbilical cord mesenchymal stem cells in gel (10% SM-hUCMSC gel) for chronic wounds (diabetic and trophic ulcer) – phase 2 clinical trial. J *Multidiscip Healthc*. **16**:1763–77.

Tilotta V, Vadalà G, Ambrosio L, Cicione C, Giacomo G, Russo F, et al. 2023. Mesenchymal stem cell-derived secretome enhances nucleus pulposus cell metabolism and modulates extracellular matrix gene expression in vitro. *Front Bioeng Biotechnol*. **11**.

Tofiq SA, Azeez HA, Othman HH. 2021. Wound healing activities of *Moringa oleifera* leaves extract cultivated in Kurdistan region-Iraq. *Jordan J Biol Sci*. **14(4):**1–6.

Tombultürk F, Soydaş T, Kanıgür-Sultuybek G. 2023. Topical metformin accelerates wound healing by promoting collagen synthesis and inhibiting apoptosis in a diabetic wound model. *Int Wound J*. **21(1)**.

Tran-Nguyen TM, Le KT, Nguyen LGT, Tran TLT, Hoang-Thai PC, Tran TL, et al. 2020. Third-degree burn mouse treatment using recombinant human fibroblast growth factor 2. *Growth Factors*. **38(5-6)**:282-90.

Uchiyama T, Li X, Nakajima K, Teranaka A, Liu Y, Bhawal U, et al. 2021. Differential inflammatory responses in the healing of oral mucosa and skin wounds. *Int J Oral Med Sci*. **20(1)**:19–23.

Vaidyanathan, L. 2021. Growth factors in wound healing—a review. *Biomed Pharmacol J*, **14(3)**:1469-80.

Wang Y, Chen X, Cao W, Shi Y. 2014. Plasticity of mesenchymal stem cells in immunomodulation: pathological and therapeutic implications. *Nat Immunol.* **15(11)**:1009–16.

Widowati W, Faried A, Adam A, Rahmat D, Kusuma HSW, Dewi NSM, et al. 2024. Potential antiaging activity of secretome gel of human Wharton's jelly mesenchymal stem cells (hWJ-MSCs) in UV-induced mice models. *Iran J Basic Med Sci.* **27(7)**:868.

Widowati W, Faried A, Gunanegara RF, Rahardja F, Zahiroh FH, Sutendi AF, et al. 2024. The Potential of Human Wharton's Jelly Mesenchymal Stem Cells Secretome Based Topical Gel for Therapeutic Application. *Avicenna J Med Biotechnol.* **16(4)**:233.

Widowati W, Faried A, Gunanegara RF, Rahardja F, Zahiroh FH, Sutendi AF, et al. 2024. Wound Healing Potent of Lyophilized-Secretome Gel from Human Wharton's Jelly Mesenchymal Stem Cells. *Trends Sci.* **21(10)**:8028–8028.

Yin H, Chen C, Liu Y, Tan Y, Deng Z, Yang F, et al. 2019. Synechococcus elongatus PCC7942 secretes extracellular vesicles to accelerate cutaneous wound healing by promoting angiogenesis. *Theranostics.* **9(9)**:2678–91.

Zhang Y. 2011. Role of c-jun N-terminal kinase and p38/activation protein-1 in interleukin-1β-mediated type I collagen synthesis in rat hepatic stellate cells. *APMIS.* **120(2)**:101–7.

Zukhiroh Z, Putra A, Chodidjah C, Sumarawati T, Subchan P, Trisnadi S, et al. 2022. Effect of secretome-hypoxia mesenchymal stem cells on regulating SOD and MMP-1 mRNA expressions in skin hyperpigmentation rats. *Open Access Maced J Med Sci.* **10(A)**:1–7.

JJBS

Volume 19, Number 1,March 2026
ISSN 1995-6673
Pages 169 – 176
https://doi.org/10.54319/jjbs/190116

Jordan Journal of Biological Sciences

Shoot Induction of *Agathis borneensis* Warb in *in vitro* Culture

Irni Furnawanthi Hindaningrum[1], Andhika Rahmansani[2], Linda Novita[1], Roni Kartiman[1], Mardoni Elya[1], Restu Siwi Muharromah[1], Kassandra Budiarni[1], Yelnititis[1], Rendie Prasetyo[2], Sugiyono[2*]

[1] *Applied Botany Research Center, Life Science and Environment Research Organization, National Research and Innovation Agency, Indonesia 16911;*[2] *Department of Botany, Faculty of Biology, Jenderal Soedirman University, Indonesia 53122*

Received: January 10, 2025; Revised: May 10, 2025; Accepted: June 3, 2025

Abstract

Agathis borneensis Warb., a member of the *Araucariaceae* Family, is listed as an Endangered *A4cd* plant. *A. borneensis* population in its natural habitat is decreasing due to habitat destruction and uncontrolled harvesting. *A. borneensis* propagation remains challenging due to slow growth, recalcitrant seed, low natural regeneration, and uneven germination, which can take months. Vegetative propagation through cutting is also difficult to root, and success depends on the age of the mother tree. To provide alternative *A. borneensis* ex-situ conservation and propagation, the plant's *in vitro* culture technique can be applied, as it produces many seedlings in a shorter time. This research aimed to evaluate the effects of cytokinins on A. borneensis shoot growth and to determine the optimal cytokinin and its concentration to stimulate *A. borneensis* shoot growth. A completely randomized split-plot design has been used in this study. The treatments included three types of cytokinin (BAP, Kinetin, and TDZ) and cytokinin concentrations at 0, 1, 2, 3, and 4 µM. The observed variable was *A. borneensis* shoot growth, with the parameters measured as shoot emergence, shoot and leaf numbers, and shoot length. The data gained were analyzed using DSAASTAT VER 1.514 software through an Analysis of Variance at 95% and 99% significance levels. The means were compared using the Duncan Multiple Range Test (DMRT) at a 95% confidence level. This study showed that MS media supplemented with 1 µM kinetin produced the fastest shoot emergence time. Meanwhile, *A. borneensis* shoots grown on MS media without cytokinin resulted in the formation of the most leaves.

Keywords: *Agathis borneensis*, 6-Benzylaminopurine, *in vitro*, Kinetin, Thidiazuron.

1. Introduction

Agathis borneensis Warb., a member of the Araucariaceae family, originated from the island of Borneo, Indonesia. *A. borneensis* can grow at low and high altitudes in tropical rainforests (Darma *et al*., 2022; Farjon, 2017). *A. borneensis* trees can reach 50-55 m and up to 3.5 m in diameter at breast height. *A. borneensis* is considered the king of wood in Borneo, a highly valuable timber. Its large and smooth wood is popular for light construction, household items, panel boards, chopsticks, matches, veneers, fuel wood, and charcoal. The resin exudate from the stem bark is a widely traded Non-Timber Forest Product (NTFP) known as copal. The Dayak communities of highland Borneo traditionally used resin for lighting (Stalin & Franco, 2021). Essential oils from *Agathis borneensis* contain α-pinene, δ-limonene, β-pinene, terpinen-4-ol, and α-terpineol. Adam *et al*. (2017) identified 60 chemical compounds in the leaves and stem bark, including monoterpene hydrocarbons, oxygenated monoterpenes, oxygenated diterpenes, oxygenated sesquiterpenes, and sesquiterpene hydrocarbons. These compounds exhibit antitumor, anticancer, anti-inflammatory, antimalarial, antibacterial, and anesthetic properties (Stalin & Franco, 2021).

According to the IUCN Red List, *A. borneensis* is categorized as Endangered A4cd due to *overexploitation*, which has halved the total habitat area and is ongoing. These conditions are exacerbated by the decline of Agathis' natural habitat quality due to climate change and human activities (Adam *et al*., 2017; Farjon, 2013). Therefore, conservation efforts must be inclusive and comprehensive, using available approaches. However, its propagation remains challenging due to slow growth, seed dormancy issues, and habitat loss. Seeds are recalcitrant (losing viability quickly when dried) and have low natural regeneration due to irregular seed production and slow, uneven germination, which can take months. Cuttings are difficult to root, and success depends on the age of the mother tree.

In vitro culture methods can be applied to propagate rare plants such as *A. borneensis* (Widyatmoko, 2019) to obtain large numbers of contaminant-free seedlings. Ishii and Mohsin (1994) identified the shoot tip of Agathis as a suitable explant for tissue culture initiation. Multiple shoots were produced when Agathis borneensis shoot tips were cultured on half-strength Gamborg's medium (0.5 G) with 1 mg/L zeatin. When the shoot tip was subsequently cultured on 0.25 G with 1 mg/L IBA, shoot elongation occurred.

* Corresponding author. e-mail: sugiyono@unsoed.ac.id.

Plant growth and differentiation *in vitro* culture are influenced by several factors, including plant genotype, nutrients, growth environment, and growth regulators (PGRs) (Biradar, 2022; George *et al*., 2008; Park, 2021). Cytokinins are often used for shoot propagation in vitro. Cytokinins can induce shoot initiation and proliferation. Some commonly used cytokinins include BAP (6-Benzylaminopurine), Kinetin (6-furfurylaminopurine), and Thidiazuron (TDZ). BAP is the most frequently used cytokinin because it is effective for stimulating shoot formation, stable on heating, resistant to oxidation, and the cheapest among cytokinins (Agustina *et al*., 2019). Kinetin is stable and more resistant to high temperatures (Andriani *et al*., 2023; Putriana *et al*., 2019). Meanwhile, TDZ is a growth regulator that functions like auxin and cytokinin, producing responses such as callus induction, embryogenesis, and organogenesis (Taha *et al*., 2021).

Only a few reports on both *A. borneensis in vitro* culture and PGRs application have been published. Therefore, it is crucial to evaluate the effect of cytokinin application on *A.* borneensis shoots' growth in *in vitro* culture and determine the best cytokinin and its concentration to stimulate this growth. This research is expected to produce high-quality seedlings to support both seedling production and conservation efforts.

2. Methods

2.1. Research design

This study was conducted in the Plant Tissue Culture Laboratory of the Applied Botany Research Centre at Indonesia's National Research and Innovation Agency. The study has been carried out experimentally using a completely randomized split-plot design. The main plot applied was cytokinin types, including BAP, TDZ, and Kinetin. The subplot was the cytokinin concentration, with four levels: 0, 1, 2, 3, and 4 µM. All treatment combinations were replicated 5 times, resulting in 45 experimental units. The variable observed was *A. borneensis* shoot growth, with the parameters measured including shoot emergence, shoot and leaf numbers, and shoot length.

2.2. Explant preparation and sterilization

The lateral shoots of *A. borneensis* were collected from a three-year-old mother plant of the Bogor Botanical Garden (collection number vak. XX.D.5.4 originated from Central Kalimantan (Central Borneo). The lateral shoot apexes with five leaves were collected, wrapped in cotton moistened with a vitamin B1 solution at the base of the cut, and placed in an airtight plastic bag to avoid stress and maintain explant freshness and vigor.

Upon arrival in the laboratory, the leaves were excised from the explants, and the shoots were gently cleaned with a cotton swab and detergent. The shoots were then rinsed in running water for 15-30 minutes. The clean shoots were then cut, and the second internode, measuring 3-4 cm, was used as an explant. Explants were soaked in sterile water supplemented with 3 drops of Tween 80 per 100 mL, then shaken for 30 minutes. The explants were subsequently rinsed for 10 seconds with sterile water, which was repeated 3 times. After rinsing, the explants were immersed in citric acid ($C_6H_8O_7$) solution for 30 minutes. Explants were transferred and soaked in bactericide and fungicide solutions without rinsing for 60 minutes. Explants were thoroughly rinsed with sterile water for 10 seconds and 3 times.

The next step was conducted in the Laminar Air Flow cabinet, in which explants were soaked for two minutes in a 70% ethanol solution with agitation, followed by a rinse in sterile water for three ten-second intervals. Explants were soaked in 0.1% HgCl2 for 2 x 7-minute intervals while shaking, then rinsed with sterile water for 3 x 10-second intervals. The use of 0.1% HgCl2 following 70% ethanol sterilization has also been reported by Chukwu *et al*. (2025), Justine *et al*. (2022), Kulkarni *et al*. (1996) and Yadav *et al*. (2021). Sterile explants were blotted on sterile filter paper. The tips of the explants in contact with the sterilizing agent were excised, resulting in an explant size of ± 2 cm. The explants were soaked again in sterile water and blotted on sterile filter paper.

2.3. Plant in vitro culture procedures

Preculture. The sterile explants were planted onto sterilized testing media (MS0) consisting of an MS medium supplemented with 3% sucrose, 100 mg/L myo-inositol, solidified with 0.7% Agar, and incubated for 7 days. This medium was used to test whether the explants were sterile.

Treatment application. The basic medium used is MS with 3% sucrose and 100 mg/L myo-inositol. A total of 750 mL of basic medium was prepared and divided into 15 flasks of 50 mL each. Cytokinins and their concentrations were then added according to the treatment combination. The media pH was measured and set to 5.8 before sterilization, and 0.7% Agar was added to each flask. The media were heated until agar was completely dissolved. Each treatment medium was divided into 5 test tubes and sterilized in an autoclave at 0.15 MPa and 121°C for 20 minutes. Sterile media were then cooled until use. The sterile explants from the preculture stage were planted onto the treatment medium and sealed tightly. They were incubated at 24 oC with continuous tube luminescent light for 16 weeks.

2.4. Data collection

Shoot emergence, shoot and leaf numbers, and shoot length were measured when shoot size was > 2 mm. Shoot emergence was observed and recorded at weekly intervals. Shoot and root numbers were counted at week 16. Shoot length was measured at week 16 by measuring the shoot from the shoot base until the tip of leaf number 1. The data were recorded, and the explant was photographed.

2.5. Data analysis

The data were analyzed using DSAASTAT VER 1.514 software to generate an Analysis of Variance (ANOVA) at 95% and 99% significance levels. The means were compared using a Duncan Multiple Range Test (DMRT) at a 95% confidence level.

3. Results and Discussion

At 16 weeks after planting (WAP), the *A. borneensis* Warb. explants exhibited growth, as shown by increases in shoot and leaf number and shoot length, even when grown in media without cytokinin. The increase in plant size, measured by organ size and height, is a sign of plant

growth, while changes in the shape of stem organs, roots, leaves, and the appearance of flowers and fruits on plants are signs of plant development (Prasetyo *et al*., 2020; Sitompul & Guritno, 1995; Tamyiz *et al*., 2022). Figure 1 illustrates the growth of explants cultivated in media without any growth regulators after 16 weeks of culture. Ahmed & Mohamed (2022) stated that kauri or resin trees are perennial, long-lived plants with moderate growth rates. Moreover, Steward *et al.* (2014) indicated that kauri exhibits modest growth at its juvenile stage.

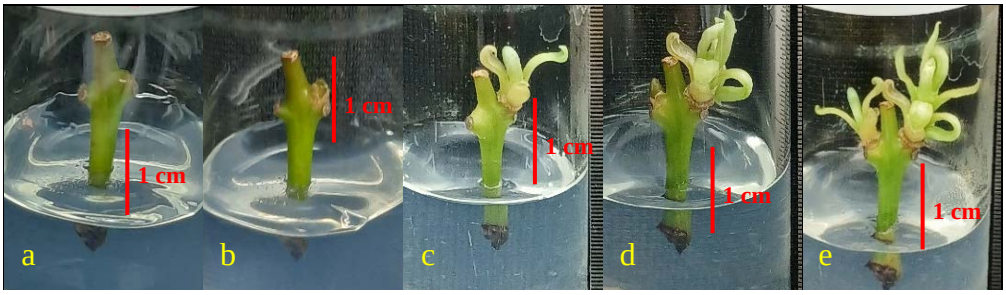

Figure 1 *A. borneensis* shoots appearance on media without cytokinin addition. (a) At age 0 weeks after planting; (b) 4 weeks after planting; (c) 8 weeks after planting; (d) 12 weeks after planting; (e) 16 weeks after planting.

The research results (Table 1) revealed that the types of cytokinin used (BAP, Kinetin, and TDZ) have no significant effect on shoot emergence time, shoot number, shoot length, and leaf number ($p > 0.05$). Table 1 also showed that cytokinin concentrations controlled the leaf number parameter; meanwhile, the interaction between cytokinin types and concentrations strongly controlled shoot emergence time. Plant responses to plant growth regulators can differ depending on the type and concentration used. According to Ružić *et al*. (2016), the optimal type and concentration of cytokinin for woody plants may vary depending on species and genotype.

Table 1. Summary of ANOVA results on the effects cytokinin of types and concentrations on A. borneensis shoots 16 weeks after planting.

Source of Variety	Significance (p-value)			
	Shoot Emergence	Shoot Number	Shoot Length	Leaf Number
p - Types of cytokinin	0,301	0,103	0,208	0,104
p - Concentrations of Cytokinin	0,055	0,093	0,215	0,017*
p - Interaction between cytokinin type and concentration	0,001**	0,306	0,472	0,113

Notes: Numbers followed by ** indicate highly significant differences in the F-test with 99% confidence level; * indicates significant differences in the F-test with 95% confidence level.

Shoot emergence is the time when a plant organ begins to grow. This growth is closely related to the development of meristematic tissues and to growth regulators that act in plants (Fajar *et al*., 2018). The results of DMRT (Table 2) revealed that *A. borneensis* explants cultured on media added with 1 µM Kinetin produced the fastest shoot emergence with an average time of 37.00±11.79 days after planting (dap). However, no significant differences were found among those cultured on BAP 1 µM, BAP 2 µM, Kin 3 µM, Kin 4 µM, TDZ 0 µM, and TDZ 4 µM. The longest shoot emergence was observed on explant culture on TDZ 3 µM (92.00±0.00). These non-significant differences in some treatments indicate that all cytokinins can stimulate shoot emergence at each optimal concentration. Kher *et al*. (2014) stated that bud formation on plant nodes varies with the type and concentration of growth regulators used.

Cytokinin influences shoot formation, cell division, and shoot proliferation in plants. Adding cytokinins to the media is crucial for inducing shoot formation and proliferation in node explants (Bala et al., 2018; J. Zhao et al., 2024). Cytokinins can regulate gene expression related to the cell division cycle. It suggests that growth regulators promote shoot growth by affecting the cell division cycle (Zhao *et al*., 2020). Kinetin is a type of cytokinin effective in shoot formation and rejuvenation. Kinetin can stimulate the growth of lateral buds and break apical (Fathy *et al*., 2022; Thorat *et al*., 2022; Zhao *et al*., 2024).

Table 2. The DMRT results of the average of A. borneensis shoot emergence time in response to the interaction between cytokinin types and concentrations at 16 wap. Note: means followed by the same letter indicate no significant difference at 95% DMRT level of confidence.

Treatments	Shoot emergence time (day)
BAP 0 µM	71.00 ± 32.14^{abcd}
BAP 1 µM	54.00 ± 4.00^{de}
BAP 2 µM	52.67 ± 12.22^{de}
BAP 3 µM	76.50 ± 3.50^{abcd}
BAP 4 µM	89.50 ± 16.50^{ab}
Kin 0 µM	78.00 ± 28.00^{abcd}
Kin 1 µM	37.00 ± 11.79^{e}
Kin 2 µM	90.33 ± 2.89^{ab}
Kin 3 µM	54.00 ± 4.00^{de}
Kin 4 µM	59.67 ± 24.01^{cde}
TDZ 0 µM	62.33 ± 21.36^{bcde}
TDZ 1 µM	76.50 ± 3.50^{abcd}
TDZ 2 µM	87.00 ± 7.81^{abc}
TDZ 3 µM	92.00 ± 0.00^{a}
TDZ 4 µM	58.00 ± 8.00^{de}

According to Sarmast *et al.* (2012), cytokinins at low concentrations are more effective in inducing shoots in *A. excelsa* R. Br. In addition, Kinetin produced better shoot

proliferation and height than other cytokinins. Additionally, Gogoi *et al*. (2017) observed that shoot initiation of *Morus indica* L. performed optimally on Murashige and Skoog media supplemented with Kinetin at different concentrations. Kinetin is needed in the late stages of the G2 phase of the cell division cycle. Cells that did not have enough Kinetin will be stuck in the G2 phase. Kinetin stimulates phosphate release, thereby activating enzymes, which then trigger the synchronous and rapid entry of cells into the mitotic phase (Barciszewski *et al*., 2007).

Several studies have reported that BAP and TDZ were more effective than Kinetin for shoot induction. BAP was more effective in axillary bud formation of *Balanites aegyptiaca*, *Citrus limon*, and *Syzygium cuminii* (Rathore *et al*., 2004). BAP promotes shoot formation by releasing axillary buds from the dormancy phase (Li *et al*., 2021; Neogy *et al*., 2020). Thidiazuron was more effective for shoot formation in node explants of three *Vitex* species (*Vitex trifolia*, *Vitex negundo*, and *Vitex doniana*) as well as *Syzygium cuminii* and did not show any abnormal morphology (Ahmad & Faisal, 2018; Naaz *et al*., 2021). TDZ promotes shoot formation by inducing cell division and proliferation and rearranging meristematic regions to differentiate axillary buds (Ram *et al*., 2022).

In this study, explants cultured in media supplemented with TDZ showed browning at the base of the explants (Figure 2). In some cases, TDZ has serious adverse effects on in vitro growth. Although TDZ has high cytokinin activity, vitrified shoots and the return of shoots to callus or tissue necrosis can occur due to prolonged exposure to TDZ (Vinoth & Ravindhran, 2018). The ability of thidiazuron to both inhibit cytokinin oxidase enzyme and trigger cytokinin biosynthesis will lead to cytokinin accumulation in plant cells. Excessive cytokinin accumulation during prolonged TDZ exposure can lead to necrosis or cell death (Nisler, 2018; Pai & Desai, 2018).

The increased number of shoots indicates *in vitro* plant propagation success (Akbar *et al*., 2017). ANOVA results (Table 1) showed no significant difference in shoot number and length. Nevertheless, adding 6-Benzylaminopurine at 0 and 2 µM; Kinetin at 0, 1, 2, and 4 µM gave rise to the highest axillary bud growth percentage (100%) (Figure 3). In comparison, the supplementation of thidiazuron at 2 µM produced the smallest percentage of axillary bud appearance (33.3%). According to Pallardy & Kozlowski (2008) and Sarmast *et al*. (2012), most conifers produce few or no axillary buds. Members of the *Araucariaceae* family, such as Araucaria, Agathis, and Wollemia, have unique axillary buds with undifferentiated meristems that lack leaf primordia and contain vascular tissue. In *pines*, *cypresses*, oaks, and hickories, shoots originate from the expansion of apical buds of the main stem and branches. There is a period of dormancy after the apical bud extends until a new terminal bud is formed and developed. Due to strong apical dominance, the apical bud extends more yearly than the lateral buds below it. Removal of the apical bud, which then removes apical dominance in conifers, can significantly affect the growth of axillary buds (Pallardy & Kozlowski, 2008).

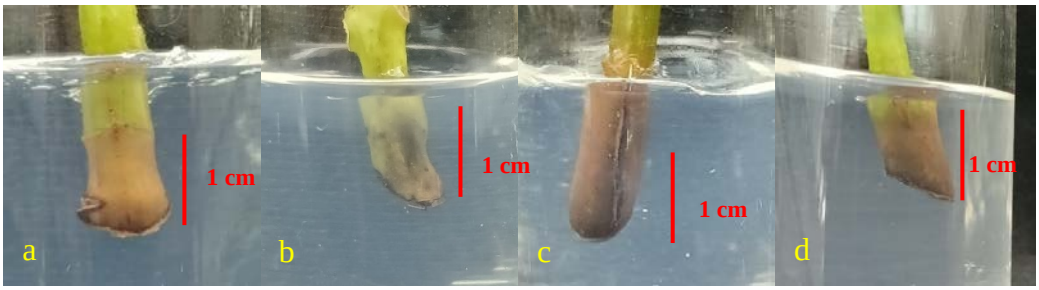

Figure 2. Condition of *A. borneensis* explants on media with the addition of TDZ at the age of 16 wap: (a) 1 µM TDZ; (b) 2 µM TDZ; (c) 3 µM TDZ; (d) 4 µM TDZ.

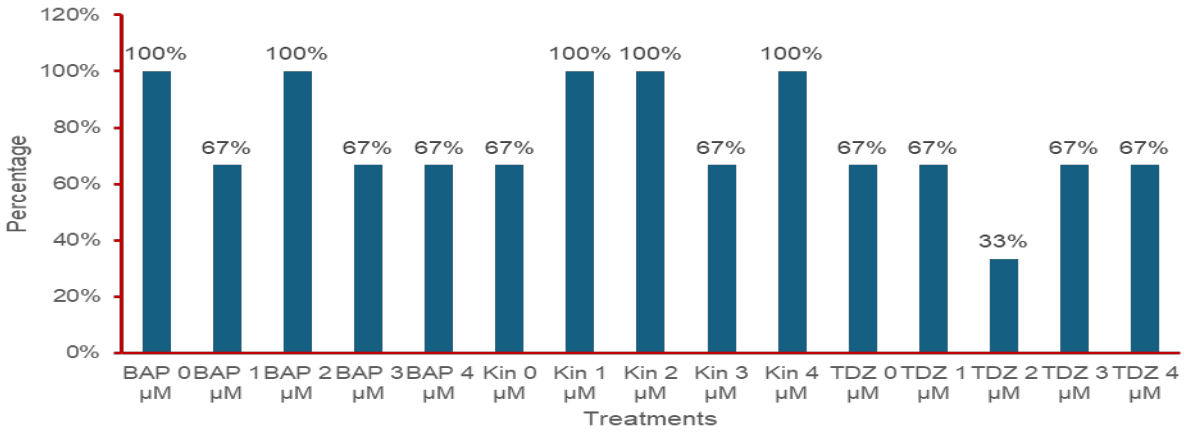

Figure 3. Percentage of *A. borneensis* sprouting explants in response to cytokinin types and concentrations at 16 wap.

Leaf formation is a form of vegetative growth in plants. Leaf formation in plants is susceptible to environmental changes and growth regulators, both endogenous and exogenous (Magdhalena *et al*., 2021). The ANOVA results

(Table 1) showed that *A. borneensis* Warb leaf formation was controlled by cytokinin concentration. Moreover, DMRT results (Figure 4) showed that explants of *A. borneensis* cultured on media without cytokinin produced the largest number of leaves (2.74±0.31 leaves/explant), which was not significantly different to those cultured on media supplemented with cytokinin at 1 µM and 4 µM, which produces 2.53±1.50 and 1.98±1.10 leaves/explant, respectively. Figure 4 also revealed that increasing the cytokinin concentration to 3 µM significantly reduced leaf number. Shoot's response to 3 types of cytokinin at 4 different concentrations is shown in Figure 5. According to Sarmast *et al*. (2012), axillary buds can be produced from *Araucaria excelsa* R.Br. orthotropic stems, even when growth regulators were absent. In other studies, cytokinin-free MS media also increased plant height with more leaves and shoots in *Guazuma ulmifolia* (Hernandez-Santana *et al*., 2021), *Cedrela fissilis* (Bonfá *et al*., 2021), *Citrus hystrix* (Handayani *et al*., 2024), and *Morus nigra* (Phillips & Garda, 2019) cultures because *in vitro* culture media contain sufficient nutrients for plant development.

MS medium is commonly used in *in vitro* plant propagation. MS media contains high nitrogen content (nitrate and ammonium), suitable for plant regeneration (Phillips & Garda, 2019). MS medium's macro-element composition (K+, Mg2+, N, NO3-, and NH4+) may balance nitrogen uptake, osmotic regulation, pH, and cation-anion balance in plant growth. At high nitrate levels, *Eucalyptus* hybrid cultures showed average shoot growth with green leaves, no hyperhydration, and produced an average shoot length of more than 1.4 cm (Máximo *et al*., 2015).

The growth of *A. borneensis* on MS media without additional growth regulators could also be attributed to endogenous growth regulators in *the A. borneensis* shoot. According to Li *et al*. (2021) and Rai *et al*. (2022), success or failure in in vitro culture can result from variations in endogenous growth regulator levels in plants. In plants, endogenous cytokinin levels are well-regulated in response to growth events, such as axillary bud formation, and to environmental factors, such as light and nutrients (Bredmose & Costes, 2017). Regulation of growth and organogenesis is associated with balancing endogenous and exogenous growth regulators (Aremu *et al*., 2014; Boston *et al*., 2013; George, 1993; Park, 2021).

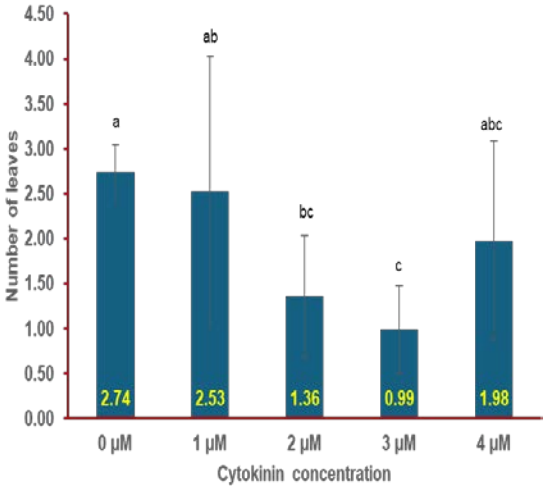

Figure 4 DMRT results of the average number of *A. borneensis* shoots at different cytokinin concentrations at 16 wap. Note: Means followed by the same letter indicate no significant difference at 95% DMRT level of confidence.

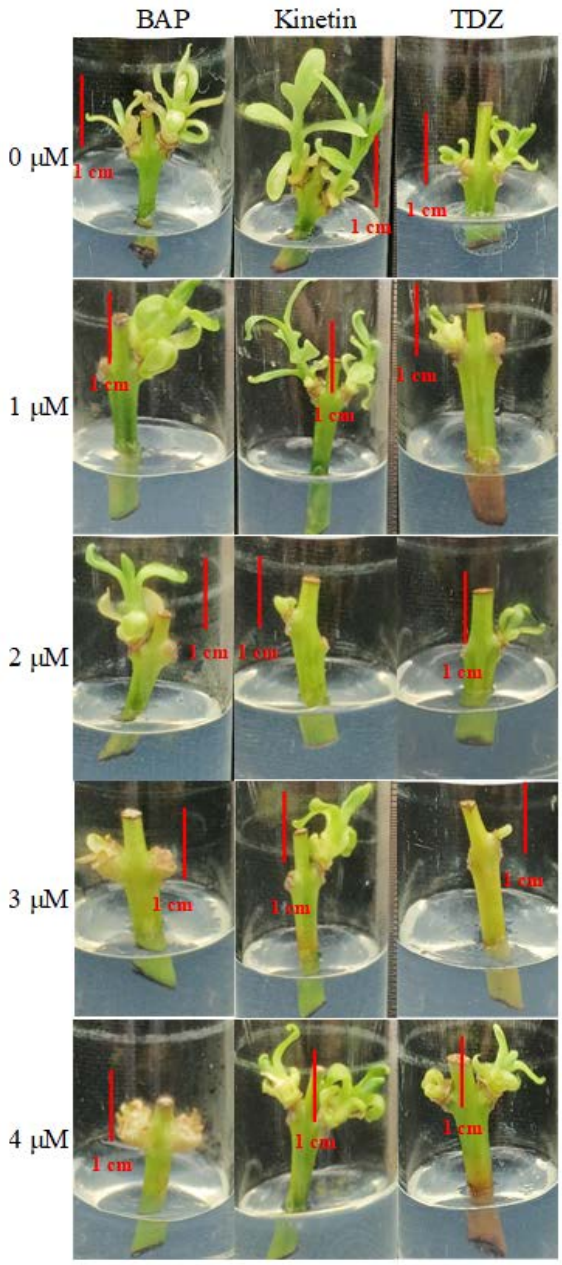

Figure 5. Conditions of *A. borneensis* shoots grown in 3 types of cytokinins on 5 concentrations at 16 wap.

In *in vitro* culture, the need to modify nutrient media composition, types and concentrations of cytokinins depends on plant species, genotype, explant type, ontogeny phase, and stage of the micropropagation process (Iliev, 2017). In this study, *A. borneensis* explants that grew in MS media without growth regulators suggest that the nutrient content, vitamins, organic components, and carbon sources were sufficient to support *A. borneensis* growth and differentiation. Kinetin at 1 µM induced the fastest shoot emergence. It is suggested that the application of kinetin interacts with endogenous growth regulators in *the A. borneensis* shoot. According to Bredmose & Costes (2017), increased growth of axillary buds results from the decrease of auxin and increase of cytokinin concentrations, thus increasing the ratio of cytokinin to auxin. Therefore, it is suggested that 1 µM kinetin could accelerate the production of *A. borneensis* seedlings.

Plant growth regulators affect many processes and conditions, including enzymatic activity, membrane permeability, cell wall relaxation, cell division and elongation, and tissue and organ senescence. Many pieces of evidence suggest that plant growth and differentiation are controlled more by interactions between plant growth regulators (Pallardy & Kozlowski, 2008).

4. Conclusion

The lateral shoot apex of *A. borneensis* collected from the Bogor Botanical Garden was sterilized and cultured on MS medium, supplemented with 3% sucrose, 100 mg/L myo-inositol, and solidified with 0.7% agar. Different types and concentrations of cytokinin were tested to induce shoot formation. It was found that cytokinin type and concentration controlled *the time of A. borneensis* shoot emergence in *in vitro* culture. *A. borneensis* explants cultured on MS media supplemented with 1µM kinetin produced the fastest shoot emergence. Meanwhile, *A. borneensis* shoots grown on MS media without cytokinin yielded the highest leaf number. Shoot multiplication and subsequent plantlet formation must be done to produce a large quantity of *A. borneensis* seedlings.

Acknowledgments

The authors wish to thank the Deputy for Research and Innovation Infrastructure (DIRI) and the Directorate of Talent Management, National Research and Innovation Agency, for providing the grant via the BARISTA Program, and the Directorate of Scientific Collection Management of Bogor Botanical Garden for providing the explants.

References

Adam, A. Z., Juiling, S., Lee, S. Y., Jumaat, S. R., & Mohamed, R. (2017). Phytochemical Composition of Agathis borneensis (Araucariaceae) and Their Biological Activities. *Mal. For.*, **80(2)**, 169–177.

Agustina, D., Tarwotjo, U., Rahadian, R., & Article, H. (2019). The Effectiveness of Plastic Mulch for Maintaining the Potato Farmland in Dieng Plateau Using Soil Biological Quality Index. *Biosaintifika*, **11(1)**, 125–131.

Ahmad, N., & Faisal, M. (2018). Thidiazuron: From urea derivative to plant growth regulator. In **Thidiazuron: From Urea Derivative to Plant Growth Regulator.** https://doi.org/10.1007/978-981-10-8004-3

Ahmed, A. H., & Mohamed, S. A. (2022). Triterpenoids from Agathis robusta Aerial Parts and Their Hepatoprotective Activity. *Phcog J*, **14(4)**, 362–366. https://doi.org/10.5530/pj.2022.14.108

Akbar, A. M., Faridah, E., Indrioko, S., & Herawan, T. (2017). Induksi Tunas, Multiplikasi dan Perakaran Gyrinops versteegii (Gilg.) Domke Secara In Vitro. *JPTH*, **11(1)**, 1–13.

Andriani, C., Kadapi, M., Suminar, E., & Nuraini, A. (2023). Perbandingan Efek BAP dan Kinetin Terhadap Laju Multiplikasi Stroberi Kultivar Sweet Charlie. *JA*, **14(1)**, 13. https://doi.org/10.24014/ja.v14i1.18824

Aremu, A. O., Plačková, L., Bairu, M. W., Novák, O., Plíhalová, L., Doležal, K., Finnie, J. F., & Van Staden, J. (2014). How Does Exogenously Applied Cytokinin Type Affect Growth and Endogenous Cytokinins in Micropropagated Merwilla plumbea? *PCTOC*, **118(2)**, 245–256. https://doi.org/10.1007/s11240-014-0477-5

Bala, R., Laura, J. S., & Beniwal, V. S. (2018). Efficient In vitro Direct Regeneration From Nodal Explants of Simmondsia chinensis (Link) Schneider-A Potential Multipurpose Plant. *PCBMB*, **19(7–8)**, 256–265. https://ikprress.org/index.php/PCBMB/article/view/1358

Barciszewski, J., Massino, F., & Clark, B. F. C. (2007). Kinetin-A multiactive molecule. *Int. J. Biol. Macromol.*, **40(3)**, 182–192. https://doi.org/10.1016/j.ijbiomac.2006.06.024

Biradar, S. R. (2022). **An Introduction of Plant Tissue Culture** (5th ed.). RUT printer and publisher. https://www.researchgate.net/publication/361304964

Bonfá, Y. S., De Laia Nascimento, V., & Terra Werner, E. (2021). In Vitro Multiplication of Cedrela fissilis Vell.: A Threatened Brazilian Hardwood Forest Tree. *PCCM*, **17**, 1–11. https://doi.org/10.46526/pccm.2021.v17.165

Boston, A. •, Heidelberg, •, London, •, San, P. •, San, D., Singapore, F. •, Tokyo, S. •, & Smith, R. H. (2013). **Plant Tissue Culture Techniques and Experiments**, Third Edition. Elsevier. www.elsevierdirect.com/rights

Bredmose, N., & Costes, E. (2017). Axillary Bud Growth. In **Reference Module in Life Sciences** (p. B9780128096338051000). Elsevier. https://doi.org/10.1016/B978-0-12-809633-8.05056-1

Chukwu, S. C., Awala, · S K, Angombe, · S, Valombola, · J S, Nanhapo, · P I, Mberama, · C, Mohd, ·, Rafii, Y., Oladosu, Y., Thomas, · B, Okporie, E. O., & Musa, I. (2025). Recent progress in tissue culture techniques and biotechnological innovations for banana production (Musa spp.): a review. *Discov. Plant.*, *2025* **2(1)**, 1–24. https://doi.org/10.1007/S44372-025-00099-2

Darma, I. D. P., Iryadi, R., Rahayu, A., Hanum, S. F., & Sutomo, S. (2022). Keragaman Jenis Agathis di Dunia dan Riap Tahunan Agathis dammara (Lamb.) Poir. dan Agathis borneensis Warb. di Kebun Raya Eka Karya, Bali. *BKR*, **25(1),** 34–43.

Fajar, D., Cahyanto, T., & Fadillah, A. (2018). Waktu Tumbuh Mata Tunas Daun Mangifera indica L. Pada Berbagai Tingkatan. *Edubiotik* **3(01)**, 19–25. https://doi.org/10.33503/ebio.v3i01.73

Farjon, A. (2013). Agathis borneensis. **IUCN Red List of Threatened Species**. https://doi.org/10.2305/IUCN.UK.2013-1.RLTS.T202905A2757743.EN

Farjon, A. (2017). **A Handbook of the World's Conifers** (rerevised Brill, Vol. 1).

Fathy, M., Saad Eldin, S. M., Naseem, M., Dandekar, T., & Othman, E. M. (2022). Cytokinins: Wide-Spread Signaling Hormones from Plants to Humans with High Medical Potential. *Nutrients*, **14(7)**, 1495. https://doi.org/10.3390/nu14071495

George, E. F. (1993). **Plant propagation by Tissue Culture Part I. The Technology Exegetics**.

George, E. F., Hall, M. A., & Klerk, G.-J. de. (2008). ***Plant Propagation by Tissue Culture*** (3rd ed). Springer.

Gogoi, G., Borua, P. K., & Al-Khayri, J. M. (2017). Improved Micropropagation and In Vitro Fruiting of Morus indica L. (K-2 cultivar). *J. Genet. Eng. Biotechnol.*, **15(1)**, 249–256. https://doi.org/10.1016/j.jgeb.2017.02.005

Handayani, R. S., Nilahayati, N., Ismadi, I., Akmal, A., Aprilia, D., & Sevia, E. D. (2024). Growth Response of Sweet Kaffir Lime (Citrus hystrix) Seeds Due to Kinetin and Coconut Water Application Using Tissue Culture Technique. *IOP Conf. Ser. Earth Environ. Sci.*, **1297(12–15)**, 1–7. https://doi.org/10.1088/1755-1315/1297/1/012015

Hernandez-Santana, V., Perez-Arcoiza, A., Gomez-Jimenez, M. C., & Diaz-Espejo, A. (2021). Disentangling the link between leaf photosynthesis and turgor in fruit growth. *Plant J.*, **107(6),** 1788–1801. https://doi.org/10.1111/tpj.15418

Iliev, I. A. (2017). Factors Affecting The Axillary and Adventitious Shoot Formation in Woody Plants In Vitro. *Acta Hortic.*, **1155(2)**, 15–28. https://doi.org/10.17660/ActaHortic.2017.1155.2

Ishii, K., & Mohsin, R. B. H. (1994). Tissue Culture of Some Dipterocarps and Agathis in Brunei. *Bull. Forestry Forest Prod. Res. Inst.*, **366**, 115–127.

Justine, A. K., Kaur, N., Savita, & Pati, P. K. (2022). Biotechnological interventions in banana: current knowledge and future prospects. *Heliyon*, **8(11),** 1–14. https://doi.org/10.1016/j.heliyon.2022.e11636

Kher, M. M., Joshi, D., Nekkala, S., Nataraj, M., & P. Raykundaliya, D. (2014). Micropropagation of Pluchea lanceolata (Oliver & Hiern.) Using Nodal Explant. *J. Hort. Res*., **22(1)**, 35–39. https://doi.org/10.2478/johr-2014-0004

Kulkarni, A. A., Thengane, S. R., & Krishnamurthy, K. V. (1996). Direct in vitro regeneration of leaf explants of Withania somnifera (L.) Dunal. *Plant Sci.*, **119(1–2)**, 163–168. https://doi.org/10.1016/0168-9452(96)04462-7

Li, S. M., Zheng, H. X., Zhang, X. S., & Sui, N. (2021). Cytokinins as central regulators during plant growth and stress response. *Plant Cell Rep.*, **40(2)**, 271–282. https://doi.org/10.1007/s00299-020-02612-1

Magdhalena, A. P., Asmanto, B. P., Sulandjari, S., & Yunus, A. (2021). The Effect of Concentration and Time Interval of Kinetin Application on the Growth of Daun Duduk (Desmodium triquetrum L.) Seeds. *JBB*, **1(1)**, 29. https://doi.org/10.20961/jbb.v1i1.50418

Máximo, W. P. F., Santos, P. A. A., Mendonça, E. G., Santos, B. R., & Paiva, L. V. (2015). Nitrate (NO3-) and Ammonium (NH4+) Ratios for Propagation of Eucalyptus Hybrid in Two Different In Vitro Cultivation Systems. *AJCS*, **9(12)**, 1242–11248.

Naaz, A., Siddique, I., & Ahmad, A. (2021). TDZ-Induced Efficient Micropropagation from Juvenile Nodal Segment of Syzygium cumini (Skill): A Recalcitrant Tree. In I. Siddique (Ed.), **Propagation and Genetic Manipulation of Plants**. Springer Singapore. https://doi.org/10.1007/978-981-15-7736-9

Neogy, A., Singh, Z., Mushahary, K. K. K., & Yadav, S. R. (2020). Dynamic cytokinin signaling and function of auxin in cytokinin-responsive domains during rice crown root development. *Plant Cell Rep.*, **1(0123456789)**. https://doi.org/10.1007/s00299-020-02618-9

Nisler, J. (2018). TDZ: Mode of action, use, and potential in agriculture. In **Thidiazuron: From Urea Derivative to Plant Growth Regulator** (pp. 37–59). Springer Singapore. https://doi.org/10.1007/978-981-10-8004-3_2

Pai, S. R., & Desai, N. S. (2018). Effect of TDZ on Various Plant Cultures. In N. Ahmad & M. Faisal (Eds.), **Thidiazuron: From Urea Derivative to Plant Growth Regulator** (pp. 439–454). Springer Singapore. https://doi.org/10.1007/978-981-10-8004-3_25

Pallardy, S. G., & Kozlowski, T. T. (2008). **Physiology of Woody Plants** (3rd ed). Elsevier.

Park, S. (2021). ***Plant Tissue Culture Techniques and Experiments*** (Fourth Edition). Academic Press Elsevier.

Phillips, G. C., & Garda, M. (2019). Plant Tissue Culture Media and Practices: An Overview. *In vitro Cell Dev Biol Plant*, **55(3)**, 242–257. https://doi.org/10.1007/s11627-019-09983-5

Prasetyo, R., Sugiyono, & Prayoga, L. (2020). INDUKSI TUNAS MIKRO PISANG KULTIVAR AMBON NANGKA (Musa sp .) SECARA IN VITRO. *Vigor*, **5(2)**, 45–50.

Putriana, Gusmiati, Restu, M., Musriati, & Aida, N. (2019). Respon Kinetin dan Tipe Eksplan Jabon Merah (Antocephalus macrophyllus (Roxb.) Havil) Secara In Vitro. *BIOMA*, **4(1)**, 48–57.

Rai, A. C., Kumar, A., Modi, A., & Singh, M. (2022). **Advances in Plant Tissue Culture**. Elsevier.

Ram, K., Patel, A. K., Choudhary, S. K., & Shekhawat, N. S. (2022). Synergetic Effects of TDZ With Various Phytohormones on High-Frequency Plant Regeneration From Mature Nodal Explants of Capparis decidua and Their Ex vivo Implications. *PCTOC*, **149(3)**, 621–633. https://doi.org/10.1007/s11240-022-02234-3

Rathore, J. S., Rathore, V., Shekhawat, N. S., Singh, R. P., Liler, G., Phulwaria, M., & Dagla, H. R. (2004). Micropropagation of Woody Plants. In **Plant Biotechnology and Molecular Markers**. Springer. https://link.springer.com/chapter/10.1007/1-4020-3213-7_13

Ružić, Đ., Vujović, T., & Cerović, R. (2016). In Vitro Multiplication of Semi-Dwarfing Pear Rootstock 'Pyrodwarf' in Relation to Cytokinin Types. *Acta Hortic.*, **1139**, 279–284. https://doi.org/10.17660/ActaHortic.2016.1139.49

Sarmast, M. K., Salehi, H., & Khosh-Khui, M. (2012). Micropropagation of Araucaria excelsa R. Br. var. glauca Carrière from Orthotropic Stem Explants. *Physiol Mol Biol Plants*, **18(3)**, 265–271. https://doi.org/10.1007/s12298-012-0115-9

Sitompul, S. M., & Guritno, B. (1995). **Analysis of Plant Growth**. Universitas Gadjah Mada Press.

Stalin, A. N., & Franco, F. M. (2021). Agathis borneensis Warb. Araucariaceae. In F. M. Franco (Ed.), **Ethnobotany of the Mountain Regions of Southeast Asia** (pp. 65–71). Springer International Publishing. https://doi.org/10.1007/978-3-030-38389-3_163

Steward, G. A., Kimberley, M. O., Mason, E. G., & Dungey, H. S. (2014). Growth and Productivity of New Zealand kauri (Agathis australis (D.Don) Lindl.) in Planted Forests. *NZJFS*, **44(1)**, 27. https://doi.org/10.1186/s40490-014-0027-2

Taha, R. A., Allam, M. A., Hassan, S. A. M., Bakr, B. M. M., & Hassan, M. M. (2021). Thidiazuron-induced direct organogenesis from immature inflorescence of three date palm cultivars. *J. Genet. Eng. Biotechnol.*, **19(1)**, 14. https://doi.org/10.1186/S43141-021-00115-4

Tamyiz, M., Prayoga, L., Prasetyo, R., Murchie, E. H., & Sugiyono. (2022). Improving Agarwood (Aquilaria malaccensis Lamk.) Plantlet Formation Using Various Types and Concentrations of Auxins. *Caraka Tani J. Sustain. Agric.*, **37(1)**, 142–151. https://doi.org/10.20961/carakatani.v37i1.58370

Thorat, S. A., Kaniyassery, A., Poojari, P., Rangel, M., Tantry, S., Kiran, K. R., Joshi, M. B., Rai, P. S., Botha, A.-M., & Muthusamy, A. (2022). Differential Gene Expression and Withanolides Biosynthesis During In Vitro and Ex Vitro Growth of Withania somnifera (L.) Dunal. *Front. Plant Sci.*, **13**, 917770. https://doi.org/10.3389/fpls.2022.917770

Vinoth, A., & Ravindhran, R. (2018). In Vitro Morphogenesis of Woody Plants Using Thidiazuron. In N. Ahmad & M. Faisal (Eds.), **Thidiazuron: From Urea Derivative to Plant Growth Regulator** (pp. 211–229). Springer Singapore. https://doi.org/10.1007/978-981-10-8004-3_10

Widyatmoko, D. D. (2019). Strategi Dan Inovasi Konservasi Tumbuhan Indonesia Untuk Pemanfaatan Secara Berkelanjutan. *Prosiding Seminar Nasional Pendidikan Biologi dan Saintek (SNPBS)*, **4**, 1–22.

Yadav, A., Prasad, Y., Kumar, M., Pandey, S., Maurya, R., & Pandey, P. (2021). Effects of Mercuric chloride and Ethanol for surface sterilization under in vitro plant growth in banana (Musa paradisiaca L.) variety "Udhayam." *J. Pharmacogn. Phytochem.*, **10(1)**, 2281–2283. https://www.phytojournal.com/archives/2021.v10.i1.13693/effects-of-mercuric-chloride-and-ethanol-for-surface-sterilization-under-in-vitro-plant-growth-in-banana-musa-paradisiaca-l-variety-8220udhayam8221

Zhao, J., Wang, J., Liu, J., Zhang, P., Kudoyarova, G., Liu, C.-J., & Zhang, K. (2024). Spatially Distributed Cytokinins: Metabolism, Signaling, and Transport. *Plant Commun.*, **5(100936)**, 1–16. https://doi.org/10.1016/j.xplc.2024.100936

Zhao, X., Han, X., Wang, Q., Wang, X., Chen, X., Li, L., Fu, X., & Gao, D. (2020). Early Bud Break 1 Triggers Bud Break in Peach Trees by Regulating Hormone Metabolism, The Cell Cycle, and Cell Wall Codifications. *J. Exp. Bot.*, **71(12)**, 3512–3523. https://doi.org/10.1093/jxb/eraa119

Subscription

Jordan Journal of Biological Sciences

An International Peer – Reviewed Research Journal

Published by the Deanship of Scientific Research, The Hashemite University, Zarqa, Jordan

Name: ..... الاسم:

Specialty: ..... التخصص:

Address: ..... العنوان:

P.O. Box: ..... صندوق البريد:

City &Postal Code:..... المدينة: الرمز البريدي:

Country: ..... الدولة:

Phone: ..... رقم الهاتف

Fax No.: ..... رقم الفاكس:

E-mail: ..... البريد الإلكتروني:

Method of payment: ..... طريقة الدفع:

Amount Enclosed: ..... المبلغ المرفق:

Signature: ..... التوقيع:

Cheque should be paid to Deanship of Research and Graduate Studies – The Hashemite University.

I would like to subscribe to the Journal

For

- ☐ One year
- ☐ Two years
- ☐ Three years

One Year Subscription Rates

	Inside Jordan	Outside Jordan
Individuals	JD10	$70
Students	JD5	$35
Institutions	JD 20	$90

Correspondence

Subscriptions and sales:

The Hashemite University
P.O. Box 330127-Zarqa 13115 – Jordan
Telephone: 00 962 5 3903333
Fax no. : 0096253903349
E. mail: jjbs@hu.edu.jo

المجلة الأردنية للعلوم الحياتية
Jordan Journal of Biological Sciences (JJBS)

http://jjbs.hu.edu.jo

المجلة الأردنية للعلوم الحياتية: مجلة علمية عالمية محكمة ومفهرسة ومصنفة، تصدرعن الجامعة الهاشمية وبدعم من صندوق دعم البحث العلمي والإبتكار – وزراة التعليم العالي والبحث العلمي.

ترسل البحوث الى العنوان التالي:

رئيس تحرير المجلة الأردنية للعلوم الحياتية
الجامعة الهاشمية
ص.ب , 330127 , الزرقاء, 13115 , الأردن
هاتف: 0096253903333
E-mail: jjbs@hu.edu.jo, Website: www.jjbs.hu.edu.jo

المملكة الأردنية الهاشمية

المجلة الأردنية

للعلوم الحياتية

مجلة علمية عالمية محكمة

تصدر بدعم من صندوق دعم البحث العلمي و الابتكار

http://jjbs.hu.edu.jo/